

2010

annual progress report

Lightweighting Material

Contents

A. Acronyms and Abbreviations

Acronyms and Abbreviations.....	A-1
---------------------------------	-----

1. Introduction

Introduction.....	1-1
-------------------	-----

2. Automotive Metals

A. Processing and Manufacturability - Oak Ridge National Laboratory.....	2-1
B. Processing and Manufacturability - Pacific Northwest National Laboratory.....	2-8
C. Modeling and CMS - Oak Ridge National Laboratory.....	2-31
D. Modeling and Computational Material Science - Pacific Northwest National Laboratory.....	2-35
E. Southern Regional Center For Lightweight Innovative Designs - Mississippi State University.....	2-39
F. Multi-material Enabling - Oak Ridge National Laboratory.....	2-67
G. Multi-Material Enabling - Pacific Northwest National Laboratory.....	2-80
H. A Study of the Effects of Microstructure on the Mechanical Properties and Failure Mechanisms of Advanced High-Strength Steels.....	2-89
I. Development of Nano-Acicular Duplex Steels.....	2-95

3. Polymer Composites

A. Polymer Composite Development - Pacific Northwest National Laboratory.....	3-1
B. Polymer Composite Development - Oak Ridge National Laboratory.....	3-10
C. Low Cost Carbon Fiber Development - Oak Ridge National Laboratory.....	3-28
D. Carbon Fiber Technology Center.....	3-50

4. USMP Cooperative Research

A. Automotive Composites Consortium.....	4-1
B. Automotive Metals Division - U.S. Automotive Materials Partnership.....	4-16
C. Auto/Steel Partnership - U.S. Automotive Materials Partnership.....	4-57
D. Nondestructive Evaluation Steering Committee - U.S. Automotive Materials Partnership.....	4-85
E. Multi-Material Vehicle - U.S. Automotive Materials Partnership.....	4-91

5. Recycling

A. Recycling End-of-Life Vehicles Of The Future - Argonne National Laboratory.....	5-1
--	-----

6. Crosscutting

A. Cost Modeling - Oak Ridge National Laboratory.....	6-1
B. Safety Data and Analysis - Lawrence Berkeley National Laboratory.....	6-6

ALM 2010 Acronyms and Abbreviations

μm	micrometer (micron)
1D	one dimensional
2D	two dimensional
3D	three dimensional

A

ABS	acrylonitrile-butadiene-styrene
ACC	Automotive Composites Consortium
ACC-PD	American Chemistry Council–Plastics Division
ACTS	Advanced Concepts Test Stand
AET	Applied Engineering Technologies, Inc.
AHSS	advanced high-strength steel
Al	aluminum
AMD	Automotive Metals Division
AMI	Autodesk Moldflow Insight
ARL	U.S. Army Research Laboratory
ARD-RSC	anisotropic rotary diffusion–reduced strain closure
A/SP	Auto/Steel Partnership
ASTM	American Society for Testing and Materials

B

bcc	body centered cubic
BIW	body-in-white
BN	boron nitride

C

C	carbon
CA	cellular automaton
CAD	computer aided design
CAE	computer aided engineering
CALPHAD	CALculated PHase Diagrams
CAVS	Center for Advanced Vehicular Systems
CC	continuous cast

CCD	charge-coupled device
CeCC	cerium based conversion coating
CF	carbon fiber
CFSL	carbon fiber semi-production line
CFTC	Carbon Fiber Technology Center
CLSM	confocal laser scanning microscope
CMH-17	Composite Materials Handbook 17
CNW	cellulose nanowhisker
CMS	computational materials science
CO2	carbon dioxide
CPI	Composite Products, Inc.
CRO	Community Reuse Organization
CSUV	car-based SUV
CT	computed tomography
CUV	crossover utility vehicle
CY	calendar year

D

DCT	dual clutch transmission
DFT	discrete Fourier transform
DI	direct injection
DIC	digital image correlation
DLFT	direct injected LFT
DMG	(coupled) elasto-viscoplastic-damage
DOE	U.S. Department of Energy
DOHC	dual overhead camshaft
DOHV	dual overhead valves
DP	dual phase
DRIFT	Direct Reinforcement Fabrication Technology
DSC	differential scanning calorimetry

E

EBSD	electron backscatter diffraction
e-coat/coating	electrocoat/electrocoating

EC	eutectic constituent
ED	extruded direction
EDS	energy dispersive spectroscopy
EHF	electrohydraulic forming
ELV	end-of-life vehicle
EMTA	Eshelby-Mori-Tanka
EMP	electromagnetic pump
EPA	US Environmental Protection Agency
EPFL	École Polytechnique Fédérale de Lausanne
EPMA	electron probe microanalysis
ESEM	environmental scanning electron microscope
ESPEI	extensible, self-optimizing magnesium phase equilibrium infrastructure
ETD	extruded transverse direction
ETW	equivalent test weight

F

FARS	Fatality Analysis Reporting System
fcc	face centered cubic
Fe	iron
FE	finite element
FEA	finite element analysis
FEM	finite element modeling
FFI	full frontal impact
FGPC	Future Generation Passenger Compartment
FISIPE	Fibras Sinteticas de Portugal S.A.
FLCA	front lower control arm
FLD	forming limit diagram
FM	flexural modulus
FPI	fluorescent penetrant inspection
fps	frames per second
FRPMC	fiber-reinforced polymer-matrix composite
FS	flexural structure
FSSW	friction stir spot weld/welding
FSW	friction stir welding

FTIR	Fourier transform infrared spectroscopy
FY	fiscal year

G

GBCE	grain boundary cohesion energy
GCWR	gross combined weight rating
Gen	generation
GHG	greenhouse gas
GM	General Motors
GMAW	gas-metal arc welding
GSF	generalized stacking fault
GVWR	gross vehicle weight rating

H

H&E	hematoxylin and eosin
HAZ	heat-affected zone
hcp	hexagonal close packed
HDG	hot-dip-galvanized
HP	high pressure
HSS	high-strength steel

I

I4	inline (architecture), four cylinders
IACS	International Annealed Copper Standard
ICAF	intergranular corrosion area fraction
ICME	Integrated Computational Materials Engineering
IISI	International Iron and Steel Institute
I/M	inspection and maintenance
IR	infrared
ISF	intrinsic stacking fault
ISV	internal state variable

K

K-PhD	kindergarten through doctoral level
KR	kriging

L

LB	lattice Boltzmann
LBNL	Lawrence Berkeley National Laboratory
LCA	life-cycle analysis
LDH	limiting dome height
LCCF	low cost carbon fiber
LENS	laser engineered net shaping
LFT	long fiber thermoplastic
LGK	Lipton-Glickson-Kurz
LM	Lightweight Materials
LP	low pressure
LPPM	low pressure permanent mold (casting process)
LSEM	large strain extrusion machining
LSTC	Livermore Software Technology Corporation

M

MCTS	Materials Compatibility Test Stand
MD	molecular dynamics
MEAM	modified embedded atom method
MEARS	Mass Efficient Architecture for Roof Strength
MFED	Magnesium Front End Design and Development
MFERD	Magnesium Front End Research and Development
MIG	metal inert gas
Mg	magnesium
MgO	magnesium oxide
Missouri S&T	Missouri University of Science and Technology
MMV	multi-material vehicle
Mn	manganese
MSF	multistage fatigue
MSST	Mississippi State University

MTR1	Multiple Tow Reactor 1
MY	model year

N

NA	naturally aspirated
NASS GES	National Automotive Sampling System General Estimates System
NCMS	National Center for Manufacturing Science
NDE	nondestructive evaluation
NHTSA	National Highway Traffic Safety Administration
NIST	National Institute of Standards and Technology
NLA	nonlinear analysis
NPSS	nanosize precipitate strengthened steel
NSF	National Science Foundation
NSP	nonlinear strain path
NTRC	National Transportation Research Center
NVH	noise, vibration, and harshness

O

OEM	original equipment manufacturer
OFI	offset frontal impact
OHV	overhead valve
OM	optical microscopy
ORNL	Oak Ridge National Laboratory
OU	Oakland University
OVT	Office of Vehicle Technologies (DOE)

P

PAN	polyacrylonitrile
PB	paint-baked
PCB	polychlorinated biphenyl
PCBN	polycrystalline cubic boron nitride
PE	polyethylene
PEL	precursor evaluation line
PEO	polyethylene oxide

PET	polyethylene terephthalate
PFI	port fuel injection
phr	parts per hundred parts resin
PI	principal investigator
PFSL	precursor fiber semi-production line
PM	powder metallurgy
PMC	polymer-matrix composite
PNNL	Pacific Northwest National Laboratory
POD	probability of detection
PP	polypropylene
PPF	pulse pressure forming
PS	polystyrene
PSC	Project Steering Committee
PSHPB	polymeric split Hopkinson pressure bar
PTC	project technical committee

R

R&D	research and development
RBF	radial basis function
RD	rolling direction
RI	resonant inspection
RSW	resistance spot welding
RT	radiographic testing
RTM	resin transfer molding
RUC	representative unit cell

S

S	Sulfer
SABIC-IP	SABIC Innovative Plastics
SBSS	short beam shear strength
SCC	stress corrosion cracking
SCRLED	Southern Regional Center for Lightweight Innovative Designs
SDS	state data system
SEA	specific energy absorption

SEM	scanning electron microscopy
SFE	stacking fault energy
SGL	SGL Group
SI	side impact
Si ₃ N ₄	silicon nitride
SIMS	secondary ion mass spectrometry
SMC	sheet molding compound
SO ₂	sulfur dioxide
SOC	substances of concern
SOHC	single overhead camshaft
SOM	solid oxygen-ion conducting membrane
SOW	statement of work
SPF	superplastic forming
SRIM	structural reaction injection molding
SUV	sport utility vehicle
SVDC	super vacuum die casting
SVR	support vector regression
SWE	spot weld element

T

TC	turbocharged
TCLP	toxicity characteristic leaching procedure
TD	transverse direction
TEM	transmission electron microscopy
Ti	titanium
TMAC	testing machine for automotive composites
TM	tensile modulus
TMS	The Minerals, Metals & Materials Society
TOF- SIMS	time-of-flight secondary ion mass spectrometry
TRC	textile reinforced composite
TRIP	transformation-induced plasticity
TS	tensile strength
TTMP	thixomolded thermomechanical processing
TWIP	twining induced plasticity

U

UHV	untrahigh vacuum
USAMP	U.S. Automotive Materials Partnership
USCAR	United States Council for Automotive Research
USF	unstable stacking fault
USW	ultrasonic welding
UTS	ultimate tensile strength
UV	ultraviolet

V

V6	V-architecture, six cylinders
VA	vinyl acetate
VE	vinyl ester
VGCNF	vapor grown carbon nanofiber
VIC	video image correlation
VIN	vehicle identification number
VTP	Vehicle Technologies Program

W

WPS	Welding Procedure Specification
WSU	Wayne State University

X

XPS	x-ray photoelectron spectroscopy
XRD	x-ray diffraction

Y

YSZ	yttria-stabilized zirconia
-----	----------------------------

Z

Zn	zinc
----	------

Introduction

As a component of the U.S. Department of Energy's (DOE's) Vehicle Technologies Program (VTP), the Lightweight Materials activity (LM) focuses on the development and validation of advanced materials and manufacturing technologies to significantly reduce light and heavy duty vehicle weight without compromising other attributes such as safety, performance, recyclability, and cost. Because it takes less energy to accelerate a lighter object, replacing cast iron and traditional steel components with lightweight materials such as high-strength steel (HSS), magnesium (Mg), aluminum (Al), and polymer composites can directly reduce a vehicle's fuel consumption. For example, a 10% reduction in vehicle weight can result in a 6%–8% fuel economy improvement. Reducing vehicle weight has other benefits such as allowing cars to carry advanced emissions control equipment, safety devices, and integrated electronic systems without becoming heavier. Lightweight materials are especially important for improving the efficiency and range of hybrid electric, plug-in hybrid electric, and electric vehicles as lightweight materials offset the weight of power system components such as batteries and electric motors.

LM focuses on the research and development (R&D) required to achieve reduced vehicle fuel consumption. The primary LM goal is to realize a 50% reduction in total vehicle weight by 2015 in ways that are cost-effective and maintain safety, performance, and reliability when compared to a 2002 baseline vehicle.

In the short term, vehicle weight reduction can be achieved by replacing heavy steel components with materials such as HSS, Al, or glass fiber reinforced polymer composites. The properties and manufacturing of these materials are well established, but better and more cost effective technologies and processes are needed for joining, modeling, and recycling the materials. In the longer term, even greater weight savings are possible (50%–75% weight reduction for some components) through use of advanced materials such as Mg and carbon fiber reinforced composites. However, more extensive R&D is needed to better understand the properties of these materials and reduce their costs.

R&D work conducted within LM is broken down into three categories: Properties and Manufacturing, Modeling and Computational Materials Science (CMS), and Multi-material Enabling. Properties and Manufacturing activities aim to improve properties (such as strength, stiffness, or ductility) and manufacturability (such as material cost, production rate, or yield) of a variety of metal and polymer composite materials. The focus of the Modeling and CMS and Multi-material Enabling work is to provide the supporting technologies necessary for full system implementation such as joining methods, corrosion prevention techniques, predictive models, and other computational tools. This introduction summarizes the highlights of the program in all of these areas during the 2010 fiscal year. The remainder of the report discusses the specific technical accomplishments in LM, broken down into five areas: Automotive Metals, Polymer Composites, United States Automotive Materials Partnership (USAMP) Cooperative Research, Recycling, and Crosscutting.

Carbon Fiber Reinforced Polymer Composites

The focus for this area continued to be lowering the cost of carbon fiber through different low cost starting materials, including textile grade polyacrylonitrile, lignin, and polyolefins, and advanced processing techniques such as stabilization, oxidation, and carbonization/graphitization that promise to improve the rate and cost of conversion to carbon fiber. The process improvements are enabling validation of successfully converting larger volumes (tows) of precursor to carbon. This section includes detailed reports on the progress made under each aspect of cost reduction toward realization of the goal of carbon fiber at \$5 per pound.

In the area of lowering the cost of processing, predictive modeling has enabled development of tools for prediction of fiber length and orientation of long fiber injection molded thermoplastic composites. From this information, mechanical properties can be predicted. The focus has shifted from model development to validation of prediction of stiffness and strength in progressively complex shaped parts. The detailed report for predictive engineering documents the advances made in developing and understanding this aspect so that industry may use this robust capability to accelerate product development of injection molded composites and lower the technical risk by optimizing tool design and injection molding conditions to optimized properties.

Magnesium Alloys

Magnesium (Mg) alloys, with the lowest density of all structural metals, have the potential to reduce component weight by more than 60%. However, significant technical barriers limit the use of Mg to about 1% of the average vehicle by weight. These barriers include high raw material cost and price volatility, relatively low specific stiffness, difficulty in forming sheet at low temperatures, low ductility of finished components (**Figure 1**), and a limited alloy set. In addition, using Mg in multi-material systems introduces joining, corrosion, repair, and recycling issues that must be addressed.

As described in Sections 2 and 4 of this report, Mg R&D conducted through LM has addressed metallurgical, manufacturing, and design challenges in both cast and wrought Mg. Research conducted at Pacific Northwest National Laboratory (PNNL) and Oak Ridge National Laboratory (ORNL) has improved our understanding of Mg; this includes characterizing Mg behavior at high strain rates and exploring novel methods of manufacturing highly formable sheet. Development and design work conducted in collaboration with the U.S. Automotive Materials Partnership (USAMP) has demonstrated high rate warm forming of Mg sheet and yielded a preliminary design for a Mg intensive vehicle front end that reduces weight by more than 44% compared to a steel baseline.



Figure 1. Mg extrusion exhibiting low ductility failure.

Aluminum Alloys

Aluminum alloys represent a middle ground in the structural light metals spectrum. Years of development within the aerospace, construction, and automotive industries have led to a well-developed and reasonably well understood alloy and processing set. Applications of Al in automotive design include hoods and panels, powertrain components, and even entire vehicle body-in-white structures. There are several barriers to the increased use of Al in vehicle weight reduction applications such as material cost, room temperature formability, and limitations within the existing manufacturing infrastructure. As with Mg, the addition of significant amounts of Al to the automotive manufacturing stream presents added multi-material challenges in joining, corrosion, paint and coatings, repair, and recycling.

LM supported work in Al includes exploration of increased formability processing techniques, improved post-form properties of superplastically formed panels, and demonstration of high strength cast Al components.

Advanced High-Strength Steel

Conventional iron and steel alloys are prominent in existing vehicle architectures, making up more than 70% of the weight of a vehicle. Despite the relatively high density of iron based materials, the exceptional strength and ductility of advanced high-strength steel (AHSS) offers the potential for efficient structural designs and reduced weight. Application of a new generation of AHSSs has the potential to reduce component weight by up to 25%, particularly in strength limited designs. Steel components are also generally compatible with existing manufacturing processes and vehicle materials, making them a likely candidate for near-term weight reduction. Steel development and research in LM are focused on introducing the so-called “third generation AHSSs.” As shown in Figure 2, third generation AHSSs are targeted to properties in between first and second generation AHSSs, with high strength, improved ductility, and low cost.

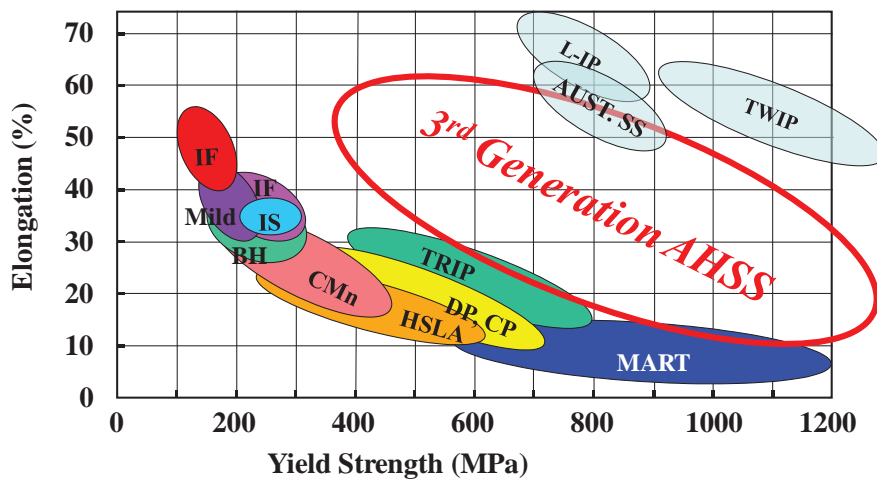


Figure 2. Yield strength versus uniform elongation for a variety of steel types.

Steel development in LM is occurring at all levels of the technology spectrum, from fundamental university research to industry collaboration. PNNL and ORNL have also played a significant role in increasing understanding and improving the properties and manufacturability of advanced steels.

Multi-Material Enabling

Improving the properties and manufacturability of lightweight materials such as carbon fiber reinforced polymer composites, Mg, and Al will allow increasing use in automotive applications. The increased use of mixed materials in vehicle systems is accompanied by technological hurdles in areas such as joining, corrosion, nondestructive evaluation, and recycling.

In the area of joining, significant work has been dedicated to evaluating new solid-state joining techniques such as friction stir welding and ultrasonic welding. Fusion welding of joints between materials with significant melting temperature differences can lead to a variety of metallurgical challenges. Solid state joining methods circumvent these issues by relying on different joining mechanisms.

Corrosion issues in multi-material systems can limit durability and add cost during vehicle construction. Several research groups are investigating corrosion mechanisms and prevention techniques as part of LM. Developing a better understanding of how lightweight materials corrode in hostile automotive environments will enable better predictions and designs for durability.

Modeling and Computational Materials Science

Developing new, lightweight vehicle structures will require advances in areas such as structural design, processing, and alloy chemistry. Classical approaches to these advancements such as experimental, analytical, or Edisonian techniques can often yield the desired results but with limited efficiency. Computational approaches to materials engineering offer the potential to short-circuit the development cycle through predictive engineering and simulated experimentation. Advanced modeling techniques can also be used to optimize designs in well-established materials, further reducing component weights such as in Figure 3. By reducing the time and resources necessary to advance lightweight materials toward vehicle applications, it is possible to introduce relatively immature materials such as Mg without the decades (or centuries) of development applied toward conventional steel and Al.

Projects conducted within LM focus on several different aspects of modeling and CMS. Some work, such as “High Strain-Rate Characterization of Mg Alloys” and “Diffusion Databases for ICME” (Chapter 2) provides valuable data and models necessary for accurately predicting material behavior. Other research, such as “MFERD Phase 1” (Chapter 4), has made extensive use of modeling and simulation for design and optimization. Substantial development in the core materials science and modeling methods for lightweight materials implementation is demonstrated in “Modeling and CMS—Mississippi State University” in Chapter 2. Beyond the major focus projects, most research conducted in LM contains at least a small element of modeling or CMS.

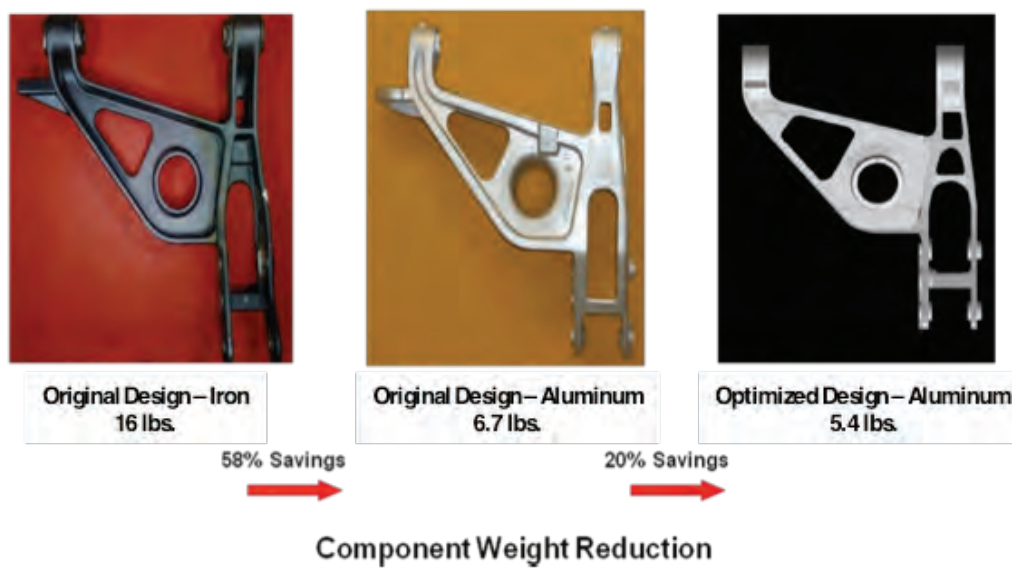


Figure 3. Example of using CMS to optimize a lightweight design.

Looking Forward

The following reports provide a detailed description of LM activities and technical accomplishments during the 2010 fiscal year. The work shown here has produced technologies that make today's vehicles more efficient, safe, and affordable. In collaboration with industry, universities, and national laboratories, VTP continues to develop the next generation of lightweight components. These efforts are building the foundation of technologies—and technology manufacturers—that tomorrow's vehicles need to achieve ultrahigh efficiency and resulting reductions in petroleum use and greenhouse gas emissions.

2. Automotive Metals

A. Processing and Manufacturability - Oak Ridge National Laboratory

Field Technical Monitor: C. D. Warren
Oak Ridge National Laboratory
1 Bethel Valley Road, Oak Ridge, TN 37831
(865) 574-9693; e-mail: warrencd@ornl.gov

Technology Area Development Manager: William Joost
U.S. Department of Energy
1000 Independence Ave., S.W., Washington, DC 20585
(202) 287-6020; e-mail: william.joost@ee.doe.gov

Contractor: Oak Ridge National Laboratory (ORNL)
Contract No.: DE-AC05-00OR22725

This project consists of two separate tasks. The first is an effort to characterize the high strain rate response of automotive grade magnesium (Mg) alloys. The second is focused toward developing a fundamental understanding of the austenite-ferrite transformation in steels, which will be necessary to develop the next generation of advanced high-strength steels (AHSSs) that will overcome difficulties in use associated with the second generation AHSSs.

Objective

High Strain Rate Characterization of Mg Alloys

- Characterize the mechanical material properties of Mg alloys for automotive applications.
- Determine the material model parameters for various constitutive models available in crash codes.
- Experimentally determine the evolution of material properties for various loading situations and strain rates.
- Formulate experimental findings into constitutive models based on continuum damage mechanics.
- Establish test and property database for automotive Mg alloys.

R&D Fundamental Study of the Relationship of Austenite-Ferrite Transformation Details to Austenite Retention in Carbon (C) Steels

- Support the development of third generation (Gen III) AHSSs through fundamental studies of the ferrite austenite phase transformation during steel finishing operations and its relationship to stabilizing and retaining austenite in finished microstructures.
- Use unique facilities like the Advanced Photon Source, available through the DOE Office of Science, to characterize in situ the austenite-ferrite phase transformation behavior of C steels under the rapid heating/cooling conditions that typify modern sheet steel production.

- Determine the extent to which retained austenite can be increased in commercial and experimental low C (< 0.2 wt %) steels.
- Formulate experimental alloys and analyze them for the possibility of increasing retained austenite over commercial steel grades, which generally contain around 10%.

Accomplishments

- Designed a fixture for interrupted strain rate tests in tension of Mg alloys.
- Performed strain rate tests in tension for Mg AM60 and AZ31 alloys up to 1,000/s strain rate.
- Developed World Wide Web database for test data analysis for Mg alloys.
- Developed measurement system based on digital image correlation at high strain rate and applied that measurement system to Mg alloys.
- Demonstrated the ability to continuously measure phase fractions and lattice parameters by synchrotron diffraction during simulated steel heating/cooling process cycles for steels.

Future Direction

- Measure strain rate properties of Mg alloys in tension and shear.
- Develop and optimize methods for interrupted strain rate tests for Mg alloys.
- Make improvements to the experimentation used for diffraction experiments such as developing a procedure to minimize decarburization in steels.
- Make improvements to streamline data reduction and analysis techniques.
- Analyze data from additional experiments on DP780 steel for transformation behavior and retained austenite.
 - Identify alloy compositions that promote higher amounts of retained austenite for preparation of laboratory scale heats and incorporate into future diffraction experiments.

Introduction

The low density of Mg alloys makes them good candidates for lightweight construction of components in the automotive industry. However, they exhibit much more complex mechanical behavior than more commonly used automotive materials. Preliminary tests indicate there is significant strain rate sensitivity among certain Mg alloys, but the lack of strain rate sensitivity information coupled with the lack of understanding of loading-induced property degradation for Mg alloys adds to the reservations for using them as structural materials.

Metals compose about 80% of all the materials used for light-duty vehicle construction, and by a wide margin, the largest fraction of the metals is steels. The traditional sheet steels used for chassis and body constructions are the so-called “mild” steels; however, high strength, low alloy steels are increasingly being used. The combined interests of improving crashworthiness and reducing vehicle weights were at least partially responsible for the development of the first generation (Gen I) of AHSSs. What is now desired is Gen III AHSSs that borrow from previous alloy development efforts to achieve intermediate strengths and ductilities but at costs that would make acceptance for automotive construction feasible. One task in this project is aimed at laying the fundamental groundwork for developing this new generation of high-strength steels.

High Strain Rate Characterization of Magnesium Alloys

Principal Investigator: Srdjan Simunovic, ORNL
(865) 241-3863; e-mail: simunovics@ornl.gov

Principal Investigator: J. Michael Starbuck, ORNL
(865) 576-3633; e-mail: starbuckjm@ornl.gov

Principal Investigator: Don Erdman, ORNL
(865) 576-4069; e-mail: erdmandl@ornl.gov

Introduction

The low density of Mg alloys makes them good candidates for lighter weight constructions of components in the automotive industry. Mg alloys, however, exhibit much more complex mechanical behavior than more commonly used automotive materials. The mechanical response of Mg alloys involves notable anisotropy, nonisotropic hardening, yield asymmetry, lower ductility, and significant degradation of effective properties due to the formation and evolution of microdefects. The intense fracturing that occurs during crash is notably different from the progressive folding in conventional automotive steel structures and requires in-depth material and structural understanding for effective automotive structural design. Accordingly, the necessary characterization procedures and constitutive models are more complex than commonly used uniaxial tests and isotropic plasticity material models for steel. Another issue of concern for automotive designers is the strain rate sensitivity of various properties of Mg alloys. Preliminary tests indicate there is significant strain rate sensitivity in Mg alloys, but the lack of experimental data coupled with the lack of understanding of loading-induced property degradation for Mg alloys adds to the reservations for using this new material for automotive applications.

Approach

In support of the U.S. Automotive Materials Partnership project AMD 604, Mg Front End Research and Development, we are investigating rate dependent properties of automotive Mg alloys. The experiments are conducted under various strain rates ranging from quasi-static up to 1,000/s. This range of strain rates is important to automotive design because it corresponds to strain rates experienced during high speed forming and vehicle crash.

Measurement of mechanical properties in the strain rate range between 1/s and 1,000/s (intermediate strain rate regime) is inherently difficult because of the wave reflections and difficulty in establishing dynamic equilibrium in the sample and the sensors. Test methods in this range have not been standardized and are subjects of intensive research and development. In addition, the deformation of Mg alloys is accompanied by significant internal damage (void nucleation, growth, coalescence) as a result of the complex deformation behavior inherent in its crystal structure (hexagonal close packed). It is, therefore, important to investigate how these mechanisms change under different rates of loading.

The main scientific and technical goals of this research project are (1) development of detailed information about Mg alloy mechanical properties in the intermediate strain rate regime, (2) characterization of corresponding property degradation by the control of imparted strain during the tests, (3) development of tightly controlled strain rate test procedures, and (4) correlation of manufactured and ideal material properties.

Results and Discussion

Data from the tests conducted so far on the project are available on the World Wide Web as described in the previous reports (http://thyme.ornl.gov/Mg_Main/description/home.cgi). The web interface allows for quick dissemination of experimental data and interaction with project participants.

Tensile High Strain Rate Tests on Hydraulic Equipment

We have developed techniques to generate reliable stress strain curves within the intermediate strain rate regime for the sheet form of Mg alloys. The stresses are calculated from the elastic strain of the specimen measured in the tab region. The displacements and strains of the tensile specimens were successfully resolved with a video image correlation (VIC) three-dimensional (3D) high speed imaging system.

This technique has major advantages over conventional indirect measurements which significantly improve the quality of the experimental data and test control. The new method will be described in a journal article that is under preparation. Figure 1 shows schematics for tensile sheet tests.

For most tests, machine transducers include a dc strain gage load cell and a charge amplified piezoelectric load cell. Actuator displacement is measured with a Temposonics acoustic transducer because the high velocities would be outside the range of standard displacement measurements. The strains in the specimen are measured using VIC on one face on the specimen and high elongation strain gages (SG1&2) on another. The system is equipped with two high speed digital cameras which provide 7,500 frames per second (fps) at a resolution of 1,024 by 1,024 pixels and reduced resolution operation to 1,000,000 fps. These two cameras are staged so that the area of interest on the test sample is visible to both cameras.

With the VIC system, a 3D full field deformation map is generated within the area of interest using the speckle pattern on the specimen. At low loading rates the stress can be evaluated from the load washer or calculated from the elastic strain on the tab. However at higher speeds, there is significant noise and ringing in the load washer. Figure 2 depicts the strain analysis for a sample that was loaded at 10 in./s (strain rate of 10 s⁻¹).

Figure 3 shows an example of the specimen loaded at 93 s⁻¹; ringing in the load washer signal is so significant that generation of a meaningful stress strain curve is difficult. However, the response from the strain gages is shown to be much more reliable, especially when the average values are used.

Characterization of Damage Evolution in Mg Alloys

We have developed procedures for quantification of evolving stages of damage based on image processing and mechanical tests. Figure 4 shows the stages in the procedure going from the optical microscope image to the void size distribution plot in the specimen. As noted in previous reports, the deformation is almost exclusively driven by void formation and growth.

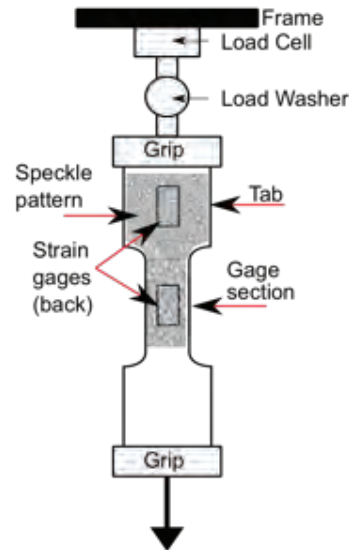


Figure 1. Tensile specimen configuration.

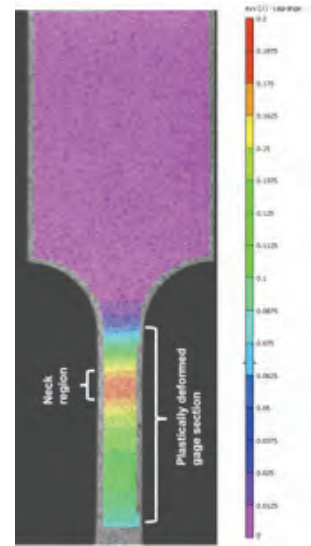


Figure 2. Measured strain distribution using VIC.

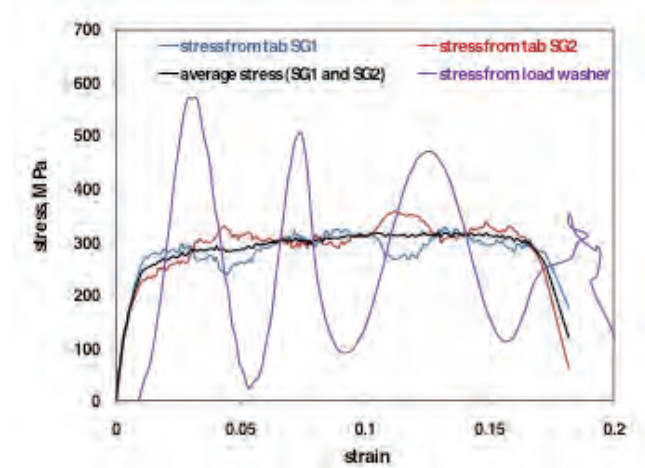


Figure 3. Stress strain curves using different methods.

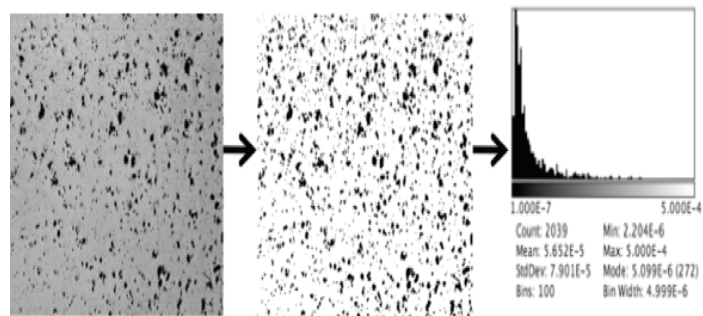


Figure 4. Measurement of porosity in the material. Porosity is used as a parameter in the constitutive model.

Conclusions

We have developed new methods for characterization of Mg alloys under intermediate (automotive) strain rates of loading. When fully developed, the tests will provide needed data for more effective design with Mg alloys and lightweight automotive designs.

R&D Fundamental Study of the Relationship of Austenite-Ferrite Transformation Details to Austenite Retention in Carbon Steels

Principal Investigator: Michael Santella, ORNL
(865) 574-4805; e-mail: santellaml@ornl.gov

Introduction

Steels represent about 62% of average vehicle weight. Of the various steel mill products used for auto construction, about 70% of the total, or 839 kg of the 1,970 kg average light vehicle weight, is supplied as flat-rolled C steel for chassis parts and body panels. The traditional sheet steels used for chassis and body constructions are the so-called “mild” steels. The combined interests of improving crash worthiness and reducing vehicle weights were at least partially responsible for the development of Gen I AHSSs. What is now desired is Gen III AHSSs that borrow from previous alloy development efforts to achieve intermediate strengths and ductilities at costs that would make acceptance for automotive construction feasible. Controlling cost will likely require that Gen III AHSSs be no more than modestly alloyed compared to Gen I AHSSs and capable of being produced within existing steel mill infrastructures.

The majority of the experimental part of this work will be done using the Advanced Photon Source to provide synchrotron radiation for high speed diffraction. Diffraction patterns can be collected at rates of one every second, possibly even higher. Capabilities exist for integrating diffraction with rapid heating/cooling cycles. Control of temperatures and heating/cooling rates are sufficient for replicating most of the processing steps used to produce existing AHSSs. Analysis of the diffraction data can determine volume fractions of the ferrite and austenite phases, lattice parameters, and how the phases vary under dynamic temperature/time conditions.

Approach

It is well known that retaining austenite in automotive sheet steels can markedly improve ductility at high strength through the TRIP effect (i.e., transformation-induced plasticity). Better fundamental understanding of austenite-ferrite transformations will enable a more scientific approach to improving properties through novel processing that can be achieved with existing infrastructure. Technical issues being addressed include the following.

- Making direct, in situ observations of the time dependence of austenite-ferrite transformation behavior at elevated temperatures, during rapid heating/cooling, and during low temperature treatments designed to maximize retained austenite.
- Measuring partitioning of C between austenite and ferrite during processing.
- Understanding effects of critical alloying elements such as C, manganese, and silicon on transformation behavior and retention of austenite.

Results and Discussion

Most of the experiments are being conducted with the uncoated dual phase steel DP780 (ArcelorMittal).

Diffraction experiments are being conducted on the UNICAT X-33 bending magnet beam line at the Advanced Photon Source (Argonne National Laboratory, Argonne, Illinois). X-ray data are captured by a charge-coupled device (CCD) on which the diffracted beams were integrated over a 1 s exposure. Diffraction patterns are acquired at a maximum rate of about 1/s. Data

analysis begins by converting the two-dimensional images recorded by the CCD detector into one-dimensional (1D) plots of diffracted intensity versus d-spacing. The 1D plots were then analyzed for texture effects and ferrite and austenite phase volume fractions using published methods.

Previous results showed that during diffraction at 800°C there was a significant and continuous decrease of austenite fraction from about 66% to 44%. Thermodynamic equilibrium calculations suggested that there should be 75%–80% of austenite in DP780 at 800°C, and this amount was verified by independent heat treating experiments. The inconsistency between phase fractions determined by synchrotron diffraction and those measured in independent experiments and predicted by thermodynamic analysis is the focus of current activities. Failure to resolve the inconsistency will indicate that the current approach to determining phase fractions is inappropriate and that an alternate method is needed to continue this type of phase transformation analysis. Possible causes of the inconsistent behavior are as follows.

- Equilibrium is not being achieved in 120 s at 800°C.
- Decarburization is occurring during diffraction. This will locally decrease the C concentration, which has a significant effect on phase fractions.
- Some step in the data analysis is not being handled accurately. Data analysis routines are being reexamined and validated.
- Other experimental issues related to heating stage are also being reevaluated.

These issues are being systematically addressed with experiments aimed at better controlling the atmosphere used during diffraction experiments and the surface condition of the specimens. **Figure 1** shows the overall response of DP780 to being heated to 970°C and held for 2 min followed by holding at 800°C for 2 min, holding for 460°C for 2 min, and then cooling to room temperature. This is basically a repeat of the previous experiment where the austenite amount decreased from 66% to 44% during the hold at 800°C. As before, the transformations between the ferrite (body centered cubic crystal structure) and austenite (face centered cubic crystal structure) phases are clearly evident. Results of the analysis to quantify the phase fractions are shown in **Figure 2**. In the repeat experiment, the austenite fraction decreased from 80% to 68%. In terms of being consistent with corroborating data, the repeat diffraction experiment was a significant improvement. The tendency of the austenite fraction to decrease with time is still a concern because it could be caused by experimental factors that are impractical to control with the current setup. Additional experiments and analyses are continuing to address this issue because resolving it is critical for establishing confidence in the diffraction results.

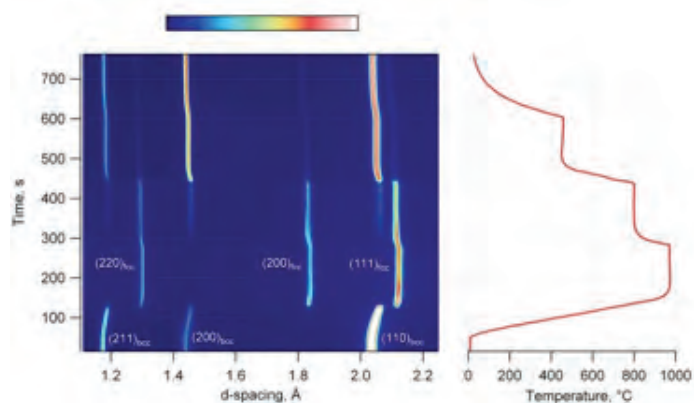


Figure 1. Intensity image plot (a) of DP780-APS103 overall ferrite-austenite transformation behavior; time-temperature cycle (b) approximates typical steel processing during cooling.

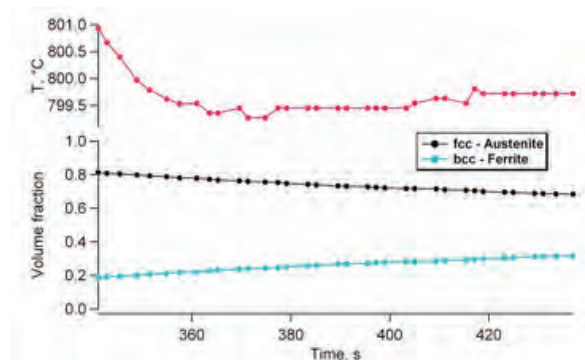


Figure 2. Phase fractions of DP780-APS103 during an isothermal hold in the intercritical temperature region: cooled to 800°C from 970°C followed by 120 s hold at 800°C.

Conclusions

Initial experiments demonstrate that phase fractions and lattice parameters can be continuously measured during heat treatments similar to those used in processing automotive sheet steels. However, inconsistencies were observed between phase fractions determined by diffraction and those measured by independent experiments. Analysis is continuing to resolve the differences and to extract additional information from the experimental diffraction data that would establish this approach as a unique capability in the development of Gen III AHSSs.

Conclusions

New methods for characterization of Mg alloys under intermediate loading strain rates are being developed. When fully developed, the tests will provide needed data for more effective design with Mg alloys for lightweighting automotive designs. The future work remaining to be completed includes (1) development of high strain rate tests for compression and shear, (2) measurement of evolving damage in Mg, and (3) development of constitutive models for Mg alloys.

In the quest to begin development of the next generation of AHSSs, initial experiments demonstrate that phase fractions and lattice parameters can be continuously measured during heat treatments similar to those used in processing automotive sheet steels. However, inconsistencies were observed between phase fractions determined by diffraction and those measured by independent experiments. Analysis is continuing to resolve the differences and to extract additional information from the experimental diffraction data that would establish this approach as a unique capability in the development of Generation III AHSSs.

Presentations/Publications/Patents

Wang, Y.; Xu, H.; Erdman, D. L.; Starbuck, M. J.; Simunovic, S. Characterization of High Strain Rate Mechanical Behavior of AZ31 Mg Alloy Using 3D Digital Image Correlation. In preparation.

References

Schultz, R. A.; Schnatterly, J. Presentations contained in Great Designs in Steel, 2007.

Nyberg, E. A.; Luo, A. A.; Sadayappan, K. Mg for Future Autos, Advanced Materials & Processes 2008, pp 35–37.

B. Processing and Manufacturability - Pacific Northwest National Laboratory

Field Technical Monitor: Dean Paxton
Pacific Northwest National Laboratory
902 Battelle Boulevard; P.O. Box 999; Richland, WA 99352
(509)375-2620; e-mail: dean.paxton@pnl.gov

Technology Area Development Manager: William Joost
U.S. Department of Energy
1000 Independence Ave., S.W.; Washington, DC 20585
(202) 287-6020; e-mail: william.joost@ee.doe.gov

Contractor: Pacific Northwest National Laboratory (PNNL)
Contract No.: DE-AC05-00OR22725 & DE-AC06-76RLO1830

The Processing and Manufacturability project consists of six tasks focused on research and development (R&D) activities advancing the basic mechanical properties, manufacturability, and cost of lightweight materials toward the levels needed for increased implementation in automotive applications. The tasks include the following.

1. First Generation AHSS's Deformation Fundamentals
2. Ultrafine Grain Foils and Sheet by Large Strain Extrusion Machining
3. Development of High Strength Superplastic Forming Al
4. Formability of Continuous Cast Mg Sheet
5. Pulse Pressure Forming of Lightweight Materials
6. Mg Research and Technology Development

The objectives, accomplishments, and future direction for these tasks are provided below.

Objective

First Generation AHSS's Deformation Fundamentals

- Develop fundamental understanding of key mechanical properties and microstructural features influencing the local formability of first generation AHSSs.
- Establish a set of more relevant material acceptance criteria and the associated screening methods to address the local formability of first generation AHSSs, which will allow faster and wider application of AHSSs in vehicle bodies.

Ultrafine Grain Foils and Sheet by Large Strain Extrusion Machining

- Demonstrate the feasibility of producing Mg sheet and shaped products with superior formability and strength properties through the application of severe plastic deformation developed by large strain extrusion machining (LSEM) and peeling techniques.
- Demonstrate the ability to scale up the LSEM process to make Mg strip in commercially suitable thickness and width dimensions to address the cost barrier of implementing Mg sheet alloys

Development of High Strength Superplastic Forming Al

- Develop a cost-effective superplastic sheet with a post-formed ultimate tensile strength greater than that of the commonly used 5083 Al alloy for use in automotive outer body panels and closures.

Formability of Continuous Cast Mg Sheet

- Evaluate the effects of lubricants on friction and formability of continuous cast (CC) Mg alloy AZ31B sheets under warm forming conditions to evaluate this lower cost alternative to conventional wrought-processed sheet
- Characterize the post-formed properties of CC AZ31B sheets provided by the United States Automotive Materials Partnership (USAMP) Warm Forming Team [Automotive Metals Division (AMD) 602].
- Characterize the post-formed microstructure of Mg pans and relate it to their formability.
- Determine the forming limits of CC AZ31B sheets under biaxial conditions [limiting dome height (LDH) test] at warm forming temperatures.

Pulse Pressure Forming of Lightweight Materials

- Develop pulse pressure forming (PPF) sheet metal forming techniques [e.g., electromagnetic forming, electrohydraulic forming (EHF)] to manufacture cost-effective body-in-white (BIW) and closure panels from Al alloys, high-strength steels, AHSSs, and Mg alloys.
- Overcome technical barriers to using PPF for more cost-effective lightweight vehicles by
 - quantifying the formability and strain rates that develop during PPF processing,
 - developing validated constitutive relations for 5182-O Al and dual phase (DP) 600 steel during PPF processing, and
 - developing validated finite element simulation of PPF process.

Mg Research and Technology Development

- Provide technical assistance on Mg related topics to the DOE Office of Vehicle Technologies (OVT).
- Acting as a liaison for DOE, work together with the project members of the Mg Front End Research and Development (MFERD) demonstration project in collaboration with China and Canada to meet the DOE lightweighting goals/objectives.
- Increase awareness of and familiarity with Mg as a viable option for automotive applications.
- Compile, document, and evaluate state-of-the-art Mg R&D around the world as a resource for determining where U.S. government resources should be directed.

Accomplishments

First Generation Advanced High-Strength Steels Deformation Fundamentals

- Acquired eight different DP980 steels from different suppliers' models of first generation AHSSs.
- Completed chemical composition analyses for the obtained DP980 steels using samples from the center/edge regions.
- Performed static tensile tests for the obtained DP980 steels using samples cut from the center/edge regions along the rolling/transverse directions.
- Identified TiC carbides inside grains and M₂₃C₆ carbides along grain boundaries and inside grains from transmission electron microscopy (TEM) observations on nanosize precipitate strengthened steel (NPSS).
- Identified the strengthening mechanism of NPSS from a series of TEM observations on the samples deformed with different strain levels.

Ultrafine Grain Foils and Sheet by Large Strain Extrusion Machining

- Overcame segmentation observed in preliminary experiments by tuning machining conditions to produce continuous AZ31 foils about 25 mm wide by 2 mm thick by the LSEM process.
- Produced, using LSEM, a microstructure with fine, uniform grain size which will provide enhanced ductility and strength in Mg AZ31B alloy.
- Obtained the ability to control strip thickness between 1 mm and 2 mm, which is a key step in demonstrating the scale-up of the LSEM process and provides guidance for equipment design and cost.

Development of High Strength Superplastic Forming Al

- Determined that the primary strengthening precipitate in the newly developed Al alloy, when subjected to superplastic forming (SPF) conditions and a paint-bake aging treatment, is the needle-/plate-like copper containing phase; other potential strengthening precipitate phases are not formed due to the low solution heat treat temperature. This strengthening effect will be limited by the automotive industries willingness to use copper as an alloying element.
- Initiated discussions with three Al suppliers interested in participating in this project to evaluate the willingness of each supplier to work on a cooperative project for commercial development of a new alloy for SPF.

Formability of Continuous Cast Mg Sheet

- Determined post-formed basal texture and tensile strength of AZ31B Mg pans (Mg sheet vendor “A”) followed a similar trend in texture and strength when plotted as a function of pan-forming temperature. Maximum post-formed strength was observed in pans formed at roughly 175°C–200°C and was associated with about 40% area fraction of basal texture along sheet normal direction.
- Verified that results from LDH tests support previously suggested tungsten disulfide as a suitable alternative to conventional boron nitride/graphite based lubricants for Mg warm forming.

Pulse Pressure Forming of Lightweight Materials

- Established in-house capability to image and quantify high-strain-rate forming of lightweight metals. Time evolution of sheet deformation (displacement, velocity, strain, and strain rate) associated with peak strain rates of about 2,000/s were quantified for EHF under free-forming conditions and in a conical die.
- Characterized strain-rate dependence of texture in biaxially deformed regions of 5182-O Al and DP600 steel deformed using EHF (high rate) or quasi-static bulge techniques.
- Modeled Al sheet deformation during EHF using Johnson-Cook equation and failure criteria to describe the material constitutive behavior. The effect of die angle on strain rate and ductility was modeled to identify test parameters that may enable enhanced formability.

Mg Research and Technology Development

- Updated the Mg technology bibliographic database which now includes more than 1,700 Mg-related citations (Mg.pnl.gov).
- Monitored Mg development and facilitated communication among national and international organizations with an interest in Mg development.
- Organized the MFERD Phase 1 Review Meeting in Seattle, Washington; compiled the 2009 MFERD Annual Progress Report; and organized the 2010 MFERD Annual Project Review Meeting.

Future Direction

First Generation Advanced High-Strength Steels Deformation Fundamentals

- Complete static tensile tests, microstructural analyses, hole expansion tests, three-point bending tests, and forming limit diagram (FLD) tests for DP980 steels.
- Analyze the experimental test results (noted above) together with the microstructural features and chemical compositions and determine parameters for the subsequent studies.
- Perform in situ x-ray diffraction (XRD) tests during tensile deformation of DP980 steels and determine volume fractions and properties of the constituent phases for the subsequent micromechanics based finite element analyses.

Ultrafine Grain Foils and Sheet by Large Strain Extrusion Machining

- Demonstrate scale-up of the LSEM process and equipment to produce Mg strip of about 250 mm width. This width will provide sufficient demonstration of the process scale up that commercial development of the LSEM process can be pursued.
- Demonstrate the use of a commercially cast Mg feedstock to directly produce Mg strip with thickness up to 2 mm.
- Provide updated processing and equipment information and specifications so that the continuous casting cost model [S. Das, Oak Ridge National Laboratory (ORNL)] can be updated and cost analysis results provided to DOE and interested commercial companies. The cost model work is reported separately in this report by S. Das (ORNL).

Development of High Strength Superplastic Forming Al

- Focus on the Al alloy 6T-2, cast additional book mold materials, and process to sheet for superplastic and room temperature tension test evaluation using alternate thermomechanical processing designed to develop adequate superplasticity.
- Identify industrial Al mill to support process scale-up.

Formability of Continuous Cast Mg Sheet

- The Mg Warm Forming Task was completed in FY 2010.

Pulse Pressure Forming of Lightweight Materials

- Develop an FLD for 5182-O Al and DP600 steel at deformation at high strain rates similar to the rates observed during EHF.
- Develop constitutive relations for lightweighting metals (5182-O Al, DP600 steel, and AZ31B Mg) to enhance understanding of the EHF process and metal formability and development of modeling capability to predict formability behavior.
- Numerically model sheet-die interactions during EHF, and evaluate them in terms of their influence on sheet formability.

Mg Research and Technology Development

- Continue to oversee, as technical chairman, Phase 2 MFERD project activities.
- Coordinate the 2010 MFERD Annual Meeting that will be held in the United States (October 2010). This annual meeting requires contracting for hotel, dining, and meeting space. It also requires contracting for translation and production of the bilingual 2009 annual report/book.
- Support national and international collaboration for Mg R&D.

- Continue to evaluate and propose Mg R&D activities to DOE OVT that are unique and necessary.
- Participate in national and international conferences dealing specifically with Mg R&D, in particular the 5th International Light Metals Technology Conference 2011 to be held in July in Germany.

Introduction

The Processing and Manufacturability project consists of six tasks focused on R&D activities advancing the basic mechanical properties, manufacturability, and cost of lightweight materials toward the levels needed for increased implementation in automotive applications. The first task is focused on developing fundamental understandings of key mechanical properties and microstructure features influencing the local formability of AHSSs. Only after these fundamental understandings are established can a set of more relevant material acceptance criteria and associated screening methods be developed to address the local formability of first generation AHSSs. The ultimate goal of this task is to reduce launch time and promote wider application of AHSSs in vehicle bodies.

The second task seeks to overcome the cost barrier of implementing Mg sheet alloys in automotive applications through a novel technique known as LSEM. Pioneered by Purdue University, LSEM is a hybrid cutting-extrusion process in which sheet metals can be produced in a single-stage deformation process. The initial phase of the work has established the feasibility of producing nominal 2 mm thick sheet of MgAZ 31B via the LSEM process.

In the third task, the objective is to develop a cost-effective superplastic Al sheet with a post-formed yield strength greater than 250 MPa for use in automotive outer body panels and closures. Current SPF techniques for Al alloys such as alloy 5083 require forming at elevated temperatures, which results in lower post-formed yield strength (~150 MPa) and thus limits the use in BIW and under hood applications where higher strength is required.

The goal of the fourth task is to develop a fundamental understanding of the microstructure-formability relationship and post-formed properties of twin-roll, CC Mg sheet, which is being evaluated as a lower cost alternative to conventional wrought-processed sheet. This task focused on understanding the relationships between (1) the tribology at the sheet-die interface during warm forming and the resulting formability of the Mg sheets and (2) the forming process parameters and the post-formed mechanical properties and microstructure of the formed parts.

The fifth task objective is to extend the formability of lightweight metals (e.g., Al and Mg) and AHSSs using PPF techniques such as EHF. However, there is a lack of understanding of practical forming limits in PPF processes and their dependence upon process parameters and tooling design. This task seeks to quantify the deformation behavior of sheet metals during the EHF process and develop validated constitutive relations and models for Al and AHSSs to enhance understanding of the EHF process and metal formability.

The final task provides technical and programmatic support to DOE OVT efforts to increase the use of Mg in automotive and other transportation applications, including liaising with the international MFERD project for DOE OVT; organizing and hosting multi-country meetings for this project in the United States during CY 2010; and coordinating, translating, and publishing the MFERD Annual Report.

The following sections outline specific task work conducted at PNNL in the area of processing and manufacturability of lightweight metals. Each task supports one or more goals within the Processing and Manufacturability Agreement as outlined below.

First Generation Advanced High-Strength Steels Deformation Fundamentals

Principal Investigator: Xin Sun, PNNL
(509) 372-6489; e-mail: xin.sun@pnl.gov
Principal Investigator: Richard W. Davies, PNNL
(509) 375-6474; e-mail: rich.davies@pnl.gov
Key Contributors: Kyoo Sil Choi and Ayoub Soulami, PNNL
Yongfeng Shen, Northeastern University, China
Industry Partners:
Donald L. Jordan, Ford Motor Company
(313) 805-4829; e-mail: djorda19@ford.com
Paul J. Belanger, General Motors Corporation
(586) 209-1224; e-mail: paul.belanger@gm.com
Dajun Zhou, Chrysler Corporation
(248) 944-1197e-mail: djz13@chrysler.com

Introduction

AHSSs are being increasingly used by the automotive industry to cost-effectively reduce vehicle weight. However, a noticeable degree of inconsistent forming behaviors has been observed for first generation AHSSs in production, and they appear to be associated with the inherent microstructure-level inhomogeneities for various AHSSs. This indicates that the basic material property requirements and screening methods currently used by the automotive industry for the mild steels and high strength, low alloy steels are no longer sufficient for qualifying the AHSSs currently used in vehicle manufacturing applications. This task is focused on developing fundamental understandings of key mechanical properties and microstructure features influencing the local formability of AHSSs. Only after these fundamental understandings are established can a set of more relevant material acceptance criteria and associated screening methods be developed to address the local formability of first generation AHSSs. The ultimate goal of this task is to reduce launch time and promote wider application of AHSSs in vehicle bodies.

The effects of nanosize precipitates in strengthening low alloy steels were examined in FY 2010. NPSSs are single phase ferritic steels strengthened by precipitates in the nanometer size range. Because of their excellent combination of mechanical properties, NPSSs are also under consideration for use in various vehicle components in the automotive industry. In this task, the fundamental strengthening mechanisms of an NPSS, bearing Ti and Mo, are investigated to explore the possible directions for future generation high-performance AHSSs.

Approach

In FY 2010, the task started with eight different types of DP980 sheet steels, with thicknesses ranging from 1 mm to 2 mm, acquired from various steel suppliers, including both domestic and foreign producers. The task was delayed for 6 months because of unforeseen delays in acquiring different materials from various steel producers. The eight different steels were labeled with generic designations (A to H) for the purpose of this study. Chemical composition analyses were first performed on seven different DP980 materials using inductively coupled plasma-atomic emission spectroscopy following the American Society for Testing and Materials (ASTM) E 1019-08 standard. Static tensile tests ($\epsilon = 10^{-4} / s$) along the rolling and transverse directions (RD and TD) were also performed on all the obtained materials using subsize ASTM E8 samples. For these experiments, the samples were cut from both center and edge areas of the sheets to examine the possible differences in microstructures, basic material properties, and chemical compositions between the two areas.

Three-dimensional (3D) microstructure analyses are scheduled for all the obtained DP980 materials using scanning electron microscopy (SEM). In-plane microstructures, both at the surface and at mid-thickness, will be obtained for both the center and the edge of each DP980 material. In addition, SEM pictures along the RD and TD will be obtained at these locations for the as-received materials to obtain detailed 3D microstructural features of the different materials. The information obtained

from these tests for all the materials will be used together with the results from different experiments, such as hole expansion and three-point bending, to determine the material parameters for the subsequent study to determine the key factors influencing the local formability of these materials. The final goal of the task is to design an effective screening test for localized formability to accelerate the material qualification process for these materials to be used in the automotive industry.

For NPSSs, XRD analysis, optical microscopy, and electron backscatter diffraction (EBSD) observations were performed on the as-received steel for phase purity and structural characterizations and for determination of the grain size, morphology, and orientation. TEM was also performed on the as-received and deformed samples to investigate the strengthening mechanisms of nanosize precipitates.

Results and Discussion

Table 1 lists the results of the chemical composition analyses of the seven different DP980 steels studied in FY 2010. Receipt of the eighth DP980 steel was delayed, and thus it was not included in the compositional analyses performed to date. The results in Table 1 are from the center region of the samples because the materials did not show a noticeable difference in chemical composition between the center and the edge areas. All of the materials have similar and relatively high C and manganese contents, and they also have similar Al contents. Other alloying elements, such as Cr, Cu, Mo, Si, are generally different in content for different materials as they have their own roles in achieving the required DP980 properties through different thermal mechanical processes.

Table 1. Chemical compositions of the investigated DP980 steels.

DP980 [thickness (mm)]	Al	C	Cr	Cu	Mn	Mo	Ni	P	S	Si
A (2.0)	0.04	0.1	0.02	0.21	2.47	0.07	<0.01	0.007	0.01	0.63
B (1.0)	0.06	0.13	0.28	0.08	2.22	0.21	0.01	0.011	0.017	0.08
C (1.6)	0.04	0.1	0.22	0.01	2.12	0.28	<0.01	0.008	0.015	0.31
D (1.2)	0.05	0.13	0.27	<0.01	2.42	0.37	<0.01	0.016	0.02	0.02
E (1.8)	0.04	0.11	0.46	0.09	2.04	0.28	0.01	0.006	0.015	0.31
F (1.3)	0.04	0.12	0.47	<0.01	2.05	0.27	0.01	0.007	0.027	0.17
G (1.3)	0.04	0.1	0.03	<0.01	2.11	0.18	0.01	0.012	0.022	0.46

Figure 1 shows the engineering stress-strain curves and the ultimate tensile strengths (UTSs) obtained from the tests for DP980 A and B steels. Four stress-strain curves for the samples cut from the center and the edge areas along the RD and TD are shown in each figure. Note here that the samples with the same testing conditions (i.e., the samples cut from the same area along the same direction) show quite consistent stress-strain curves, and therefore, only one representative curve for each testing condition is plotted in the figures. DP980 A steel generally shows split-type in-plane failure mode and exhibited quite consistent behaviors between the four different testing conditions in terms of strength as well as ultimate ductility as shown in Figure 1(a). This may indicate that DP980 A steel sheets have quite homogeneous microstructure distributions in all areas within the sheet, and also the microstructures along the RD and TD are quite similar to each other. These deductions will be validated in FY 2011 with the SEM observations at different locations for this steel. However, DP980 B steel shows different in-plane failure modes (i.e.,

shear-type failure in RD samples and split-type failure in TD samples) and exhibits different stress-strain behaviors depending on the sample's location and loading direction. The observations on Figure 1(b) may indicate that DP980 B steel has relatively banded microstructures along the RD, and the edge area has quite different microstructures (i.e., possibly less of the martensitic phase) from that of the center. Again, the microstructural features from SEM analyses can be used to explain the characteristics of these observed macroscopic behaviors.

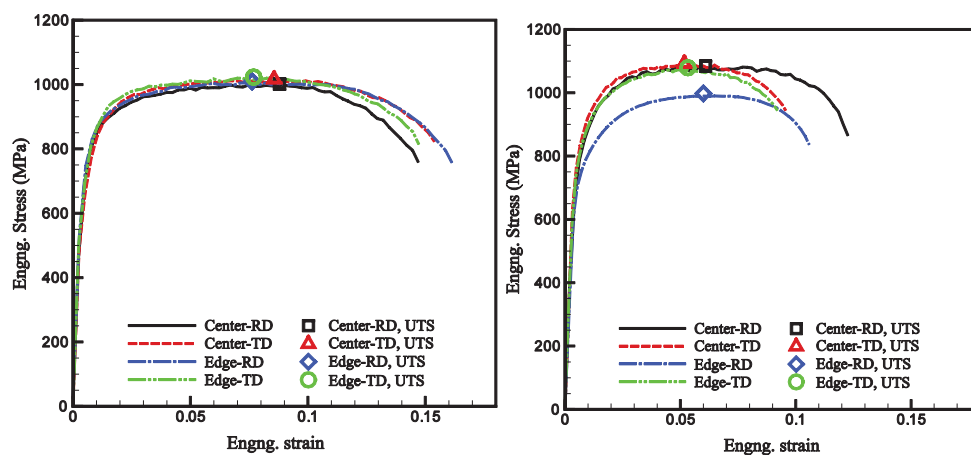


Figure 1. Stress-strain curves of the samples from the center and edge regions along the rolling and transverse directions (RD and TD) for (a) DP980 A and (b) DP980 B.

Figure 2 shows the morphology of the undeformed NPSS from optical microscopy and EBSD. Based on XRD analysis, optical microscopy, and EBSD observations, the examined NPSS was found to be a single phase ferritic steel with an average grain size of about 6 μm and showed fully recrystallized microstructure with many nanosize precipitates inside the grains. Figure 3(a) shows TiC carbide particles, which are homogeneously distributed throughout the material. These carbide particles have an average size of 7 nm and an average spacing of 15 nm. Figure 3(b) shows a few spherical M_{23}C_6 carbides, with a diameter of tens of nanometers, lined up along the grain boundary. M_{23}C_6 carbides are not restricted to the grain boundaries but also occur inside the grains, as shown in Figure 3(c). Dense populations of small particles often have significant influence on the strength of metallic materials because they act as obstacles for the movement of dislocations. Therefore, the dual precipitate structure, consisting of dispersed TiC carbides in the matrix and M_{23}C_6 carbides along the grain boundaries, can provide combined matrix and grain boundary strengthening. Figure 4(a) shows the typical morphology of TiC carbide and dislocations at the strain level of 5.5%. Compared to Figure 3, increased dislocation density is observed, and the finely dispersed carbides can be found tangling with dislocations. As shown in Figure 4(b), the dislocation density increases significantly with the increase of strain. In Figure 4, most carbides are tangled with dislocations, and it is hard to find unpinned dislocations moved away from the carbides. This suggests that the finely dispersed nanosize precipitates are beneficial for the increase of dislocation density during plastic deformation by restraining the recovery and annihilation of dislocations.

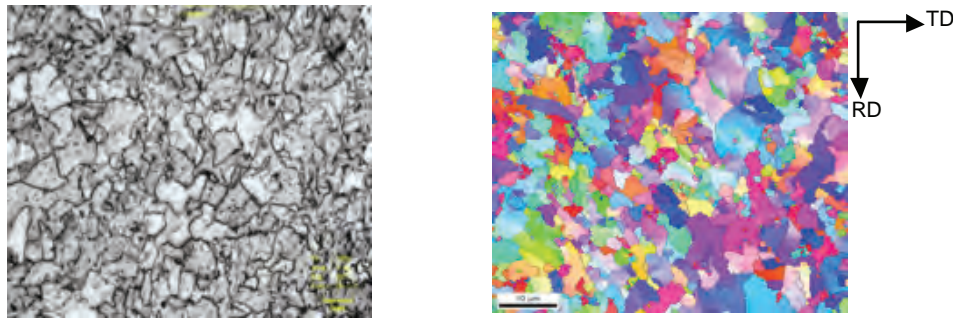


Figure 2. The morphology of as-received NPSS from (a) optical microscopy and (b) EBSD.

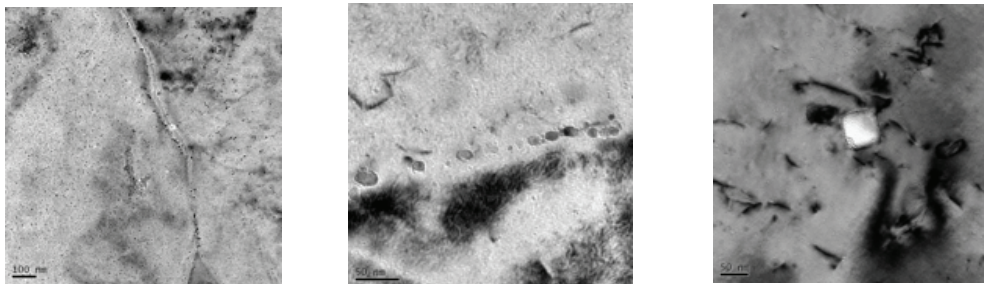


Figure 3. TEM images of as-received NPSS showing (a) TiC carbides inside grain, (b) M_{23}C_6 carbides at grain boundary, and (c) M_{23}C_6 carbide inside grain.

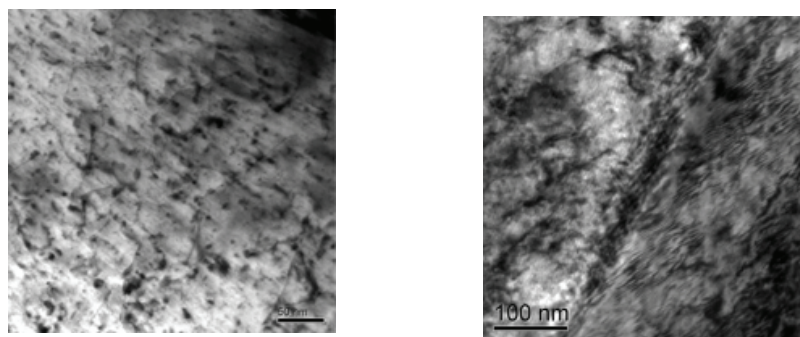


Figure 4. TEM images of deformed NPSS showing interactions between carbides and dislocations at strains of (a) 5.5% and (b) 22%.

Conclusions

Different DP980 steels were acquired from different suppliers and tested at different locations in different directions to establish the fundamental understandings on key mechanical properties and the microstructure features influencing the local formability of AHSSs.

Chemical composition analyses were first performed on different DP980 steels acquired to date. The results from these analyses show that different steels generally have somewhat different alloying elements; however, the chemical composition of a specific steel is quite consistent for the different regions. Static tensile tests have also been performed for samples cut from two different locations (center and edge) along the RD and TD. The results suggest that the behaviors of DP steels vary depending on locations and directions. This is possibly due to the inhomogeneous microstructure features within the specific sheet and/or along the RD and TD. Microstructural analyses using SEM are scheduled in FY 2011 to obtain the detailed 3D microstructural features of the different DP980 steels. The results from SEM analyses are expected to explain the characteristics of observed macroscopic behaviors.

A series of TEM observations have been performed to understand the fundamentals of the strengthening mechanisms of NPSSs. Finely dispersed TiC carbides were observed inside the grains and some M₂₃C₆ carbides were also found along the grain boundary and inside the grains. These finely dispersed precipitates can strengthen the steel by pinning dislocations as well as retarding the recovery and annihilation of dislocations.

Ultrafine Grain Foils and Sheet by Large Strain Extrusion Machining

Principal Investigator: Mark T. Smith, PNNL

(509) 375-4478; e-mail: mark.smith@pnl.gov

Srinivasan Chandrasekar, School of Industrial Engineering, Purdue University

(765) 494-3623; e-mail: chandy@ecn.purdue.edu

Kevin Trumble, School of Materials Engineering, Purdue University

(765) 494-4114; e-mail: driscoll@ecn.purdue.edu

Introduction

This PNNL-Purdue collaboration seeks to overcome the cost barrier of implementing sheet Mg alloys in automotive applications. LSEM, under development by the Purdue group, is a hybrid cutting-extrusion process in which sheet metals can be produced in a single-stage deformation process. The initial phase of the work has established the feasibility of producing nominal 2 mm thick sheet of MgAZ 31B using the LSEM process.

Approach

A rotary LSEM configuration implemented on a lathe (**Figure 1a**) was used for this phase of the work. In the LSEM process, a constraining edge is used in addition to a cutting edge to impose large shear strains while controlling the product thickness. The chip thickness ratio, $\lambda = tc/t$, and cutting tool rake angle (α) determine the deformation levels in the sheet. The shear strain is given by an upper-bound model as

$$\gamma = \frac{\lambda}{\cos \alpha} + \frac{1}{\lambda \cos \alpha} - 2 \tan \alpha \quad (1)$$

Figure 1b shows the variation of strain with λ and α . The shear strain increases with both increasing and decreasing λ , affording two different deformation paths to the same strain. Significant to the present task is that larger hydrostatic pressures are imposed for smaller λ (also shown in **Figure 1b**). The capability for imposing high hydrostatic pressures, together with the localized adiabatic heating, is an attractive feature of LSEM for producing sheet in alloys of low workability such as Mg.

In Phase 1 of this work, LSEM trials were conducted under systematically varying conditions to establish the feasibility of producing 2 mm thick sheet from extruded MgAZ-31B billets. The main experiments were designed to establish the

interactive effects of hydrostatic pressure and deformation zone temperature on the ability to suppress segmentation and produce continuous sheet. The rake angle was fixed at 5° for all experiments. The shear strain was held constant at $\gamma = 2$, with λ varying from 0.7 to 1.4 and the cutting velocity varying from 0.2 m/s to 2 m/s, giving deformation temperatures ranging

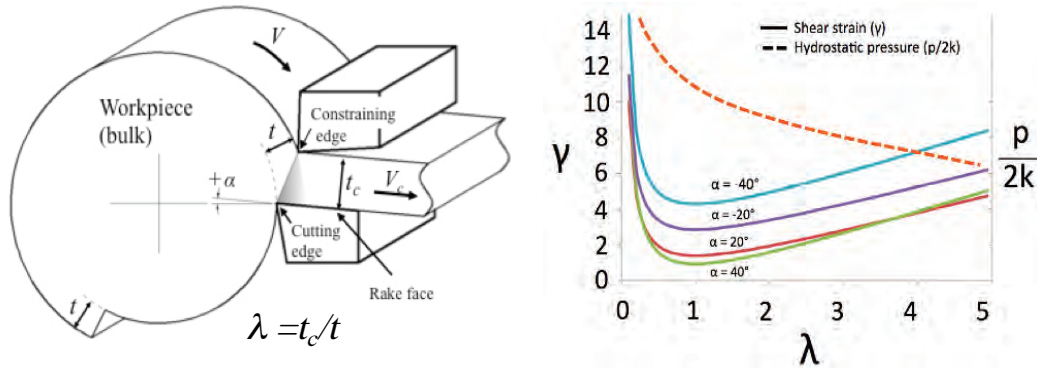


Figure 1. (a) LSEM in rotary configuration. λ is the chip thickness ratio. (b) Upper-bound model results showing how shear strain (γ) and hydrostatic pressure (dotted curve) vary with λ . Note that the hydrostatic pressure (p), which is normalized by the yield strength in the plot, increases monotonically with decreasing λ .

from about 70°C to 250°C . Metallographic analysis of the resulting specimens is also reported.

Results and Discussion

Application of the LSEM process to MgAZ31B is clearly demonstrated in Figure 2. Here, the normally broken, needle-like chips of a low pressure LSEM (LP LSEM) process (Figure 2a) is compared with the continuous, defect free strip of a high pressure LSEM (HP LSEM) process (Figure 2b). The figure shows what can be accomplished by a modest increase in

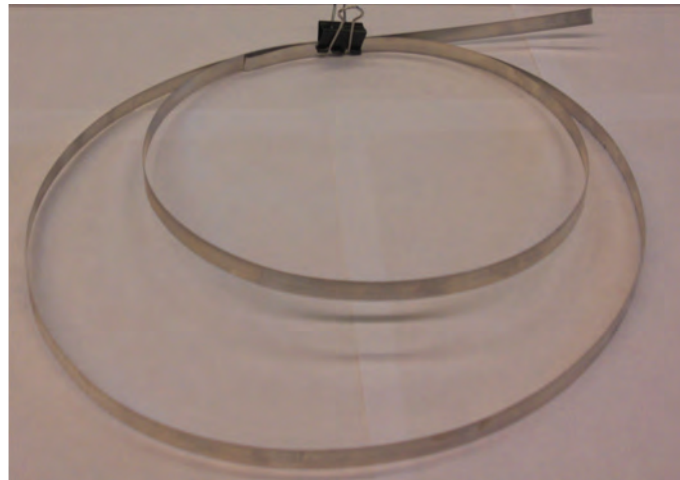


Figure 2. Sample MgAZ31B processed by LSEM. (a) LP LSEM ($p/2k = 1.2$, $T = 70^\circ\text{C}$) and (b) HP LSEM ($p/2k = 1.7$, $T = 230^\circ\text{C}$). In both cases, $\gamma \sim 2$. The deformation zone temperature, T , was achieved naturally, without any work material or tool preheating.

hydrostatic pressure, from $p/2k = 1.2$ (LP LSEM) to $p/2k = 1.7$ (HP LSEM) and temperature (70°C to 230°C).

To explore the hydrostatic pressure effect at increasing sheet thickness, the undeformed chip thickness (t in Figure 1a), was increased progressively in both the HP LSEM and the LP LSEM until broken chips were obtained (Figure 3). For this experiment, the workpiece was not preheated ($T_{\text{amb}} \sim 25^\circ\text{C}$). Because the deformation rate was also kept constant ($V_o = 1$ m/s), the deformation zone temperature for each hydrostatic pressure was about constant. The transition from continuous chip formation to serration occurs at a much larger undeformed chip thickness in HP LSEM ($t \sim 0.5$ mm) than in LP LSEM ($t \sim 0.1$ mm).

A case of HP LSEM was then tried at the largest possible undeformed chip thickness for the available machine tool. The resulting sheet was 2.5 mm thick and essentially free of defects. While for this case, the workpiece was preheated to 250°C, the hydrostatic pressure was reduced somewhat ($p/2k = 1.4$) to reduce the burden on the machine tool. The experiment shows that LSEM can be tailored to produce large section sheet material and, at the limit of the current experimental tooling, can reach the nominal 2 mm thickness goal. Although these results have clearly established the controlling parameters and feasibility of producing MgAZ31B sheet at the 2 mm thickness by LSEM, substantial work remains to make the process robust for scale-up.

The microstructure of the material processed by HP LSEM ($T = 230^\circ\text{C}$) is shown in Figure 4. Similar structures were observed for the LP LSEM sheet produced at similar temperatures. The grain size decreases from $16\ \mu\text{m}$ in the starting material (extruded billet) to about $4\ \mu\text{m}$ in the processed material. Another distinguishing feature of these structures was a relatively narrow grain size distribution, as measured by the linear intercept method. The microstructure seems to be a result of dynamic recrystallization. While not shown, the grains of the material processed by HP LSEM at $T = 130^\circ\text{C}$ could not be resolved with the optical microscope. It is suspected that grains for this condition are of a submicrometer scale, as is normally the case when this strain level ($\gamma = 2$) is achieved at sufficiently low temperature.

Technology Transfer

This task is primarily focused on demonstration of the LSEM process concept and scaling up of equipment to produce a suitable 250 mm wide strip. If scale-up is successful, results will be presented to a number of materials and metals product suppliers in an attempt to transfer technology into the automotive materials supplier base.

Conclusions

Continuous sheet of Mg AZ31B at thickness up to about 2 mm thick has been produced directly from billet in the single-stage LSEM process, with minimal or no preheating of the workpiece. The process takes advantage of its ability to produce relatively high hydrostatic pressures and local deformation heating and is characterized by a critical temperature for continuous sheet formation that decreases with increased hydrostatic pressure and increases with increased sheet thickness. Through systematic experiments and modeling of the deformation field, the controlling ranges of these parameters have been elucidated. The process is capable of producing homogeneous microstructures showing considerable grain refinement (~fourfold decrease).

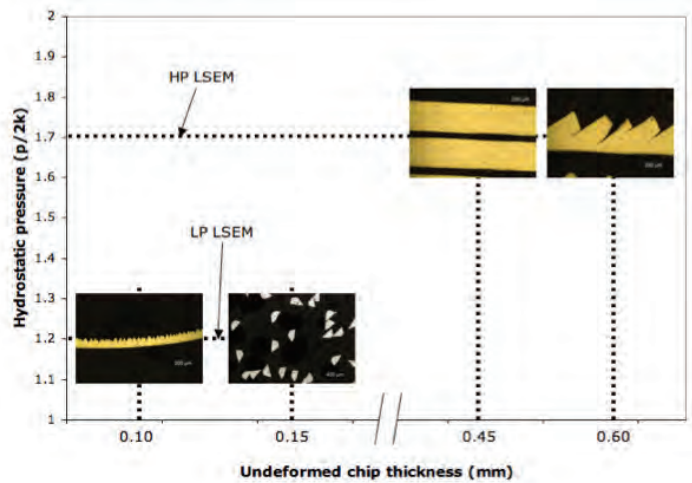


Figure 3. Hydrostatic pressure vs undeformed chip thickness. The work material was initially at ambient temperature. Deformation rate = 1 m/s.

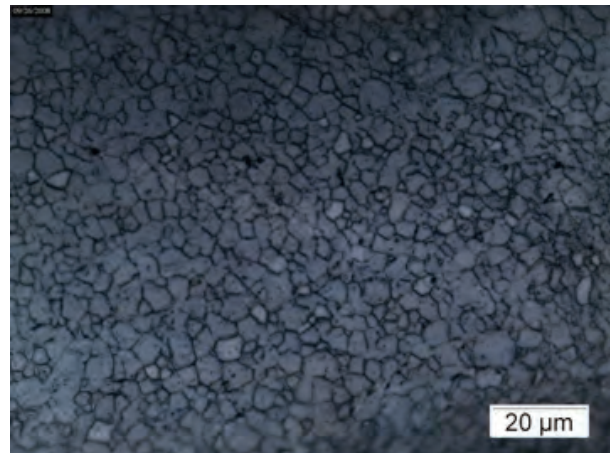


Figure 4. Optical micrograph of HP LSEM ($T = 230^\circ\text{C}$) showing uniform, equiaxed grain structure with grain size $3.6 \pm 0.3\ \mu\text{m}$.

Development of High Strength Superplastic Forming Aluminum Sheet for Automotive Applications

Principal Investigator: Curt A. Lavender, PNNL
(509) 372-6770; e-mail: curt.lavender@pnl.gov

Principal Investigator: Daniel Edwards, PNNL
(509) 371-7184; email: dan.edwards@pnl.gov

Principal Investigator: Jung-Pyung Choi, PNNL
(509)276-3380; email: jung.choi@pnl.gov

Introduction

The objective of this task is to develop a cost-effective superplastic sheet with a post-formed yield strength greater than 250 MPa. SPF of Al alloys has been used in the forming of automotive outer body panels and closures. Because SPF involves forming the Al sheet at elevated temperatures, the final formed material strength is similar to that of an annealed (soft) Al sheet. Current automotive SPF applications have focused on the use of Al 5083 alloy, which, with relatively high Mg content, develops a post-formed yield strength of around 150 MPa that has restricted its use in BIW and under hood applications where higher strength is required.

Approach

The technical approach is to develop a heat-treatable alloy that with the proper thermomechanical processing will exhibit fine grained superplasticity with a post-forming heat-treat response. The development of a fine grain microstructure that remains stable at SPF temperatures generally requires a unique alloy chemistry combined with a very specific combination of homogenization and hot and cold rolling. Previous PNNL SPF alloy development work will be leveraged and chemistry and thermomechanical process modifications within known practical ranges will be used to optimize SPF microstructures. The focus of the task will be to develop a heat-treatable alloy that has a post-forming age-strengthening response that is compatible with automotive BIW thermal cycles (E-coat, paint-bake). The result of the task will be development of a cost-effective, high-strength SPF Al alloy sheet that can be used in higher strength and elevated temperature automotive applications, extending the use of SPF Al to BIW and underhood sheet components.

Technology Transfer Path

Technology transfer for this activity will be accomplished by engaging the automotive superplastic component manufacturers by sharing information. The task parameters have been largely defined by the superplastic industry and will easily transfer to the existing infrastructure. The development of the alloy and commercial production has been more difficult. However, in the last 6 months PNNL has been approached by three Al companies, all expressing interest in participating in the alloy processing. Their participation should facilitate technology transfer of the alloy processing techniques being developed at PNNL.

Results and Discussion

The initial phases of this activity were focused on development of an Al alloy that responded to the thermal history expected during high-volume SPF part manufacture to achieve the 250 MPa yield strength. As previously reported, an alloy system was identified that demonstrated the desired mechanical properties. However the alloy was not processed to achieve superplasticity and as a result exhibited poor superplastic elongation. The next phases of the activity, the initial results of which are reported here, will focus on (1) development of the thermomechanical processing to achieve fine grained superplasticity, (2) identification of the strengthening phases present in the alloy, and (3) engaging an Al supplier to support low cost commercial production.

Fine Grained Alloy Processing

Fine grained superplasticity is achieved by developing a grain size in Al that is less than 15 μm and relatively equiaxed. To achieve fine grain sizes in Al, there must be particles in the structure in the size range from 10 μm to 15 μm to act as nuclei, finer particles on the order of 1 μm to 5 μm to pin grain boundaries and suppress growth, and a large amount of strain to facilitate the nucleation process. For the alloys under development, the larger eutectic constituent (EC) particles will be

of the Al_6Mn (Cr, Si, Fe) or Mg_2Si type, shown in Figure 1 as the light and dark phases, respectively. In the previous year, alloys were produced to evaluate mechanical properties and did not have an ideal EC distribution due to the relatively low amount of rolling reduction used to produce the sheet Al from which the micrograph in Figure 1 was taken. For the next phase of the activity, ingots 75 mm thick (200 mm by 300 mm) and weighing about 7 kg are to be rolled entirely to the final gage of 1.5 mm. This increased rolling reduction should redistribute the particles in a more homogeneous manner and provide a more uniform distribution of nucleation sites, ultimately resulting in a more equiaxed grain morphology

The second particle phase to be developed is the finer precipitate, often called “dispersoid,” intended to pin boundaries and prevent grain growth. The dispersoid size and volume fraction are developed during the homogenization and hot rolling steps and, when combined with sufficient nuclei and cold work, are critical to the development of fine grain size. Samples from the as-cast ingots were subjected to high-temperature aging, slow cooling, and eddy-current testing to develop an understanding of the kinetics of the dispersoid formation by measuring the conductivity change associated with depletion of the solute. As the solute is depleted, dispersoids are formed and the conductivity increases, as shown in Figure 2 where conductivity as a percentage of the International Annealed Copper Standard (% IACS) is plotted against time. The importance of the homogenization temperature is shown in Figure 3 where two samples were homogenized to the same conductivity (% IACS), presumably developing the same volume fraction of dispersoids, at 450°C and 516°C. After cold work and anneal, the samples homogenized at 510°C for 10 hours developed grain sizes nearly an order of magnitude smaller than the sample homogenized at 450°C. Preliminary analysis and kinetic calculations suggest that for the SPF alloy under development about 85 hours at 400°C will be required to develop the same conductivity as achieved at 500°C for 10 hours. This value will be confirmed experimentally, and ingots with each homogenization treatment will be rolled to verify the impact of dispersion size on final grain size.

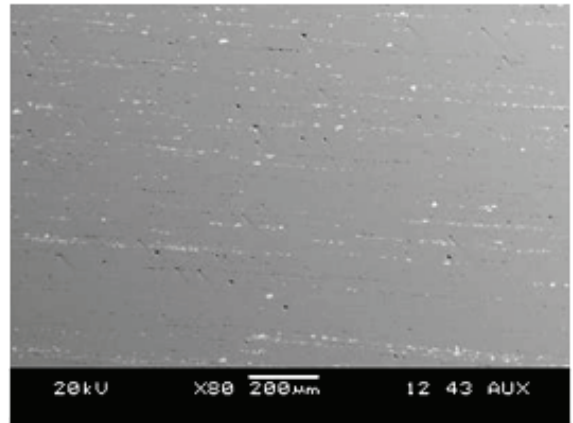


Figure 1. Scanning electron micrograph of the SPF alloy showing the distribution of ECs: Al_6Mn (Cr, Si, Fe) (light phase) and Mg_2Si (dark phase).

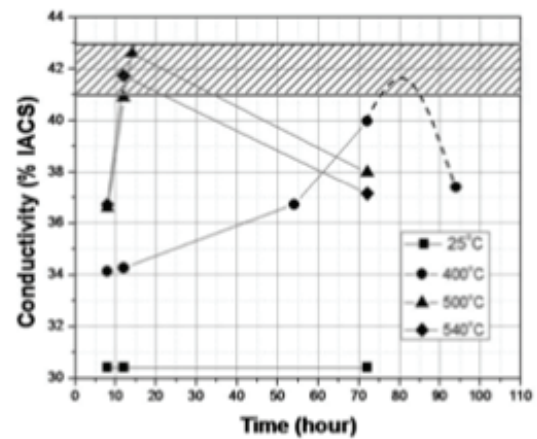


Figure 2. Conductivity as a function of time for four temperatures that will be used to determine homogenization heat treatment.

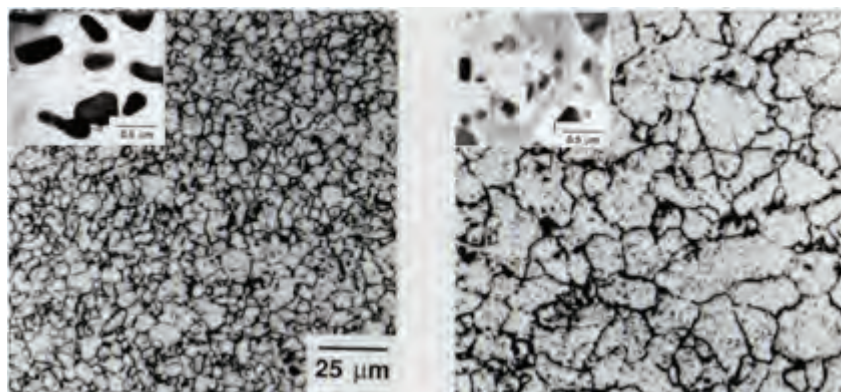


Figure 3. Optical metallography showing the grain size developed in an Al alloy homogenized at (a) 510°C and (b) 450°C. The inset micrographs show the difference in the dispersoid size where the larger dispersoids, (a), were more effective at suppressing grain growth than the finer dispersoids, (b).

Strengthening Mechanisms

During the previous reporting period, an alloy identified as 6T-2 was developed that demonstrated the 250 MPa yield strength requirements with the limited solution heat treat and paint-bake process. The alloy contained, in weight percent, 0.7 Mg, 1.5 Si, and 0.4 Cu. The 6T-2 alloy is considered to be “excess Si,” meaning that more Si is available than is required to consume the 0.7 Mg in Mg₂Si at an ideal stoichiometric ratio, and therefore the alloy is potentially hardened by excess Si and Mg₂Si and AlCu precipitates. Samples from the alloy were processed as follows: (1) heat treated at 510°C, water quenched, and aged to peak hardness to achieve the T6 and (2) heat treated at 450°C, air cooled, and paint-baked (called SPF/PB). Samples from each process were evaluated by SEM and TEM to determine the precipitates that harden the alloy. The results are summarized in the TEM micrograph in Figure 4 for the T6 and SPF/PB conditions. The T6 condition, Figure 4(a), exhibits a number fine precipitates, strain associated with lattice distortion, and even some limited dislocation structure. This microstructure produced an alloy with a yield strength in excess of 300 MPa. The alloy subjected to SPF/PB, Figure 4(b), exhibits a limited number of precipitation types and no lattice distortion and dislocation structure. As a result, the yield strength is close to 250 MPa.

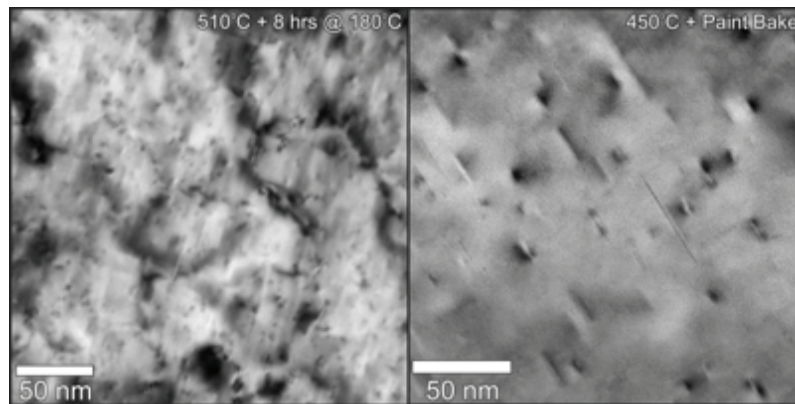


Figure 4. TEM micrographs of alloy 6T-2 (a) heat treated to the peak hardness and (b) paint-baked (SPF/PB) showing the difference in precipitate structure.

Based on the TEM image, the fine, nanometer sized precipitates in the T6 sample are likely the Mg₂Si and are not found in the SFP/PB treatment due to the low-solution, heat-treat temperature. The larger plate /needle-type precipitates are the theta AlCu phase and are found in both alloys along with another, yet to be identified, phase that is likely to be Si particles (expected in an excess Si alloy). The interesting result is that Cu content had little effect on the hardening response of the 510°C solution heat treat but a strong effect on the low temperature solution heat treat, indicating that most of the strengthening in the T6 is associated with the Mg₂Si while in SPF/PB treatment the hardening is due to the Cu phase. There is likely a contribution of the Si to strength for both heat treatments given that during the previous work lower Si alloys were shown to have lower strengths.

Material Supplier Development

One of the more important aspects of this activity is transfer of the alloy and process development knowledge to an Al company to (1) make the alloy available to a large consumer base and (2) ensure that the alloy and process being developed can be produced in a commercial Al mill. During previous years, no Al company expressed interest in participating in the task. However, in the last 6 months, PNNL has been approached by POSCO of Korea; Superform USA (Spectralite Al); and, most recently, Sky Al of Japan. During the next phase, one or more of these companies will be engaged in the task.

Conclusions

- The thermomechanical process development is still ongoing and focused at producing the fine grain size needed for superplasticity by controlled development of second phase particles. Progress has been made toward understanding the kinetics and particle phases present in the alloy.
- The primary strengthening precipitate in the SPF/PB process alloy is the needle-/plate-like Cu containing phase. At the

reduced-solution heat-treat temperature associated with the SPF cycle, the Mg₂Si precipitate was not developed. This, combined with a limit of 0.4 wt % Cu, restricts the alloy to the 250 MPa strength level. Under ideal heat-treat conditions, the alloy will form at least two additional precipitates and develop a yield strength in excess of 300 MPa.

- Three Al suppliers have approached PNNL and are now interested in participating in the activity. PNNL will discuss the task with each supplier and determine which supplier to pursue with cooperative work.

Formability of Continuous Cast Magnesium Sheet

Principal Investigator: Aashish Rohatgi, PNNL
(509) 372-6047; e-mail: aashish.rohatgi@pnl.gov

Key Contributors:

Darrell R. Herling and Eric A. Nyberg, PNNL

Industry Participants:

Paul E. Krajewski, General Motors Corporation

(248) 912-8395; e-mail: paul.e.krajewski@gm.com

Peter A. Friedman, Ford Motor Company

(313) 248-3362; e-mail: pfriedma@ford.com

Jugraj Singh, Chrysler Corporation, LLC

(248) 512-0029; e-mail: js329@chrysler.com

Introduction

Mg sheet, a lightweight alternative to steel or Al sheet, has potential applications in BIW, body closures, interior frames/brackets, and tubular components. However, a major barrier to using Mg sheet is the high cost of conventional wrought processing due to the hexagonal crystal structure of Mg and its poor hot-short characteristics. Continuous casting of Mg alloy sheet using twin-roll casting techniques offers the potential to reduce the cost of Mg sheet. However, the formability, forming process window, and post-formed properties of CC Mg sheet need to be evaluated to determine its viability as a low-cost alternative to conventional wrought-processed sheet. Therefore, the goal of this work is to develop a fundamental understanding of the microstructure-formability relationship and post-formed properties of CC Mg sheet. The work scope for this agreement was developed in conjunction with the USAMP Warm Forming Team (AMD 602) and was performed in conjunction with the University of Virginia and Canada Center for Mineral & Energy Technology–Materials Technology Laboratory.

Approach

The overall approach of the task comprised understanding the relationships between (1) the tribology at the sheet-die interface during warm forming and the resulting formability of the Mg sheets and (2) the forming process parameters and the post-formed mechanical properties and microstructure of the formed parts. Mg alloy AZ31B sheets from five undisclosed vendors, identified only by letters A, M, N, O, and X, were provided by the AMD 602 team. The tribology at the sheet-die interface was studied through measurements of average surface roughness parameters of the Mg sheet and through determination of elevated temperature coefficient of friction for as-received Mg sheets and lubricant combinations. The surface roughness was determined following American National Standards Institute standards; lubricants were down-selected (following a market survey) using criteria such as thermal stability ($\geq 300^\circ\text{C}$), ease of removal, and cost; and coefficient of friction was determined using PNNL's bending-under-tension fixture. The sheet formability data were obtained from trials conducted by the AMD 602 team. Post-formed mechanical property and microstructural characterization were performed on samples machined from the Mg pans that had been warm formed by the AMD 602 team. Finally, elevated temperature LDH tests were performed to evaluate the effect of different warm forming lubricants on the formability of Mg sheets (vendor: Mg Elektron, North America).

Results and Discussion

The primary activity in FY 2010 was the microstructural characterization of warm formed Mg pans (AZ31B sheets from vendor "A") using the EBSD technique. Elevated temperature LDH tests were also performed to evaluate warm forming lubricants. The results of these efforts are described below.

Figure 1 shows the {0001} pole figures, from the pan-base center, of warm formed Mg pans (forming temperature and binder pressure listed with each pole figure). The pole figures are generally similar with the basal poles concentrated around, but slightly tilted off, the sheet-normal direction. Figure 2a shows that the proportion of the indexed area from the pan-base center, with {0001} poles oriented within 20° about the sheet-normal direction, increases somewhat with increasing forming temperature to 225°C followed by a decrease upon subsequent increase in forming temperature to 325°C. Finally, the curve shows an increasing trend with further increases in warm forming temperature to 350°C. Figure 2b plots the post-formed mechanical strength of samples machined from pan-base as a function of pan-forming temperature (FY 2009). Comparing Figures 2a and 2b, it is interesting to note that the trend in the {0001} basal texture [Figure 2(a)] as a function of pan-forming temperature is similar to that observed in post-formed tensile properties [Figure 2(b)]. The respective curves increase with increasing forming temperature, with a maximum around 175°C–225°C, followed by a decrease at 300°C–325°C and increasing further at 350°C. It is also worth noting that the crystal orientation image maps (from which the pole figures in Figure 1 were obtained) showed an average grain size of about 5 μm and an absence of deformation twins for all pan-forming temperatures. Thus, the variation of post-formed room-temperature tensile strength with pan-forming temperature [Figure 2(b)] appears to be more influenced by the variation in texture [Figure 2(a)] than by the initial grain size or twins.

Elevated temperature LDH tests (~300°C) showed that tungsten disulfide (proposed alternative to conventionally used boron nitride/graphite based lubricants) performed as well as or better than boron nitride lubricant and was relatively easier to clean

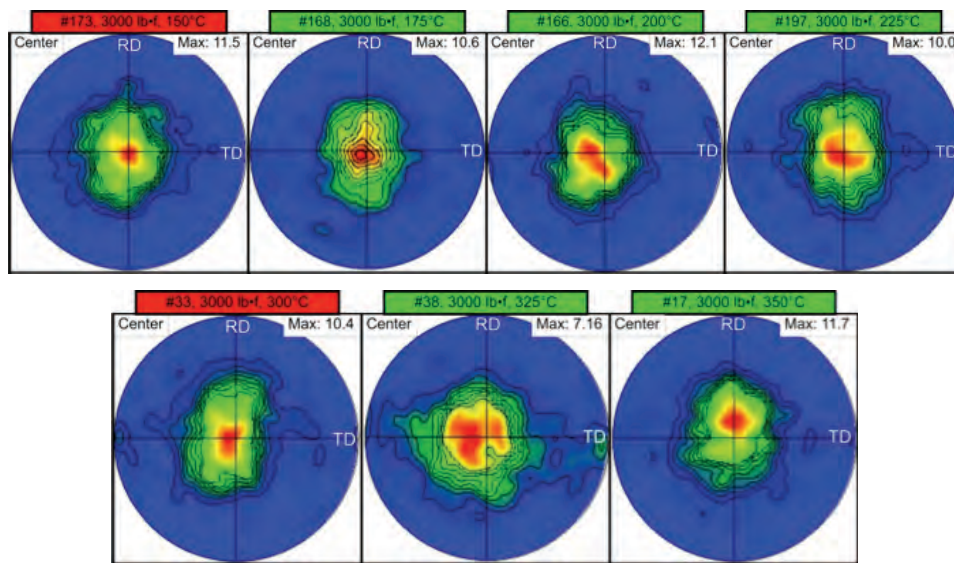


Figure 1. {0001} pole figures of AZ31B pans (pan-base center, vendor “A” sheets); the forming temperature and binder pressure are listed above each pole figure; RD and TD imply rolling and transverse directions of the sheet, respectively; the maximum value (“Max” on the top-right of each figure) refers to the contours concentrated around the centers of the pole figures (i.e., sheet normal direction). Pans were formed successfully at all temperatures except 150°C and 300°C.

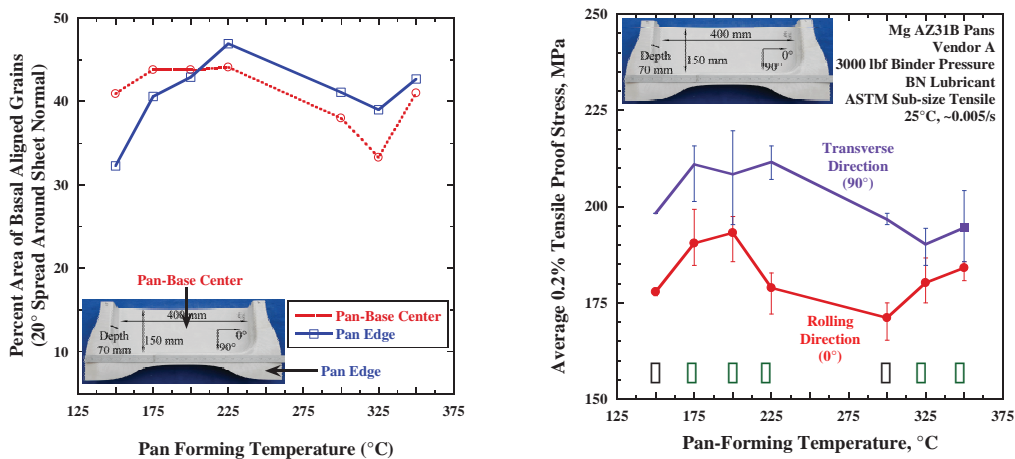


Figure 2. Dependence of Mg post-formed (a) texture and (b) strength on pan-forming temperature.

off (than boron nitride). Since plastic deformation in Mg is quite temperature sensitive, uniformity in temperature across the surface of the sheet sample and in the heated punch and die was found to be critical to ensure repeatable tests and to avoid premature failure near the die radius. The results also indicated greater formability when both faces of the sheet (as opposed to only the face in contact with the punch) were lubricated, presumably by preventing premature failure where the sheet contacts the die shoulder.

Conclusions

The post-formed basal texture and room-temperature tensile strength of AZ31B pans (Mg sheet vendor “A”) follow a similar trend as a function of prior warm forming temperature. For the pans formed between 150°C and 350°C at a binder pressure of 3,000 lbf, a maximum is observed in both the area fraction with basal {0001} texture (sheet normal direction) and post-formed strength (RD and TD) when forming is carried out at about 175°C to 200°C.

Under the test conditions used in this research, tungsten disulfide was found to demonstrate similar/better performance in LDH tests compared to boron nitride and was also relatively easier to clean off of the Mg sheets. Thus, tungsten disulfide is an attractive alternative to conventional boron nitride lubricant for Mg warm forming.

Pulse Pressure Forming of Lightweight Materials

Principal Investigator: Richard W. Davies, PNNL
(509) 375-6474; e-mail: rich.davies@pnl.gov
Principal Investigator: Aashish Rohatgi, PNNL
(509) 372-6047; e-mail: aashish.rohatgi@pnl.gov
Principal Investigator: Mark T. Smith, PNNL
(509) 375-4478; e-mail: mark.smith@pnl.gov

Key Contributors:

Elizabeth V. Stephens and Ayoub Soulami, PNNL
Gary L. Vanarsdale, Science Applications International Corporation

Industry Partners:

Sergey F. Golovashchenko, Ford Motor Company
(313) 337-3738; e-mail: sgolovas@ford.com
John R. Bradley, General Motors Corporation
(248) 912-8539; e-mail: john.r.bradley@gm.com
Ajit K. Desai, Chrysler Corporation
(248) 576-7455; e-mail: akd11@chrysler.com

Introduction

The ultimate goal of the task is to extend the formability of high-strength, lightweight metals (e.g., Al and Mg) and AHSSs using PPF techniques such as EHF. PPF techniques have the potential to enhance formability of difficult to form metals, minimize/eliminate springback after forming, and use less expensive single-sided tooling. However, there is a lack of understanding of practical forming limits in PPF processes and their dependence upon process parameters and tooling design. This task will quantify the deformation behavior of sheet metals during the EHF process and develop validated constitutive relations and models for Al and AHSS to enhance understanding of the EHF process and metal formability.

Approach

High-rate deformation behavior of 5182-O Al (1 mm) and DP600 steel (0.6 mm and 1 mm) sheets during EHF, under free-forming conditions and in a 48° conical die, was quantified using high-speed imaging and digital image correlation (DIC) techniques. Microstructures of the EHF and quasi-statically formed domes were characterized to study strain-rate effects on texture evolution. Sheet deformation during EHF was modeled in Abaqus using 3D and axi-symmetric two-dimensional (2D) models with numerical pulse-pressure profiles and employing the Johnson-Cook equation to describe the material’s constitutive behavior. Selection of the Johnson-Cook constitutive equation was motivated by its ability to incorporate the

effects of strain rate, strain, and temperature on the flow stress. The dependence of strain-to-failure (an indicator of sheet formability) and of peak strain rates on the angle of the conical die were analyzed. Future work includes development of high-rate (EHF) forming-limit diagrams, constitutive modeling of sheet metals, and modeling of sheet-die interactions.

Results and Discussion

Figure 1(a) shows selected images of strain distribution at the apex of the dome formed during EHF (9,000 V) of 5182-O Al inside the 48° conical die. Figure 1(b) shows the time evolution of strain at specific locations at the apex. Contours and plots similar to those in Figures 1(a) and 1(b) were also obtained for displacement, velocity, and strain rate under various test conditions. Figure 2 shows a major strain of roughly 50% in the “safe” region adjacent to the fracture in a 5182-O Al sample (EHF, 9,900 V, 48° conical die). This safe strain was associated with a strain rate (at the apex) of about 2,000/s and, when plotted on an FLD (Figure 3), indicates enhanced formability relative to safe strain under quasi-static forming. Such experimentally determined data on strain distribution and its evolution with time (Figure 1) and strain rates associated with enhanced formability (Figure 3) are unique and have not been reported in the existing literature.

Figures 4(a) and 4(b) compare the textures of Al and DP steel that were free-formed quasi-statically and via EHF to about 12%–14% true strain (at the apex). The pole figures in Figure 4 correspond to the equi-biaxially deformed region at the dome apex. The Al sample (Figure 4a) shows almost no effect of strain rate (peak strain rate ~300/s) on the texture. However, the texture in steel shows strain-rate sensitivity: quasi-static deformation led to strengthening of the preexisting {111} fiber

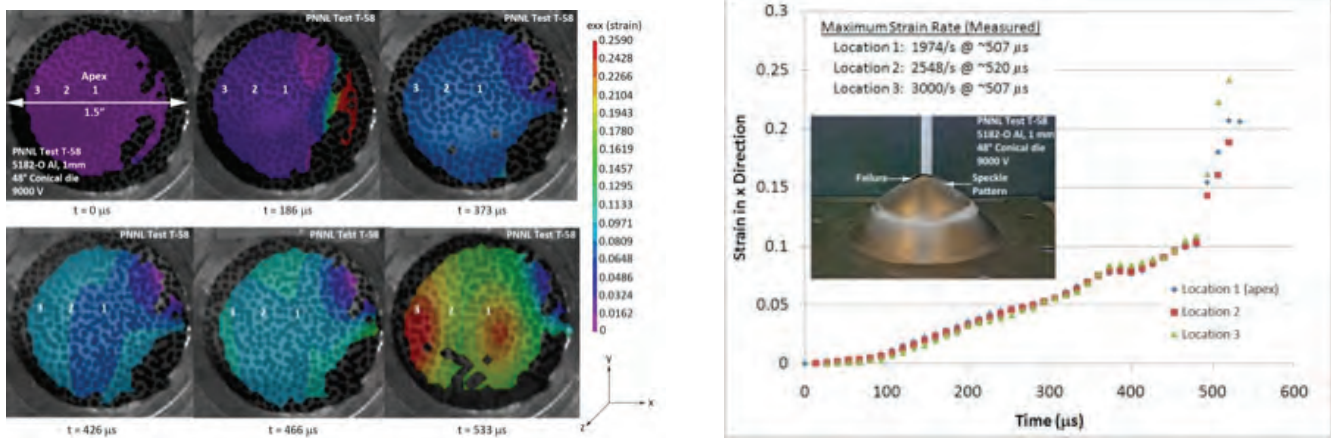


Figure 1. (a) Speckle-patterned images showing strain distribution at the dome apex of a 5182-O Al sheet deformed in a 48° conical die; (b) strain-time evolution for the test duration at locations marked in (a).

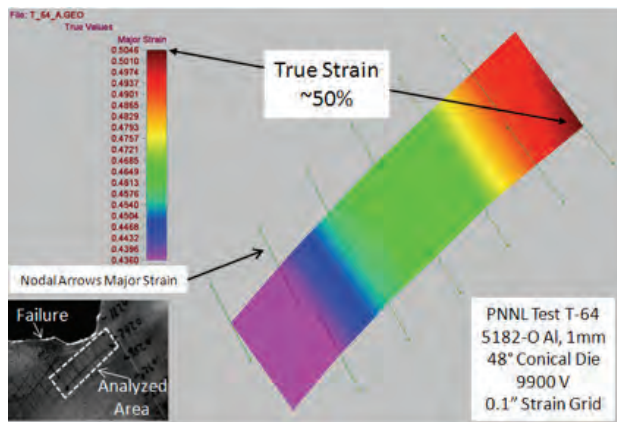


Figure 2. Postmortem strain measurement, near failure EHF location, using traditional (Taylor, 1988) strain-gridding method

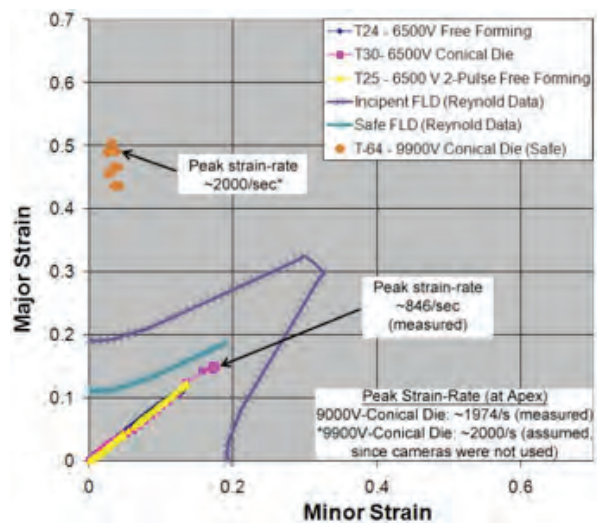


Figure 3. Forming limit diagram (FLD) with strain data (Figure 2) superimposed on the quasi-static forming limit curve.

texture in the ferrite phase while the high-rate EHF process had less influence. Although further investigation is needed to understand the strain-rate effects and different trends in texture evolution in these two materials, it is likely that the DP microstructure (i.e., soft ferrite + hard martensite) may be responsible for the strain-rate sensitivity of texture in DP600 steel.

The symmetry of the EHF apparatus used in this research enabled sheet deformation to be modeled as a computationally less intensive 2D axi-symmetric case instead of a 3D model. The influence of the die angle on sheet deformation (e.g., dome height, strain and strain rate at the apex, and failure strain) was modeled, and the apex-strain and strain-rate data (see Table 1) for the 48° case show good agreement with the experiments [see Figure 1(b)]. In some tests, sheet failure may occur at a location inside the die and, therefore, not visible to the cameras. In such cases, the model-predicted failure strains can be validated against postmortem strain data while the data at the dome apex (visible to the cameras) can be used to validate the strain rate and strain history before failure. Future work will examine the influence of the stress state and strain path associated with the sheet's impact with the die on ductility.

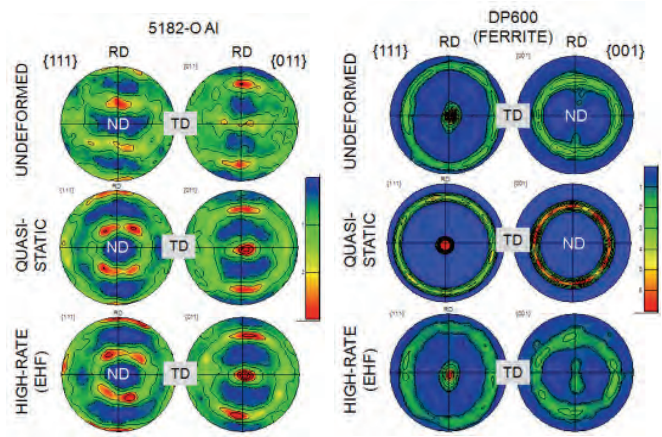


Figure 4. Pole figures comparing textures (at the dome apex) of undeformed, quasi-statically free-formed, and electrohydraulically free-formed sheet metals: (a) 5182-O Al and (b) DP600 steel.

Table 1. Predicted (2D model) deformation behavior of 5182-O Al in a conical die.

<i>Angle (with horizontal)</i>	<i>Dome height (mm)</i>	<i>In-plane strain at apex (%)</i>	<i>Max. in-plane strain rate at apex (1/s)</i>	<i>Failure strain (%)</i>
90 ^o	62.3	31.25	4465	36.7
55°	64.5	35.35	5400	39.85
48°	52.4	22.5	2300	32.41

Conclusions

An in-house capability for high-speed imaging has been established which, in combination with the DIC technique, has been successfully used to quantify the deformation behavior of Al and steel sheet materials formed at strain rates greater than 103/s using EHF.

Preliminary evidence of enhanced ductility was observed in 5182-O Al (1 mm) during deformation in a 48° conical die (peak in-plane strain rate of ~2,000/s at apex). Unlike Al, DP600 steel (0.6 mm) did not show evidence of enhanced ductility when formed in the conical die.

Under the experimental conditions used in this task, the texture in equi-biaxially deformed regions (at the dome apex) of 5182-O Al and DP600 steel (ferrite phase) show different trends and different strain-rate sensitivities. The DP microstructure (i.e., soft ferrite + hard martensite) of the DP steel is likely one of the reasons for the observed strain-rate sensitivity of ferrite deformation texture.

A 2D axi-symmetric model of sheet deformation during EHF was developed and validated against experimentally measured strain and strain rate at the dome apex.

Magnesium Research and Technology Development

Principal Investigator: Eric A. Nyberg, PNNL
(509) 375-2103; e-mail: Eric.Nyberg@pnl.gov

Introduction

The Mg Research and Technology Development task supports and manages efforts to increase the use of Mg in automotive and other transportation applications. These efforts look at property improvements while reducing costs associated with existing or new processes and manufacturing technologies. Ultimately, the goal is to advance the manufacture of economically viable Mg-intensive transportation vehicles.

Approach

- Support the DOE OVT on requested information and data related to the latest in Mg processing and property R&D worldwide.
- Provide the DOE OVT member of the U.S. MFERD Project Steering Committee (PSC) with information as it relates to funding or technical developments and challenges of the MFERD project. Review the monthly U.S. MFERD task leaders' progress and note any financial issues relevant to DOE funding.
- Attend and evaluate U.S. MFERD task leaders' review meetings and assess effectiveness of the U.S. tasks of the MFERD project.
- Conduct quarterly teleconferences with the Chinese and Canadian Project Technical Committee cochairs for the organization of the annual MFERD report and annual review meeting.
- Report on significant technical progress presented at technical conferences or published, identifying gaps in international research related to Mg R&D.
- Promote efforts to leverage R&D funding through interagency coordination [e.g., DOE-National Science Foundation (NSF)].
- Develop and maintain the Mg R&D Bibliographic Database located at Mg.pnl.gov.

Milestones, Metrics, and Accomplishments

- Milestone 1: Annually Update the Mg R&D Bibliographic Database located at Mg.pnl.gov (June 2010). This milestone was completed by periodically updating the bibliographic database which now includes more than 1,700 Mg-related citations.
- Milestone 2: Provide a framework for a U.S. Mg Fundamental and Applied R&D Program that crosses government offices and international boundaries. There were multiple facets to completing this milestone. Trip reports document international conferences; laboratory site visits; and continued interactions with the U.S. Army Research Laboratory (ARL), the University of Virginia, the University of Michigan, NSF, and DOE. In June 2010, ARL funded a workshop to identify areas of interest for both basic and fundamental Mg research. Principal Investigator Eric Nyberg assisted in identifying key participants for this meeting, not only for the Mg area but also for Al and titanium topics. Professor Sean Agnew from the University of Virginia and NSF continue to investigate a meaningful framework with which to form a collaborative U.S. research program. NSF has expressed an interest in funding an initiative on basic Mg R&D beginning in calendar year (CY) 2012 following a scheduled program development meeting in CY 2011.
- Milestone 3: Support MFERD in developing enabling technologies. This milestone was completed in a number of ways. Mr. Nyberg participated in the U.S. Task Leaders' Annual Meeting. He organized the PSC-Phase 1 Review Meeting in Seattle, Washington; compiled the 2009 MFERD Annual Progress Report; and organized the 2010 Annual Project Review Meeting. Mr. Nyberg also advised DOE of any issues that developed from multiple quarterly teleconference meetings for the technical committee or from weekly communications among project colleagues.

- Milestone 4: Organize the 2010 MFERD Annual Meeting (Ann Arbor, Michigan). This milestone was completed by reviewing, selecting, and contracting a meeting and hotel venue. A venue (the University of Michigan) within driving distance of the U.S. automaker team members was selected to maximize meeting attendance. A registration website was developed that allowed participants to conveniently register for the meeting online. The U.S. technical reports were translated and compiled with the Canadian and Chinese reports to create the 529-page 2010 Annual Report.

Conclusions

In FY 2010, the Mg Research and Technology Development task was successful in its objectives. Programmatic success of Phase 1 of the MFERD project was achieved. Awareness of the state-of-the-art R&D conducted both nationally and internationally was made through presentations and participation in a number of conferences, program reviews, and research center visits. Detailed trip reports summarized these activities. Invitations to present overview lectures, internationally, on the subject of Mg R&D indicate recognized expertise and knowledge at the forefront of the research communities. In addition, successful management of Phase 1 for the U.S. portion of the three-country MFERD project has contributed to the successful continuation of this demonstration project into Phase 2.

Conclusions

Lightweight metals offer significant weight savings potential in numerous automotive BIW and closure panel applications. The major barriers to their implementation are the cost-effective processing and manufacturing of these materials and gaps in the fundamental understanding of processing parameters versus properties needed to predict performance. This project consists of six tasks which each have work scope aimed at reducing key barriers to greater implementation of AHSSs, Al alloys, and Mg alloys.

Presentations/Publications/Patents

First Generation Advanced High-Strength Steels Deformation Fundamentals

Choi, K. S.; Soulami, A.; Liu, W. N.; Sun, X.; Khaleel, M. A. Influence of Various Material Design Parameters on Deformation Behaviors of TRIP Steels. *Computational Materials Science* 2010, doi:10.1016/j.commatsci.2010.10.002.

Soulami, A.; Choi, K. S.; Shen, Y.; Liu, W. N.; Sun, X.; Khaleel, M. A. On Deformation Twinning in a 17.5%Mn-TWIP Steel: A Physically-Based Phenomenological Model. *Materials Science and Engineering A* 2010, doi:10.1016/j.msea.2010.10.031.

Soulami, A.; Choi, K. S.; Liu, W. N.; Sun, X.; Khaleel, M. A.; Ren, Y.; Wang, Y. D. Predicting Fracture Toughness of TRIP 800 Using Phase Properties Characterized by In-Situ High Energy X-Ray Diffraction. *Metallurgical and Materials Transactions A* 2010, 41, 1261–1268.

Sun, X.; Choi, K. S.; Soulami, A.; Liu, W. N.; Khaleel, M. A. On key factors influencing ductile fractures of dual phase (DP) steels. *Materials Science and Engineering A* 2009, 526, 140–149.

Choi, K. S.; Liu, W. N.; Sun, X.; Khaleel, M. A.; Fekete, J. R. Influence of Manufacturing Processes and Microstructures on the Performance and Manufacturability of Advanced HSS (AHSS). *Transactions of ASME, Journal of Engineering Materials and Technology* 2009, 131, #041205.

Sun, X.; Choi, K. S.; Liu, W. N.; Khaleel, M. A. Predicting Failure Modes and Ductility of Dual Phase Steels Using Plastic Strain Localization. *International Journal of Plasticity* 2009, 25, 1888–1909.

Choi, K. S.; Soulami, A.; Liu, W. N.; Sun, X.; Khaleel, M. A. Effects of Retained Austenite Stability and Volume Fraction on Deformation Behaviors of TRIP Steels. In *Proceedings of Materials Science and Technology 2010 Conference and Exhibition*, The American Ceramic Society, 2010.

Choi, K. S.; Liu, W. N.; Sun, X.; Khaleel, M. A. Predicting Ductility and Failure Modes of TRIP steels under Different Loading Conditions. In *Proceedings of 10th International Conference on Numerical Methods in Industrial Forming Processes, NUMIFORM 2010*, 2010.

Liu, W. N.; Choi, K. S.; Soulami, A.; Sun, X.; Khaleel, M. A. Effects of Forming Induced Phase Transformation on Crushing Behavior of TRIP Steel. SAE Technical Paper no. 2010-01-0216 of SAE 2010 World Congress, Society of Automotive Engineers, 2010.

Sun, X.; Choi, K. S.; Soulami, A.; Liu, W. N.; Khaleel, M. A. Effects of Voids on Ductility of Dual Phase (DP) Steels. In Proceedings of 16th International Symposium on Plasticity & Its Current Applications, International Journal of Plasticity, 2010.

Choi, K. S.; Soulami, A.; Liu, W. N.; Sun, X.; Khaleel, M. A. Fracture Driven by Phase Inhomogeneity in Higher Grade Dual Phase Steels. In Proceedings of International Automotive Body Congress 2009, International Automotive Body Congress, 2009.

Ultrafine Grain Foils and Sheet by Large Strain Extrusion Machining

Efe, M.; Moscoso, W.; Chandrasekar, S.; and Trumble, K. P. Production of Mg AZ31B Foils by Machining-Based Processes. In Materials Science and Technology (MS&T) 2009 Conference (ACerS, ASM, AIST and TMS), Pittsburgh, Pennsylvania, October 25–29, 2009.

Saldana, C.; Swaminathan, S.; Brown, T. L.; Moscoso, W.; Mann, J. B.; Compton, W. D.; and Chandrasekar, S. Unusual Applications of Machining: Controlled Nanostructuring of Materials and Surfaces. ASME Journal of Manufacturing Science and Engineering 2010, 132-3, 030908 (12 pages) doi:10.1115/1.4001665.

Moscoso, W.; Efe, M.; Trumble, K. P.; Chandrasekar, S. “Direct production of MgAZ31B sheet by large-strain extrusion machining,” to be submitted to Acta Materialia in November 2010.

Sagapuram, D, Trumble, K.P, and Chandrasekar, S., “Texture development in MgAZ31B foil produced by large-strain extrusion machining,” to be submitted to Metallurgical and Materials Transactions, November 2010.

Moscoso, W.; Efe, M.; Compton, W. D.; Trumble, K. P.; and Chandrasekar, S. Direct Production of Sheet from Alloys of Limited Workability Using Machining-Based Processes. Presented at the 2011 TMS Symposium on Functional and Structural Nanomaterials: Fabrication, Properties, Applications and Implications.

Mann, J. B.; Saldana, C.; Swaminathan, S.; Moscoso, W.; Murthy, T. G.; Compton, W. D.; Trumble, K. P.; and Chandrasekar, S. Severe Plastic Deformation by Machining and Production of Nanostructured Alloys. In Nanostructured Metals and Alloys: Processing, Microstructure, Mechanical Properties and Applications; Whang, S. H., Ed.; Woodhead Publishing, in press.

Development of High Strength Superplastic Forming Al

Lavender C. A. and Smith M. T. Development of High Strength Superplastic Al Sheet for Automotive Applications. Presented at DOE VTP Annual Merit Review, Washington, DC, June 10, 2010.

Formability of Continuous Cast Mg Sheet

Rohatgi, A.; Herling, D. R.; and Nyberg, E. A. Characterization of Continuous-Cast AZ31B Mg Alloy Sheets and Lubricants for Warm-Forming Friction Effects. In 2010 TMS Annual Conference Proceedings; Agnew, S. R., Neelameggham, N. R., Nyberg, E. A., Sillekens, W. H., Eds.; Mg Technology 2010; TMS (The Minerals, Metals & Materials Society): 2010; pp. 573–578.

Pulse Pressure Forming of Lightweight Materials

Rohatgi, A.; Stephens, E. V.; Soulami, A.; Davies, R. W.; and Smith, M. T. High-Strain-Rate Forming of Al and Steel Sheets for Automotive Applications. In Proceedings of IDDRG Conference 2010; Kolleck, R., Ed.; IDDRG, Austria, 2010; pp. 441–450.

Davies, R. W.; Stephens, E. V.; Rohatgi, A.; Smith, M. T.; and Vanarsdale, G. L. Strain Rates and Formability of Al Alloys Under Pulse Pressure Metal Forming. Presented at the International Symposium on Plasticity 2010, St. Kitts, January 3–8, 2010.

Mg Research and Technology Development

Nyberg, E. A. Global Mg Research and Development Needs of Tomorrow. Presented at the Korean International Mg Symposium for Advanced Industry Trends, Seoul, South Korea, May 11, 2010, Pacific Northwest National Laboratory, Richland, WA. PNNL-SA-72637, 2010.

Nyberg E. A. Mg Research and Technology Development: A Perspective from the Pacific Northwest National Laboratory. Presented at the MagNET Program Annual Group Meeting, Vancouver, British Columbia, Canada, June 22, 2010. PNNL-SA-73505, 2010.

Editor of the 2010 TMS Annual Conference Proceedings; Eds. Agnew, S. R., Neelameggham, N. R., Nyberg, E. A., Sillekens, W. H., Eds.; Mg Technology 2010; TMS (The Minerals, Metals & Materials Society) 2010.

Mathaudhu, S. N. and Nyberg, E. A. In 2010 TMS Annual Conference Proceedings; Agnew, S. R., Neelameggham, N. R., Nyberg, E. A., Sillekens, W. H., Eds.; Mg Technology 2010; TMS (The Minerals, Metals & Materials Society): 2010; pp. 27–32.

References

Taylor, B. Formability Testing of Sheet Metals. Metals Handbook—Forming and Forging. ASM International: Metals Park, Ohio, 1988; 877–879.

C. Modeling and CMS - Oak Ridge National Laboratory

Field Technical Monitor: C. D. Warren
Oak Ridge National Laboratory
1 Bethel Valley Road; Oak Ridge, TN 37831
(865) 574-9693; e-mail: warrencd@ornl.gov

Technology Area Development Manager: William Joost
U.S. Department of Energy
1000 Independence Ave., S.W.; Washington, DC 20585
(202) 287-6020; e-mail: william.joost@ee.doe.gov

Contractor: Oak Ridge National Laboratory (ORNL)
Contract No.: DE-AC05-00OR22725

Objective

- Develop a tracer diffusion database in the Mg-Al-zinc-manganese (Mg Al Zn-Mn) system using secondary ion mass spectrometry (SIMS) for measurements of diffusion depth profiles of isotopes.

Accomplishments

- Established process parameters for accurate and reproducible depth profiling in Mg using the latest Cameca IMS 7f-GEO SIMS system. A primary requirement of the project is the capability to quickly and accurately measure isotopic ratios in Mg samples using SIMS. A suitable process recipe for depth profiling in Mg was established with the IMS 7f-GEO SIMS system for this purpose. Control over the instrument parameters in the IMS 7f SIMS system was found to be superior to the previous IMS 3f SIMS system for minimizing sputter topography during depth profiling and obtaining reliable results.
- Completed construction of an ultrahigh vacuum (UHV) system for thin film deposition of Mg. A UHV sputter deposition system for thin film deposition of high purity (low oxygen) Mg using enriched isotopic sputter target foils of Mg was constructed. X-ray photoelectron spectroscopy (XPS) results of a deposited Mg thin film indicated that the level of oxygen was less than a few atomic percent, which is expected to be reduced further with the installation of a titanium sublimation getter system.
- Performed interdiffusion studies in Mg-Al. Interdiffusion between pure Mg and pure Al was examined using solid-to-solid diffusion couples annealed at various temperatures (below 450°C) and times (several days). Concentration profiles were determined by energy dispersive spectroscopy (EDS) and electron probe microanalysis (EPMA). The interdiffusion coefficients will be computed from these.

Future Direction

- Measure Mg self-diffusivities in single-crystal and polycrystalline Mg. Compare with published radiotracer data.
- Develop a phase field simulation for modeling tracer diffusion in polycrystalline Mg alloys with input from molecular dynamics (MD) simulations to model volume and grain boundary diffusion.
- Measure Mg and Zn tracer diffusivities in the Mg-Al-Zn and Mg-Al-Mn systems. For Mn and Al tracer diffusivities, use the radioisotopes of Mn and Al (if available) for measurements. ORNL support will be used for the design and construction of a time-of-flight-SIMS system for measurements involving radioisotopes.
- Determine interdiffusion coefficients in the hexagonal close packed single phase of the Mg-Al-Zn and Mg-Al-Mn systems, and use diffusion theory to extract the tracer diffusivities of Al and Mn in these alloys.

High Throughput Isotopic Diffusion Databases for Magnesium Integrated Computational Materials Engineering

Principal Investigator

Nagraj Kulkarni, Oak Ridge National Laboratory
(865) 576-0592; e-mail: kulkarnins@ornl.gov

Industrial Partner

U.S. Automotive Materials Partnership Integrated Computational Materials Engineering (ICME) Team

Collaborators

Peter Todd, Oak Ridge National Laboratory
(865) 574-6824; e-mail: toddpj@ornl.gov
Balasubramaniam Radhakrishnan, Oak Ridge National Laboratory
(865) 241-3861; e-mail: radhakrishnb@ornl.gov
Yongho Sohn, University of Central Florida
(407) 882-1181; e-mail: ysohn@mail.ucf.edu
Kevin Coffey, University of Central Florida
(407) 823-2175; e-mail: krcoffey@mail.ucf.edu
Jerry Hunter, Virginia Tech
(540) 391-0366; e-mail: hunterje@vt.edu

Introduction

The objective of this project is to create an isotopic (tracer) diffusion database in the Mg-rich phase of the Mg-Al-Zn-Mn system. This database and a thermodynamic database that is being continuously updated will be provided to participants involved in various tasks in the Mg-ICME (Allison et al., 2006) program.

Approach

The procedure for obtaining tracer diffusion data first requires the preparation of homogeneous single phase alloy samples in the desired Mg-Al-Zn-Mn system. This is followed by deposition of stable isotopes or radioisotopes of these elements in the form of thin films on the sample surfaces. After diffusion annealing at various temperatures below the melting temperatures of these alloy samples, the isotopic diffusion depth profiles in these samples are measured using SIMS. Analysis of the diffusion depth profile data using the thin film solution (Shewmon, 1989) provides the tracer diffusivity for the selected sample composition at the annealing temperature. At higher temperatures the tracer diffusion in polycrystalline alloy samples is likely to be dominated by volume diffusion, while at lower temperatures there will likely be an additional contribution from grain boundary diffusion. The SIMS diffusion data will be analyzed to extract both types of diffusion contributions. By repeating such measurements for different compositions and temperatures, a significant amount of tracer diffusion data for Mg, Al, Zn, and Mn in the single phase Mg-Al-Mn-Zn system will be obtained. These data can then be fitted using suitable functions to generate the tracer diffusion database. A phase field simulation will be used to model the effective tracer diffusivity in polycrystalline Mg alloy samples with input from MD computations for grain boundary diffusivities.

Results and Discussion

Sample Preparation and Control of Instrument Parameters in the Cameca IMS 7f-GEO SIMS System for Depth Profile Measurements in Mg

A suitable process recipe (3.5 kV primary and 1.5 kV secondary voltage for a net impact energy of 2.0 kV, sputter angle ~42 degrees, and use of an oxygen leak with pressure of 2×10^{-6} torr in the sample chamber) for depth profiling in Mg was established with the IMS 7f-GEO SIMS system to obtain high precision and accurate isotopic ratio measurements for

tracer diffusion studies (Figure 1). In comparison to the older system (IMS 3f) used previously, the IMS 7f-GEO has significantly improved primary column optics and secondary ion mass analysis and detectors and higher stability electronics. Control over these instrument parameters was found to be critical in reducing sputter topography during depth profiling. The experience with SIMS depth profiling in electronic materials and reactive elements such as Al proved to be useful in this regard (Hunter, 2009).

Ultrahigh Vacuum System for Thin Film Deposition of Mg

The construction of a new UHV sputter deposition system (Figure 2) for high purity (oxygen free) Mg isotopic film deposition was completed successfully in FY 2010. This system uses a short-target substrate spacing for high rate deposition, UHV bakeable vacuum components and pumping, hot metal getter purification, all metal sealed argon process gas components, and shielding in chamber to provide gettering during sputtering for improved purity. Oxygen levels near the detection limit (few atomic percent) for XPS analysis were measured in the Mg films deposited with this system.

Interdiffusion Studies

Interdiffusion between pure Mg (99.9%) and pure Al (99.999%) was examined using three solid-to-solid diffusion couples annealed at 300°C, 350°C, and 400°C for 30, 15, and 10 days, respectively. The interaction layers that developed were examined by optical and scanning electron microscopy. Figure 3(a) shows a backscatter electron micrograph of the diffusion couples annealed at 400°C. Concentration profiles [Figure 3(b)] were determined by EDS and EPMA for measuring the interdiffusion coefficients. A thick layer of β (Al_3Mg_2) and a thin layer of γ ($\text{Al}_{12}\text{Mg}_{17}$), both with measurable concentration gradients, formed in all three couples. Measured thicknesses were normalized to determine the activation energy for the growth of these two layers.

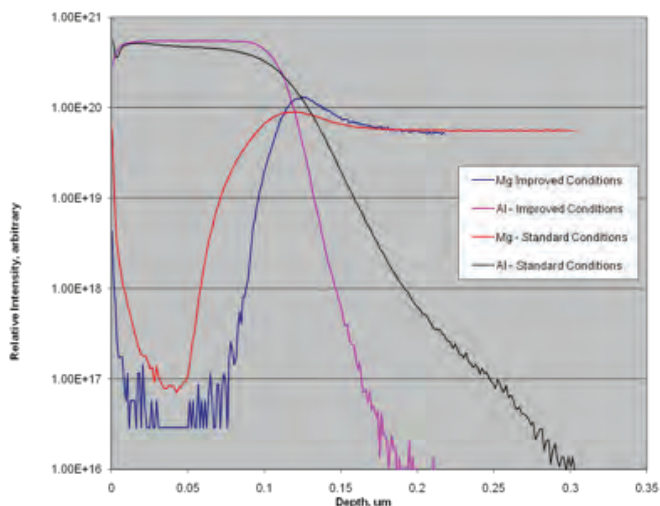


Figure 1. Improved depth profiling of Al on Mg using the IMS 7f SIMS system at Virginia Tech resulted in a steeper and more accurate depth profile.

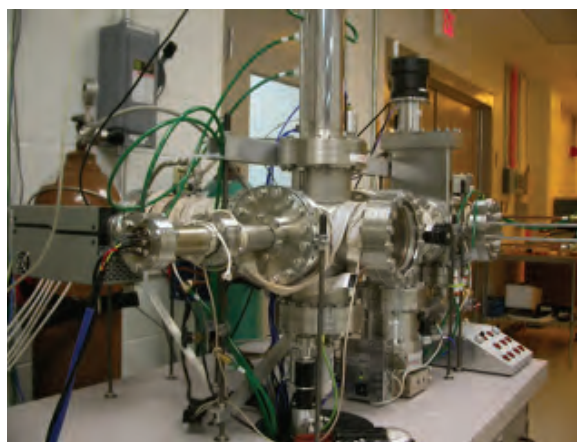


Figure 2. UHV system at the University of Central Florida for deposition of high purity isotopic Mg thin films.

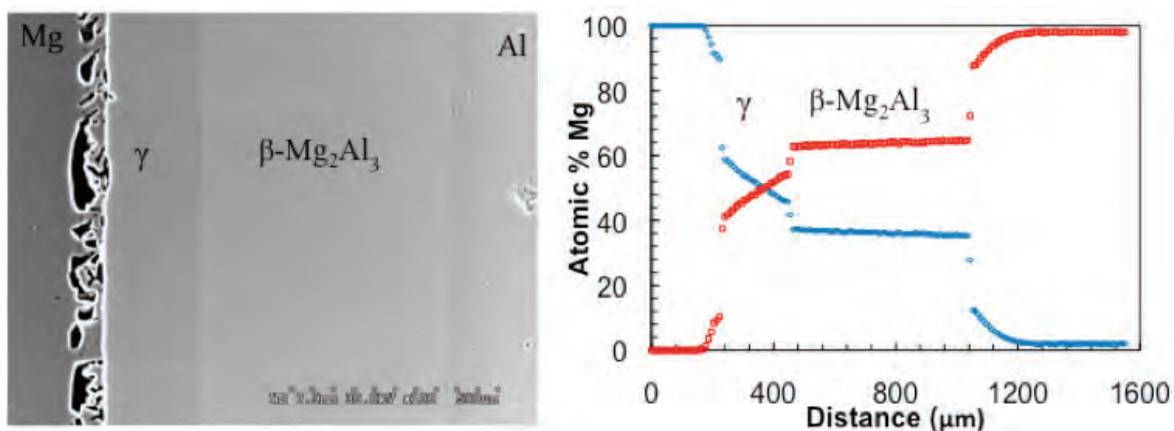


Figure 3. Backscatter electron micrograph and concentration profiles of Al and Mg measured by EDS from a solid-to-solid diffusion couple annealed at 400°C for 10 days.

Conclusions

The instrument parameters in the latest Cameca IMS 7f-GEO SIMS system were optimized for accurate diffusion depth profiling measurements in Mg. A UHV deposition system for isotopic thin films of Mg was constructed, and XPS results demonstrated very low oxygen levels. Interdiffusion measurements in Mg-Al were carried out for computing interdiffusion coefficients.

Presentations/Publications/Patents

Belova, I. V.; Allnatt, A. R.; Sohn, Y. H.; Kulkarni, N. S.; Murch, G. E. Enhancement Factors for Interdiffusion in FCC Alloy Diffusion Couples. Presented at the 6th International Conference on Diffusion in Solids and Liquids (DSL-2010), July 5–7, 2010, Paris, France.

Brennan, S.; Warren, A. P.; Coffey, K. R.; Sohn, Y. H.; Kulkarni, N. S.; Todd, P. J. Tracer Diffusion Studies of Mg and Zinc in Mg-Al-Zn Alloys. Presented at the 2010 TMS Annual Meeting & Exhibition: Symposium on Mg Technology 2010, February 14–18, 2010, Seattle, Washington.

Brennan, S.; Warren, A. P.; Klimov, M.; Coffey, K. R.; Sohn, Y. H.; Kulkarni, N.; Todd, P. Determination of Al, Zn and Mn Impurity Diffusion Coefficients in Mg. Presented at the Materials Science and Technology 2009 Conference, October 25–29, 2009, Pittsburgh, Pennsylvania.

Brennan, S.; Warren, A. P.; Coffey, K. R.; Sohn, Y. H.; Kulkarni, N.; Todd, P. Impurity Diffusion Studies of Al in Mg. In Mg Technology 2010; Agnew, S. R., Neelameggham, N. R., Nyberg, E. A., Sillekens, W. H., Eds.; The Minerals, Metals & Materials Society: Warrendale, Pennsylvania, 2010; pp 537–538.

References

Allison, J.; Backman, D.; Christodoulou, L. Integrated Computational Materials Engineering: A New Paradigm for the Global Materials Profession. *J. Met.* 2006, 58, pp 25–27.

Hunter, J. L., Jr. Chapter 6: Improving Depth Profile Measurements of Natural Materials: Lessons Learned from Electronic Materials Depth-Profiling. In *Secondary Ion Mass Spectrometry in the Earth Sciences*; MAC Short Course Series 41; Mineralogical Association of Canada: Québec, Canada, 2009; pp 132–148.

Shewmon, P. *Diffusion in Solids*, 2nd ed.; The Minerals, Metals & Materials Society: Warrendale, Pennsylvania, 1989; pp 15–19.

D. Modeling and Computational Material Science - Pacific Northwest National Laboratory

Field Technical Monitor: Dean Paxton
Pacific Northwest National Laboratory
902 Battelle Boulevard, P.O. Box 999, Richland, WA 99352
(509)375-2620; e-mail: dean.paxton@pnl.gov

Technology Area Development Manager: William Joost
U.S. Department of Energy
1000 Independence Ave., S.W., Washington, DC 20585
(202) 287-6020; e-mail: william.joost@ee.doe.gov

Contractor: Pacific Northwest National Laboratory (PNNL)
Contract No.: DE-AC05-00OR22725 & DE-AC06-76RLO1830

The Modeling and Computational Materials Science (CMS) project is targeted at developing techniques and methods for predicting and describing the structure-property-processing relationships in lightweight materials with specific application to the automotive industry. This project currently includes one task entitled Materials Informatics for the Integrated Computational Materials Engineering (ICME) Cyberinfrastructure. The objectives, accomplishments, and future directions for this task are provided below.

Objectives

- Provide material informatics capability to the U.S. Automotive Materials Partnership (USAMP) ICME lightweight alloy workgroups. Develop a toolkit for the assessment of materials data consistency and completeness (data support) for model development and disseminate to workgroups.
- Assess the consolidation or federation of multiple heterogeneous data sources into a single contextual resource for interrogation of materials properties. Identify information weaknesses and gaps in lightweight alloy data resources as individuals and collectives.
- Develop method for knowledge augmentation in data repositories based upon multiphysics models. Perform analysis to determine whether local correlations could potentially lessen constraints imposed by incomplete data sets and system definitions.

Accomplishments

- Developed first generation informatics toolkit to identify weaknesses in data support for model development from individual data repositories. Algorithms and protocols developed and approach disseminated to Mg-lightweight alloy workgroup.
- Applied method to the lightweight alloy data in the repositories at the Mississippi State University (MSST) Center for Advanced Vehicular Systems (CAVS) and the Metals Bank (Korea); identified weaknesses in system definitions and property coverage. Reported results at 2010 August USAMP review meeting.
- Developed new approach for feature selection of data elements to facilitate data support sufficiency for multiscale models.

Future Directions

- Develop informatics tool to support data assessment and fusion across multiple repositories; apply to the MSST CAVS and Metals Bank/Korea Institute of Metals repositories. Assess potential benefits and barriers for fusing the Materials Atlas (Defense Advanced Research Projects Agency) and Canadian metals data resources with CAVS and Metals Bank resources.
- Identify information weaknesses for model development in data resources; recommend new repository data or updates to improve design capabilities. Develop contextual framework for thermodynamic properties of lightweight alloys based upon knowledge content.
- Join framework which identifies incomplete system definitions with multiphysics models for knowledge augmentation.

Introduction

The use of modeling and CMS can greatly accelerate the introduction of lightweight materials and improve properties of existing materials. Greater implementation of modeling and CMS can guide experimental work and process modifications that improve material properties and performance and make such information more available to system designers. The current and future research conducted in this project is targeted at developing and validating modeling and CMS techniques for lightweight materials. The objective of this research is to demonstrate methods for predicting and describing the structure-processing-properties relationship in lightweight materials through the length scale continuum. The following sections summarize work performed at PNNL on specific tasks in the area of materials informatics that supports the cyberinfrastructure impacting lightweight materials development for automotive applications.

Activity and Developments

Materials Informatics for the Integrated Computational Materials Engineering (ICME) Cyberinfrastructure

Principal Investigator: Kim Ferris, Pacific Northwest National Laboratory
(509) 375-3754; e-mail: Kim.Ferris@pnl.gov

Principal Investigator: Dumont Jones, Proximate Technologies, LLC
(614) 258-8835; e-mail: dumont.jones@prxt.com

Introduction

As a prerequisite for information-driven multiscale alloy design, repositories of alloy information should be evaluated to understand their suitability as platforms for informatics-based design. With this in mind, the project milestones for FY 2010 were to establish metrics for evaluating property data consistency and completeness in a repository for information-driven design and to present results to the DOE and ICME teams. Metrics and evaluation protocols for repositories were established and tested against individual repositories as reported below. The results suggest that while current repositories have design utility, they also have significant data consistency and completeness gaps, limiting a full information-based design program.

Approach

Assessment criteria can be summarized by the requirement that the repository data underlying structure-property relations be complete and well-defined. The first and most basic requirement for information-based modeling is that a system definition map to well-defined property values. Data completeness is a second, but often more flexible, requirement. Nominally, all structure-property combinations should be covered; however in practice, noteworthy and problematic gaps are often observed. The need for true completeness is reduced when property correlations can be inferred. Identifying potential property correlations is a third assessment component. Correlations help define true completeness requirements, have intrinsic value to later informatics models, and offer suggestions for repository augmentation.

Results and Discussion

We have examined the information on Mg alloys in two materials repositories: the CAVS repository associated with MSST and the publicly available portion of the Metals Bank repository, associated with the Korea Institute of Metals. The CAVS repository is in an early stage of content development and has been used thus far to explore the feasibility of a self-service model for uploading the results of materials characterization experiments. The CAVS repository is promising but not yet compliant with design work. The CAVS materials content is limited, and its current system definitions (alloy designation only) do not hold sufficient information to resolve properties in the fashion discussed below. Therefore, the following discussion will focus on the Metals Bank repository.

Data Coverage and Measurement Density

To assess the degree to which properties and systems have been covered in the Metals Bank repository, the repository was queried for the number of measurements for each possible structure-property combination, with results presented in contour-plot form. The portion of this plot with the highest measurement densities appears as Figure 1. This simple picture can be used as a way to quickly compare the content of different repositories. The strong measurement bias toward the Mg AZ alloy series (Mg-Al-zinc) and a few mechanical properties is noteworthy and will ultimately constrain information-based design.

Ambiguities in System Definition

Next, questions of system definition are considered. Here, the Metals Bank system definition is used (alloy + post-treatment + processing + shape), and the analysis database is queried for system-property combinations that show an abnormally high degree of fractional error. Key results are summarized in Figure 2.

The presence of a system-property combination in Figure 2 suggests that the system definition (or possibly the property measurement) should be refined. Figure 2 shows that tensile properties and grain size in particular are subject to high degrees of error for a fixed system definition. Because the modes of measurement are standardized for these properties, Figure 2 suggests the problem lies with the system definition itself.

Ascertaining the Contributions to System-Definition Ambiguities

Figure 3 shows the results of a principal components analysis in which the relative contributions of system-definition components toward Metals Bank property errors are assessed. Here, negative values indicate reduction in error from a particular component of the system definition. This approach appears to be a promising, if still incompletely refined, tool for system-definition assessment. Several features can be noted. First, differing system definitions can be used depending on the properties of interest. For example, grain size shows equal reduction in error from all definition components. However, thermodynamic property errors are dominated by the alloy type,

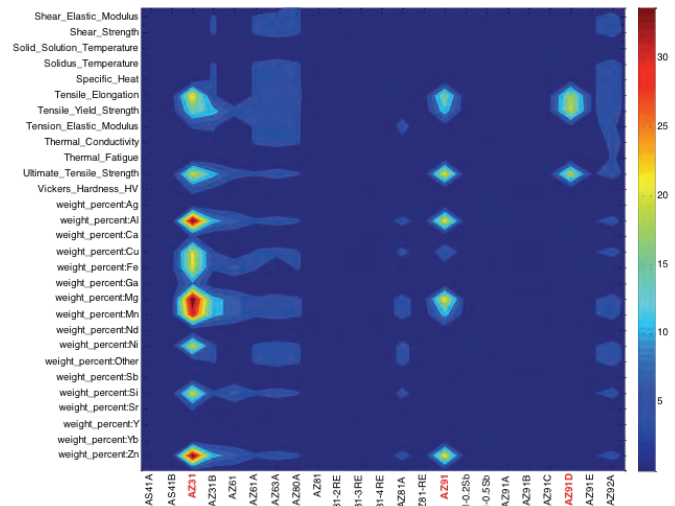


Figure 1. Measurement density per alloy system reported for Mg alloys in the Metals Bank alloy database.

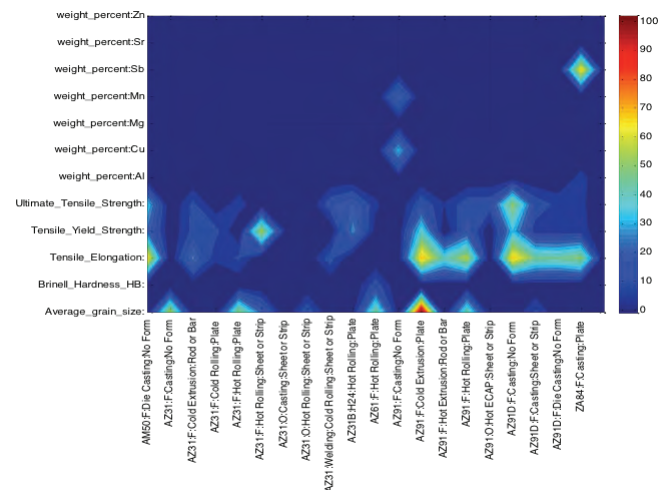


Figure 2. Significant errors ($100 \times \text{standard deviation} / \text{mean value}$) for Mg alloy system properties and properties reported in the Metals Bank alloy repository. Tensile properties and average grain size show the greatest deviations (at least 50%), suggesting that the current system definitions do not resolve these property measurements.

indicating (as expected) that the post-treatment, processing, and shape components do not reduce error significantly in these properties. Also as expected, processing is important to resolving the system definition for mechanical properties. We observe that a poorly defined system-definition component can make errors worse: qualitative definitions of processing and post-treatment actually add to the system-definition error for certain properties.

Early Stage Association Development and Hypothesis Generation

We have also begun to examine potential correlations between properties (not shown here due to space constraints) with a view toward generating design hypotheses. In many cases the amount of supporting data for potential correlations is limited; validation of hypotheses and improvement of system definition for mechanical properties can be suggested as a directed program of augmentation for alloy repositories such as the Metals Bank.

Technology Transfer

The informatics tools provide data joining and analysis technology for the specific alloy property problems of the lightweight materials group and multiple data resources like the Metals Bank and CAVS. The first generation toolkit has been deposited at CAVS and is generally available to ICME interested parties. The current developmental version of the toolkit is available at https://spteamsl.pnl.gov/sites/mat_informatics/default.aspx. The results generated at different stages of the project are shared with the workgroups and data repositories participating in this work.

Conclusions

We have examined two current alloy databases in an effort to assess their suitability as platforms for information-based design. Analysis of these data suggests that the Metals Bank repository is already useful as a design tool. However, our results also show that the system-definition metadata in the Metals Bank do not consistently resolve property values. Refined system definitions and validation of design hypotheses resulting from property correlations suggest a directed method to enhance the design value of repositories like CAVS and the Metals Bank.

Presentations/Publications/Patents

Ferris, K. F.; Jones, D. M. Towards Informatics Tools and Information Assessments for the Development of Lightweight Mg-Alloys. In Proceedings of the 2010 Materials Science and Technology Conference Tools, Models, Databases and Simulation Tools Developed and Needed to Realize the Vision of Integrated Computational Materials Engineering: ICME: Informatics and Infrastructure, Houston, Texas, October 17–21, 2010.

Ferris, K. F.; Jones, D. M. Materials Informatics Approaches for the Accelerated Development of New Materials. Invited Talk, CAVS/Mississippi State University, October 2009.

Ferris, K. F.; Jones, D. M. Assessing Data in Support of Structure-Processing-Property Relationships in Mg-Alloy Design. Presentation at the TMS 2010 Annual Meeting: Mg Technology 2010, Seattle, Washington, February 14–18, 2010.

Jones, D. M.; Ferris, K. F. Generic Materials Property Data Storage and Retrieval for Alloy Material Applications. Presentation at the TMS 2010 Annual Meeting: Mg Technology 2010, Seattle, Washington, February 14–18, 2010.

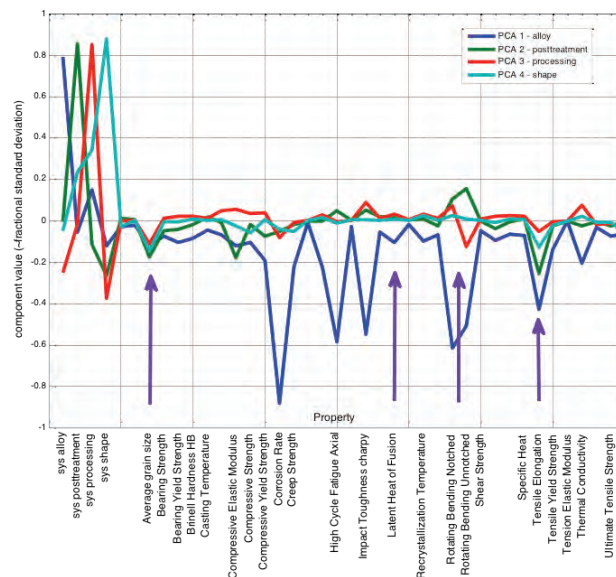


Figure 3. The impact of various elements of the system definition in the Metals Bank repository on system error.

E. Southern Regional Center For Lightweight Innovative Designs - Mississippi State University

Field Technical Monitor: Dr. Mark Horstemeyer
Carpenter Engineering Building, Room 206
Mississippi State University, MS 39762
(662) 325-7308; e-mail: mfhorst@cavs.msstate.edu

Technology Area Development Manager: William Joost
U.S. Department of Energy
1000 Independence Ave., S.W.; Washington, DC 20585
(202) 287-6020; e-mail: william.joost@ee.doe.gov

Contractor: Mississippi State University (MSST)
Contract No.: DE-FC-26-06NT42755

Objectives

The three major objectives of this project are

- to develop experimentally validated cradle-to-grave modeling and simulation tools to optimize automotive and truck components for lightweighting materials (Al, steel, and Mg) alloys and polymer based composites) with consideration of uncertainty to decrease weight and cost and yet increase the performance and safety in impact scenarios,
- to develop multiscale computational models that quantify microstructure-property relations by evaluating various length scales from the atomic through component levels for each step of the manufacturing process for vehicles, and
- to develop an integrated kindergarten through doctoral level (K–PhD) educational program to educate students on lightweighting designs and impact scenarios.

Accomplishments

- Created strong ties with companies from various sectors (e.g., automotive, software, and local manufacturers), and they have embraced the technology being developed in this program.
- Received additional cost sharing support from several companies: MSC, Alpha Star, SAC, POSCO, and Mitsubishi Motors. As a result of extensive interaction with these sponsors, we collectively increased our sponsorship funding to \$1,100,000.
- Provided a strong support role to the U.S. Automotive Materials Partnership (USAMP) Integrated Computational Material Engineering program, including establishing several focused research teams with USAMP members and developing 10 year draft roadmaps of Mg, steel, and polymers with DOE.
- Developed a physics based multiscale internal state variable (ISV) model that includes uncertainty.
 - Validated the model for Al and steel alloys and began to validate it for Mg alloys.
 - Established a number of atomistic potentials (i.e., Fe, C, Si, Al, Mg) that will be used in development of high-strength steel alloys.
 - Initiated optimization methods in conjunction with the multiscale ISV model, including ISV and process-structure-property with finite element (FE) analysis and design.

- Received recognition from The Minerals, Metals & Materials Society and USAMP for our cyberinfrastructure, which integrates our software and experimental information in a wiki.
- Correlated the multistage fatigue (MSF) model with different Mg alloy strain-life curves.
- With uncertainty under low strain rate, variable temperature, and high strain rate tension-compression-torsion tests, characterized several structural materials for lightweighting (i.e., Al, steel, and Mg alloys) throughout their manufacturing and life-cycle history.
 - Tested these materials in crash simulations and safety performance evaluations.
- Used multiscale material models to develop process-product concepts for the composites effort.
- Produced quality samples for evaluation in the natural fiber program.
- In the biomechanics program, advanced to incorporating polymeric ISV models for tissues and evaluating damage phenomena for brains subject to high rate impact using FE analyses. (The biomechanics projects were included because we wanted to include human effects as objectives in the multi-objective design of metal and composite materials.)
- Produced a number of high quality students and graduated 12 students with MS and PhD degrees. For the K–12 program, we have developed crash kits and run K–2 and 3–6 grade “Mission Eggcellence” competitions in multiple counties throughout Mississippi in an effort to inspire interest in science and engineering. All of the computational and experimental databases can be found at the MSST cyberinfrastructure at <https://ccg.hpc.msstate.edu>.

Future Directions

- Continue developing the structure-property relationships and multiscale models for Mg alloys with a focus on demonstrating the technology through the Mg front end project sponsored by DOE.
- Move forward to develop material specific multiscale models, validated by critical experiments, for the composite, biomechanics, and natural fiber research projects.
 - Use these materials in crash simulations to generate new data generated. We will then update the cyberinfrastructure to have a national and an international user base.
 - Extend the MSF model to describe joint behavior.

Introduction

The Southern Regional Center for Lightweight Innovative Designs (SRCLID) plans to reduce emissions and position the United States for less reliance on foreign oil through focusing our research and educational enterprise on lightweighting vehicles.

We develop multiscale physics-based material models that are experimentally validated and account for uncertainty variables. This entails theory development, experimental characterization, and large scale computing. Our design methodologies then guide design optimization of components, systems, and materials in engineering practice throughout the southern automotive corridor of the United States. Specifically, the development of new materials and math based tools is sought for use in development of next generation vehicles, particularly under various crash and high-speed impact environments.

SRCLID goals are threefold: (1) develop an experimentally validated cradle-to-grave modeling and simulation effort to optimize automotive and truck components for various materials (Al, high strength steel, Mg alloys, and polymer based composites) with consideration of uncertainty in order to decrease weight and cost, yet increase the performance and safety in impact scenarios; (2) implement a multiscale modeling philosophy (“from atoms to autos”) in which we quantify the microstructure-property relations by evaluating various length scales, starting at the atomic level, for each step of the

manufacturing process for vehicles; and (3) develop an integrated K-PhD educational program to educate students on lightweight designs and impact scenarios.

To accomplish these overarching goals, we have divided the project into 12 tasks. The following sections summarize the activities and developments for each of these tasks.

Activity and Developments

Multiscale Microstructure-Property Plasticity Considering Uncertainty

Principal Investigator: Kiran N. Solanki, Center for Advanced Vehicular Systems (CAVS), MSST
(662)325-5454; email: kns3@cavs.msstate.edu

Participants: D. J. Bammann, E. B. Marin, M. F. Horstemeyer, P. T. Wang, E. B. Marin, Y. Hammi, A. Oppedal, H. El Kadiri, C. Bouvard, A. Antonyraj, Q. Ma

Approach

We are developing a material database, ISV material models, and process models for extruded (AM30 and AZ61) and warm formed (AZ31) Mg alloys. We plan to

- quantify structure-property relations with consideration of uncertainty for AZ31 sheet metal,
- quantify structure-property relations with consideration of uncertainty for pre-extruded and extruded AM30 and AZ61,
- perform laboratory-scale extrusion experiments on Mg alloys AM30 and AZ61 to generate data for validation of simulation tools,
- develop crystal plasticity and ISV macroscopic models to model microstructure evolution during extrusion processes,
- construct FE models and perform analysis of stamping for Mg alloys,
- develop robust process models for laboratory-scale and industrial extrusion processes using Eulerian-ALE FE formulations, and
- develop methods which consider uncertainty for the optimum design of extrusion/stamping processes.

Results and Discussion

An elasto-viscoplastic model was extended to include damage. The coupled elasto-viscoplastic-damage model, named the DMG model, was implemented in the user material subroutine VUMAT of ABAQUS/Explicit for both three-dimensional and shell elements using a fully implicit integration scheme. The model assumes that the damage process of ductile fracture in Mg occurs mainly as a result of the void nucleation, growth, and coalescence into a microcrack (Figure 1).

The isotropic hardening part of the material constitutive law reflects the effect of the global dislocation density, and it is represented by the growth in size of the yield surface while the center remains at a fixed point in stress space. The kinematic hardening part, which models the Bauschinger effect, reflects the effect of anisotropic

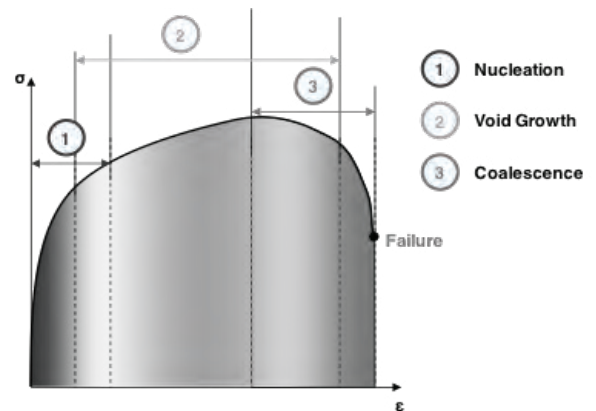


Figure 1. Sequences in a ductile fracture mechanism.

dislocation density, and it is represented by the translation of the center of the yield surface in stress space while the size remains fixed.

Extrusion Simulations

A laboratory-scale indirect extrusion fixture was designed at CAVS through an iterative procedure, achieving a final rigid design of the fixture which could withstand repeated extrusion runs. Once the fixture design was finalized, a rigorous experiment execution protocol was developed with the goal of achieving repeatability and validity in the testing results. This protocol was used to perform indirect extrusion experiments on aluminium alloy A11100 to generate data for model validation. The commercial code HyperXtrude was used to model and simulate the experiments. A good agreement between thermomechanical extrusion simulation results and experimental measurements was achieved by fully considering the real-world physics of laboratory-scale extrusion for flat dies.

Laboratory-scale extrusion experiments were also performed on Mg alloy AZ61 at 454°C with ram velocities of 5 mm/min and 10 mm/min. HyperXtrude was used to simulate the experiments. In particular, the prediction of the microstructure evolution (texture) during extrusion was obtained using streamline data from the HyperXtrude simulations (velocity gradient and time steps) and the crystal plasticity code VPSC. The VPSC simulations revealed twinning systems, slip activation, and corresponding critical resolved shear stress (CRSS) evolution during extrusion. Experimental microtextures at various locations in the partially extruded billet were measured by the electron backscatter diffraction (EBSD) technique. The computed textures from HyperXtrude and VPSC simulations match well the experimental textures observed using EBSD, as shown in Figure 2.

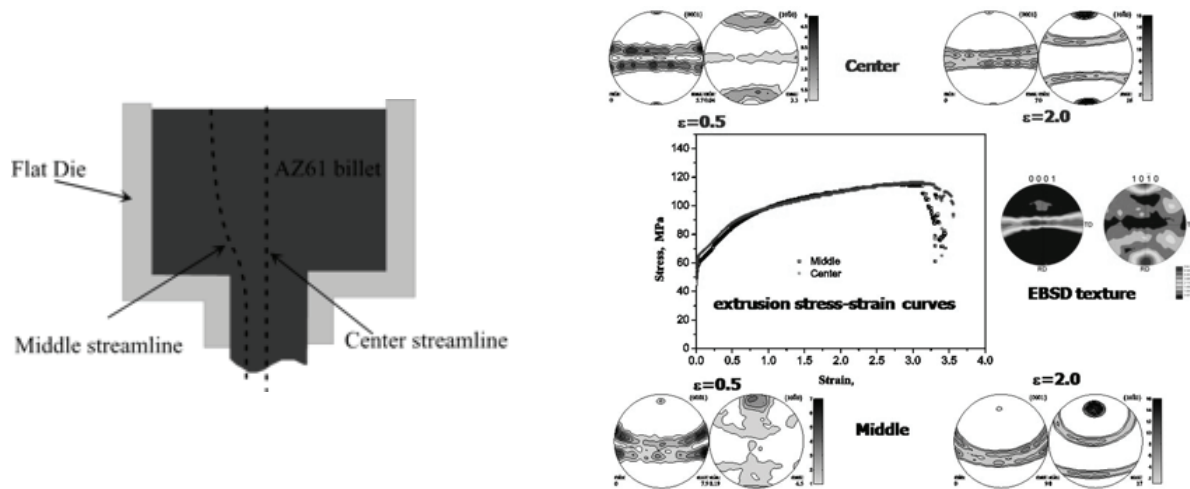


Figure 2. (a) The center and middle streamline in the flat die; (b) the extrusion stress-strain curves and the textures in the flat die based on HyperXtrude and VPSC simulations.

Sheet Forming Simulations of Mg Alloys

The simulations were performed using the FE code ABAQUS/Explicit with the DMG material model implemented into the user material subroutine VUMAT. The goal of these simulations was to compare simulation results between viscoplastic material models with and without damage. Results showed that the coupled plasticity-damage DMG model can give a better prediction of the thickness distribution and the onset of localized necking, which is a common failure mode in metal forming (Figure 3).

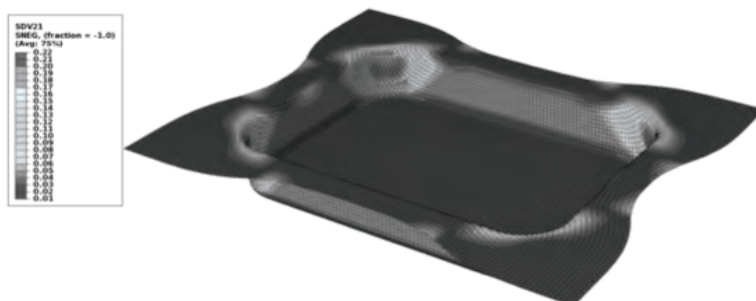


Figure 3. Damage distribution in a pan forming simulation.

Conclusions

We have established the fundamental framework of extrusion processes for Mg alloys, including laboratory-scale experiments to quantify processing–structure–property relations, extrusion modeling to validate texture evolution, and exploration of twinning mechanisms using the associated VPSC models. In addition, we have developed sheet forming numerical capabilities which include damage-induced plasticity models with uncertainty. Particular alloys studied were AZ61 and AM30 extrusions and AZ31 sheets.

Cyberinfrastructure

Principal Investigator: Tomasz Haupt, CAVS, MSST
(662)325-4524; email: haupt@cavs.msstate.edu
Co-Principal Investigators: R. Carino, F. M. Ciorba

Approach

The objective of this effort is to design and develop a cyberinfrastructure to exploit the recent transformative research in material science involving multiscale physics based predictive modeling, multiscale experiments, and design. We are proceeding with a two-stage development model: phase one was to leverage existing software and tools to bring up a working software infrastructure, and phase two was to evaluate and further develop missing or insufficient software, as needed, to support the project requirements.

The experience developing the cyberinfrastructure for SRCLID [including Mg Front End Research and Development (MFERD)/Integrated Computational Materials Engineering (ICME)] in phases I and II indicates that the user-expected functionality comprises four major components integrated through a single-access web portal, as shown in [Figure 1](#).

The components are: database of experimental data and material constants, online model calibration tools, repository of codes, and run time environment for efficient and fault tolerant execution of multiscale simulations.

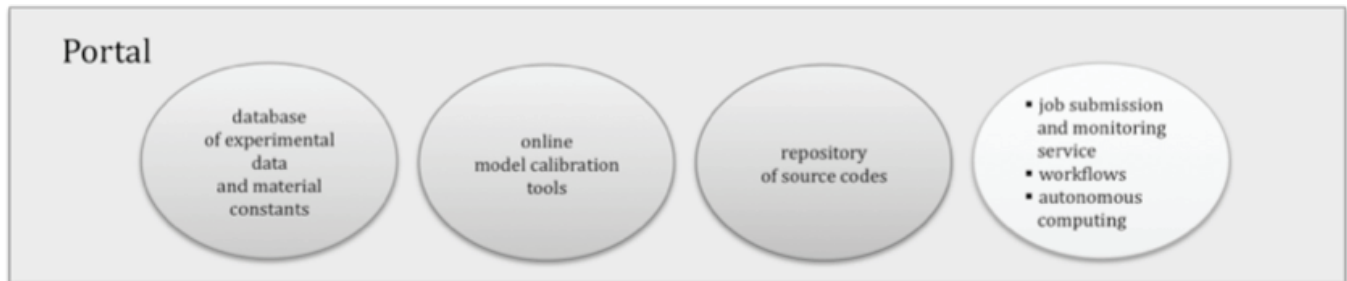


Figure 1. Cyberinfrastructure for SRCLID (<https://csg.hpc.msstate.edu>).

Results and Discussion

The Wiki

The wiki (<http://csg.hpc.msstate.edu>) became the façade for the portal. The main purpose of it is to accumulate the knowledge pertaining to ICME. In addition, it provides access to all portal components: the repository of the experimental data and material constants, the online model calibration tools, and the repository of the open source codes. In the near future it will also provide access to an autonomic run time environment for composing and executing multiscale workflows directly from the web browser. The wiki is currently populated with information, tutorials, data, and results coming from the other SRCLID tasks.

Validation and Computational Optimization of Codes

This effort aims at optimizing the computational performance of existing simulation codes on multicore computers as well as on high performance parallel computer clusters. To achieve this, a performance analysis environment (PAE) has been established and tailored to match the requirements of the simulation codes in use at CAVS/MSST. PAE is based on open-

source performance profiling and tracing tools such as Tuning and Analysis Utilities (TAU), (Performance Application Programming Interface (PAPI), Eclipse, Jumpshot, and Scalable performance Analysis of Large Scale parallel Applications (SCALASCA). A first success of this effort is the optimization of a microstructure mapping code with an improvement factor of 100x (Carino, 2009) and the parallelization of microMegas (Ciorba, 2010).

Conclusions

We continue to focus on the development of the wiki in which the material database and multiscale models of lightweight metals, polymers, and steel will be included.

Fatigue of Lightweight Automotive Material

Principal Investigator: Mark F. Horstemeyer, CAVS, MSST

(662)325-7308; e-mail: mfhorst@cavs.msstate.edu

Co-Principal Investigator: J. B. Jordon

Approach

The primary factor controlling fatigue life in lightweight metals is the incubation and growth of a microstructurally small crack, which is profoundly influenced by the material's microstructural features, such as void or intermetallic inclusions, grain size, orientation or dendrite size, second arm spacing, etc. This work was decomposed into the following main tasks: fatigue testing and characterization, simulations of fatigue crack initiation and growth, fatigue life model development and predictions, modeling calibration and validation, and transfer of the experimental data and fatigue models (industrial partners for this task are General Motors and Ford).

Results and Discussion

Effect of Twinning, Slip, and Inclusions on the Fatigue Anisotropy of Extrusion-Textured Mg AZ61 Alloy

Using an MSF model, experiments were conducted with extruded Mg AZ61 alloy to quantify structure-property relations with respect to fatigue. These experiments were conducted in the extruded direction (ED) and extruded transverse direction (ETD) under low and high cycle strain control fatigue conditions.

Structure-property relations were quantified by examining the fracture surfaces of the fatigued specimens using a scanning electron microscope. In terms of crack incubation, fatigue cracks were found to initiate from intermetallic particles (inclusions) that were typically larger than the mean size. Quantified sources of fatigue crack incubation, microstructurally small cracks, and cyclic stress-strain behavior were correlated to the MSF model. Based on the specific material parameters, the MSF model was able to predict the difference in the strain-life results of the Mg AZ61 alloy in the ED and ETD, including the scatter of the experimental results. Finally, the MSF revealed that the inclusion size was more important in determining the fatigue life than the anisotropic effects from the texture, yield, and work hardening.

Figure 1 shows the correlations of the MSF model to experimental data for both ED and ETD.

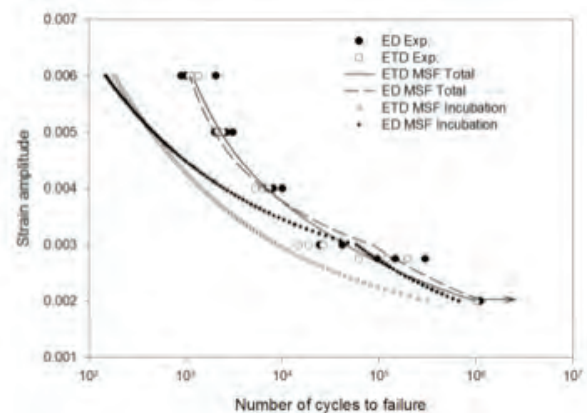


Figure 1. A comparison of the multistage fatigue (MSF) model of total and incubation life with experimental data for extruded AZ61 Mg alloy in both the extruded direction (ED) and the extruded transverse direction (ETD).

For validation purposes, components were made by cutting through the cross section of the extruded Ford rail. These components were 25.4 mm wide and were the same Mg AZ61 alloy presented earlier. These components were tested under fully reversed displacement control at a frequency of 3 Hz. A total of four components were tested at two different displacement amplitudes: 2 mm and 3 mm. The specimens tested at 2 mm were switched from displacement control mode to load control mode at 10,000 cycles and continued until failure at 30 Hz.

Three-dimensional FE simulations were performed (Figure 2a) with the ISV plasticity/damage constitutive model and a mesh refinement study was used to determine the appropriate element size. The maximum principal strain amplitude from the FE results was used as equivalent uniaxial strain amplitude for the input to the MSF model. Figure 2b shows the comparison of the component fatigue specimens to the MSF prediction. The MSF showed good correlation to the fatigue life at the lower amplitude but showed a more conservative prediction for the higher amplitude.

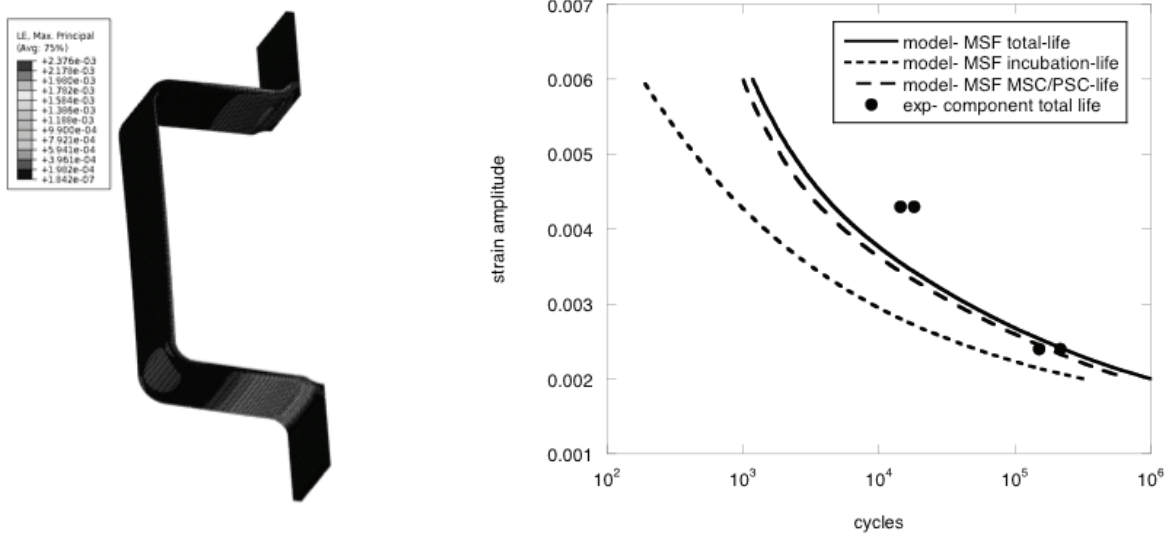


Figure 2. Results of three-dimensional FE simulations: (a) maximum principal strain contour plot of the FE analysis of the Mg AZ61 components; (b) comparison of the multistage fatigue (MSF) model to the experimental fatigue results of the AZ61 component test.

Microstructure and Damage Evolution during Tensile Loading in a Wrought Mg Alloy

The damage evolution in a wrought Mg alloy under uniaxial tensile deformation was investigated. Sectioned specimens subjected to interrupted tensile deformation were examined under optical microscopy to quantify the number density of cracked intermetallic particles as a function of applied strain. Digital image analysis of the optical images was used to quantify damage by separating cracked from noncracked particles. Finally, an ISV damage model was shown to adequately capture the experimentally observed damage progression due to the intermetallics.

Figure 3 shows the number of cracked particles per volume versus applied tensile strain. Damage in this type of alloy is due mainly to slip and twinning occurring in the matrix Mg adjacent to the particles. However, Figure 3 shows a strong correlation between progression of cracking particles and damage. The damage nucleation model predicted results that are in good agreement with the observed damage progression of the AZ61 Mg alloy.

Conclusions

Three extruded Mg alloys, AM30, AZ31, and AZ61, and a cast AZ91 alloy provided by our automotive partners have been investigated. Experiments and simulations were conducted to quantify structure-property relations with the intent to develop a microstructure-sensitive fatigue model for Mg alloys. For extruded Mg alloys, an in-depth experimental study was conducted to calibrate a physics based MSF model to Mg AZ61 alloy. For additional modeling purposes, monotonic damage in Mg AZ61 was characterized and modeled. Experiments were also conducted on cast AZ91 to quantify sources of fatigue initiation. Regarding fatigue modeling for joints, a FE analysis study was conducted on friction stir spot welds to determine the stress state and the stress intensity factors.

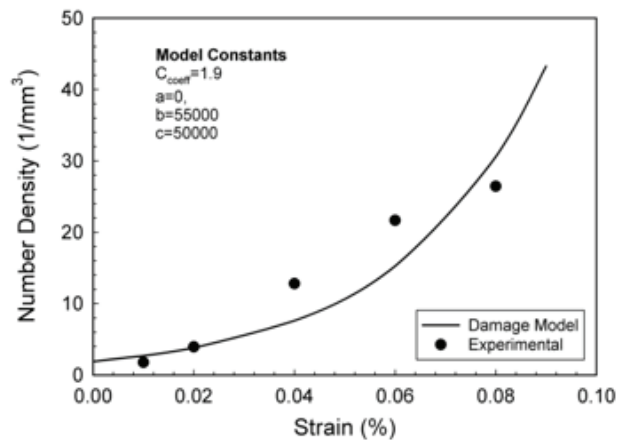


Figure 3. Number density versus strain of an AZ61 Mg alloy showing a comparison of the Horstemeyer-Gokhale (1999) void nucleation model with experimental data.

Corrosion of Magnesium Alloy

Principal Investigator: Mark F. Horstemeyer, CAVS, MSST
(662)325-7308; email: mfhorst@cavs.msstate.edu
Participants: H. Martin, C. Walton, J. Danzy, A. Hicks

Approach

The goal of this research is to study various Mg alloys in as-cast or extruded form in order to develop a model that accurately describes pit nucleation, pit growth, and pit coalescence. Ultimately, the data gathered will be used to calibrate an ISV model that will be used to predict the corrosion of Mg alloys.

Results and Discussion

Comparing Immersion and Salt Spray Environments

Figures 1(a) and 1(b) show the average weight and thickness loss, respectively, over the five exposure times for the immersion and salt spray surfaces on the various Mg alloys being compared. As one can see, all surfaces follow similar logarithmic trends for weight loss [Figure 1(a)] and thickness loss [Figure 1(b)]. However, the samples exposed to the salt spray environment gained weight, while all samples exposed to the immersion environment lost weight [Figure 1(a)]. The samples exposed to the salt spray environment also lost the most thickness for each Mg alloy as compared to the immersion environment [Figure 1(b)].

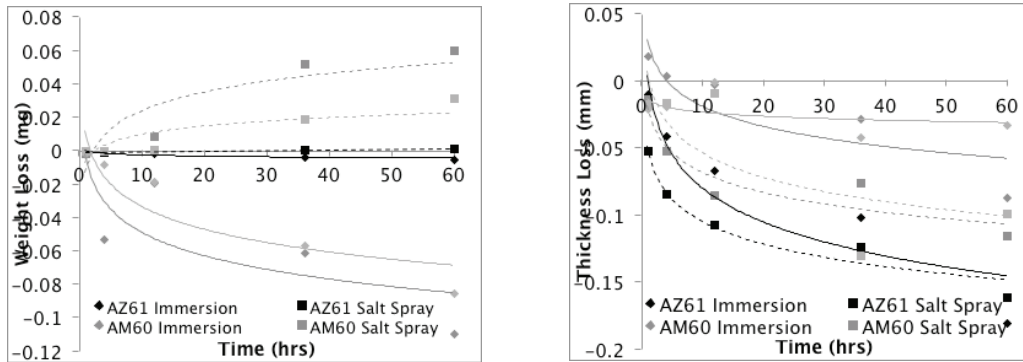


Figure 1. (a) Average weight loss and (b) average thickness loss of the various Mg coupons based on testing environment as a function of time. Notice that all surfaces followed logarithmic trends.

Figure 2a shows the pit number density over the five exposure times for the immersion and salt spray surfaces on the various Mg alloys being compared. As can be seen, all surfaces followed second-order polynomial trends. The AZ61 surfaces showed the highest amount of pit formation compared to the other surfaces, while the as-cast AM60 surfaces showed the lowest amount of pit formation. In addition, all immersion surfaces had higher pit number densities compared to the respective salt spray surfaces. Figure 2b shows the changes in the pit area, which is the two-dimensional area covered by the pits as seen by micrographs for the immersion and salt spray surfaces on the various Mg alloys being compared.

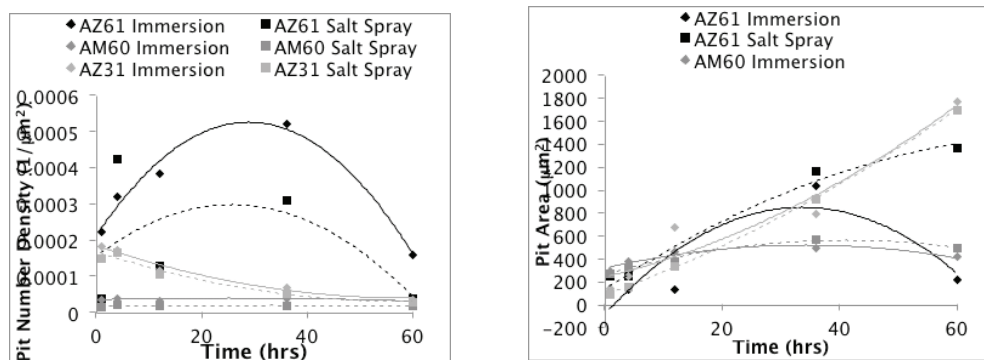


Figure 2. Average pit number density (a) and surface area (b) of the various Mg coupons based on testing environment as a function of time.

Figure 3a shows the changes in the nearest neighbor distance, which is the distance between two pits, for the immersion and salt spray surfaces on the various Mg alloys being compared. As with the pit number density and the pit area, the surfaces followed second-order polynomial trends, although in reverse of the pit number density and pit area. The extruded AZ61 surfaces showed the smallest nearest neighbor distance while the as-cast AM60 surfaces showed the largest nearest neighbor distance. Figure 3b shows the intergranular corrosion area fraction (ICAF), which is the fraction of the surface that shows the corrosion that occurs in the β -phase precipitate phase of the alloy, for the immersion and salt spray surfaces on the various Mg alloys being compared.

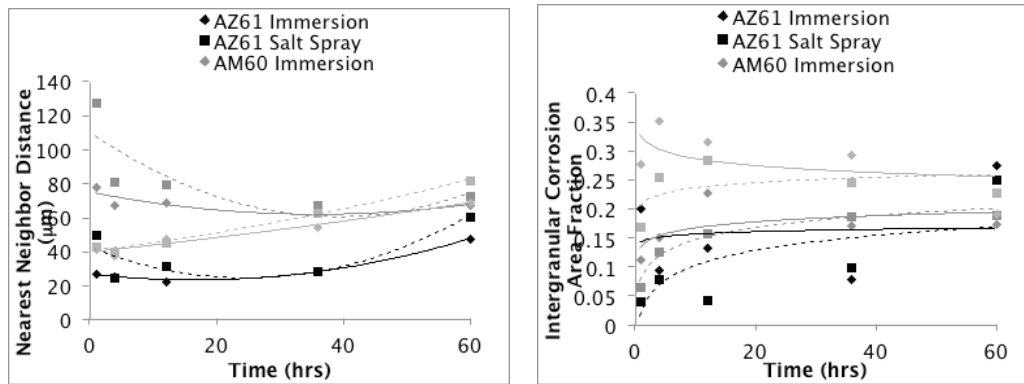


Figure 3. Average nearest neighbor distance (a) and intergranular corrosion area fraction (b) of the various Mg coupons based on testing environment as a function of time.

Conclusions

Three Mg alloys in two forms, as-cast AM60, extruded AZ61, and extruded AZ31, were examined in two corrosive environments, immersion and salt spray. General corrosion characteristics, weight loss and thickness loss, surface characteristics, pit number density, pit area, nearest neighbor distance, and ICAF were quantified over 60 hours. The most heavily corroded Mg alloy, determined by combining general and pitting corrosion, was AZ61, followed by AZ31 and then AM60. When comparing environments, more pits formed on all surfaces exposed to the immersion environment, while the pits were larger for the salt spray environments.

High Rate Damage and Fracture, Experimentation, Simulation and Visualization

Principal Investigator: Philip Gullett, Civil & Environmental Engineering, MSST

(662)325-5486; email: pmgullett@enr.msstate.edu

Participants: M. F. Horstemeyer, T. N. Williams, W. R. Whittington, S. Simunovic (Oak Ridge National Laboratory)

Approach

The aim is an enhanced multiscale microstructure-property model that can be implemented into commercial codes and that can be used in high-fidelity crash simulations for the design and optimization of structural Mg components. We plan to characterize material behavior using split Hopkinson bar experiments in compression and develop damage evolution based fracture criteria.

Results and Discussion

Strain Rate Response of Cast Mg Components

The strain rate sensitivity of cast AZ91 Mg automotive control arms produced using four different casting processes was examined. The casting processes included squeeze casting and low pressure permanent mold (LPPM) casting and the ablation and T-Mag processes. The compressive stress-strain behavior of specimens was evaluated at quasi-static and high strain rates. All of the specimens were tested to fracture. The specimens were obtained from as-received control arms and extracted from the region indicated by Figure 1.

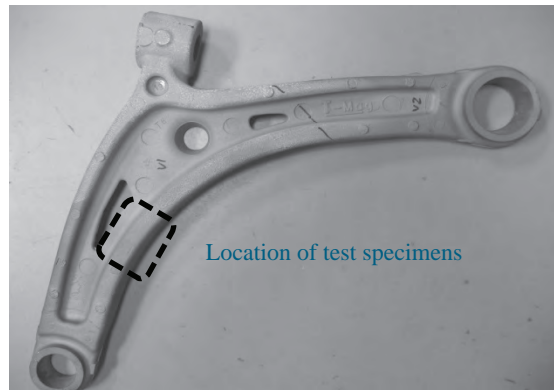


Figure 1. Cast Mg automotive control arm. Control arms were cast from AZ91 and AM60B alloys. Specimens taken from the rib section indicated by the dashed line were tested under high rate loading conditions.

Figure 2 shows the results at strain rates of 1,000/s–3,000/s. At these strain rates the observed yield strengths varied from 90 to 110 MPa, with the T-Mag process having the lowest yield strength and squeeze casting the highest. As strain rates increased (Figure 2) all processes exhibited an increase in yield and ultimate strength with an increase in strain rate. The T-Mag in the T-6 condition exhibited the highest yield strength in all cases yet appeared to soften much sooner than all the other cases as compared to their respective strain rates. The squeeze cast control arm had the second highest yield strength in all cases and had the highest ultimate strength at 3,000/s strain rate. The yield strength of all castings at high strain rates varied between 150 MPa and 300 MPa while the ultimate strength narrowed the gap to between 365 MPa and 410 MPa.

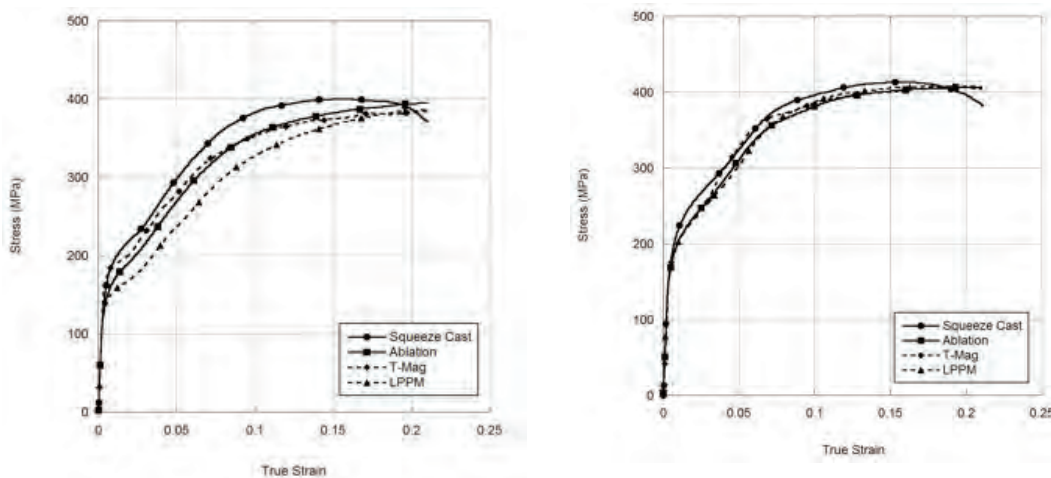


Figure 2. The compressive response of AZ91 specimens produced using four different casting processes were tested using the split Hopkinson pressure bar. The compressive response is shown for strain rates of 1,000/s (a) and 3,000/s (b).

Macroscale Fracture and Modeling

While there are many methods used to predict fracture, very few tie measurable material parameters to the physical processes that control ductile crack growth. The approach taken here uses an FE framework (Rashid, 1997, 1998) capable of incorporating material-specific ductile fracture mechanisms into the failure model and that is independent of mesh topology.

Damage nucleation and evolution is predicted using the MSST Microstructure-Property Model. The model incorporates nonlinear isotropic and kinematic hardening, temperature, damage, and rate dependence of the material. Because the material model incorporates damage, the crack advance should take into account the damage present. In the current effort, damage was used to define a crack advancement criterion and normal opening force for crack advance direction. The formulation was tested using a Mode-I fracture simulation (Figure 3). The results show that the predicted crack path matches the theoretical (straight ahead), while the J2 based damage evolved perpendicular to the crack path before crack growth.

Conclusions

This report summarizes the state of experimental and numerical simulation of failure mechanisms in structural Mg alloys. The aim is an enhanced multiscale microstructure-property model that can be implemented into commercial codes and that can be used in high-fidelity crash simulations for the design and optimization of structural Mg components.

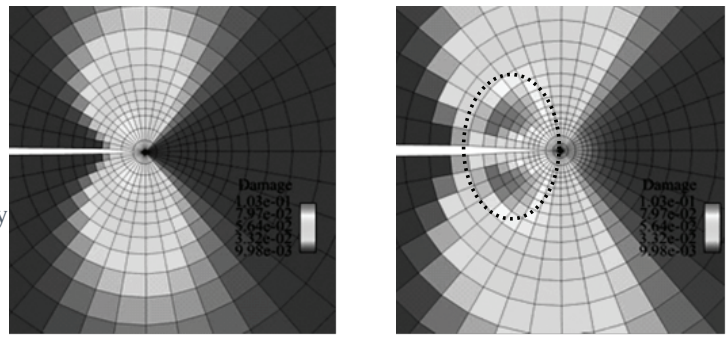


Figure 3. Mode-I fracture simulation: (a) Mode-I damage field before crack advance (the light area in this image is the region of increasing J_2 damage); (b) Mode-I damage field after crack advance (the dark area in the dashed line is the region of highest J_2 damage evolution).

Materials Design for Steel Alloys

Principal Investigator: Seong-Gon Kim, Physics & Astronomy, MSST

(662) 325-8031; email: kimsg@hpc.msstate.edu

Co-Principal Investigators: M. F. Horstemeyer, H. Rhee, S. Kim

Approach

We propose to perform compositional design of steel alloys with a better understanding of the quantum-mechanical and atomistic structure of various constituent composite crystal structures and their interactions, the influence of alloying additions, and the effects of thermomechanical treatments on wrought materials during and after processing. We use a hierarchical multiscale methodology to investigate the effect of nanoscale precipitates and additives on the overall strength and ductility in steel alloys designed for automotive applications.

Results and Discussion

MEAM Potentials for Fe-C Alloys

We developed a new modified embedded atom method (MEAM) potential for iron-carbon (Fe-C) alloys using the multi-objective optimization procedure based on the MEAM potentials for pure Fe and C. Figure 1 shows the cohesive energy of Fe-C alloy systems in the B1 and L12 crystal structures as a function of the nearest neighbor distance. Our results show that the MEAM potential for the Fe-C alloy system reproduces discrete Fourier transform (DFT) calculations reasonably accurately for these two structures over a wide range of nearest neighbor distances.

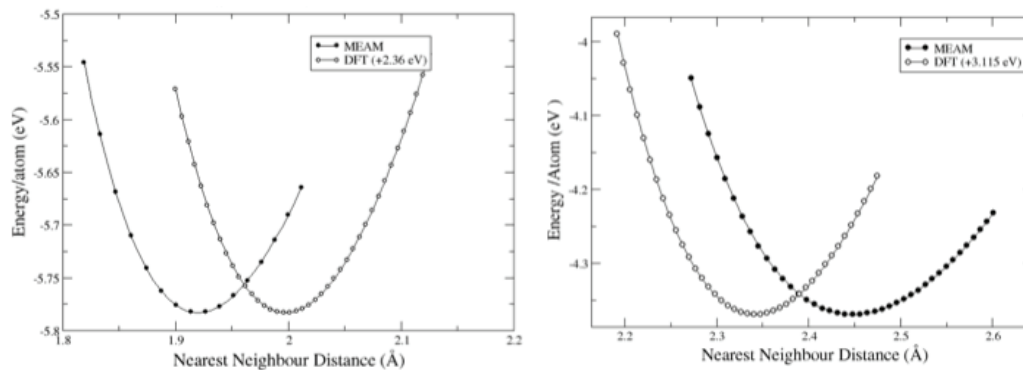


Figure 1. The cohesive energy of an Fe-C alloy system as a function of the nearest neighbor distance: (a) Fe-C in B1 crystal structure and (b) Fe-C in L12 crystal structure. The results by MEAM potential (filled circles) are compared with those of the DFT calculations (open circles).

We found that the new Fe-C MEAM potential demonstrates excellent agreement with DFT calculations for many important physical quantities.

MEAM Potentials for Fe-V Alloys

We developed a new MEAM potential for Fe-Vanadium alloys using the multi-objective optimization procedure (Kim et al., 2009) based on the MEAM potentials for pure Fe and V (Baskes, 2009). Molecular dynamics (MD) simulations were performed to observe the materials properties of Fe with increasing amounts of Vanadium (V) substitution. V atoms were substituted randomly in the bcc Fe matrix. Figure 2 shows the performance of the developed potential. Energy versus lattice parameter curves are in good agreement with the DFT calculated results. Also the variation of lattice parameter with increasing amounts of V substitution has better agreement with experiment compared to the previous potential, as shown in Figure 2(c).

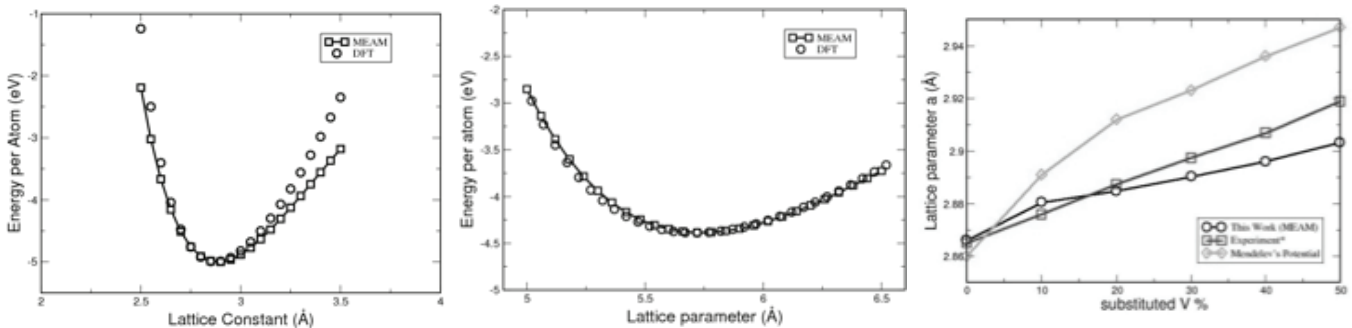


Figure 2. Energy versus lattice parameter for (a) Fe-V and (b) Fe-15 V. Figure 2(c) shows variation of the lattice parameter with increasing percentage of V substitution.

The Effect of V on the Grain Boundaries in Ferrite

V is one of the most important micro-alloying elements for steels. We used DFT to study the effect of V atoms in ferrite. Because grain boundaries are commonly present in the ferrite phase of most (AHSS) alloys, we investigated the effect of V atoms on the strength of grain boundaries in ferrite. We obtained the optimized grain boundary structure of Fe bcc $\Sigma 3$ (111) $[1(-1)0]$ shown in Figure 3.

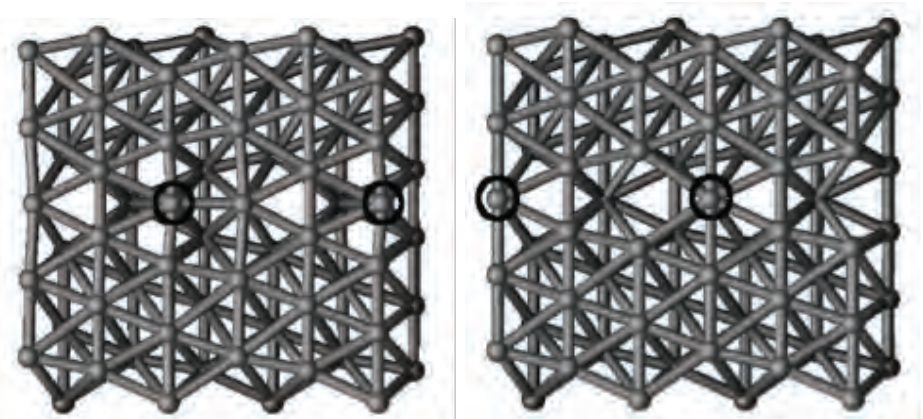


Figure 3. The optimized structure of V defects in Fe bcc grain boundaries showing (a) interstitial and (b) substitutional defects. V atoms are circled to distinguish them from Fe atoms.

We focus on the substitutional segregation on the grain boundary in this project. The V segregation energy in the grain boundary is the difference of the grain boundary formation energy from V defect formation energy in bulk. The substitutional defect formation energies are again lower than interstitial ones by 4.70 eV. From the calculated energies we can conclude that V atoms exist mostly as substitutional defects in bulk and segregate into substitutional defects in grain boundaries. The grain boundary cohesion energy (GBCE) without V is calculated as 1.43 eV while the GBCE with segregated V is 1.54 eV. The V

segregation increases GBCE by 0.11 eV. Therefore, from our DFT calculation results we can conclude that the segregated V atoms in the grain boundary significantly strengthen the grain boundary against brittle grain boundary fracture.

Experimental Results

Thermomechanical treatments were performed to investigate effects of modified structures on the mechanical behavior of dual phase (DP) steels. For a bake-hardening heat treatment, flat dog-bone-shaped tensile specimens machined from steel sheets were deformed by an Instron machine at different prestrainings of 0 (as-received condition), 1%, 2%, and 5% and then heat treated at 170°C for 20 min. After finishing the heat treatment, the specimens were cooled down to room temperature in air. By using these specimens, high strain rate Hopkinson tensile tests were carried out at similar strain rates (~550/s). Figure 4 shows stress versus strain curves obtained from high strain rate tensile tests on the as-received and baked specimens, which underwent different prestrainings.

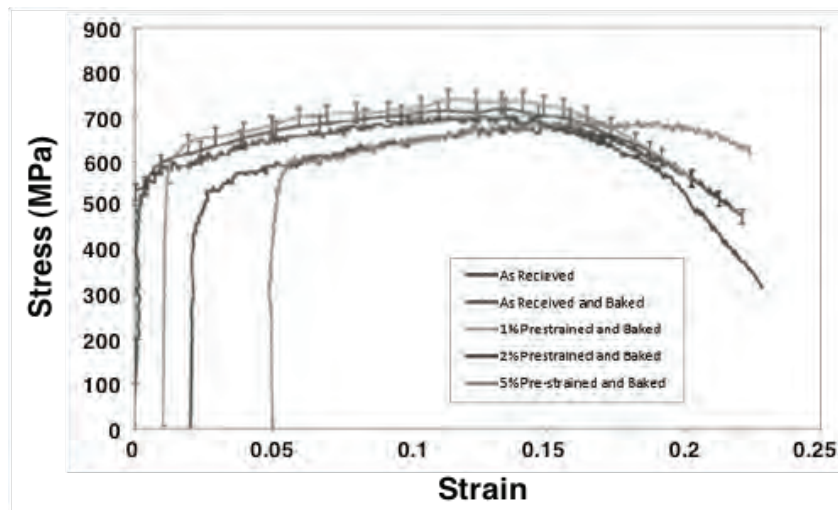


Figure 4. Stress versus strain curves obtained from high strain rate Hopkinson bar tests in tension on the as-received and baked specimens, which underwent different prestrainings.

Conclusions

We developed new MEAM potentials for Fe-C and Fe-V alloy systems and tested their validity against experimental measurements and quantum mechanical first-principles calculations. Quantum mechanical first principles simulations based on DFT were performed on the main phases of AHSSs to investigate the microalloying effect of V on the grain boundaries in ferrite. We obtained the structure of V defects in one of the most common grain boundaries in ferrite and their formation energies. We performed thermomechanical treatments on DP steels to investigate effects of modified structures on their mechanical behavior. Our results show that yield strength, flow stress level, and maximum tensile strength strongly depend on the prestrained and heat treated conditions.

Simulation-Based Design Optimization

Principal Investigator: Masoud Rais-Rohani, Aerospace Engineering, MSST
(662)325-7294; email: masoud@ae.msstate.edu

Participants: K. Motoyama, A. Najafi, M. Rouhi, C. Tamasco, A. Parrish, M. Kiani, A. Yildiz

Approach

We plan to investigate computational techniques for modeling mechanical properties of welded joints, perform sheet-forming process simulation and optimization using ISV based material models, conduct multi-objective design optimization using full-vehicle response simulations with ISV based material models, investigate computational techniques for modeling interphase properties in nano-enhanced polymer composites, and perform multi-objective design optimization of a vehicle model with composite structural components.

Results and Discussion

Welding Simulation and Validation

With a focus on the shielded metal arc welding (SMAW) process, FE analyses were conducted using Simufact.welding software. Before using Simufact.welding in design optimization framework, a series of welding tests was performed to compare simulation predictions with measured responses. Two different test components were considered (). The first test piece consisted of two rectangular plates that were welded together to form a simple lap joint whereas the second test piece was a multipart automotive component with complex welded joints.

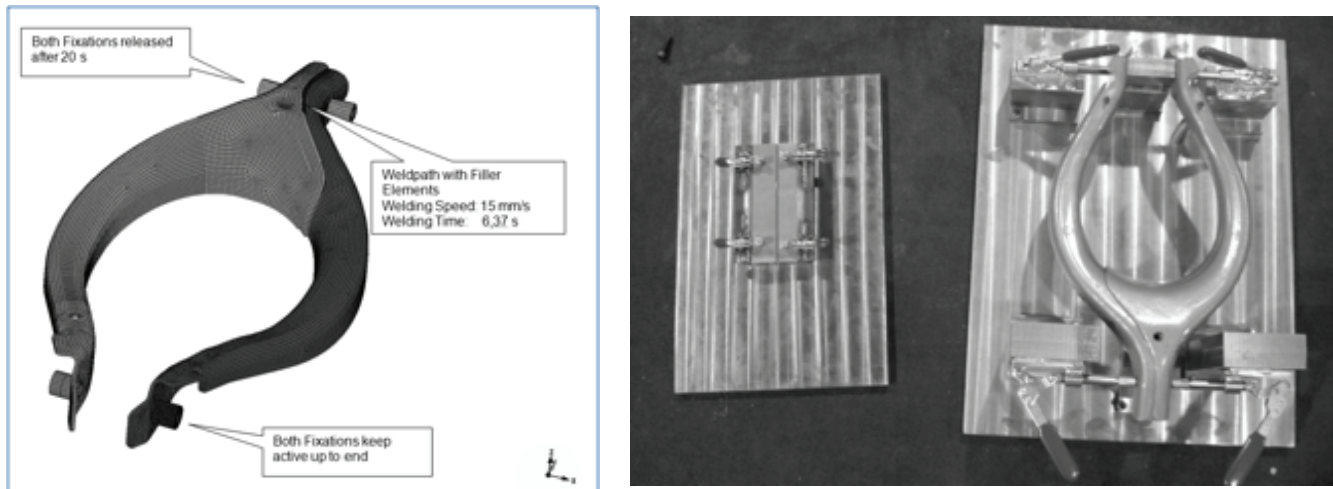


Figure 1. Comparison of (a) welding simulation model and (b) two welded test pieces.

Preliminary findings indicate that the simulation predictions are in reasonably good agreement with the experimental observations, and work is under way to perform sensitivity analysis focused on process parameters and process-product optimization tied to welding simulation.

Full-Vehicle Response Simulation and Approximation

A 1996 Dodge Neon model is being used as a test bed for performing full-vehicle crash simulations and multi-objective design optimization of vehicle structures. The three specific objectives pursued this year included (1) substitution of Mg AZ31 alloy for steel in specific crash components, (2) response approximation using advanced metamodeling techniques, and (3) application of ISV based material models.

We used the MAT-124 material card in LS-DYNA for modeling all AZ31 sheet parts (shell elements). MAT-124 allows for separate stress-strain relationships in tension and compression for Mg. AZ31 tension properties were determined from experimental data. To capture the compression behavior, we multiplied the tension data by the ratio of compression to tension of AM30 cast Mg.

With the goal of performing multi-objective optimization involving both crash and stiffness properties of the structural model, we selected 22 separate components with significant influence on the rigidity and/or crash energy absorption of the vehicle in both frontal and side impacts. To maintain roughly the same level of energy absorption and toughness as the baseline (steel) model, the thickness of each Mg component was modified. For the Mg model, we examined both 19% and 38% plastic strain values as the point of failure. The collapsed shapes of the vehicle model at 84 ms after full frontal impact (FFI) for the three cases considered are shown in Figure 2. The crash pulse at the midpoint of the B-pillar is compared for the three cases in Figure 3. The Mg models show a reduction of about 24% in the peak acceleration. However, the result shows a significant increase in intrusion distance at two different locations when steel components are switched to Mg.

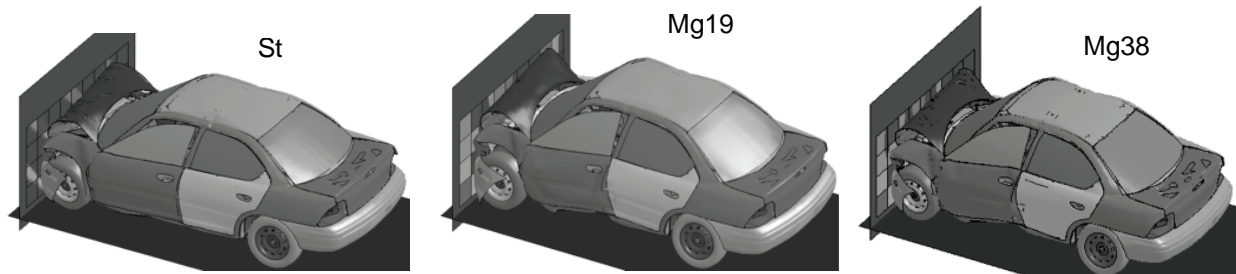


Figure 2. Crash modes in FFI with (a) steel structural components and Mg structural components with two fracture criteria: (b) 19% (Mg19) and (c) 38% (Mg38) plastic strain to failure.

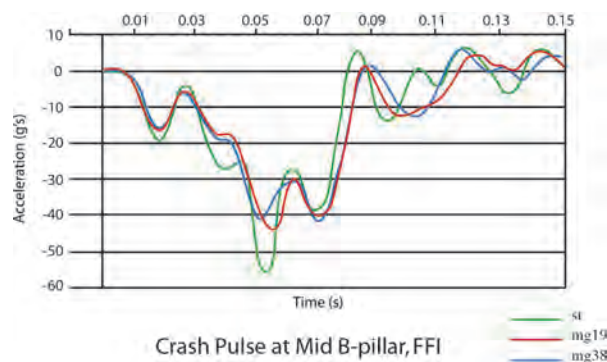


Figure 3. Comparison of the crash pulse at the midpoint of the B-pillar in the baseline and modified Neon models (the three cases shown in Figure 2).

Metamodeling techniques were used to approximate crash responses in lieu of direct coupling of noisy and computationally expensive crash simulations with design optimization. Optimization requires numerous function calls and metamodels are a more cost efficient way of obtaining a crash response at a design point of interest. Eight responses are currently being approximated using metamodels, with stiffness responses soon to be added. The eight current responses come from three impact scenarios: FFI, offset frontal impact (OFI), and side impact (SI). FFI and OFI responses are intrusion distances at the toeboard and dashboard on the driver side of the car as well as acceleration on the B-pillar at the approximate height of the driver's head. SI responses are the acceleration on the B-pillar as with FFI and OFI and the intrusion distance of the driver side door (driver side impact). These responses were chosen to approximate effects on the driver in the absence of a dummy in the current Dodge Neon model. Stiffness responses will be added to include vehicle stiffness as a constraint on the optimization problem to minimize mass.

Five metamodels were developed and tuned for each of the eight responses. These five were then used to construct an ensemble of metamodels and the most accurate metamodel is chosen for each response individually. The metamodels considered were polynomial response surface, Gaussian process, radial basis function (RBF), kriging (KR), and support vector regression (SVR). RBF, KR, and SVR have tuning parameters that can be modified when the model is constructed. These three models are tuned for each response and the most accurate combination of parameters is selected for each individual response. An ensemble of metamodels was created using all five stand-alone metamodels including the tuned results of RBF, KR, and SVR. The ensemble method assigns a weighting factor to each metamodel and the response is determined by the sum of the metamodels times their weighting factors.

Conclusions

Good progress has been made in multiple areas including forming process simulation and optimization, welding simulation and validation, full-vehicle response (i.e., crash and stiffness) analysis and approximation, and interphase modeling of nano-enhanced polymer materials. There are some remaining challenges that need to be addressed to achieve the stated objectives for this phase of the SRCLID project.

A Modified LENS® Process for Controlled Net Shaping-Induced Local Microstructure and Properties

Principal Investigator: Sergio Felicelli, Mechanical Engineering, MSST
 (662)325-1201; email: felicelli@me.msstate.edu
 Co-Principal Investigator: L. Wang

Approach

In this work, a solidification model is developed to simulate dendritic growth under convection. The cellular automaton (CA) technique for interface tracking is coupled with a transport model—the lattice Boltzmann (LB) method—for calculating heat and solute transfer by both convection and diffusion during solidification.

Our approach will proceed in the following two main subtasks: (1) model the solidification phenomena occurring in the molten pool during the LENS process to predict the microstructure of the deposited material, including the formation of dendrites, grains, and pores, and (2) develop an in-house capability to build parts with the LENS machine at MSST.

Results and Discussion

Currently, the LB method has been adopted to numerically calculate fluid flow, solute transport, and heat transfer. The governing equations and boundary conditions for transport phenomena and fluid flow can also be found in the literature.

The energy and solute transport simulated by the LB method was validated by comparing the simulation results of temperature and composition distribution to analytical solutions. Also, the LB-CA model was validated by modeling the free growth of a single dendrite and comparing the tip velocity and equilibrium liquid composition to those obtained by the analytical Lipton-Glickson-Kurz (LGK) model with various undercoolings. Figure 1 shows the tip growth velocity and equilibrium concentration of the steady-state growth of an Al-3 wt % Cu dendrite as a function of undercooling. As observed, a good agreement is obtained between LB-CA and the values calculated by the LGK theory and those obtained by an FE-CA model previously developed by the authors.

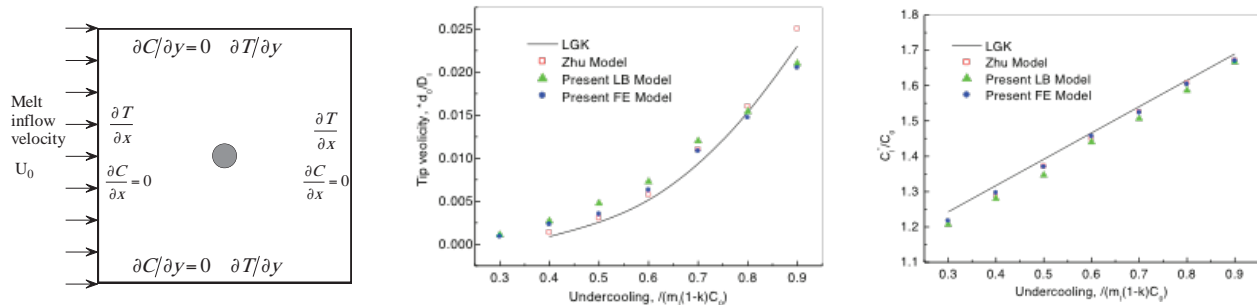


Figure 1. Tip growth velocity and equilibrium concentration for the growth of an Al-Cu dendrite: (a) schematic of dendrite growth model and boundary conditions (changed to achieve different undercoolings); comparison between numerical simulations and LGK model predictions of the steady-state (b) tip velocity and (c) tip equilibrium liquid composition for Al-3.0 wt % Cu alloy.

Simulation Results

All the performed simulations of dendrite growth were done for a binary Al-3 wt % Cu alloy. In the example of Figure 1, a single nucleus with 0-degree preferential direction was placed at the center of a calculation domain of 90 by 90 μm discretized with a 300 by 300 grid.

Three cases were studied for different boundary condition: case 1—constant undercooling and no convection, case 2—constant temperature gradient (400 K/m) imposed on the four sides. Figures 2(a)–2(c) show the single dendrite morphologies and composition fields for simulation cases 1–3 by the LB-CA model. The dendrite morphologies shown in Figures 2(a) and 2(b) demonstrate that the cooling rate due to the heat extraction from the boundaries enhances the side branching and thus the formation of secondary arms. The dendrite morphologies shown in Figures 2(a) and 2(c) demonstrate that the growth of dendrite arms is enhanced in the upstream side. As the dendrite grows, solute rejected to the liquid ahead of the solid liquid interface is washed away by the upstream fluid flow, which leads to an asymmetrical solute distribution and dendrite morphology.

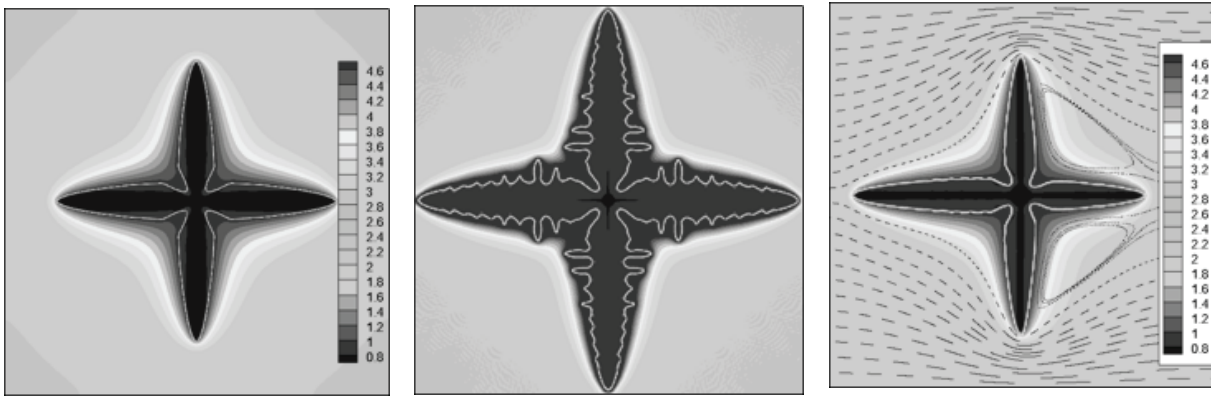


Figure 2. Dendrite morphology and solute map with various boundary conditions: (a) solute diffusion only, (b) constant heat flux at boundaries, (c) constant inflow velocity at left side, and (d) inflow velocity and constant heat flux at boundaries.

A multiple dendrite case is considered in the next example. Figure 3 presents the simulated evolution of equiaxed multidendrite growth. The domain is assumed to have uniform initial and random preferred growth orientations ranging from 0 to 90 degrees with respect to the horizontal direction were randomly distributed in the calculation domain.

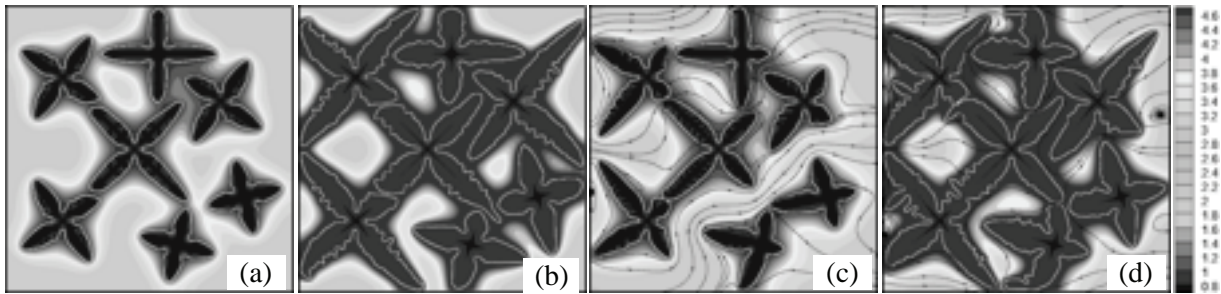


Figure 3. Equiaxed growth of multiple dendrites of Al-3.0 wt % Cu alloy solidified with (a) solute transport only, (b) a constant heat flux at boundaries, (c) constant inflow velocity at left side, and (d) inflow velocity and constant heat flux at boundaries.

Figure 3(a) shows the simulated dendrite morphologies considering only solute transport. It is observed that the dendrites develop the main primary arms along their crystallographic orientations but without secondary arms. The growth of some primary arms is suppressed by nearby dendrites. A cooling rate due to heat flux imposed at the boundaries enhances the side branching as shown in Figure 3(b). Figure 3(c) is similar to the simulation of Figure 3(a) but with convection added, due to an imposed inflow on the left boundary. Compared to Figure 3(a), the primary dendrite arms shown in Figure 3(c) are coarser and longer in the upstream direction than those in the downstream direction. Finally, Figure 3(d) shows the simulated dendrite morphologies when both solute and heat transfer with convection are included in the model. The melt flow washes away the interdendritic composition and enhances the dendrite growth and the merging between dendrites. The figures demonstrate that convection promotes the removal of solute from the solid liquid interface in the upstream side and thus increases the interface stability, resulting in coarsening of the dendrite morphology.

Conclusions

This work presented a new solidification modeling technique to simulate dendrite growth that uses the LB method to solve the transport equations and the CA technique to track the interface. Simulations of single- and multiple-dendrite growth with the binary Al-3.0 wt % Cu alloy were performed showing good stability and accuracy. When compared with an FE-CA model, the LB-CA model showed significant improvement in scalability for problems involving solidification under convection.

Structural Nanocomposite Design

Principal Investigator: Thomas E. Lacy, Aerospace Engineering, MSST
(662) 325-2754; email: lacy@ae.msstate.edu
Participants: H. Toghiani, C. U. Pittman, Jr., S. Gwaltney

Introduction

Specimens of varying weight fractions (phr—parts per hundred parts resin) were fabricated using a dispersing agent to facilitate nanocomposite dispersion and ultrasonication and/or high-shear mixing (Lacy et al., 2008).

Approach

For this study a thermoset resin (Derakane 441-400 VE from Ashland Co.) was used along with two distinct vapor grown carbon nanofibers (VGCNFs) (typical diameters, 60–200 nm; typical lengths, 20–100 μm) from Applied Science, Inc. as nanoreinforcements: (1) unmodified (“pristine”) VGCNFs (PR 24-XT-LHT) and (2) surface-oxidized VGCNFs (PR-24-XT-LHT-OX). Key aspects of nanocomposite fabrication, testing, modeling, and validation are addressed in this project, including dispersion and interfacial adhesion of nanoreinforcements. A multiscale design methodology is being used to investigate the effects of nanoreinforcements on the mechanical properties of fiber-reinforced composites for automotive structural applications.

Results and Discussion

MD simulations, analytic and numerical micromechanics models, and FE simulations are being used to establish an empirically validated multiscale material model for predicting effective properties of VGCNF–vinyl ester (VE) nanocomposites.

All MD simulations were performed with Materials Studio v5.0 software using a cell of size $60 \times 50 \times 60 \text{ \AA}$ with triply periodic boundary conditions applied. VE resin monomers (VE1, VE2, and styrene) were initially randomly packed around the graphene sheets to yield a final simulation cell density of 1.18 g/cm^3 , agreeing with the density experimentally measured for 1 phr VGCNF in a VE resin (Figure 1).

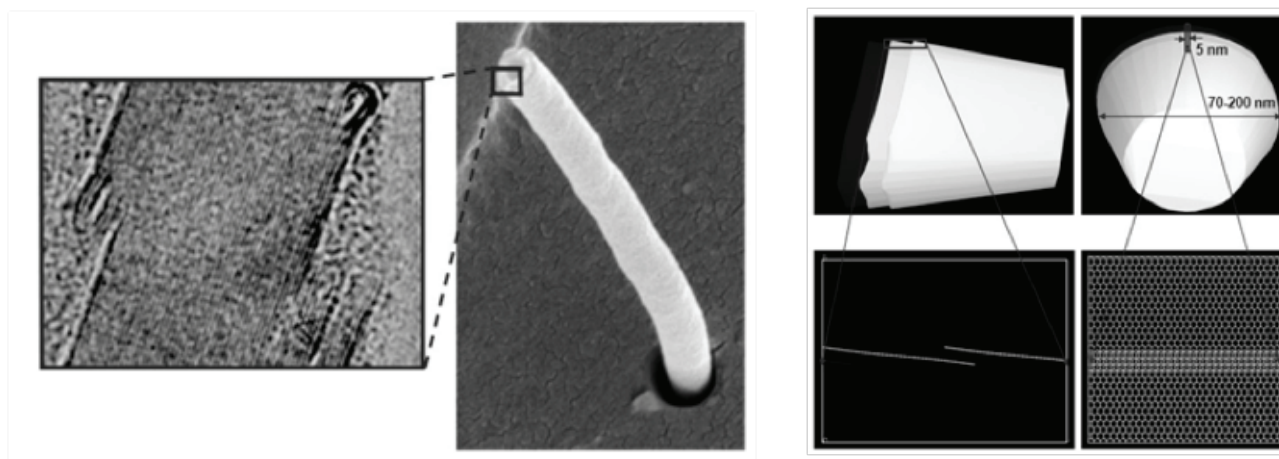


Figure 1. View of a single carbon nanofiber with stacked-cone structure (a) and schematic of overlapping graphene sheets along the outer edge of VGCNF stacked nanocones (b).

Figure 2 shows two snapshots of the simulation: (a) after the geometry optimization step and (b) at the end of the simulation run (~15 ns). Notice in the final frame the packing of molecules around the graphene sheets.

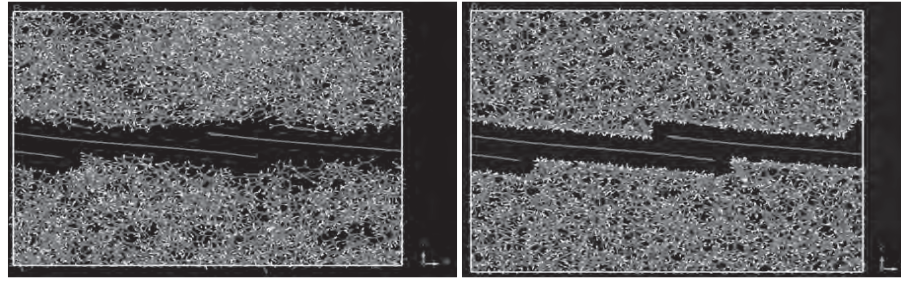


Figure 2. Snapshots of (a) the initial frame after geometry optimization and (b) the final frame after dynamics simulation for a total time of about 15 ns.

A parametric study was performed to investigate the effect of nanofiber-matrix interphase properties and dimensions on bulk nanocomposite properties where the interphase modulus was expressed as a fraction of the matrix modulus (i.e., E_i/E_m). The average thickness, t , and elastic modulus, E_i , of the interphase are strongly influenced by nanofiber surface chemistry, resin type and properties, and curing protocol. Figure 3 shows a plot of the effective longitudinal modulus, E_L , as a function of average interphase thickness for straight solid fibers ($R_i/R_o = 0$, $L/D = 100$) and hollow nanofibers ($R_i/R_o = 0.3$, $L/D = 100$) based upon the MTM where the interphase properties were varied over the range $0.5 \leq E_i/E_m \leq 20$ to encompass both relatively compliant and stiff interphases. With the exception of $E_i/E_m = 0.5$ (i.e., a relatively compliant interphase), the predicted effective nanocomposite modulus increased as the interphase thickness increased. As can be seen from Figure 3(b), the calculated effective longitudinal moduli over the range of observed nanofiber wall thicknesses (Yu et al., 2010b) are significantly greater than the modulus for a nanocomposite with solid nanofibers ($R_i/R_o = 0$). This underscores the importance of using realistic VGCNF geometry data when calculating effective properties. A comparison of Figures 3(a) and 3(b) suggests that the use of very small amounts of VGCNFs (0.63 vol %) results in an improvement of more than 70% in the predicted effective longitudinal modulus of the nanoreinforced resin for the case where no interphase exists ($t/R = t/R_o = 0$). Similar results were obtained when calculating the effective transverse modulus (Yu et al., 2010a).

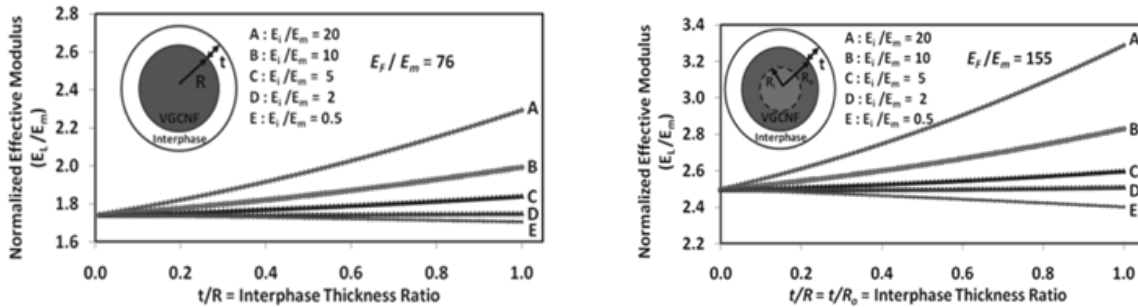


Figure 3. Effect of interphase thickness on effective longitudinal modulus for nanocomposites containing (a) solid straight nanofibers ($R_i/R_o = 0$, $L/D = 100$, EFS = 240 GPa) and (b) hollow straight nanofibers ($R_i/R_o = 0.3$, $L/D = 100$, EF = 490 GPa) at 0.63v% VGCNF.

Figure 4 contains a plot of the effective nanocomposite longitudinal modulus, E_L , as a function of nanofiber waviness ratio (h/λ). At the same carbon volume fraction and $L/D = 50$, straight hollow ($R_i/R_o = 0.3$) fibers induced a 41% greater effective normalized modulus than solid fibers (Yu et al., 2010a). Interestingly, the predicted modulus for nanocomposites with a fixed amount of short, straight hollow fibers ($L/D = 10$, $R_i/R_o = 0.3$) was roughly the same as that for a composite composed of the same weight fraction of longer straight solid fibers ($L/D = 50$, $R_i/R_o = 0$). Effective VGCNF-VE properties from

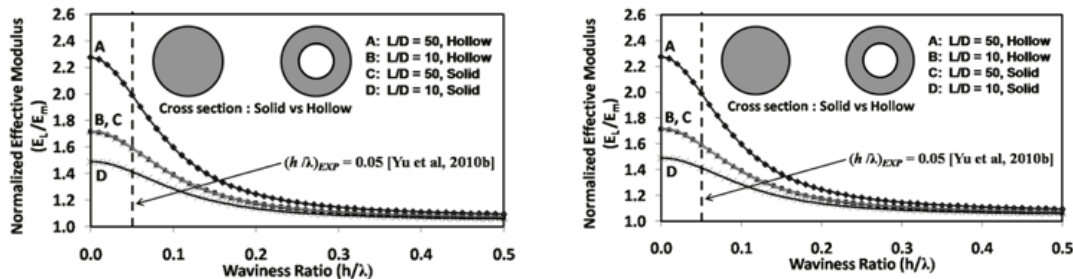


Figure 4. Effect of fiber waviness on effective longitudinal modulus for nanocomposites containing aligned (a) solid ($R_i/R_o=0$, EFS = 240 GPa) and hollow ($R_i/R_o=0.3$, EF = 490 GPa) nanofibers with no interphase and (b) solid ($R_i/R_o=0$, EFS = 240 GPa) and hollow ($R_i/R_o=0.3$, EF = 490 GPa, $R_i/R_o=0.3$) nanofibers with interphase ($t/R = 0.3$, $E_i/E_m=10$) at 0.63v% VGCNF.

micromechanics simulations and/or bulk structure property tests will be used in the development of computationally efficient material and geometric nonlinear FE models for predicting progressive failure of nanoreinforced continuous fiber composite structures. The National Aeronautics and Space Administration special purpose multiscale composite failure analysis code MAC/GMC (Bednarczyk and Arnold, 2002) is being used in conjunction with the ABAQUS FE solver to predict failure of E-glass (i.e., electrical grade glass) plain-weave woven fabric laminates.

Conclusions

A crucial aspect of this work is the establishment of appropriate handshake protocols for efficient data transfer between multiscale calculations performed over a series of fundamentally distinct spatial scales. This study should facilitate the development of engineered multiscale materials design by providing insight into relationships between nanomaterial fabrication/processing, chemical and physical characteristics, and interaction and evolution of structure across disparate spatial and temporal scales that lead to improved macroscale performance.

Natural Fiber Composites for Structural Component Design

Principal Investigator: Sheldon Q. Shi, Forest Products, MSST
(662)325-3110; email: sshi@cfr.msstate.edu

Participants: M. Qatu, K. Liang, M. Tschopp, J. Wang, D. Ward, D. Nicolas, D. Zhang, J. Shi, I. Fulton, W. Che

Approach

An exploratory study of the effects of pressure and layup on a hybrid composite of randomly oriented woven kenaf fibers and fiberglass/polyester sheet molding compound (SMC) was conducted. We plan to investigate natural fiber retting, natural fiber treatment, nanotechnology and/or chemical modification on the natural fibers, composite fabrication and testing, natural fiber SMC fabrication techniques, and composite modeling.

Results and Discussion

Chemical Components and Morphologies of the Kenaf Bast Fibers Obtained from Chemical Processes

Kenaf bast fibers were treated as follows. Alkaline retting treatment followed by bleaching treatment was applied to remove the hemicellulose and lignin from the raw kenaf bast fibers, and retted fibers and bleached fibers were obtained. Acidic hydrolysis was conducted on the bleached fibers, and the microfibrils and cellulose nanowhiskers (CNWs) were obtained. The CNWs had been applied to fabricate polyvinyl alcohol (PVA)-CNW composites and exhibited excellent reinforcement efficiency for tensile properties. The functional groups and crystallinities of the fibers were measured. This study focused on the chemical components and morphologies of these fiber types.

Scanning electron microscopy (SEM, Zeiss Supra TM 40) was applied to analyze fiber morphology. Seventy fibers were randomly chosen for their dimension measurement using “Smart SEM User Interface.” The CNW samples for morphology analysis were obtained by placing a drop of the CNW suspension onto a grid without any staining and drying it in air at ambient temperature. The dried samples were examined by transmission electron microscopy (TEM, JEOL JEM-2000 EX-II). The dimensions of 70 randomly chosen CNWs were measured from the TEM images. The morphology of the raw kenaf bast fiber, retted fiber, bleached fiber, microfibril, and CNW was studied from their SEM or TEM images (Figures 1 and 2). The statistics of the fiber lengths and diameters were quantified.

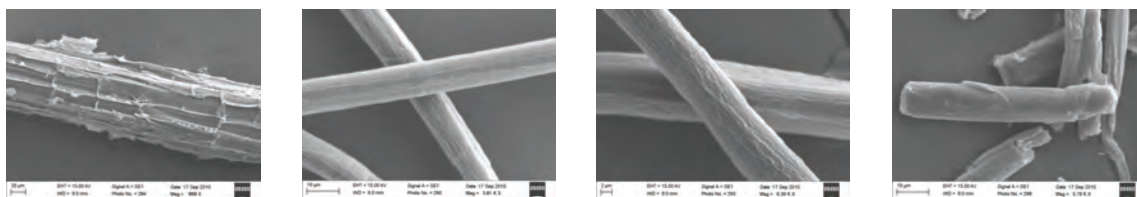


Figure 1. SEM images of (a) the raw kenaf bast fibers, (b) retted fibers, (c) bleached fibers, and (d) microfibrils.

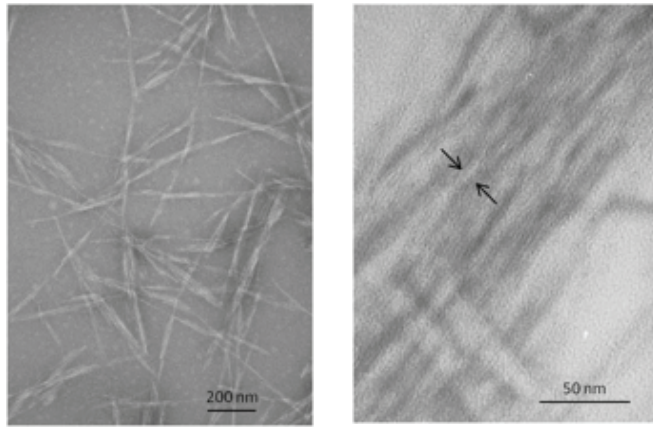


Figure 2. TEM images of CNWs: (a) magnification = 50,000X, accelerating voltage = 100 kV; (b) magnification = 370,000X, accelerating voltage = 100 kV.

A Microtension Test Method for Measuring Four Representative Individual Cellulosic Fibers

We developed an experimental technique to stress the microcellulosic fibers and to evaluate mechanical properties of several representative individual fibers. A microtension testing system was devised to measure the mechanical properties of individual cellulosic fibers. The system can measure tensile modulus, strength, creep, relaxation, and cyclic loading characteristics and the effect of moisture on mechanical properties of a microfibril.

Morphology of Natural Fibers

The typical cross-sectional images of an individual fiber by a confocal laser scanning microscope (CLSM) and environmental scanning electron microscope (ESEM) are shown in Figures 3 and 4. Both kenaf and bamboo have a thick secondary cell wall with a very small lumen in polygonal shape, which indicates that both fibers undergo extensive cell-wall thickening during maturation. Ramie individual fiber is flattened and typically hexagonal or oval in shape, while fibers of Chinese fir are rectangular in cross section.

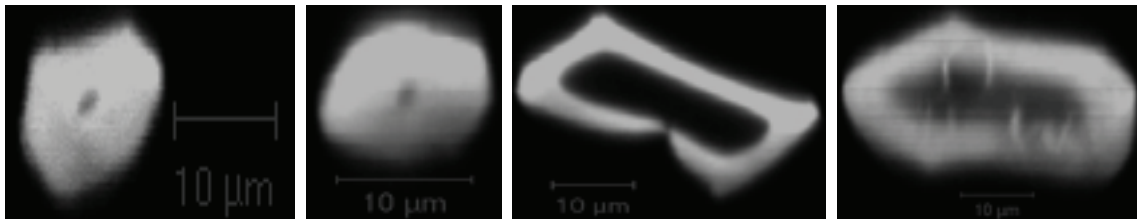


Figure 3. Typical CLSM images of cross sections of individual fibers: (a) bamboo, (b) kenaf, (c) Chinese fir, and (d) Ramie.

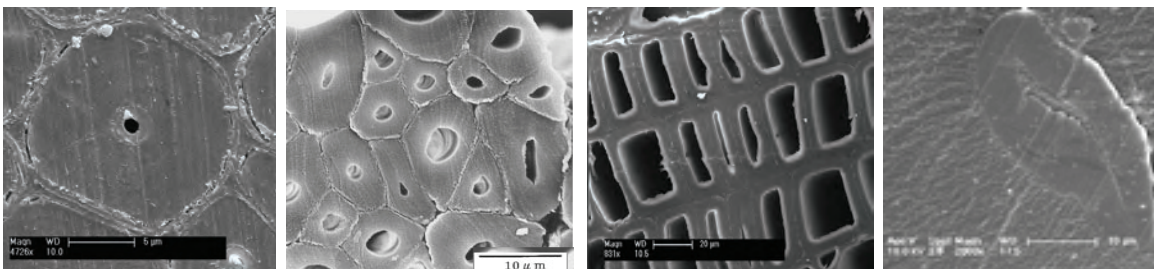


Figure 4. Typical ESEM images of cross sections of individual fibers: (a) bamboo, (b) kenaf, (c) Chinese fir, and (d) ramie.

We established MD models to understand many of the variables associated with deformation of thermoplastic polymers using atomistic modeling (e.g., chain length, number of chains, strain rates, temperature). MD simulations were used to study the deformation mechanisms during uniaxial tensile deformation of amorphous polyethylene. The stress-strain behavior included elastic, yield, strain softening and strain hardening regions that were qualitatively in agreement with previous simulations and experimental results (Figure 5). The chain lengths, number of chains, strain rate and temperature dependence of the stress-strain behavior were investigated. The energy contributions from the united atom potential were calculated as a function of strain to help elucidate the inherent deformation mechanisms within the elastic, yield, and strain hardening regions.

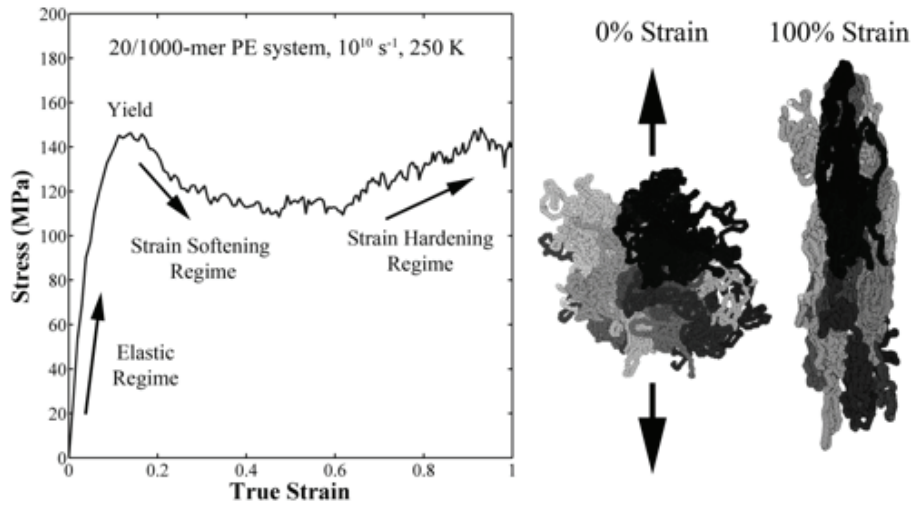


Figure 5. Stress-strain response for amorphous polyethylene deformed by uniaxial tensile loading.

Current work is focusing on the deformation behavior of polypropylene and glucose interfaces as a model for the composite materials used in this work. MD and molecular statics simulations will be used to examine elastic and plastic properties of amorphous cells of both glucose and polypropylene and the interface mechanical properties between the two materials.

Conclusions

Our kenaf natural fiber SMC has properties comparable to commercial glass fiber SMC, and the impregnated kenaf SMC was not degraded during weathering. The newly designed SF-I microtester is well suited for measuring mechanical properties of individual microfibrils. A detailed procedure was given to describe fabrication of a laminated natural fiber kenaf based composite. Various samples have been manufactured with modulus of elasticity up to about 10 GPa and modulus of rupture up to about 270 MPa. Simulations showed that temperature increase of polymer in high rate tests can be reproduced by augmenting the deformation boundary conditions. This might shed light on the fundamental mechanisms associated with the generation of heat in thermoplastic polymers under high rate deformation.

Bio-Inspired Design

Principal Investigator: Lakiesha N. Williams, Agricultural & Biological Engineering, MSST
(662)325-3282; email: lwilliams@abe.msstate.edu

Approach

The purpose of the present work is to build and validate a numerical model of the human scalp that will realistically model the skin, connective tissue, aponeurosis, and underlying areolar tissue in an FE head model. The model will be validated by evaluating pressure and stress distributions in the scalp due to impact. Using FE modeling software allows us to create a highly detailed graph (or mesh) which we can use to assign mechanical properties to individual layers. We will create an anatomically correct human head (including neck and shoulders). To date, no computational human head scalp model has been developed to include these features.

Results and Discussion

Porcine Skin

A customized polymeric split Hopkinson pressure bar (PSHPB) apparatus was used for evaluating strain rate sensitivity; samples were extracted along direction 1 (Figure 1). To evaluate directional dependency of tissue behavior, samples were dissected along three orthogonal directions (directions 1, 2, and 3; $n=4$ for each direction) and tested at a strain rate of 350 s^{-1} . Porcine scalp histology was used to determine the makeup of the porcine scalp tissue structure. The sample shown in Figure 2 was placed under tension and pulled to 10% strain, fixed with paraformaldehyde, and stained using hematoxylin and eosin (H&E). By performing H&E staining, using a method of paraffinization on fixed samples, the separate skin layers were clearly distinguishable.

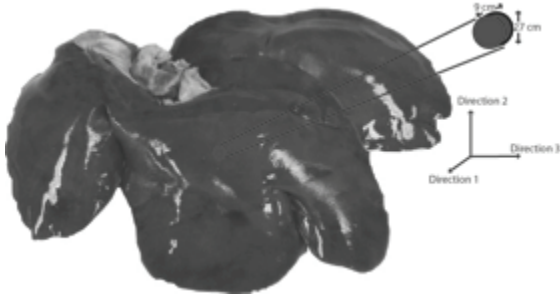


Figure 1. Three orthogonal directions (1, 2, and 3) based on porcine liver anatomy. Representative sample geometry and size



Figure 2. Structural representation of different layers of the skin shown via H&E staining.

The mechanical response of liver tissue was accurately calibrated for the MSST thermoplastic (TP) material model (Figure 3). Stress status in the cylindrical liver sample was revealed by FE modeling of the PSHPB test at a strain rate of 1,000 s^{-1} (Figure 4). The contour plots of s_{33} (axial stress) and s_{Mises} were found to vary dramatically at the initial stiffening, maximum stress of the peak, softening phase, valley stress, subsequent hardening, and failure stress.

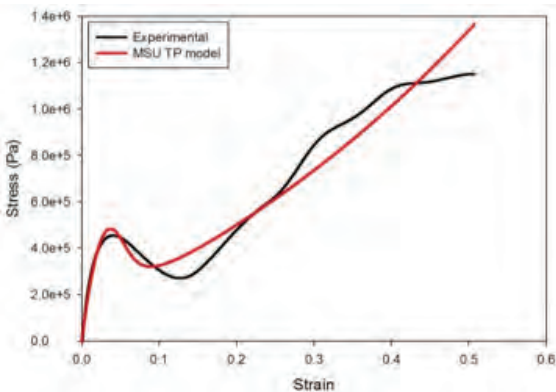


Figure 3. The MSST TP model shows a good fitting with the experimental data. The theoretical curve and experiment data at 1,000 s^{-1} were plotted as a representation.

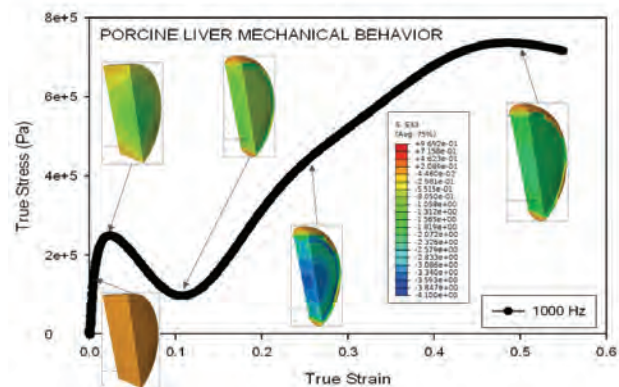


Figure 4. FE simulation results showing the contour plots of axial stress, σ_{33} , at various stages along true stress-true strain curve at 1,000 s^{-1} .

The stress contours of the sample also revealed a nonuniform stress state throughout testing. The wave propagation observed via computational modeling was consistent with the experimental results of the striker and transmitted bars, thereby validating the testing procedure.

Conclusions

The use of a PSHPB apparatus for high strain rate testing of porcine liver tissue reveals the inelasticity, isotropy, and strain rate sensitivity of the tissue. A composite skin FE model was developed. Also, all four layers were evaluated to examine the differences in mechanical properties and ultimately correlate the structure and function of the skin tissue.

K–12 Outreach Program

Principal Investigator: Mark F. Horstemeyer, CAVS, MSST
(662)325-7308; email: mfhorst@cavs.msstate.edu
Participants: R. C. Cuicchi, P. M. Cuicchi

Approach

The K–12 Outreach Program, also referred to as Mission Eggcellence, provides students with a hands-on introduction to vehicular crashworthiness through applying basic concepts of physics (students are provided with simple definitions from physics such as mass, velocity, momentum and energy, and how they are used during a crash), explanations of what actually happens during a crash (using the physics terms and defining what is necessary to enable passengers to survive a crash), and examples of safety devices (explanations and examples of some devices such as bumpers, seatbelts, airbags and safety cages used in cars and trucks with simulations to demonstrate how they work). Following are the objectives of the K–12 Outreach Program.

- Create a grade appropriate curriculum with experiments and problems associated with the physics of car crashes for grades K–2, 3–5, 6–8, and 9–12. (Objective 1)
- Develop a teacher workshop for teachers of grades K–2, 3–5, 6–8, and 9–12 for training in use of the grade appropriate curriculum in the regular classroom. Equipment necessary to conduct the experiments and compete in the competitions is given to each teacher participant. (Objective 1)
- Design a competition for grades K–2, 3–5, 6–8, and 9–12 incorporating bumper design for passenger safety. (Objective 2)
- Design a competition for grades K–2, 3–5, 6–8, and 9–12 incorporating car design for passenger safety. (Objective 2)
- Publish a book containing the experiments, illustrations, competitions, and safety chapter. An electronic version will be included with the book and will contain videos of the teacher training and competitions. (Objective 3)

Results and Discussion

Contributions to the Long-Term and Sustainable Engagement of the Team/Unit

MSST is developing an “automotive experience” strategic program that includes K–12, undergraduate work, and graduate level work. A new course and certificate are being developed in real time for this endeavor.

Thirty-three school districts in 22 counties have had 127 teachers participate in the teacher workshops. Five hundred sixty-four students have competed in the student competitions. Seventy-five percent of the teachers who attended the workshop had students compete in both the bumper design and car design competitions.

We are planning on including ASM to broaden the program further. Nissan North America (Canton, Mississippi) and Vista Engineering Inc. have both donated in-kind contributions to the SRCLID program with specific interest in the educational development aspects of the program.

Conclusions

The Mission Eggcellence Program has been developed for grades K–2, 3–5, 6–8, and 9–12. The Teacher workshop for these grades has been very successful. Feedback was excellent.

Presentations / Publications / Patents

Task 1

1. Solanki, K. N.; Horstemeyer, M.F.; Steele, G.W.; Hammi, Y.; Jordon J. B. Calibration, validation, and verification including uncertainty of a physically motivated internal state variable plasticity and damage model. IJSS 2010;47(2),186-203.

- Solanki, K. N.; Moitra, A.; Bhatia, M. (2010). Effect of Substituted Al in Mg Tension Twin, *Journal of Computational Material* (Accepted for publication).
- Bammann, D. J.; Solanki, K. N. (2010). On Kinematic, Thermodynamic and Coupling of a Damage Theory for Polycrystalline Material, *International Journal of Plasticity*, 26(6), 775–793.
- Solanki, K. N.; Bammann, D. J. (2010). A Thermodynamic Framework for a Gradient Theory of Continuum Damage. *Acta Mechanica*, 213, 27–38.
- Acar, E.; Solanki, K. N.; Rais-Rohani, M.; Horstemeyer, M. (Mar 2010). Stochastic Uncertainty Analysis of Damage Evolution Computed through Microstructure-Property Relations. *Probabilistic Engineering Mechanics Elsevier*, 25(2), 198-205.

Task 2

- Tomasz Haupt, “Cyberinfrastructure for Integrated Computational Material Engineering,” in *Mg Technology 2010: Proceedings of a Symposium Sponsored by the Mg Committee of the Light Metals Division of TMS S. Agnew* (Editor), Neale R. Neelameggham (Editor), Eric A. Nyberg (Editor), W. Sillekens (Editor), Wiley, 2010.
- Ciorba, F. M.; Groh, S.; Horstemeyer, M. F. “Parallelizing discrete dislocation dynamics simulations on multi-core systems,” *International Conference on Computational Science (ICCS 2010)*, to be presented at the Workshop on Tools for Program Development and Analysis in Computational Science, May 31st-June 2nd, Amsterdam, NL.

Task 3

- Jordon, J. B.; Horstemeyer, M. F.; Daniewicz, S. R.; Badarinarayan, H.; Grantham, J. “Material Characterization and Modeling of Friction Stir Spot Welds in a Mg AZ31 Alloy,” *Journal of Engineering Materials and Technology*, 132, 4, <http://dx.doi.org/10.1115/1.4002330> (2010)

Task 4

- Martin, H. J.; Danzy, J.; Horstemeyer, M. F.; Wang, P. T. “Comparing the Corrosion Effects of Two Environments on As-Cast AM60 and AZ91,” 2010 American Institute of Chemical Engineers Annual Meeting; Salt Lake City, UT; 2010 November.
- Martin, H. J.; Walton, C.; Danzy, J.; Hicks, A.; Horstemeyer, M. F.; Wang, P. T. “Modeling the Corrosive Effects of Various Mg Alloys Exposed to Two Saltwater Environments,” 2010 American Institute of Chemical Engineers Annual Meeting; Salt Lake City, UT; 2010 November.

Task 6

- Jelinek, Bohumir; Houze, Jeffrey; Groh, Sebastian; Kim, Seong-Gon; Horstemeyer, M. F.; Wagner, G. J.; Baskes, M. I. “MEAM potentials for Al, Si, Mg, Cu, and Fe alloys,” 2010 SEAPS Meeting, Baton Rouge, LA, October 20–23, 2010.
- Kim, Sungho; Kim, Seong-Gon; Horstemeyer, M. F. “Vanadium effects on a BCC iron sigma 3 grain boundary strength,” 2011 TMS Annual Meeting, San Diego, CA, March 2011.
- Liyanage, L.; Moitra, Amitava; House, J.; Kim, Seong-Gon; Tschopp, Mark; Kim, Sungho; Horstemeyer, M. F. “A modified embedded-atom-method potential for Fe-C alloy systems,” 2011 APS March Meeting, Dallas, TX, March 2011.
- Moitra, Amitava; Kim, Sungho; Kim, Seong-Gon; Park, Seong Jin; German, Randall; Horstemeyer, M. F. “Atomistic Scale Study on Effect of Crystalline Misalignment on Densification during Sintering Nano Scale Tungsten Powder,” book chapter in *Advances in Sintering Science and Technology*, eds. Rajendra K. Bordia and Eugene A. Olevsky, pp. 149-160, ISBN:9780470408490 (2010).
- Moitra, Amitava; Kim, Sungho; Kim, Seong-Gon; Park, Seong Jin; German, Randall; Horstemeyer, M. F. “Investigation on sintering mechanism of nanoscale tungsten powder based on atomistic simulation,” *Acta Materialia* 58, 3939–3951 (2010).

6. Kim, Sungho; Kim, Seong-Gon; Horstemeyer, M. F. "Vanadium effects on a BCC iron sigma 3 grain boundary strength," Proceedings: Collected Proceedings: Deformation, Damage, and Fracture of Light Metals and Alloys (2011).
7. Kim, Seong-Gon; Horstemeyer, M. F.; Rhee, Hongjoo; Kim, Sungho. "Task 6: Materials Design for Steel Alloys in the Southern Regional Center for Lightweight Innovative Designs (SRCLID)," DOE Southern Regional Center for Lightweight Innovative Designs (SRCLID) Phase II Final Report, Chap 6 (2010).

Task 7

1. Motoyama, K. "Implications of Welding Simulation Techniques to Optimize Manufacturing Processes," Technical Presentation, DETC2010-29105, 2010 ASME International Design Engineering Technical Conferences & Computers and Information In Engineering Conference, Montreal, Canada, August 15–18, 2010.

Task 8

1. Yin, H.; Wang, L.; Felicelli, S. D. "Solidification model coupling lattice Boltzmann method with cellular automaton technique," 4th International Shape Casting Symposium, 2011 TMS Annual Meeting and Exhibition, San Diego, California, February 27–March 3, 2011.
2. Yin, H.; Felicelli, S. D.; Wang, L. "Simulation of dendritic microstructure with lattice Boltzmann and cellular automaton methods," Acta Materialia, submitted November 2010.
3. Yin, H.; Felicelli, S. D. "Dendrite Growth Simulation during Solidification in the LENS Process," Acta Materialia, Vol. 58, 2010, pp. 1455–1465.

Task 9

1. Nouranian, S; Toghiani, H.; Lacy, T. E.; Pittman Jr., C. U.; Dubien, J. 2010. "Dynamic Mechanical Analysis and Optimization of Vapor-Grown Carbon Nanofiber/Vinyl Ester Nanocomposites Using Design of Experiments," J. Compos. Mater., Prepublished November, 22, DOI: 10.1177/0021998310385027.
2. Du, Y.; Zhang, J.; Toghiani, H.; Lacy, T. E.; Xue, Y.; Horstemeyer, M. F.; Pittman Jr., C. U. 2010. "Kenaf Bast Fiber Bundle-Reinforced Unsaturated Polyester Composites I: Processing Techniques for High Kenaf Fiber Loading," Forest Products Journal, 60(3), 289–295.
3. Du, Y.; Zhang, J.; Wang, C.; Lacy, T. E.; Xue, Y.; Toghiani, H.; Horstemeyer, M. F.; Pittman Jr., C. U. 2010. "Kenaf Bast Fiber Bundle-Reinforced Unsaturated Polyester Composites II: Water Resistance and Composite Mechanical Properties Improvement," Forest Products Journal, 60(4), 366–372.
4. Yu, J.; Lacy, T. E.; Toghiani, H.; Pittman Jr., C. U. "Material Property Estimations for Nano-Reinforced Polymer Composites Using Classical Micromechanics and the Generalized Method of Cells," in the Proceedings of the 51st AIAA/ ASME/ ASCE/ AHS/ ASC Structures, Structural Dynamics, and Materials Conference, Orlando, Florida, May 12–15, 2010.
5. Yu, J.; Lacy, T. E.; Toghiani, H.; Pittman Jr., C. U. "Micromechanical Modeling of Nanoreinforced Composites with Carbon Nanofibers and Interphase," in the Proceedings of the American Society for Composites 25th Annual Technical Conference, Dayton, Ohio, September 20–22, 2010.
6. Nouranian, S.; Jang, C.; Toghiani, H.; Pittman Jr., C. U.; Lacy, T. E.; Gwaltney, S. "Investigation of Vinyl Ester Resin/ Vapor-Grown Carbon Nanofiber Surface Interactions Using Molecular Dynamics Simulations," in the Proceedings of the 2010 Annual Meeting of the American Institute of Chemical Engineers (AIChE), Salt Lake City, Utah, November 7–12, 2010.

Task 10

1. Shi, S. Nanotechnology for Natural Fiber Based Composites. Harbin Engineering University, Harbin, China, March 10, 2010.
2. Liang, K.; Shi, S. Q. Modified soybean oil/polyhedral oligomeric silsesquioxane (POSS) bio-nanocomposites: Synthesis and characterization. 11th International Conference on Biocomposites, Toronto, Canada, May 2–4, 2010.
3. Castillo, H.; Lee, S.; Shi, S. Q.; Srinivasan, R.; Shi J. “Semi-crystalline polymer-based composites with corn fiber (separated from DDGS) as an interfacial reagent.” 11th International Conference on Biocomposites, Toronto, Canada, May 2–4, 2010.
4. Liang, K.; Shi, S. Q. “Kenaf bast fiber sheet molding compound (SMC) composites with acrylated epoxidized soybean oil.” 64th Forest Products Society (FPS) International Convention, Madison, WI, June 20–22, 2010.
5. Shi, S. Q.; Zhang, S.; Jiang, D.; Che, W.; Shi, J. “Graphitization of natural fiber cellulose into carbon fiber.” 64th Forest Products Society (FPS) International Convention, Madison, Wisconsin, June 20–22, 2010.
6. Liang, K.; Shi, S. Q. 2010. “Modified soybean oil/polyhedral oligomeric silsesquioxane (POSS) bio-nanocomposites: Synthesis and characterization.” In Proceeding of 11th International Conference on Biocomposites: Transition to Green Materials, Toronto, Canada, May 2–4, 2010.
7. Peng, Y.; Shi, S. Q. 2010. Effect of cloisite clay on the dynamic mechanical properties of resin film. Proceedings of Wood Adhesives 2009. September 28–30, Lake Tahoe, Nevada, USA.
8. Liang, K.; Shi, S. Q. 2010. Nanoclay filled soy-based polyurethane foam. Journal of Applied Polymer Science. 119 (3): 1857–1863.

Patent

1. Shi, S. Q.; Zhang, D.; Shi, J.; Jiang, D. 4/30/2010. Functional natural fiber nanocomposites and their fabrication techniques. Docket Number: 2009.0734 PROV.

Patent disclosures

1. Zhang, D.; Shi, S. Q. 2/23/2010. Magnetic charcoal and its fabrication. MSU Tech ID: 2010.0767
2. Zhang, D.; Shi, S. Q. 8/27/2009. Carbon fiber and functional charcoal from natural cellulosic material. MSU Tech ID: 2009.0744
3. Shi, S. Q.; Zhang, D.; Shi, J.; Jiang, D. 7/9/2009. Functional natural fiber nanocomposites and their fabrication techniques. MSU Tech ID: 2009.0734

Task 11

1. “A comparison study on the structures and mechanical behaviors of sandwich composite biological structural materials”, MS&T 2010 Conference & Exhibition, Houston, TX, Oct. 18, 2010.
2. “Structure-Property relationships of the scalp”. Biomedical Engineering Society, Austin, TX, October 6, 2010.
3. Clemmer, J.; Liao, J.; Davis, D.; Horstemeyer, M.; Williams, L. N. “A Mechanistic Study for Strain Rate Sensitivity of Rabbit Patellar Tendon,” Journal of Biomechanics, 43, 2010: 2785–2791.

References

Baskes, M. I. "Modified embedded-atom potentials for Fe," unpublished.

Bednarczyk, B. A.; Arnold, S. M. 2002. Micromechanics Analysis Code with Generalized Method of Cells (MAC/GMC), User's Manual: Version 4.0. NASA-TM-2002-212077.

Carino, R.; Ciorba, F. M.; Ma, Q.; Marin, E. Improving the Performance and Usability of a Microstructure Mapping Code. MSU.CAVS.CMD.2009-R0023, Mississippi State University: Center for Advanced Vehicular Systems (2009).

Ciorba, F. M.; Groh, S.; Horstemeyer, M. F.; "Parallelizing discrete dislocation dynamics simulations on multi-core systems." International Conference on Computational Science (ICCS 2010), Workshop on Tools for Program Development and Analysis in Computational Science, May 31–June 2, 2010, Amsterdam (2010).

Kim, Seong-Gon; Horstemeyer, Mark F.; Baskes, M. I.; Rais-Rohani, Masoud; Kim, Sungho; Jelinek, B.; Houze, J.; Moitra, Amitava; Liyanage, Laalitha. "Semi-empirical potential methods for atomistic simulations of metals and their construction procedures." *J. Eng. Mater. Technol.*, 131(4), 041210 [9 pages] (2009).

Lacy, T.E.; Pittman Jr., C.U.; Toghiani, H.; Nouranian, S.; Hutchins, J.; Zhou, Y.; Jeelani, S.; Carpenter, J.A. 2008. Structural Nanocomposite Design. DOE SRCLID FY 2008 Progress Report.

Rashid, M. M. 1997a. "A new theory for free-surface formation in solid continua." *Int. J. Solids Struct.* 34:2303-20.

Rashid, M. M. 1998. "The arbitrary local mesh replacement method: An alternative to remeshing for crack propagation analysis." *Compu. Meth. Appl. Mech. Eng.* 154(1):133–150.

Yu, J.; Lacy, T.E.; Toghiani, H.; Pittman Jr., C. U. 2010a. "Classical micromechanics modeling of nanoreinforced composites with carbon nanofibers and interphase." Submitted to *Journal of Composite Materials* (Submitted July 2010, Reviewer's comments received September 2010, accepted pending minor revisions; revisions were submitted October 2010).

Yu, J.; Lacy, T. E.; Toghiani, H.; Pittman Jr., C. U.; Schneider, J. 2010b. "Determination of carbon nanofiber morphology in polymer nanocomposites," in preparation. To be submitted to the *Journal of Composite Materials*.

F. Multi-material Enabling - Oak Ridge National Laboratory

Field Technical Monitor: C. D. Warren
Oak Ridge National Laboratory
1 Bethel Valley Road; Oak Ridge, TN 37831
(865) 574-9693; e-mail: warren cd@ornl.gov

Technology Area Development Manager: William Joost
U.S. Department of Energy
1000 Independence Ave., S.W.; Washington, DC 20585
(202) 287-6020; e-mail: william.joost@ee.doe.gov

Contractor: Oak Ridge National Laboratory (ORNL)
Contract No.: DE-AC05-00OR22725

This project consists of four tasks critical for the welding of lightweighting metal structures. The tasks include (1) development of an understanding of dynamic loading on spot welds in AHSS's; (2) development of friction stir spot welding (FSSW) methods for AHSSs; (3) development of friction stir and ultrasonic welding methods for Mg (Mg) alloys; and (4) development of a rapid, reliable spot weld inspection method for use in manufacturing plants.

Objectives

- In order to design with spot welds in advanced HSS (AHSSs), develop a new, robust spot weld element (SWE) and incorporate the SWE in advanced crashworthiness computer-aided engineering (CAE) codes used by automotive crash modelers. The resulting SWE must accurately model the deformation and fracture modes of spot welds in AHSSs as a function of impact loading, welding, and steel chemistry while maintaining computational efficiency and ease of use.
- In order to better facilitate the joining of transformation-induced plasticity (TRIP) and high-strength steels, demonstrate the feasibility of producing acceptable friction stir spot weld (FSSW) joints in those materials and resolve technical obstacles to the use of FSSW to joining higher performance steels.
- The technical issues to be resolved for FSSW of higher performance steels include (1) characterizing the effects of liquid-metal embrittlement on both the steel materials and the friction stir weld tooling; (2) evaluating the wear and durability performance of polycrystalline cubic boron nitride (PCBN) to silicon nitride (Si3N4) tooling as well as other potential tool materials; and (3) identifying and documenting equipment limitations that could prevent the use of FSSW on TRIP steels or any other specialty steel alloys identified by automotive manufacturers.
- Develop methods to produce robust joints between Mg alloys and steel using the solid-state processes of friction stir welding (FSW) and ultrasonic welding (USW). This includes development of an understanding of the fundamental relationships influencing metallurgical, mechanical, and chemical aspects of bond formation for Mg-steel and Mg-Mg joints produced by FSW and USW. It also includes evaluating the responses of the processes to changing alloys, product forms, and surface conditions.
- Develop an infrared (IR) thermography based weld quality detection technology capable of reliable and cost effective online nondestructive monitoring and feedback control of the welding assembly operation in a high-volume automotive production environment.

Accomplishments

- An initial version of the SWE covering two different steel grades was developed that is capable of handling weld geometry and weld property gradients and also of predicting different fracture modes and fracture load limits which are experimentally observed in impact tests.
- The experimental task to develop the SWE collected and characterized the effects of impact speeds and loading modes

on the failure of spot welds of DP780 and DQSK steels. The team also licensed the integrated electrical-thermal-mechanical-metallurgical weld model to original equipment manufacturers (OEMs) and developed a web based database of spot weld testing results for user-friendly interactive data analysis and retrieval. Lastly, the weld process model was extended to three layers of sheet steel stackup, sheet-to-sheet gaps, and other ultra high-strength steel grades and demonstrated the capability of predicting heat-affected zone (HAZ) softening in ultra-high-strength steels.

- The experimental task to develop FSSW demonstrated that FSSWs of TRIP steel can achieve minimum strength property values specified for resistance spot welds.
- The experimental task to develop mixed material joining methodologies demonstrated the ability to effectively join Mg to steel using both FSW and USW solid-state joining techniques. The task compared the lap-shear strengths of spot-welded Mg-steel joints made with bare steel to those made with zinc-coated steel to determine the strength increase associated with chemical reactions between Mg and zinc. The ability to achieve strength levels exceeding the decision gate of 1.5 kN was demonstrated.
- The nondestructive evaluation (NDE) task demonstrated that a low cost IR camera is capable of both postmortem and real-time weld quality assessment to establish a rapid nondestructive inspection technique for spot welds. That team applied advanced multiphysics model for revealing temperature and deformation evolution during resistance spot welding (RSW) of AHSSs in two and three layer stackups. The prediction was used to improve the data analysis algorithm used in IR inspection techniques.

Future Direction

- Spot weld element development and experimental validation of a weld process modeling framework for various AHSS spot weld configurations and structural components commonly expected in auto body structures will be completed. This will include determining the weld failure criteria necessary for different loading and fracture modes for spot-welded AHSSs. The CAE models will be validated and optimized and then implemented as a stand-alone element for incorporation into commercial finite-element method codes used by OEMs.
- Future work to develop FSSW for AHSSs will include a more comprehensive characterization of mechanical behavior including fatigue strength, T-peel strength, cross-tension strength, and metallurgical examinations as part of the FSSW of AHSSs task. It will also include work to identify and characterize the liquid-metal embrittlement phenomena and evaluate candidate materials for friction stir tools.
- The joining of dissimilar metal will include the determination of the fundamental aspects of Mg-steel bond formation in ultrasonic spot welding. This will include analysis of joint microstructures to better characterize features that contribute to making strong bonds. The task team will also evaluate weld bonding (combinations of adhesive bonding with the solid-state welding processes) as a means to improve mechanical properties. Research plans include placing more emphasis on fatigue testing in the FSW and USW task with the goal of determining stress levels that can support a fatigue life of 10⁶ loading cycles. Strategies for providing corrosion protection for Mg-steel joints will also be examined, and this will be coordinated with other projects that have greater emphasis on corrosion mitigation.
- Future work aimed toward developing an affordable nondestructive evaluation method for resistance spot welds will include utilizing a low cost IR camera based inspection system to different steels, thicknesses, and surface coatings and evaluating performance of the resulting welds in the cross tension and other mechanical tests commonly used by OEMs. This includes improving the data analysis software so that it can analyze data in real time and developing a prototype IR weld quality monitoring expert system for field demonstration.

Introduction

This project comprises four distinct tasks that are related to the welding of metals. The first task is to characterize the impact of highly dynamic load rates on the integrity of spot welds in AHSSs. The prediction of spot weld failure in crashworthiness CAE simulations has been generally unsatisfactory for AHSSs. Redesigning, to prevent weld failures, has frequently resulted in design compromises that can adversely affect the weight savings available by using AHSSs. Further lightweighting

opportunities from optimized use of AHSSs are not possible without an improved understanding of the failure phenomena and the development of validated spot-weld CAE tools.

The second task is to develop friction stir spot welding (FSSW) methods for AHSSs, including TRIP steels and others to be identified by industry partners. This task is a collaborative effort between ORNL and Pacific Northwest National Laboratory (PNNL) and includes a committee of consultants from Chrysler, Ford, General Motors (GM), Kawasaki (robot manufacturer), MegaStir (producer of PCBN friction stir tooling), and Ceradyne (producer of Si₃N₄ tooling). More comprehensive characterization of joint mechanical behavior will be done including tests of fatigue strength, T-peel strength, cross-tension strength, and microstructure.

The third task is geared toward the evaluation and development of friction stir welding (FSW) and ultrasonic welding (USW) processes to join Mg to steel and Mg to Mg. That task will develop an improved understanding of the interaction of each unique energy source with appropriate alloy combinations. It will also investigate the fundamental aspects of bond formation (metallurgical and/or mechanical) during solid-state processes and investigate the response to changing alloys, product forms (wrought, castings), and surface conditions (coatings). The materials being joined (Mg and steel) form a strong galvanic couple. Strategies to prevent corrosion of Mg-steel joints include potentially unbroken interlayers or transition materials, complete encapsulation, and coatings or hermetic adhesives that are welded through during the joining process (weld bonding). The feasibility of effectively controlling corrosion will be assessed.

The fourth task under this project is aimed at developing a quantitative, rapid, in-plant, NDE process for ensuring the quality of spot welds. The development of the resistance spot welding (RSW) process for joining AHSS is crucial for assembling the AHSS intensive automotive body structure. The approach being taken is to develop an IR thermography based weld quality detection technology capable of reliable and cost-effective online, nondestructive monitoring and feedback control of the welding assembly operation in a high-volume, automotive production environment.

Activity and Developments

Dynamic Characterization of Spot Welds in Advanced High Strength Steels

Principal Investigator: Zhili Feng, Oak Ridge National Laboratory
(865) 576-3797; e-mail: fengz@ornl.gov

Principal Investigator: Srdjan Simunovic, Oak Ridge National Laboratory
(865) 241-3863; e-mail: simunovics@ornl.gov

Introduction

The primary driver for increased use of AHSSs in auto body structures is the drastic improvements in performance while reducing the vehicle weight. Resistance spot welding is by far the most common joining process used in automotive manufacturing. Typically, there are several thousand spot welds in a vehicle. Because the separation of spot welds can affect the crash response of welded structural components, the static and dynamic behavior of the spot welds has been one of the critically important considerations in vehicle design and manufacturing.

The computer aided engineering (CAE) based simulation of the crash behavior of auto body structures is an indispensable tool that enables rapid and cost-effective design and engineering of crashworthy auto body structures. The prediction of spot weld failure in crashworthiness CAE simulation has been generally unsatisfactory for AHSS and other lightweight materials [such as Al and Mg alloys]. The lack of the fundamental understanding and predictive capability of the spot weld behavior is a critical barrier that hinders rapid and optimum insertion of lightweight materials in auto body structures. Weld failures, detected in later stages of the new model car development cycle, have frequently resulted in design compromises that can

adversely affect the weight savings available by using AHSS. Further lightweighting opportunities from optimized use of AHSS and other lightweighting materials are not possible without an improved understanding of the phenomena and the development of respective spot weld CAE tools.

Approach

This project will develop a new and robust approach to reliably predict the deformation and failure of spot welds in advanced crashworthiness CAE. These developments will provide the solutions to the barriers for the design and engineering of crashworthiness for welding-intensive auto body structures. The project will cover the range of AHSSs, weld configurations, welding conditions, and loading modes required for industry CAE implementation. The outcome is an optimized model that can be implemented in crash simulation FEA codes used by the automotive crash modelers.

A three-pronged approach, supported by experimental data, was used to develop the new spot weld modeling methodology:

- a spot weld element (SWE) formulation and associated constitutive models optimized for robustness in CAE simulation, with the complexity to incorporate weld geometry and microstructure effects;
- a physics based, integrated, electrical-thermal-mechanical-metallurgical spot weld process model to generate the weld geometry, microstructure, and residual stress results needed by SWE; and
- a companion weld characterization and impact test database for development and validation of the new spot weld modeling approach.

Figure 1 shows the overall research and development (R&D) plan and approach to develop the SWE for advanced crashworthiness CAE.

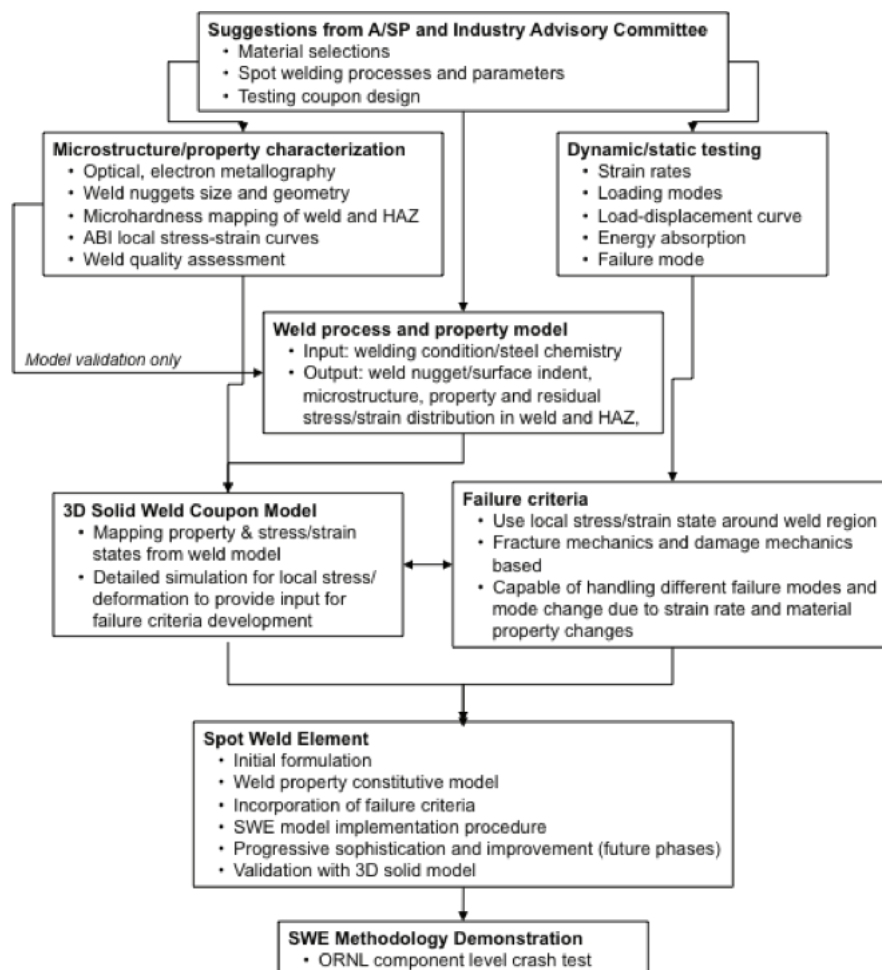


Figure 1. Organization and relationship among different R&D tasks.

Because of the complexity and the scope of the efforts required to develop and mature this new modeling methodology, this project was divided into two phases. Phase I, completed in FY 2009, was a concept feasibility effort aimed at developing the initial version of the SWE modeling approach and generating the companion testing data for an initial set of steels, weld configurations, and impact testing conditions. Phase II, started in FY 2010, is a comprehensive technical feasibility R&D effort which covers a wide range of AHSSs, thickness ranges, weld configurations and microstructures to refine, improve, mature, validate, and demonstrate the SWE methodology for eventual implementation in CAE by the industry users.

Results and Discussion

In FY 2010, we extended the integrated electrical-thermal-mechanical-metallurgical weld process and property model to successfully simulate 3T (i.e., three layers of sheet metal) stackups, sheet-to-sheet gaps, and ultra-high-strength steels (such as boron steel) in which heat-affected zone (HAZ) softening is of concern in crash performance.

Figure 2 shows the simulation of temperature evolution during RSW of a three-layer stackup of an uncoated DP600 steel. The initial interfacial heating at the faying surfaces of the sheet metal was clearly observed, which suggests the roles of interface contact resistance in the formation of weld. As the temperature increases, the bulk electric resistance of the material increases. The dominant heating mode is the bulk joule heating.

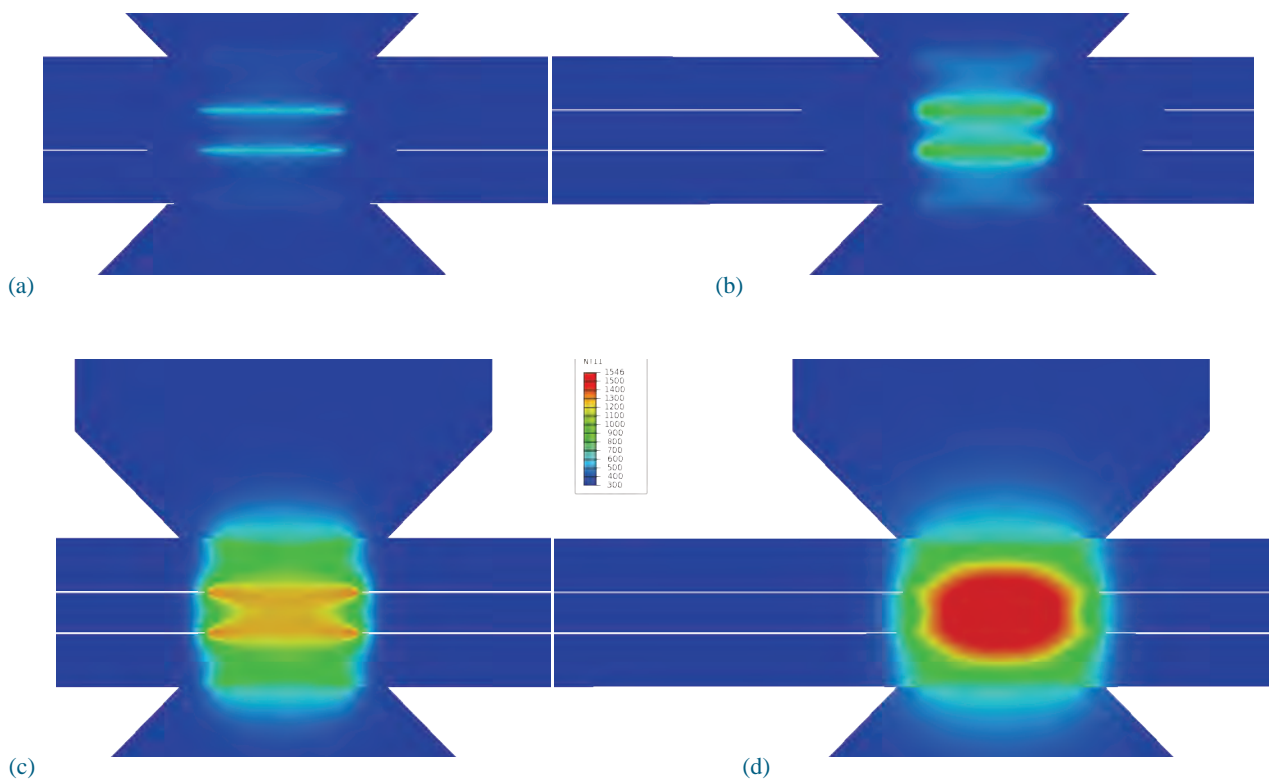


Figure 2. Temperature evolution in a 3T stackup resistance spot weld made of a DP600 steel (a) after one welding cycle, (b) after two and a half welding cycles, (c) after four and a half welding cycles, and (d) after nine welding cycles.

Figure 3 presents the predicted distributions of microhardness in a DP600 AHSS (3T stackup) and a boron AHSS (2T with 0.5 T initial gap). The DP600 steel (initial hardness of 200 Hv) exhibited considerable hardening of the weld nugget (>350 Hv) due to the formation of martensite. The hardness in the HAZ outside the weld nugget exhibits complex hardening and softening partners, although the extent of hardening and softening is relatively small (within the range of 180–290 Hv). The boron steel weld shows a narrow but considerably softened HAZ (~360 Hv) surrounding the moderately hardened weld nugget (~520 Hv) compared to a base metal hardness of 490 Hv. The above model predictions are consistent with the general observations of weld hardness variations in AHSS. More rigorous experimental validation of the model and necessary refinement are planned in FY 2011.

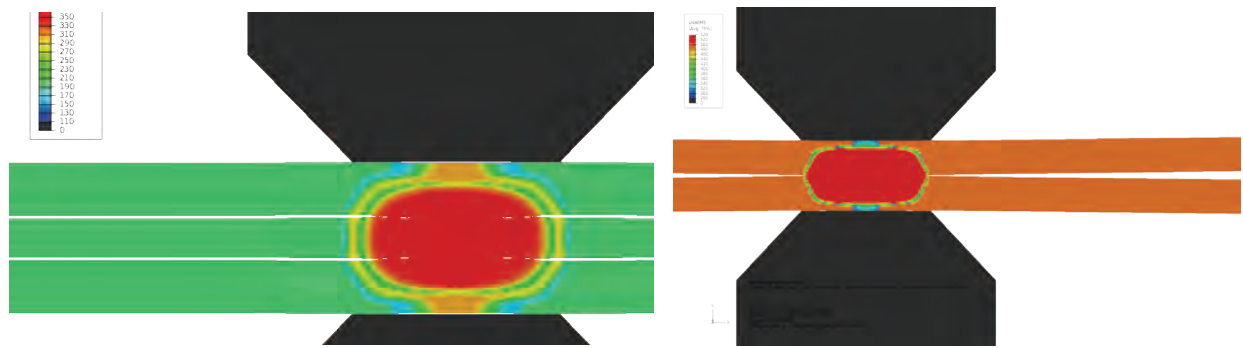


Figure 3. Predicted microhardness distribution in (a) DP600 steel, 3T stackup, and (b) boron steel, 2T stackup with an initial 0.5 T sheet-to-sheet gap.

In addition to the above modeling development, the project had extensive communications and meetings with the industry advisory committee, OEMs, and steel suppliers to finalize a companion experimental and impact testing program to support the development and validation of the developed models.

Conclusions

The integrated electrical-thermal-mechanical-metallurgical resistance spot weld process and performance model formulation have been successfully extended to handle the 3T stackup and sheet gap situations that are commonly encountered in auto body structure welding. The integrated formulation has been shown to be stable and robust and can be used to provide the microstructure and local property variations (including the HAZ softening) as input to the SWE model.

Friction Stir Spot Welding of Advanced High-Strength Steels II

Principal Investigator: Michael Santella, Oak Ridge National Laboratory
(865) 574-4805; e-mail: santellaml@ornl.gov

Introduction

An initial project on FSSW of AHSSs addressed some basic questions such as whether FSSW of AHSSs can be accomplished with currently available tool materials and whether FSSWs made in HSSs could develop acceptable tensile lap-shear strengths. Efforts were also made to improve joint strength through systematic investigations into weld process parameters and tool design. This was accomplished primarily by using redesigned tools and refined operating parameters, the selection of which was guided by analysis of process output data, microstructure analysis, and strength testing.

Two important conclusions of the initial project related to process cycle time and tooling costs. For FSSW to be accepted as a reasonable alternative to RSW in automobile manufacturing, it must not impose too large of a penalty in weld cycle time. Resistance spot welds on steels like DP780 can be made in a fraction of a second. This is largely due to the high welding currents used and the fact that contact resistance at the sheet-sheet interfaces promotes rapid heating and melting at those locations. The rapid melting at sheet-sheet interfaces is an essential feature of bonding in RSW. In contrast, FSSWs rely on the conduction of heat from tool-sheet interfaces and viscous dissipation to raise the temperature of the sheet-sheet interfaces. Rather than melting, it is the combined effects of time, temperature, pressure, deformation, and recrystallization that lead to metallurgical bonding in FSSW. It is unlikely that this process will ever have spot welding times competitive with those of RSW.

Secondly, analysis of FSSW total process costs indicated that at \$100 per tool, stir tools would need to survive for about 26,000 welds for FSSW to be equivalent in cost to RSW. Higher stir tool costs would demand significantly higher lives to meet the same criterion. On the other hand, as the cost of stir tools drops, the difference in process costs decreases, making FSSW more competitive with RSW. The cost of PCBN tools used for the initial project was considerably higher than \$100 per tool. While no systematic study of tool durability was done, experience suggests that PCBN tool life would likely be

on the order of 500–1,000 spot welds on steels like DP780. Based on these observations, reducing the cost of tooling or significantly increasing durability are the critical hurdles for FSSW to compete directly with RSW of steels. Alternatively, there must be other compelling technical reasons to use FSSW on steels rather than RSW.

Approach

This task is a 50-50 collaboration between ORNL and PNNL. It includes a panel of consultants with representatives from Chrysler, Ford, and GM. Consultants from MegaStir (PCBN friction stir tool manufacturer), Ceradyne (Si3N4 manufacturer), and Kawasaki (robot manufacturer) also participate on an as-needed basis. Initial studies will use existing inventories of TRIP590, TRIP780, and hot-stamp boron steel (sourced from a Swedish supplier, the parent of US Hardtech). Additional alloys of interest to the OEMs will be included.

The FSSW will be done using both PCBN and Si3N4 tools. The spot welding is done in displacement-control mode by varying the parameters of tool plunge depth and tool plunging rate. In addition to these control parameters, other process variables are typically recorded for each weld including weld time, spindle torque, normal force, and temperature on the back side of the two-sheet stackups. This additional information is archived for future use and analysis.

Joint properties will be evaluated initially by tension testing lap joints to determine their shear-tension strengths. Depending on those results, more extensive testing will be done to measure fatigue strength, T peel strength, and cross-tension strength. Typical metallographic techniques and microhardness mapping will be used to further assess joint characteristics and properties.

Results and Discussion

Several series of spot welds were made using a 1.5 mm thick TRIP steel provided by GM. The steel was reported to be uncoated. The stir tools used for these welds included existing designs of PCBN as well as newly acquired tools manufactured from Si3N4. Welds were made using both one-step and two-step procedures, and tool rotation speeds of 800 and 1,600 rpm. The welding time was fixed at 4 s so that strength results could be compared with existing datasets. The various welding details and lap-shear strength results are presented in Table 1.

A total of five spot welds were made for each condition. Four of the welds were tested for lap-shear strength and one was reserved for metallographic analysis. The strength values in Table 1 represent averages for the four specimens. The boron nitride (BN) tools are made of PCBN; the silicon nitride tools are made of Si3N4. This TRIP steel had a nominal strength of 780 MPa; thus, the BN97 welds at 1,600 rpm and the two-step BN46 welds exceeded American Welding Society Specification D8.1 minimum values. Initial testing of FSSWs made with an uncoated TRIP780 steel indicated they are capable of exceeding the minimum values required of resistance spot welds.

Tooling ^a	rpm	Steps	Lap-Shear Strength (kN)
BN97	800	1	9.7
	1,600	1	11.3
	1,600	2	15.1
BN46	1,600	1	8.1
	1,600	2	12.5
SN77	1,600	1	6.14
SN97	1,600	2	5.3

^aBN = boron nitride tooling; SN = silicon nitride tooling.

Table 1. Initial results for FSSW of uncoated TRIP steel.

Conclusions

Initial testing of FSSWs made with an uncoated TRIP780 steel indicated they are capable of exceeding the minimum values required of resistance spot welds.

Friction Stir and Ultrasonic Solid-State Joining of Magnesium to Steel

Principal Investigator: Michael Santella, Oak Ridge National Laboratory
(865) 574-4805; e-mail: santellaml@ornl.gov

Introduction

Increasing the use of lightweight materials and implementing manufacturing technologies that enable the use of lightweight materials are the two primary paths toward passenger vehicle weight reduction. In some situations, lightweight materials can be directly substituted for higher density materials, but there are barriers to direct substitution. In a modern, multi-material vehicle, lightweight materials such as Al and Mg alloys can be a challenge to attach to the underlying substructure, which is usually composed of steel. Joining methodologies available in the cost range amenable to automotive manufacturing include RSW, adhesives, linear fusion welding, hemming, clinching, bolting, and riveting. However, because of the highly dissimilar natures of the materials, Mg-steel joints are problematic. Mg-to-steel joints cannot be simply fusion welded due to the extreme differences in their melt temperatures, and solid-state methods that require large amounts of plastic strain such as riveting suffer from the poor ductility of Mg due to its hexagonal crystal structure.

Alternative joining methodologies such as FSW, FSSW, and USW may be able to overcome traditional barriers to join and construct hybrid Mg-steel components. These solid-state joining methods provide unique joining capabilities that if realized may potentially produce faster and more economical alternatives to current technologies (bolting/riveting). However, FSW and USW for dissimilar Mg-steel combinations are significantly underdeveloped for broad deployment.

The purpose of this project is to develop an applied understanding of the

- localized metal forming and metallurgical bonding that develops during FSW, FSSW, and USW;
- influence of process parameters on joint strength and performance; and
- properties of joints made with both types of process (i.e., friction stir type and USW) including lap-shear strength, fatigue properties, corrosion issues, and microstructural characteristics.

Approach

This project is designed to overcome many of the technical barriers to implementing FSW and USW technologies. Task 1 focuses on systematically evaluating the application of ultrasonic spot welding to make lap joints of Mg to steel. It features a decision gate of achieving lap-shear strengths of at least 1 kN as an indication of technical feasibility of the approach. Task 2 concentrates on improving joint strength through modification of process controls and on investigating the fundamental metallurgical aspects of bond formation. An initial evaluation by metallographic examination and lap-shear testing of ultrasonic spot welding of cast Mg alloys will also be done. The objectives of Task 3 are to evaluate fatigue properties of Mg-steel ultrasonic spot welds and to consider strategies to control corrosion in the joints. The tasks are oriented to developing information useful to manufacturers in their decision making processes. However, the intention is to develop a basic understanding of the feasibility of making Mg steel joints and of the general usefulness of USW.

Results and Discussion

The ultrasonic welds were made with a Sonobond CLF2500 using a pedestal welding station. The rated conditions at the welding tip on this equipment are 20 kHz frequency with 25 μm amplitude. The sonotrode tips are made from T1 steel. They typically have flat, rectangular faces with dimensions of either 5 mm by 7 mm or 7 mm by 7 mm. The line pressure to the tip clamping mechanism was adjusted to make the welds under a constant nominal pressure of 39 MPa.

The materials used for the current experiments were sheets of 0.8 mm thick hot-dip-galvanized (HDG) mild steel and 1.6 mm thick AZ31B-H24. The zinc coating on the steel is about 9 μm thick. The surfaces of the AZ31B sheet are buffed with nonmetallic abrasive pads (Scotch-Brite) before welding to remove surface oxides and produce shiny surfaces. Both metals were also degreased with acetone followed by isopropyl alcohol to remove lubricants and surface debris.

Coupons of AZ31 nominally 30 mm wide by 100 mm long were welded to mild steel coupons of the same size to produce specimens for mechanical testing and metallographic analysis. A 25 mm overlap was used for making lap-welded coupons with spot welds centered in the overlap regions. Specimens were positioned for welding so that the primary vibration

direction of the sonotrode was perpendicular to their long axes. Spot welding is typically performed using powers of 1,500–2,500 W. Welding times typically range from 0.2–1.2 s.

The results of the tensile lap-shear testing are presented in Figure 1, where the variations of failure load with welding time are plotted. With both tips there was an initial rapid rise in lap-shear failure load from around 0.5 kN to near 2.9 kN as the welding times increased from 0.2 to 0.4 s. After the rapid increase, failure loads continued increasing with welding times but at a much lower rate. From 0.4 to 1.2 s, failure loads increased to a maximum average value of 3.7 kN for the 5 mm by 7 mm tip and 4.2 kN for the 7 mm by 7 mm tip. Welds of the AZ31 to bare steel were unsuccessful. Weak bonding occurred in this case, but joints could be easily broken by hand.

The lap-shear strength results can be placed in perspective by comparison with data from resistance spot welds and FSSWs of AZ31. The pioneering work of Klain and coworkers (Klain, Knight, and Thorne, 1953) confirmed that AZ31 could be resistance spot welded with lap-shear strengths ranging up to 5.7 kN. Lap-shear strengths increased with spot diameters and were about 4.0 kN for diameters with areas equivalent to the 7 mm by 7 mm USW tip. More recent work by Lang and coworkers (Lang et al., 2008) measured lap-shear strengths up to 3 kN for spot welds of AZ31 with nugget diameters of about 7 mm. Pan and coworkers (Pan et al., 2007) showed that AZ31 sheet could be friction stir welded, and some joints had lap-shear strengths as high as 4.75 kN. No comparable published data could be found for Mg steel spot-welded joints made by these two processes. Nevertheless, strengths for ultrasonically welded joints at times greater than about 0.5 s consistently exceeded 3 kN, and so they are generally consistent with values found for Mg-Mg spot welds.

The results of the fatigue testing are shown in Figure 2, where the fatigue life expressed as cycles to failure is plotted against the load range for testing. The USW spot welds were tested at constant values of $R = 0.1$ and $R = 0.2$, where $R = \text{minimum load}/\text{maximum load}$. There is little published information for similar or dissimilar spot welds involving Mg alloys, and Figure 2 compares the USW data to similar data for FSSWs of AZ31-to-AZ31. Regression analysis was used for the lines drawn through the USW data at $R = 0.1$ and the FSSW data of $R = 0.0$. However, a single line could have been fit through the entire combined data set. This suggests the fatigue properties of the AZ31-steel USW spots welds will not differ significantly from FSSW welds made using AZ31.

Conclusions

Spot welds with lap-shear strengths up to 4.2 kN can be made between sheets of AZ31-H24 and HDG steel by USW. These lap-shear strengths are comparable to those of Mg-Mg joints made by both RSW and FSSW. The fatigue properties of the AZ31-steel USW spot welds appear comparable to those of FSSWs of AZ31-AZ31.

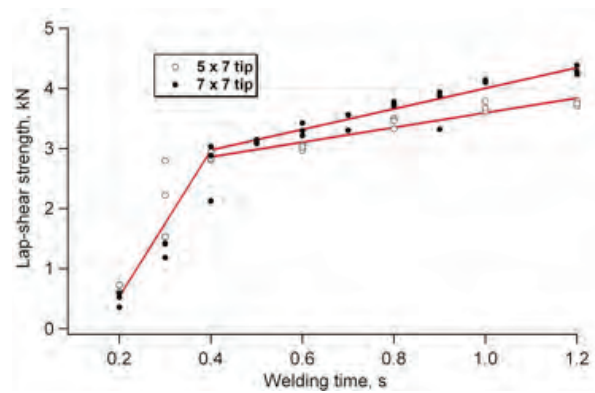


Figure 1. Variations of lap-shear strength with welding time and tip size.

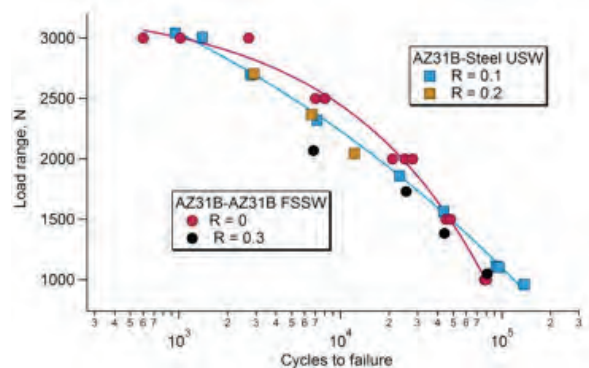


Figure 2. Variations of fatigue life expressed as cycles to failure with loading range.

Online Weld Quality Monitor and Control with Infrared Thermography

Principal Investigator: Zhili Feng, Oak Ridge National Laboratory
(865) 576-3797; e-mail: fengz@ornl.gov

Principal Investigator: Hsin Wang, Oak Ridge National Laboratory
(865) 576-5074; e-mail: wangh2@ornl.gov

Principal Investigator: Wei Zhang, Oak Ridge National Laboratory
(865) 241-4905; e-mail: zhangw@ornl.gov

Introduction

Welding is an essential enabler for multi-material vehicles for lightweight and fuel economy improvement. For instance, the development of the RSW process for joining AHSSs is crucial for assembling the AHSS intensive automotive body structure, resulting in a 16% weight reduction for body-in-white (BIW) [Lotus, 2010]. Variations in welding conditions, part fit-up, and other production conditions inevitably occur in the complex, high-volume BIW assembling process. These variations can result in out-of-tolerance joints that impair the quality and performance of the vehicles. The increasing usage of multi-materials is expected to pose even more stringent requirements on the joint quality. Reliable quality inspection techniques are crucial for ensuring high-quality joints on the assembly line. The high-volume, mass production nature of an automotive plant dictates that any new quality inspection technology needs to be low cost, have a fast cycle time, and be highly accurate to be successfully adopted by the automotive industry. In Phase I of this project, the proof-of-principle study, the feasibility and effectiveness of IR thermography for weld quality inspection were successfully demonstrated. However, a research-grade IR camera was used, and the cost of the IR camera was very high. In this phase, a weld inspection system based on a low cost IR camera was demonstrated for both postmortem and real-time applications. To accurately correlate the recorded temperature-time profiles to weld quality characteristics, an advanced multiphysics model was used to provide fundamental understating of the heat transfer during RSW of different materials and thicknesses.

Approach

A major component of the field-deployable quality inspection system is the IR camera. Based on Phase I results, key specifications for the IR camera performance matrix (such as temperature sensitivity and sample frequency) were formulated. A comprehensive market survey was conducted to understand the state of the art of low cost IR cameras. A low cost, commercially available off-the-shelf camera which met or exceeded the performance specifications was acquired. This camera costs a small fraction (about one-sixth) of research-grade cameras, and it is expected to significantly decrease the capital cost of the entire inspection system. The camera was thoroughly evaluated for both postmortem and real-time quality inspection applications. A filter is installed to allow the camera to operate in either standard-temperature range (-20°C to 120°C) or high-temperature range (250°C to $1,200^{\circ}\text{C}$). The former is suitable for the postmortem application where the surface temperature change is less than 30°C . The latter works well for the real-time application, where the weld cools down rapidly from near melting to room temperature.

The IR camera records an extremely large amount of temperature-time history data, where a wealth of information related to weld quality is buried deeply. Temperature fingerprints (or thermal signatures) are used as accurate indicators for weld quality characteristics. A validated multiphysics model, developed at ORNL (Feng, 2003; Feng, 1998), is used to calculate the heat transfer during RSW of different materials and

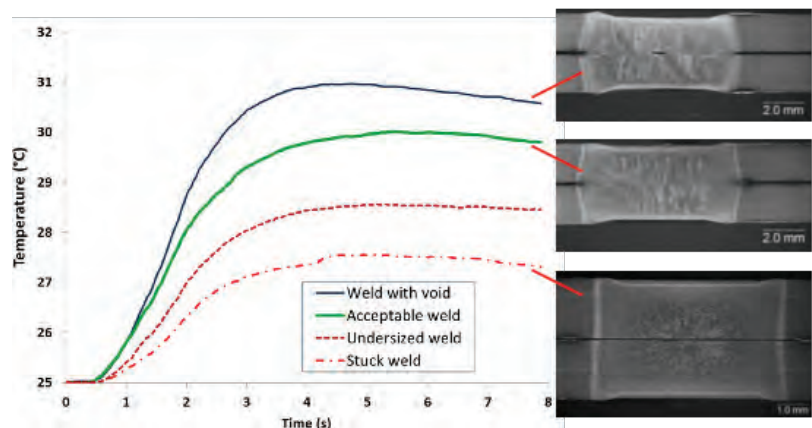


Figure 1. Postmortem weld quality inspection based on temperature-time profiles recorded using the low cost IR camera for the controlled welds with different weld quality attributes.

thicknesses. This advanced numerical model is based on finite-element analysis of coupled thermal-electrical-metallurgical-mechanical phenomena. The calculated results provide insight into the temperature evolution during welding, which is crucial to identifying reliable temperature fingerprints.

Results and Discussion

The evaluation of the low cost IR camera for postmortem inspection applications was performed on a set of existing reference samples which were used for the high cost research camera in Phase I. These reference samples were made of dual phase (DP) 590 zinc-coated steel with a thickness of 1.8 mm, commonly used in the automotive BIW. As shown in Figure 1, welds with different defects and geometry attributes exhibit highly distinguishable transient temperature profiles. Temperature fingerprints such as peak temperature, heating rate, and cooling rate can be readily used to differentiate weld quality attributes.

The experimental setup for evaluating the low cost IR camera for real-time inspection is shown in Figure 2. The joint is a 2T stackup consisting of two 1.5 mm thick uncoated DP 780 steel sheets. A series of spot welds was made by varying the heating time from 0.03 to 1 s while keeping all other welding parameters unchanged. The “stuck” weld, a major defect where the weld appears normal on the surface but fails prematurely under loads, shows lower peak temperature and slower cooling rate compared to the weld with minimal nugget size. Data analysis is ongoing to identify additional temperature fingerprints for quantitatively evaluating the weld quality characteristics.

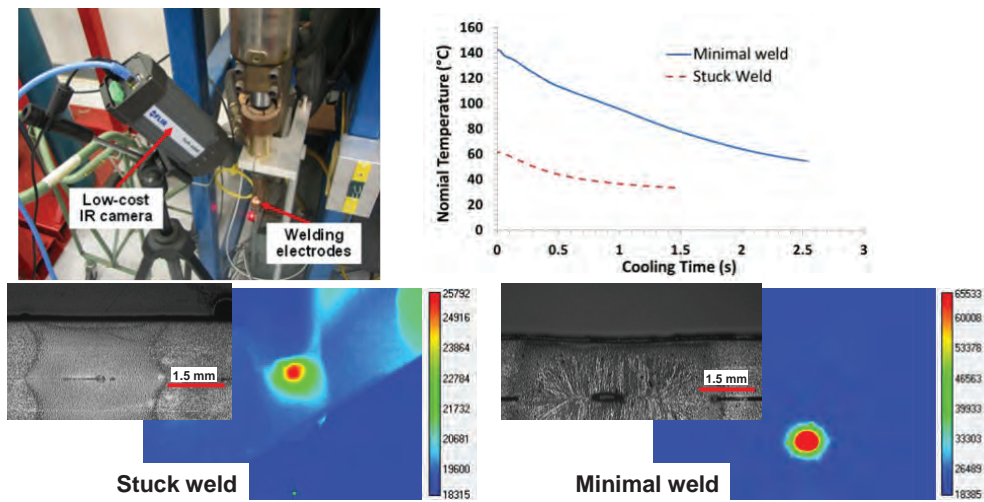


Figure 2. Real-time weld quality inspection using the low cost IR camera.

Using the multiphysics model for RSW, the evolution of temperature, deformation, and stress was quantitatively calculated. Figure 3 shows the distribution of peak temperature in two joint configurations (2T vs 3T) commonly encountered in BIW. In the 2T configuration, the heat generated from the faying surfaces of the two steel sheets was sufficient to soften the material. The electrodes were able to indent the steel surfaces. In the 3T configuration, the steel surfaces, which were in contact with the electrodes, remained at a relatively low temperature. The material was still hard enough to prevent the electrode from causing any indentation.

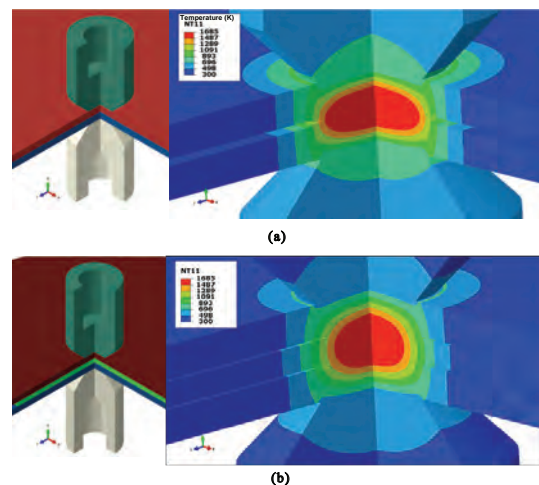


Figure 3. Predicted temperature distribution in two joint configurations of DP 590 steel sheets: (a) two sheet stackup configuration (2T); (b) three-sheet stackup configuration (3T).

Figure 4 plots the predicted cooling curves at three monitoring locations on the sheet top surface with different distances to the weld center. The peak temperature at the same distance to the weld center is lower in 3T configuration than 2T configuration, while the cooling rate is faster. The predicted temperature-time data shown in Figures 3 and 4 will be further analyzed to identify temperature fingerprints for the weld quality attributes.

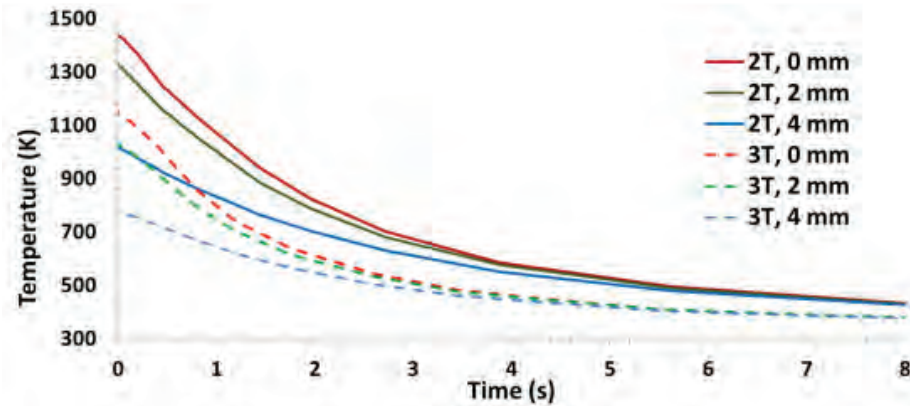


Figure 4. Predicted cooling curves at three monitoring locations on the sheet top surface with different distances (0 to 4 mm) to weld center in the 2T and 3T joint configurations.

Conclusions

In this first year of the 3-year-long Phase II task, a low cost IR camera was acquired and demonstrated to have sufficient temperature sensitivity, spatial resolution, and sampling rate for both postmortem and real-time applications. The advanced multiphysics model provided quantitative understanding of the evolution of temperature and deformation during RSW. These major advances, along with continued support from industrial advisors (automotive OEMs and steel suppliers), lay the solid foundation for further development of the reliable and cost-effective weld quality inspection system. Resistance spot weld tests, to be conducted at ArcelorMittal as part of the industry participation and cost sharing, were originally planned for this fiscal year to study steel grades, sheet thicknesses, and surface coatings that are typical in auto BIW structures. Due to unforeseen circumstances, the testing schedule was postponed to the late October–November 2010 time frame. This delay in the testing is not expected to significantly impact the progress and milestones originally planned for the second and third years of the Phase II task.

Conclusions

This project comprises four tasks aimed at developing the computational tools, process methodologies, and inspection methods for welding lightweighting metals. The integrated electrical-thermal-mechanical-metallurgical resistance spot weld process and performance model formulation has been successfully extended to handle the 3T stackup and sheet gap situations that are commonly encountered in auto body structure welding. The integrated formulation has been shown to be stable and robust and can be used to provide microstructure and local property variations (including HAZ softening) as input to the SWE model. This model will be used by designers to aid in vehicle structural designs using AHSSs.

Methods are being developed for FSSW of martensitic hot-stamp boron steel and TRIP steels. Those efforts include looking at potential tool materials and assessing their durability and economics. Liquid metal embrittlement of sheet steels and stir tools by zinc is also being characterized. Initial testing of FSSWs made with an uncoated TRIP780 steel indicates that they are capable of exceeding the minimum values required of resistance spot welds.

Solid-state joining between automotive sheet steel and Mg alloys is under development. Both FSW and USW are used to study the potential for creating structural bonds between these dissimilar materials. Detailed investigations into the joint characteristics include an evaluation of joint strength, microstructure, chemical structures, and alloy formation. Spot welds with lap-shear strengths up to 4.2 kN can be made between sheets of AZ31-H24 and HDG steel by USW. These lap-shear strengths are comparable to those of Mg-Mg joints made by both RSW and FSSW. The fatigue properties of the AZ31-steel USW spot welds appear comparable to those of FSSWs of AZ31-AZ31.

An NDE method is under development as a reliable, robust, low cost, and affordable means to quantitatively inspect spot weld quality in an automotive manufacturing plant. To date, a low cost IR camera has been acquired and demonstrated to

have sufficient temperature sensitivity, spatial resolution, and sampling rate for both postmortem and real-time applications. The advanced multiphysics model for data interpretation provides a quantitative understanding of the evolution of temperature and deformation during RSW. Because of unforeseen circumstances, the testing schedule has been postponed to November 2010. This delay in the testing is not expected to significantly impact the progress and milestones originally planned in the second and third years of this Phase II task.

Presentations / Publications / Patents

Chao, Y. J.; Kim, Y.; Feng, Z.; Simunovic, S.; Wang, K.; Kuo, M. Dynamic Spot Weld Testing. 2009 SAE World Congress, Detroit, Michigan, USA, Paper 2009-01-0032.

Feng, Z.; Simunovic, S.; Chao, B.; Wang, K.; Belwafa, J.; Chen, M. Impact Modeling and Characterization of Spot Welds. International Auto Body Congress (IABC) 2009, Nov 4–5, 2009, Troy, Michigan.

Feng, Z.; Wang, H.; Zhang, W. Expert System For Non-contact Weld Quality Inspection Using Infrared Imaging, ORNL Invention Disclosure, September 2010.

Hovanski, Y.; Santella, M. L.; Grant, G. J. Friction Stir Spot Welding of Advanced HSS. Presented at and published in the proceedings of Materials Science & Technology, October 2009.

Hovanski, Y.; Santella, M. L.; Grant, G. J. Friction Stir Spot Welding of Advanced HSS. Presented at IABC, Troy, Michigan, November 2009, and published in conference proceedings of International Automotive Body Conference, 2009.

Santella, M. L.; Franklin, T.; Pan, J.; Pan, T.Y.; Brown, E. Ultrasonic Spot Welding of AZ31B to Galvanized Mild Steel. SAE Paper 2010-01-0975, April 2010 (also accepted for SAE Transactions journal).

Santella, M. L.; Hovanski, Y.; Frederick, A.; Grant, G. J.; Dahl, M. E. Friction Stir Spot Welding of DP780 Carbon Steel. Science and Technology of Welding and Joining 2010, 15(4), pp 271–278.

Wang, H.; Feng, Z.; Zhang, W. Non-destructive Inspections of Welds and Joints using Infrared Imaging and Induction Heating, ORNL Invention Disclosure, March 2010.

References

Feng, Z.; Babu, S. S.; Riemer, B. W.; Santella, M. L.; Gould, J. E.; Kimchi, M. Modeling of Resistance Spot Welds—Process and Performance. Weld Res Abroad, 2003, 49, pp 29–35.

Feng, Z.; Gould, J. E.; Babu, S. S.; Santella, M. L.; Riemer, B. W. An Incrementally Coupled Electrical-Thermal-Mechanical Model for Resistance Spot Welding. In ASM Proc. Int. Conf. 5th Trends Weld. Res.; Vitek, J. M., Ed.; et al., Pine Mountain, Georgia, 1998, pp 599–604.

Joost, W. Vehicle Technologies Program – Lightweight Materials. Presentation. p. 12.

Klain, P.; Knight, D. L.; Thorne, J. P. Spot Welding of Mg with Three-Phase Low Frequency Equipment. Welding Journal. 1953, 32, pp 7–18.

Lang, B.; Sun, D. Q.; Li, G. Z.; Qin, X. F. Effects of Welding Parameters on Micro-Structure and Mechanical Properties of Resistance Spot Welded Mg Alloy Joints. Science and Technology of Welding and Joining. 2008, 13, pp 698–704.

Lotus Engineering Inc., An Assessment of Mass Reduction Opportunities for a 2017 – 2020 Model Year Vehicle Program, March 2010.

Pan, T.-Y.; Santella, M. L.; Mallick, P. K.; Frederick, A.; Schwartz, W. J. A Feasibility Study on Spot Friction Welding of Mg Alloy AZ31. In Friction Stir Welding and Processing IV, Minerals, Metals and Materials Society (TMS), Warrendale, Pennsylvania, 2007.

G. Multi-Material Enabling - Pacific Northwest National Laboratory

Field Technical Monitor: Dean Paxton
Pacific Northwest National Laboratory
902 Battelle Boulevard; P.O. Box 999; Richland, WA 99352
(509)375-2620; e-mail: dean.paxton@pnl.gov

Technology Area Development Manager: William Joost
U.S. Department of Energy
1000 Independence Ave., S.W.; Washington, DC 20585
(202) 287-6020; e-mail: william.joost@ee.doe.gov

Contractor: Pacific Northwest National Laboratory (PNNL)
Contract No.: DE-AC05-00OR22725 & DE-AC06-76RLO1830

The Multi-Materials Enabling project consists of two tasks focused on research and development that can lead to greater implementation and manufacturing of multi-material lightweight components/systems in automotive applications. The tasks include: 1) Friction Stir Spot Welding of Advanced HSS (follow-on) and 2) Friction Stir and Ultrasonic Solid-State Joining of Mg to Steel. The objectives, accomplishments and future direction for these tasks are provided below:

Objectives

- Establish the applied technical understanding necessary to produce robust joints between Mg alloys and steel using the solid-state processes of friction stir welding (FSW) and ultrasonic welding (USW) such that structural joining of Mg products may be accomplished without the need for mechanical fastening.
- Develop the fundamental relationships influencing metallurgical, mechanical, and chemical aspects of bond formation. Evaluate the responses of the processes to changing alloys, product forms, and surface conditions.
- Demonstrate the feasibility of producing acceptable friction stir spot welding (FSSW) joints in high-strength steels with the transformation-induced plasticity (TRIP) effect and other difficult-to-join steels to facilitate additional down gauging and usage of high-strength ductile steel alloys.
- Characterize the effects of liquid-metal embrittlement on both the steel work materials and on the friction stir tooling such that joining of coated AHSSs may be further enabled as part of a near-term lightweight solution.
- Compare the wear and durability performance of polycrystalline boron nitride (PCBN) to silicon nitride (Si₃N₄) tooling.

Accomplishments

- Completed initial investigation into bond formation and performance of Mg to steel joints, including microanalysis procedures to begin establishing bonding mechanisms.
- Completed secondary milestones demonstrating the ability to structurally join Mg to steel using both FSW and USW solid-state techniques.
- Completed initial evaluation of FSSW in TRIP, DP980, and dissimilar AHSS alloys.

Future Directions

- Identification and characterization of liquid-metal embrittlement phenomena in AHSS.
- Interaction with equipment suppliers so that their constraints help guide decisions about welding parameters and tooling.
- Concentrated evaluation of candidate materials for friction stir tools, including comparative wear testing and durability studies.
- More comprehensive characterization of mechanical behavior including fatigue strength, T-peel strength, cross-tension strength, possibly impact behavior, and metallurgical examinations.
- Understanding the effects of mixed AHSS systems on FSW joint properties.
- Evaluation of fatigue, corrosion, coatings, and adhesives on solid-state joints between Mg and steel.

Introduction

The realization of significant weight savings in passenger and commercial vehicles is likely to occur through the use of a variety of advanced materials. While improvements in the properties, manufacturability, and cost of advanced materials are critical in achieving vehicle weight reduction, technologies that support the use of these materials in a multi-material system are equally important. Unlike a single-material system, structures composed of different metals and polymer composites present significant challenges in areas such as joining, corrosion, recycling, and nondestructive evaluation. Work conducted in this agreement seeks to overcome these challenges by developing new techniques, establishing standards, and preparing advanced technologies for a production environment.

Joining in advanced material systems requires significant changes in process and technique as compared to conventional structures. The use of fusion welding is limited by thermal conductivity or microstructural sensitivity in single advanced-material joints; fusion welding can be nearly impossible for many multi-material joints due to differences in melting temperature or the potential for formation of brittle intermetallics.

The following sections outline specific task work conducted at Pacific Northwest National Laboratory (PNNL) in the area of multi-material enabling technologies. Each task supports one or more goals within the Multi-Material Enabling Agreement.

Activity and Developments

Friction Stir Spot Welding of Advanced High-Strength Steel Follow-on

Principal Investigator: Yuri Hovanski, Pacific Northwest National Laboratory
(509) 375-3940; e-mail: Yuri.Hovanski@pnl.gov

Principal Investigator: Michael L. Santella, Oak Ridge National Laboratory
(865) 574-4805; e-mail: santellaml@ornl.gov

Introduction

An initial project on FSSW of AHSSs addressed some basic questions such as whether FSSW of AHSS can be accomplished with currently available tool materials, and FSSW made in high-strength steels could develop acceptable tensile lap-shear strength. Efforts were also made to improve joint strength through systematic investigations into weld process parameters and tool design. This was accomplished primarily by using redesigned tools and refined operating parameters, the selection of which was guided by analysis of process output data, microstructure analysis, and strength testing.

This follow-on project is designed to address several of the conclusions of the initial project, including characterization of tool life and durability, and to address the overall cost and availability of tooling and equipment capable of producing friction stir spot welds in AHSS alloys. Work also continues in developing the appropriate process parameters for AHSS that are problematic to resistance spot welding (RSW), including coated TRIP steels and dissimilar thickness and alloy combinations.

Approach

The project is a 50/50 collaboration between ORNL and PNNL. Additionally, it includes a panel of consultants including representatives from Chrysler, Ford, and General Motors (GM). Consultants from companies such as MegaStir (PCBN friction stir tool manufacturer), Ceradyne (Si₃N₄ manufacturer), and Kawasaki (robot manufacturer) also participate on an as-needed basis.

The primary focus of this project is the development of FSSW parameters, tooling, and equipment for AHSS alloys that cannot be acceptably resistance spot welded. Using previous work as a guide, parametric studies will be done to attempt optimization of FSSW in alloys that cannot be acceptably resistance spot welded based on a balance of joint strength properties and weld cycle time. The influence of stir tool design will be included in the effort. Joint properties will be evaluated initially by tension testing lap joints to determine their shear-tension strengths. Depending on those results, more extensive testing will be done to measure fatigue strength, T-peel strength, cross-tension strength, and possibly impact behavior. The usual metallographic techniques and microhardness mapping will be used to further assess joint characteristics and properties.

Additionally, the effects of zinc coatings applied to C steel sheets for corrosion protection will be evaluated. Liquid zinc can embrittle steel through a process known as liquid-metal embrittlement (LME), and zinc can similarly attack stir tool materials. The effects of both liquid and solid zinc being stirred into spot welds, in addition to their influence of microstructure, strength properties, and fracture behavior, are not well characterized. Initial studies will use existing inventories of TRIP590, TRIP780, and hot-stamp boron steel (HSBS, sourced from a Swedish supplier, the parent of US Hardtech). Additional alloys of interest to the original equipment manufacturers (OEMs) will be included as they are acquired.

The initial project demonstrated that PCBN stir tools are effective for welding steels. However, their cost is high relative to their apparent durability. In addition, there appears to be a limited number of suppliers of PCBN stir tools. The material formulations on PCBN used for stir tools are evolving with manufacturers such as MegaStir claiming improved performance. In addition, other ceramic-based materials such as silicon nitride appear to have some potential as lower-cost tool stock. Identifying the intrinsic limitations of candidate tool materials is an essential aspect of developing more effective, durable, economical tooling. As such, tool durability will be performed as part of this study.

Technology Transfer Path

The main focus of technology transfer is related to tooling and equipment. Thus a process database with effective loads, temperatures, and operating parameters is being shared with tool providers to allow them to more efficiently design and manufacture appropriate tooling for FSSW of AHSS. Additionally, the same data is being supplied to machine manufacturers and automotive OEMs to help distinguish the needs associated with implementation of this process, leading to appropriate deployment.

An additional arm of the technology transfer is associated with the front of the process, as the near-term need for AHSS have been supplied from the OEMs and AHSS providers. This knowledge is critical to identify those alloys and combinations that would lead to near-term lightweight solutions, while addressing areas that currently do not have effective solutions.

Results and Discussion

Several series of spot welds were made using 1.5 mm thick TRIP steel provided by GM. The steel was reported to be uncoated. The stir tools used for these welds included existing designs of PCBN and newly acquired tools manufactured from

Si3N4. As for previous evaluations, welds were made using both one-step and two-step procedures, and tool rotation speeds of 800 rpm and 1600 rpm. The welding time was fixed at 4 s so that strength results could be compared with existing datasets. The various welding details and lap shear strength results are presented in Table 1.

A total of five spot welds were made for each condition. Four of the welds were tested for lap-shear strength, and one was reserved for metallographic analysis. The strength values in Table 1 represent averages for the four specimens. The BN tools are made of PCBN; the SN tools are made of Si3N4. This TRIP steel had a nominal strength of 780 MPa; thus, the BN97 welds at 1600 rpm and the two-step BN46 welds exceeded American Welding Society (AWS) D8.1 minimum values.

Table 1. Initial results for FSSW of uncoated TRIP steel

Tooling	rpm	Steps	kN
BN97	800	1	9.7
	1600	1	11.3
	1600	2	15.1
BN46	1600	1	8.1
	1600	2	12.5
SN77	1600	1	6.14
SN97	1600	2	5.3

Tool durability testing was initiated utilizing hybrid-PCBN tools. Durability tests were performed on 1.5 mm DP980 sheet using baseline performance data developed for PCBN tools during the initial project. Test evaluating tools containing a blend of PCBN and tungsten–rhenium, including 70% PCBN, 80% PCBN, and 90% PCBN, where the balance in each case will be tungsten–rhenium are currently under way. Lap-shear tensile tests are performed to characterize the continued ability to produce consistent joint strengths throughout the life of the tool. Figure 1 shows the characteristic wear profiles of a 70% PCBN tool during the first 1200 welds. Joint strengths were fairly uniform during the first 850 welds, with a trend for decreasing lap-shear strength beyond that point.

During fiscal year (FY) 2010, further development of low-cost tooling was pursued with tool manufacturers. This included the combined efforts of industry and the researchers at the national laboratories working together to incorporate data obtained

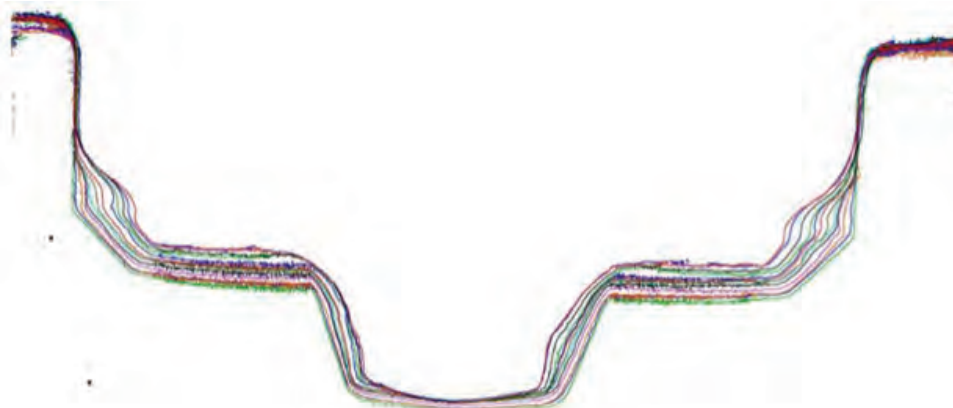


Figure 1. Representative profiles of 70% PCBN tool tip for FSSW of DP980. Wear profiles from 0 to 1200 welds.

from the previous project into the design of future tooling, potentially resulting in significant reductions in the overall prices of tooling for FSSW of AHSS. One example of this effort is demonstrated by work done with process engineers from Ceredyne Inc. to design silicon nitride tools that minimize the overall product volume, allowing for direct powder injection molding of the tools. This process is much less expensive than the precision grinding, which is the industry standard today. The final tool design, currently under evaluation and shown in Figure 2, demonstrates volume-sensitive pricing that ultimately led to tool prices less than \$30 per tool for large orders (precision-ground tooling exceeds \$500 per tool).

Conclusions

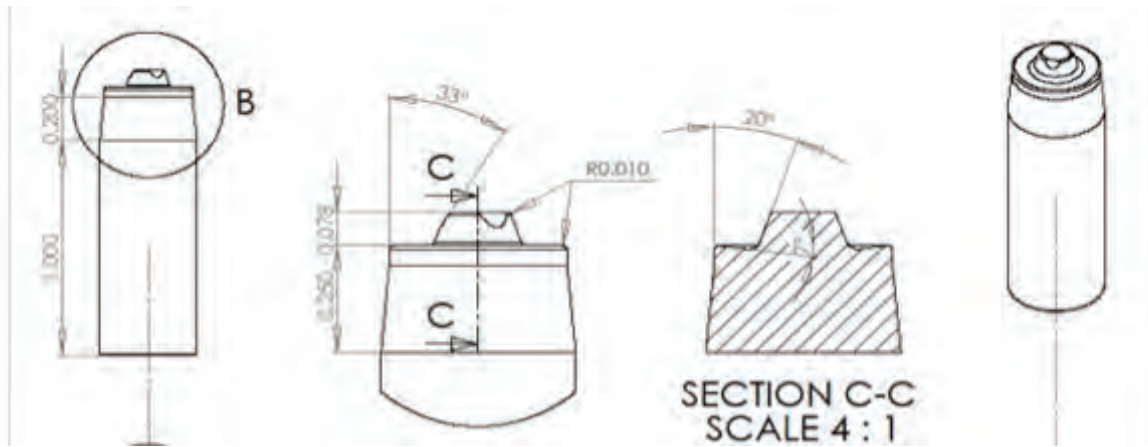


Figure 2. Drawings of the direct injection moldable silicon nitride tool for FSSW of AHSS.

Initial lap-shear testing of FSSW produced in TRIP steels showed promise, with several process parameters leading to joint strengths in excess of the AWS minimum specified for RSW of AHSS. Further characterization continues in the effort to evaluate the response of FSSW on TRIP alloys.

Progress toward understanding the durability, wear rates, and effects of tool life on mechanical properties is under way. Evaluation of the first of several PCBN hybrid alloys has been completed, allowing for characterization of wear for 1000 welds. These data are leading to a better understanding of material life, tool design, and process durability. Work in tool characterization and process development led to additional progress by industry and the national laboratories that shows the potential for implementing technology that would significantly reduce the overall cost of tooling for FSSW of AHSS.

Friction Stir and Ultrasonic Solid-State Joining of Magnesium to Steel

Principal Investigator: Yuri Hovanski, Pacific Northwest National Laboratory
(509) 375-3940; e-mail: Yuri.Hovanski@pnl.gov

Principal Investigator: Michael L. Santella, Oak Ridge National Laboratory
(865) 574-4805; e-mail: santellaml@ornl.gov

Principal Investigator: Glenn J. Grant, Pacific Northwest National Laboratory
(509) 375-6890; e-mail: Glenn.Grant@pnl.gov

Introduction

Structural applications of Mg alloys are growing at a fast pace. While much of this growth is in the area of die-cast components, there is also significant interest in Mg-wrought products. A key combination of low density and high specific strength makes Mg alloys excellent candidates for automotive applications because of the associated effect of weight reduction on better fuel economy. Though currently there are no adequate wrought Mg alloys available to meet the requirements of automotive body applications, extensive research is taking place to enhance the properties of Mg sheet products. Steel, on the other hand, is currently the automaker's material of choice. This is because cold rolled mild steel offers excellent ductility, consistent properties, and low overall component production costs. Decreasing the weight of automobiles can directly contribute to the goal of reducing fuel consumption. Increasing the use of lightweight materials and implementing manufacturing technologies that enable the use of lightweight materials are the two primary paths toward weight reduction. In some situations, lightweight materials can be directly substituted for higher density materials, but in most situations, barriers exist to direct substitution. In a modern multi-material vehicle, lightweight materials such as Al and Mg alloys can be a challenge to join and attach to the underlying substructure, usually composed of steel. Even in Al- and Mg-intensive designs, where entire substructures may be constructed of lightweight metals, there remains a need to join the substructure with other parts of the body-in-white (BIW), such as the predominantly steel passenger safety cage. Joining

methodologies available in the cost environment relevant to automotive manufacturing include RSW, adhesives, linear fusion welding, hemming, clinching, bolting, and riveting.

As alternative joining methodologies, FSW, FSSW, and USW may be able to overcome traditional barriers to join and construct hybrid Mg/steel components. These solid-state joining methods provide unique joining capabilities that, if realized, have the potential to produce faster and more economical alternatives to current technologies (e.g., bolting/riveting). However, FSW and USW for dissimilar Mg/steel combination are significantly underdeveloped for broad deployment.

The purpose of this project is to develop an applied understanding of:

- localized metal forming and metallurgical bonding that develops during FSW, FSSW, and USW;
- the influence of process parameters on joint strength and performance; and
- the properties of joints made with both types of process including lap-shear strength, fatigue properties, corrosion issues, and microstructural characteristics.

Approach

This project is designed to overcome many of the technical barriers to implementing FSW and USW technologies. Task 1 focused on systematically evaluating the application of USW to make lap joints of Mg to steel. It features a decision gate of achieving lap-shear strengths of at least 1 kN as an indication of technical feasibility of the approach. Task 2 will concentrate on improving joint strength through modification of process controls and investigating the fundamental metallurgical aspects of bond formation. An initial evaluation by metallographic examination and lap-shear testing using ultrasonic spot welding for cast Mg alloys will also be done. Task 3 will evaluate fatigue properties of Mg–steel ultrasonic spot welds and consider strategies to control corrosion in the joints. The tasks are oriented toward developing information useful to manufacturers in their decision making processes. However, the intention is to develop a basic understanding of the feasibility to produce Mg–steel joints and of the general usefulness of each of the solid-state welding methods previously outlined.

Technology Transfer

As the overall intent of the project in solid-state joining of Mg to steel is intended to be a technology development effort, the overall scope of technology transfer is limited. Nevertheless, the work being developed will be made available to the public via publications, presentations, and international conferences. Additionally, a database containing all appropriate process windows, tooling, and their associated mechanical properties will be turned over to participants of the industrial advisory committee.

Results and Discussion

Ultrasonic Welding

The ultrasonic welds are made with a Sonobond CLF2500 using a pedestal welding station. The rated conditions at the welding tip on this equipment are 20 kHz frequency with 25 micrometer (μm) amplitude. The sonotrode tips are made from T1 steel. They typically have flat, rectangular faces with dimensions of either 5 mm \times 7 mm or 7 mm \times 7 mm. The line pressure to the tip clamping mechanism was adjusted to put the welds under a constant nominal pressure of 39 MPa.

The materials used for the current experiments were sheets of hot-dip-galvanized (HDG) mild steel that were 0.8 mm thick and 1.6-mm-thick AZ31B-H24. The zinc coating on the steel is about a 9 μm thick. Prior to welding, the surfaces of the AZ31B sheet are buffed with non-metallic abrasive pads (Scotch-Brite™) to remove surface oxides and produce shiny surfaces. Both metals are also degreased with acetone followed by isopropyl alcohol to remove lubricants and surface debris.

Coupons of AZ31, nominally 30 mm wide \times 100 mm long, were welded to mild steel coupons of the same size to produce specimens for mechanical testing and metallographic analysis. A 25 mm overlap was used for making lap-welded coupons with spot welds centered in the overlap regions. Specimens were positioned for welding so that the primary vibration direction of the sonotrode was perpendicular to their long axis. Spot welding was typically performed using power of 1500–2500 W. Welding times typically ranged from 0.2–1.2 s.

The results of the tensile lap-shear testing are presented in [Figure 3](#) where failure load vs welding time is plotted. With both tips there was an initial rapid rise in lap-shear failure load from around 0.5 kN to near 2.9 kN as the welding times increased

from 0.2–0.4 s. After the rapid increase, failure loads continued increasing with welding times but at a much lower rate. From 0.4–1.2 s, failure loads increased to a maximum average value of 3.7 kN for the 5 mm × 7 mm tip and 4.2 kN for the 7 mm × 7 mm tip. Welds of the AZ31 to bare steel were unsuccessful. Weak bonding occurred in this case, but joints could be easily broken by hand.

The lap-shear strength results can be placed in perspective by comparison with data from resistance spot welds and friction stir spot welds of AZ31. Published work confirmed that AZ31 could be resistance spot welded with lap-shear strengths ranging to 5.7 kN. Lap-shear strengths increased with spot diameters and were about 4.0 kN for diameters with areas equivalent to the 7 mm × 7 mm USW tip. More recent published work measured lap-shear strengths up to 3 kN for spot welds of AZ31 with nugget diameters of about 7 mm. Another published study showed that AZ31 sheet could be friction stir welded, and some joints had lap-shear strengths as high as 4.75 kN. No comparable published data could be found for Mg–steel spot-welded joints made by these two processes. Nevertheless, strengths for ultrasonically welded joints at times greater than about 0.5 s consistently exceeded 3 kN, so they are generally consistent with values found for Mg–Mg spot welds.

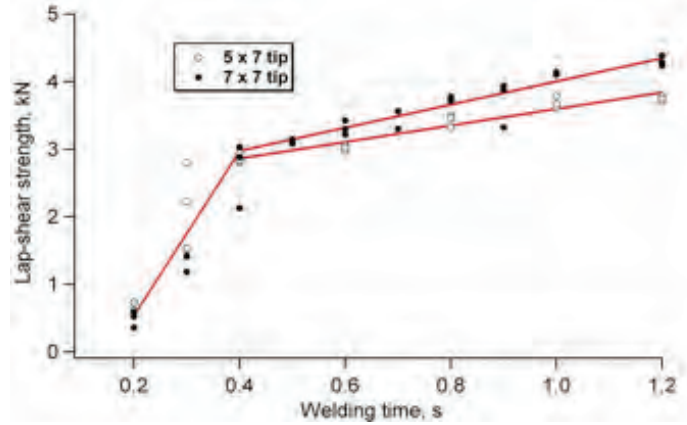


Figure 3. Lap-shear strength vs welding time for two tip sizes

The results of the fatigue testing are shown as Figure 4 where the fatigue life expressed as cycles to failure is plotted against the load range for testing. The USW spot welds were tested at constant values of $R = 0.1$ and $R = 0.2$, where $R = \text{minimum load}/\text{maximum load}$. There are few published data for similar or dissimilar spot welds involving Mg alloys, and Figure 4 compares the USW data to similar data from friction stir spot welds of AZ31-to-AZ31 lap welds. Regression analysis was used for the lines drawn through the USW data at $R = 0.1$ and the FSSW data of $R = 0.0$. However, a single line could have been fit through the entire combined data set, which suggests that the fatigue properties of the AZ31–steel USW spots welds will not differ significantly from other types of spot welds made using AZ31.

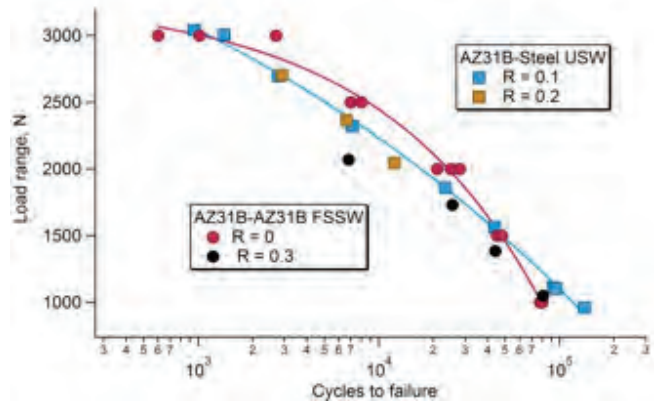


Figure 4. Fatigue life expressed as cycles to failure vs loading range for AZ31–steel USW.

Friction Stir Welding

Following our work reported in 2009, an effort was made to find the effect of tool features on the joint strength of a Mg alloy to steel in a lap configuration. Two tool designs were tested in this study. The first tool had a convex scrolled shoulder and a stepped spiral pin. The second tool had identical features as the first tool except for a short, hard insert on the tool pin bottom. It was anticipated that the short, hard insert would help in deforming the bottom steel sheet and, therefore, would enhance the joint strength. Schematic drawings of both the tools are shown in Figure 5.

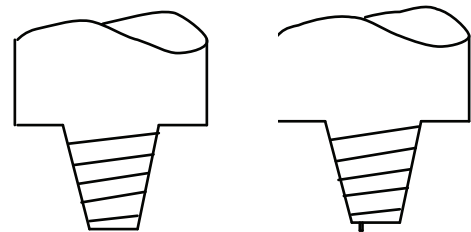


Figure 5. Schematic drawings of the tools. (a) Tool 1 and (b) Tool 2 with the short, hard insert on the pin bottom.

To obtain better insight into joint strength, the weld efficiency of all the joints was calculated by comparing the failure load of the joint when pulled in lap-shear tensile testing with the maximum load-carrying capacity of the weaker parent sheet section. It was found that the 0.8 mm steel is weaker for AZ31-to-0.8 mm steel welds, and the AZ31 sheet is weaker for AZ31-to-1.5 mm steel welds. In the current study, a weld efficiency >90% was achieved in the case of AZ31-to-0.8 mm steel welds at 500 tool rpm and 2.47 mm plunge depth. With joint strengths in excess of 6 kN, one of the AZ31-to-0.8 mm steel weld specimens at this particular combination of process parameters showed failure of the steel sheet, leaving the weld intact. An example of such a lap-shear specimen is shown in Figure 6.

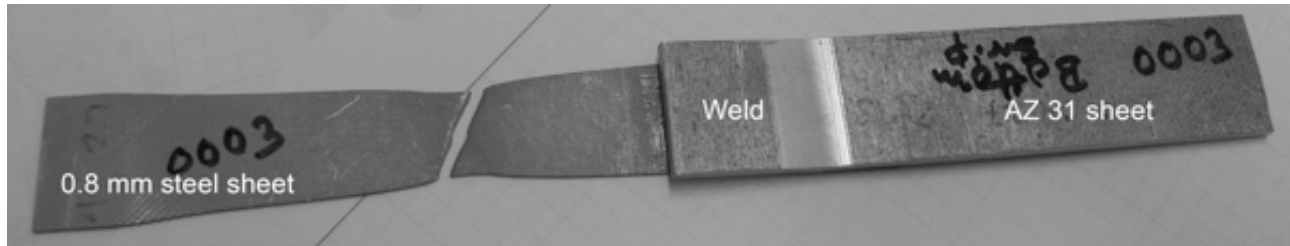


Figure 6. A lap-shear specimen: failure occurred by steel sheet fracture, leaving the weld intact.

Interface characteristics were observed via optical and scanning electron microscopes (SEMs). An example of a joint made by Tool 1 is shown in Figure 7a. Penetration of the tool into the steel sheet is evident in this image, resulting in hook-like features along the joint interface as marked by B and B¹. Higher magnification SEM images obtained from various locations along the joint interface are shown in Figure 7b–d. Microstructural features observed in these images indicate melting of the zinc coating present on the steel sheet due to process heat. For example, Figure 7b shows the presence of numerous bright particles in a lamellar/spiral matrix, which is typical of a solidification microstructure. These particles were found to be zinc–Mg intermetallics, which were embedded in a zinc–Mg eutectic matrix. The hexagonal shape of one such particle is evident in Figure 7c. However, no such solidification product was found along the region where the steel sheet showed signs of deformation due to the penetrating action of the tool (Figure 7d). As a result, Mg and steel remain in intimate contact along the width of the weld where the tool penetrates into the bottom steel sheet. Moreover, absence of any Zn–Mg alloy layer along the Mg–steel interface implies that the Zn coating could not act as a brazing material.

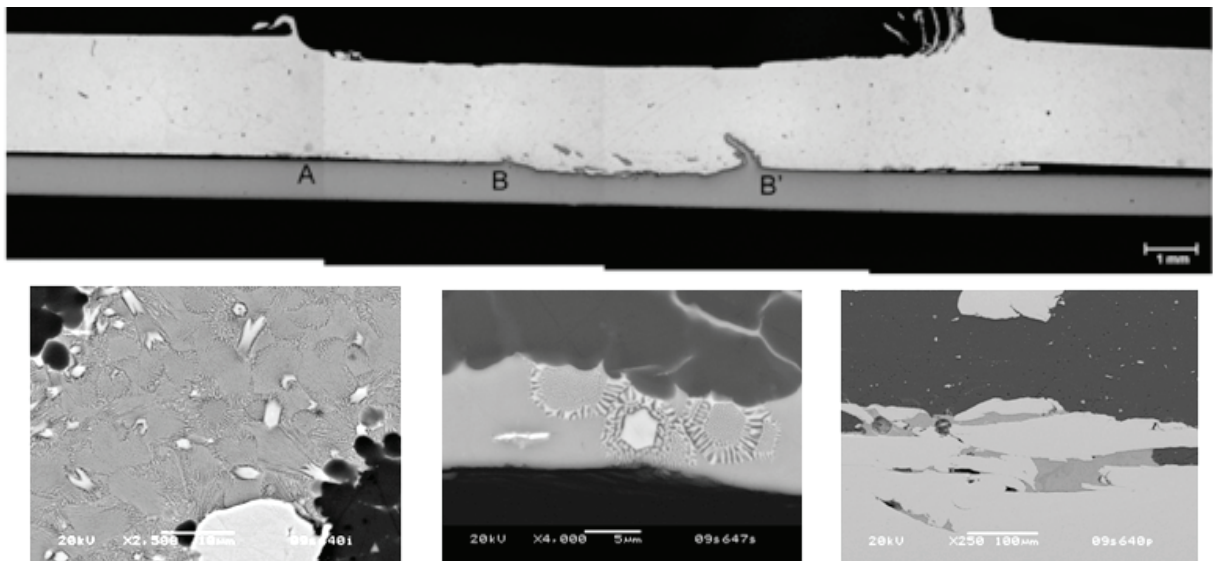


Figure 7. (a) Cross section of a joint made by Tool 1, where bottom steel sheet deformation is evident; (b), (c), and (d) are higher magnification SEM images of the joint shown in Figure 7a.

To compare the effects of tool features, a typical cross section of a joint fabricated by Tool 2 is shown in Figure 8. The effect of the tungsten carbide insert on the tool pin bottom is clearly evident on this image. The presence of the insert resulted in the machining of the bottom steel sheet. Further, it led to the formation of two dovetail-like features on both ends, as noted by the arrows. Comparison of Figures 7a and 8 shows that the interlocking features are not very well defined when Tool 1 is used. In contrast, when Tool 2 is used, there are well-defined, sharp, interlocking features, which lead to increased joint strength with lower variability.

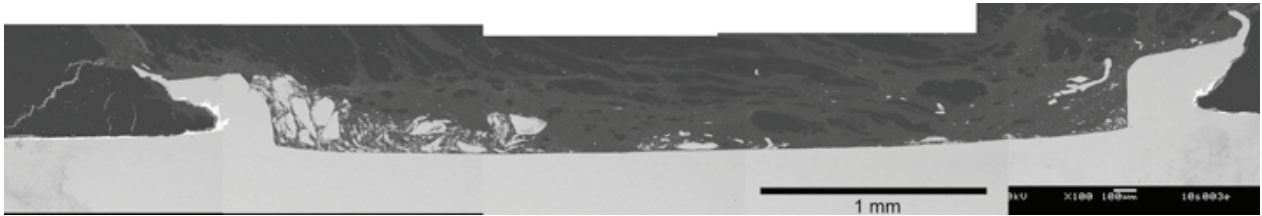


Figure 8. Cross section of a joint fabricated by Tool 2.

Conclusions

Project performance throughout this year allowed for all FY 2010 milestones to be successfully achieved. Thanks to continued support from several industrial advisors and the collaborative effort between PNNL and ORNL researchers, increased understanding of the joining mechanisms possible between Mg and steel was achieved. Progress during this period has ultimately allowed the joint efficiencies of solid-state welds between Mg and steel to be increased from 60% to beyond 90%, surpassing the goals set for FY 2010 milestones. Successful progress was made on both FSW and USW fronts, albeit the mechanisms involved in each improvement were process specific.

Conclusions

Further implementation of lightweight materials as part of multi-material vehicle designs will only be achieved by advancing their ability to be successfully joined. Projects developing near-term joining solutions for AHSS that necessitate microstructural preservation during the joining process are paving the way for improving overall fleet efficiency. Furthermore, research in joining technologies that would enable structural joining of vastly dissimilar metals such as Mg and steel are providing the knowledge base needed to make sure such improvements continue into the next few decades.

Publications/Presentations/Patents

Hovanski, Y.; Grant, G.; Jana, S.; Santella, M. Solid State Joining of Mg to Steel. Presented at the TMS annual meeting, February 2010.

Hovanski, Y.; Grant, G. J.; Jana, S.; Mattlin, K. Friction Stir Welding Pin Tool with Scribe. Patent application filed 2010.

Hovanski, Y.; Jana, S.; Grant, G. J.; Santella, M. L. Friction Stir Welding of Mg to Steel. Presented at MS&T 2010, October 2010.

Hovanski, Y., Santella, M. L.; Grant, G. J. Friction Stir Spot Welding of Advanced HSS. Presented at MS&T, October, 2009.

Hovanski, Y.; Santella, M. L.; Grant, G. J. Friction Stir Spot Welding of Advanced HSS. Presented at IABC, Troy, Michigan, November 2009, and published in the 2009 conference proceedings of IABC 2009.

Jana, S.; Hovanski, Y.; Grant, G. Friction Stir Welding of Mg to Steel: A Preliminary Investigation. *Met. Trans. A.*, in press 2010.

Santella, M.; Franklin, T.; Pan, J.; Pan, T.; Brown, E. Ultrasonic Spot Welding of AZ31B to Galvanized Mild Steel. SAE Paper 2010-01-0975 (also SAE Transactions), 2010.

Santella, M. L.; Hovanski, Y.; Frederick, A.; Grant, G. J.; Dahl, M. E. Friction Stir Spot Welding of DP780 C Steel. *Science & Tech. of Welding & Joining*, May 2010, 15(4), 271–278.

H. A Study of the Effects of Microstructure on the Mechanical Properties and Failure Mechanisms of Advanced High-Strength Steels

Principal Investigator: Warren M. Garrison Jr.
Carnegie Mellon University
5000 Forbes Avenue; Pittsburgh, PA 15213
(412) 268-3593; e-mail: wmg@andrew.cmu.edu

Technology Area Development Manager: William Joost
U.S. Department of Energy
1000 Independence Ave., S.W.; Washington, DC 20585
(202) 287-6020; e-mail: william.joost@ee.doe.gov

Field Project Officer: Adrienne Riggi
National Energy Technology Laboratory
3610 Collins Ferry Road; Morgantown, WV 26507
Phone: (304)285-5223; e-mail: adrienne.riggi@netl.doe.gov

Contractor: Carnegie Mellon University
Award Number: National Science Foundation Award CMMI 0726949

Objectives

- To understand the effect of complex, multiphase microstructures on the mechanical behavior and formability of advanced high-strength sheet steels.
- To investigate the effect of void nucleation resistance of inclusion particles on the mechanical behavior and formability of HSS steels.

Accomplishments

Defined four steel compositions to be used in investigating mixtures of lower bainite and ferrite and mixtures of martensite and ferrite on mechanical behavior and formability. (FY 2008)

- Defined two steel compositions to be used to assess void nucleation resistance of inclusions on mechanical behavior and formability. (FY 2008)
- Melted the four heats of the compositions selected to examine the effects of mixtures of lower bainite and ferrite and mixtures of martensite and ferrite on mechanical behavior and formability. Portions of these four heats were processed to one-half-inch-thick plate and to sheet material. This was done at U.S. Steel research facilities in Pittsburgh. (FY 2008)
- Prepared four heats to examine the effect of inclusion void nucleation resistance on mechanical behavior and formability. The first such heat was prepared to have inclusions which were not resistant to void nucleation. Portions of this heat were rolled to one-half-inch plate and other portions to sheet. However, two heats were made in succession to getter the sulfur (S) as particles of titanium carbosulfide. Neither heat was successful due to calcium contamination since the S was gettered as particles of calcium sulfide, and such particles are not resistant to void nucleation. A third heat was prepared in which titanium additions were made to getter the S as particles of titanium carbosulfide. This heat was prepared by vacuum induction melting followed by vacuum arc remelting at Carpenter Technology. U.S. Steel's research center rolled this material to one-half-inch plate and to sheet. (FY 2008, FY 2009, FY 2010)
- Obtained the hardness, Charpy impact energy, and all tensile properties, including the uniform elongation as a function of annealing temperature, for the four alloys being used to assess the effect of mixed microstructures on mechanical

behavior and formability. We found that as the annealing temperature is decreased, the uniform strain increases, reaches a maximum, and then decreases. A high uniform strain is desirable as it indicates high work hardening capacity and good formability. (FY 2009, FY 2010)

- Measured the amounts of retained austenite in the four alloys prepared to study the effect of microstructure on formability as a function of annealing temperature. We found that as the annealing temperature is decreased, the amount of retained austenite increases, reaches a maximum, and then decreases as the annealing temperature is decreased further. The annealing temperatures associated with the high uniform strains are the annealing temperatures associated with the maximum amounts of retained austenite. (FY 2010)
- Determined the inclusion volume fraction, sizes and spacings, and chemistry for the heat prepared to get the S as particles not resistant to void nucleation. These sulfides were primarily calcium sulfide. Void generation studies were carried out, and it was found these inclusions were not resistant to void nucleation. In addition, the Charpy impact energy and tensile properties were determined. (FY 2009, FY 2010)
- Examined the final heat made to get the S as particles of titanium carbosulfide with respect to sulfide type, and it appears the S in this heat was gettered as particles of titanium carbosulfide. The tensile properties and Charpy impact energy of this heat were determined. The Charpy impact energy of the heat in which the S was gettered as particles of titanium carbosulfide was 176 J, while the Charpy impact energy of the heat in which the S was gettered as particles of calcium sulfide was 124 J. The higher toughness of the heat in which the S was gettered as particles of titanium carbosulfide is consistent with our experience that gettering S as particles of titanium carbosulfide significantly increases toughness. (FY 2010)

Future Directions

- Need to examine the microstructures of the heats used to obtain complex microstructures in more detail. We will use transmission electron microscopy to examine the microstructures of these four alloys as a function of annealing temperature. A major objective would be to determine the morphology and size scale of the retained austenite in the four heats as a function of annealing temperature.
- Need to quantify the sulfide distribution in the heat in which the S was successfully gettered as particles of titanium carbosulfide. This would include particle chemistries and the particle volume fraction, average size, and average spacing. We also need to obtain a void generation curve for the inclusions in this heat to assess the degree to which the particles of titanium carbosulfide are more resistant to void nucleation than particles of calcium sulfide for these compositions.
- Need to carry out tensile tests for the six heats using flat tensile specimens from sheet material as up to now we have used round tensile specimens. We will assess the tensile properties using flat tensile specimens for the four heats containing complex microstructures as a function of annealing temperature. We will obtain the tensile properties of the two heats being used to assess the effects of inclusion void nucleation resistance on formability for the simple quench and temper we having been using for these two materials.
- Need to start examining formability of these six heats using sheet material. We will begin with bending tests and hole expansion tests.

Introduction

The purpose of this work is to examine the effects of heat treatment and composition on the microstructure and mechanical properties of high-strength steels with the ultimate goal of producing microstructures which would have ultimate tensile strengths of at least 1,200 MPa and which would be suitable for use in automotive applications, especially for steel sheets to be used in forming operations.

Several factors should be considered when assessing the formability of steel. The first is that the work hardening capacity and characteristics be sufficient to ensure formability in the sense that strain localization and/or local thinning does not take place in the forming process; thus, the strains which can be tolerated before local thinning increase with work hardening rate. The uniform strain is often taken as a measure of this characteristic; thus, high uniform strains are desired in steels that are

intended for applications in which they must be formed. The second is that the material has sufficient ductility that fracture does not take place during the forming operation. The latter characteristic is important because it has been found that as the strength levels of steels for forming applications are increased there is a tendency for fracture to take place before the forming operation is complete, at least in some forming operations. Thus, not only are the work hardening characteristics important, in that the work hardening rates should be high, but resistance to fracture should also be high. In addition to their formability characteristics, higher strength steels are of interest for their weight reduction and impact energy absorption characteristics.

Our approach has been strongly influenced by two papers. The first paper is a note by Bhadeshia (2002), which was inspired by a paper by Jacques et al. (2001). Jacques et al. found that one could obtain excellent uniform elongations in multiphase steels which did not contain silicon or Al to promote the existence of mechanically stable retained austenite which is free from carbide formation. Bhadeshia suggested, based on these results, that the 8 to 15 vol % retained austenite commonly found in TRIP (transformation-induced plasticity) steels contributed about 2% to a total uniform elongation of roughly 25%. Bhadeshia suggested that the high work hardening rates in the multiphase steels typical of TRIP steels might be instead due to a mixture of soft and hard phases. In his discussion, Bhadeshia went on to say that the high work hardening rates might be associated with initial deformation of the ferrite, which would not work harden at a high rate, but at some point the as-quenched martensite in the microstructure would start to deform and the high work hardening rate of the as-quenched martensite is what determines the high work hardening rate of the structure and the high uniform elongations. The second paper is one by Lee et al. (2004) in which void generation in multiphase steels was investigated. They found that voids are generated during plastic deformation not only at inclusions and carbide particles but at interfaces between strong and weak microstructural elements; for example, voids could be generated at interfaces between ferrite and martensite. The rate at which voids are formed during deformation can have important consequences in terms of tensile ductility and possibly on formability. The slower the rate at which voids are generated can improve tensile ductility. Thus one would want to minimize the volume fraction of voids at each point of the deformation process and to make void nucleation as difficult as possible.

In this work, we have prepared four compositions for which we felt we could use variations in the annealing temperature to vary the amounts of ferrite and martensite. The objective was to obtain microstructures which were entirely martensite, which were 25% ferrite and 75% martensite, and which were 50% ferrite and 50% martensite and to assess how these different microstructures influenced work hardening behavior and formability. This approach is suggested by the paper by Bhadeshia.

In addition, we will assess the effects of inclusion resistance to void nucleation on formability. We have found that by getting the S as particles of titanium carbosulfides we can increase the fracture toughness and Charpy impact energy in some steels by more than a factor of 2. This is because the particles of titanium carbosulfide are very resistant to void nucleation. It is our thesis that by getting the S as particles of titanium carbosulfide one can improve the toughness of steels used in automotive sheet, which would improve energy absorption in a crash, and that one can also improve formability by making the inclusions very resistant to void nucleation.

The compositions of the heats made for this work are given in Table 1. The first four heats represent the compositions selected to assess the influence of complex microstructures and in which we hope to achieve mixtures of ferrite and martensite to assess work hardening rate and formability. The other four heats were made to produce two heats in which the inclusions were not resistant to void nucleation. In Heat E the inclusions were CaS particles, and they had very little resistance to void nucleation. Heats F and G were failed attempts to produce a heat in which the S was gettered as particles of

Table 1. Compositions of Experimental Heats (wt %)

Alloy	Heat ID	C	Mn	Ni	Cr	Mo	Ti	Al	Si	P	S	O ₂	N ₂
MP1	D	0.188	3.84	<0.002	0.01	0.002	<0.002	0.021	0.015	0.005	0.0037	0.0021	0.0041
MP2	B	0.183	3.73	<0.002	0.01	0.021	<0.002	1.437	0.021	0.005	0.0024	0.0033	0.0041
MP3	C	0.197	4.22	<0.002	0.011	0.003	<0.002	0.030	1.46	0.005	0.0031	0.0013	0.0056
MP4	A	0.205	4.27	<0.002	0.010	0.003	0.002	0.033	2.84	0.004	0.0025	0.0027	0.0055
M1	E	0.180	0.49	3.01	0.98	0.24	<0.002	0.031	1.98	0.003	0.0027	0.0015	0.0018
M2	F	0.158	0.007	2.93	0.97	0.25	0.038	0.025	1.95	0.002	0.0034	0.0013	0.0014
M2B	G	0.15		3	1	0.25	0.025						
M2C	H	0.15		3	1	0.25	0.025						

titanium carbosulfide; these heats were contaminated by calcium of an unknown source. Heat H was our final attempt to prepare a heat otherwise the same as Heat E but in which the sulfides were titanium carbosulfides. Heat H seems to have been successful in this regard. All heats but one were made by U.S. Steel, and all were processed to plate and sheet by U.S. Steel.

Activity and Developments

We completed our study of the effect of annealing temperature on the tensile properties of these four alloys, and we measured the amounts of retained austenite in these alloys as a function of annealing temperature. The ultimate tensile strengths of the four alloys are plotted as a function of annealing temperature in Figure 1. The important point is the ultimate tensile strengths remain high as the annealing temperature is decreased.

Figure 2(a) is a plot of the uniform strain during a tensile test as a function of annealing temperature for the four multiphase alloys. Again, at the higher annealing temperatures the steels are austenitic before quenching, but at the lower annealing temperatures the steels are within the ferrite and austenite two phase field. The uniform strain is the strain at which necking begins. The higher the uniform strain the higher the work hardening capacity of a material and the higher the formability. The data in Figure 2(a) show that the uniform strains reach a maximum at low annealing temperatures.

In Figure 2(b) the amounts of retained austenite in the multiphase alloys are plotted as a function of annealing temperature. For all four alloys the amounts of retained austenite reach high levels at low annealing temperatures. The results in Figure 2(b) strongly suggest that the desirable high uniform strains are due to the large amounts of retained austenite. At this time we do not know why the maximum amount of retained austenite content of the alloy containing 3 wt % silicon is lower than that of the alloy containing 1.5 wt % Al. This measurement of austenite content will be redone.

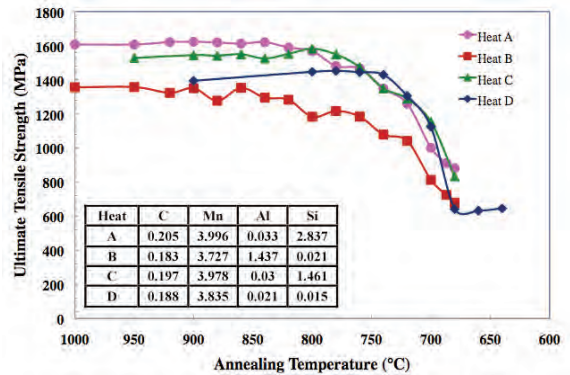


Figure 1. The ultimate tensile strengths of the four multiphase alloys plotted as a function of annealing temperature. At the higher temperatures the alloys are austenitic before quenching, but at the lower annealing temperatures the alloys are well within the ferrite and austenite two phase field.

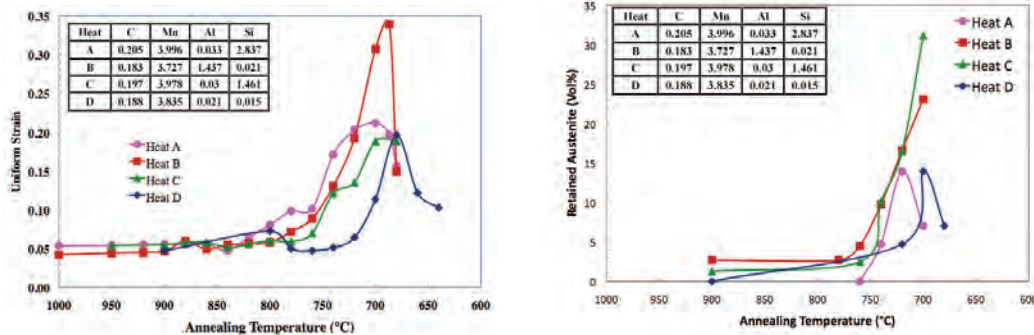


Figure 2. In (a) the uniform strain of the multiphase alloys is plotted as a function of annealing temperature. In (b) the amount of retained austenite in the multiphase alloys is plotted as a function of annealing temperature.

Figure 3 consists of two plots of the total percent elongation to fracture as a function of ultimate tensile strength for different types of steel. Figure 3(a) shows the desired range of properties for the “Third Generation of AHSS” for automotive applications. In Figure 3(b) we have plotted some of our results for the multiphase alloy with 3 wt % silicon and the multiphase alloy with 1.5 wt % silicon. This plot of our data suggests that these two alloys have desirable properties in terms of ductility at high strength levels. It would be more meaningful if all of the data consisted of the uniform strain as a function of strength, but it seems that the typical plot is the percent total elongation as a function of strength.

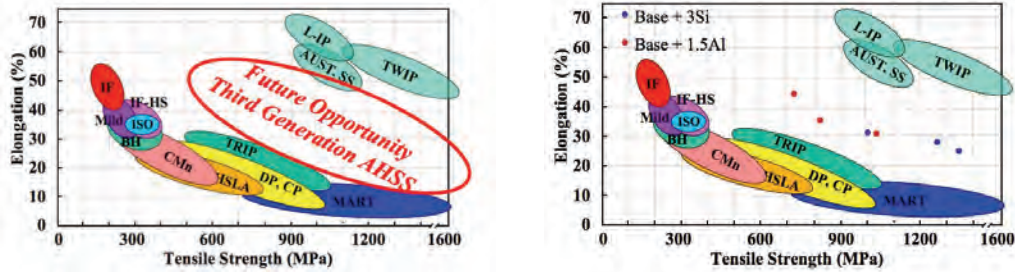


Figure 3: In (a) the total percent elongation to fracture is plotted as a function of ultimate tensile strength for different types of steels. The objective of this program is to develop steels whose properties fall in the region labeled “Future Opportunity Third Generation AHSS.” In (b) we have included results for the multiphase alloys containing 3 wt % silicon and 1.5 wt % Al. The properties of these two alloys suggest they would have better formability than currently available steels in this strength range.

Regarding the two heats which have been prepared to examine the degree to which the resistance of inclusions to void nucleation influences formability, we have completed the following.

- Heat E, the heat in which the inclusions are not resistant to void nucleation, has been completely characterized in terms of tensile properties, Charpy impact toughness, and inclusion characteristics, including the inclusion volume fraction, average size, average spacing between inclusions, and inclusion chemistries.
- A void generation curve has been obtained for Heat E.
- Heat H, in which the S has been gettered as particles of titanium carbosulfides, has been characterized in terms of tensile properties and Charpy impact energy.

The Charpy impact energy of Heat H was 176 J, and it was 124 J for Heat E, in which the S was gettered as particles of CaS; this difference in toughness was anticipated. We need to characterize the titanium carbosulfide inclusions in Heat H in detail and develop a void generation curve for this material.

Conclusions

At this point we believe that the two multiphase alloys, Heats A(3Si) and B(1.5Al), have tensile properties, a high uniform strain, and a high total percent elongation to fracture, which suggest they would be useful from the standpoint of having improved formability at high strength levels. These improved tensile properties are believed to be a result of the large amounts of retained austenite found in these alloys after annealing at low temperatures.

Presentations/Publications/Patents

Garrison, W. M., Jr. A Study of the Effects of Microstructure on the Mechanical Properties and Failure Mechanisms of Advanced HSS. Presented at the AISI review of projects on Advanced HSS, July 19–20, 2010, Detroit Michigan.

Reference

Bhadeshia, H.K.D.H. TRIP-Assisted Steels. *ISIJ International*, 2002, 42, pp. 1059–1060.

Hosford, W. F.; Caddell, R. M. *Metal Forming: Mechanics and Metallurgy*, Prentice-Hall, Englewood Cliffs, N.J., 1983, p. 299.

Iorio, L. E.; Garrison, W. M., Jr. The Effects of Titanium Additions on AF1410 Ultra-high Strength Steel. *Metallurgical and Materials Transactions A*, 2006, 37A, pp. 1165–1173.

Jacques, P. J.; Girault, E.; Harlet, P.; Delannay, F. The Developments of Cold-Rolled TRIP-Assisted Multiphase Steels. Low Silicon-assisted Multiphase Steels. *ISIJ International*, 2001, 41, pp. 1061–1067.

Lee, S. B.; Speer, J. G.; Matlock, D. K. The Influence of Phase Distributions and Interfaces on Fracture and Formability of High Strength Sheet Steels. In *International Conference on AHSS Steels for Automotive Applications Proceedings*, Winter Park, Colorado, June 6–9, 2004, Baker, Margaret A., ed., Association for Iron and Steel Technology: Warrendale, Pennsylvania, 2004, p. 383.

Maloney, J. L.; Garrison, W. M., Jr. The Effect of Sulfide Type on the Fracture Behavior of HY180 Steel. *Acta Materialia*, 2005, 53, pp. 533–551.

Marciniak, Z.; Kuczynski, K. Limit Strains in the Processes of Stretch-Forming Sheet Metal. *Int. J. Mech. Sci.*, 1967, 9, pp. 609–620.

Nishimoto, A.; Hosoya Y.; Nakaoka, K. Relation Between Hole Expansion Formability and Metallurgical Factors in Dual-Phase Steel Sheets. In *Proceedings of the Conference Symposium on the Fundamentals of Dual Phase Steels*, held at Chicago, February 23–24, 1981, Kot, R. A., and Bramfitt, B. L., eds., Metallurgical Society of AIME: Warrendale, Pennsylvania, 1981, pp. 447–463.

Park, Y. J.; Coldren, A. P.; Morrow, J. W. Effect of Martensite Bands and Elongated Manganese Sulfide Inclusions on the Formability of Dual-Phase Steels. In *Proceedings of the Conference Symposium on the Fundamentals of Dual Phase Steels*, held at Chicago, February 23–24, 1981, Kot, R. A., and Bramfitt, B. L., eds., Metallurgical Society of AIME: Warrendale, Pennsylvania, 1981, pp. 485–497.

Schmitt, J. H.; Jalinier, J. M. Damage in Sheet Metal Forming—I. Physical Behavior. *Acta Metall.*, 1982, 30, pp. 1789–1798.

Schmitt, J. H.; Jalinier, J. M. Damage in Sheet Metal Forming—II. Plastic Instability. *Acta Metall.*, 1982, 30, pp. 1799–1809.

Sugimoto, K.; Sakaguchi, J.; Iida, T.; Kashima, T. Stretch-Flangeability of High-Strength TRIP Type Bainitic Sheet Steel. *ISIJ International*, 2000, 40, pp. 920–926.

Sugimoto, K.; Yu, B.; Mukai, Y.; Ikeda, S. Microstructure and Formability of Al Bearing TRIP-Aided Steels with Annealed Martensite Matrix. *ISIJ International*, 2005, 45, pp. 1194–1200.

Sumimoto, K.; Kanda, A.; Kikuchi, R.; Hasimoto, S.; Kashima, T.; Ikeda, S. Ductility and Formability of Newly Developed High Strength Low Alloy TRIP-aided Sheet Steels with Annealed Martensite Matrix. *ISIJ International*, 2002, 42, pp. 910–915.

Yamazaki, K.; Oka, M.; Yasuda, H.; Mizuyama, Y.; Tsuchiya, H. Recent Advances in Ultrahigh-Strength Sheet Steels for Automotive Structural Use, *Nippon Steel Technical Report*, No. 64, January 1995, p. 37.

I. Development of Nano-Acicular Duplex Steels

Principal Investigator: David C. Van Aken
Missouri University of Science and Technology
Materials Science and Engineering
1400 N. Bishop; Rolla, MO 65409-0340
(573) 341-4717; e-mail: dcva@mst.edu

Co-Principal Investigator: Julia E. Medvedeva
Missouri University of Science and Technology
Physics
1315 N. Pine St.; Rolla, MO 65409-0640
(573) 341-4789; e-mail: juliaem@mst.edu

Co-Principal Investigator: Von L. Richards
Missouri University of Science and Technology
Materials Science and Engineering
1400 N. Bishop; Rolla, MO 65409-0340
(573) 341-4730; e-mail: vonlr@mst.edu

Technology Area Development Manager: William Joost
U.S. Department of Energy
1000 Independence Ave., S.W.; Washington, DC 20585
(202) 287-6020; e-mail: william.joost@ee.doe.gov

Field Project Officer: Adrienne Riggi
National Energy Technology Laboratory
3610 Collins Ferry Road; Morgantown, WV 26507
(304) 285-5223; e-mail: adrienee.riggi@netl.doe.gov

Contractor: Missouri University of Science and Technology (Missouri S&T)
Contract No.: National Science Foundation Award CMMI-0726888

Objectives

- Use a first-principles density functional approach by the projector augmented wave method as implemented in the Vienna Ab-initio Simulation Package (VASP) to examine solution enthalpy of Fe-Mn-(Al,Si)-C alloys; examine chemical defect formation; and determine the effect of C, manganese, and Al on the generalized stacking fault energies.
- Develop a third generation AHSS that is both lighter and stronger than current automotive steels. The new steel will be a duplex steel composed of austenite and bainitic ferrite that will be stronger and exhibit greater formability than current first generation AHSSs that are based upon ferritic microstructures.

Accomplishments

- Identified defect structures in austenite that suggest short range ordering in Fe-Mn-Al-C solid solutions. These defect structures have the same coordination as is observed for κ -carbide. Calculations of the generalized stacking fault energy (SFE) show that Al increases the intrinsic SFE and stabilizes austenite with respect to hexagonal martensite.
- Produced 10 lightweight steels that meet mechanical property goals for third generation AHSSs with compositions (in weight percent) ranging from Fe-(13.5–15.4)Mn-(2.4–5.6)Al-(0.8–2.9)Si-(0.06–0.23)C. These steels consisted of microstructures containing various combinations of retained austenite, bainitic ferrite, primary ferrite, and martensite.

- Used FactSage to predict the stabilization of primary ferrite during solidification and at hot-working temperatures for a nominal composition of Fe-xAl-14Mn-1.8Si-0.15C with Al content varied in the model.
- Performed preliminary analysis to explain the differences observed in deformation behaviors in bainitic ferrite and austenite alloys based on microstructural characterization.

Future Directions

- Extend first principle calculations to include the effect of silicon on the generalized SFE. In addition, study the silicon and Al effects on cleavage and tensile characteristics.
- Investigate serrated plastic flow observed during work hardening in light of the short-range order of Mn-C-Al clusters predicted by the first principle studies.
- Create a thermodynamic database to help predict phase equilibria and experimentally verify predictions in Fe-Mn-Al-C steels.
- Use orientation imaging microscopy and transmission electron microscopy to characterize deformation and phase transformations in lightweight Fe-Mn-Al-C steels.

Introduction

Lightweight steel is produced by alloying with Al and silicon to produce a composition having greater than 4 wt % of these 3p elements. In terms of atomic percent, this level of alloy represents more than 10 at. %, and these steels are expected to demonstrate new physical and mechanical behaviors. The enhanced plasticity in austenitic Fe-Mn-Al-C alloys is related to two mechanisms known as TRIP (transformation induced plasticity) and TWIP (twinning induced plasticity). The observed mechanism (TRIP vs TWIP) is controlled by SFE (γ_{ISF}), and the face centered cubic (fcc) to hexagonal close packed (hcp) ϵ -martensitic transformation is believed to occur in steels with low SFE ($\gamma_{\text{ISF}} \leq 20 \text{ mJ/m}^2$), whereas twinning is a contributing deformation mechanism in steels with higher SFE (Frommeyer et al., 2003; Vitek, 1974). The magnitude of SFE also determines the width of the dislocation core and controls the splitting of a dislocation into two partials.

Activity and Developments

Effect of Carbon, Manganese, and Aluminum on the Generalized Stacking Fault Energies in Austenite

Alloying may strongly affect the SFEs, and thus it is a way to achieve improved plasticity and strength. The effect of solute on SFE is complex and depends on many factors such as volume, temperature, strain, solute concentration, and magnetic interactions. Therefore, to determine the microscopic origin of mechanical behavior of austenitic Fe-Mn-Al-C steels it is necessary to estimate the value of intrinsic SFE, which is formed by planar shear and changes the atomic stacking sequence from ABCABCAB to ABCACABC, which corresponds to stable intrinsic stacking faults (ISFs). In fcc metals the favorable slip is $\langle 112 \rangle$ (111), and the planar shift is produced by the partial dislocation with Burgers vector $b_p = 1/6 \langle 112 \rangle$, which produces the minimum (ISF) on the generalized stacking fault (GSF) energy curve (Figure 1, black curve). A displacement of $1/12 \langle 112 \rangle$ ($0.5 b_p$) corresponds to an unstable stacking fault (USF, γ_{US}); this energy controls the barrier for dislocation movement. The third important energy characteristic of planar shear is the displacement at $1/3 \langle 112 \rangle$ ($2 b_p$), which corresponds to the maximum in GSF curve (MAX, γ_{max}) and determines the barrier for the movement of the full dislocation. These GSF energies are the key parameters which determine the structure and mobility of dislocations (Vitek, 1974).

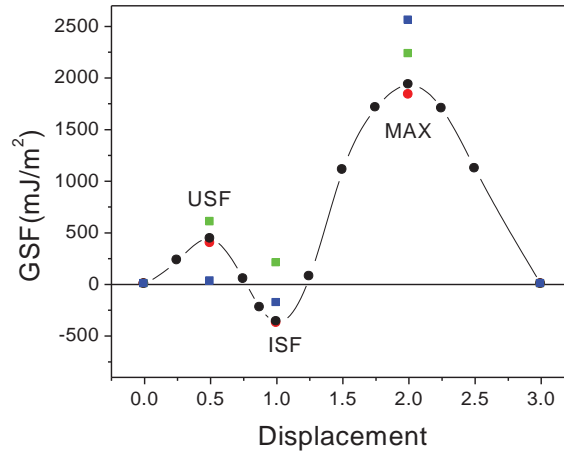


Figure 1. Generalized stacking fault (GSF) energies for $1/6\langle 112 \rangle(111)$ displacements in austenitic Fe (black), Fe 4 at. % Mn (red), Fe-8 at. % C (green) and Fe-8 at. % Al (blue). The extreme GSF energies corresponding to impurity positions $n=0$, 0 at the stacking fault are shown for Fe-C and Fe-Al.

We modeled the stacking fault defects using a 24-atom supercell, and GSF energies were calculated as a total energy change caused by a rigid shift of a half of the crystal along $\langle 112 \rangle$ direction in the (111) slip plane. The calculated GSF energies for pure fcc iron (Figure 1, Table 1) are in accord with previous ab initio results (Hickel et al., 2009; Kibey et al., 2006). We determined the energy of intrinsic stacking fault γ_{ISF} to be equal to -347 mJ/m^2 , which shows the preference of the hcp structure for the ISF for pure Fe. We found that manganese substituted for iron has a negligible effect on γ_{US} , γ_{ISF} , and γ_{max} (Figure 1 and Table 1). Subsequent calculations do not take into account the manganese addition.

Table 1. The SFEs (mJ/m^2) for pure fcc Fe and the averaged values for fcc Fe-4 at. % Mn, Fe 4 at. % C and Fe-4 at. % Al.

GSF (mJ/m^2)	Fe	Fe-Mn	Fe-C	Fe-Al
γ_{US}	439	428	544	370
γ_{ISF}	-347	-339	-48	-277
γ_{max}	1,932	1,916	2,072	2,155

For the interstitial C, we considered different octahedral interstitial positions in the n th layer (with $n = 0, 1, 2, 3$) below the stacking fault and at two concentrations: 4 at. % and 8 at. %. C increases all three stacking fault energies, and the differences in γ_{US} , γ_{ISF} and γ_{max} are gradually reduced to their values for pure Fe as n increases. C located in the third layer below ($n=3$) has a small influence on the stacking fault energies. Thus, there is a strong dependence of γ_{ISF} on both C location and concentration, whereas the variations in both γ_{US} and γ_{max} are less significant. Interstitial C located at the stacking fault sharply increases γ_{ISF} , making it positive. An even larger increase would occur in the case $n = 0,0$ when two C atoms are at the stacking fault. However, as it was demonstrated previously, the C-C interaction is repulsive and C atoms tend to be located farther away from each other in austenite. Therefore, the case $n = 0,0$ (Table 2) is unlikely. Taking into account that C is distributed randomly, we averaged γ_{ISF} on three layers and determined that the average value is about 300 mJ/m^2 higher than that in pure iron. This implies that the fcc phase is more favorable than the hcp in the Fe-C alloy, C is a strong austenite stabilizer, and C cannot promote the $\gamma \rightarrow \epsilon$ -martensite transformation (TRIP).

Table 2. The SFEs (mJ/m^2) for the position of one C atom in the n th layer below the stacking fault in Fe-4 at. % C and two C atoms at the stacking fault ($n = 0,0$) in Fe-8 at. % C.

GSF (mJ/m^2)	$n = 0$	$n = 1$	$n = 2$	$n = 3$	$n = 0,0$
γ_{US}	547	541	493	435	601
γ_{ISF}	49	-51	-145	-320	203
γ_{max}	2,120	2,024	2,018	1,964	2,229

For Al we considered the substitutional sites in the n th layer ($n = 0, 1, 2, 3$) below the stacking fault and with two concentrations, 4 at. % and 8 at. % (Table 3). We determined that Al also increases γ_{ISF} and that its effect depends on the Al distribution and content. The increase in the average value of γ_{ISF} is about 70 mJ/m² when compared with the pure fcc iron. The effect is more pronounced for the higher Al concentration (Table 3, $n = 0, 0$). For this atomic configuration, γ_{ISF} increases by 170 mJ/m². Thus, Al is an austenite stabilizer and suppresses the $\gamma \rightarrow \epsilon$ -martensite transformation. It should be noted that γ_{US} sharply decreases with Al concentration, and the lowering of the energy barrier for dislocations may favor enhanced plasticity. Further calculations on the effect of Al concentration on the USF energy γ_{US} and similar investigations for silicon are in progress.

Table 3. The SFEs (mJ/m²) for the position of the Al atom in the n layer below the stacking fault in Fe-4 at. % Al and two Al atoms in the k and l layers ($n = k, l$) in Fe-8 at. % Al.

GSF (mJ/m ²)	$n = 0$	$n = 1$	$n = 2$	$n = 0, 0$
γ_{US}	289	452	414	26
γ_{ISF}	-280	-275	-343	-182
γ_{max}	2,355	1,955	1,935	2,753

Lightweight Steel Using Al

Lightweight steels have been cast at Missouri S&T, and their microstructure-property behavior is being studied. In total, 10 different lightweight steels have been produced that meet the third generation property goals. Four types of microstructures have been produced with various combinations of manganese, silicon, Al, and C. Steels with austenite and ϵ -martensite microstructures have been formulated and exhibit TRIP where both austenite and ϵ -martensite transform to α' -martensite. Here we will report on three steels that have the targeted microstructure consisting of bainitic ferrite and austenite and report the influence of Al content on the deformation behavior. Table 4 lists the chemistries in weight percents. Al concentrations were above 3.4 wt % but were varied to observe how Al affects ferrite stability. The combination of Al and silicon was kept above 4 wt % (~10 at. %) to reduce density, while the manganese levels were kept about 13 wt % to ensure austenite stabilization. The silicon content was above 1 wt % to suppress cementite formation (Grassel et al., 1997) and therefore induce stasis of ferrite growth. Cast materials were homogenized at 1,100°C for 2 hours before being air cooled to ambient temperature. The castings were subsequently milled to produce 13.6 mm \times 126 mm \times 50 mm plates for hot rolling. Hot rolling occurred incrementally, starting at 900°C, with reheating between reductions when the temperature fell below 700°C. The plates were reduced 80% to a thickness of 2.8 mm. After the final rolling pass the plates were reheated to 900°C for 10 minutes before being water quenched. All of the alloys contained primary ferrite formed during solidification, which produced stringers of ferrite parallel to the rolling direction (see Figure 2).

Table 4. Chemistry of lightweight steels being reported.

Constituent	Alloy 1 (wt %)	Alloy 2 (wt %)	Alloy 3 (wt %)
Carbon	0.14	0.2	0.11
Manganese	13.87	13.56	13.92
Aluminum	3.51	3.44	4.53
Silicon	1.42	2.1	1.28
Phosphorus	0.022	0.012	0.017
Sulfur	0.005	0.018	0.011
Nitrogen	0.017	0.013	0.045
Calculated γ_{SFE} , mJ/m ²	26.4	26.7	35
Density, g/cm ³	7.44 \pm 0.03	7.47 \pm 0.04	7.31 \pm 0.04

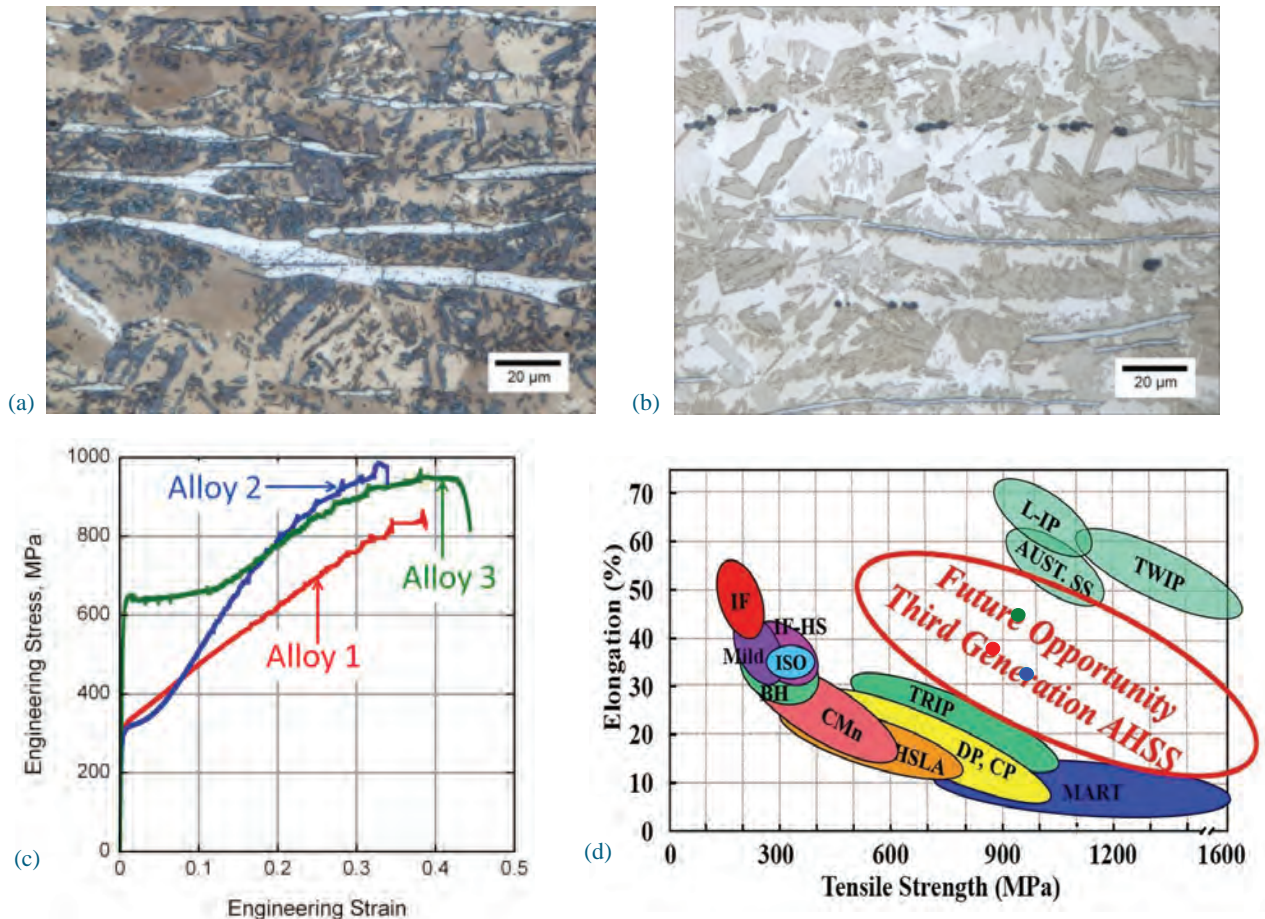


Figure 2. (a) Microstructure of Alloy 1 consisting of ferrite stringers parallel to the rolling direction (white contrast), bainitic ferrite (darkest contrast), and austenite. (b) Microstructure of Alloy 2 showing coarser blocks of bainitic ferrite. (c) Tensile-elongation curves for the three alloys (Table 4). (d) Property distribution plot for first and second generation AHSSs compared with tensile results from (c).

Increasing the C content in Alloy 2 produced a microstructure with less primary ferrite, whereas Alloy 3 had the highest Al content and the most primary ferrite. Alloy 1 produced a linear work hardening behavior after yielding at 300 MPa, whereas Alloy 2 had a yield plateau for 3% to 4% strain before rapid work hardening. Alloy 3 exhibited discontinuous yielding at about 2% strain (650 MPa upper yield stress and 640 MPa lower yield stress) and showed a yield plateau for 2% to 12% strain before rapid work hardening. All three alloys exhibited TRIP behavior with austenite transforming to α' -martensite. The retained austenite in Alloy 2 transformed at a faster rate than either Alloy 1 or Alloy 3. Alloy 2 also had a coarse block structure of bainitic ferrite. Timokhina et al. (2004) observed similar trends in an Fe 0.2C-1.55Mn-1.5Si alloy and suggested the stability of the austenite depended on its interaction with bainitic ferrite or martensite. Furthermore, as predicted by the SFE calculations, hexagonal ϵ -martensite was not observed. In our studies, it was noted that the size and distribution of bainitic ferrite had a strong influence on work hardening behavior. Microstructures with coarse blocky ferrite laths (Alloy 2) transformed to α' -martensite at a faster rate compared to the austenitic regions near refined degenerate ferrite. Serrated flow was also observed during work hardening for all three alloys and may indicate dynamic strain aging caused by short range ordering. A similar observation has been reported by Owen and Grujicic (1999) in austenitic Hadfield manganese steels. These findings may be explained by Mn-Al-C clustering.

Alloy 3 demonstrated the highest yield strength (>600 MPa) and an elongation greater than 40%. It has been suggested that as the disparity in strength between microstructural constituents decreases, the overall ductility of the composite structure will increase. It is well known that nitrogen can produce strain aging and discontinuous yielding in ferritic steels, and Alloy 3 had the highest nitrogen level and the most primary ferrite. This effect is still under investigation with first principle calculations being performed to study the effect of nitrogen on the formation of defect structures in Fe-Mn-Al-Si solid solutions. We are also in the process of characterizing the chemistry of the ferrite and austenite structures to better understand the role of Al in the ductility and TRIP behavior of the austenite.

Conclusions

First principle calculations are providing critical insight as to the roles of Al and silicon in high manganese steels that are formulated for reduced density. Short range ordering to form Mn-C-Al defects as shown by our first principle calculations may increase the strength of the austenite and increase the ductility in TRIP steels by reducing the strength disparity in composite microstructures. Evidence of these defect clusters was observed in the tensile behavior, which demonstrated dynamic strain aging.

Presentations / Publications / Patents

McGrath, M. C.; Van Aken, D. C.; Richards, V. L. Mechanical properties and their dependence on microstructure in hot-rolled 3rd generation advanced HSS. Presented at the 2010 TMS Annual Meeting, Seattle, Washington, February 14–18, 2010.

McGrath, M. C.; Van Aken, D. C.; Richards, V. L. Effect of cerium on the inoculation of acicular ferrite in hot-rolled FeMnAlC steel. Presented at AISTech 2010, Pittsburgh, Pennsylvania, May 3–6, 2010.

Medvedeva, N. I.; Howell, R. A.; Van Aken, D. C.; Medvedeva, J. E. Effect of phosphorus on brittle fracture in α -carbide. Phys. Review B, 2010, 81, 012105.

Medvedeva, N. I.; Van Aken, D.; Medvedeva, J. E. Magnetism in bcc and fcc Fe with C and manganese. J. Phys. Cond. Matter, 2010, 22, 316002.

References

Frommeyer, G.; Brux, U.; Neumann, P. Supra-ductile and high-strength manganese TRIP/TWIP steels for high energy absorption purposes. ISIJ Int. 2003, 43, 438.

Grassel, O.; Frommeyer, G.; Derder, C.; Hofmann, H. Phase transformations and mechanical properties of Fe-Mn-Si-Al TRIP-steels. J. Phys. IV France, 1997, 7, C5-383.

Hickel, T.; Dick, A.; Grabowski, B.; Kormann, F.; Neugebauer, J. Steel design from fully-parameter-free ab-initio computer simulations. Materials Technology, 2009, 80, 4.

Kibey, S.; Liu, J. B.; Curtis, M. J.; Johnson, D. D.; Sehitoglu, H. Effect of nitrogen on generalized stacking fault energy and stacking fault widths in high nitrogen steels. Acta Mater. 2006, 54, 2991.

Owen, W. S.; Grujicic, M. Strain aging of austenitic Hadfield manganese steel. Acta Mater. 1999, 47, no. 1, 111.

Timokhina, I. B.; Hodgson, P. D.; Pereloma, E. V.; Effect of microstructure on the stability of retained austenite in transformation-induced-plasticity steels. Met Trans A, 2004, 35A, no. 8, 2331.

Vitek, V. Theory of core structure of dislocations in body-centered cubic metals. Cryst. Latt. Def. 1974, 5, 1–34.

3. Polymer Composites

A. Polymer Composite Development - Pacific Northwest National Laboratory

Field Technical Monitor: Dean Paxton
Pacific Northwest National Laboratory
902 Battelle Boulevard, P.O. Box 999; Richland, WA 99352
(509)375-2620; e-mail: dean.paxton@pnl.gov

Technology Area Development Manager: Carol Schutte
U.S. Department of Energy
1000 Independence Ave., S.W.; Washington, DC 20585
(202)287-5371; e-mail: carol.schutte@ee.doe.gov

Contractor: Pacific Northwest National Laboratory (PNNL)
Contract No.: DE-AC05-00OR22725 & DE-AC06-76RLO1830

The Polymer Composite Development project consists of two tasks focused on research and development that can lead to greater implementation and manufacturing of polymer composite materials for automotive applications. The tasks are (1) Natural Fiber Composite Retting, Preform, Manufacture, and Molding and (2) Evaluation of Composite Natural Fiber-Resin Compatibility. The objectives, accomplishments, and future directions for these tasks are provided as follows.

Objective

- Fabricate 150 mm × 150 mm kenaf–vinyl ester compression-molded panels with standard deviation in density, moisture uptake, tensile, and flexural properties of <10% among five 25 mm specimens cut from the panel to enable meaningful evaluation of strategies to improve the interface between fibers and resin in bio-fiber composites.
- Accomplish 30% reduction in loss of flexural modulus of 50 fiber volume % kenaf–vinyl ester compression-molded composite specimens following 24 hr immersion in water at 25°C to address the major barrier to use of bio-fiber composites: loss of bio-fiber composite mechanical performance with exposure to moisture.
- Demonstrate scalability of the bio-fiber composites fabrication process by producing 50 kg of kenaf non-woven material to validate mechanical properties to within 10% of lab-scale testing.

Accomplishments

- Processed more than 50 kg of kenaf non-woven material for composite fabrication and mechanical property validation. Composite panel density was demonstrated to have a variation of 1.7% and a moisture uptake a variation of 13.8%. Variation in mechanical properties was found to be 14.9% for tensile strength, 8.1% for tensile modulus, 10.5% for flexural strength, and 10.3% for flexural modulus. (FY 2010)
- Achieved 70% improvement in kenaf fiber composite mechanical properties following 24 hr water immersions using a novel resin additive technology. Specifically, the flexural modulus of untreated fiber composite was reduced from 10.61 to 3.09 GPa after the soak treatment, whereas the modulus of treated fiber composite was only reduced from 10.55 to

5.31 GPa, representing a 30% lower impact. Retention of mechanical performance with exposure to moisture is essential for use of bio-fiber composites in the reduction of cost and weight and the increase of renewable content in vehicle components. (FY 2010)

- Completed the Natural Fiber Composite Retting, Preform, Manufacture, and Molding task in FY 2010.
- Completed the Evaluation of Composite Natural Fiber-Resin Compatibility task in FY 2010.

Future Direction

- Details of the fiber-formatting and composite-molding processes for kenaf fiber, hybrid kenaf/glass fiber, and kenaf/carbon fiber composites will be published in peer-reviewed journals to make this information widely available.
- Details and results of the developed resin additive fiber treatments will be published in peer-reviewed journals to facilitate continued development of natural fiber composites for structural, exterior applications.

Introduction

Plant based natural bio-fibers have the opportunity to address all three of the 2010 Technology-Specific Research Goals for Materials identified by the U.S. Department of Energy (DOE) for material and manufacturing technologies for high-volume production vehicles (FreedomCAR and Fuel Partnership Plan). Through displacement of glass fiber in fiber-reinforced polymer composites, natural fibers can enable the simultaneous attainment of reduction in the weight of vehicle structure, increase in material affordability, and increase in renewable material content. At 1.4 g/cm³, natural fibers such as kenaf are 40% lighter than currently used 2.6 g/cm³ E-glass fiber, translating to a potentially significant component weight savings. The cost and energy to produce a kilogram of natural plant fiber [\$0.20–1.00, 4 megajoules (MJ)] is much less than that required to produce glass fiber (\$1.10–1.80, 30 MJ) or carbon fiber (\$11.00/kg, 130MJ) (Huda, 2008). Especially with the use bio based resin, natural fibers can drastically increase the renewable content of current thermoset composites from 0% to more than 50%.

Most natural fiber composite components on vehicles today consist of fiber-filled thermoplastics, such as polypropylene, and are nonstructural interior parts. The potential for vehicle weight savings can be dramatically increased if natural fibers can be used in structural and semi-structural exterior automotive parts where glass fiber is used today. These new applications will likely involve thermoset resins and will require environmentally durable performance. The mechanical robustness of these parts must persist at the temperature and moisture extremes encountered by the vehicle during its operational lifetime.

For natural fibers to penetrate the glass fiber composite market, cost-effective methods for fiber retting (extraction of fibers from the plants), fiber formatting, and natural fiber composite molding must be developed. In addition, the crucial barrier of moisture-induced mechanical property degradation in natural fiber composite must be overcome.

The objective of the first task of this project is to develop and demonstrate scalable methods to format fibers for compounding and molding into composite with consistent physical and mechanical performance. The second task of the project builds on the success of the first to investigate the compatibility of natural fiber reinforcements with polymer systems applicable to automotive structural and semi-structural composites. The project seeks to evaluate and characterize the stiffness, strength, and failure modes of selected candidate natural fiber-reinforced material systems under standard and wet conditions. Novel fiber surface treatments and material processing variables are designed and evaluated in an effort to optimize the durability of natural fiber composite mechanical performance in the presence of moisture. The project focuses on a limited number of natural fiber and polymer systems that meet basic requirements for automotive applications, including fiber cost and availability, strength and stiffness, and high-volume processing compatibility. These include kenaf fiber, epoxy vinyl ester resin, and standard and bio based unsaturated polyester resins.

Inherent limitations to the mechanical and environmental performance of natural fibers are overcome through development of methods to blend natural with synthetic fibers to form hybrid composites with intermediate material costs, performance, and density.

The following sections outline specific task work conducted at Pacific Northwest National Laboratory (PNNL) in the area of polymer composite development technologies. Each task supports one or more goals within the Polymer Composite Development Agreement, as outlined below.

Activity and Developments

Natural Fiber Composite Retting, Preform, Manufacture, and Molding

Principal Investigator: Kevin L. Simmons, Pacific Northwest National Laboratory
(509) 375-3651; e-mail: Kevin.Simmons@pnl.gov

Principal Investigator: Leonard S. Fifield, Pacific Northwest National Laboratory
(509) 375-6424; e-mail: Leonard.Fifield@pnl.gov

Key PNNL Contributors: Sachin Laddha, Matt Westman, Tyler Kafentzis

Industrial Participants: Dan Houston (Ford Motor Company), Libby Berger (General Motors), Rob Seats, Bob Moffit (Ashland), Steve Hardebeck (Reichold), Rob Plaunt (AOC), Bob Hughes (BioTech Mills), Hugh McKee (Bast Fibers LLC)

Introduction

Natural fibers have the opportunity to displace glass fibers in high-volume production automotive thermoset composites if methods to format, layup, and compression mold the fibers can be developed. For maximum acceptance, natural fiber molding processes must be compatible with current glass fiber composite production and infrastructure. This activity supports the goals of kenaf–vinyl ester composite fabrication with cross-panel property deviation below 10% and demonstrated scale-up of laboratory kenaf processing to >50 kg of non-woven fiber material.

Approach

Conventional sheet molding compound composite fabrication requires chopped fibers to freely flow with a matured thermoset resin to evenly fill a hot mold during compression. Retted kenaf fibers tend to entangle with each other, preventing free material flow. This limitation was overcome through the development of a kenaf fiber net-shape preform that can be wet with resin, stacked into laminate layers, and directly compression molded. Chopped fibers of 5 cm length were arranged into non-woven mats using an electric carding machine (Louet North America) with no binder and no additional needle punching.

Process variables were explored through production of a series of 150 mm × 150 mm × 3 mm test panels (>250 produced) from the non-woven mats using unsaturated polyester (Aropol 7030), bio based unsaturated polyester (Envirez 1807, 25% bio based), and epoxy vinyl ester (Derakane 782) resins. The effects of chopped fiber length, fiber loading, filler choice and loading, molding conditions, maturation conditions, and other process conditions were determined. In addition, non-woven mats and molded composites were produced from glass fibers, carbon fibers, and hybrids of kenaf with glass fiber and kenaf with carbon fiber.

Success of this task in developing fiber-formatting and molding techniques was critical to the completion of the project as it facilitated the meaningful development of fiber treatments to improve resin interfacing and wet composite mechanical performance in the second task. Each compression-molded panel was cut into five test specimens. These were equilibrated at 50% relative humidity for 48 hr before being tested “dry” or soaked for 24 hr in deionized water following equilibration before being tested “wet.” The weight gain of soaked samples and the flexural and tensile properties of the wet and dry samples were measured toward addressing the goals of the project.

Results and Discussion

The effects of fiber length and loading on the tensile and flexural properties of vinyl ester composites made from kenaf non-woven mats were investigated. Composites reinforced with 25 mm kenaf fiber (Table 1) exhibited similar dry mechanical properties to those reinforced with 50 mm kenaf fiber (Table 2), indicating that 25 mm is longer than the critical fiber length in this system. Tensile and flexural properties of dry-tested specimens were observed to increase with fiber loading up to the

approximate production method limit of 60 fiber volume % kenaf. Effects of fiber type and fiber treatment for the project were investigated on panels consisting of 50 fiber volume % and no inorganic filler. The non-woven mat preform process for panel fabrication facilitates fiber loadings much higher than the around 15 fiber volume % that is commonly used for glass fiber sheet molding compounds. In addition to increasing mechanical properties, high natural fiber loadings can help to displace relatively expensive resin similar to inorganic fillers, but with a much lower negative impact on composite density. Natural fiber wet specimen properties decreased with fiber loadings above 40–50 fiber volume % kenaf in a fiber loading regime in which the higher moisture content associated with the higher fiber content dominates the mechanical performance (Table 3).

Table 1. Effect of 25 mm kenaf fiber loading on dry-tested vinyl ester composites.

Nominal 25 mm Fiber Loading	Tensile Modulus (GPa)	Tensile Strength (MPa)	Flexural Modulus (GPa)	Flexural Strength (MPa)
30 vol% kenaf	8.22	71.39	8.15	90.04
40 vol% kenaf	10.21	75.08	9.78	108.67
50 vol% kenaf	10.69	81.92	11.71	126.15

Table 2. Effect of 50 mm kenaf fiber loading on dry-tested vinyl ester composites.

Nominal 50 mm Fiber Loading	Tensile Modulus (GPa)	Tensile Strength (MPa)	Flexural Modulus (GPa)	Flexural Strength (MPa)
30 vol% kenaf	8.11	61.80	7.47	89.34
40 vol% kenaf	8.24	66.36	8.91	98.90
50 vol% kenaf	11.54	83.46	10.61	118.29
60 vol% kenaf	12.40	92.62	11.21	134.51

Table 3. Effect of 50 mm kenaf fiber loading on wet-tested vinyl ester composites.

Nominal 50 mm Fiber Loading	Tens. Modulus (GPa)	Tens. Strength (MPa)	Flex. Modulus (GPa)	Flex. Strength (MPa)	Weight Gain (%)
30 vol% kenaf	4.39	42.79	3.05	48.53	8.35
40 vol% kenaf	5.22	51.96	3.25	50.10	9.71
50 vol% kenaf	5.47	35.60	3.09	42.33	13.39
60 vol% kenaf	4.48	32.77	3.24	25.83	17.11

Combining kenaf fiber with glass or carbon fiber in production of the non-woven mats for composite reinforcement enables an optimization of the properties of each: the lower moisture uptake and higher mechanical properties of glass or carbon and the lower density and lower cost of kenaf. For 50 total fiber volume % panels, kenaf and glass fibers were in hybrid with densities ranging from 1.3 g/cm³ for all kenaf fiber to 1.8g/cm³ for all glass fiber (Table 4). Fiber ratios in assembled non-woven kenaf/glass hybrid fiber mats were confirmed with burn-out tests. Scanning electron micrographs qualitatively reveal the extent of fiber blending and the increased fiber/resin interface in a kenaf/glass hybrid composite (Figure 1). Similar to the kenaf/glass fiber hybrid panels, kenaf/carbon fiber hybrid panels exhibited corresponding increases in tensile and flexural properties relative to the kenaf-only panels (Table 5).

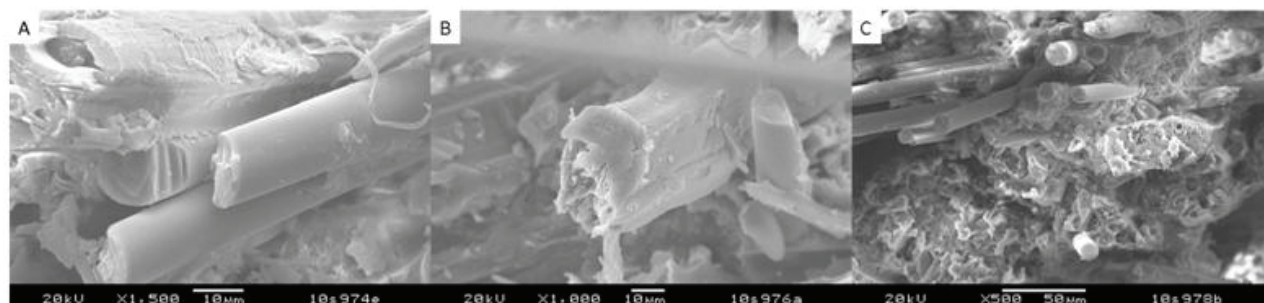


Figure 1. Scanning electron micrographs of kenaf/glass hybrid panels showing proximity of glass and kenaf fibers: (A) Untreated hybrid; (B) and (C) hybrid panels with two different resin additive fiber treatments.

Table 4. Glass loading in dry (wet)-tested 50 total fiber volume % kenaf/glass hybrid vinyl ester composites.

Fiber Weight Ratio	Tens. Modulus (GPa)	Tens. Strength (MPa)	Flex. Modulus (GPa)	Flex. Strength (MPa)	Density (g/cm ³)
0% Glass/kenaf	11.54 (5.47)	83.46 (35.60)	10.61 (3.09)	118.29 (42.33)	1.29
25% Glass/kenaf	10.57 (6.44)	87.21 (43.75)	9.25 (4.02)	81.91 (58.74)	1.47
50% Glass/kenaf	12.77 (8.69)	98.87 (73.79)	13.71 (7.21)	148.37 (106.60)	1.59
100% Glass	20.75 (16.20)	148.79 (81.60)	20.18 (14.85)	243.57 (118.40)	1.78

Table 5. Kenaf/carbon 50 total fiber volume % dry (wet)-tested hybrid vinyl ester composites.

Panel	Tens. Modulus (GPa)	Tens. Strength (MPa)	Flex. Modulus (GPa)	Flex. Strength (MPa)	Weight Gain (%)
Kenaf	11.54 (5.47)	83.49 (35.60)	10.61 (3.09)	118.29 (42.33)	(13.39)
1:2 w/w carbon/kenaf	15.44 (11.99)	124.37 (84.87)	14.52 (7.91)	166.70 (100.63)	(6.95)

The mechanical properties measured for kenaf and kenaf/glass hybrid panels made with the Derakane 782 vinyl ester and the Envirez 1807 bio based unsaturated polyester were similar, although the bio based polyester composites generally exhibited higher tensile strength (Table 6).

Table 6. Kenaf and kenaf/glass hybrid dry (wet)-tested vinyl ester (Derakane 782) (VE) and bio based unsaturated polyester (Envirez 1807) (PE) composite performance. Panels are 50 total fiber volume %.

Panel Description	Resin	Tensile Modulus (GPa)	Tensile Strength (MPa)	Flexural Modulus (GPa)	Flexural Strength (MPa)	Weight Gain (%)
Kenaf	VE	11.54 (5.47)	83.46 (35.60)	10.61 (3.09)	118.29 (42.33)	(13.39)
Kenaf	UP	10.57 (5.44)	92.22 (67.27)	7.96 (2.13)	102.87 (24.08)	(7.47)
1:1 w/w kenaf/glass	VE	12.77 (8.69)	98.87 (73.79)	13.71 (7.21)	148.37 (106.60)	(3.51)
1:1 w/w kenaf/glass	UP	13.85 (7.52)	106.57 (39.30)	12.19 (5.42)	153.88 (55.74)	(7.88)

Conclusions

Chopped kenaf fiber was assembled into integral non-woven mats and laminated with resin to produce net-shape natural fiber preforms for compression molding in sheet molding compound-type process. Panels were produced with high fiber loadings, minimal voids, and good fiber wet-out and low cross-panel variation in fiber density. The carding process for assembled of non-woven mats was demonstrated as amenable to the production of hybrid mats combining kenaf fiber with glass fiber or carbon fiber in any desired ratio.

Five test specimens were cut from each panel and conditioned under controlled humidity to produce dry samples prior to testing or conditioned and then soaked overnight to produce wet samples. The tensile and flexural properties of dry and wet specimens were determined along with the moisture uptake of the soaked samples.

The developed preform production and molding processes were successfully applied to multiple natural fiber types, fiber lengths, filler contents, and thermoset resins including an epoxy vinyl ester resin, an unsaturated polyester resin, and a bio based unsaturated polyester. The 25% renewable content of the Envirez 1807 combined with a 50% kenaf fiber loading resulted in composite panels with 75% renewable content and >20% lower density than corresponding glass fiber composite panels. More than 50 kg of kenaf fiber was molded into nearly 250 composite panels using the developed process with <15% average variation in mechanical and moisture uptake properties among the five specimens taken from each panel.

Evaluation of Composite Natural Fiber-Resin Compatibility

Principal Investigator: Leonard S. Fifield, Pacific Northwest National Laboratory
(509) 375-6424; e-mail: Leonard.Fifield@pnl.gov

Principal Investigator: Kevin L. Simmons, Pacific Northwest National Laboratory
(509) 375-3651; e-mail: Kevin.Simmons@pnl.gov

Key PNNL Contributors: Sachin Laddha, Matt Westman, Tyler Kafentzis

Industrial Participants: Dan Houston (Ford Motor Company), Libby Berger (General Motors), Rob Seats, Bob Moffit (Ashland), Steve Hardebeck (Reichold), Rob Plaunt (AOC), Bob Hughes (BioTech Mills), Hugh McKee (Bast Fibers LLC)

Introduction

A major barrier to the displacement of glass fiber with lower density natural fiber in reinforcement of exterior and semi-structural transportation composites is the tendency of natural fiber composites to absorb moisture and for their mechanical properties to rapidly degrade in the presence of moisture. In addition to being less inherently hydrophilic, synthetic fibers currently used in automotive composites undergo surface treatments to facilitate a favorable resin interface. This activity focuses on the development of natural fiber surface treatments that improve the fiber-resin interface and inhibit fiber moisture uptake to support the goal of 70% improvement in the tensile and flexural properties of kenaf fiber reinforced–vinyl ester composite following a 24-hour soak.

Approach

The fabrication process developed as a part of this project, including kenaf fiber formatting into non-woven mats and molding of the preformed mats into 50 fiber volume % composites, was used to establish a baseline of untreated kenaf fiber composite properties and to evaluate the fiber treatment variable. Under guidance from automotive manufacturers, a set of screening tests was selected for the purpose of evaluating and comparing fiber treatments relative to application in semi-structural exterior parts. While impact toughness and coefficient of thermal expansion were understood to be of eventual application importance, this project focused on measurement of tensile and flexural properties for composites before and after 24 hr immersion in deionized water. In addition to these standard mechanical tests, several spectroscopic means were employed including scanning electron microscopy (SEM) and time-of-flight secondary ion mass spectrometry (TOF-SIMS) to gain understanding of the action of the fiber treatments.

Various chemical and physical fiber treatments were considered as well as fiber treatment application methods in order to reduce fiber moisture uptake and maintain composite mechanical properties after overnight soak. Loose fibers were treated before carded assembly into non-woven mats and assembled mats of fibers were treated. Chemical treatments were applied to the fibers through bath solution “dips,” spraying using a carrier solvent, and through direction addition to the resin formulation along with low-profile additive, modifiers, catalyst, etc., before introduction of the resin mixture to the fiber. Several classes of standard and novel chemical agents were investigated including silane based (PNNL-S), small molecule based (PNNL-X), dual component (PNNL-D), and polymer based (PNNL-P) agents.

Technology Transfer Path

The success of this activity in demonstrating chemical resin additives for existing commercial thermoset resins systems, described in two PNNL invention disclosure reports, has garnered interest from the automotive industry including a top-tier automotive resin supplier. Details of the technology have been communicated under nondisclosure agreement, and the supplier is performing internal evaluations of the resin additive technologies.

The resin additive approach for mitigating natural fiber moisture uptake is low cost and simple to implement, especially relative to strategies for fiber treatment prior to the molding process. The technology developed and demonstrated at PNNL significantly increases opportunities for natural fiber vehicle composite manufacturers to take advantage of low-density, bio based materials that have been limited by moisture uptake and wet mechanical performance.

Results and Discussion

Degradation of properties with exposure to moisture was generally observed to track with the magnitude of the moisture-induced weight gain. Among the explored chemical treatment methods, the resin additive approach was found to be the most effective, benefitting from having minimal organic solvent use (no additional solvent) and minimum number and difficulty of process steps (simply added and stirred with the resin formulation). **Table 1** compares the effect of the spray and resin additive methods for two reactive small molecule fiber treatments on the properties of composite panels following 24 hr soak (wet).

Table 1. Effect of fiber treatment application method on wet-tested 50 vol% kenaf–vinyl ester panels.

Treatment/Method	Tensile Modulus (GPa)	Tensile Strength (MPa)	Flexural Modulus (GPa)	Flexural Strength (MPa)	Weight Gain (%)
PNNL-X11A / Spray	6.05	38.03	2.46	36.66	11.01
PNNL-X11A / Additive	8.89	63.44	5.22	91.62	4.36
PNNL-X11B / Spray	6.4	51.58	2.92	35.69	12.08
PNNL X11B / Additive	8.86	61.84	5.94	85.9	5.19

The effect on dry and wet mechanical and water uptake performance of a series of 50 fiber volume % vinyl ester composite panels fabricated using examples from each class of chemical fiber treatment agents is displayed in **Table 2**, along with data from a panel fabricated with untreated fiber. Without fiber treatment, panel properties are seen to degrade by 53%, 57%, 71%, and 64% for tensile modulus (TM), tensile strength (TS), flexural modulus (FM) and flexural strength (FS), respectively, following 24 hr soak. The panel with untreated fiber was observed to increase in weight by >13% during that time. Reactive small-molecule (PNNL-X) and polymer based (PNNL-P) agents demonstrated the greatest effect in counteracting this moisture degradation. In contrast to the panel with untreated fiber, the TM, TS, FM, and FS performance of the panel with PNNL-X12 fiber treatment degraded by only 20%, 10%, 52%, and 26%, respectively. The moisture uptake was reduced to <4%, a >71% improvement over the panel made from untreated fiber. For the PNNL-PL fiber treatment, TM, TS, FM, and FS performance degraded following soak by 19%, 12%, 49%, and 32%, respectively. Moisture uptake for a panel with this fiber treatment was <5%, a 65% improvement over that of a panel made with untreated fiber.

Table 2. Effect of chemical fiber treatment on dry (wet)-tested 50 vol% kenaf–vinyl ester composites.

Fiber Treatment	Tens. Modulus (GPa)	Tens. Strength (MPa)	Flex. Modulus (GPa)	Flex. Strength (MPa)	Weight Gain (%)
None	11.54 (5.47)	83.49 (35.60)	10.61 (3.09)	118.29 (42.33)	(13.39)
PNNL-SS	(5.94)	(52.56)	(3.59)	(48.71)	(13.14)
PNNL-X12	10.37 (8.25)	84.48 (76.35)	10.02 (4.77)	102.36 (75.80)	(3.80)
PNNL-D0	12.2 (6.47)	101.07 (60.28)	10.61 (2.94)	118.29 (40.83)	(9.81)
PNNL-PL	10.26 (8.34)	92.97 (82.20)	9.3 (4.71)	124.84 (84.61)	(4.65)

Blending of glass fibers with kenaf fibers in production of non-woven mats resulted in composite panels with increased tensile and flexural properties and reduced moisture uptake. Chemical fiber treatments developed for kenaf fiber panels were also applied to the hybrid fibers. Example results of dry and wet testing of untreated and treated 50 total fiber volume %, 1:1 w/w kenaf/glass hybrid vinyl ester panels are displayed in **Table 3**. The combined use of fiber blending and chemical treatment resulted in 24 hr soak moisture uptake values below 2% for panels with densities of 1.5 g/cm³.

Table 3. Effect of treatment on dry (wet)-tested 50 fiber volume % 1:1 w/w kenaf/glass vinyl ester composites.

Fiber Treatment	Tens. Modulus (GPa)	Tens. Strength (MPa)	Flex. Modulus (GPa)	Flex. Strength (MPa)	Weight Gain (%)
None	12.77 (8.69)	98.87 (73.79)	13.71 (7.21)	148.37 (106.60)	(3.51)
PNNL-X11A	12.13 (10.60)	90.96 (60.96)	11.37 (7.10)	142.30 (107.82)	(3.29)
PNNL-X11B	(11.10)	(100.72)	(8.62)	(126.19)	(1.67)
PNNL-X12	12.19 (10.09)	93.80 (71.21)	11.04 (6.53)	144.84 (88.17)	(2.76)
PNNL-PL	13.53 (10.12)	108.01 (90.23)	12.23 (8.64)	161.88 (120.48)	(3.44)

The developed chemical fiber treatments were similarly seen to be effective for kenaf/carbon fiber hybrid vinyl ester panels (Table 4) and kenaf/glass fiber hybrid panels made with bio based unsaturated polyester (Table 5). Degradation of TM, TS, FM, and FS properties for the PNNL-PL-treated kenaf/glass fiber bio-based unsaturated polyester composite following 24 hr soak were reduced to 9%, 4%, 45%, and 38% from the 46%, 63%, 56%, and 64% observed for the untreated hybrid fiber composite, respectively. Moisture uptake for this treated hybrid fiber panel was close to 3%, a 60% improvement over the untreated hybrid fiber panel.

Table 4. Effect of treatment on dry (wet)-tested 50 fiber volume % 2:1 w/w kenaf/carbon vinyl ester composites.

Fiber Treatment	Tens. Modulus (GPa)	Tens. Strength (MPa)	Flex. Modulus (GPa)	Flex. Strength (MPa)	Weight Gain (%)
None	15.44 (11.99)	124.37 (84.87)	14.52 (7.91)	166.70 (100.63)	(6.94)
PNNL-X11A	(13.68)	(117.62)	(8.51)	(120.91)	(2.52)

Table 5. Dry (wet) test data for 50 fiber volume % 1:1 w/w kenaf/glass bio based unsaturated polyester composites.

Fiber Treatment	Tens. Modulus (GPa)	Tens. Strength (MPa)	Flex. Modulus (GPa)	Flex. Strength (MPa)	Weight Gain (%)
None	13.85 (7.52)	106.57 (39.30)	12.19 (5.42)	153.88 (55.74)	(7.88)
PNNL-PL	12.98 (11.83)	108.75 (103.99)	15.82 (8.78)	174.37 (108.92)	(3.11)

Near-, mid-, and long-term targets for natural fiber composite properties in transition to exterior and semi-structural applications were developed with input from Ford Motor Company and General Motors during FY 2010. These are displayed in Table 6 along with the PNNL-determined baseline values and the technology status following PNNL development of fiber treatments in FY 2010.

Table 6. Targets for natural fiber structural composites, baseline values, and PNNL technology status. (Values are for 50 fiber volume %, compression-molded vinyl ester composites with no inorganic filler tested following 24 hr soak at room temperature in deionized water.)

		Weight Gain	Tensile Modulus (GPa)	Tensile Strength (MPa)	Flexural Modulus (GPa)	Flexural Strength (MPa)	Density (g/cm ³ dry)
<i>Structural Targets</i>	<i>2011 Targets (1 year)</i>	5%	7	50	4	75	1.5
	<i>2015 Targets (5 years)</i>	2%	8	75	5	100	1.4
	<i>Ultimate Targets</i>	1%	9	100	10	150	1.3
<i>Baseline</i>	<i>Untreated Kenaf</i>	13.39%	5.47	35.60	3.09	42.33	1.27
	<i>Untreated Glass</i>	0.22%	19.37	205.24	15.63	258.04	1.78
<i>PNNL Status</i>	<i>Treated Kenaf</i>	4.65%	8.25	76.35	4.77	75.80	1.25
	<i>Untreated 1:1 Kenaf/Glass</i>	3.51%	8.69	73.79	7.21	106.6	1.50
	<i>Treated 1:1 Kenaf/Glass</i>	1.67%	11.1	100.72	8.62	126.19	1.47

Conclusions

Chemical fiber treatments developed in FY 2010 reduced the moisture uptake and subsequent degradation of tensile and flexural mechanical properties of kenaf natural fiber composites and hybrid composites containing kenaf and glass or carbon fiber. Treatment by resin additive resulted in a 70% improvement in wet mechanical properties of 50 volume fiber % kenaf-vinyl ester composites.

In FY 2010, the PNNL-developed technologies met or exceeded the 5 year mechanical and moisture uptake performance goals for natural fiber structural composites established in January of 2010 in collaboration with industry leaders.

Conclusions

Natural fibers can offer significant weight and cost benefits to automotive composites if their application can be extended to exterior and structural or semi-structural vehicle applications. The major barriers to this transition are formatting and molding technologies for the fibers and development of fiber systems that have adequate mechanical properties and environmental durability. This project's two tasks have directly addressed these technology gaps and have achieved results surpassing mid-term technology targets established in collaboration with the automotive industry. The promise and progress of natural fiber composite technology warrants continued investment to enable lighter-weight, lower-cost materials with increased renewable content.

Presentations/Publications/Patents

Fifield, L. S.; Simmons, K. L. Compression Molded, Bio-fiber Reinforced, High Performance Thermoset Composites for Structural and Semi-Structural Applications. In Proc. of 10th Annual Automotive Composites Conference & Exhibition—Composites: Shaping New Vehicles, Society of Plastics Engineers, 2010.

Fifield, L. S.; Simmons, K. L. Keeping Sponges Dry in a Puddle: Reducing Moisture Uptake and Sustaining Mechanical Properties in High Natural Fiber-Content Thermoset Composites. Presented at Natural Fibers in Thermoset Composites: Opportunities, Barriers and Enabling Technologies, Ohio Bioproducts Innovation Council Workshop, Dublin, Ohio, August 11, 2010.

Fifield, L. S.; Simmons, K. L.; Laddha, S. G.; Kafentzis, T. A. Performance Enhancement of Compression Molded Kenaf Fiber Reinforced Vinyl Ester Composites through Resin Additive. In Proc. of SAMPE 2010 Spring Conference and Exhibition: New Materials and Processes for a New Economy, Society for the Advancement of Materials and Process Engineering, 2010.

Fifield, L. S.; Simmons, K. L.; Westman, M.; Kafentzis, T. A. Polymer Resin Additives for Natural Fiber Thermoset Composites. PNNL Invention Disclosure 16795-E.

Fifield, L. S.; Simmons, K. L.; Laddha, S.; Westman, M.; Kafentzis, T. A. Resin Additives for Natural Fiber Composites. PNNL Invention Disclosure 16734-E.

Qiu, R.; Ren, X.; Fifield, L. S.; Simmons, K. L.; Li, K. Hemp-Fiber-Reinforced Unsaturated Polyester Composites: Optimization of Processing and Improvement of Interfacial Adhesion. *J. Appl. Polym. Sci.* Accepted 2010

Simmons, K. S.; Fifield, L. S.; Laddha, S. G.; Chen, F.; Wright, K. M. Effect of Sodium Hydroxide and Supercritical Fluid Treatments on Unretted Kenaf Fibers. In Proc. of SAMPE 2010 Spring Conference and Exhibition: New Materials and Processes for a New Economy, Society for the Advancement of Materials and Process Engineering, 2010.

References

FreedomCAR and Fuel Partnership Plan:

www.eere.energy.gov/vehiclesandfuels/pdfs/program/materials_team_technical_roadmap.pdf

Huda, M. S.; Drzal, L. T.; Ray, D.; Mohanty A. K.; M. Mishra. Natural-fiber composites in the automotive sector. In *Properties and Performance of Natural-Fibre Composites*; Pickering, K. L. Ed.; Woodhead Publishing Ltd.: Cambridge, UK, 2008; pp 221–268.

B. Polymer Composite Development - Oak Ridge National Laboratory

Field Technical Monitor: C. Dave Warren
Oak Ridge National Laboratory
1 Bethel Valley Road; Oak Ridge, TN 37831
(865) 574-9693; e-mail: warrencd@ornl.gov

Technology Area Development Manager: Carol Schutte
U.S. Department of Energy
1000 Independence Ave., S.W.; Washington, DC 20585
(202) 287-5371; e-mail: Carol.Shutte@ee.doe.gov

Contractor: Oak Ridge National Laboratory (ORNL)
Contract No.: DE-AC05-00OR22725

This project consists of five tasks critical for the manufacture and implementation of composite materials in automotive structures. The tasks are (1) development of advanced preform technologies; (2) development of predictive models for long fiber thermoplastic (LFT) injection molding; (3) development of standard test methods for composite crashworthiness; (4) conducting intermediate-strain-rate crush experiments on composites; and (5) development of rapid, reliable joining methods for composites. These projects are aimed at developing methods for low cost manufacturing and design for crashworthiness of composites in automotive structures. They include lower cost directed-fiber placement technologies and development of reliable models for LFT injection molding, along with development of an understanding of the material response of composites in automotive crash loadings and joints comprised of composite materials.

Objective

In support of the development of advance perform technologies; objectives for this year include the following.

- Develop rapid, low cost fiber-placement technologies based on programmable, robotic-controlled, directed chopped-fiber processes for the application of reinforced thermoplastics, hybrid glass-carbon fiber, and low cost carbon fiber.
- Develop the supporting technologies required to successfully implement the advanced preforming process technology including preform characterization and preform process modeling.

In support of the development of predictive models for LFT injection molding, objectives for this year include the following.

- Develop technologies to enable the use of injection-molded LFT composites by ORNL and PNNL. This objective includes the characterization of fiber length and orientation distributions as well as developing processing models to enable computer-aided design of molds and parts.
- Develop models for the molding of LFT composites, implement those models in Autodesk Moldflow Insight (AMI), and validate the models (by PNNL). This objective includes validation of the basic property prediction models implemented in the Eshelby-Mori-Tanka (EMTA) and EMTA-nonlinear analysis (NLA) codes for elastic properties, quasi-static stress strain responses, and strengths of LFT sample components.

In support of the development of standard test methods for composite crashworthiness and conducting intermediate-strain-rate crush experiments on composites, objectives for this year include the following.

- Develop both coupon-level and element-level standardized test methods for characterizing the specific energy absorption (SEA) associated with the progressive crushing of composites and other materials. This objective includes studying the deformation and failure mechanisms of automotive materials subjected to crush forces as a function of impact velocity. These test methods will be used in the design of crashworthy components for automotive applications.

In support of the multi-material joining and enabling capabilities development of rapid, reliable joining methods for composites, objectives for this year include the following.

- Develop a method to predict the effects of environmental exposures and mechanical loadings on the durability of composite-adhesive-metal (i.e., multi-material) joints. The focus application for this task is the joining of a polymer-matrix composite (PMC) underbody to an automotive body structure.
- Develop and validate analytical models and tools capable of predicting multi-material joint performance and durability under multiple loading scenarios including the generation of an experimental database on the multi-material joint's performance and durability under various loading and environmental conditions. This objective will support and validate the modeling approach so that it can be used in automotive structural design.

Accomplishments

Significant accomplishments supporting the development of advanced perform technologies include the following.

- Completed deposition uniformity study and used upgraded chopper to fabricate preforms for the Automotive Composites Consortium (ACC) Composite Seat Focal Project 4 program.
- Completed installation and initiated operations with the new infrared (IR)/convective charge heating system as a more industry-representative and effective means of heating and transferring blanks of reinforcing fibers mingled with thermoplastic fibers into the press for compression molding. This enhanced material transfer rates and reduced press closure times to improve overall molding operations and reduce performing costs.

Significant accomplishments supporting the development of predictive models for LFT injection molding include the following.

- Established Autodesk Moldflow Insight models for SABIC Innovative Plastics (SABIC-IP) and ACC LFT injection-molded plaques. This included generating a database of experimental results for model comparison and future use for sample plaques produced by LFT molding.
- Performed analyses and microstructure measurements to validate fiber length and orientation distribution models for SABIC-IP LFT plaques and ACC plaques to support their future molding.
- Performed EMTA computations and experimental measurements to validate the EMTA elastic property predictions and performed ABAQUS/EMTA-NLA (nonlinear analysis) to validate the EMTA-NLA stress-strain response predictions against the experimental stress-strain results for the LFT plaques.

Significant accomplishments supporting development of standard test methods for composite crashworthiness and conducting intermediate-strain-rate crush experiments on composites include the following.

- Completed literature review on element-level test methods and initiated testing of coupon-level composites subjected to crush loading.
- Developed a dynamic full-field measurement system based on high-speed video and image correlation methods for assessing the crashworthiness of composites.
- Developed the capability to conduct high-speed tensile tests on structural components in the testing machine for automotive composites (TMAC). Completed preliminary investigations on using TMAC for flat-panel ballistic toughness tests.

Significant accomplishments in support of the muti-material joining and enabling capabilities development of rapid, reliable joining methods for composites include the following.

- Developed reliable methods for joining composites to other composites and to metals, welding coupled with adhesive bonding (weld bonding). ORNL is supporting the joining methods developed by the ACC for the composite underbody and seat demonstration project. During the last year, ORNL completed tension tests with weld-bond specimens of LFT composites provided by ACC.

- Completed tensile fatigue tests of super lap shear, multi-material joint specimens fabricated both with and without spot welds at room temperature, 80°C, and –40°C and designed test fixtures and equipment to evaluate composite-to-steel joint specimens via torsion. This mode is considered a significant load case in the automotive body structure (by ORNL).
- Tested quasi-static torsion tests of joint specimens prepared with weld-bonded and adhesively bonded joint configurations (by ORNL). Results showed that the weld-bonded joints are more robust and sustain higher levels of torsional loading and angular rotation than the adhesively bonded specimens. ORNL initiated cyclic torsion fatigue tests of specimens prepared with weld-bonded and adhesively bonded joint configurations.
- Initiated dynamic (high strain rate) tensile tests of joint specimens using the testing machine for TMAC. These tests are important to understanding the effects of dynamic loading on the performance of composite-to-steel joints in an automotive application.

Future Directions

In support of the development of predictive models for LFT injection molding, objectives for the future may include the following.

- Complete validation of models developed for LFT injection molded composites in the coming year (by ORNL and PNNL). This will include characterization of fiber length and orientation for ACC moldings produced using LFT processes and validation of fiber length and orientation distribution models for LFT-molded materials.
- Validate Eshelby-Mori-Tanka (EMTA) and EMTA-NLA modeling approaches for elastic properties and stress-strain responses of ACC materials which are two-dimensional parts.

In support of the development of standard test methods for composite crashworthiness and conducting intermediate-strain-rate crush experiments on composites, objectives for the future may include the following.

- Further understanding of composites in crash by developing and evaluating second-generation flat-coupon test fixture for crush of composites and metals. The team will also evaluate rate effects and trigger effects using circular and square tube specimens for crush of composites.

In support of the multi-material joining and enabling capabilities development of rapid, reliable joining methods for composites, objective for the future may include the following.

- Advance methodologies for material joining by completing modifications of super lap shear specimen geometry and test methodology to enable evaluation of joint durability via cantilever bending and torsion test methods in support of the underbody project. The team will also conduct dynamic tensile tests of composite-to-steel joint specimens using TMAC.
- Move from developing test methods for two-dimensional parts to developing test methods for three-dimensional parts. This effort will include design of specimens, tests, fixtures, and equipment for evaluating multi-material joint durability in three-dimensional composite parts.

Introduction

This project consists of five tasks critical for the manufacture and implementation of composite materials in automotive structures. The first task is aimed at developing high-rate preforming technologies for the automotive environment. The materials under consideration for making preforms are glass fiber, carbon fiber, thermoplastic fibers, and hybrid combinations of these materials. These fibers are also used in combination with thermoplastic resins that have been placed on the fiber. Experiments involve equipment modifications to achieve significantly enhanced chopping speeds, better preform uniformity, and blending of multiple materials.

The second task is aimed at the development of predictive computational models for LFT injection-molded components. LFT composites have attracted significant interest in the automotive industry as candidate materials for structural applications due to the high-speed, low cost manufacturing processes that can be used. Predictive engineering capabilities are needed to assist

in design of these materials and the molding process. This project takes an integrated approach, linking process to structural modeling using new fiber orientation and length distribution models, advanced property prediction models for linear and nonlinear responses, advanced microstructural characterization methods, and mechanical testing.

The third task has a goal of developing standard test methods for composite crashworthiness and works closely with other composite material standards organizations to accomplish that goal. The research task is focused on developing dynamic crush test protocols for flat and tubular composite specimens. A new prototype flat-coupon test fixture had been developed and is being modified, while a comprehensive literature review on element-level test methods has been completed and testing initiated.

The fourth task is aimed at performing intermediate-rate crush tests on composites and involves the use of a uniquely designed apparatus, TMAC. Understanding the influence of impact velocity on the crush response of materials and structures is critically important for crashworthiness modeling inasmuch as collisions occur at a range of velocities. While the equipment was initially designed for equipment crush, it has now been modified to allow for tensile testing at intermediate strain rates, allowing for more comprehensive material assessment. The TMAC has the capability for constant-strain-rate loading, which is not available on typical tension loading machines.

The final task is aimed at development of a method to predict the effects of environmental exposures and mechanical loadings on the durability of a composite-adhesive-metal (multi-material) joint. The focus application for this project is the joining of a PMC underbody to the rest of the vehicle structure. This effort includes the development and validation of analytical models and tools capable of predicting multi-material joint performance and durability under multiple loading scenarios. It also includes the generation of an experimental database on a multi-material joint's performance and durability under various loading and environmental conditions to support and validate the modeling approach.

Activity and Developments

Development of Next-Generation Programmable Powder Preforming Process (P4)

Principal Investigator: Bob Norris, ORNL
(865) 576-1179; e-mail: norrisrejr@ornl.gov

Introduction

Polymer matrix composite (PMC) materials offer a number of benefits in lightweighting of automotive and heavy vehicles, including greater stiffness and strength per unit weight than conventional materials, easier formability, less corrosion susceptibility, the ability to tailor properties to specific load requirements, and enhanced noise and vibration damping. However, widespread implementation of carbon fiber composites, which are among the materials with the greatest weight-saving potential, will require lower cost materials and manufacturing processes than are currently available.

Use of advanced preforming processes could lead to more widespread use of composites. Robotic-controlled, programmable, directed-fiber preforming processes have demonstrated exceptional value for rapidly preforming, large, glass-reinforced, automotive composite structures. Due to their unique features and flexibility, and their inherently low scrap rate, they are among the most viable candidate processes for making affordable carbon fiber preforms for a variety of structural automotive components. The ACC has successfully demonstrated preforming in both Focal Project 2 (a composite pickup bed design) and Focal Project 3 (a carbon-fiber-intensive, body-in-white structural design), and the technology has been used in production of the General Motors Silverado pickup box and the Aston Martin Vanquish body side.

The Focal Project 3, carbon-fiber-intensive, body-in-white design, indicated a potential for greater than 60% weight savings under the assumption of a thickness design constraint of 1.5 mm. The analyses also indicated the potential for saving an additional 15% in mass if the thickness constraint is reduced to 1 mm. Unfortunately, evidence suggests that 1.5 mm may

be a practical limit for liquid molding. However, thermoplastics preforms, in which the reinforcing fiber and matrix (in the form of thermoplastic fiber during deposition) are both deposited in the preforming step, offer a potential path to obtaining thinner sections and, consequently, additional weight savings, as well as greater potential for recyclability. Hybrid-fiber preforms that can effectively take advantage of using carbon and glass fibers concurrently offer another potential benefit in terms of economics and property enhancement and may be a good route for introducing more carbon fiber in somewhat lower quantities than necessary for all-carbon components in automotive applications.

Approach

The objective of this project is to advance directed-fiber preforming processes to effect a further reduction in vehicle weight—relative to metals and conventional glass fiber composites—while maintaining the economic advantages of net-shape preforming. The project is pursuing three focus areas corresponding to three materials systems: reinforced thermoplastics, carbon fiber, and hybrid glass-carbon fiber.

A research-focused preforming system has been installed in the polymer composites laboratories at ORNL to serve as the base for hardware and associated technology developments. The P4 (programmable powdered preform process) machine is currently being used to build preforms for evaluation using the Twintex product (glass fiber commingled with thermoplastic fiber to serve as the matrix), glass impregnated with thermoplastic resin using Direct Reinforcement Fabrication Technology (DRIFT), and various forms of carbon and glass reinforcement. Although the near term focus is on demonstrating advances with glass fiber and existing industrial grades of carbon fiber, the long-term goal is to establish the groundwork for large-scale introduction of low cost carbon fiber for significant impact in automotive lightweighting.

Results and Discussion

The ACC Materials and Processing working groups had initiated work with École Polytechnique Fédérale de Lausanne (EPFL) in Switzerland to study processing effects and material properties of commingled glass and thermoplastic fibers leading to cost-model comparisons of various thermoplastic-composite processes. EPFL analysis indicated economics can also be attractive for some of these competitive processes at improved chopping speeds in the 12 to 15 kg/min range (Wakeman, 2006), leading to our focus on demonstrating the technical and economic feasibility of higher speed chopping processes. In the previous reporting period, the capability to meet and exceed this deposition rate was demonstrated for a representative liftgate perform. During the current period, the high-speed deposition uniformity was evaluated at similar rates.

A series of tests was run assuming that the robot would be depositing a six-pass pattern (three passes down and back, each without stopping) over lengths of 0.5 m, 1.0 m, and 1.5 m. Tests were run at three different robot speeds and three different chopper output levels corresponding to 50%, 75%, and 100% of rated capability each. The amount of material deposited was weighed for each test to judge deposition uniformity. After normalizing to 75% chopper speed and 75% robot speed with the other data calculated by speed ratios, the data differences at each point are shown in Table 1 as a percent difference from the expected value. As might be somewhat expected, there tends to be slightly more fiber deposited than predicted at the lower chopper speeds and slightly less than predicted at the higher chopper speeds. The trends appear to be mixed versus the robot speed as slightly more fiber is deposited at both higher robot and lower chopper speeds versus the reverse at both higher robot speeds and higher chopper speeds. The table shows the deviation from predicted amount of fiber deposited compared to what was actually deposited. No effort has been made to adjust robot “dispenseware” programming gains or other settings to this point.

Table 1. Percentage difference of measured output from predicted output.

Chopper Speed	Robot Speed	100%	75%	50%
	Section Length (m)	Mass (kg)	Mass (kg)	Mass (kg)
100%	1.5	□2.7%	3.0%	0.1%
	1	□4.7%	□4.2%	□0.6%
	0.5	□5.5%	□5.6%	□1.5%
75%	1.5	0.5%	1.5%	2.4%
	1	□2.3%	0.0%	2.6%
	0.5	□2.0%	□1.6%	1.8%
50%	1.5	2.9%	3.6%	0.3%
	1	1.6%	3.1%	0.5%
	0.5	4.6%	1.7%	1.2%

The ACC Focal Project 4 Composite Seat baseline design uses glass fiber with a polypropylene (PP) matrix. ACC is using the direct-injected LFT (DLFT) manufacturing process as the baseline for this work. For comparative purposes, ORNL manufactured preforms, as shown in [Figure 1](#), from the current Twintex baseline material using the existing preforming screens and upgraded chopper for evaluation in the seat project. The first goal was to demonstrate the technical feasibility of this product form for this application before working towards optimizing robot and chopping speeds and preform quantities per cycle. ORNL supplied both relatively unconsolidated preforms and largely consolidated preforms to the ACC DLFT molding trial. Unfortunately, the charge heating system at the DLFT molder was inadequate for heating either preform variant, and only a few of the preforms were actually molded. The conclusion was that the deficiencies were indeed due to the heating system and that the material did show positive flow characteristics worthy of further work with an improved heating system. To allow for this work, the seat pan outer mold has been shipped to ORNL for this work. ORNL will continue collaboration with ACC to evaluate this product form as well as the economics involved in this process.



Figure 1. Composite seat preforms from Twintex.

Because it is believed that hybrid-fiber preforms can effectively take advantage of carbon and glass fibers currently being used and offer potential benefits in terms of economics and property enhancement, ORNL has obtained standard lower cost carbon fiber alternatives from Zoltek and Toho to evaluate in conjunction with glass-fiber reinforcement previously acquired from Owens Corning. ORNL has also procured PP fiber from Fiber Science to serve as the composite matrix in initial trials to evaluate and demonstrate in situ blending of these hybrid blends at the preforming machine.

In late FY 2009, ORNL procured a convection oven modified to incorporate IR heating, taking advantage of a system produced by Wisconsin Infrared. It was installed and operations initiated during this reporting period to facilitate compression molding of traditional thermoplastics and sheet molding compounds (SMCs) with thermosets and work with in situ blended materials. It has been used for consolidating preforms for moldings such as those shipped to ACC for their molding trials and for compression molding samples for testing at ORNL. Taking advantage of this equipment and its proximity to our press, we have significantly improved our material transfer speeds. We also have improved the press closing process. Although the overall processing is improved well beyond where we were with the previous setup, at the close of the period we have not gotten a level of molded panel quality worthy of extensive panel mechanical testing and are working to improve both the uniformity of the charge heating and the fiber blending. We are using the remaining funding to tweak both processes to determine whether to continue looking at in situ blending with this approach or to switch our focus to structural reaction injection molding (SRIM) in future preform developmental and demonstration work.

Conclusions

During this reporting period, a deposition uniformity study was completed on the upgraded chopper demonstrating relatively consistent output with a slight dependency on speed. The upgraded chopper was used to fabricate preforms for the ACC Composite Seat Focal Project 4 program. Molded panels will be used to evaluate the technical and economic feasibility of this process for that application and to evaluate the demonstration articles.

Installation of the new IR-convective charge heating system was completed and operations initiated with this equipment, which is a more industry-representative and effective means of heating and transferring blanks of reinforcing fibers mingled with thermoplastic fibers into the press for compression molding. Enhanced material transfer rates and reduced press closure times were achieved to improve overall molding operations. This will facilitate compression molding of traditional thermoplastics and SMCs with thermosets and work with in situ blended materials.

Effort was continued with in situ blended PP and hybrid blends of commercially available industrial grades of carbon fiber and glass fiber, making additional blending improvements. Even with substantial improvements, molded panels are not yet adequate for extensive characterization, at least partially due to nonuniformity of heating. Although the focus of this approach

is to facilitate evaluation of alternative material combinations, especially hybrids, in situ blending may prove economically attractive. As the variety of forms of commingled materials is extremely limited, this allows evaluation of materials not available at all in commingled form and in a much broader array of blending alternatives.

Collectively, the technologies under development in this project will advance low cost processing on two fronts. First, they will provide the opportunity to use additional materials in the net-shape preforming process, which is expected to lead to additional weight reduction and/or better performance. Second, they will provide the requisite tools to evaluate the effects of process parameters on the utility and performance of preforms and molded parts.

Engineering Property Prediction Tools for Tailored Polymer Composite Structures

Principal Investigator: Vlastimil Kunc, ORNL
(865) 574-8010; e-mail: kuncv@ornl.gov

Principal Investigator: Ba Nghiep Nguyen, PNNL
(509) 375-3634; e-mail: Ba.Nguyen@pnl.gov

Introduction

In past years, process and property prediction models were developed for injection-molded LFTs. The process models involved a fiber orientation model, termed the anisotropic rotary diffusion–reduced strain closure (ARD-RSC) model (Phelps and Tucker, 2009), and a fiber length attrition model (Phelps, 2009) that captures fiber breakage in the mold during filling. These models were implemented in the University of Illinois ORIENT code and also in a research version of AMI. AMI is a computer-aided engineering tool for predicting mold fill and material deposition during injection molding. The property prediction models comprise a series of micromechanical models using the standard and improved EMTA approaches to capture the linear and nonlinear behaviors of LFTs (Nguyen et al., 2008, 2009, 2010). The computer capabilities, named EMTA and EMTA-NLA, were developed at PNNL to implement these property prediction models. While EMTA is stand-alone software for computation of thermoelastic properties, EMTA-NLA presents the capabilities implemented in the ABAQUS finite-element packages (via user subroutines) for NLA of LFT structures. The experimental methods to characterize microstructure and mechanical properties of LFTs were developed and validated at ORNL. This project task is aimed at validating the process and basic property prediction models for SABIC-IP and ACC moldings of LFTs against the measured experimental data..

Approach

At the time of this report, only preliminary tests on some ACC-molded plaques had been performed after the August 2010 plaque delivery; therefore, complete data for the model validation for these plaques are not available. However, measurements of fiber length distribution and AMI analyses were performed to support the actual molding of ACC plaques.

Validation outlined in this report was performed on SABIC-IP plaques. The experimental data were collected using methods and techniques developed in previous years of this project. The test matrix for the model validation was selected in input from industry experts. AMI was applied to simulate the injection molding of the SABIC IP plaques to predict the fiber orientation and length distributions in these structures. The predicted results at selected locations were compared with the experimental data. Based on the advice of the industry experts, the validation is satisfactory if the averaged through-thickness values agree with the measured data within 15%. Next, to validate the predictions of EMTA and of EMTA-NLA, measured fiber orientation and length data at some selected locations were used to compute the local elastic properties and stress-strain responses up to the point of failure. Finally, demonstration of the integrated tool was carried out in process-linked structural analyses using AMI, EMTA-NLA, and ABAQUS to predict damage accumulation and stress-strain responses of specimens removed from molded plaques in the flow and cross-flow directions. All the predictions were compared with the experimental results to validate the models.

Results and Discussion

Consistent material properties and an understanding of the material microstructure are important for model validation. Test specimens were SABIC-IP-molded 2 mm, 3 mm, and 4 mm thick plaques with 20, 30, and 40 wt % glass in PP. Molding conditions included slow and fast fill speeds, and low and high back pressures. Plaques with 30% glass loading were evaluated first, and plaques with matrices of 20% and 40% glass/PP materials were evaluated later in the year based on the approved testing matrix. Microstructure characterization and mechanical property measurements provided a consistent picture, indicating suitability of these plaques for the model validation. Figure 1 outlined sampling locations and dog-bone test specimen orientation with respect to the plaque.

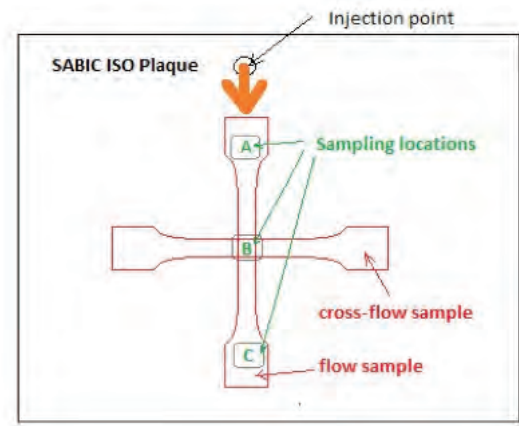


Figure 1. Sampling locations A, B, and C; orientation of dog-bone test samples centered at location B.

Figure 2(a) shows that a low back pressure during molding resulted in the retention of longer fibers. Higher stiffness values in the cross-flow direction in Figure 2(b) for low back pressure samples indicate the existence of wider cores in these samples compared to samples molded with a high back pressure.

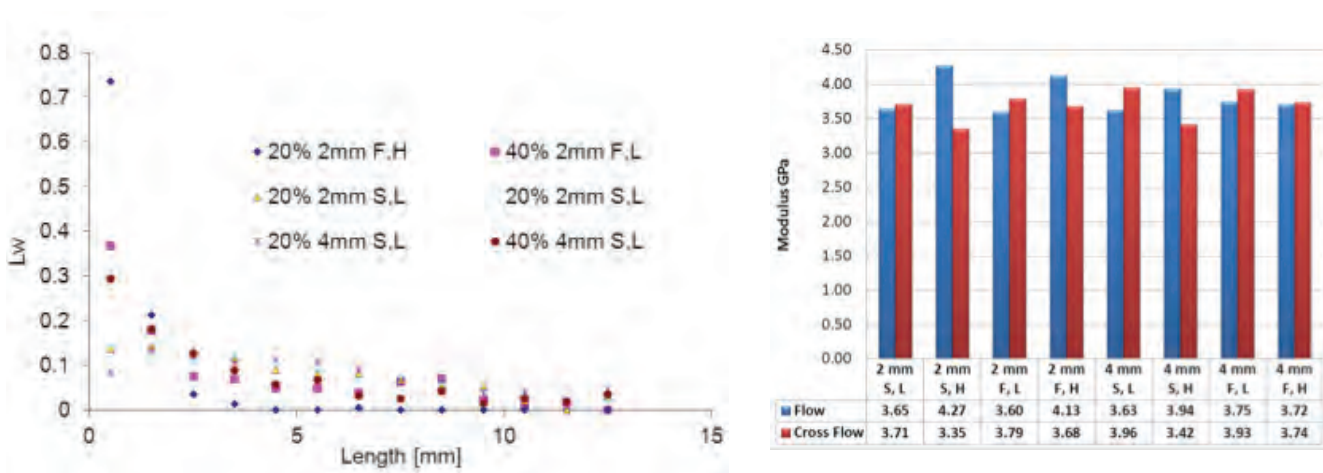


Figure 2. S/F–slow/fast fill speed, H/L–high–/low back pressure: (a) weight-based fiber length distribution of selected plaques; (b) modulus for 20% glass/PP plaques.

Figure 3(a) shows the finite-element model for a 40 wt % glass fiber/PP plaque (270 mm × 310 mm × 2 mm) molded under fast fill and high back pressure conditions. Figures 3(b) and 3(c) illustrate the through-thickness A_{11} and A_{22} components of the second-order orientation tensor for the locations selected on the centerline at 100 mm (Region B) and 50 mm (Region C) from the plaque end, respectively. The averaged values of the predicted A_{11} and A_{22} for the skin/shell and core layers agree well with the measured data (within 10%).

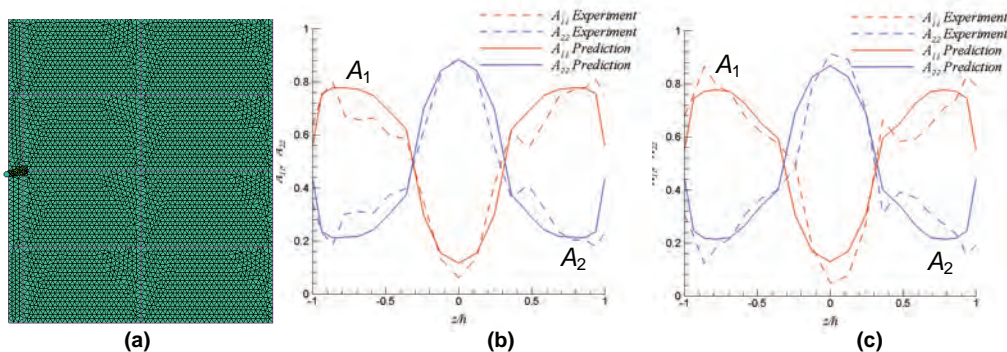


Figure 3. AMI injection molding analysis of a SABIC-IP plaque: (a) finite-element model, (b) through thickness variations of A_{11} and A_{22} in Region A, and (c) through thickness variations of A_{11} and A_{22} in Region B.

Figure 4 shows the through-thickness variation of the weight-average length at Region B. The averaged value of the predicted weight-average lengths at this region is 1.03 mm, which agrees fairly well with the experimental weight-averaged length value of 1.38 mm.

The measured and predicted fiber orientation and length distributions at Region B for the same plaque were used in the EMTA computation to predict the local elastic properties. The elastic moduli in the flow and cross-flow directions are presented in Table 1, which also provides the experimental results averaged over three test values. The predicted and measured moduli are in good agreement, as indicated by the deviation percentages given in Table 1.

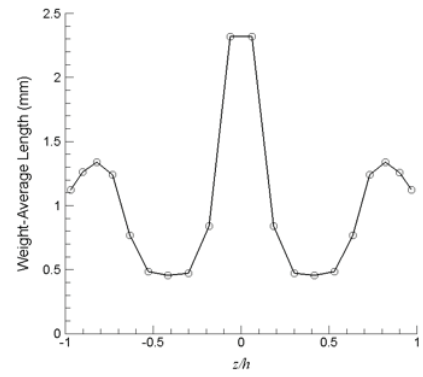


Figure 4. Predicted through-thickness weight-average length in Region B.

Table 1. Predicted and measured elastic moduli in the flow and cross-flow direction at Region B.

Elastic moduli (MPa)	EMTA results using measured FLD and FOD ^a	EMTA results using predicted FLD and FOD	Experiment
E_{11} (flow direction)	7891 (2.1 %)	7769 (0.54%)	7727
E_{22} (cross-flow direction)	5740 (10.1 %)	5848 (12.2%)	5213

^aFLD = fiber length distributions; FOD = fiber orientation distributions.

The damage model of EMTA-NLA was used in the ABAQUS analyses to simulate the tensile responses of the specimens removed along the flow and cross-flow directions of the plaques in the same series. The specimens' centers were located 100 mm from the plaque end. EMTA-NLA mapped fiber orientation and length distributions from AMI to ABAQUS. Figure 5(a) shows the predicted failure location in the flow-direction specimen which corresponds to the experimental failure area also illustrated in this figure. Figure 5(b) presents the predicted and experimental stress-strain responses recorded at the specimen center (Region B). To closely assess the predicted stress-strain response, EMTA-NLA/ABAQUS analysis was also conducted using one element representing Region B for which measured fiber length and orientation were used. The predicted responses for the whole specimen using predicted fiber length and orientation and for the single element globally agree with the experimental results also shown in Figure 5(b). Since the single-element analysis captured the response at the specimen center, it is to be expected that this analysis would predict higher strength as the specimen failure did occur earlier near one dog-bone shape corner instead of at the specimen center [Figure 5(a)].

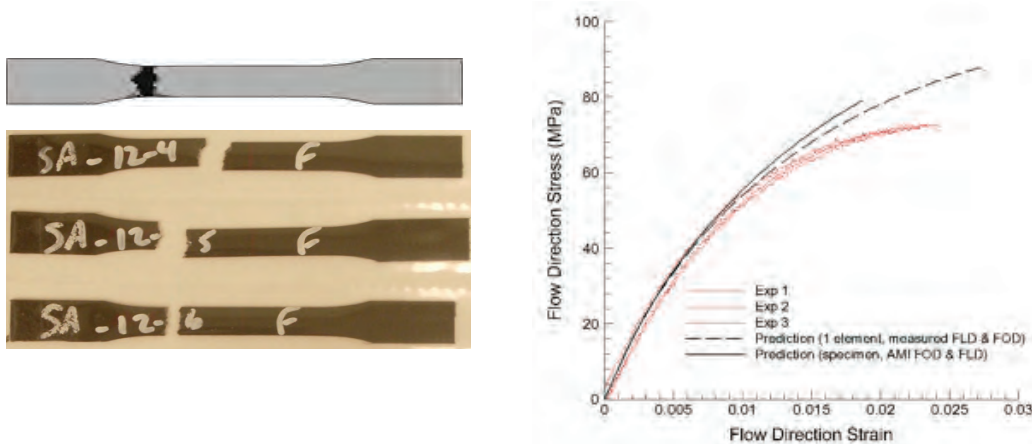


Figure 5. (a) Predicted and experimental failure locations of flow-direction specimens and (b) predicted and experimental stress-strains responses of these specimens up to failure.

The strength predicted for the flow-direction specimen is 79.2 MPa compared to the averaged experimental value of 71.6 MPa [Figure 5(b)]. The agreement of results is within 11%. EMTA-NLA/ABAQUS analysis was also conducted for the cross-flow direction specimen. Damage and strength predictions were also in good agreement with the experimental observations [Figure 6(a) and 6(b)].

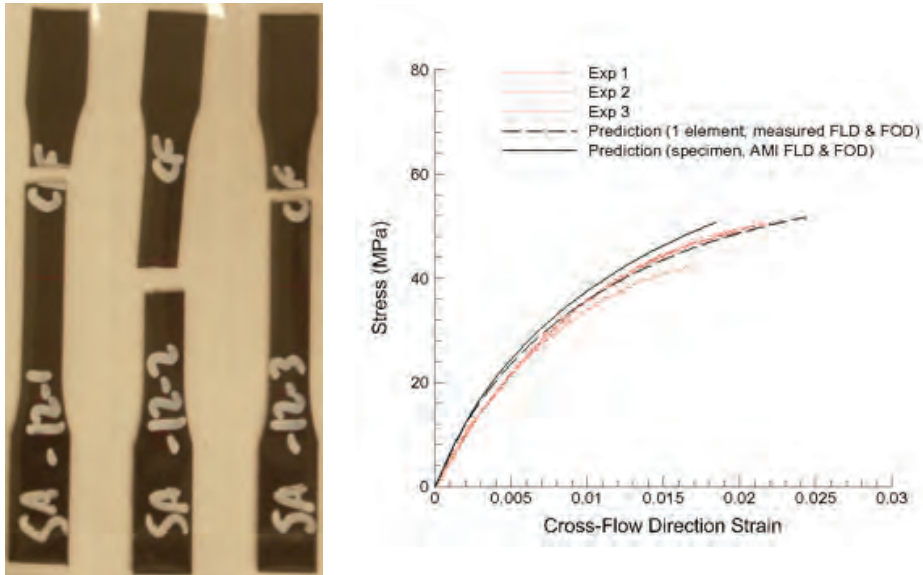


Figure 6. (a) Predicted and experimental failure locations of cross-flow-direction specimens and (b) predicted and experimental stress-strains responses of these specimens up to failure.

Finally, the AMI injection molding simulations were performed for the ACC plaques made of the Ticona 40 wt % glass fiber/ polyamide 6 (PA6) and the Dow 40 wt % glass fiber/ PP to support the actual plaque moldings using these materials. Figure 7(a) shows the predicted pressure distribution for the glass/PA6 plaque at the end of molding. The clamp force evolution is presented in Figure 7(b). The maximum clamp force was predicted to be less than 1,100 tons, which is within the press capacity of the ACC injection molding machine.

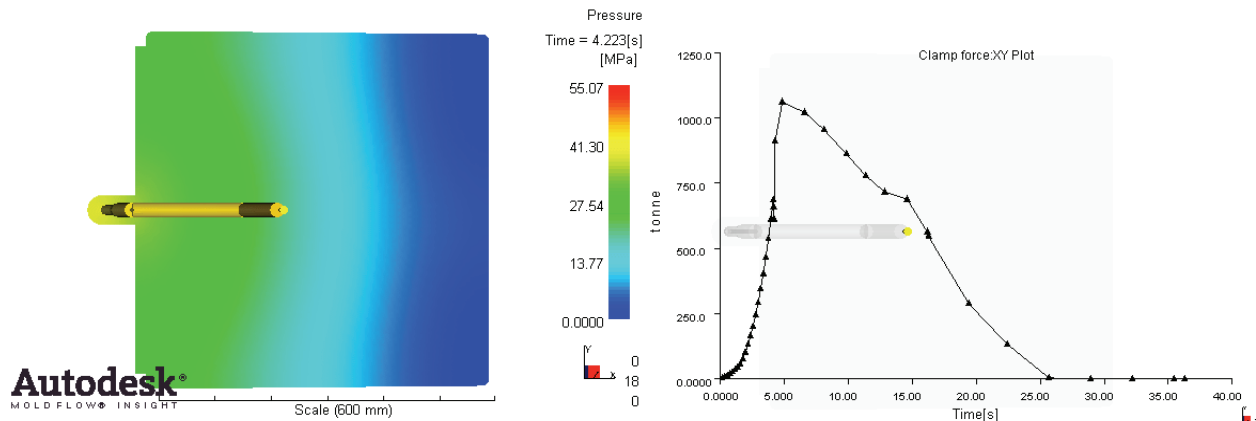


Figure 7. (a) Predicted pressure distribution in the ACC glass/PA6 plaque and (b) clamp force evolution.

Conclusions

The validations of process and property prediction models were conducted for SABIC-IP plaques. Measured fiber orientation and length distributions as well as mechanical property data were used for the model validation. The ARD-RSC model correctly captures fiber orientation in these plaques. The fiber length distribution model predicts the length distribution at selected locations on the plaque centerline fairly well. Additional length data are needed to further assess this model. The property prediction models for elastic properties and quasi-static responses of EMTA and EMTA-NLA accurately predict the local elastic properties, damage accumulation, and stress-strain responses up to failure of the studied specimens. Preliminary work was conducted to analyze the injection molding of ACC plaques. We will pursue the experimental characterization of the composite microstructure and measurement of mechanical properties to support model validation for the ACC plaques.

Development of Standardized Test Methods for Characterizing the Crashworthiness of Composites

Principal Investigator: J. Michael Starbuck, ORNL
(865) 576-3633; e-mail: starbuckjm@ornl.gov

Principal Investigator: Daniel O. Adams, University of Utah, Department of Mechanical Engineering
(801) 585-9807; e-mail: adams@mech.utah.edu

Other Team Members: Graham Barnes, Engenuity Limited

Introduction

The mechanisms governing the progressive crush response of composite materials proposed for automotive applications are not well understood. Additionally, many of these materials are known to exhibit crush characteristics that are sensitive to rate of loading. Understanding the influence of loading rate, fiber and matrix materials, and laminate design on the energy absorption during dynamic crush loading is critically important for crashworthiness design. To date, however, there is no standard by which either coupon-level or element-level testing may be performed. Thus, test data on different material systems, laminates, and loading rates that have been produced by different laboratories are generally not comparable. The objective of this research program is to develop both coupon-level and element level standardized test methods for assessing and comparing energy absorption characteristics of candidate composite materials. This report is for the first year of this multi-year project.

Results and Discussion

Using an initial prototype test fixture developed at the University of Utah, as shown in **Figure 1(a)**, a series of tests were performed on carbon epoxy specimens fabricated from a large number of laminates. The use of high-speed video photography provided for the identification of failure modes associated with energy absorption. These initial tests led to several findings regarding desired ply orientations and stacking sequences to produce different failure modes. Oscillations in the resulting force data, originally believed to be associated with “ringing” of the fixture during drop-weight testing, were determined to not be due to fixture design but were characteristic of the drop tower data acquisition system. However, a second-generation fixture design has been proposed, **Figure 1(b)**, which provides a reduced-mass upper loading plate and a more compact design. Additionally, the researchers have consulted with Engenuity Limited regarding alternative specimen loading methods and are in the process of procuring a test fixture of this design. It is expected that two second-generation flat coupon test fixtures will be developed based on input from the initial University of Utah and Engenuity prototypes. Additionally, research has focused on suitable methods of data reduction and methods of directly obtaining fixture-based crush displacement during testing for use in calculating energy absorption. Such direct measurement eliminates the need for calculation and calibration of factors such as friction losses.

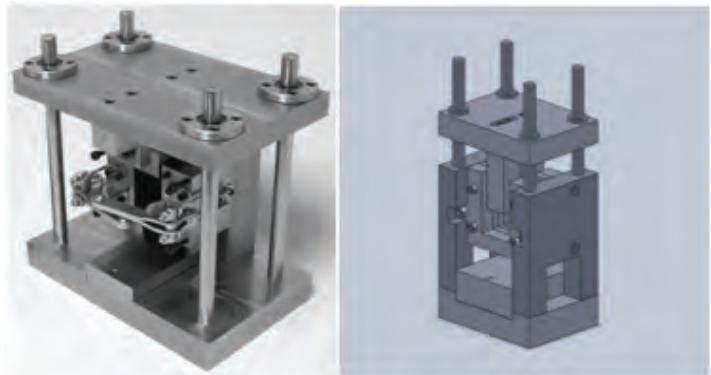


Figure 1. Prototype coupon-level test fixtures: (a) initial prototype developed at the University of Utah and (b) proposed second-generation fixture design.

Before development of an element-level test method, a comprehensive literature review was performed and a 40-page draft report was completed. More than 100 references on the topic of energy absorption, failure modes, and the effects of testing parameters on composite structures were considered. Based on this review, two aspects of tube testing have been selected for initial evaluation: strain-rate effects and triggering effects on the energy absorption of composite structures. Based on the existing literature and the experience of the principal investigators (PIs), it is hypothesized that both of these effects are related to the primary failure mode produced during crushing. To investigate these effects, circular and square tube specimens need to be designed to fail in each of the three primary failure modes. Specimens will then be tested at strain rates up to 8 m/s

using bevel and tulip triggers. Three initial composite layups have been designed using unidirectional carbon/epoxy prepreg material. Preliminary testing performed at a quasi-static load rate using the bevel trigger has been performed. The desired failure modes for each composite layup were produced in the specimens, as shown in [Figure 2](#).



Figure 2. Failure modes produced in circular tube specimens during crush: (a) fiber splaying and (b) fragmentation.

In FY 2010, the PIs attended the Composite Materials Handbook 17 (CMH-17) meeting in Costa Mesa, California, and Dr. Starbuck briefed the Crashworthiness Working Group on the progress of this research. Additionally, a Work Item was initiated in ASTM Committee D30 (Composites) for the development of standardized crashworthiness test methods, and Dr. Adams briefed the committee both in St. Louis (March) and Dayton (September) on progress and plans for future work.

Conclusions

Prototype test fixtures for a coupon-type test method have been developed and evaluated. Modifications are under investigation for a second-generation fixture. A comprehensive literature review has been completed to support the development of a structural tube-type test. This review has identified strain-rate effects and trigger effects as initial parameters for investigation using both circular and square tube specimens. The two development efforts involve coordinated activities and use of the same composite materials and layups for crush testing. The PIs have briefed both the CMH-17 Crashworthiness Group and the ASTM D30 Committee on accomplishments to date and future plans.

Intermediate-Rate Crush Response of Crash Energy Management Structures

Principal Investigator: J. Michael Starbuck, ORNL
(865) 576-3633; e-mail: starbuckjm@ornl.gov

Principal Investigator: Don Erdman, ORNL
(865) 576-4069; e-mail: erdmandl@ornl.gov

Introduction

Progressive crush is an important mechanism by which the kinetic energy of a traveling automobile is dissipated in a collision to protect the safety of occupants. Unfortunately, the mechanisms governing the progressive crush response of some emerging automotive materials are not well understood. Additionally, many of these materials are known to exhibit responses that are sensitive to rate of loading. Understanding the influence of impact velocity on the crush response of materials and structures is critically important for crashworthiness modeling inasmuch as collisions occur at a range of velocities. Additionally, from a structural standpoint, the deformation (or strain) rate is generally not unique from either a spatial or temporal standpoint. Consequently, it is important to quantify the behavior of materials at various strain rates.

Approach

Typically standard test machines are used for experiments at quasi-static rates, whereas drop towers or impact sleds are the convention for dynamic rates. These two approaches bound a regime within which data for experiments at constant impact velocity are not available by conventional experimental practice. This regime is termed the intermediate-rate regime and is defined by impact velocities ranging from 1 m/s to 5 m/s. Investigation of rate effects within this regime requires experimental equipment that can supply a large force with constant velocity within these rates.

Using a drop tower or sled at intermediate rates, although technically possible, is problematic due to the prohibitively large mass required to maintain constant velocity during the crush. Consequently, ORNL and the ACC collaborated to define specifications for a unique experimental apparatus that mitigates the shortcomings of existing equipment. MTS Systems Corporation designed and built the servohydraulic test machine, referred to as the Testing Machine for Automotive Crashworthiness (TMAC). TMAC is uniquely capable of conducting controlled progressive crush tests at constant velocity in the intermediate-velocity range (i.e., less than 5 m/s) because of the large energy available at those rates and the sophisticated simulation and control software that permits velocity uniformity to within 10%.

The experimental facility is used to understand the crush behavior between the static and dynamic (8 m/s) conditions. The TMAC is shown in Figure 1. The approach taken for measuring the intermediate response of materials included the development of a unique high-force (500 kN), high-velocity (8 m/s) servohydraulic machine to conduct progressive crush experiments on structural components at intermediate rates and the development of a low-force (40 kN), high-velocity (18 m/s) servohydraulic machine for conducting tensile strain rate characterization tests. It also included the use of high-speed imaging to observe and document deformation and damage mechanisms during the crush event.

Results and Discussion

For FY 2010, activities have focused on supporting user programs, developing and promoting user interactions, improving data acquisition, and developing high-rate tension tests on TMAC. In addition to promoting user programs, continued support was provided to the development of a crashworthiness chapter for the military's composite design guide, CMH-17 (formerly MIL-HDBK-17), and the start of a technical division on the Dynamic Response of Materials within the Society for Experimental Mechanics. Constant-strain-rate test data have been measured by multiple users and incorporated into their design methodologies.

United States Council for Automotive Research (USCAR)/ACC: High-Rate Testing of the Weld-Bond Super Lap Shear Specimen

In FY 2009 USCAR/ACC in conjunction with Multimatic Engineering Services Group ran preliminary high-rate tensile tests at two different rates (1 mm/s quasi-static and 4 m/s) on TMAC. The information from these tests, primarily load-displacement trace, and the high-speed video were used to evaluate a hybrid joint being considered for the composite automotive underbody project. At the higher rates, the "cage-type" grips that were used were overloaded, and although several tests were successful, there was excessive specimen slippage and testing was terminated until new grips could be obtained. In FY 2010 the grips and specimens were redesigned to eliminate these problems.

TMAC was designed primarily for crush testing, which is a compression type of test; however, it can be used for tensile testing provided the appropriate slack adapter and grips are installed. This user project was the first attempt at this. The gripping difficulties were described above, and a second issue was discovered when trying to correctly generate the drive file for tension tests. After this user project was completed, the drive file for the machine was updated to provide synchronized



Figure 1. TMAC as originally installed in the NTRC Composites Laboratory.

high-rate tensile capabilities and custom-built 30,000 pound grips were designed. In FY 2010, the new grips were fabricated and additional work was completed on developing drive and data files for tension tests on TMAC. The final test setup is shown in Figure 2. Additional weld-bond tests were completed that identified a problem with the piezoelectric load washer in tension. The regional MTS service technician was brought to the ORNL site for trouble shooting, and it was determined that the preload on the load washer was incorrect and had to be reset and recalibrated.

Ballistic Toughness

Additional test capabilities were developed in FY 2010 to conduct flat-panel testing and thus expand and broaden the TMAC user projects database. The test setup has an instrumented impact bar that penetrates a specimen that is clamped between two plates. Piezoelectric load washers were mounted at four corners of the plate so as to have a secondary force measurement. The test setup is shown in Figure 3.



Figure 3. Flat-panel test setup for ballistic toughness testing on TMAC.



Figure 2. TMAC tension setup for testing the ACC super lap shear weld-bond specimen.

Conclusions

TMAC provides a unique capability to measure SEA on crush tubes and other specimen geometries as a function of (constant) impact velocity within a range from quasi-static to 8 m/s. To complement this capability, a high-rate tension machine can be used for conducting coupon-level tests up to 18 m/s. Large-scale specimens and structural components can also be tested in tension on TMAC by adding a slack adapter and appropriate grips. Fixtures also exist for flat-panel and beam-type specimen geometries. User interest in this equipment remains very high, with follow-on projects and new projects currently in the draft stage. Constant-strain-rate tests were conducted and the data were used by several users to aid in their design of composites energy management structures.

Composite Underbody Attachment

Principal Investigator: Barbara Frame, ORNL
(865) 576-1892; e-mail: framebj@ornl.gov

Introduction

This project is a collaborative effort on the Composite Underbody project (Focal Project 4) between ACC; Multimatic, Inc.; and ORNL. The objective of this project is to develop a method to predict the effects of environmental exposures and mechanical loadings on the durability of a composite-adhesive-metal joint. The focus application is joining a PMC underbody to an automotive body structure and validating the assembly's long-term durability and performance.

Approach

This project has six key elements to accomplish the goals: (1) design of the multi-material joint tests, (2) material characterization, (3) test article manufacture, (4) mechanical performance of joint specimens for durability, (5) synergistic durability from multiple environmental stressors, and (6) computer-aided engineering (CAE) model validation and development. Test program specifics are determined based on an analysis of an underbody design project.

The underbody geometry was simplified to allow extraction of test data representative of the performance of this type of multi-material joint, and a method for coupon-level testing of combined environmental and mechanical loading on the joint will be developed. The validity of existing automotive CAE durability tools for this application is being evaluated. Inputs for model validation and development are based on test results obtained as part of this project and previous research on similar materials.

As part of this approach, experimental durability test data derived from tensile, bending, and torsional coupon tests, along with appropriate material durability data, are being generated by ORNL and ACC and are being used by Multimatic, Inc., to develop the appropriate modeling techniques for this project. This, followed by testing and correlation using data derived from a larger three-dimensional structural specimen subjected to two unique loading conditions that produce different types of stress concentrations in the joint, will provide a high level of confidence in the validity of the models.

Contributions from the project team include the following.

ORNL: Project lead, test method development, durability testing, TMAC dynamic tension testing.

ACC: Technical consultation regarding automotive industry needs and requirements, material characterization, test specimen fabrication.

Multimatic, Inc.: Joint finite-element analyses, CAE model validation and development.

Deliverables include a composite-to- steel joint coupon-testing protocol, test data, CAE model validation results, and final report. Recommendations to improve the methodology (testing and analytical) will be proposed as deemed appropriate.

Results and Discussion

Durability Modeling (Multimatic, Inc.)

Multimatic, Inc., conducted analyses in which quasi-static structural coupon tests were simulated for test analysis correlation and modeling methodology development. Analysis correlation studies were conducted for the tensile testing of fiberglass fabric SMC composite-to-steel super lap shear coupons for both an adhesively bonded and a weld-bonded joint configuration. The results have been reported in conference proceedings (Fuchs, 2010).

Tension-Tension Fatigue Tests

Tension-tension fatigue tests were conducted with super lap shear test specimens prepared using techniques and materials proposed for joining a composite underbody to the vehicle structure. The two types of joint configurations evaluated included specimens that were weld bonded (joined with combination adhesive and spot welds) and adhesively bonded (no spot welds). The milestone "Complete tensile fatigue tests of super lap shear specimens fabricated both with and without spot welds at ambient, 80°C, and -40°C" was completed before September 2010. Results have been reported in conference proceedings (Shah, 2010). All data have been forwarded to Multimatic and ACC to be used for the joint model validation and development efforts associated with Composite Underbody Focal Project 4.

Cantilever Bend Test and Torsion Test Method Development

Test equipment and fixtures to evaluate joint specimens via torsional loading have been prepared, and testing with specimens prepared with weld-bonded and adhesively bonded joint configurations has been initiated. Quasi-static tests have shown that the weld-bonded joints are more robust and sustain higher levels of torsional loading and angular rotation than the adhesively bonded only specimens. Cyclic torsion fatigue testing with both type specimens is in progress.

Low-amplitude cantilever bend fatigue tests have been demonstrated with composite-to-steel weld-bonded specimens for millions of cycles. None of the specimens showed detectable signs of peel or other damage at the weld-bonded joint. Observations are that to enable testing at higher load levels and for fatigue failures to occur in the joint, the thickness of the steel substrate must be increased.

TMAC Dynamic Tension Testing

Preliminary dynamic tensile tests of composite-to-steel specimens were conducted using TMAC. These tests are important to understanding the effects of dynamic loading on the performance of composite-to-steel joints in an automotive application. Results were indeterminate and suggest that additional investigations will be required to interpret the high-strain-rate tensile data generated with these type specimens.

Three-Dimensional Composite Joint Specimens

Layup and molding trials of the composite underbody being conducted by ACC are progressing. These trials may produce the composite to be used to fabricate the 3D composite joint specimens. Design of the 3D composite joint specimens is on hold pending results of the single-load case coupon tests and model validation work.

Conclusions

Analyses were conducted by Multimatic, Inc., in which quasi-static structural coupon (super lap shear) tests were simulated for test-analysis correlation and modeling methodology development. Tension-tension fatigue tests were conducted with super lap shear test specimens prepared using techniques and materials proposed for joining a composite underbody to the vehicle structure. The milestone “Complete tensile fatigue tests of super lap shear specimens fabricated both with and without spot welds at ambient, 80°C, and -40°C” was completed.

Test equipment and fixtures to evaluate joint specimens via torsional loading were prepared. Quasi-static tests have been conducted with specimens prepared with joint configurations that were weld bonded and adhesively bonded only. Cyclic torsion fatigue testing with both type specimens is in progress.

Initial dynamic tensile tests of composite-to-steel specimens were conducted using TMAC. Results suggest that additional investigations will be required to interpret the high-strain-rate tensile data generated with these type specimens. Layup and molding trials of the composite underbody are progressing. These trials may produce the composite to be used to fabricate the 3D composite joint specimens. Design of the 3D composite joint specimens is on hold pending results of the single-load case coupon tests and model validation work.

Conclusions

P4 has been used to fabricate preforms for the ACC composite seat focal project, and a new heating system has been installed to facilitate molding trials. Efforts to evaluate various fibers, fiber mixes, and mixes with thermoplastic fibers and resins are continuing. The technologies under development in this project will advance low cost processing on two fronts. First, they will provide the opportunity to use additional materials in the net-shape preforming process, which is expected to lead to additional weight reduction and/or better performance. Second, they will provide the requisite tools to evaluate the effects of process parameters on the utility and performance of preforms and molded parts.

Validation of process and property prediction models was conducted for SABIC-IP plaques made from LFTs. Measured fiber orientation and length distributions and mechanical property data were used for the model validation. The ARD-RSC model correctly captures fiber orientation in these plaques. The fiber length distribution model fairly predicts the length distribution at the selected locations on the plaque centerline. Additional length data are needed to further assess this model. The property prediction models for elastic properties and quasi-static responses of EMTA and EMTA-NLA accurately predict the local elastic properties, damage accumulation, and stress-strain responses up to failure of the studied specimens.

Prototype test fixtures for a coupon-type crush test method have been developed and evaluated. Modifications are under investigation for a second-generation fixture. A comprehensive literature review has been completed to support the development of a structural tube-type test. This review has identified strain-rate effects and trigger effects as initial parameters for investigation using both circular and square tube crush specimens. TMAC has been used to crush test and

obtain data for a variety of materials in support of numerous efforts. Large-scale specimens and structural components can now be tested in tension on TMAC by adding a slack adapter and appropriate grips. User interest in this equipment remains very high with follow-on projects and new projects currently in the draft stage.

Multi-material joining has been ongoing in support of ACC Focal Project 4. Tension-tension fatigue tests were conducted with super lap shear test specimens prepared using techniques and materials proposed for joining a composite underbody to the vehicle structure. Tensile fatigue tests of super lap shear specimens “fabricated both with and without spot welds at ambient, 80°C, and –40°C” were completed. Quasi-static torsional tests have been conducted with joint specimens prepared with joint configurations that were weld bonded and adhesively bonded only. Cyclic torsion fatigue tests with both type specimens are in progress. Initial dynamic tensile tests of composite-to-steel specimens were conducted using TMAC. Results suggest that additional investigations will be required to interpret the high-strain-rate tensile data generated with these type specimens.

Presentations / Publications / Papers

Adams, D. Crashworthiness Test Method Development Activities. Presented at the ASTM D30 Committee Meeting, Dayton, Ohio, September 23, 2010.

Adams, D. Test Methods for Crashworthiness Assessment of Composite Laminates. Presented at the ASTM D30 Committee Meeting, St. Louis, Missouri, April 21, 2010.

Fuchs, H.; Conrod, B. Super Lap Shear Joint Structural Test-Analysis Correlation Studies. Presented at the Society of Plastics Engineers, Automotive Composites Conference and Exhibition, Troy, Michigan, September 15–16, 2010 (<http://www.speautomotive.com/aca.htm>).

Nguyen, B. N.; Jin, X.; Wang, J.; Phelps, J. H.; Tucker III, C. L.; Kunc, V.; Bapanapalli, S. K.; Smith, M. T. Implementation of New Process Models for Tailored Polymer Composite Structures into Processing Software Packages. PNNL-19185. Pacific Northwest National Laboratory, 2010.

Nguyen, B. N.; Kunc, V. An Elastic-Plastic Damage Model for Long-Fiber Thermoplastics. *Inter. J. Damage Mech*, 2010, 19, pp 691–725.

Nguyen, B. N. Multiscale Modeling of Injection-Molded Short- and Long-Fiber Filled Thermoplastics. Presented by Nguyen, Ba Nghiep (Invited Speaker) at the American Chemistry Council Plastics Division Workshop on Mechanical Performance of Short Fiber and Long Fiber Filled Injection Molded Thermoplastic Parts—A State of the Art, Troy, Michigan, December 9, 2009.

Norris, R. E.; Lomax, R. D.; Xiong, F.; Dahl, J. S.; Blanchard, P. J. Advanced High Speed Programmable Preforming. Presented at SAMPE 2010, Seattle, Washington, May 17–20, 2010.

Shah, B.; Frame, B.; Dove, C.; Fuchs, H. Structural Performance Evaluation of Composite-to-Steel Weld Bonded Joint. Presented at the Society of Plastics Engineers, Automotive Composites Conference and Exhibition, Troy, Michigan, September 15–16, 2010.

Starbuck, J. M.; Adams, D.; Barnes, G. Crashworthiness Test Method Development Activities. Presented at the CMH-17 Crashworthiness Working Group Meeting, Costa Mesa, California, July 19, 2010.

References

Nguyen, B. N.; Bapanapalli, S. K.; Holbery, J. D.; Smith, M. T.; Kunc, V.; Frame, B. J.; Phelps, J. H.; Tucker III, C. L. Fiber Length and Orientation Distributions in Long-Fiber Injection-Molded Thermoplastics—Part I: Modeling of Microstructure and Elastic Properties. *J. Compos. Mater.* 2008, 42, pp 1003–1029.

Nguyen, B. N.; Bapanapalli, S. K.; Kunc, V.; Phelps, J. H.; Tucker III, C. L. Prediction of the Elastic-Plastic Stress/Strain Response for Injection-Molded Long-Fiber Thermoplastics. *J. Compos. Mater.* 2009, 43, pp 217–246.

Nguyen, B. N.; Kunc, V. An Elastic-Plastic Damage Model for Long-Fiber Thermoplastics. *Inter. J. Damage Mech.* 2010, 19, pp 691–725.

Phelps, J. H. Processing-Microstructure Models for Short- and Long-Fiber Thermoplastic Composites. PhD Thesis, 2009, University of Illinois at Urbana-Champaign, Urbana, Illinois.

Phelps, J. H.; Tucker III, C. L. An Anisotropic Rotary Diffusion Model for Fiber Orientation in Short- and Long-Fiber Thermoplastics. *J. Non-Newt. Fluids Mech.* 2009, 156(3), pp 165–176.

Wakeman, M. D.; Francois, G.; Manson, J. E. Cost Modeling of Thermoplastic P4 Process Technology. Progress Report 1 for the Automotive Composites Consortium, École Polytechnique Fédérale de Lausanne, April 2006.

C. Low Cost Carbon Fiber Development - Oak Ridge National Laboratory

Field Technical Monitor: C. Dave Warren
Oak Ridge National Laboratory
1 Bethel Valley Road, Oak Ridge, TN 37831
(865) 574-9693; e-mail: warrencd@ornl.gov

Technology Area Development Manager: Carol Schutte
U.S. Department of Energy
1000 Independence Ave., S.W., Washington, DC 20585
(202) 287-5371; e-mail: Carol.Shutte@ee.doe.gov

Contractor: Oak Ridge National Laboratory (ORNL)
Contract No.: DE-AC05-00OR22725

This project consists of five tasks critical for the development and industrial implementation of lower cost carbon fiber. Fifty-one percent of the cost of producing carbon fiber is attributable to the cost of the precursor; therefore, a significant share of effort is expended on developing lower cost precursors. The precursor development tasks include (1) development of lignin based carbon fiber precursors; (2) commercialization of a previously developed lower cost textile based polyacrylonitrile (PAN) precursor; and (3) development of lower cost polyolefin precursors. Thirty-nine percent of the cost of producing carbon fiber is attributable to the cost of conversion of the precursor into carbon fiber; therefore, significant effort is expended to develop lower cost, higher-rate-production technologies. The fourth task, conversion, includes development of a higher speed, lower cost oxidative stabilization process and development of microwave-assisted plasma processing methods, which are funded under a separate program. While accounting for only 4% of the cost of manufacturing carbon fiber, appropriate surface treatment and sizings targeted at automotive (not epoxy) resin systems are critical for the production of high-quality automotive components. The fifth task is aimed at the development of carbon-fiber surface treatments and sizing specifically targeted at resin systems of interest to the automotive industry.

Objective

Develop and transition to the marketplace lower cost carbon fiber precursors using lignin, a sustainable resource, as the base material.

Demonstrate that one or more lignin based precursor formulations can be expected to produce commodity-grade carbon fibers at a selling price of near \$5–7 per pound and have a modulus of at least 25 Msi.

Develop precursors from textile based PAN containing vinyl acetate (VA) for conversion into carbon fiber. Textile PAN is a material commonly used in knitting yarn and can reduce carbon fiber manufacturing costs by more than \$2.00 per pound of carbon fiber.

Develop the conversion protocol (time-temperature-tension) needed for conversion of textile PAN precursors into finished carbon fiber.

Provide assistance in scale-up of production facilities to commercially produce textile based carbon fiber precursor and aid current and future carbon fiber producers in the incorporation of new textile precursors into manufacturing plants.

Develop time-temperature-tension profiles for users of alternate precursors and assist in optimization of the manufacturing parameters.

Develop polyolefin based carbon fiber precursors that can be rendered infusible before carbonization by an economical accelerated stabilization route. Polyolefin precursors offer a higher carbon yield, lower cost raw material, and can be processed more inexpensively because they are melt spinnable.

Manufacture carbonized fiber from stabilized polyolefin precursors by developing an optimal conversion protocol.

Characterize the carbon fiber from polyolefin precursors and show that the mechanical properties meet program goals of at least 250 ksi strength and 25 Msi modulus are achievable.

Estimate the cost of polyolefin based carbon fiber precursors and show that they are likely to be less expensive than other potential precursors.

Provide the capability for production of small quantities of fiber or composite material samples using carbon fiber made from alternative precursors or manufacturing processes.

Provide the capability to test the convertibility of alternate precursors and develop their conversion protocols while also integrating the developments done in other tasks.

Provide the capability to test new concepts that can potentially lower carbon fiber cost.

Develop an improved technique for oxidizing carbon fiber precursors with a reduced residence time, equipment footprint, and resultant carbon fiber manufacturing cost.

Evaluate the cost impact of the new carbon fiber production techniques and materials.

Scale up all developed technologies to both pilot scale and preproduction prototype scale and transition them to industry. Completing technology scale-up reduces the risk to potential industries of applying the cost-lowering technologies.

Develop surface treatment techniques and sizing material for low cost carbon fibers (LCCFs) compatible with vinyl ester and nylon.

Develop sizing materials and finishes that will increase the adhesion of carbon fiber to vinyl ester resins and nylon.

Obtain a minimum of 11 ksi of short beam shear strength (SBSS) in composite materials derived from carbon fiber treated and sized by ORNL. Commercial fibers in the same resin system have short SBSSs below 10 ksi.

Accomplishments

- Completed initial work on full-scale development of a textile PAN precursor with Fibras Sinteticas de Portugal S.A. (FISIPE). Supported efforts to improve tow-splitting technology of textile precursors for reducing tow sizes to 40,000 or 20,000 filament tows in the precursor plant.
- Achieved fiber properties for strengths of 450 ksi on full-scale tows of carbonized textile PAN precursors (program requirement is 250 ksi). Modulus properties values of 35 Msi have been achieved, which are well above the program goals of 25 Msi.
- Consulted with the SGL Group (SGL) on the applicability of FISIPE precursors in their manufacturing systems and provided small samples to BMW and SGL to assist in their evaluations of FISIPE precursor potential.
- Obtained polyolefin fiber with diameters low enough to yield a faster functionalization (< 1 hr). Set up a semi-continuous functionalization module for polyolefin fibers and processed fiber tows of 288 and 1,500 filaments continuously, demonstrating varying degrees of functionalization.
- Semi-continuously processed a tow of 1,500 filaments of polyolefin precursor and demonstrated carbonized fiber properties 150 ksi and 15 Msi, meeting the program milestone.
- Developed a cooperative research and development agreement project with an industrial partner for commercialization of the polyolefin precursor technology.
- Established the melt-spinning conditions for appropriate blends of lignin with copolymers. Processed those into carbon fibers and measured properties. Unfortunately, none of the lignin blends met the mechanical targets for continued evaluation (tensile strength >150 ksi, modulus >20 Msi). Tensile strengths reached 140 ksi, but modulus was low at about 10 Msi, which is likely due to a lack of tensioning.

- Began establishment of processing conditions for conversion of lignin precursor fibers into carbon fiber on the precursor evaluation line (PEL). Encountered significant difficulty in tensioning fibers to allow them to be processed through the system.
- Installed a new 1,750°C carbonization furnace, five-pass box oxidation oven to simulate the configuration and conditions of industrial oxidation ovens, and tensioning/stretching equipment for the precursor evaluation system.
- Completed installation of and began operations with the 2,500°C furnace for the precursor evaluation system.
- Developed plans and cost estimates for major upgrades to the 1 ton per year pilot line to be used for integrating and commercializing lower cost carbon fiber technologies.
- Finished construction and began operation of the reactor materials compatibility test stand for determining optimal material composition to be used with the advanced oxidation process.
- Successfully processed textile-grade PAN with the advanced oxidation.
- Evaluated energy demand and residence time characteristics of the advanced oxidation module under development.
- Obtained two patents for the advanced oxidation process.
- Demonstrated the ability to achieve highly active surface functionality on 3 K aerospace, 26 K textile, and 50 K commodity-grade carbon fiber tows for the conventional interfacial task. Demonstrated a twofold increase in surface atomic oxygen concentration, which is indicative of a higher degree of functionality.
- Continuously surface treated more than a thousand feet of single-tow carbon fiber using ORNL's advanced surface treatment techniques. The efficacy of these surface treatment techniques was demonstrated with the testing of mechanical properties of composite materials, which showed an increase in SBSS from 6 ksi to 10 ksi.
- Identified potential sizing chemistries compatible with vinyl ester and nylon resin systems. Chemistry formulation development efforts were started and applied at ORNL.
- Evaluated and reported on commercially available carbon fiber surface treatment and sizing methods for vinyl esters.
- Designed, constructed, and optimized laboratory-scale continuous-process surface treatment applicator, sizing equipment, and drying heater system.

Future Direction

Revisit the fundamentals of lignin precursor fiber spinning, including spinneret design, lignin chemistry, and molecular weight, increasing fiber drawdown time to obtain better molecular alignment in the fiber and less physical handling of fiber at all stages, with a specific goal of being able to tension the precursor during the early stages of oxidation.

Continue to optimize the FISIFE precursor processing conditions and to support FISIFE scale-up. Will require adding prestretching and tensioning to the pilot line to yield more precise fiber stretching during stabilization and oxidation.

Pursue commercialization of lower cost textile based precursors with current industrial carbon fiber suppliers and potential future carbon fiber suppliers to high-volume industries.

Evaluate potential collaborations in all areas of carbon technology development with potential, new, high-volume entrants into the carbon fiber market.

Incorporate textile precursors into the Carbon Fiber Technology Center demonstration line, which is being constructed with funds from the American Recovery and Reinvestment Act, and support scale up of textile precursor technology from pilot-line scale to production-line scale in U.S. facilities.

Demonstrate carbonized fiber properties ≥ 200 ksi strength and ≥ 20 Msi modulus by FY 2011 and ≥ 250 ksi strength and ≥ 25 Msi modulus by FY 2012 using polyolefin based precursors.

Understand the carbonization process and optimize carbon yield from polyolefin precursors.

Explore nontraditional stabilization methods for the polyolefin precursors.

Scale and transition the polyolefin technology to an industrial partner.

Complete a major pilot-line upgrade that will yield higher production volumes and more process control through the addition of a greater degree of stretching control during oxidative stabilization.

Continue refining and scaling the reactor design and processing protocols of the advanced oxidation system to achieve a high-speed, multiple-large-tow, semi-continuous (multiple pass) plasma oxidation process.

Conduct rate-effect studies and update cost analysis for the advanced oxidation system.

Develop the capability to oxidize nontraditional precursors in the advanced oxidation system.

Scale the process and equipment for the advanced oxidation.

Demonstrate 10 ksi (~70 MPa) or more composite SBSS using the surface treatments and sizing developed in this program and automotive resin systems identified by automotive partners.

Generate data on the quality of adhesion between carbon fibers and nylon in automotive-grade composites with an emphasis on long fiber injection-molded composite applications.

Introduction

The first task under this project addresses the cost of carbon fiber by demonstrating the use of lignin, a sustainable resource, as a new precursor material. The project is evaluating the use of low cost, high-volume lignin feedstocks that have the potential to meet the demand requirements and product performance needs of the automotive market. The task goal is to demonstrate that one or more lignin based precursor formulations can be expected to produce commodity-grade carbon fibers at a selling price near \$5–7 per pound and with a modulus of at least 25 Msi and a strength of at least 250 ksi.

The purpose of the second task is to develop and commercialize textile based PAN. A collaborative international program led by ORNL and FISIFE is working to render textile based PAN suitable for conversion into carbon fiber. Textile fiber sells for half the cost of conventional carbon fiber precursors and would result in a savings of more than \$2.00 per pound in the finished carbon fiber manufacturing costs.

The goal of the third task is to develop the technology for the production of LCCF from melt-spun polyolefin precursor fibers. Polyolefin based fibers [polyethylenes (PEs) and polypropylene (PP)] are industrially produced in United States and are very low cost commodity plastic fibers (\$0.50–0.7 per pound). The cost of precursor fibers from polyolefin is projected to be less than half of that of the PAN-based precursor fibers, yet the carbon yield will be significantly higher than with PAN precursors. The combination of lower raw material cost, higher material yield, and process savings from melt spinning of the precursor makes the polyolefin precursor the most cost-advantageous alternative.

The purpose of the fourth task is to develop a plasma processing technique to rapidly and inexpensively oxidize PAN precursor fibers. Conventional oxidation is a slow thermal process that typically consumes more than 80% of the processing time in a conventional carbon fiber conversion line. A rapid oxidation process could dramatically increase the conversion line throughput and appreciably lower the fiber cost. A related project has already demonstrated the potential for significantly accelerating carbonization.

The quality of the fiber-matrix interface is often a critical factor in determining composite mechanical properties and durability. Carbon fibers are typically surface treated and sized to make them compatible with aerospace resin systems. The final task under this project is developing surface treatments and fiber sizings that will make carbon fibers compatible with vinyl ester and nylon. Research at ORNL is targeting the control of surface functional groups, the creation of highly energetic surfaces, and the development of appropriate sizings.

The costs of manufacturing carbon fiber are shown in Figure 1 along with the range that each of these tasks affects in that production process.

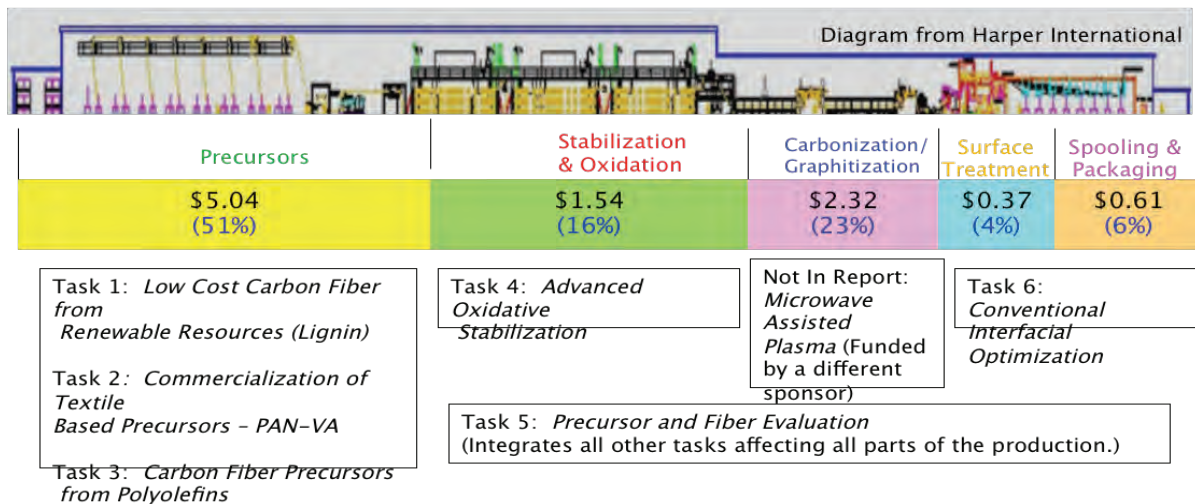


Figure 1. Program coordination between different tasks.

The strategy for transitioning each of these technologies to industry is to involve industry as early in the development process as is practical from the risk-benefit standpoint as is possible. It is realized that trying to incorporate multiple technologies into production lines simultaneously would be a very high risk for industries; therefore, the project teams seeks to involve industry in each of the tasks as that technology becomes sufficiently mature to be of interest for commercialization. The textile precursor has reached that level and has both precursor manufacturers and carbon fiber manufacturers involved. The lignin and polyolefin precursor efforts are premature for precursor and carbon manufacturers but are well enough understood for raw material suppliers (lignin and polyethylene) to be involved. The advanced oxidation is nearing a maturity stage to involve oxidation oven manufacturers, and the surface treatment and sizing development efforts have automotive suppliers involved because they are the missing links to being able to use both lower cost and currently available carbon fiber in automotive structures.

Activity and Developments

Low Cost Carbon Fiber from Renewable Resources

Principal Investigator: Fred Baker, ORNL
(865) 241-1127; e-mail: bakerfs@ornl.gov

Principal Investigator: Nidia Gallego, ORNL
(865) 241-9459; e-mail: gallegonc@ornl.gov

Introduction

This project addresses the cost of carbon fiber by demonstrating the use of lignin, a sustainable resource, as a new precursor material. The project is evaluating the use of a low cost, high-volume lignin feedstock that has the potential to meet the demand requirements and product performance needs of the automotive market. The project goal is to demonstrate that one or more lignin based precursor formulations can be expected to produce commodity-grade carbon fibers at a selling price of near \$5–7 per pound with a corresponding modulus of at least 25 Msi and strength of at least 250 ksi.

Approach

The development of lignin based precursors will be accomplished using laboratory-scale equipment and pilot-scale melt-spinning and carbon fiber production lines. The project will construct the technical database necessary to facilitate commercial production of lignin based carbon fiber, including knowledge in the following areas.

- Isolation and purification of lignin to obtain appropriate precursor properties for carbon fiber production.
- Melt-spinning technology, including compounding/pelletization of precursor feed material, extruder and spinneret configuration, spinning conditions, copolymers, and plasticizing agents.
- Thermal processing of precursor fiber into carbon fiber.
- Advanced processing of lignin based carbon fiber.
- Mechanical properties of lignin based carbon fiber.
- Surface treatment and sizing technology for relevant resin systems.
- Development of process flow sheets and economics for lignin based carbon fiber production for presentation to companies considering entering the business of LCCF production.

This task seeks to develop materials and methods for the manufacture of lignin based carbon fiber. Industrial partners and collaborators include Lignol Innovations (Vancouver, BC, Canada), Kruger Wayagamack (Trois-Rivières, QC, Canada), INNVENTIA, formerly STFI Packforsk (Stockholm, Sweden), University of Tennessee (Knoxville), and the Institute of Paper Science and Technology (IPST) at the Georgia Institute of Technology (Atlanta).

Results and Discussion

Identification of Appropriate Blends (Alloys) of Lignin with Synthetic Polymers and Pitches

Lignin obtained from Alcell was used for this subtask. Based on Hildebrand and Hansen solubility parameters, PP, polyethylene oxide (PEO), polyethylene terephthalate (PET), PAN, and mesophase pitch were selected for blending with lignin (in various proportions), and rheology, thermal analysis, and single fiber spinning tests were conducted. Despite the apparently favorable solubility parameters, several of the polymers and mesophase pitch blends resulted in complete phase separation in the spun fiber, including PP and PEO. The most promising polymer appeared to be PET, and several formulations of varying ratios of lignin and polymer (5–20 wt % PET) were melt spun on the multifilament equipment and the precursor fibers thermally processed into carbon fibers for mechanical testing and scanning electron microscope (SEM) evaluation. None of the Alcell lignin–PET blends met the mechanical targets for continued evaluation. Tensile strength reached 140 ksi, but modulus was low at about 10 Msi. Further work on lignin polymer blends was put on hold to revisit more fundamental studies.

Continuous Conversion of Lignin Based Precursor into Carbon Fiber

This project subtask sought to establish the processing conditions for conversion of lignin precursor fibers into carbon fibers and measurement of the mechanical properties of the carbon fibers. Much of the work was focused on developing a satisfactory technique for anchoring bundles of lignin precursor filaments (many thousands) to the PAN based carbon fiber tow used to pull the precursor fiber through the PEL and establishing appropriate processing conditions. Many different anchoring techniques were tried, ranging from mechanical clamping to high-temperature ceramic cements of different chemistries. A silica based cement appeared to be best, and several conversion runs were made with and without tensioning of the fiber. Tensioned fiber yielded the highest tensile strength obtained to date, 175 ksi, but the modulus still fell well short of the milestone target of 20 Msi.

Demonstration of Sustained Melt Spinning of Lignin Precursor Fibers as a Non-woven Mat

This project subtask is focused on establishing the melt-spinning conditions for production of a non-woven mat of lignin precursor fibers for subsequent thermal processing into carbon fiber using bulk transport (belt) systems. In late FY 2010, using commercial-scale melt spinning equipment at a vendor's facility, it was demonstrated that hardwood lignin (Alcell) can be readily melt spun into a mat. Processing of selected samples of the precursor fibers into carbon fiber for evaluation of properties is planned for FY 2011.

Melt Spinning of Alcell Lignin

Process development work during FY 2010 was focused on the only source of lignin readily available in the quantity required, the Alcell product produced by Lignol Innovations as a by-product of the organosolv pulping of waste hardwood materials for cellulosic ethanol fuel production. This lignin, as furnished, meets the purity specifications for carbon fiber production, is readily melt spinnable without the aid of a plasticizing agent, and is being furnished in 100 kg quantities under nondisclosure and material transfer agreements in effect between UT Battelle and Lignol Innovations.

Through careful manipulation of the trace level of residual solvent in the Alcell lignin, the glass transition temperature (T_g) and melting point (T_m) were progressively raised to values close to the limits of melt spinnability, but more importantly, rapid stabilization of the precursor fiber was facilitated. All published work to date on lignin based carbon fiber, including the ORNL work, has involved very long stabilization times for the precursor fiber (e.g., upwards of 3 days). As exemplified by the data in Figure 1, work on modifying lignin chemistry through the first half of FY 2010 very substantially reduced stabilization time (to 10–15 min) and significantly increased carbon fiber yield (from 46–53%).

As shown in Figure 2, further heat treatment of the carbon fiber obtained at 1,000°C to temperatures up to 2,700°C resulted in a high degree of graphitization of the carbon fiber.

These x-ray diffraction (XRD) data demonstrated a substantial enhancement of lattice parameters: d_{002} (graphene layer spacing) decreased from 3.88 to 3.41 Å at 2,700°C; correspondingly, L_c (height of graphene stacking layers) increased from 9 to 33 Å. As a point of reference, a T300-grade PAN based carbon fiber exhibited d_{002} and L_c values of 3.47 Å and 13 Å, respectively, significantly lower lattice parameters than the lignin based carbon fiber treated at 2,700°C. However, whereas the mechanical properties of the T300 carbon fiber are close to the target for lightweighting of vehicles, the properties of even the 2,700°C lignin based carbon fiber still fell short, particularly modulus. In essence, the modulus of the heat-treated, lignin based carbon fiber did not track the degree of graphitic structure introduced into the fibers. Much more detailed and time-consuming XRD analyses subsequently revealed that, in marked contrast to T300 fiber, there is no preferred orientation of the graphitic crystallites in the lignin based carbon fiber, a significant deficiency with respect to obtaining target properties.

Conclusions

Lignin sources have been identified that meet the purity qualifications required for making carbon fiber. Work toward identifying and producing precursor fiber with appropriate plasticizers is continuing. Difficulty in handling the precursor fibers during carbonization is presenting obstacles to obtaining satisfactory mechanical properties. The mechanical properties achieved to date do not meet the required program minimums. The ability to spin lignin precursors as a mat product has been demonstrated.

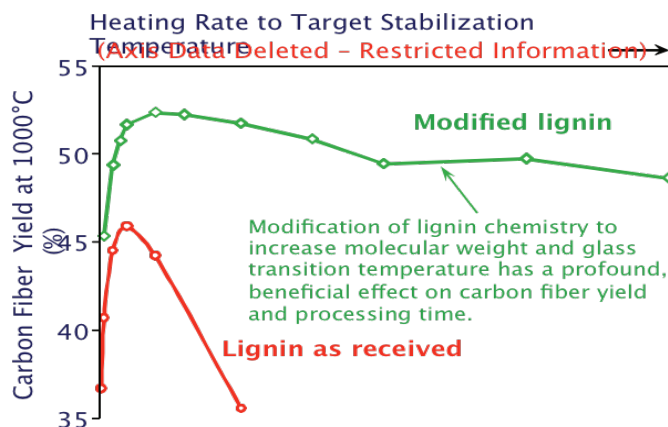


Figure 1. Rapid stabilization of lignin and carbon fiber yield.

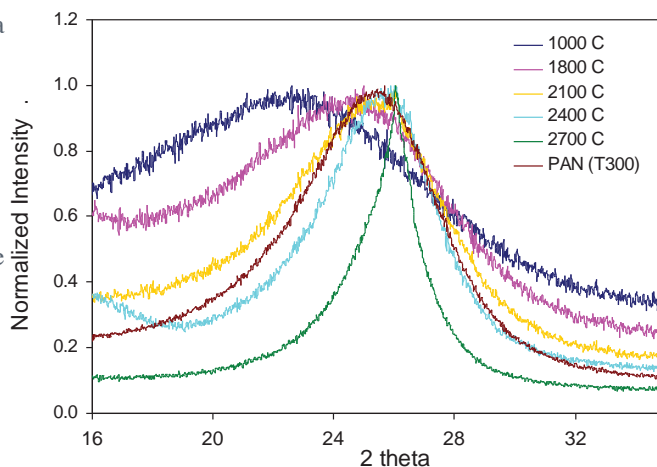


Figure 2. Graphitization of lignin based carbon fiber.

Commercialization of Textile Based Precursors—Textile Polyacrylonitrile–Vinyl Acetate

Principal Investigator: Dave Warren, ORNL
(865) 574-9693; e-mail: warrencd@ornl.gov

Principal Investigator: Soydan Ozcan, ORNL
(865) 241-2158; e-mail: ozcans@ornl.gov

Principal Investigator: Felix Paulauskas, ORNL
(865) 576-3785; e-mail: paulauskasfl@ornl.gov

Principal Investigator: Bob Norris, ORNL
(865) 576-1179; e-mail: norrisrejr@ornl.gov

Principal Team Members:

Ronny Lomax, Amit Naskar, Fue Xiong, Kenneth Yarborough, Oak Ridge National Laboratory
Mohamed Abdallah, MGA Advanced Composites and Engineering
Ana Paula Vidigal, Paolo Correia, and José Contreiras, FISIFE SA

Introduction

Over the past few years, the DOE Automotive Lightweighting Materials program has been developing technologies for the production of lower cost carbon fiber for use in body and chassis applications in automobiles. Program requirements target materials that have tensile strengths in excess of 250 ksi and moduli of at least 25 Msi. Past work included the development of alternate, lower cost precursors and alternate, lower cost methods for manufacturing precursors into finished carbon fiber. The purpose of this project is to take one precursor technology, textile based PAN, from the technical feasibility stage and scale up to commercial implementation. The technology being pursued for the textile based precursor is the chemical modification of textile PAN containing VA using a proprietary solution bath while the fiber is still in the uncollapsed state.

This project has resulted in the determination of the optimum concentration-temperature-exposure profiles to render the fiber carbonizable by conventional processes and also readily and inexpensively manufactured in existing textile PAN plants. Successful completion of this project will result in a manufacturer being ready to sell precursors to carbon fiber converters and ORNL providing to those producers specific instructions for precursor conversion, subject to export control limitations. Deliverables include samples of partially or fully carbonized carbon fiber.

Approach

Previously, under a separate contract as part of the Automotive Lightweighting Materials program, Hexcel Corporation developed the basic science necessary to render textile based PAN polymers carbonizable. That science included subjecting the textile precursor to a chemical pretreatment bath while the fiber was still in the uncollapsed state. That work was conducted offline from the textile fiber manufacturing. Fiber samples were split off from the line by hand, packaged, and processed in their laboratory. Hexcel obtained satisfactory samples but under only one set of processing conditions and with one specific textile fiber. Certain issues needed to incorporate the technology into manufacturing plants were not addressed but are being addressed for VA-containing precursors in this project.

Results and Discussion

ORNL has established a highly interactive and mutually beneficial partnership with a Portuguese textile fiber manufacturer, FISIFE, which produces VA-comonomered polyacrylonitrile (PAN) for textile applications. FISIFE is a high-volume manufacturer that produces a commodity fiber that is roughly one-half the cost of conventional acrylic carbon fiber precursors. Our efforts are aimed at developing a chemical pretreatment to be added in their manufacturing line to render one of their textile formulations oxidizable, carbonizable, and satisfactory as a carbon fiber precursor.

During this reporting period, FISIFE has continued formulating and spinning improved precursor fiber variants (examples shown in Figure 1) and providing extensive samples to ORNL for conversion and evaluation. They also processed (Figure 2) and evaluated larger-sized tows internally as part of their scale-up efforts. Note the golden color of this precursor fiber, which differs from the traditional white color of typical carbon-fiber-grade PAN. The color is indicative of the specialized pretreatment developed and implemented by ORNL and FISIFE, which is key to the success of this alternative product.

ORNL has been using both the precursor and fiber evaluation line and the pilot line to determine time-temperature-tension processing profiles for the FISIFE precursor. Program requirements are to develop fibers with strengths of at least 250 ksi and moduli of at least 25 Msi. Figure 3 shows the evolution of the strength and modulus during development of processing conditions over time. We have currently reached strengths of 450 ksi, which exceed program goals, and a current modulus value of 35 Msi, which is well above program goals. Property levels have varied, and significant effort is being devoted to both achieving these property levels consistently at the small scale and establishing robust processes capable of reproducing these properties as the process is being scaled for production. Although the August 17 data points (Figure 3) are significant in terms of both strength and modulus, we do not have enough experience at this point to know whether these properties are consistently achievable. The pilot line has been modified to provide process flexibility in evaluation of these developmental products, and additional modifications to greatly expand these capabilities are anticipated in the next reporting period. This is a very useful tool in the scale-up effort and will certainly complement the larger Carbon Fiber Demonstration Line initiative currently being established to provide semi-production quantities for industrial acceptance testing.



Figure 1. Textile tow precursor as produced by FISIFE and supplied to ORNL on spools for evaluation.



Figure 2. Textile tow precursor as produced by FISIFE and evaluated internally.

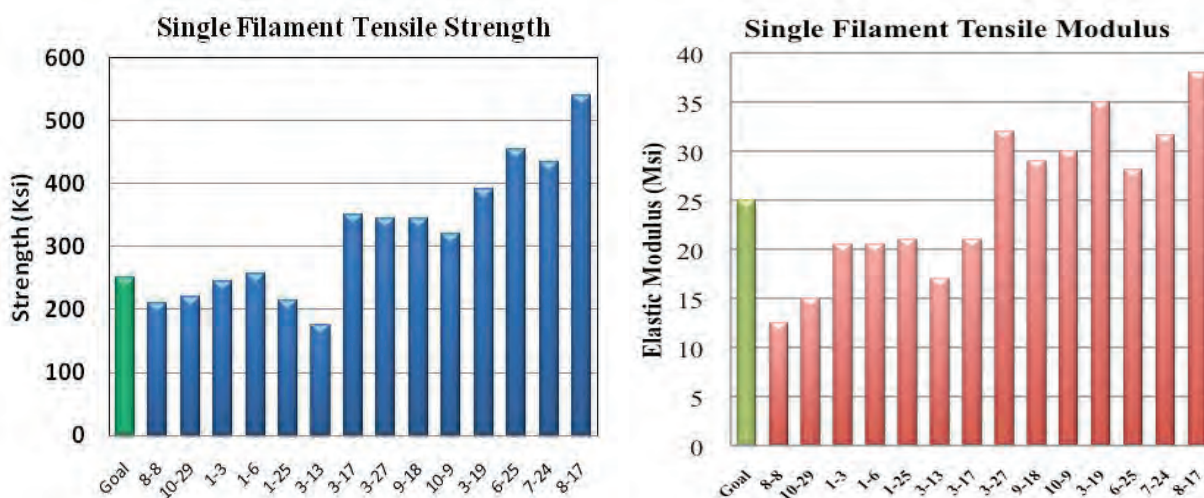


Figure 3. Strength (a) and modulus (b) data from FISIFE precursor converted and tested at ORNL showing substantially improvement trends.

The capabilities and approach developed and demonstrated in this project can be applied to both facilitate the ongoing scale-up of the FISIFE precursor and the commercialization of that precursor. This approach can be used to assist other potential producers in similar efforts.

Conclusions

The development of VA PAN textile precursors has been a success. Strength values (450 ksi) exceed program requirements (250 ksi), and modulus values (35 Msi) are above program requirements (25 Msi). The chemical pretreatment equipment has been installed in the production facility, and final verification of production-quality material is in progress. FISIFE is pursuing additional support for its ongoing commercialization efforts.

Carbon Fiber Precursors from Polyolefins

Principal Investigator: Amit Naskar, ORNL
(865) 576-0309; e-mail: naskarak@ornl.gov

Principal Investigator: Rebecca Brown, ORNL
(865) 574-1553; e-mail: brownrh@ornl.gov

Other Participants: Marcus Hunt and Fue Xiong, ORNL

Introduction

The goal of this project is to develop the technology for the production of LCCF from melt-spun polyolefin precursor fibers. At present, common commodity-grade carbon fibers are produced from PAN based precursors. PAN based textile precursors are a potential candidate for low cost carbon fibers, with projected cost savings of about \$2.00 per pound for finished carbon fiber. Currently, however, there are no domestic producers of textile PAN, and so supply and price stability may become an issue. Textile fibers are solution spun, and the manufacturing process involves multiple unit operations to produce the precursors. Also, in solution spinning the mass throughput rate is significantly less than that of the relatively simpler conventional melt-spinning process. Polyolefin based fibers (polyethylene and polypropylene) are industrially produced in the United States and are very low cost commodity plastic fibers (\$0.50–0.75 per pound). The cost of precursor fibers from polyolefin is projected to be less than half that of the PAN based textile precursor fibers. Because polyolefin fibers are melt spun, a stabilization route needs to be developed to render the precursor fibers infusible prior to carbonization. In subsequent carbonization steps, optimal processing parameters need to be identified for desired carbon fiber morphology and properties.

Approach

The technical approach in developing carbonized filaments from a melt-processable precursor involves modification of filaments by a chemical reaction to render them infusible. In the case of PAN based fiber, thermal oxidation (incorporation of oxygen heteroatom in the polymer) cross-links the fiber and increases the glass transition temperature above its melting point and pyrolysis temperature. In the case of polyolefin fibers, chemical functionalization is required after melt spinning to form a thermoset plastic. This may be achieved by either modifying the polyolefin resin before spinning without affecting its melt rheology (spinnability) or through post-spinning modification of fibers from neat resins.

An accelerated functionalization method (using sulfur as the heteroatom) is being developed to meet the above objective. A chemical reactor was constructed for continuous functionalization of the precursor fibers. The target functionalization time is 1 hr or less because the residence time inside the reactor is important for commercial viability of this technology.

Carbonization runs under various operating conditions, and optimization of processing parameters are under way to tailor the fiber morphology and properties. Tensile properties of the filaments were measured and thermal analysis, elemental analysis, diffraction studies, and analysis of electron micrographs have been conducted at each step of the fiber processing to understand thermal-mechanical-chemical changes in the filaments. Critical technical criteria of this technology include achieving ≥ 25 Msi tensile modulus, ≥ 250 ksi breaking strength, and $\geq 1.0\%$ ultimate strain in the finished fiber by the end of FY 2012.

Results and Discussion

Tensile properties of the precursor filaments at various stages are summarized in Table 1. It is well known that the tensile properties of melt spun fibers can be tailored by altering draw-down ratio during melt spinning. As-spun filaments (spun drawn) were cold drawn in a draw frame to increase filament orientation and mechanical properties. Table 1 shows that upon application of a high degree of draw, from precursor batches 1 to 3, filament diameter remains constant and tensile strength and modulus increase. Filaments from various draw ratios have different thermomechanical properties. Thermal shrinkage force increases with increasing draw ratio. The temperature associated with maximum shrinkage force is critical for the functionalization reaction. After optimization of time, temperature, and dimensional stability during the chemical reaction, a protocol for semi-continuous functionalization of the polyolefin fiber tow was developed (tested with tows of 36, 288, and 1,500 filaments). A representative photograph of the processing run is shown in Figure 1. Once the filaments were stabilized (as indicated by thermal analysis data, shown later in this report), they were carbonized under specific processing conditions. Tensile properties were tested using single-filament test method, and the cross-sectional areas of the fibers were measured under SEM to obtain the stress data of the carbonized filaments. Carbonized filaments with 160 ksi tensile strength, 15 Msi modulus, and 1.1% ultimate elongation were produced. (To comply with export control regulations, processing parameters are not disclosed in this report.)

Table 1. Tensile properties of PE fibers and their carbonized filaments.

Fiber type	Filament Diameter (μm)	Max. Filament Stress (ksi)	Max. Modulus. (Msi)	Ultimate Elongation (%)	Remarks
Precursor-1	16	14	0.02	190	Resin-1
Precursor-2	16	20	0.06	120	Resin-1
Precursor-3	16	25	0.10	115	Resin-1
Precursor-4	19	22	0.15	100	Resin-2
Stabilized-1	21	10	0.20	25	From precursor-1
Stabilized-2	19	8	0.20	17	From precursor-2
Stabilized-4	28	7	0.20	12	From precursor-4
Carbonized-1	15 ^a	92	4	1.6	Difficult to process under tension
Carbonized-4	15 ^a	160	15	1.1	Carbonized under specific conditions

^aEffective filament diameter (i.e., equivalent diameter without any core).

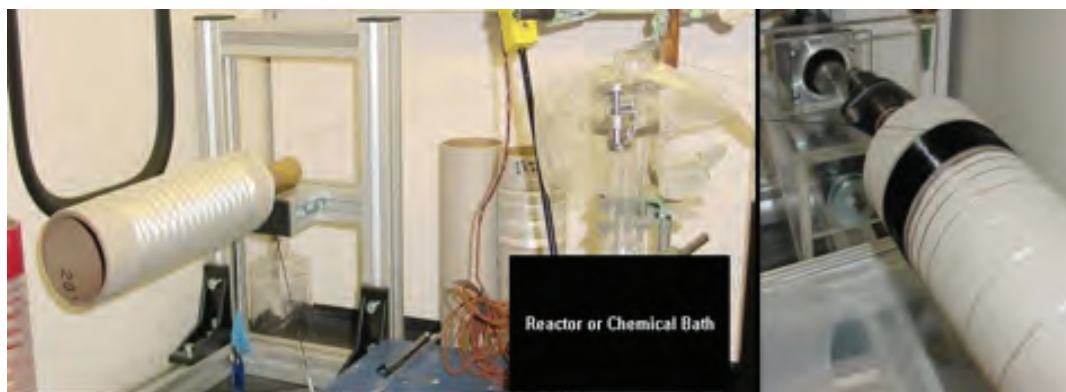


Figure 1. Photograph showing semi-continuous precursor functionalization run.

Thermal analyses of the precursors that were partially stabilized demonstrated a slight crystallinity, as observed in differential scanning calorimetry (DSC), XRD, and dynamic mechanical thermal analysis. A high degree of functionalization eliminated this crystallinity. The elimination of crystallinity is a process-controlled phenomenon (i.e., the elimination of crystallinity in the thermoplastic fibers is a function of multiple process parameters). All of the functionalization runs summarized in this report involve less than 1 hr of processing time. Usually, heteroatom (S) concentration across the functionalized filament radius follows a gradient. The core of the filament shows the least S concentration. Figure 2 shows the energy dispersive spectroscopy (EDS) mapping (backscattered x-ray) of S elements in a stabilized Precursor-4 fiber. It is apparent that the

representative filament has high S concentration at about 2–4 μm depth along the circumference of the cross section. The quantitative values of elemental S concentration at different filament radii are not reported in this summary. It was believed that the decrease in filament diameter would increase the diffusion rate of S across the filament diameter. However, in spite of the increased diffusion rate, filaments with high surface area (due to smaller filament diameter) impose increased hydrogen bonding and subsequent interfilament bonding during thermal treatment. During FY 2010 the team focused on two aspects of filament stabilization: (a) improved handling of small-diameter filament tow and (b) carrying out experiments with large-diameter filament tow to demonstrate carbonized filament properties. The first processing aspect remains inconclusive at this stage. A modified functionalization route may be required, and this will be explored during FY 2011.

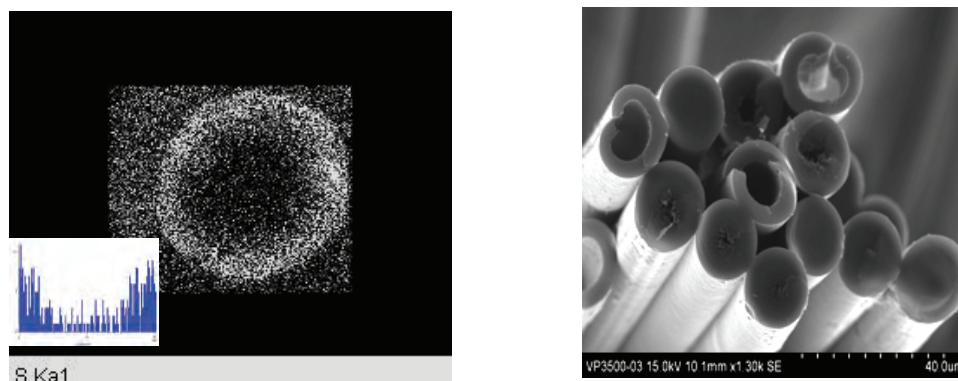


Figure 2. (a) Mapping elemental S on the fiber cross sections during EDS study in an SEM and quantitative linescan of elemental S across the filament diameter (inset) and (b) carbonized filaments from such stabilized fibers with no core or weak amorphous core

DSC shows elimination of crystallinity in some polyolefin precursors with increased degree of functionalization. Figure 3(a) shows the DSC thermograms of Precursor-1 at various functionalization levels (degree of functionalization: R1S3 > R1S2 > R1S1 > neat R1 \sim 0). The wide-angle XRD patterns of the corresponding filaments are shown in Figure 3(b). It is clear that with increasing degree of functionalization the peak intensities due to PE crystallites decrease; however, filaments retain a slight degree of order at high degree of functionalization, as is apparent from XRD data of R1S3. This could be due to the presence of an orientated amorphous phase in the functionalized fibers.

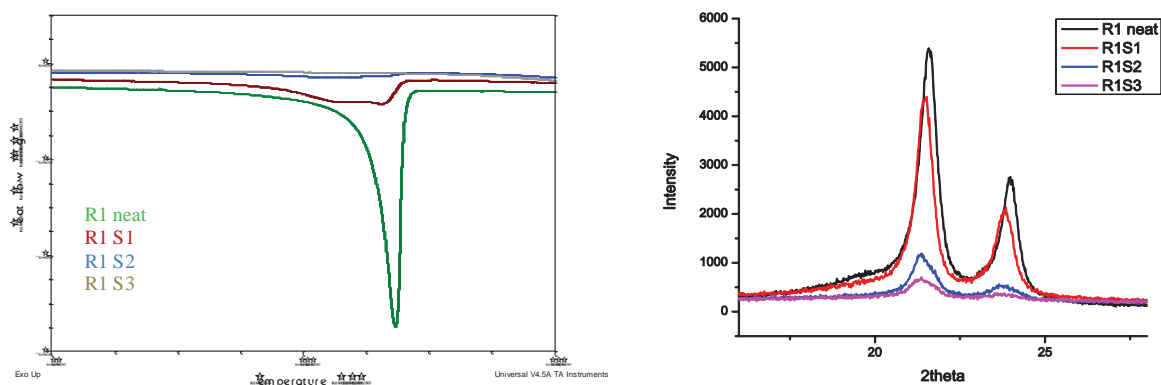


Figure 3. (a) DSC thermograms of precursor-1 fibers at different degrees of functionalization and (b) wide-angle XRD patterns (2θ profile) of the corresponding fiber tow. (R1S* are proprietary sample designations.)

The Fourier transform infrared spectroscopy (FTIR) spectra of the fibers before and after functionalization are shown in Figure 4(a). After functionalization the peaks due to C-O-S (900 cm^{-1}), C = C (1630 cm^{-1}), and O-H ($3,000\text{--}3,500\text{ cm}^{-1}$ broad peak) vibrations appear (Kaneko, 2004). This confirms chemical functionalization of the neat fibers. The dynamic mechanical data of the corresponding neat, partly stabilized, and fully stabilized filaments are shown in Figure 4(b). The neat fiber melts at 130°C . Partly stabilized filaments show reduction in modulus at 130°C due to partial melting of filaments. Fully stabilized filaments show a steady plateau modulus that is relatively higher than that of the precursors.

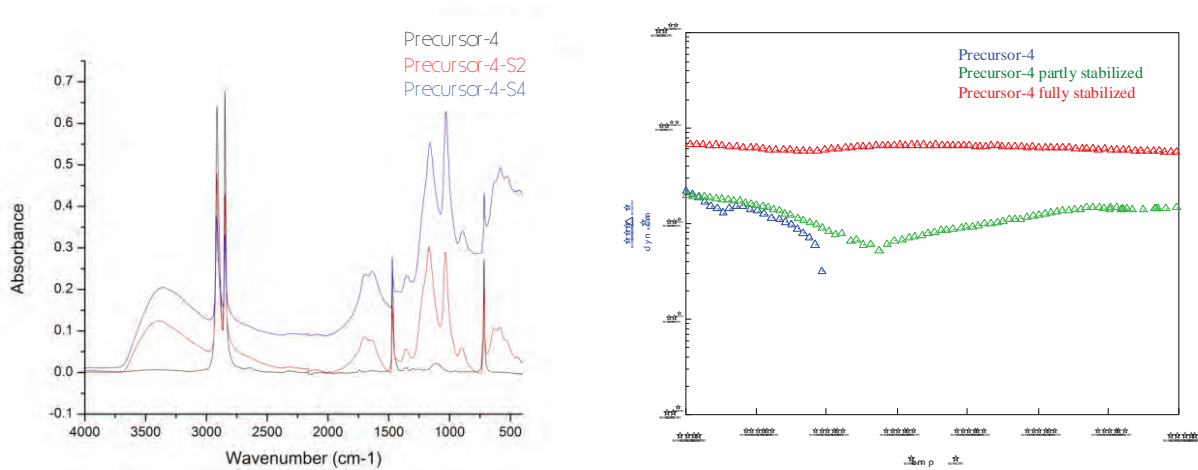


Figure 4. (a) FTIR spectra of neat and stabilized fibers and (b) dynamic mechanical storage modulus profile of the filaments with complete and incomplete stabilization.

The wide-angle XRD data of carbonized PE fiber and a corresponding carbon fiber from PAN are shown in Figure 5. It is clear that the PE based fiber produced a (002) peak due to graphitic planes. However, this peak is not as intense as that for the PAN fiber primarily due to lower filament count in the PE based carbon fiber mass studied in the XRD experiment.

Conclusions

During FY 2010, significant progress was made toward the production of LCCFs from PE. Only minor work has been conducted on PP precursors. The effects of draw ratio and degree of functionalization on fiber crystallinity and tensile properties are understood. PE fibers were made infusible through continuous processing in less than 1 hr, and processing parameters were optimized to form carbonized filaments exhibiting tensile strength of 160 ksi, modulus of 15 Msi, and 1.1% elongation. However, issues of interfilament bonding during thermal treatment and incomplete sulfonation of the fiber core were identified as major obstacles to be addressed in FY 2011 to achieve the targeted carbon fiber properties. The team met the milestones for FY 2010.

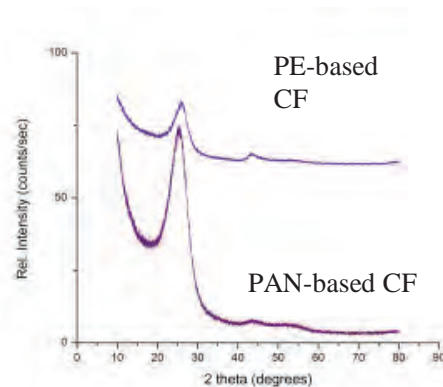


Figure 5. XRD patterns of PE based and PAN based carbon fibers.

Advanced Oxidative Stabilization of Carbon Fiber Precursors

Principal Investigator: Felix Paulauskas, ORNL
(865) 576-3785; e-mail: paulauskasfl@ornl.gov

Principal Investigator: Bob Norris, ORNL
(865) 576-1179; e-mail: norrisrejr@ornl.gov

Other Participants:
Soydan Ozcan, and Kenneth D. Yarborough, ORNL
Professor Joseph Spruiell, University of Tennessee
Truman Bonds, Sentech

Introduction

The advanced oxidative stabilization project is a critical element in the Low Cost Carbon Fiber program in terms of meeting ultimate technical and economic goals. The objective of this task is to develop an improved technique for oxidizing carbon fiber precursors with reduced residence time, cost, and equipment footprint. To meet these objectives, technology developed in this task should be capable of processing economically attractive precursor fiber chemistries and being scaled to process sufficiently large tow sizes and numbers of tows such that the entire integrated material and process system can meet program goals for fiber performance and costs. Significant advances in demonstrating process feasibility have been achieved at the bench scale previously.

The purpose of this project is to develop a plasma processing technique to rapidly and inexpensively oxidize precursor fibers. Conventional oxidation is a slow thermal process that typically consumes more than 80% of the processing time in a conventional carbon-fiber conversion line. A rapid oxidation process could dramatically increase the conversion line throughput and appreciably lower the fiber cost. A related project has already demonstrated the potential for significantly accelerating carbonization. Critical technical criteria include (1) ≥ 25 Msi tensile modulus, ≥ 250 ksi breaking strength, and $\geq 1.0\%$ ultimate tensile strain in the finished fiber; (2) uniform properties over the length of the fiber tow; (3) repeatable and controllable processing; and (4) significant unit cost reduction compared with conventional processing. The current work phase is aimed at developing this technology to be able to continuously process small tows of fiber in short periods of time (hours) and achieve properties equivalent to industrial grades of carbon fibers. This is being done by using a 3 K commercial precursor, processing it in the advanced oxidative stabilization unit, and then carbonizing it conventionally. The goals also include significantly reducing the time required for oxidative stabilization (conventionally 80–120 min), which will permit greater fiber production rates and improved economics. Once this phase is concluded, the scientific basis will be sufficiently mature to allow for the scale-up of the process using lower cost precursors in larger tow sizes on a continuous basis.

Approach

For this task, the researchers are investigating PAN precursor fiber oxidation using nonequilibrium (with respect to plasma volume population), nonthermal plasma at atmospheric pressure. As illustrated in Figure 1, conventional oxidative stabilization produces a “core-shell” geometry with a distinct interphase between the (slowly growing) fully oxidized shell and the (shrinking) stabilized inner core. Plasma processing enhances oxygen diffusion and chemistry in the PAN oxidation process, accelerating the oxidized layer growth rate, and oxidizing the fiber more uniformly, with a considerably less pronounced interface between the two regions. Previous work has shown this approach can reduce residence time.

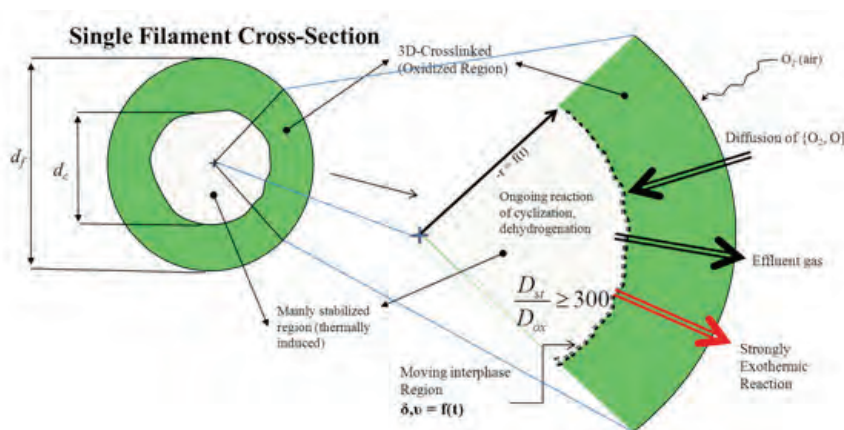


Figure 1. Single-filament cross section during conventional oxidative stabilization process.

Atmospheric-pressure plasma provides better control over the thermal environment and reaction rates than low-pressure plasma. It greatly reduces the sealing challenges inherent to low-pressure processing. In addition, a modified approach begun this fiscal year introduces the advantage of improved internal heat and flow distribution and the use of short-lived reactive species in the oxidation process.

Results and Discussion

At the end of FY 2009, the research had been brought to a point where scaling up to multiple tow processing with the advanced oxidation process had been demonstrated using the Multiple Tow Reactor 1 (MTR1), as shown in Figure 2. This reactor is capable of processing up to six small tows simultaneously while maintaining the proper temperature gradient, tension per tow, and chemistry. The bulk of the experimental work in FY 2010 was conducted with this device. The key focus areas for this past year are discussed as follows. It should be noted that the research is now at a point where, after some additional work, it is on the verge of a rapid scalability stage.

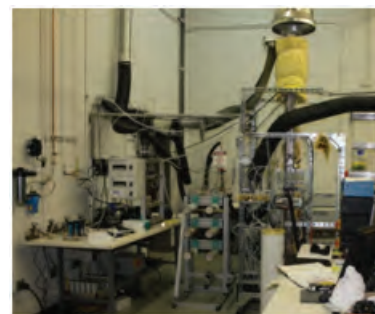


Figure 2. MTR1 used in this research.

Oxidized–Carbonized Fiber Mechanical Properties Analysis

During the ongoing testing in MTR1, it became evident that certain processing conditions that produced high-density results at the lower residence times were also resulting in damage to the oxidized fiber. Therefore, an exhaustive study was launched to examine the cause-and-effect relationships of this damage. During the course of this study, it was discovered that under certain conditions the nature of the damage being done was very unique, producing physical properties that could be beneficial for certain applications but detrimental to others. A systematic testing procedure was established where a series of processed fiber tows would be sent to ORNL for mechanical testing of individual filaments. This study soon became tied to the program milestone on the mechanical properties of fibers produced from the advanced oxidation process. Selected samples of results are shown in Tables 1 and 2. The program requirements are included in Table 2. The modulus requirement was quickly achieved, while the tensile and elongation requirements were more difficult. It became evident that the damage being done to the fiber was affecting the mechanical properties. Over the course of testing, the mechanical properties were improved using refined methods. Eventually the mechanical properties of the advanced oxidized fibers were equivalent to, and then exceeded, the corresponding values of the conventional oxidized fibers, yet the properties of the subsequently carbonized fibers were not reaching similar levels. At the time of this report, mechanical properties are being measured, and it is anticipated that the program properties for carbonized fiber will be surpassed.

Table 1. Oxidized mechanical properties.

	Processing Date	Tensile Strength (ksi)	Modulus (Msi)	Elongation (%)
Conventional	-	38–44	0.5–1.4	13–20
Summary Results	6/18–8/23/10	16–50	0.4–1.1	4–20
Example 1	7/12/10	35.2	1.1	11.6
Example 2	8/17/10	50.3	0.8	17

Table 2. Carbonized mechanical properties.

	Processing Date	Tensile Strength (ksi)	Modulus (Msi)	Elongation (%)
Program Metrics	-	250	25	1
Conventional	-	380–425	25–30	1.3–1.6
Summary Results	6/18–8/17/10	120–186	19–28	0.42–0.77
Example 1	6/18/10	174.1	27.8	0.61
Example 2	8/17/10	186.0	23.2	0.75

Chemical Analysis

Another focus area for the FY 2010 period was expanding and better defining the stoichiometry of the advanced oxidative process. Special attention was initially given to the negative effect certain chemical species had on the quality of the fiber (creation of pits and other damage). After an intensive evaluation, it was concluded that this issue was not the main culprit, but in fact new beneficial species were identified in the oxidation process. The details of this work cannot be reported here, but two new sets of useful chemical mixtures were discovered that resulted in significant increases in such properties. One

set produced a greater than 50% improvement in tensile strength and a doubling of elongation over average test results for oxidized fiber. Another set produced a nearly 50% improvement in tensile strength, a greater than 10% increase in modulus, and a greater than 20% increase in elongation over conventional test results for carbonized fiber. Further work is being planned that will determine the optimal balance of these new sets.

Unit Energy and Residence Time Analysis

An essential requirement of this task is the one-third to one-half reduction in residence time and significant reduction of unit energy demand to lower the cost of carbon fibers. Sufficient data are not currently available to directly compare the unit energy demand of the advanced oxidation process to a similarly scaled conventional oxidation process. In addition, the unit energy demand of the laboratory-scale MTR1 is far less energy efficient than a full-scale industrial oxidation oven, which usually incorporates additional energy-saving features. The MTR1 was not designed with thermal efficiency in mind but as a laboratory unit for for feasibility studies, data acquisition, and parametric investigations. Nearly half of the reactor is uninsulated for diagnostic purposes. Nevertheless, a calculation was made in the MTR1 where the unit energy demand on average was 2.9 MJ/g (based on six tows of 3 K filaments each for 60 min residence time). If six 50 K tows were processed at a 30 min residence time, the estimated unit energy demand would be about 90–100 kJ/g. As a reference, a quick estimation of energy consumption from the Kline (Friedman, 2007) report showed a range of 25–50 kJ/g of oxidized material. The residence times have varied, depending on process parameters, final desired fiber properties, and type of precursor.

Material Compatibility Analysis

A milestone for initial results from materials compatibility was achieved in December 2009. The purpose of this test was to investigate the effect of the advanced oxidation process on typical furnace materials used in industry. The initial set of tests was conducted inside the MTR1 and was carried out over a period of 2 weeks. For this set of tests, the samples were hung inside as a vertical sample train. The results revealed interesting corrosion effects on certain materials, while others were left undamaged. Based on these findings, a permanent Materials Compatibility Test Stand (MCTS, Figure 3) was designed and constructed to conduct long-term materials compatibility testing with the advanced oxidation process currently being used. This system includes an automated data acquisition system; a sealed, inert test chamber inside a remotely controlled convection oven; and independent plasma generation for independent chemistry control. The test chamber was designed to withstand a higher temperature range than that required in the advanced oxidation process. This flexible, independent system will generate many hundreds of hours of data over the course of the oxidation research. The corroded samples will be subjected to a basic corrosion evaluation periodically.



Figure 3. MCTS used for corrosion tests.

Textile Polyacrylonitrile Oxidation

In March 2010, a milestone on reporting the bulk properties of textile PAN oxidized using the advanced oxidation process was achieved. A comparison of aerospace- and textile-grade PAN is shown in Figure 4. A 2-month investigative study into adapting the advanced oxidation process to textile PAN from aerospace PAN found that despite the lesser chemical and physical properties of textile PAN, the process could be adapted to achieve similar density results to those of aerospace PAN. The textile PAN used was found to be more unstable than the aerospace PAN but could consistently be processed once the optimal parameters were identified.



Figure 4. Comparison of aerospace and textile PAN precursors subjected to the advanced oxidation process.

Additional Accomplishments

Additional accomplishments included designing and construction an additional winder system, the Advanced Concepts Test Stand (ACTS), and retrofitting the Single Tow Reactor 2 (STR2) for concurrent testing with the MTR1. During the course of experimentation, it was decided that an additional winder system with improved capabilities over the existing system was needed for additional experiment flexibility. This system was built from 100% off-the-shelf components and has higher torque capacity, larger speed range, and was LabVIEW compatible. The ACTS was built to allow for rapid prototyping of new ideas and concepts for furthering the advanced oxidation work. It provides an environment for testing bench-scale quick assemblies and establishing proper operation ranges. Finally, the STR2, which originally was used for bench-scale conventional oxidation work, was retrofitted for simultaneous testing with the MTR1. This was done based on experimental results, suggesting the degree of temperature control in the MTR1 may not have been sufficient. The STR2 used a different thermal control configuration, so it was tied into the MTR1 plasma generation system so that identical chemistry could be used, and any differences could be attributable to the different thermal control schemes. This series of tests produced very useful data that contributed to the optimization of the MTR1 testing results. Finally, additional work was performed to improve the control software using LabVIEW, and various hardware improvements were made. Additional enhancements were made in controlling the input chemistry, resulting in better control, a wider range of chemistry, and easier determination of chemistry mix. A new plasma power supply was designed and built, yielding a wider operating range and more stable operation over time. Additional safety routines and hardware were added to address various worst-case scenarios and improve response times to thermal events.

Conclusions

In this fiscal year, several important objectives were met that produced valuable knowledge on the scaled-up advanced oxidation process. The relationship between fiber density and quality and process parameters in the MTR1 was better defined. A wider range of chemical parameters was explored and understood. Textile PAN was processed for the first time in the MTR1. The MCTS that will provide essential information on reactor material compatibility with the advanced oxidation process became operational. Energy demand and residence time factors were evaluated and summarized. Work in this fiscal year has brought the technology closer to demonstrating that it is adequately robust for further development and eventual future commercialization.

At the conclusion of this project, the researchers will be positioned to procure, install, test, and operate a pilot-scale plasma oxidation module in an advanced technology pilot line. The follow-on of this project will be the design and construction of the advanced technology pilot line that will then be installed in the Carbon Fiber Technology Center. It will be used to validate system performance and scalability and to produce the required quantities of advanced technology carbon fibers to support the Lightweighting Materials program's advanced development activities.

Conventional Interfacial Optimization of Reinforcement Fibers for Polymeric Systems

Principal Investigator: Soydan Ozcan, ORNL
(865) 241-2158; e-mail: ozcans@ornl.gov

Principal Investigator: Felix Paulauskas, ORNL
(865) 576-3785; e-mail: paulauskasfl@ornl.gov

Other Participants:

Frederic Vautard, Chris Janke, Amit K. Naskar, Harry M. Meyer, ORNL
Truman Bonds, Sentech Inc.
Will McCarvill, Commercial Chemistries Inc.
Ronald Allred, Adherent Technology Inc.
Andy Brink, Michelman Inc.

Introduction

Carbon fiber composites are attractive materials for automotive structures because of the opportunity they present to realize substantial weight savings and fuel economy. Low cost carbon fibers are currently being developed at ORNL for automotive applications. These fibers are likely to be combined with low cost, high-volume resins such as vinyl esters, polyesters, or nylons as the matrix materials for automotive applications.

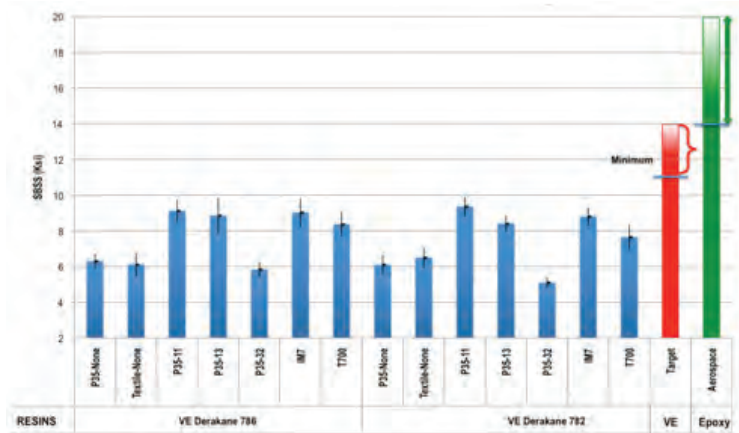
The quality of the fiber-matrix interface is often a critical factor in determining composite mechanical properties and durability. It has been observed that the interface in commercially available carbon–vinyl ester composites is poor (Xie, 1993; Hamerton, 1997; Juska, 1993). It is likely that the interface will be of equally low quality in the carbon fibers under development. Conventional carbon fibers are too expensive to be used in large-volume applications, yet their superior properties would enable lightweighting in current glass-fiber based industrial composite applications. Because of the cost barrier, carbon fiber producers have not developed their products for large-volume processes such as sheet molding compounding and injection molding. The goal of this research is to remove the barrier to using LCCFs with automotive resins due to the lack of fiber matrix compatibility.

Approach

A novel gaseous surface treatment and alternative sizings are being developed at ORNL to use in carbon fiber production targeted at large-volume, low cost vinyl ester and nylon resin systems common to automotive applications. Present common practice is to surface treat carbon fibers in an electrooxidative bath. After surface treatment, the fibers are sized with a waterborne polymer (usually epoxy) by immersion in a sizing bath. Electrooxidative treatments form a wide range of acidic and basic oxygen-containing moieties on carbon surfaces including ethers, hydroxyls, lactones, ketones, carboxylic acids, and carbonates at crystallite edges and defects (Fitzer, 1987; Ishitani, 1981). The electrooxidative process cannot be controlled to emphasize only a particular surface species. For this reason, it cannot be tailored for forming acid/base or chemical bonds with vinyl esters. Research at ORNL is targeting the control of surface functional groups and the creation of highly energetic surfaces that not only change the type of surface treatment used but also present different requirements for sizing techniques that diverge from the traditional approach. Carbon fiber surfaces can be functionalized with narrow distributions of moieties centered on desired groups by properly choosing source gases and application parameters. The flexibility of the surface treatment method that is being developed at ORNL permits the use of a variety of sizing chemistries and components. It also will allow an array of surface functionality designs to be used with various reactive coupling agents, film-forming polymers, radical inhibitors, and surfactants. Traditional surface treatment and sizing materials will not provide sufficient bonding between fibers and the new-generation matrix polymers.

Results and Discussion

Short beam shear test (SBSS) results of commercially available products are shown in Figure 1. Baseline data have been generated from composites made from commercial-grade carbon fibers (either surface treated and sized by the manufacturer or not surface treated but with sizing applied). Carbon fibers exhibited about 6 ksi SBSS without any surface treatment and sizing. Samples surface treated and sized by different manufacturers showed SBSS in the range of 7.5 to 9.5 ksi. Results indicated that carbon fiber and vinyl



Key: P35: Zoltek Panex 35 ; Textile: tTextile based carbon fiber (not commercially available, developed by FISIFE and ORNL); IM7: Hexcel brand carbon fiber; T700: Toray brand carbon fiber; None: no surface treatment and sizing; -11 and -13: Zoltek epoxy based sizings; -32: Zoltek polyester based sizing; VE: Vinyl ester resin

Figure 1. Short beam shear test results of commercially available carbon fibers bonded with vinyl ester resin. Baseline data generated from composites prepared from carbon fibers from different manufacturers with their standard surface treatment and sizing (blue bars). ORNL's research target is indicated by the second-to-last bar. The last bar shows the typical range with aerospace epoxy resins and high-performance fibers.

ester adhesion was significantly lower when traditional surface treatment and sizing were used compared to aerospace-grade carbon fiber/epoxy composite products (Harvey, 1987; Keming, 2010), which usually range between 14 and 20 ksi.

ORNL's surface treatment system is capable of efficiently treating tows up to 50 K. The current surface treatment method is the processing of a continuous single tow at a residence time of around 75 s. This method is compared with commercially treated and untreated samples in Figure 2. Up to 22% atomic oxygen content has been achieved at laboratory scale by continuous treatment with an ability to focus around the combination of desired functional groups. Raman spectroscopy

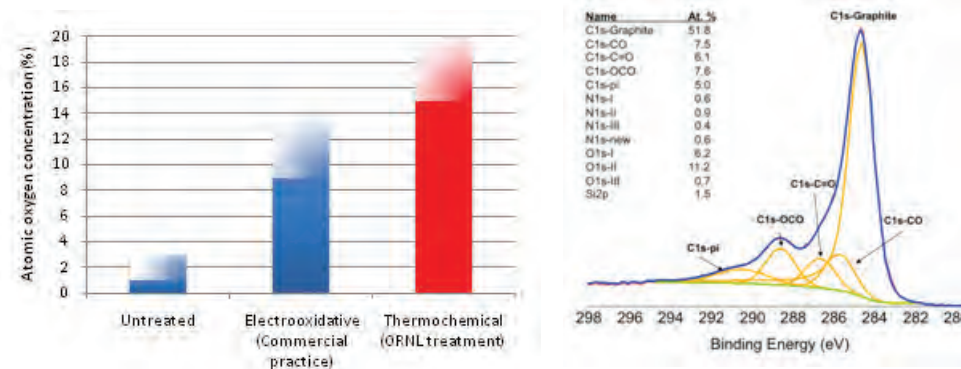


Figure 2. (a) Comparison of surface atomic oxygen concentration of untreated fibers (measured), commercial electrooxidative surface-treated fiber (compiled from literature), and thermochemical treatment at ORNL (measured); (b) typical functional groups after oxygen treatment by ORNL system. [Results were obtained by x-ray photoelectron spectroscopy (XPS).]

results (not shown) indicated that the weak layers and debris left from the carbonization furnace had been partially removed from the surface using this method.

Short beam shear results of vinyl ester composites before and after ORNL surface treatment are shown in Figure 3(a). Although the surface treatment development is ongoing, preliminary results show that surface treatment by itself improved the interface adhesion significantly. The SEM image in Figure 3(b) shows the composite fracture surface made from non-

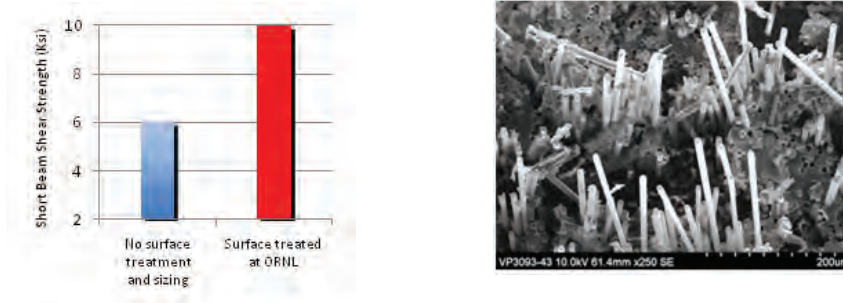


Figure 3. (a) Short beam shear test results of composites prepared from Zoltek Panex 35 fiber with vinyl ester resin (AOC 3045) before and after surface treatment at ORNL; (b) SEM image of fractured surfaces of non-surface-treated and unsized fibers with vinyl ester composites.

surface-treated and unsized fibers. The exposed fibers show no visible resin stick or, significantly, fiber pullout, indicating failure is mainly in the interface.

Conclusions

A new thermochemical method of surface treating carbon fibers was developed and tested. In just a short time, the concept has been proven and significant progress has been made in increasing the oxygen content on the surface of carbon fibers (from 6% to more than 22%), which improves the adhesion of carbon fibers to low cost vinyl resins used in industry.

Mechanical testing of the SBSS of composites manufactured from ORNL surface-treated carbon fibers confirmed the significant improvement. Although thermochemical surface treatment is still in development, it is sufficiently advanced that sizing research can be started. Several sizing chemistries are being evaluated. These chemistries will be tested with the present thermochemical surface treatment. It is anticipated that a final surface treatment and sizing process will be developed that will dramatically increase the SBSS of composites made with LCCF and low cost resin systems and meet a key need in ORNL's Low Cost Carbon Fiber program—the use of low cost resin systems in carbon fiber composite structures.

Conclusions

This project comprises five separate tasks that are aimed at developing technologies to lower the cost of carbon fibers, making them more attractive to the automotive industry. The fibers must have a minimum strength of 250 ksi and a minimum modulus of 25 Msi and be compatible with automotive-grade resin systems. Three alternative precursors are being developed, two alternative production methods are under development (one by a sister DOE program), and one surface compatibility project is being developed.

In the development of a lignin based precursor, lignin sources have been identified which meet the purity levels required for making carbon fiber. Work toward identifying and producing precursor fiber with appropriate plasticizers is continuing. The mechanical properties achieved to date do not meet the required program minimums. Spinning of lignin precursors as a mat product has been demonstrated.

The second precursor development project involves the modification of textile-grade PAN to render it as a suitable carbon fiber precursor. This task is nearing completion and has been a success. Strength values (450 ksi) exceed program requirements (250 ksi), and modulus values (35 Msi) are above program requirements (25 Msi). The chemical pretreatment equipment has been installed in the production facility, and final verification of production-quality material is in progress.

During FY 2010, significant progress was made toward the production of LCCFs from polyolefin precursors. The effects of draw ratio and degree of functionalization on fiber crystallinity and tensile properties are understood. PE fibers were made infusible through continuous processing in less than 1 hr, and processing parameters were optimized to form carbonized filaments exhibiting tensile strength of 160 ksi, modulus of 15 Msi, and 1.1% elongation. However, issues of interfilament bonding during thermal treatment and incomplete sulfonation of the fiber core were identified as major obstacles to be addressed in FY 2011 to achieve the targeted carbon fiber properties. The team met the milestones of FY 2010. Polyolefin precursors are the lowest cost potential precursors due to their low raw material cost, low production cost (melt spinning), and inherently high carbon content which gives greater production yield.

The precursor evaluation system and pilot line continue to function as essential tools for the development and validation of new precursor technologies, having been used for the initial evaluation and/or development of polyolefin, textile PAN, and proprietary precursors. Significant new capabilities have been acquired for the precursor evaluation system. Important upgrades to the pilot line are scheduled for implementation during the next year.

In the development of a more rapid oxidative stabilization process, several important objectives were met that produced valuable knowledge on the scaled-up advanced oxidation process. We are now completing the work necessary to design a pilot-scale unit under that task. At the conclusion of this project, the researchers will be positioned to procure, install, test, and operate a pilot-scale plasma oxidation module in an advanced technology pilot line.

A new thermochemical method of surface treating carbon fibers was developed and tested during this fiscal year. In just a short time, the concept has been proven and significant progress has been made in increasing the oxygen content on the surface of carbon fibers (from 6% to over 22%), which improves the adhesion of carbon fiber to low cost vinyl resins used in industry. Mechanical testing of the SBSS of composites manufactured from ORNL surface-treated carbon fiber confirmed the significant improvement. Nylon resin systems will be considered in future work.

Presentations/Publications/Patents

- Baker, D.A.; Gallego, N.C.; Gallego; Baker, F.S. On the characterization and spinning of an organic-purified lignin towards the manufacture of low-cost carbon fiber, *J. Appl. Polymer Sci.*; Accepted for publication, 2010.
- Baker, F.S. Activated Carbon Fibers and Engineered Forms from Renewable Resources, U.S. Patent 7,727,932, June 1, 2010.
- Baker, F.S. American Carbon Society Graffin Lecture, University of Washington, Washington, November 2009.
- Baker, F. S.; Eberle, C. C.; Mielenz, J. R.; Naskar, A. K.; Norris, R. E.; Pickel, J. M. Genetically-Modified Lignin-Derived Bio-Thermoplastics for Polymer Matrix Composites, selected for U.S. Patent application, May 24, 2010.
- Baker, F. S.; Gallego, N. C.; Baker, D. A. Utilization of Sustainable Resource Materials for Production of Carbon Fiber Materials for Structural and Energy Efficiency Applications. Presented at SAMPE 2010, May 17–20, 2010, Seattle, Washington; CARBON 2010, July 11–16, 2010, Clemson University, South Carolina; Ontario BioAuto Council Annual Conference, September 23, 2010, Windsor, Ontario, Canada.
- Baker, F. S. Lecturer at the Carbon Fiber 2009 Conference ORNL Short Course on Carbon Fiber for Tomorrow: A Review of Current Technologies and the Path to Wide Spread Industrial Growth. Two presentations entitled Production of Carbon Fiber from Pitch Precursors: Spinning and Conversion and Low Cost Production of Carbon Fiber from Ligni. Carbon Fiber 2009, December 8–11, 2009, San Diego, CA.
- Baker, F. S.; Menchhofer, P. A.; Baker, D. A. Carbon Nanotube (CNT)-Enhanced Precursor for Carbon Fiber Production and Method for Making a CNT-Enhanced Continuous Lignin Fiber, U.S. Patent Application, filed May 19, 2010.
- Baker, F. S. Production of Composite Cellulose/Carbon Fiber Filters for HVAC Systems. Invention Disclosure selected for U.S. Patent Application, September 23, 2010.
- Bhat, V. V.; Contescu, C. I.; Gallego, N. C.; Baker, F. S. Atypical Hydrogen Uptake on Chemically Activated, Ultramicroporous Carbon, *CARBON*, 48, pp 1331–1340, 2010.
- Brown, R. H.; Pickel, J. M.; Naskar, A. K. Stress relaxation behavior and mechanical properties of functionalized polyolefins. PMSE Preprints, 2010, ACS National Meeting, Boston, Massachusetts, August 22–26, 2010.
- Lara-Curzio, E.; Kiggans, J.; Dudney, N. J.; Contescu, C. I.; Baker, F. S.; Armstrong, B. L. Lightweight, Durable Lead-Acid Batteries, U.S. Patent Application 2009/0260666, published October 29, 2009.
- Naskar et al. Precursor Compositions and Stabilization Methods for Polyolefin-Based Carbon Fiber Manufacturing, invention disclosure, September 2010, UT-Battelle ID# 2462.
- Ozcan, S.; Janke, C.; Paulauskas, F. L.; Naskar, A. K.; McCarvill, W. Method of Improving Adhesion of Vinyl Esters and Polyesters to Carbon Fibers, Invention Disclosure DOE S-NUMBER:S-124,028, 2010.
- Ozcan, S.; Paulauskas, F. Surface Compatibility of Carbon Fibers. In Composite World Conference, Carbon Fiber Outlook, San Diego, California, 2009.
- Paulauskas et al. Apparatus and Method for Oxidation and Stabilization of Polymeric Materials. U.S. Patent 7,534,854 B1, filed January 31, 2006, and issued May 19, 2009.
- Paulauskas et al. Apparatus and Method for Oxidation and Stabilization of Polymeric Materials. U.S. Patent 7,786,253 B2, filed May 14, 2009, and issued August 31, 2010.
- Paulauskas et al. Apparatus and Method for Stabilization or Oxidation of Polymeric Materials. U.S. Patent 7,649,078 B1, filed March 28, 2006, and issued January 19, 2010.
- Paulauskas, F. L. Advanced Oxidative Stabilization. Presented at the Carbon Fiber 2009 Conference; December 9–11, 2009. San Diego, California.
- Paulauskas, F. L. Microwave Assisted Plasma Carbonization. Presented at the Carbon Fiber 2009 Conference; December 9–11, 2009. San Diego, California.

References

- Fitzer, E.; Weiss R. Effect of surface treatment and sizing of C-fibres on the mechanical properties of CFR thermosetting and thermoplastic polymers, *Carbon*, 1987, 25, pp 455–467.
- Friedman, B. Cost Assessment of Pan-Based Precursor And Carbon Fiber, Kline & Company, Final Report, November 2007.
- Hamerton, I.; Hay, J. N.; Howlin, B. J.; Jones, J. R.; Lu, S.Y.; Webb, G. A. ToF SIMS and XPS Studies of Carbon Fiber Surface during Electrolytic Oxidation in 17O/18O Enriched Aqueous Electrolytes, *Chem. Mater.* 1997, 9, pp 1972–1977.
- Harvey, J.; Kozlowski, C.; Sherwood, P. M. A. X-ray photoelectron spectroscopic studies of carbon fibre surfaces. Part 6 Pilot plant surface treatment and epoxy resin composites, *J. Mater. Sci.* 1987, 22, pp 1585–1596.
- Ishitani, A. Application of X-ray photoelectron spectroscopy to surface analysis of carbon fiber, *Carbon*, 1981, 19, pp 269–275.
- Juska T., Carderock Div-SME-92-38, R&D Report, January 1993.
- Kaneko, M.; Kumagai, S.; Nakamura T.; Sato, H. Study of sulfonation mechanism of low-density polyethylene films with fuming sulfuric acid. *J Appl Polym Sci* 2004, 91, pp 2435–2442.
- Keming, M.; Ping, C.; Baichen, W.; Guiling, C.; Xinmeng, X. A Study of the Effect of Oxygen Plasma Treatment on the Interfacial Properties of Carbon Fiber/Epoxy Composites, *J. Appl. Polym. Sci.* 2010, 118, pp 1606–1614.
- Xie, Y.; Sherwood, P. M. A. AS4 Pan-based Carbon Fiber by Core Level and Valence Band XPS, *Surf. Sci. Spec.*, 1993, 1, pp 306–311.

D. Carbon Fiber Technology Center

Field Technical Monitor: C. David Warren
Oak Ridge National Laboratory
1 Bethel Valley Road; Oak Ridge, TN 37831
(865) 574-9693; e-mail: warrencd@ornl.gov

Technology Area Development Manager: Dr. Carol Schutte
U.S. Department of Energy
1000 Independence Ave., S.W.; Washington, DC 20585
(202) 287-5371; e-mail:carol.schutte@ee.doe.gov

Contractor: Oak Ridge National Laboratory (ORNL)
Contract No.: DE-AC05-00OR22725

Objectives

- Demonstrate scalability of low cost carbon fiber (LCCF) technologies.
- Produce LCCF quantities needed for large-scale material and process evaluations.
- Foster industrial collaborations for LCCF technology development and transition.
- Partner with educational institutions and use these physical resources for workforce training.

Accomplishments

- Secured the award and established the project scope and plan.
- Established building requirements and evaluated existing buildings.
- Selected potential building sites; prepared a technical specification; executed solicitation; and evaluated proposals for the design, construction, and lease of an off-site building to house the facility.
- Established requirements; prepared a technical specification; executed a solicitation; and evaluated proposals for the design, manufacture, and installation of a carbon fiber semi-production line (CFSL).
- Established requirements; prepared a technical specification; executed a solicitation; and commenced evaluation of proposals for the design, manufacture, and installation of a melt spun precursor fiber semi production line (PFSL).

Future Directions

- Complete procurement, construction, manufacturing, installation, and commissioning of building and equipment.
- Commence operations by January 2013.

Carbon Fiber Technology Center

Principal Investigator: Craig Blue, ORNL
(865) 574-4351; e-mail: blueca@ornl.gov

Deputy Principal Investigator: Cliff Eberle, ORNL
(865) 576-0302; e-mail: ecc@ornl.gov

Introduction

The Carbon Fiber Technology Center (CFTC) was proposed by ORNL in FY 2009 in response to the DOE Office of Energy Efficiency and Renewable Energy's Lab Call for Facilities and Equipment, Lab Call 09 002 (American Recovery and Reinvestment Act funds). According to the Mission Need Statement that authorized this project,

low-cost carbon fiber will likely have different mechanical properties than the carbon fiber grades currently produced for the aerospace industry. End-use industries are unlikely to commit to using lower cost carbon fiber without significant efforts to validate that low-cost carbon fiber meets their needs while fiber manufacturers are unlikely to commit to investing in large scale manufacturing technologies without purchasing commitments. . . . In order to address these issues, it is necessary to acquire a flexible capability for advanced research, development, and demonstration of carbon fiber to achieve EERE's long-term program goals. This capability combines the ability to handle various feedstock materials, the integration of advanced energy efficient conversion technologies, and the ability to produce sufficient quantities of finished fiber to supply end-users for validation trials. . . . The successful completion of this activity will remove the obstacles for accelerated adoption of this light-weight, enhanced performance material in multiple high volume industries.

The primary tasks to be undertaken in this effort are as follows.

- Lease a suitable general purpose building at a former government site that is being reindustrialized.
- Deploy a highly flexible CFSL designed to handle all LCCF precursor chemistries and material formats with capacity to carbonize 25 tons per year of polyacrylonitrile (PAN) fibers in 24k tow format.
- Deploy a melt-spun PFSL for producing melt-spun low cost precursor fibers in both tow and bulk material formats with production capacity matched to the carbon fiber line throughput.
- Make space and utility provisions for the future deployment of semi-production scale advanced conversion technologies.

Approach

To satisfy this mission need, ORNL will design, construct, and operate the CFTC to be a highly flexible, highly instrumented LCCF technology facility for demonstrating and evaluating new low cost manufacturing processes and technologies at pilot scale. The CFTC will promote successful commercialization of LCCF technologies. A new building will be designed and constructed to house a thermal (conventional) conversion line and a melt-spinning precursor fiber production line. It will provide the capabilities to

- demonstrate the scalability of LCCF;
- produce and make available up to 25 tons per year of conventionally converted fibers, made from low cost precursors, for large-scale material and process evaluations;
- accommodate the future deployment of advanced conversion technologies;
- produce precursor fibers made from a variety of precursor materials (e.g., lignin and polyolefin) on a melt-spinning line in sufficient quantity to feed the conversion lines;
- foster industrial collaborations for LCCF technology development and transition; and

- host workforce training for LCCF implementation.

Previous and ongoing LCCF developments must be demonstrated in the CFTC to achieve successful transfer of these technologies to industry, as illustrated in Figure 1. The CFTC will serve as a bridge from research to commercialization.

The CFTC is designed to be readily accessible to domestic industry and universities. It will be located on a reindustrialization

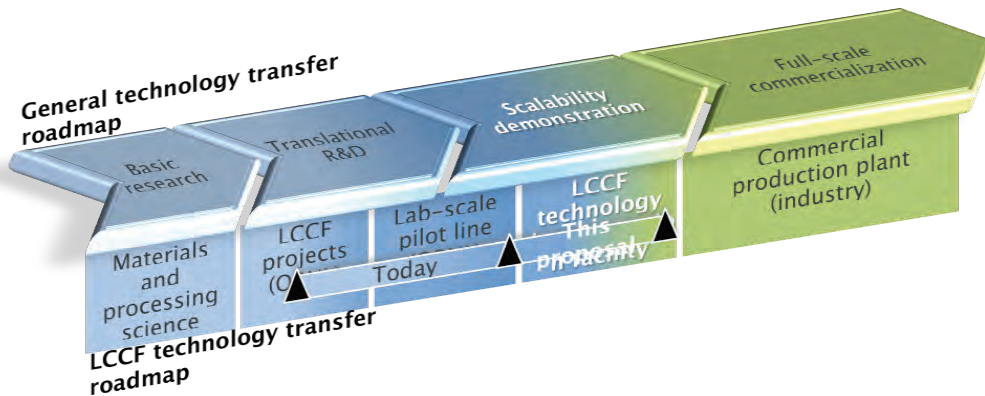


Figure 1. Roadmap for technology transfer and commercialization.

site that has available space where industry partners can locate leveraging facilities.

The CFTC technical scope includes the specification, procurement, and commissioning of (1) a CFSL, (2) a melt-spun PFSL, and (3) a building to house these lines plus an advanced technology CFSL that will be deployed in the future. The facility should be able to produce various carbon fiber grades including standard modulus commercial grades, intermediate modulus aerospace grades, and fiber grades that are in development at both ends of the cost and performance spectrum.

The CFSL will be a highly instrumented conventional conversion line capable of processing several kinds of precursor fibers including those based on PAN, pitches, lignin, polyethylene, and rayon in tow, non-woven mat, or discontinuous loose fiber form. The CFSL will have an output of up to 25 tons per year of standard modulus carbon fibers made from PAN precursor. This is sufficient capacity to provide the estimated material needs for large-scale material and process evaluations for several applications including automotive [1–2 total tons for each separate, original equipment manufacturer (OEM)], wind energy (5–10 total tons for each OEM), and oil and gas (1–5 total tons for each new application). The PFSL will be capable of melt spinning filaments from lignin, polyolefins, and pitches, with capacity matched to that of the CFSL. The CFSL and PFSL will both be designed to produce materials in tow and bulk material formats. While both the CFSL AND PFSL are based on conventional technology, each has flexibility (and therefore complexity) that considerably exceeds the current state of the art. When the advanced conversion processes that are presently in development become sufficiently mature, they will also be scaled and deployed in CFTC as an advanced technology conversion semi-production line with a scale similar to that of the CFSL. A rendering of the equipment in the facility is shown in Figure 2. The primary deliverable of this project is an operational facility capable of manufacturing up to 25 tons per year of carbon fibers made from PAN, lignin, or polyolefin precursor materials.

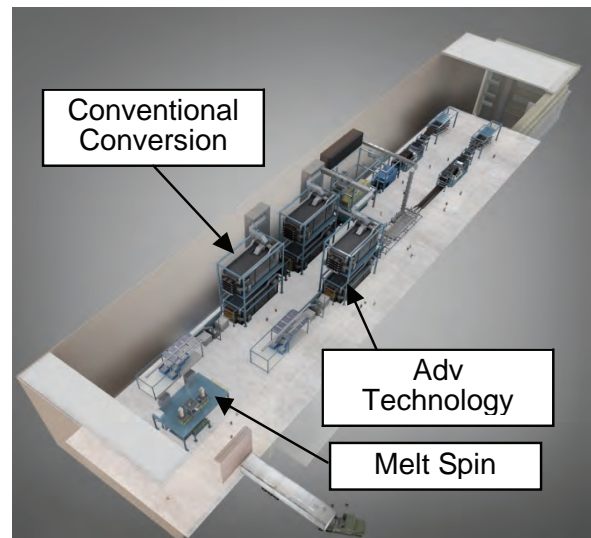


Figure 2. Facility and equipment perspective of the Carbon Fiber Technology Center.

Results and Discussion

The project award was announced on 18 November 2009. The proposed budget was \$40 million, and the award was budgeted at \$34.7 million. The early months were spent evaluating existing buildings and potential sites for new buildings, conducting value engineering, and finalizing the project's scope and key design parameters to harmonize the technical basis, budget, and mission need. In December, it was decided to site the equipment in a leased building that would be constructed on a Community Reuse Organization (CRO) site. The facility production capacity was set at 25 tons per year, and a building was to be constructed on the ORNL campus that would consolidate the composites research equipment (now housed in multiple, scattered buildings) into a single building. However, equipment bids and rigorous building cost estimates came in well over budget, so the on-site building was cancelled to ensure that there would be adequate funding for the higher priority semi-production equipment to fully satisfy the mission need.

The leased building will have about 40,000 gross square feet, including support spaces, and a high bay with net usable area 400 feet long by 72 feet wide. The process equipment will be housed in the high bay. The building will be designed and constructed by a private development team, in accordance with ORNL's specifications, and leased to ORNL. A design criterion was developed in the spring and a solicitation issued in early June, closing in late July. The bidders could choose to propose a building on one of three CRO sites. Multiple proposals were received, and the winning bidder has been selected. Contract negotiations are currently ongoing, so at the time of this writing the procurement information, including the bidder's identity and selected site, could not be released. An announcement will be made in the first quarter of FY 2011.

A technical specification was prepared for the CFSL, and the solicitation was issued in early June, closing on 6 July. Multiple bids were received and evaluated, and the winning bidder has been selected. Some initial bid clarifications and value engineering have been completed. Negotiations are scheduled for early October 2011. No further information can be released at this time, but announcements are expected in the first quarter of FY 2011.

A technical specification was prepared for the PFSL, and the solicitation was issued in early July, closing on 20 August. Multiple bids were received, and bid evaluation is under way. Bid selection and negotiations are scheduled for October and November 2011. No further information can be released at this time, but announcements are expected in the first quarter of FY 2011.

In FY 2011, the primary activities will be advanced engineering and construction/manufacturing of the building and the semi-production lines. The equipment is scheduled to be installed and commissioned in FY 2012, with commencement of operations in January 2013 or sooner.

Conclusions

ORNL was awarded \$34.7 million in November 2009 to design, construct, and operate the CFTC. The project scope, schedule, and budget have been established. Procurements were initiated for the building and the major equipment items. Bid evaluations are complete for the building and the carbon fiber line, with negotiations ongoing or imminent. Bid evaluations are ongoing for the precursor fiber line. We expect to award all three of these contracts in the first quarter of FY 2011.

4. USAMP Cooperative Research

A. Automotive Composites Consortium

Field Technical Monitor: Jim deVries
Ford Motor Company
2101 Village Road; Dearborn, MI 48121
(313)322-3494; email: jdevries@ford.com

Field Technical Monitor: Khaled W. Shahwan
Chrysler Group LLC—Chrysler Technology Center
Experimental & Computational Mechanics Department
CIMS: 483-05-1, 800 Chrysler Drive; Auburn Hills, MI 48326-2757
(248) 576-5609; e-mail: kws8@chrysler.com

Field Technical Monitor: Hamid Kia
General Motors Holdings LLC, GM Global R&D
Mail Code 480-106-2224; 30500 Mound Road; Warren, MI 48090-9055
(586)986-1215; e-mail: hamid.g.kia@gm.com

Technology Area Development Manager: Carol Schutte
U.S. Department of Energy
1000 Independence Ave., S.W.; Washington, DC 20585
(202) 287-5371; e-mail: carol.schutte@ee.doe.gov

Field Project Officer: Joseph Renk
National Energy Technology Laboratory
626 Cochran Mill Road; P.O. Box 10940; Pittsburgh, PA 15236
(412)386-6406; e-mail: joseph.renk@netl.doe.gov

Contractor: U.S. Automotive Materials Partnership (USAMP)
Contract No.: DE-FC26-02OR22910

Objective

- Develop and demonstrate high-volume manufacturing (molding) processes to produce lightweight composite automotive components.
- Collaborate with suppliers to develop low cost, high volume molding processes that enable production of minimal weight components.
- Develop and document new test methods where required to fully understand material performance.
- Develop direct compounding of automotive thermoplastic polymers to reduce cost and increase performance benefits offered over conventional long fiber injection or compression molding.
- Develop methodologies and data for each Automotive Composites Consortium (ACC) member company (Chrysler, Ford, and General Motors) to implement lightweight, cost-effective structural composites in high volume vehicles.

- Design and fabricate structural automotive components with reduced mass and cost and with equivalent or superior performance to existing components.
- Understand the mechanical behavior of composites and develop the computational methods needed to model and predict the crash-energy management response of structural composites.

Approach

- Investigate and develop an improved carbon fiber sheet molding compound (SMC) material amenable to cost-effective high volume applications, working in conjunction with a Tier One automotive composites supplier.
- Explore the root causes of bond-line read-through (BLRT) through application of developed quantification tool to enable use of reduced thickness panels.
- Investigate direct compounding of automotive thermoplastic polymers to reduce cost and increase performance offered over conventional long fiber injection or compression molding.
- Use shape memory polymers as a means of addressing geometry issues such as die lock in composites preforming tooling.
- Use direct compounding of polyamide based composites to eliminate the cost of producing injection molding pellets and allow for higher fiber length.
- Design, analyze, fabricate, and test
 - a structural composite underbody, focusing on cycle time, structural joining of composite to steel, and using continuous oriented fibers, and
 - a second row composite seat (without an integrated restraint system) which will combine the functions of a seat and a load floor.
- Develop robust predictive modeling methodologies and validate them against experimental test data.

Accomplishments

- Developed both epoxy and vinyl ester/polyester resin based carbon fiber SMC systems that produced properties close to targets, including using low cost, large tow carbon fibers.
- Completed a final component validation experiment to demonstrate that the lessons learned in the BLRT project could be applied to an actual component.
- Implemented material models in the BLRT finite element (FE) code, resulting in predicted magnitudes for BLRT-induced distortion that correlated with experimental data.
- Demonstrated the concept of using shape memory based tooling technology as an alternative to traditional preforming techniques for improved preform dimensional control.
- Evaluated experimental long fiber thermoplastic formulations against commercially available formulations. The results of this test program were encouraging, indicating that the formulation developed for direct compounded material either met or exceeded properties of the commercial precompounded product.
- Demonstrated full part molding for the composite underbody with anticipated savings of 11.3 kg.
- Achieved full characterization of the glass fabric SMC materials.
- Optimized structure of weld bond joints, including saving mass by decreasing adhesive and doubler gage.

- Analyzed weld bond joints of composite-steel joints, showing good agreement with experiment.
- Analyzed mold and crush surrogate structure and compared experiment and model, demonstrating validity of model.
- Completed molds for all four composite parts of the seat.
- Molded, trimmed, and plasma treated composite seat parts for assembly. All metal reinforcements and brackets have been fabricated and e-coated (electrocoated).
- Made significant progress toward understanding the complex behavior of fiber-reinforced composites under various impact speeds. Experimental characterizations of materials have been developed and adopted within predictive tools. Modes of energy absorption and basic physics, including effects of size, curing, and manufacturing, have been characterized and modeled and are in the process of being verified and validated.

Future Direction

- Refine material formulation and compounding processing parameters for improved physical properties.
- Mold demonstration component from carbon fiber SMC
- Complete BLRT project in the first quarter of FY 2011.
- Work with an identified supplier for making the resin transfer molding (RTM) screen mold and work with tool suppliers for developing and manufacturing screen deformation shape memory tooling.
- Optimize the selection and dosing of additives used in the long fiber thermoplastic polyamide 66 formulations.
- Mold composite underbodies to design specifications. Assemble underbodies into structure mimicking portion of body-in-white.
- Test underbody assemblies with loads similar to the 40 mph offset deformable barrier. Compare test data to analytical predictions, and redesign as needed to provide original targets.
- Assemble seats for testing and verify design through testing and correlation to analytical prediction.
- Repeat the composite seat cost modeling exercise with the final design and materials.
- Document projects in technical reports.
- Complete the development of computational tools and modeling methodologies.
- Use vehicle components/subassemblies to verify and validate the developed computational tools.

Introduction

ACC is a compilation of three focal projects, each delivering cost-effective, high performance composite solutions for high volume automotive applications. These projects focus on developing the reinforced polymer materials (thermoplastics and thermosets) and manufacturing methods to produce component level systems that meet crash and durability requirements.

Focal Project 4: Structural Automotive Components from Composite Materials

Principal Investigator: Libby Berger, General Motors
(248) 930-5018; e-mail: libby.berger@gm.com

Principal Investigator: John Jaranson, Ford Motor Company
(313) 390-5842; e-mail: jjaranso@ford.com

Introduction

ACC Focal Project 4 is divided into two parts: a structural composite underbody and a lightweight composite seat. For both, our primary objective is to develop analytical and manufacturing methodologies and data for each ACC member company to be able to implement lightweight, cost-effective structural composites in high-volume vehicles.

The underbody project was divided into the following three phases.

- Phase 1—Preliminary design and material and process system selection
- Phase 2—Full design of part and tooling, including material development and scenario for component manufacture and vehicle assembly
- Phase 3—Fabrication and validation of the full underbody

As shown in [Figure 1](#), our design of the composite underbody consolidates 16 stamped steel parts into one composite part, saving 11.3 kg out of the 44.9 kg initial steel underbody mass. The increased stiffness of the composite allows an additional 3.3 kg reduction in the mass of the steel “sled runner” rails. In the 2010 fiscal year, we completed Phase 2 and have begun Phase 3. We have developed processing techniques and characterized material properties for the glass fabric SMC material selected in Phase 1, designed and analyzed the underbody structure as part of a full vehicle, tested that design and analysis technique with a model structure, further developed the weld bonded joining system, designed the final test assembly, and begun molding of the full underbody.

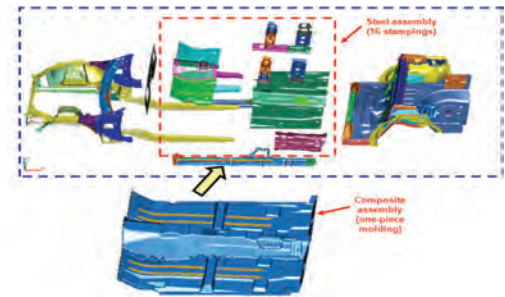


Figure 1. Preliminary design of the composite underbody, consolidating 16 steel stampings into one molded part.

Material Properties and Characterization

The glass fabric SMC material was molded as a 45/0/-45/90/-45/0/45 layup. This layup was originally selected because it gave us about a 3 mm plaque thickness, aiding in comparison to other material systems. As this required seven layers, the system would be slightly unbalanced. Our most difficult load case was determined to be the offset deformable barrier, so we selected a bias to 45°. Staying with this layup through a number of development steps has allowed us to compare material characterization from molding trial to molding trial. The results of characterization over five plaques, averaged over four specimen directions, are shown in [Table 1](#).

Table 1. Material properties for a representative layup of fabric SMC.

	Tensile	Compression	Flex
Modulus (GPa)	19.7	19.6	
Stress to failure (MPa)	247.0	264.0	357
Strain to failure (%)	1.7	1.6	
Fiber content (wt %)	63.0		
Density (g/cc)	1.92		

Thermal properties were also characterized. The coefficient of linear thermal expansion from -30 to $+30^{\circ}\text{C}$ is $13.4 \times 10^{-6}/^{\circ}\text{C}$, very similar to steel and to other structural composites. Thermal transitions as measured by dynamic mechanical analysis are Tonset of 73°C , T75 of 114°C , and Tloss of 165°C .

Design Correlation with Model Structure

Because computer aided engineering based design methods were used throughout this project, a means of testing these methods against our material and processes was needed. The double dome shape previously used for fabric drape analysis correlation was molded and used for crush testing to determine the correlation between our modeling and experimental results. The structure was crushed between two rigid plates for a total 50 mm deformation. Figure 2 shows the correlation between test data and analysis, with and without accounting for fabric shear from the deformation. Other analysis trials took into account other manufacturing effects such as the varying thicknesses and yarn spreading effects, determining that a more complete the evaluation of manufacturing effects for a given process and geometry enhances the accuracy of the model. The analysis included results with and without fabric shear. The results with the fabric shear, which mimics the actual part, match the initial peak of the experimental data very closely. Because our modeling uses an element-deletion method, post-peak modeled forces are expected to be lower than experimental, as seen in Figure 2.

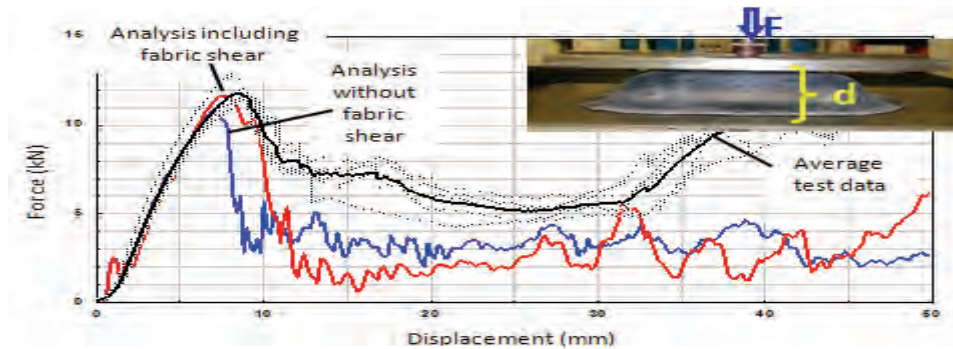


Figure 2. A comparison of experimental crush and analytical crush of a double dome structure with a 45/-45/-45/45 layup.

Joining of Composite Structure to Steel Vehicle Structure

We have selected weld bonding for joining the composite underbody to the steel of the rest vehicle. A patent for the composite-to-steel weld bond configuration was granted this year, as noted at the end of this report. Physical tests were conducted at different temperatures (-40°C , ambient, and 80°C) using 120 mm wide super lap shear coupons with various joint configurations. The test details and the results of the initial work were reported in the 2009 annual report. The data generated were used for FE analysis model development and test-analysis correlation. In Phase 2 of this study, specimens made with various combinations of steel substrates (1.5 mm DP590 and 1.2 mm HSLA 350) and doubler (0.7 mm and 1.2 mm HSLA 350) were tested under quasistatic tension loading at different temperatures. In addition, specimens made with only one layer of adhesive between the composite and the steel substrate (i.e., no layer of adhesive between the composite and doubler) were tested. For example, Figure 3 shows the average peak loads for weld bonded specimens as a function of temperature, comparing weld only, adhesive only, and adhesive on either one or both sides of the weld bond. It was concluded that further mass/cost savings could be achieved without compromising the joint strength by using thinner doublers and eliminating a layer of adhesive. These data show that bonding only one side of the weld bond joint does not significantly decrease the peak load.

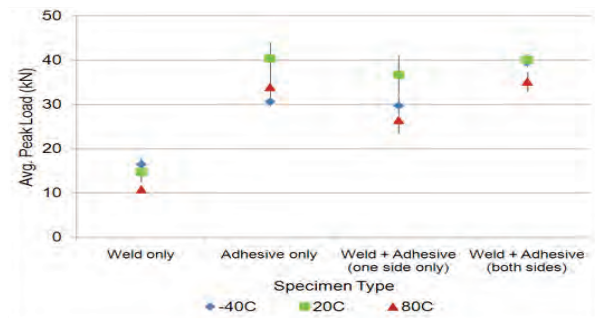


Figure 3. Comparison of weld bond strengths with adhesive on one side or on both sides, with weld only and adhesive only joints.

Molding of Composite Underbody: Summary for Fiscal Year 2010 and Future Plans

A matched metal compression tool was built to mold full underbody parts. The tool has shear edges and a 75 mm land around the part to allow for a small fabric positioning and flow region. Full parts have been molded, as shown in **Figure 4**, although these parts were not to complete design specification, pending preform design iterations. The full characterization of the fabric SMC material, including material and thermal properties, as well as fatigue, has been completed. The weld-bonded joints were optimized to save mass and cost, and the experimental results show good agreement with analysis. A surrogate structure was molded and crushed to demonstrate the validity of the structural modeling.

Our future direction is to mold parts to design specification, then to assemble them into a structure similar to the steel attachment points in the vehicle structure (**Figure 5**). This will then be tested in a manner that will mimic the offset deformable barrier test. This testing will be compared to our analytical model, and the model will be revised as necessary.

Lightweight, Low Cost Composite Seat

Four composite molding tools were completed in FY 2010. Composite parts for the seat build were successfully molded with 40% glass-filled polypropylene in both 1 in. and 0.5 in. glass fibers. All of the steel reinforcements and components were fabricated and all trim and assembly fixtures were built.

Design and Build Progression

Molds for the four composite parts that make up the composite seat structure have been completed by Century Tool & Gage in Fenton, Michigan. **Figure 6** shows a photo of the seat cushion inner mold. The molds were delivered to Composite Products, Inc. (CPI) in Winona, Minnesota for molding trials and production of the composite parts. Fifty pieces of each of the four parts were molded using 40% glass-filled polypropylene with 0.5 in. glass fibers, and 10 pieces of each part were molded with 40% glass-filled polypropylene with 1 in. glass fibers. **Figure 7** shows a mold in the press at CPI and a photo of some of the molded parts.



Figure 4. Molded composite

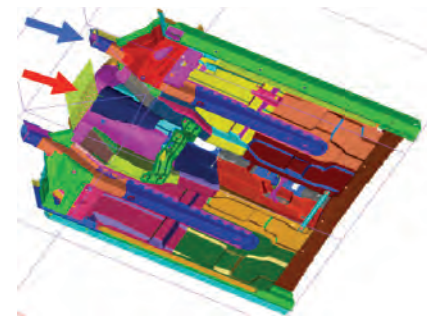


Figure 5. Design of final test assembly. Loads will be applied at the two arrow points with the structure fixed at the rear.

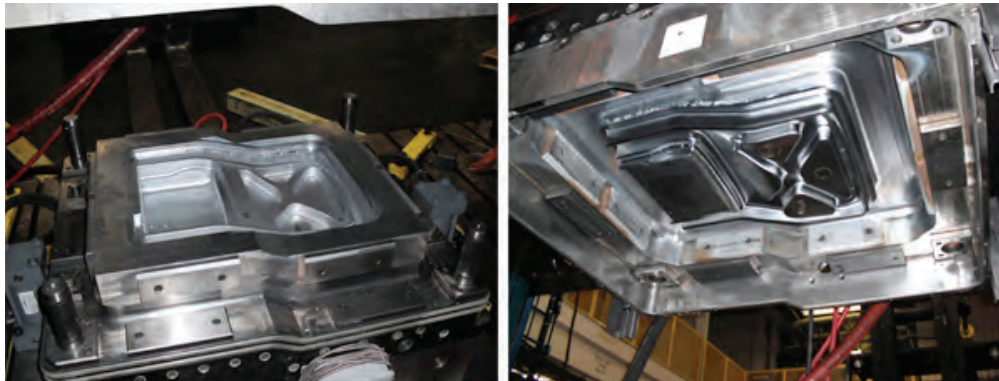


Figure 6. Seat cushion inner mold.



Figure 7. Molding press and tool and molded parts.

After molding the parts were sent for waterjet trimming and plasma treating of the bonding surfaces. Plasma treating the bonding surfaces is standard practice and recommended by the adhesive supplier to ensure an adequate bond to the polypropylene composite. Our own initial lap shear bonding study indicates nearly a 50% drop off in adhesive bond strength if plasma treating of the composite surfaces is not done. Figure 8 shows the results of this bonding study.

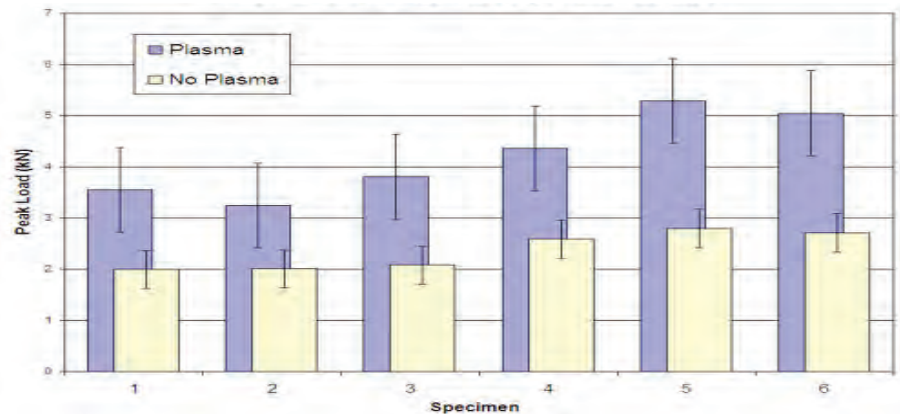


Figure 8. Adhesive lap shear bond strength with and without plasma treating.

The composite seat parts were plasma treated at Plasmatreat in Elgin, Illinois using their RD1004 plasma jet head with a 14 degree nozzle on the end of a 5 axis robot. Distance to the part (8 mm) and travel speed (65 mm/s) were controlled to achieve a minimum dyne level of 72 on the mating surfaces of the parts.

In addition to the completion of the molded composite parts, all of the steel reinforcements and brackets have been fabricated and e-coated, the assembly and drilling fixtures have been built, and the foam and trim for the complete seats have been fabricated. All that is left is assembly and testing.

Next Steps

The next steps are to complete the build of seats and verify the design through testing. Seats will be assembled at RCO Engineering in Roseville, Michigan. Quotes for testing have been received and a final decision on a testing partner will be made in early November 2010. The final step will be to document the project in a technical report including design, analysis, molding, assembly, testing, and cost modeling.

Advanced Materials and Processes of Composites for High Volume Application

Principal Investigator: Daniel Houston, Ford Motor Company
(313) 323-2879; e-mail: dhousto2@ford.com

Carbon-Fiber SMC

A major technical hurdle that the carbon fiber SMC project had to overcome in FY 2010 was to debundle current commercially available carbon fiber into a form that could be used to significantly “wet-out” the fibers with current SMC compounding equipment. The team was able to make significant progress by incorporating an air driven mechanical chopper that was installed on an SMC compounder. The chopper unit was able to deliver highly filamentized carbon fibers, which resulted in better mechanical properties, a key deliverable of this project.

Two different resin systems were successfully compounded with chopped carbon fibers, resulting in high physical properties. The first system was a high T_g epoxy resin with 6 K or 12 K tows of carbon fiber at a 30% to 45% by weight loading. These 1 in. random chopped carbon fiber SMC materials had some tensile strengths exceeding the targeted 150 MPa and a tensile modulus of 30 GPa. It should be noted that the compounding process window for achieving the better properties was narrow.

The second system was based on vinyl ester/polyester resin. It showed similar physical properties, although the modulus was lower at 25 GPa, even at a fiber loading of roughly 50% by weight. The system molded in 3 minutes at 155°C, with plaques as thin as 1.5 mm.

To improve both of these systems, efforts to debundle the carbon fiber tows were made. An air driven mechanical chopper was installed on an SMC compounder. Highly filamentized carbon fibers were obtained. Subsequent tests showed that this chopper, together with a more compatible resin-fiber system, can significantly boost the tensile strength performance. The chopper and compatible resin system provided the following tensile properties: 35 wt % 12 K rovings from Toho 120 MPa without the improved chopper vs 145 MPa for the 35 wt % 50 K rovings from Zoltek using the improved chopper system. The tensile modulus remained the same for both at 23 GPa. The use of low cost, large tow carbon fibers thus became feasible for the first time as indicated by the data obtained from 50 K tow fiber SMC.

Conclusions

Carbon fiber SMCs close to the target tensile properties and processing characteristics were successfully made with both epoxy and vinyl ester/polyester resin systems. Both systems were enhanced by developments in debundling larger carbon fiber tows, resulting in improved fiber wet-out and subsequent physical property performance.

Results and Discussion: Bond-Line Read-Through Project

Introduction

BLRT is a surface distortion that can occur in bonded assemblies. When this distortion is found in production, the outer panel is thickened to eliminate the distortion. The goal of this project was to determine other strategies for eliminating this distortion without adding weight and determine the root causes of BLRT. Two final technical gaps required for the project were to determine whether the modeling results could be reproduced during actual experimental testing at both the flat panel and actual component level. The results of this evaluation were very successful and resulted in writing design and manufacturing guidelines that will be available for DOE, original equipment manufacturers, and suppliers to use for all future adhesive bonding for SMC closure applications. This project is an outstanding example of research being implemented into the manufacturing base. The second part of the goal that was addressed during FY 2010 was to establish the root cause of BLRT, which was established to be fundamental: caused by differential shrinkage between the adhesive and the substrates.

Approach

Phase 2—Experimental Determination of BLRT Root Cause and Exacerbating Factors

The experimental work for this project was completed in FY 2010. Two experiments simulating closure panel assembly were conducted: an experiment evaluating the effect of standoff and dam design and/or hard hits on BLRT severity (Fernholz,

2010a) and an experiment evaluating whether the type of bonding fixture used to manufacture the assemblies affected the severity of the distortion (Fernholz, 2011). In two experiments laboratory-scale assemblies were built: an experiment to determine whether the time between bonding and priming and between priming and painting affects the severity of the distortion and an experiment to provide data for validating the FE model being developed in Phase 3. A final component validation experiment was completed to demonstrate that the lessons learned in this project could be applied to an actual component. In that experiment, the root cause of distortion in a current service part, the 1999–2004 Mustang deck lids, was determined to be a variation in the thickness of the inner panel that caused the thickness of the adhesive to change abruptly. The deck lid inner panel tool was modified to make the thickness of the bond flange consistent across its width. New assemblies were manufactured to demonstrate that this change eliminated the distortion.

Phase 3—Analytical Model Development

Initial FE model predictions of the severity of BLRT-induced distortions found that use of a linear elastic material model for the adhesive overpredicted the severity of BLRT-induced distortions; therefore, efforts in FY 2010 were focused on characterizing the viscoelastic properties of the adhesives of interest and implementing new material models into the FE model. Implementation of these material models in the FE code resulted in predicted magnitudes for BLRT-induced distortion that correlated with experimental data. Viscoelastic material data for the sheet molding compound used as the assembly substrate was also collected. Current FE codes, however, do not have a way to implement an orthotropic, viscoelastic material model. Fortunately, a series of analyses showed that the temperature dependency of SMC material properties is substantially more important than the time dependency of these properties; consequently, SMC properties can be adequately represented by an orthotropic, temperature dependent, linear elastic material model. An analytical analysis of the effect of the shape of the adhesive bead, along with other factors, was completed. The remaining analytical work will be completed in the first quarter of FY 2011.

Project Conclusion

BLRT is, at the most fundamental level, caused by differential shrinkage between the adhesive and the substrates. For adhesives in which the chemical shrinkage is minimal (e.g., adhesives typically used in automotive composite assemblies), the primary source of shrinkage is thermal shrinkage as the adhesive cools from the temperature at bonding to room temperature. Since adhesives must generally be cured at elevated temperature in automotive composite applications, there will be some distortion in bonded assemblies. Those distortions, however, will not necessarily be severe enough to be visible; to be visible, other factors must be present. The factors that exacerbate the severity of the naturally occurring distortions are (a) variations in the thickness of the adhesive bead across the bead width, (b) adhesive material properties, and (c) sectional stiffness of the substrate. All of these factors must be controlled in both the design and manufacture of assemblies to eliminate visible distortions in assemblies built with minimum thickness outer panels.

Shape Memory Based Tooling

The project objectives are to develop preform tooling material that can produce complex and challenging composite components quickly and cost effectively. The technology would eliminate the need for composite parts joining, reduce processing times and costs, and enable true vehicle lightweighting while maintaining structural viability. The major barriers to the implementation of the Shape Memory Tooling Project are material development and processing technologies.

The development of new shape memory based tooling was undertaken in 2010 in an effort to enable the implementation of polymer composite components in automotive applications by investigating the possibility of making complex and challenging composite part preforms quickly and cost effectively. The technical barriers for FY 2010 are material development and processing technologies for development of the preform screens.

In the initial phase of the project the concept of using shape memory technology as an alternative to traditional preforming techniques for improved preform dimensional control was demonstrated. The initial preform screens developed via the shape memory technology produced accurate component dimensional capability and compared well to more traditional preform screen technology but was much faster. [Figure 1](#) indicates what the Shape Memory Tooling Project is trying to achieve.

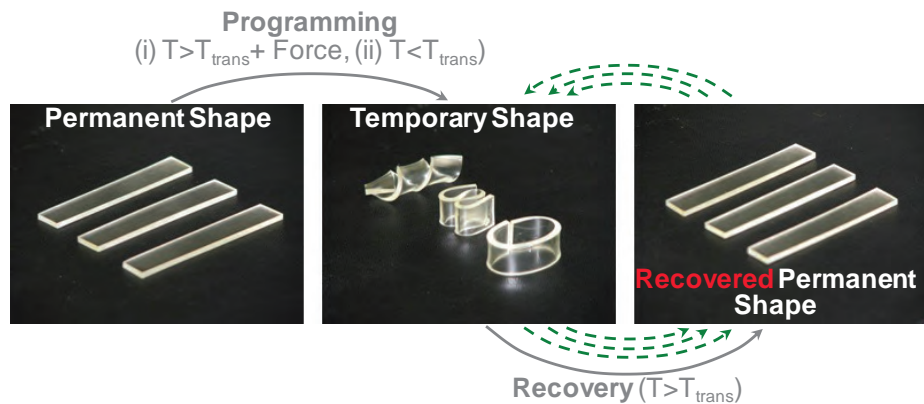


Figure 1. Flat composite panel going from a flat geometry to a part geometry and then back to a flat geometry.

Shape memory properties and durability were found to be highly dependent on their dimension, homogeneity, and perforation quality. Therefore, improvement of the preforming screen preparation process was studied. A new RTM molding tool was designed in collaboration with suppliers that will allow for preparing defect-free, dimensionally homogeneous flat shape memory epoxy plaques ($\sim 17 \times 17$ in.) with variable thickness (2 to 5 mm in 1 mm increments). Future work includes working with an identified supplier for making the RTM-type screen mold, working with tool suppliers for developing and making a screen deformation tool, and evaluating and quantifying the performance and durability of the shape memory preforming screens.

Direct Long Fiber Technology Project

Direct compounding of thermoplastic composites has become widespread within the automotive industry due to the flexibility of the process and potential economic advantages. And while successful applications have been reported for polypropylene based composites, limited development has been focused on direct compounding of engineering thermoplastics. Therefore, an experimental program was executed to test the feasibility of direct compounding for polyamide based composites. To allow a performance comparison with commercial precompounded materials, polymer formulations were compounded into a pelletized format. This approach enabled the option for subsequent processing via injection molding or extrusion compression. Once a generic formulation for the polymer constituents had been defined, a toll compounder was identified to produce pelletized materials for subsequent molding trials. In addition, for benchmarking purposes, a commercially available polyamide 66 material was molded and tested to establish target material properties.

The mechanical test program provided data for tensile and impact properties before and after long-term heat aging. The results of this test program were encouraging, indicating that the formulation developed for direct compounded material either met or exceeded properties of the commercial precompounded product. This would suggest that the technology is suited to engineering polymers although further work is planned to optimize the selection and dosing of additives used in the polyamide 66 formulations.

From a processing perspective, direct compounding technology uses continuous fiber in the material feed stream. This provides an advantage over conventional injection molding as long fiber lengths can be preserved in the molded composite. To help quantify this benefit, a fiber length measurement method was investigated to establish a length distribution within test samples. Historically, characterizing fiber length distribution has been a problem due to the innate difficulties of existing characterization methods. Most methods are extraordinarily time consuming and may not represent the true fiber length distribution. Because of the large number of fibers and their typically nonrandom dispersion, it is not feasible to count a given number of fibers to achieve a representative sample. Therefore, a new procedure was developed to segregate fibers based upon length and in turn determine distribution by mass. Fiber samples manufactured using a variety of process conditions were examined. As expected, samples processed with lower compounding screw speed exhibited higher retained fiber length. A comparison of actual fiber length data vs predictions showed good correlation. Hence, next steps are to establish the robustness of the fiber length measurement method for different material grades. The glass fibers were segregated via a series of screens that are placed on top of each other, in order, from largest screen to smallest screen. The fibers are mixed in water and poured through the screens, which allow the water to pass through and capture the fibers, from largest to smallest. The fibers are then measured for actual fiber length. The measurement process was achieved by placing the fibers on a scanner and then using software to measure fiber length. The fiber length ranged from 1 to 3mm long.

Predictive Technology Development and Composite Crash Energy Management (ACC 100)

Principal Investigator: Khaled W. Shahwan, Chrysler Technology Center
(248) 576-5609; e-mail: kws8@chrysler.com

Objective

Understand the mechanical behavior of composites that is necessary to develop the tools and methods needed to analyze and predict the crash-energy management characteristics and response of automotive structural components.

Goals and Approach

Conduct experimental tests to characterize quasistatic and dynamic properties (including coupled properties of selected structural composite materials, damage modes, and progression mechanisms); develop models based on phenomenological and advanced micromechanical approaches to predict the material and structural responses during the regimes of mechanical behavior; and verify and validate the computational tools by predicting quasistatic and dynamic behavior of experimental tests at the coupon and component levels. Further validate and correlate by predicting crash performance of automotive components, subassemblies, and systems made of composites.

Multiscale Modeling of Two-Dimensional Triaxially Braided Carbon Composite Tubes

This multiscale formulation involved the development of a reduced-order multiscale model in which the fiber-matrix interface was modeled using a traction-separation law where the values of fracture toughness in modes I, II, and III measured in quasistatic tests were used. The interface strength values were assumed to be identical to those of the matrix strength in the corresponding direction. These values were taken from prior tests. It is instructive to comment on the computational complexity of the reduced-order multiscale model with interface debonding which consists of 46 state variables. The state variables include six eigenstrain components times four phase partitions (24 total), three eigenseparation components per each of the three interface partitions (9 total), one phase damage state variable for each phase partition (4 total), and three interface damage state variables for each of the three interface partitions (9 total). In addition, in situ inelastic phase properties of matrix and tows have been recalibrated to the coupon test data from the transverse tension, longitudinal tension, and longitudinal compression—all conducted on the 45° braided composite architecture (as the calibration base).

Using the concept of “representative unit cell” [(RUC; the smallest repeating geometric unit which can be used to model the entire braid architecture (axial tows, bias tows, and matrix)], detailed FE models were built. Such detailed RUC models can include between 50,000 and 90,000 FEs per RUC depending on the material and detail levels. The structural FE models used symmetry to represent a one-quarter tube, and a comparison was made to the experimental results. Figure 1 shows the results of such a comparison between the test data and the simulation results of the reduced-order multiscale model.

The analysis proceeds by first calibrating the composite material properties (constituents) for the 45° braided architecture by using optimization techniques and coupon data obtained from experimental tests on the 45° braids. The calculated properties are estimated once and assumed to be the same for all other braided architectures, namely the 30° and 60° braids.

The limited study also investigated the effects of incorporating interface debonding (damage) and the inclusion of interlaminar delamination on the overall structural response (via simulation) and showed no remarkable improvements to the results. The studies showed that the reduced-order multiscale modeling approach can yield some agreements in trends/average values, but still does not fully predict with high level of (acceptable) accuracy some regimes of behavior.

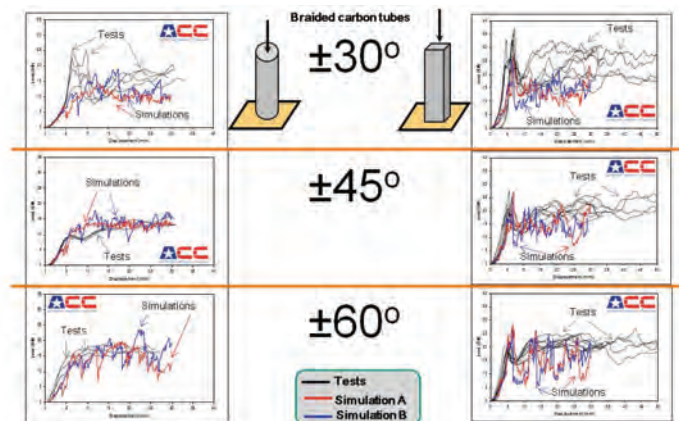


Figure 1. Simulations vs test results (load vs axial crush/displacement) for 30°, 45°, and 60° braided circular and square tubes.

Size Effects on Structural Strength in Textile Composites

This topic is focused on developing a qualitative and quantitative understanding of meso- to macro-size effects in structures made of quasi-brittle textile composite materials. “Size” refers to the size of specimen/structural dimensions relative to the size of the damage zone and/or microstructure. **Figure 2a** shows the four different structural (plaque) sizes that were selected (all plaques had the same total thickness with up to eight plies per size). “Effects” refer to those effects on damage characteristics, nominal strength, and post-peak regime in materials exhibiting such strength–size dependence. **Figure 2b** shows schematics of the classical relationship between nominal strength vs relative size (normalized measures). Such a relationship is bounded between strength and linear elastic fracture mechanics criteria. Also, “size effects” in this context do not stem from the well-known statistical distribution of micro-flaws in a material (e.g., Weibull based distribution), but rather from an energetic consideration. Such considerations are driven by the size effects quasi-brittle materials exhibit because their fracture process zone is not negligible (in size) compared with the overall structural dimensions and the size of local scales (e.g., fiber tows). The motivating question therefore is “Do the measured overall material/structural properties (e.g., strength) change when different size specimens of the same textile material are tested?”

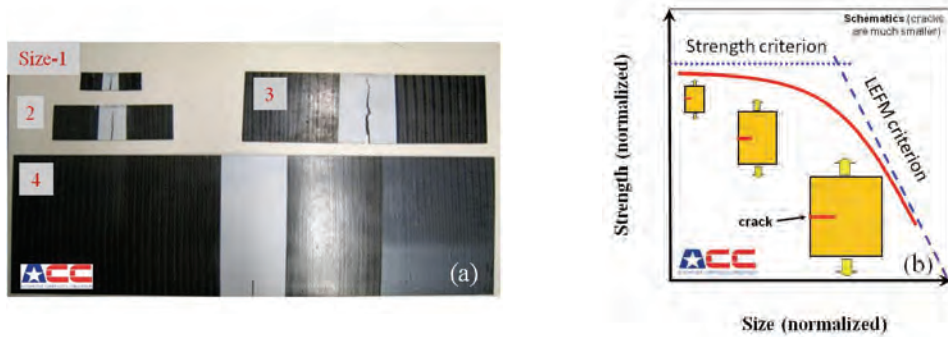


Figure 2. (a) The four different structural (plaque) sizes that were selected to study size effects on the nominal strength of braided carbon composites. (b) Schematic showing the classical relationship between nominal strength vs relative size (normalized measures).

Figure 3 shows different detailed FE modeling approaches used in investigating size effects in braided textiles. Figure 4 shows experimental vs computational results and demonstrates the strong size effects that are present in such quasi-brittle textiles. This implies that the measured strength characteristics depend not only on the material properties but also on the size of the specimen being tested. Such dependence poses special challenges to modeling and response prediction.

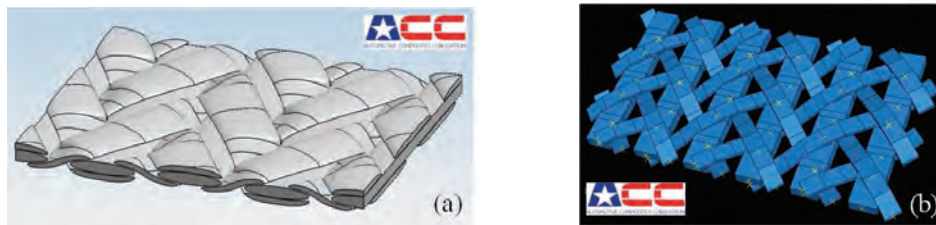


Figure 3. Two different three-dimensional models of two different sizes of a braid (1 ply): (a) detailed FE model of a 4-RUC specimen (2 by 2); (b) coarser FE mesh of a larger plaque made up of 25 RUCs (5 by 5). [For clarity only axial and braider tows are shown in (b).]

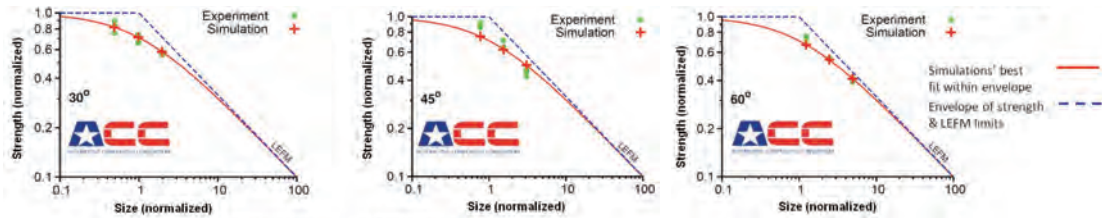


Figure 4. Experimental vs computational results showing the reduction in nominal strength (normalized) as a function of increase in size (normalized) for the three braid architectures.

Modeling the Manufacturing Process Induced Effects on the Matrix Properties of Textile Composites (In Situ Properties Predictions)

During the manufacturing process for textile reinforced composites (TRCs) the material properties of a polymer resin (matrix) do change over the curing cycle. The resin's liquid-to-solid transition, accompanied by volume change and coupled with mismatches in thermal coefficients between fibers and resin (and applied mechanical stresses), may result in inhomogeneous curing of TRC structural specimens. These spatial variations could result in built-in local residual stresses, and such local field variations within the cured material are a result of the physics of curing in materials with complex microstructures. This can result in differences between the presumed material properties (usually virgin/neat properties) and the actual in situ material properties. The actual response of a structural component made of a TRC may be accurately predicted by using well-characterized in situ material properties, not the virgin/neat properties which are commonly used as input data to analysis codes.

This topic is aimed at developing the knowledge needed and the computational tools necessary to make such assessments and estimates of in situ properties within an objective framework based on engineering mechanics and developing qualitative and quantitative methods (and modeling tools) to better understand and predict in situ properties during the manufacturing and curing processes of structural components made of TRCs.

An example of the influence of using neat/virgin matrix properties versus their in situ counterparts on the RUC response is shown in Figure 5a. It clearly demonstrates the necessity for minimizing potential "inaccuracies" in the "presumed" input material properties to improve prediction accuracy and robustness. To accomplish that, predictive models need to include effects such as stress relaxation, evolution of extent-of-cure (spatially and temporally), and thermal conductivity properties as part of the computational process. [Note: the response of one RUC represents only the response of that small region of material and may not represent the nonlinear response of the larger region (e.g., specimen, structure).] Extensive experimental and computational programs were developed including nano-indentation characterization (Figure 5b), characterization using optical techniques such as Brillouin and Raman light scattering, and FE modeling procedures. Examples of such investigations are given in Figure 6, which shows that matrix properties vary by location (i.e., proximity to a fiber/tow) and that the apparent fiber properties within a cured tow can differ depending on the type of resin.

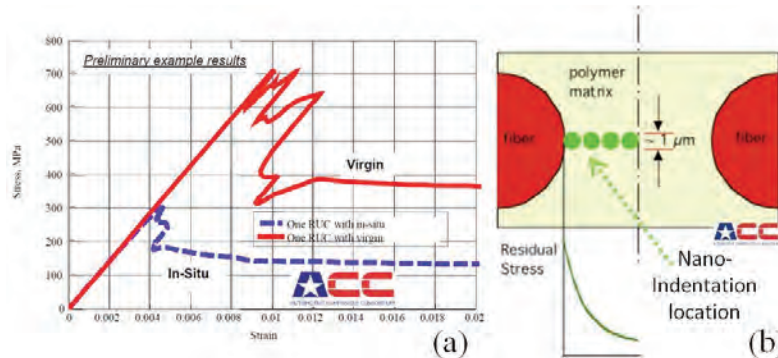


Figure 5. (a) The responses of one RUC using two different matrix properties. (b) A schematic showing examples of nano-indentation locations (four small green circles) may be used near/away from fibers (larger red semi-circles).

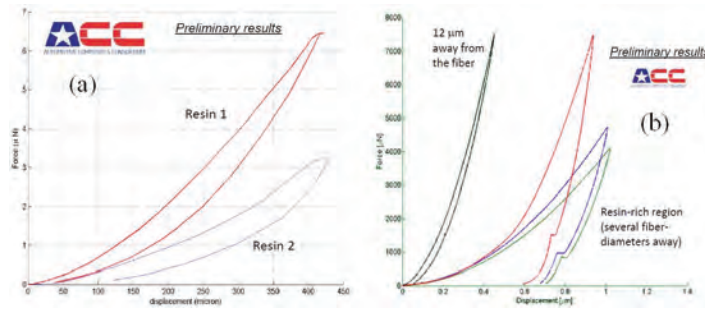


Figure 6. Experimental nano-indentation force-displacement response: (a) the same fiber embedded in two different cured resins; (b) variation in cured resin property with distance away from the fiber.

Conclusions

Full design of part and tooling, including material development and scenario for component manufacture and vehicle assembly, has been completed for the underbody project. A matched metal compression tool was built to mold full underbody parts. Full parts were molded but these parts have not yet achieved complete design specification.

Molds for all four composite parts of the composite seat were completed. Composite parts were molded, trimmed, and plasma treated for assembly. All metal reinforcements and brackets have been fabricated and e-coated.

The BLRT project demonstrated that the lessons learned could be applied to an actual component and assist engineers in the design strategy for Class A composite applications.

Efforts within the ACC have also resulted in lower cost material formulations for automotive composites.

- Epoxy and vinyl ester/polyester resin based carbon fiber SMC systems have produced properties close to targets, using low cost, large tow carbon fibers.
- Experimental long fiber thermoplastic formulations were developed for direct compounded material that either met or exceeded properties of the commercial precompounded product.

Significant progress was made toward understanding the complex behavior of fiber-reinforced composites under various impact speeds. Extensive experimental characterizations of materials have been developed and adopted within computational predictive tools. Modes of energy absorption and basic physics, including effects of size, curing, and manufacturing, have been characterized and modeled and are in the process of being verified and validated.

Presentations/Publications/Patents

ACC 007

Berger, L. "A Structural Composite Automotive Underbody," Society for the Advancement of Materials and Processing Engineering, Seattle, Washington, May 17–20, 2010.

Berger, L. "Design and Fabrication of a Structural Composites Automotive Underbody," Society of Plastics Engineers Automotive Composites Consortium, Troy, Michigan, September 15–16, 2010.

Berger, L.; Simon, D.; Dove, C.; Knakal, C. "Properties and Molding of a Fabric SMC for a Structural Composite Underbody," Society of Plastics Engineers Automotive Composites Conference and Exhibition, Troy, Michigan, September 15–16, 2010.

Dove, C. "Shear Deformation Properties of Glass-Fabric Sheet Molding Compound," Society of Plastics Engineers Automotive Composites Conference and Exhibition, Troy, Michigan, September 15–16, 2010.

Fuchs, H.; Conrod, B. "Super Lap Shear Joint Structural Test-Analysis Correlation Studies," Society of Plastics Engineers Automotive Composites Conference and Exhibition, Troy, Michigan, September 15–16, 2010.

Fuchs, H.; Deslauriers, P. "Double Dome Structural Test-Analysis Correlation Studies," Society of Plastics Engineers Automotive Composites Conference and Exhibition, Troy, Michigan, September 15–16, 2010.

Shah, B.; Frame, B.; Dove, C.; Fuchs, H. "Structural Performance Evaluation of Composite-to-Steel Weld Bonded Joint," Society of Plastics Engineers Automotive Composites Conference and Exhibition, Troy, Michigan, September 15–16, 2010.

Fuchs, J.; Fickes, J.; Banks, E.; Berger, E. "Automotive Structural Joint and Method of Making Same," U.S. Patent Application 12/119084, May 12, 2008. Notice of claims approval May 27, 2010.

Fuchs, J.; Banks, E.; Berger, E.; Fickes, J.; Oswald, D.; Foss, P. "Dynamic Load Bearing Composite Floor Pan for an Automotive Application,," U.S. Patent 7784856, August 31, 2010.

ACC 932

Fernholz, K. D.; Lazarz, K. "Effect of Cure Temperature on the Severity of Bond-Line Read-Through Induced Surface Distortion," The Adhesion Society 33rd Annual Meeting, Daytona Beach, Florida, February 21–24, 2010.

Fernholz, K. D. "The Influence of Bond Dam Design and Hard Hits on Bond-Line Read-Through Severity," SPE Automotive Composites Conference, Troy, Michigan, September 15–16, 2010.

Fernholz, K. D. "The Effect of Bond Fixture Heat Source on Bond-Line Read-Through Severity," COMPOSITES 2011, Fort Lauderdale, Florida, February 9–11, 2011.

Fernholz, K. D. "Quantifying the Visibility of Surface Distortions in Class 'A' Automotive Exterior Body Panels," submitted to Measurement Science and Technology, September 2010.

B. Automotive Metals Division - U.S. Automotive Materials Partnerships

Field Technical Monitor: Bill Charron
Ford Motor Company
Mfg. Development Center, Fairlane North 2
6100 Mercury Drive; Dearborn, MI 48126-2746
(313) 805-6628; e-mail: wcharron@ford.com

Field Technical Monitor: Steve Logan
Chrysler Group LLC
Materials Engineering
CIMS Code 482-00-13; 800 Chrysler Drive; Auburn Hills, MI 48326-2757
(248) 512-9485; e-mail: sl16@chrysler.com

Field Technical Monitor: James Quinn
General Motors Company
GM, R&D and Planning
Mail Code 480-106-212; 30500 Mound Road; Warren, MI 48090-9055
(586) 596-4395; e-mail: james.f.quinn@gm.com

Technology Area Development Manager: Carol Schutte
U.S. Department of Energy
1000 Independence Ave., S.W.; Washington, DC 20585
(202) 287-5371; e-mail: carol.schutte@ee.doe.gov

Field Project Officer: Joseph Renk
National Energy Technology Laboratory
626 Cochrans Mill Road; P.O. Box 10940; Pittsburgh, PA 15236
(412)386-6406 ; e-mail: joseph.renk@netl.doe.gov

Contractor: U.S. Automotive Materials Partnership (USAMP)
Contract No.: DE-FC26-02OR22910

Objective

- Develop a standardized cosmetic corrosion test for finished Al automotive body panels that provides a good correlation with on-vehicle testing and field performance.
- Demonstrate and enhance the feasibility and benefits of using Mg in powertrain components to cost effectively achieve more than 15% weight reduction compared to Al while meeting or exceeding all performance and durability requirements of the Al powertrain components.
- Develop an accelerated cosmetic corrosion test that demonstrates good correlation to field performance of painted Al body panels to help facilitate the increased use of Al outer panels for automobile mass reduction.
- Evaluate the technical feasibility (acceptable range of alloy compositions, acceptable casting processes, heat treatment processes, technical cost models, heat treatment and stress corrosion tests, etc.) of using the B206 Al alloy to provide a low cost casting alternative to forged Al and ductile iron for lightweight automotive suspension components.
- Develop and evaluate predictive, math based tools to describe properties (performance) of Al powder metal components to reduce the risk of lightweight material substitution.

- Evaluate/develop/validate casting process technologies needed to manufacture high integrity cast Mg automotive suspension components and address critical technology barriers inhibiting Mg application and component affordability.
- Design and develop a lightweight Mg front end body structure to enable Mg applications in vehicle body structure systems to provide a mass reduction of 50% to 60% over steel at a nearly neutral cost status while meeting all current safety and performance requirements.
- Develop and demonstrate key enabling material and manufacturing enabling technologies (e.g., high integrity casting, wrought Mg processing, improved alloys, corrosion protection, and joining processes) and expand the accompanying engineering knowledge base [e.g., crashworthiness; noise, vibration, and harshness (NVH); and durability performance] to permit design and implementation of Mg-intensive automotive-body front end structures having substantially reduced mass, but with performance and cost comparable to sheet-steel baseline structures.
- Establish an integrated computational materials engineering (ICME) capability for Mg alloys and manufacturing processes of interest to the automotive industry, with focus on wrought AZ31 and AM30 and die cast AZ91D during the FY 2010 period.
 - Contribute to the comprehensive database of processing-structure-property relationships for wrought AZ31 and cast AZ91D during FY 2010.
- Establish predictive capabilities for forming of wrought Mg (e.g., AZ31) by “warm” forming processes, and localization of microstructural-dependent mechanical properties in die casting (e.g., porosity, shrinkage and phase equilibria in AZ (1D).
- Evaluate/develop/validate ceramic coating technologies to eliminate the galvanic corrosion problems associated with the use of steel fasteners to join Mg parts and expand the applications of Mg components in the automotive industry.
- Continue developing and optimizing the warm forming process to bring the technology to an implementation ready status and develop a supply base for warm forming.
 - Develop a warm forming process that both enhances formability and allows for the use of lower cost heating methods for the die.
 - Design, build, and demonstrate the process on a full-scale door inner panel that is not feasible with conventional stamping.
 - Identify a production supplier and the design and engineering of a production warm forming process.
- Develop an automotive paint-line-compatible pretreatment process for mixed metal (Mg, Al, Zn, steel) body-in-white assemblies, where mixed metal parts are joined before painting, by incorporating corrosion inhibiting compounds into the electrocoat layer while still using the existing production paint-line facility to minimize capital investment. Successful completion will enable the use of Mg components without precoating them offline.

Accomplishments

Automotive Metals Division (AMD): Al Automotive Closure Panel Corrosion Test Program (AMD 309)

- Identified a modified version of American Society for Testing and Materials (ASTM) G85-A2 as an accelerated corrosion test that predicts the corrosion observed on Al in-service panels.
- Identified the differences in accelerated corrosion performance between different cabinets running ASTM G85-A2.
- Analyzed the correlation between in-service corrosion performance and ASTM G85-A4.

Automotive Metals Division: Improved Automotive Suspension Components Cast with B206 Alloy (AMD 405)

Objective: Define the optimum B206 Al alloy chemistry, casting process, and heat treatment that will produce safety critical suspension components free of stress corrosion cracking (SCC) at lower cost and lighter weight than forged Al and ferrous based solutions.

- Phase 1—Through a study of tensile properties versus alloy composition conducted by researchers at Alcan International using separately cast ASTM B108 permanent mold test bars, determined that best mechanical properties for the B206 Al alloy are obtained with two separate alloy compositions, depending on whether the T7 or the T4 temper is used, which are still within the overall Al Association B206 alloy composition range. These two alloy compositions are listed in the final report.
- Phase 2—Performed studies to define the relationship between chemistry, cooling rate, and resultant mechanical properties and compiled the results into a set of casting and design guidelines which can assist in casting design, process selection, and process control to better achieve desired B206 alloy mechanical properties and avoid hot cracking.
 - Twenty different B206 alloy compositions were prepared, which were within the overall B206 Al alloy range, and “wedge” castings were poured to establish the tensile properties of the alloy as the solidification rate varied from 30 seconds to 30 minutes.
 - Hot crack test castings were made to determine the effect of alloy composition on castability.
- Phase 3—Created a cost model and determined that the B206 alloy in the T7 temper has the potential for significant cost reductions compared to A356 alloy castings. The increased strength of the B206 alloy compared to the A356 alloy allows for less material to be used, which offsets the higher cost of the B206 alloy (10% more expensive than A356).

Automotive Metals Division: Powder Metal Performance Modeling of Automotive Components (AMD 410)

Objective: Develop and evaluate predictive, physics based tools to describe properties (performance) of powder metal components to reduce the risk of lightweight material substitution.

- Determined material constants for FC-0205 and FC-0208 iron-carbon powders.
- Determined material constants for Al-6061 Al powder.
- Developed compaction, sintering, and performance computer models.
- Evaluated the process history of target engine main bearing cap component.
- Validated compaction and sintering models by comparing predicted density and material properties to production engine main bearing caps.
- Validated performance model by comparing predicted fatigue performance against bench test results of a current production engine main bearing cap.
- Demonstrated lightweight material opportunities for the main bearing cap using Al-6061 powder.
- Proposed alternative designs for the main bearing cap that could yield weight savings and performance improvements.
- Submitted user guide for the math based model developed in this program for powder metallurgy (PM) component design and performance prediction.

Automotive Metals Division: Optimization of High-Volume Warm Forming for Lightweight Sheet Alloys (AMD 905)

- Investigated three promising variants of nonisothermal warm forming in terms of formability, cost, and process robustness for commodity Al alloy 5182.
- Established a low cost warm forming process which does not require die heating. Demonstrated improved formability with new pan die tool with using a heated blank and a room temperature die. Maximum local strains were increased from about 5% to more than 30%.
- Began engineering of full-scale die for demonstration of scaled up warm forming process and determined expected weight savings.

Automotive Metals Division: High Integrity Magnesium Automotive Components (AMD 601)

- Developed and then converted four different types of Al casting processes [squeeze casting, low pressure permanent mold (LPPM), ablation, T-Mag] to Mg processes and cast identical Mg control arm components using AM60 and/or AZ91 Mg alloys by each process. The technical barriers that were overcome by this project included microstructure control, porosity and hot tearing, thermal treatments, grain refinement, and controlled mold filling to effectively manufacture high integrity cast Mg components that would demonstrate high ductility, high strength, and low porosity and be free of objectionable oxides and inclusions. (FY 2006–2010)
- Developed an electromagnetic pump (EMP) process for Mg and successfully transferred molten Mg and cast control arms. EMP systems are noted for the quiescence transfer of metal thereby eliminating metal oxides and inclusions that can be produced by conventional casting methods. This is the first time that an EMP has been developed and used with molten Mg. (FY 2009–2010)
- Successfully cast hundreds of identical Mg control arms using the four processes and evaluated the material properties to determine which process could provide the best results in accordance with the statement of work (SOW) deliverables for the Mg processes. (FY 2009–2010)
- Developed modeling techniques to minimize hot tear and porosity for Mg components. The model was applied to low pressure die cast and squeeze cast Mg alloy components of interest to the High Integrity Magnesium Automotive Component (HIMAC) project (AMD 601). The squeeze casting parameters used by Meridian Lightweight Technologies were integrated into the model that was developed by the University of Iowa, and the results of the casting (porosity and hot tears) matched the predicted results of the model. (FY 2009–2010)
- Compared metallographic and material property results by examining hundreds of castings from all processes that were developed. Control arms produced by each casting process were provided by different industrial partners. Samples were extracted from the control arms to examine the microstructure, porosity size distribution, and grain size. Four point bend testing was performed to investigate the mechanical properties and a Weibull analysis was used to quantify specimen failure rate. Monotonic and cyclic testing were performed for each casting process and inclusion quantification was performed on the fracture surfaces on the failed specimens. The five casting processes were evaluated. Overall, the two best performing processes based on defect analysis, monotonic and cyclic behavior, and the subsequent scanning electron microscopy fractography are the T-Mag and ablation processes. (FY 2008–2010)
- Identical castings produced from all four Mg casting processes were evaluated in accordance with the project's SOW x-ray standard, ASTM E-155, to achieve level 2 or less. (FY 2008–2010)
- The SOW for the project indicated the goal for the x-ray requirement was to achieve ASTM E-155 (level 2 or less). The squeeze casting and EMP processes interfaced with production equipment, and there was insufficient time to fully achieve this x-ray level requirement. However, all other aspects of these processes were achieved.
- The HIMAC project was completed on 9/30/2010.

Automotive Metals Division: Magnesium Front End Design and Development

Phase I, Design and Feasibility Study (AMD 603)

- Concluded on March 31, 2010. Major accomplishments included identification of crashworthiness limitations of the Mg alloy front rails in the unibody structure and replacement with Al extrusions, and sensitivity of the cost structure to certain joining attributes and corrosion protection. Although the original weight reduction target of 60% for the unibody structure was not achieved, the 45% reduction outcome approaches the overall program target of 50%.

Automotive Metals Division: Magnesium Front End Research and Development

Phase I, Enabling Technology Development (AMD 604/904)

- Project AMD 604 was formally concluded in March 2010 and successor project AMD 904 was launched on April 1, 2010. Agreement among international partners in China and Canada on an agenda and budget for Phase II and development of supporting objectives at the national and international task team levels were achieved in March 2010. Initiation of Task 2.0 on design and acquisition of six candidate designs for the “demonstration” structure meeting selected criteria was launched.

Automotive Metals Division: Integrated Computational Materials Engineering (AMD 703)

- Augmented the SharePoint computer database maintained by Mississippi State University (MSST) with additional program data in the field of fatigue life of base materials, fatigue life of friction stir spot welds, and microstructural data from MSST.
- Conducted the first ever TMS (The Minerals, Metals & Materials Society) symposium devoted specifically to the ICME of Mg and its alloys, comprising 17 contributed papers covering a variety of topics in the field.
- Calculated the thermodynamic solution energetics for the Mg-Al-Zn system from first principles computer methods and reported as functions of solute concentration using a quasi-semirandom solid formalism to derive the energy term.
- Developed beta test capability and appraisal for the “extensible, self-optimizing magnesium phase equilibrium infrastructure” graphical user interface used in computer calculation of phase diagram data. This software permits a standardized approach to be used for optimizing thermodynamic functions from experimental or theoretical data which may be acquired by different methods and models.
- Determined only minor influence of twinning and detwinning for deformation of AZ31 at elevated temperatures in sheet forming.
- Obtained and provided extrusion billet material which can be used by modelers at MSST and Lehigh University in correlation of predicted and actual microstructures (and properties) in the extrusion of AM30.
- Conducted microstructure and fatigue property measurements of excised coupons from “super vacuum” processed and T6 heat treated AZ91D, providing the framework for predictive capability of die-casting models based on metal flow and solidification, with localized mechanical properties in resultant castings.
- Confirmed limitations on fatigue life in super vacuum die cast AZ91D primarily associated with porosity.

Automotive Metals Division: Development of Steel Fastener Nano-Ceramic Coatings for Corrosion Protection of Magnesium Parts (AMD 704)

Objective: Evaluate/develop/validate ceramic coating technologies to eliminate the galvanic corrosion problems associated with the use of steel fasteners to join Mg parts and expand the applications of Mg components in the automotive industry.

- Evaluated and rated the effect of multilayer nano-ceramic coatings on the galvanic corrosion between coated 1050 steel substrates and Mg. The criteria used to rate the coatings for galvanic and general corrosion were a combination of qualitative visual assessments, mass loss measurements, and optical measurements of corrosion products.
- The multilayer coating consisting of silicon nitride as a precoat, Al oxide as the second coat, and an ultraviolet (UV) curable topcoat performed the best with respect to limiting galvanic current between the coated steel specimen and Mg. The silicon nitride precoat is the most effective nano-ceramic coating in adhering to steel, despite the presence of surface imperfections such as grain boundaries and inclusions. The Al oxide layer enhances the ductility of the precoat and, combined with the UV curable top coat, provides the insulating barrier that reduces galvanic current which in turn reduces galvanic corrosion between coated steel substrates and Mg.

Future Directions

- AMD 309—Al Automotive Closure Panel Corrosion Test Program. The ASTM G.01 committee is reviewing the results of AMD 309 work and will determine whether a modified test method or a new annex of the ASTM G-85 standardized test method is required for Al corrosion.
- AMD 410—Powder Metal Performance Modeling of Automotive Components. General Motors and Ford are exploring whether the computer models developed by this program can be run in-house to optimize powder metal component design with respect to weight and performance.
- AMD 905—Optimization of High-Volume Warm Forming for Lightweight Sheet Alloys. Design, build, and demonstrate low cost warm forming process on full-scale door inner panel that is not feasible with conventional stamping. Achieve successful scale-up and identification of supplier partner. This will enable the production of a one-piece Al door inner design which is both lower cost and lighter weight than the conventional multipiece design.
- AMD 603—Magnesium Front End Design and Development Phase I, Design and Feasibility Study. Although this current aspect of the greater magnesium front end effort has concluded, a design task will be incorporated in the Magnesium Front End Research and Development Phase II project so that both international and supplier organizations can actively participate in the design and manufacturing technologies of a demonstration structure intended to exhibit the necessary attributes of Mg-intensive automotive substructures.
- AMD 604/904—Magnesium Front End Research and Development Phase I, Enabling Technology Development. The objective of this successor project is the design, manufacture, and testing of a demonstration structure exhibiting key attributes of the intended Mg front end vehicle substructure, including joining technologies, surface protection schemes, and durability requirements. In addition to the principal tasks identified in Phase I, there is now a design task chartered to achieve a suitable structure, which will then become the focus of scientific and technological thrusts of Phase II, including increased focus on technical hurdles such as mechanical property limitations of present Mg alloys and galvanic corrosion expected at the joints to remainder body-in-white steel structures.
- AMD 703—Integrated Computational Materials Engineering. The current project is presently targeted to conclude by September 30, 2011.
- AMD 704—Development of Steel Fastener Nano-Ceramic Coatings for Corrosion Protection of Magnesium Parts. The project will optimize the coating process parameters to deliver a nano-ceramic coating that when applied to steel fasteners will generate less galvanic current, and subsequently less galvanic corrosion, with Mg than Al to Mg. The use of Al in the form of spacers or fasteners is the current automotive strategy for isolating steel from Mg but can increase cost and require compromises in component and joint design. The ability to use nano-ceramic coated steel fasteners will facilitate the use of Mg by providing a lower cost joining solution that minimizes galvanic corrosion, which is a fundamental barrier to the use of Mg in automotive applications.

Introduction

The realization of significant weight savings in passenger and commercial vehicles is likely to occur through the use of a variety of advanced materials. While improvements in the properties, manufacturability, and cost of advanced materials are critical in achieving vehicle weight reduction, technologies that support the use of these materials in a multi-material system are equally important. Unlike a single material system, structures composed of different metals and polymer composites present difficult challenges in areas such as joining, corrosion, recycling, and nondestructive evaluation. Work conducted in this program seeks to overcome these challenges by developing new techniques, establishing standards, and preparing advanced technologies for a high volume production environment.

The mission of the AMD is to facilitate the development of improved materials and the related manufacturing technologies for the automotive application of metals through cooperative programs, including those supporting FreedomCAR. To achieve those goals, current AMD projects focus on technological hurdles faced in high volume application of Mg and Al in the alloys themselves and in the manufacturing technology and infrastructure gaps in casting, sheet and forming, and joining of these materials to themselves and to other materials.

The following sections outline specific task work conducted by AMD project teams in addressing the technology gaps and challenges.

Activity and Developments

Aluminum

With potential weight savings of roughly 35% to 50% compared to steel and iron and a relatively well developed infrastructure, Al is and will remain the most prominent lightweight structural material for the foreseeable future. However, largely because of the relative maturity level of Al and its associated manufacturing processes (compared to Mg and titanium), it has not received as much emphasis as Mg and its associated processes at AMD in recent years. Nevertheless, AMD has supported several projects focusing on Al and related processes, including the following.

- Evaluation of a high strength Al casting alloy (B-206) for automotive suspension components.
- Development of simulation tools for Al powder metal components.
- Development of warm forming processes to improve formability of challenging Al sheet metal components.

Aluminum Automotive Closure Panel Corrosion Test Program (AMD 309)

Project Cochair: Tracie Piscopink-Jafolla, General Motors Company
(248) 676-7014; e-mail: tracie.l.jafolla@gm.com

Project Cochair: Francine Bovard, Alcoa Technical Center
(724) 337-3249; francine.bovard@alcoa.com

Introduction

Although Al closure panels have been used on numerous vehicles for several years, the degree of confidence in predicting service performance has not been high due to the lack of an accelerated corrosion test that mimics field performance. Automotive manufacturers and their suppliers often rely on accelerated corrosion tests that were developed for evaluating painted steel, but these tests do not always provide performance results on painted Al sheet that are consistent with in-service Al closure panel performance.

To address the need for an accelerated Al corrosion test, a group comprising representatives from the U.S. automotive manufacturers, Al suppliers, coating suppliers, and other associated suppliers was formed in 2000. The goal of this group has been to identify and implement a standardized accelerated corrosion test for cosmetic corrosion of Al that exhibits the same appearance, severity, and corrosion products that are exhibited on in-service Al components. The purpose of this report is to provide a summary of the efforts of this group.

In-Service Exposure

It is critical when developing a laboratory based test that test-to-field correlation be performed. In an effort to capture real-world data in developing this test, it was deemed preferable to expose these panels to severely corrosive environments that represent “worst case” service environments. Five in-service exposure sites were selected for this study: (1) Detroit, Michigan; (2) Florida; (3) St. Johns, Newfoundland; (4) Montreal, Quebec; and (5) an Ohio to New York truck route. Testing at all of these sites was completed with 4 or 5 years of exposure at each site. Triplicate panels of each panel set were exposed on each vehicle per site. The panel sets are listed in Table 1 below.

Table 1. Materials.

<i>Panel code</i>	<i>Alloy substrate</i>	<i>Metal finish</i>	<i>Paint system</i>
<i>A or 1</i>	<i>AA6111-T4PD</i>	<i>Mill</i>	<i>Standard</i>
<i>B or 2</i>	<i>AA6111-T4PD</i>	<i>Mill</i>	<i>Low F-E-coat only</i>
<i>C or 3</i>	<i>AA6111-T4PD</i>	<i>Mill</i>	<i>Standard</i>
<i>D or 4</i>	<i>AA6111-T4PD</i>	<i>Sanded</i>	<i>Standard</i>
<i>E or 5</i>	<i>AA6016-T4</i>	<i>Mill</i>	<i>Standard</i>
<i>F or 6</i>	<i>AA6022-T43</i>	<i>Mill</i>	<i>Standard</i>
<i>G or 7</i>	<i>AA2036-T4</i>	<i>Sanded</i>	<i>Standard</i>
<i>H or 8</i>	<i>EG 60 Steel</i>	<i>Mill</i>	<i>Standard</i>
<i>I or 9</i>	<i>Cold rolled steel</i>	<i>Mill</i>	<i>Standard</i>

Approach

Sets of 24 panels (three each of eight material variables) were attached to a mounting panel (16 in. by 12 in.) using double-backed tape prior to mounting on the vehicle. At the Detroit, St. John’s, and Montreal sites one set was mounted on the hood of each vehicle (horizontal orientation) and one set on the right front door of each vehicle (vertical orientation). For the Ohio-New York (OH-NY) truck route the panels were mounted beneath the trailer frame behind the front wheels (vertical orientation only). Each panel contains two diagonal scribe lines which are 2 in. long and 1 in. apart. The panels were exposed for a total of 4 years of in-service exposure. Intermediate evaluations were conducted when possible.

Results and Discussion

Although the extent of corrosion in the on-vehicle exposures varied considerably from vehicle to vehicle for the various sites, panels D, G, and I typically exhibited significantly more corrosion than the other substrates, as illustrated by the images in Figure 1. The Al panels with metal finishing (D and G) generally have more corrosion than the other Al substrates, and cold rolled steel (I) has more corrosion than the electrogalvanized steel (H).

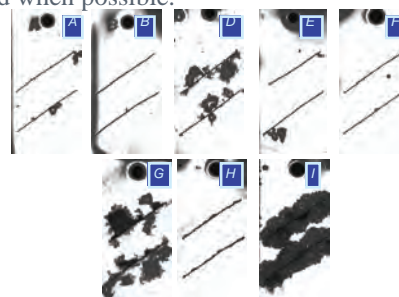


Figure 1. St. John’s on-vehicle test with 5 years’ exposure.

Conclusions

Metal finishing significantly affects the corrosion performance of Al during in-service exposure, while little corrosion is observed on panels with no metal finishing. This is an observation from all vehicle exposure sites. In subsequent analysis the Al panels were placed into two categories—metal finished panels (substrates D and G) and nonmetal finished panels (substrates A, E, and F).

Analysis of the corrosion products on the Al panels showed the presence of S. The steel panels exposed at the same sites do not show the presence of S in the corrosion products. This finding initiated a search for an accelerated corrosion test that included exposure to S in the test cycle.

Accelerated Corrosion Test

Introduction

A variety of accelerated corrosion tests are used in the automotive industry. Many of these tests were developed for the evaluation of steel substrates and often different automakers specify different accelerated corrosion tests for the evaluation of the same mix of substrates. Multiple accelerated corrosion tests were evaluated as part of this project to determine the ability of the tests to distinguish the corrosion performance of Al.

Approach

Multiple standard accelerated corrosion tests were evaluated for their ability to distinguish the cosmetic corrosion performance on painted Al sheet. The criteria for providing the ability to distinguish performance was the existence of a corrosion morphology similar to that observed in the field, the ability to rank Al panel corrosion performance consistent with that observed in the field, and the ability to provide a corrosion product similar to that found in the field.

Results and Discussion

After several rounds of laboratory tests and comparison of the results with results from on-vehicle exposures, the list of laboratory tests of interest was narrowed to two tests: modified ASTM G85-A2 and modified ASTM G85-A4. The corrosion from the modified ASTM G85-A2 test is illustrated in Figure 2. Panels D and G (sanded substrate prior to coating application) exhibit a greater degree of corrosion than the other Al panels.

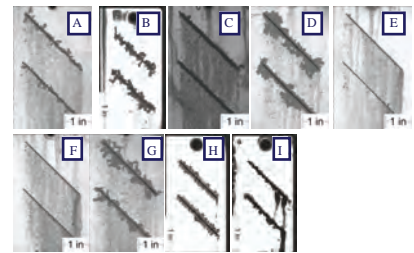


Figure 2. Modified ASTM G85-A2—3 weeks of testing.

In comparing the accelerated corrosion test to in-service performance, the average normalized corrosion area in square millimeters of mill finish substrates (A, E, F) was plotted against the average normalized corrosion area of sanded substrates (D and G). Several comparisons were made based on the type of cabinet and the length of the accelerated test. Figure 3 shows the results after 3 weeks of accelerated testing in the water jacketed cabinet. It should be noted that although the extent of corrosion is greater in the accelerated test than in-service, the ratio of corrosion of the sanded panels to the mill finish panels is close to the same.

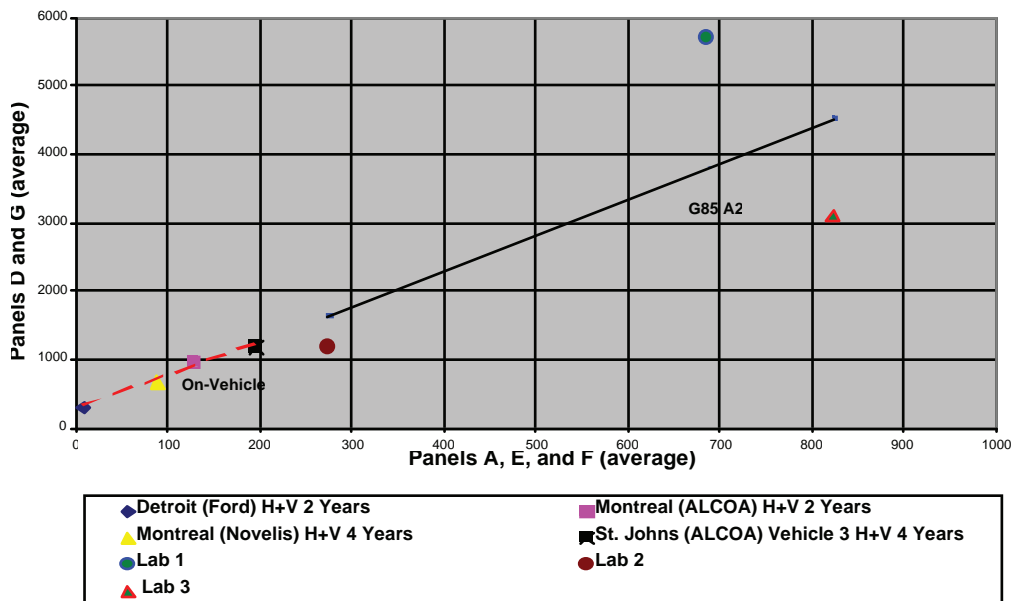


Figure 3. Comparison of ASTM G85-A2 in a water jacketed cabinet after 3 weeks of testing to in-service performance.

Figure 4 shows the comparison after 3 weeks of accelerated testing in the automated cabinet. The extent of corrosion in the automated cabinet is not as great (or aggressive) as in the water jacketed cabinet and tends to be less than the in-service panels. However, once again the ratio of corrosion of the sanded panels to the mill finish panels is close to the same.

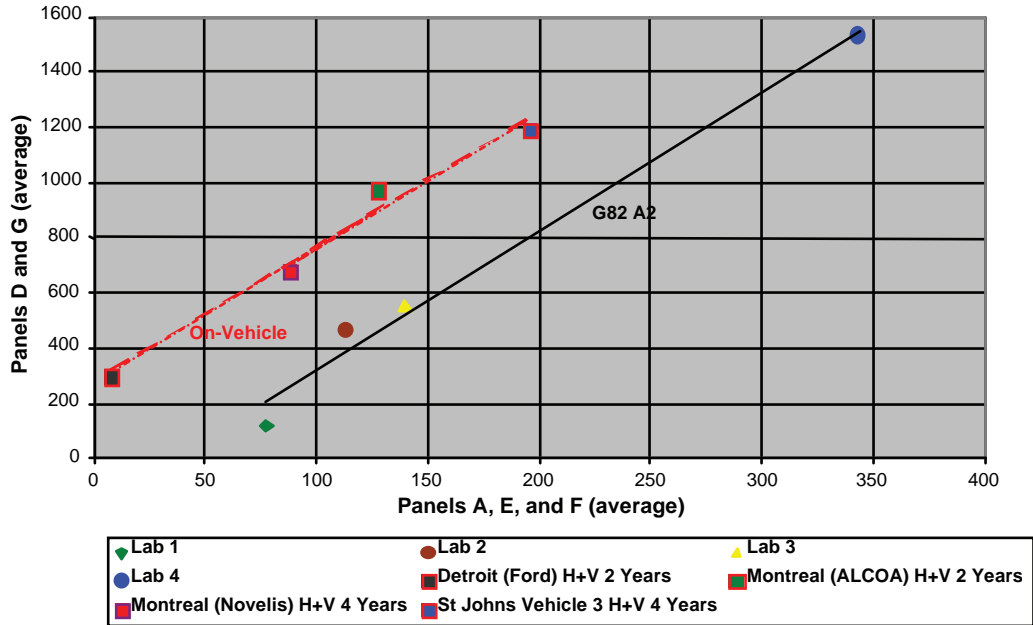


Figure 4. Comparison of ASTM G85-A2 in an automated cabinet after 3 weeks of testing to in-service performance.

Figure 5 summarizes the performance of ASTM G85-A4 compared to on-vehicle panel performance. The ASTM G85-A4 test was conducted according to three different protocols: (1) modified with acetic acid instead of sulfur dioxide (SO₂), (2) continuous spray of SO₂, and (3) intermittent spray of SO₂. Modification 1, with acetic acid, resulted in little corrosion on any of the panels. Both the continuous and intermittent spray provided accurate relative rankings of the corrosion on Al. However, the intermittent spray protocol resulted in significantly more corrosion on the Al panels compared to the continuous spray protocol. It should be noted that the laboratory to laboratory reproducibility using this test method is quite good.

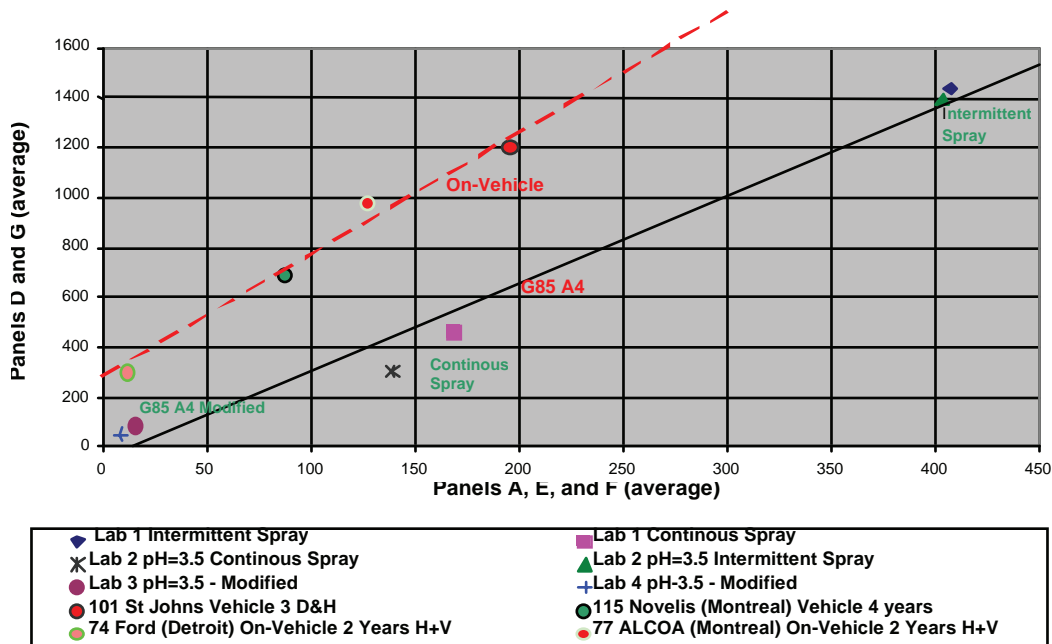


Figure 5. Comparison of the extent of corrosion of ASTM G85-A4 with three different testing protocols to the on-vehicle performance.

Conclusions

The recommended accelerated corrosion tests on painted Al sheet are modified ASTM G85–A2 and modified ASTM G85–A4. Both of these accelerated tests are acidified to a pH of 2.5–3.2. An acidic exposure environment appears to be a key parameter when trying to mimic in-service corrosion performance with an accelerated test. However, many of the industry accepted standards for accelerated corrosion tests of steel are run in neutral environments. Neutral environments evaluated in this program induced little or no corrosion on the painted Al panels. While the ASTM G85–A2 test does not include S in the exposure, the acidic exposure provides the necessary environment to induce corrosion on Al that replicates the morphology of corrosion on the in-service panels.

ASTM G85–A4 provides both the acidic exposure and the exposure to S but can be a difficult test to run due to the use of SO₂ gas. It is recognized that environmental health and safety issues associated with handling SO₂ may preclude use of this type of test at some facilities. Because of these issues there are a limited number of facilities with existing SO₂ testing capability.

A requirement in the identification of an accelerated corrosion test method for Al cosmetic corrosion that predicts in-service performance is precision in the test method. Precision of any test method is a function of test repeatability—the ability of a single laboratory using identical test equipment and identical test materials and protocols to obtain similar test results—and test reproducibility—the ability of two different laboratories using identical test materials, test equipment, test materials, and test protocols, to obtain similar test results. Many of the test methods examined in the course of this study failed to give repeatable and reproducible results and, as a result, were eliminated from further consideration.

Evaluation of in-service panel exposures shows that all of the panels that were prepared with metal finishing (sanding) prior to paint application exhibit a significantly higher level of cosmetic corrosion than those that were not sanded. Because of this observation, differentiation of the sanded panels from the nonsanded (mill finish) panels was the primary criterion for establishing correlation of accelerated corrosion test results to the in-service exposure results.

Another observation from some of the in-service panel exposures was the presence of S along with chloride in the corrosion product on Al panels. Therefore, to mimic corrosion products observed on in-service Al sheet corrosion in certain atmospheric environments, S may need to be included in the accelerated test exposure.

The accelerated corrosion tests that provided results most consistent with on-vehicle service relevant exposures for Al corrosion are modified ASTM G85–A2 and modified ASTM G85–A4. While the ASTM G85–A2 does not include S in the exposure, the acidic exposure provides the necessary environment to induce corrosion on Al that replicates the morphology of corrosion on the in-service panels.

Of all of the test methods evaluated in this project, modified ASTM G85–A2 appears to be the most reliable test for evaluating filiform corrosion of painted Al auto-body panels. The test method consistently provides the same relative ranking and cosmetic corrosion morphology as is observed in service relevant on-vehicle exposures.

Improved Automotive Suspension Components Cast with B206 Alloy (AMD 405)

Principal Investigator: Richard Osborne, General Motors Company
(248) 202-6963; e-mail: richard.osborne@gm.com

Introduction

The 206 alloy is significantly stronger than the 356 alloy and has mechanical properties approaching some grades of ductile iron and forged Al. It also has excellent high temperature tensile and low cycle fatigue strength, making the alloy an ideal candidate for suspension components. The 206 alloy is more expensive than 356, but the higher cost may be offset because less material may be required to provide the needed strength. The 206 alloy is seldom used despite its excellent properties, due to its propensity for hot cracking, need for rapid cooling rate to achieve target properties, and susceptibility to SCC in the T6 temper.

GKS Engineering has discovered a better method to grain refine this alloy through chemistry control, which reduces the tendency for hot cracking thereby improving castability. This, however, is insufficient to justify the selection of the B206 alloy for automotive applications without a complete assessment of the B206 mechanical properties across the alloy range, including heat treatment and susceptibility to stress corrosion. Stress corrosion is a primary concern as there is little literature and experience in testing and characterizing stress corrosion in Al casting alloys

The objective of this project was to provide complete technical and economic data needed to justify commercial use of this material in suspension components. High cooling rate is needed to achieve forging-like mechanical properties in the 206 alloy, but the alloy tends to be susceptible to hot cracking in processes that can achieve high cooling rates. GKS Engineering's contribution to improving grain refining has been shown to reduce hot cracking susceptibility; however, these results will not be accepted by the engineering community unless SCC and fatigue are also addressed. To provide a convincing argument, Phase 4 of this project produced and tested mule castings from an original equipment manufacturer (OEM)—forged 6082-T6 using semi-permanent mold and ablation casting processes. Testing included mechanical properties, component fatigue, and SCC. This information derived from control arm testing should be sufficiently convincing to allow automotive suspension engineers to consider and possibly select the B206 alloy as a lower cost alternative to forged Al and a lighter weight option than ferrous based solutions.

Approach

The work was conducted in four separate phases, as follows.

Phase 1: Determine the effect of alloy composition on mechanical properties in the T4 and T7 heat treated conditions and establish the feasibility of using less expensive versions of the alloy.

Phase 2: Study heat treatment of B206 alloy and establish combinations of solution and aging time and temperatures which produce desirable strength with stress corrosion immunity. This phase also evaluated improved T7 heat treatment cycles to increase elongation in this temper.

Phase 3: Create cost models for automotive suspension components produced by different processes and different materials.

Phase 4: Produce control arm castings using two different casting processes. Test components were produced in the T4 and T7 tempers, to provide required computer aided engineering (CAE) and design information, and establish the feasibility of using cast B206 alloy components to replaced forged Al parts.

Results and Discussion

Phase 4 of the project was completed during the 2010 fiscal year. During this phase of work castings, based upon an OEM forged 6082-T6 Al design, were produced from the B206 alloy to verify prior experimental findings. Prior work from Phase 1 of this project suggested using semi-permanent mold (Morel Industries) and ablation casting (Alotech) to make the control arms because both processes were believed to have sufficient cooling rates to achieve the target mechanical properties of the baseline forged control arm. Phase 1 of this project also provided optimized chemistries for both the T4 and T7 tempers of the B206 alloy. Control arms from both processes were cast and heat treated to the T4 and T7 tempers using the respective optimized B206 chemistries. Mechanical properties were measured for all four conditions (combinations of casting process and heat treatment). Semi-permanent mold T7 control arms (labeled PT7) were preselected for bench fatigue testing.

Table 1 summarizes the mechanical property results of the control arm castings. The process is identified by an "A" for ablation and a "P" for semi-permanent mold followed by the T4 or T7 heat treatment. The desired (target) properties, shown in the second column, are based on the production of forged Al control arms using the 6082 alloy in the T6 temper. With the exception of one case (the cell shaded in blue), the target properties were met or exceeded.

Table 1. Mechanical property test results from control arm castings.

	Target Values	AT4	PT4	AT7	PT7
Yield Strength (MPa)	270	278	299	277	332
UTS (MPa)	310	414	448	358	400
4D Elongation (%)	10	13.3	15.7	11.38	6.33
Modulus (Msi)	—	10.29	10.11	10.24	10.3
Poisson's ratio	—	0.331	0.326	0.332	0.325
stress constant, K (psi)	—	90,590	98,040	73,710	78,960
strain coefficient, <i>n</i>	—	0.144	0.147	0.108	0.085

Seven PT7 castings were machined and bushings and a ball joint were press fit into the control arms. The assembly was mounted on a full-scale test bench and stressed under cyclic load until fatigue failure occurred. The failure location was the same for all castings and the same as the baseline forged control arms. The castings gave a performance nearly equal to but slightly less than the forged control arms. However, these tests were made on PT7 castings, which had the lowest fatigue strength of all the castings. Better performance results would have been expected had the project bench test used PT4 castings.

A series of stress corrosion tests were also conducted on the control arm castings. The first series of tests were conducted from a relatively thick section of the casting. Eight of the AT4 samples passed the 30 day alternate immersion test. Another 12 AT4 samples failed after 2 to 5 days of exposure. All AT7 and PT7 samples failed within 5 days. These results were unexpected. There is considerable evidence to show that A206-T4 and A206-T7 are immune to stress corrosion failure, in particular, there is the study of knuckles used in several Ford models [14]. So what caused the premature failure?

The test samples were taken from a thick section of the casting where extensive microsegregation and porosity were present. The presence of significant porosity or large pores would explain the poor results. The test samples were quite small; only 3.1 mm in diameter; so large pores would significantly increase the effective stress applied to the sample and reduce stress corrosion life. Segregation is also an issue. Examination of the fracture surface in some failed specimens showed large amounts of copper- and iron-containing intermetallics. For these reasons a second series of tests was conducted from a thin section of the casting, where problems associated with intermetallics and porosity would be significantly less.

In the second series of tests all AT4 samples passed, but the AT7 and PT7 samples failed. This result show that porosity and microsegregation were important factors in the stress corrosion performance of this alloy. However there was another problem in the aged (T7) condition. In the case of the AT7 castings, an unconventional low temperature aging treatment was used. In the case of the PT7 castings, a standard T7 aging treatment was used, but these castings were subjected to a shorter solution heat treatment time and therefore contained a fair amount of undissolved copper along the grain boundaries.

A third set of tests was therefore conducted after subjecting samples to an improved heat treatment. These samples passed the 30 day test.

Conclusions

In summary, the results of this phase of study indicate the following.

- The B206 alloy can produce equivalent mechanical properties to forged 6082-T6 Al.
- Bench tests indicate that B206 will also be competitive with forged 6082-T6 Al with respect to component fatigue performance.
- The results of this phase also show that the heat treatment and thermal history of 206 alloy must be controlled carefully to avoid sensitivity to stress corrosion. Suitable heat treatments were identified, together with test procedures that may be used to establish that the desired immunity to SCC is present. This information is essential for alloy selection and product validation.

- In castings which have substantial thick sections, one must use a solution heat treatment time long enough to dissolve most of the Al₂Cu phase “decorating” the grain boundaries. The proper aging treatment for the T7 temper is 4 hours at 200°C. The use of lower temperatures will produce sensitivity to stress corrosion. Whatever heat treatment is used, it should be qualified for stress corrosion resistance before commercial production.
- Substitute sea water solution should be used for the 30 day alternate immersion tests. This gives significantly less pitting corrosion than the standard 3.5% NaCl solution and, consequently, is much less likely to give a false failure of samples because of pitting corrosion. Loading of samples at 75% of their yield stress is recommended for alternate immersion testing as long as a substantial amount of porosity is not present in the sample.

Powder-Metal Performance Modeling of Automotive Components (AMD-410)

Shekhar G. Wakade, General Motors Company
(248) 568-5845; e-mail: shekhar.g.wakade@gm.com

Paulo Rosa, Chrysler Group LLC
(248) 576-3197; e-mail: pr31@chrysler.com

Glen Weber, Ford Motor Company
(313) 322-0175; e-mail: gweber@ford.com

Eric McCarty, Materials Technologies Consulting, LLC
(248) 520-3009; e-mail: eric.mccarty@sbcglobal.net

Introduction

Unlike other material processing technologies, the PM industry lacked the simulation capability to readily evaluate design. Computer simulation models are needed to aid in the identification and risk of execution for the next generation of PM conversions. Past history has shown typical conversion savings from the current processes (forgings, stampings, castings, and machined components) to powder metal to be in excess of \$3 million. Weight savings are typically achieved via PM’s ability to produce more near-net-shaped components than competitive processes, and cost savings can be achieved through reduced post forming operations, such as machining. To properly engineer these components, it is necessary to understand the material and processing methods to obtain the mechanical behavior appropriate to the application. The accurate simulation of material behavior is vital for prediction of the performance of structural components. The approach is to develop and validate predictive models that describe the performance of nonforged PM components to reduce design time and development costs and aid in optimizing component weight and performance.

Approach

The project was divided into five tasks as described below.

Task 1: Determine current PM standards publications, component design guidelines, and manufacturing and evaluation methods and provide a selection of metal powders that can satisfy design performance requirements, component design guidelines, and manufacturing and testing specifications across industry participants.

Task 2: Evaluate and develop numerical modeling techniques to predict mechanical properties throughout PM component sections.

Task 3: Develop component and vehicle level testing to validate durability, quality control, and performance of PM parts.

Task 4: Manage and report program activities.

Task 5: Perform technology/commercial transfer throughout the product value chain.

Results and Discussion

The project ended in December 2009, and the final report was submitted in March 2010.

Conclusions

This project created powder metal compaction, sintering, and performance computer models and validated them using an engine main bearing cap. The models successfully predicted component performance by accurately predicting density and porosity through the compaction and sintering processes where traditional PM computer models failed. The new PM models were used to propose alternative designs that could reduce weight by 3.8% while increasing the monotonic strength by 5% and the fatigue life by 9.5% using the same iron-carbon powder. The project also identified opportunities to apply the models to Al and metal matrix composites using the same main bearing cap as a demonstration component.

Optimization of High-Volume Warm Forming for Lightweight Sheet Alloys (AMD 905)

Field Technical Monitor: Peter Friedman, Ford Motor Company
(313) 248-3362; e-mail: pfriedma@ford.com

Field Technical Monitor: Jugraj Singh, Chrysler Group LLC,
(248) 512-0029; e-mail: js329@chrysler.com

Field Technical Monitor: Ravi Verma, General Motors Company
(248) 807-4188; e-mail: ravi.verma@gm.com

Introduction

The need to improve fuel economy has led automakers to explore lightweight materials such as Al and Mg for automobile bodies and closures. While attractive from a mass perspective, these alloys have insufficient formability for some complex three-dimensional (3D) panels. Complex parts, such as door inners that can be stamped in mild steel, are difficult or impossible to stamp in Al or Mg using conventional methods. The lower formability of Al has led engineers to consider a variety of alternate forming methods including hydroforming[22], superplastic forming[23], quick plastic forming [24], electromagnetic forming[25], and warm forming[26].

Warm forming refers to sheet forming in the temperature range of 200°C to 350°C using heated, matched die sets similar to conventional stamping. The advantages of forming Al at warm temperatures compared to room temperature have been known for more than 30 years. Automotive industry researchers from General Motors, Ford, and Chrysler investigated warm forming and published, in varying detail, reports of successful forming trials in the late 1970s [27–32]. Other articles during the same time promoted warm forming as a technology of the future [26, 33], and a great deal of work was also done outside the automotive industry well into the 1980s [34–40]. However, emphasis on fuel economy waned in the 1980s, and as a result, interest in using Al also declined, so work on warm forming slowed. Recently, there has been an increase in work on the “warm behavior” of Al [41–47] and reconsideration of warm forming as a viable technology.[48]

Successful completion of two projects on warm forming (AMD 307 and AMD 602) has shown that this technology can be used as a cost-effective method of manufacturing complex 3D panels from both Al and Mg sheet alloys. In AMD 307, the process was demonstrated in a prototype mode on a one-piece door inner that was not feasible in either Al or Mg at room temperature. In AMD 602, a purpose built die was integrated into a fully automated forming cell to demonstrate the process under run-at-rate conditions. While the process was successfully demonstrated on both Al and low cost (twin-roll cast) Mg sheet, the die systems require complex heating strategies which will translate to high tooling costs and long lead times. The current project aimed at investigating nonisothermal methods of warm forming to further optimize the process in terms of production robustness and total cost. By controlling temperature locally on different elements of the die as well as the blank, the formability of these alloys can be significantly improved while process complexity and cost are reduced. This could include, as a technical stretch, complete elimination of heating of the forming tool.

Approach

The warm forming die developed in the previous project was designed to produce a deep draw pan as shown in [Figure 1](#). While this is a challenging part that mimics the type of deep draw needed to produce parts such as door inners, it is limited in that it does not produce a stretch condition in the interior of the stamping, as is commonly the case. This type of internal stretch is required in many production stampings, and therefore there is a need to simulate this condition in the development of new methods of warm forming. To accomplish this internal stretch, the warm forming die used in AMD 602 was modified to include a state of stretch in the middle of the panel.

A cylindrical feature was selected that would impart an axisymmetric stretch condition at the bottom of the pan. This required the fabrication of a new punch [[Figure 2\(a\)](#)] with a recessed feature in the middle. Consequently the die cavity was also modified to allow for the attachment of a cylindrical punch at the center of the tool to reverse the metal at the bottom of the pan. The new punch was designed so that it could be water cooled to help produce the nonisothermal condition targeted in this project. A schematic of the formed pan is shown in [Figure 2\(b\)](#).

The development of the automated warm forming cell in AMD 602 has created a unique capability to develop the warm forming system under production conditions.

One persistent disconnect with the development of warm forming technology is that experimental trials are typically conducted in a laboratory environment where it is difficult to simulate the fast and consistent transfer of the heated blank in to the warm forming die.

This is typically not a roadblock when exploring warm forming under isothermal conditions because the cooling of the heated blank is not an issue as the heat from the die can bring the blank back to temperature before forming. However, in nonisothermal warm forming the heat loss during transfer of the blank, idle time before forming, and the speed of the press are critical parameters in the development of the process. In the planned forming trials in this project the warm forming cell developed in AMD 602 will be used so these variables can be tightly controlled.

Results and Discussion

The first set of experiments was performed at room temperature to establish baseline formability of 1.5 mm thick AA5182 sheet using Fuchs' solid lubricant, Forge Ease 278, diluted to work with sheet metal stamping. A constant draw depth of 71 mm was used for the pan, while the feature depth was increased in steps of 1 mm. The results are shown in [Table 1](#). The maximum feature depth achieved at room temperature (with no localized thinning/necking) was determined to be 12 mm. These experiments were repeated using a conventional lubricant (Quaker Chemical's Ferrocote 6130) currently in use by the OEMs. This oil based (conventional) lube performed comparably to the solid lube and successfully made the feature depth of 12 mm.

The next set of experiments was performed with sheet blanks heated to 270°C, with cold (room temperature) die and solid lube. These results are also included in [Table 1](#). The feature depth achieved increased to 25 mm. This is a significant improvement over room temperature and should meet the formability requirements of the most demanding of automotive closure panels. Photographs in [Figure 3](#) visually depict the maximum feature depths achievable with blanks at room temperature (pan 51), and at 270°C (pan 50).



Figure 1. Photograph of the panel formed in the warm forming die in the AMD 602 project.

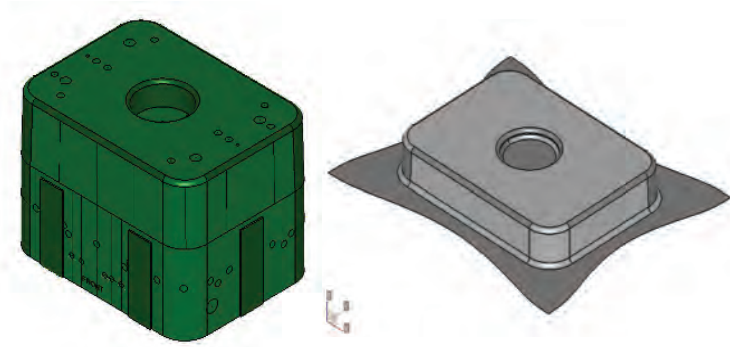


Figure 2. Computer aided design representation of (a) the new punch for the warm forming die showing the depression in the center which creates the stretch condition and (b) the formed panel.

Table 1. Forming results for cold die trial.

Panel number	Blank temp. (C)	Pan depth (mm)	Feature depth (mm)	Result
52	Room temperature 1	71	-	Good
51	Room temperature	71	12	Good
33	Room temperature	71	13	Necking
50	270	71	25	Good
49	270	71	26	Fracture
58	Room temperature	100	-	Fracture
61	270	100	-	Good
63	270	100	23	Good
62	270	100	24	Fracture

The improvement of the limiting feature depth as a function of blank temperature is plotted in Figure 4. There is no significant increase in maximum feature depth until the temperature is raised beyond 150°C. At 200°C the limiting feature depth increases to 19 mm and at 270°C to 25 mm.

These nonisothermal experiments were repeated to understand the nature of material flow (stretch vs draw) in the forming of the feature. For this purpose, blanks were marked with a circle (60 mm diameter) concentric with the feature and orthogonal lines (length 200 mm) through the center. Measurements made on the circle and lines before and after forming were used to calculate average strain locally within the feature bottom, or globally within a larger area of the pan bottom, in the two orthogonal directions (see insert in Figure 4). These results are plotted in Figure 5 as strain vs temperature plots. Global width and global length strains are very small in magnitude and show little or no dependence on temperature. On the other hand, local width and local length strains appear to be the major contributor to the feature formation and show strong relationship with temperature. The increase in these strains is very similar to the increase seen with the feature depth when blank temperature is increased from room temperature to 270°C. Because the pan draw is almost complete when the feature tool starts dipping into the pan bottom to create the feature, it is not surprising to see that the feature is a result of almost pure stretch and very little draw.

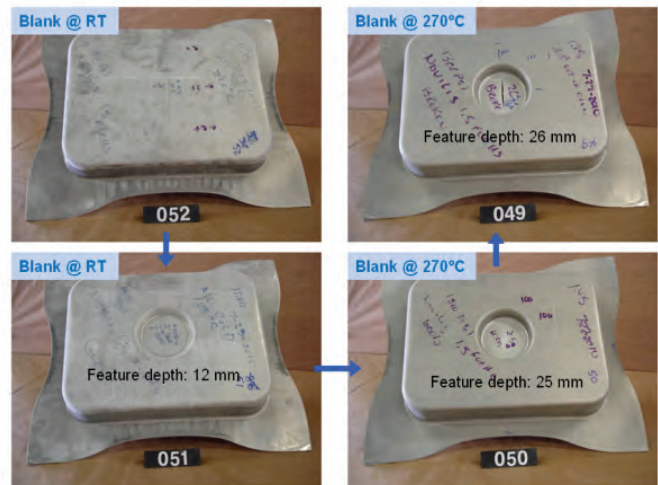


Figure 3. Photographs of pans formed at a draw depth of 71 mm showing limiting feature depth at room temperature (RT) (051) and 270°C (050).

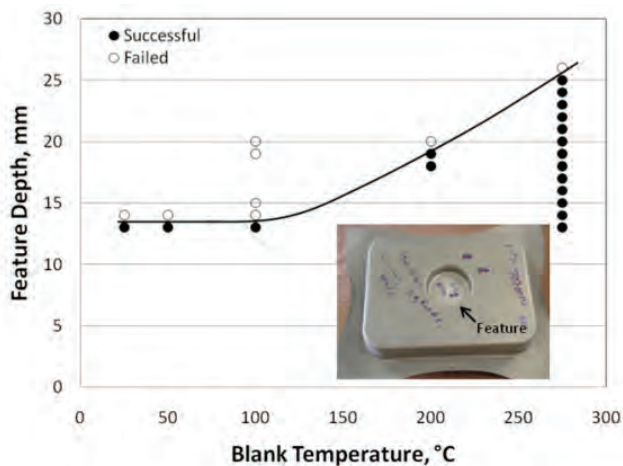


Figure 4. Feature depth plotted as a function of blank temperature for cold die trials at a pan draw depth of 71 mm.

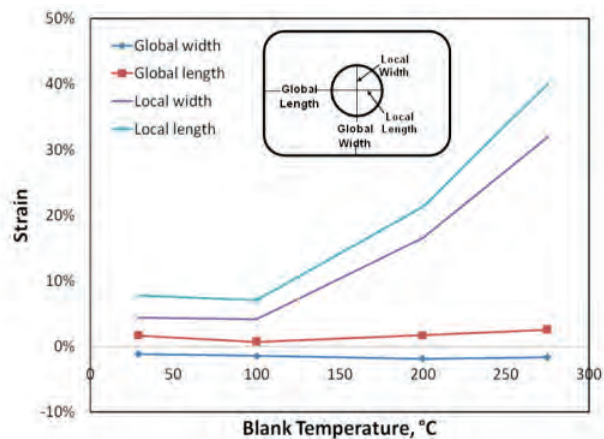


Figure 5. Measured local strains plotted as a function of blank temperature for cold die trials at a pan draw depth of 71 mm).

To further study the benefits of nonisothermal forming, the pan draw depth was increased to 100 mm and forming experiments were run again with blanks at room temperature and at 270°C. As shown in Figure 6, the panel could not be drawn successfully to 100 mm depth with the blank at room temperature (panel #58). However, at 270°C panels could be drawn successfully to 100 mm depth and achieve a maximum feature depth of 23 mm. Thus, with the blank at 270°C, the pan draw depth was increased from 71 mm to 100 mm, with only slight decrease in the maximum feature depth from 25 mm to 23 mm. It appears that the large blank size used for the 100 mm draw most likely resulted in larger strains in the bottom of the pan, which lowered the limiting feature depth. Changes to the binder to adjust the feed rate with the bigger blank would most likely result in a feature depth that is more or less independent of the panel draw depth.

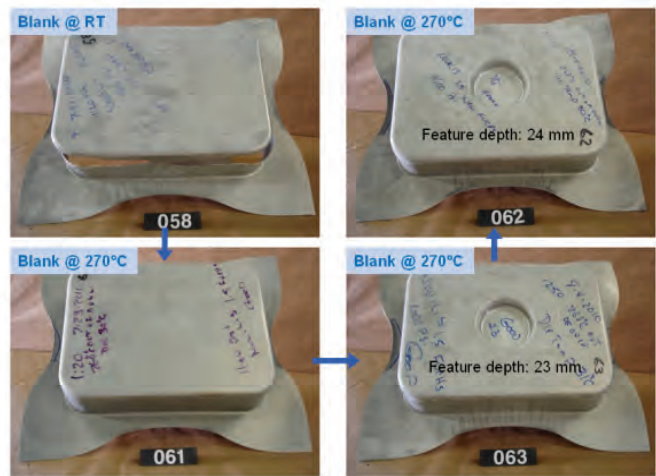


Figure 6. Pans formed to a draw depth of 100 mm at room temperature (RT) and 270°C.

Magnesium

Compared to Al, Mg has the potential for even greater weight savings over steel and iron (~40%–65%). However, the implementation of Mg in the automobile industry has significantly lagged the implementation of Al at least in part due to a weak infrastructure and a lack of maturity with respect to the processes required to implement Mg components. As a result, AMD has chosen to emphasize funding of several Mg projects over the past few years, including the following.

- A Mg powertrain cast components project.
- High integrity cast Mg suspension components development.
- A Mg front end research and development project.

Magnesium Front End Design and Development (AMD 603)

Principal Investigator: Alan A. Luo, General Motors Company
(248) 912-8254; e-mail: alan.luo@gm.com

Principal Investigator: David A. Wagner, Ford Motor Company
(313) 845-2547; e-mail: dwagner6@ford.com

Principal Investigator: Stephen D. Logan, Chrysler Group LLC
(248) 512-9485; e-mail: sl16@chrysler.com

Introduction

The Magnesium Front End Design and Development (MFEDD) project (AMD 603), which concluded on March 31, 2010, was the companion design activity to AMD 604 (Magnesium Front End Research and Development). Whereas the research portion of the Mg front end effort focused on a broad range of knowledge based, part-forming, and enabling manufacturing technologies for Mg alloys, MFEDD was strictly devoted to development of actual vehicle substructure designs implemented primarily in Mg alloys and technical cost modeling of the envisioned manufacturing and assembly processes, including the extractive metallurgy of Mg. The effort drew primarily on existing proprietary designs for two exemplary vehicle architectures and hence was limited in participation to the USAMP partners and two selected suppliers. The computer aided design (CAD) and CAE methods used permitted accurate determination of both actual weight savings and performance attributes including crashworthiness, mechanical stiffness, vibrational modes, and durability (fatigue). Technical cost modeling analysis provided insights into manufacturing aspects commanding special attention for continued research (e.g., joining and surface treatment).

Approach

Computer Aided Design and Engineering. Cosma Engineering (Troy, MI) was selected as the supplier for the Mg-intensive front end designs and concomitant CAE. Figure 1 illustrates the exemplary vehicle designs considered—(a) unibody (or body-frame-integral) architecture, used primarily in passenger cars, and (b) body-on-frame, more typical of light trucks. The overall design approach had three phases: (1) an initial or “first order” design completed rapidly, using handbook material properties and best understanding of intended manufacturing methods; (2) a second iteration using improved knowledge of material properties gleaned from the companion MFERD project; and (3) an optimized design based on improvement of material properties achieved through ongoing research within MFERD. Realistically, material property optimization remains an ongoing challenge, and current results reflect mainly the second iteration step. At each stage of development, the supplier produced structural weight reductions relative to baseline (steel), bill-of-materials, assembly sequence and methods, and performance metrics, including structural stiffness and crashworthiness obtained from CAE methods using handbook or actual mechanical properties of the materials selected. Ongoing design reviews provided the principal means by which the supplier provided concepts and updates, with opportunity for discussion and recommendations from the OEM community of experts. The final design reviews at project conclusion incorporated the culmination of all supplier deliverables over the course of the project.

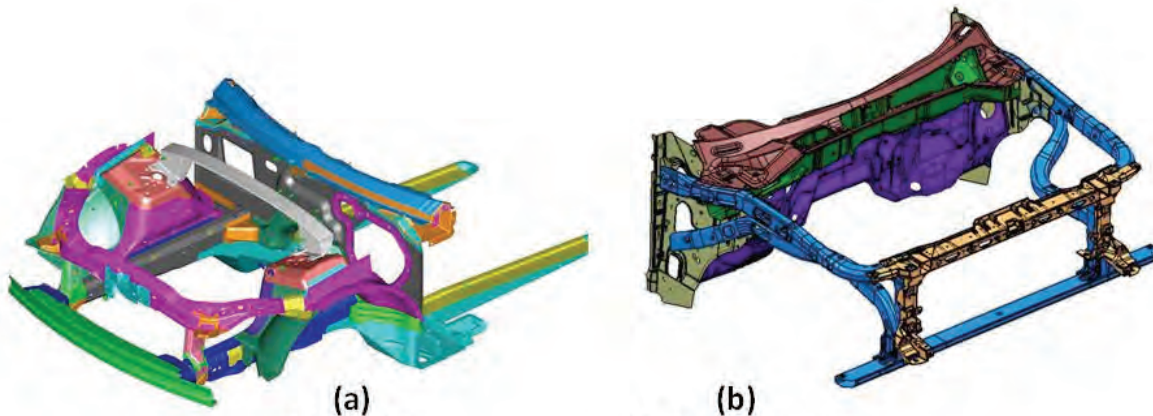


Figure 1. Baseline vehicle substructure architectures for design studies based on Mg substitution for current steel usage: (a) unibody or body-frame-integral and (b) body-on-frame.

Technical Cost Modeling. Camanoe Associates (Cambridge, Massachusetts) was selected to conduct technical cost modeling of the manufacture of the two vehicle substructures as implemented in Mg or combinations of Mg and other materials (e.g., extruded Al). The supplier used a process based cost-modeling system in which manufacture of an object is reduced to a sequence of process steps which are then independently analyzed according to commonized procedures and economic factors (e.g., labor rates, cost of capital). The model then permits calculation of “what if” scenarios typically used to gauge production volume effects and sensitivity analysis to assess impact of certain key variables (e.g., cost of electricity, base materials). For this project, the supplier was also requested to provide technical cost modeling of the two principal extractive metallurgy processes for Mg: electrolytic reduction and silicothermic reduction (i.e., the “Pidgeon” process).

Results and Discussion

The project concluded March 31, 2010, and pertinent detailed findings were presented in the DOE semiannual report of May 2010. A summary of project conclusions is included here for completeness.

For the unibody structure, the final net weight reduction relative to the all-steel baseline was 44.57 kg or 45%. This result was predicated on replacement of extruded Mg front rails with Al extrusions as required to achieve acceptable crashworthiness. Other Al components (e.g., floor pan front) were also included in the final design. The part count reduction achieved by the integration achievable through the die-casting process was 59.26% (44 pieces for the Mg structure vs 108 pieces in the steel baseline). All specifications for vehicle stiffness, durability (fatigue), vibrational modes, and crashworthiness were met or were within acceptable limits. The materials technologies used included: 15 Mg super vacuum die cast AM60B castings, one Mg AM30 extrusion, four AZ31 formed Mg sheet parts, six Al extrusions, 10 formed Al sheet parts and eight miscellaneous Al parts (weld nuts and fasteners). Joining technologies included adhesive bonding, friction stir welding (FSW), metal inert gas welding, and self-piercing and break-stem rivets. The corrosion protection strategy relied on initial pretreatment of all constituent components before the substructure assembly process (mainly due to requirements for adhesive bonding). The

ability to provide polymeric topcoating to the substructure via the conventional vehicle paint shop will be a research topic of MFERD Phase II. The cost models in this case considered a separate paint operation for the front end substructure. For 100,000 vehicles/year, the cost penalty for the Mg-intensive substructure relative to the baseline steel structure was about 44%, with an estimated penalty per kilogram of weight saved of \$5. This number was an improvement over the original project target of \$8 per kilogram of weight savings.

In the case of the body-on-frame architecture, the baseline structure was very mass efficient by virtue of using both hydroformed tubular steel members as well as a partial Mg grill surround and support. Nevertheless, the weight savings achievable through increased use of Mg was 14.19 kg or 24.8%. Two component parts of the original 20 were eliminated as a result of integration. The breakdown of technologies was seven Mg die castings, four steel stampings, six Al stampings, and one plastic injection molding. The Mg-intensive structure met all physical requirements of crashworthiness, stiffness, modal signatures, and durability. Proposed joining strategies included adhesive bonding, fasteners, rivets, and resistance spot welding of steel components. The corrosion protection strategy was nominally the same as for the unibody insofar as pretreatment of component parts, assembly, and topcoating before integration into the remainder of the body structure. The issue of galvanic isolation for the Mg structure remains under investigation and will be an item of content for MFERD Phase II. The approximate cost penalty for the increased Mg usage was 29% above baseline steel, resulting in a penalty per unit weight savings of about \$5.80 per kilogram.

The technical cost models developed included a breakdown by rough part formation (e.g., die casting, sheet forming, extrusion), joining, and finishing (corrosion protection) processes. Additionally, cost models were developed for the two principal extractive metallurgy processes for Mg: electrolysis and silicothermic reduction (the Pidgeon process). These analyses suggested “modeled” costs of production using U.S.-based economics of about \$4.90 per kilogram for the electrolytic process and \$4.10 per kilogram for the Pidgeon process. These numbers were in rough agreement with Mg ingot pricing in the United States at the time of the analysis. The roughly 20% premium attributable to the electrolytic process was largely ascribed to capital investment despite relatively higher costs of both labor and energy for the Pidgeon process.

Conclusions

At its conclusion, the MFEDD project showed via modeling and engineering studies that weight savings approaching 45% of the baseline steel unibody substructure were achievable with a geometrically equivalent Mg-intensive structure using commercially available alloys and manufacturing methods. Acceptable crashworthiness of this structure could only be warranted with substitution of extruded Al at key crush points of the structure. For the body-on-frame structure, a weight savings relative to the baseline of about 25% was realized with no compromise of any physical attribute. Cost penalties relative to baseline were about 30% for the body-on-frame and 44% for the unibody. Identifiable challenges were revealed for joining and corrosion protection technologies that impact the cost structures of the assemblies considered.

Magnesium Front End Research and Development (AMD 604, AMD 904)

Principal Investigator: Alan A. Luo, General Motors Company
(248) 912-8254; e-mail: alan.luo@gm.com

Principal Investigator: David A. Wagner, Ford Motor Company
(313) 845-2547; e-mail: dwagner6@ford.com

Principal Investigator: Stephen D. Logan, Chrysler Group LLC
(248) 512-9485; e-mail: sl16@chrysler.com

Introduction

The Magnesium Front End Research and Development (MFERD) projects (Phase I-AMD 604 and Phase II-AMD 904) incorporate ongoing technical discussions and collaborative research with counterpart organizations in the United States, Canada, and the People’s Republic of China. The technical objective is the development of engineering expertise and

manufacturing capabilities that permit the realization of integrated, Mg-intensive, automotive substructures having substantial weight reduction (target: 60%) and comparable performance to steel-based baselines. The precursor project, USAMP Project AMD 604, was launched in November 2006 and concluded on March 31, 2010. On April 1, 2010, USAMP launched Phase II (AMD 904). Whereas Phase I focused on the knowledge base for engineering with Mg and development of enabling technologies of manufacture for the intended constituent components of the envisioned front end structures, the Phase II goal is to design, fabricate, and test a demonstration structure having attributes of an idealized fabricated and finished Mg-intensive automotive front end substructure.

Approach

Phase I. Design aspects for the hypothesized Mg front end substructures were treated in a separate project (AMD 603) to protect OEM proprietary information associated with donor structures. For MFERD Phase I, vehicle attributes were broadly classified as either “knowledge-based” [i.e., crashworthiness, NVH, durability (fatigue) and corrosion] or “enabling technologies” (extrusion, sheet forming, casting, and joining), and corresponding task teams were organized both nationally and internationally to identify and address supporting objectives and work statements. A project management structure including an international project steering committee (PSC) and project technical committee (PTC) was adopted, and regular meetings of these committees were convened. The technical task committees also met both nationally and internationally during Phase I. Annual review meetings were organized and comprehensive reports were published in both English and Chinese [1, 2]. The final review for Phase I will be conducted as part of the Three-Country Annual Meeting on October 25–27 in Ann Arbor, Michigan.

Phase II. In 2009, the international project participants agreed to develop a Phase II project continuation with the primary goal of developing and producing a demonstration structure to exercise the various knowledge- and technology-based features of integrated Mg-intensive structural assemblies, of which the vehicle front end is exemplary. At a meeting of the PSC-PTC committees in March 2010, a draft work statement for Phase II was adopted and details of the task team objectives were presented. Continued planning and initial progress on Phase II will be pursued at the 2010 Annual Meeting in October 2010. **Figure 1** illustrates the principle of the conceptualized demonstration structures: (a) represents a structure using the super vacuum die casting (SVDC) “shock tower” developed and manufactured in Phase I and (b) represents an example of an entirely new approach wherein individual component pieces would be designed and fabricated specifically for the demonstration structure. Both demonstration structures are intended to use all Mg material forms of interest (e.g., sheet-formed parts, extrusions, and die castings) and permit experimentation with various joining and finishing methods. Partner countries and organizations would contribute to experimental component fabrication, assembly, finishing, and testing through a variety of mechanical, durability, and corrosion procedures.

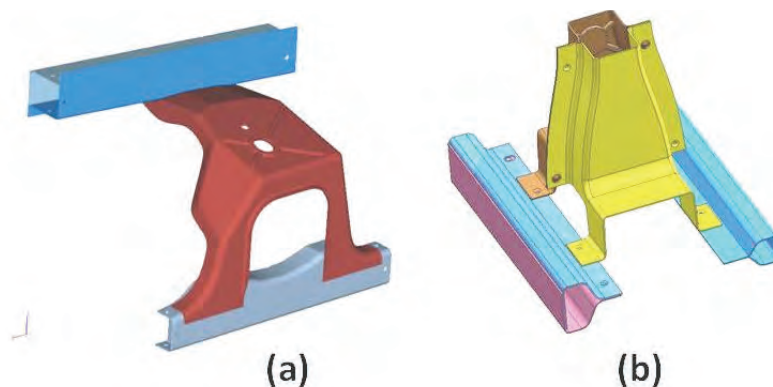


Figure 1. Exemplary Mg demonstration structures using attributes of vehicle body substructures: (a) design using existing shock tower casting; (b) entirely novel concept design.

Results and Discussion

The following section provides summary statements reflecting concluding status of AMD 604 (Task 1) and technical objectives for AMD 904 (Task 2).

Task 2.0 (Design)—(New to MFERD) Evaluated six concept designs from three automotive design and engineering firms in 2010 of which two examples are shown in Figure 1. The team will select and launch a principal approach for the MFERD

Phase II demonstration structure including final design CAD, tooling design and fabrication, component fabrication, assembly, and testing protocols.

Tasks 1.1/2.1 (Crashworthiness)—The ongoing impediment to successful implementation of current Mg alloys on the critical loading path for structural “crash” elements such as frame rails is the limited ductility of Mg (strain to fracture) in castings and the highly anisotropic nature of deformation and fracture of wrought Mg compounded by crystallographic texturing that occurs during forming. These effects derive from the basic physical metallurgy of Mg and may ultimately be addressed only through fundamental improvements in alloy design and processing. Although texturing generally does not arise in cast structures, ductility is limited more by processing artifacts such as porosity, which may be minimized through approaches such as SVDC. Phase II efforts will include investigation of novel Mg extrusion alloys intended to be more resilient under impact conditions (Task 2.5). USAMP design efforts, however, indicate that Al alloy substitution for impact members can produce effective overall structures with only nominal weight penalty relative to exclusive use of Mg.

Task 1.2/2.2 (NVH)—All Phase I work on characterization is complete. Sound transmission through Mg metal at higher frequencies (>1,000 Hz) remains a fundamental problem addressable chiefly by design and material acoustic insulation or “sandwiching,” which adds to the technical complexity of using Mg in such applications as the dashboard structure. Damping capability of Mg for lower frequency vibrations is comparable to that of Al castings. Phase II efforts will focus on characterization of sound transmission from engine to passenger compartment for an actual production vehicle Mg component (Dodge Viper front-of-dash) and developing and validating countermeasures for this specific application.

Task 1.3/2.3 (Durability/Fatigue)—Phase I focused attention on round-robin fatigue testing of extruded AM30 and AZ31 sheet, showing generally good agreement among the laboratories involved. Additionally, round-robin evaluation of friction stir spot welds was completed, again with excellent interlaboratory agreement. Phase II will focus on extending fatigue characterization of joints, seen as the critical point of concern for durability of integrated structures such as the front end. Environmentally assisted fracture including SCC and corrosion fatigue will be addressed in Task 2.4.

Task 1.4/2.4 (Corrosion and Surface Treatment)—Phase I identified preferable pretreatment and topcoat options for the Mg alloys under consideration, considered manufacturing scenarios, and offered a protocol for assessment of coatings to steel fasteners for use with Mg alloys. In Phase II the U.S. team will establish both pilot line capability for the full range of magnesium surface treating before assembly of the demonstration structure and polymer encapsulation of the entire structure after assembly. The Canadian and Chinese teams will focus their attention on matters of environmentally assisted fracture.

Task 1.5/2.5 (Extrusion)—All Phase I tasks were completed and prototype extrusions of AM30 and AZ61 were delivered to the task teams. Task 2.5 will focus on manufacture of piece parts for the demonstration structure and evaluation of novel extrusion alloys having improved mechanical properties suitable for crash-sensitive vehicle structure applications.

Task 1.6/2.6 (Sheet Forming)—This task was coordinated with AMD 602 (warm forming of Mg sheet). In Phase I mechanical properties of various commercial sheet materials at room and elevated temperatures were measured. Phase II efforts will focus on characterization of novel con-cast sheet material becoming available to the project (Canada Centre for Mineral and Energy Technology) and production of prototype component parts for the demonstration structure.

Task 1.7/2.7 (High-integrity Body Castings)—All Phase I objectives have been completed including the development and demonstration of a novel SVDC process for AM60B and investigation of improved mechanical performance from base AM60 with additional Al. Phase II will focus on establishment of suppliers for SVDC die castings; production of prototype parts for the demonstration structure; and investigation of novel die casting alloys with improved mechanical strength, ductility, heat treatability, and weldability.

Task 1.8/2.8 (Welding and Joining)—Phase I resulted in notably increased understanding of adhesive bonding and FSW (both friction stir spot and linear welding) for the Mg alloys of interest, including assessment of key parameters, measurement of sustainable loads, and limited assessment of fatigue durability. Mechanical attributes for use of threaded fasteners and thread-forming fasteners were also developed. The U.S. Phase II will focus on continued development of FSW, adhesive bonding, and self-piercing rivet technology, with emphasis on the introduction of thermally assisted processes to facilitate joining of Mg. Task 2.8 will also include activities associated with the joining of component parts into the assembled demonstration structures.

Conclusions

MFERD Phase I (AMD 604) concluded in 2010 with completion of all outstanding supplier contracts and deliverables. Phase II was launched with the specific objective of implementing Phase I knowledge and manufacturing outcomes into a physical demonstration structure suitable for validation of the principles and qualifications suitable for mass manufacture of actual vehicle structures predicated on integration of various forms of suitable Mg alloys and other constituents into complex articulated subassemblies.

Integrated Computational Materials Engineering for Magnesium (AMD 703)

Principal Investigator: Mei Li, Ford Motor Company
(313) 206-4219; e-mail:mli9@ford.com

Principal Investigator: Louis Hector, General Motors Company
(586) 651-2628; e-mail:louis.hector@gm.com

Introduction

Integrated Computational Materials Engineering (ICME) is an emerging paradigm within the materials community, wherein advanced computational tools are used over a wide range of material length scales to predict the macroscopic behavior of materials using microstructural and processing knowledge [1]. AMD 703 is a companion project to the USAMP Magnesium Front End projects (AMD 603, 604, and 904) aimed at using the tools and methodologies of ICME to address specific materials issues associated with the understanding and implementation of Mg alloys for practical applications (i.e., automotive body substructures). The project exploits a range of interactions with the international materials communities, suppliers, universities, and technical societies (e.g., TMS) with the intent of rapidly developing an integrated suite of computational tools for Mg alloy design, processing, and use.

Approach

AMD 703 launched in 2007 as a companion to AMD 604 (MFERD), with particular focus on national and international efforts devoted to ICME of Mg alloys. USAMP principals also contribute (via USAMP AMD 702) to a separate DOE project at the Center for Advanced Vehicular Studies at MSST, having various linkages to ICME topics and data for Mg alloys. The MSST activities are reported separately from this document.

For organizational purposes, the ICME of Mg has been structured as follows: Task 1—Cyberinfrastructure; Task 2—CALculated PHase Diagrams (CALPHAD), Diffusion Infrastructures, and Database; Task 3—Processing-Structure-Property Relationships for Extruded Magnesium Components; Task 4—Processing-Structure-Property Relationships for Sheet Magnesium Components; Task 5—Processing-Structure-Property Relationships for Die-Cast Magnesium Components; Task 6—Multi-Attribute Design Optimization; and Task 7—Multistage Fatigue Model. Of these tasks, 2, 3, 4, 5, and 7 receive direct support from USAMP to universities or other suppliers, while the remainder are funded chiefly through MSST's project, albeit with common reviews and interactions with the USAMP partners and suppliers. DOE laboratories (Pacific Northwest National Laboratory and Oak Ridge National Laboratory) also have principal investigators participating in Mg ICME. These efforts are reported separately.

The task teams meet semiannually to review objectives and discuss results. Certain results coming from the various tasks are also incorporated as data into the “cyberinfrastructure,” which is maintained as an internet resource by MSST. The cyberinfrastructure is apportioned into two different types of representation: (1) a SharePoint site which permits file placement and exchange and (2) a more recent “wiki” site which performs more like the familiar Wikipedia in its organization, content, and navigation.

Results and Discussion

Task 1. Cyberinfrastructure. TMS supported various initiatives contributing to Mg ICME during 2010. In particular, TMS hosted and supported an entire symposium dedicated to Mg ICME at its annual meeting, February 15–19, 2010, in Seattle,

Washington. A list of relevant presentations from that symposium is included in the “references” section at the end of this report. The majority of these works reflect interactions with and support by the USAMP program and the companion program at MSST.

Task 2. CALculated PHase Diagrams (CALPHAD), Diffusion Infrastructures, and Database (Materials Informatics, LLC). The primary objective of this work is the development and deployment of an extensible, self-optimizing magnesium phase equilibrium infrastructure (ESPEI), a computer graphical user interface, and associated software which will largely automate the thermodynamic modeling of alloy systems (e.g., Mg-Al) using existing databases for phase equilibria and accompanying thermodynamic values such as enthalpy and entropy associated with formation of solutions and multiphase systems. The work by Materials Informatics, LLC, is also linked to the use of thermodynamics databases and software for prediction of phase equilibria such as “Thermo-Calc.” Thermo-Calc Software, Inc., is also a program participant in AMD 703 and during this period has worked extensively with Materials Informatics, LLC, in achieving a demonstrable version of the ESPEI software and user interface. A beta test version of ESPEI, as developed by this project, was provided to Carpenter Technology Company, for use in assessing the performance of the software package, albeit for material systems other than Mg. In the current version of ESPEI (version 1.3), the database development phase enables the automation of solution phases (e.g., fcc, bcc, hcp, and liquid phases) and stoichiometric and nonstoichiometric compounds.

The work of Northwestern University is aimed at first principles calculation of thermodynamic and transport parameters at the atomic level (e.g., formation energies for vacancies and solute atoms) for the alloy system Mg-Al-Zn, which would govern behaviors of such practical alloys as AZ91 (a principal die casting alloy) and AZ31 (the main sheet alloy of interest to the project). The calculations are based on quantum mechanics principles as applied to various alloy and intermetallic compound crystal structures, in particular using the special quasi-random structure (SQS) approach which uses calculational “cells” which, while having some degree of order, also approximate more random solid solutions.

These calculations for the Mg-Al-Zn system suggest a more negative mixing enthalpy for the solution phase than understood from CALPHAD assessments, giving some credence to the use of such first principle methods for situations where experimental data are questionable or nonexistent due to slow kinetics.

Task 3. Processing-Structure-Property Relationships for Extruded Magnesium Components. USAMP contributes to this task through efforts at General Motors, Ford, and Chrysler and interrelated projects funded through MFERD at Lehigh University and Applied Magnesium (formerly Timminco), which consist primarily of supply and characterization of billet stock and extruded forms in alloys of interest (e.g., AM30, AZ61) and novel alloys suggested for improved extrusion behavior and resultant properties of extruded profiles.

Task 4. Processing-Structure-Property Relationships for Sheet Magnesium Components. The University of Virginia and General Motors are primary contributors to this task, with additional work being conducted at MSST and Ohio State University and through projects AMD 602, successor project AMD 905, and AMD 904 (and successor project to AMD 604). The primary thrust of this task is the development and validation of constitutive models which permit the assessment of warm-forming behavior for sheet Mg, given critical parameters of initial texture and temperature and such phenomena as crystal plasticity and dynamic recrystallization. In 2010, the University of Virginia demonstrated constitutive equations for Mg deformation at elevated temperatures which incorporated dynamic recrystallization into earlier viscoplastic, self-consistent models with good experimental agreement established through tensile-compression tests. In particular, tensile-compression tests on AZ31 sheet (1.0 mm) were conducted at elevated temperatures using special fixtures at Ohio State. The role of twinning and detwinning in warm forming of Mg (AZ31) was then assessed to be minimal. A complete constitutive equation which can be used to determine formability and properties of warm-formed components from Mg sheet remains under development.

Task 5. Processing-Structure-Property Relationships for Die-Cast Magnesium Components. The main contributors to this task are the University of Michigan, Ford Motor Company, and MAGMA Foundry Technologies, Inc. Efforts are focused on determination of phase distributions in die castings (e.g., β phase in AZ91) through the use of simulation software (property and thermal history mapping of die castings) and assessment of microstructural influences on the intrinsic strength of Mg, AZ91 (University of Michigan). The University of Michigan has also provided data and analysis for fatigue properties (Task 7) of SVDC-cast AZ91 shock towers. Within this task, the University of Michigan has determined microstructures within the prototype shock tower die casting and observed influences of the solidification and thermal history using MAGMA’s software. Ford’s efforts are directed to the assessment of β -phase (Mg₁₇Al₁₂) precipitation in AZ91 and determination

of its phase-field distribution and likely influences on mechanical properties such as may be influenced by solution and precipitation phenomena. A portion of this work is based on first-principles calculations of thermodynamic and interfacial stability for precipitation of the β -phase.

Task 7. Multistage Fatigue Model. The principal contributors to this task are the University of Michigan, Ford Motor Company, and MSST. The University of Michigan's principal subtask has been the measurement of localized microstructures, mechanical properties, and fatigue performance within super vacuum high pressure die castings of which the vehicle shock tower die casting developed in MFERD Phase I is exemplary. During this period the University of Michigan has extracted samples from differing regions of AZ91D shock towers and assessed both microstructures and fatigue properties. It was also found in these studies that T6 heat treatment had little effect on fatigue properties of AZ91D under conditions considered for the materials at hand, the greater influence on fatigue stress and associated lifetime being assigned to the localized extent of porosity, influenced largely by the nature of the die casting process. While gas-induced porosity due to the turbulent nature of the die-casting process may be reduced by techniques such as the super vacuum process, shrinkage porosity may be unavoidable.

Conclusions

In its fourth year, AMD 703 continues to enjoy good communication among the various task teams, both as subcommittees and as a collective effort through the semiannual reviews and special symposia such as that at the TMS 2010 Annual Meeting. The cyberinfrastructure as envisioned is continuing to be populated with mechanical, microstructural, and other key data as used in ICME. First principles and thermodynamics efforts are yielding key factors for basic Mg metallurgy, and efforts on wrought Mg as sheet or extrusion are providing a measure of predictive capabilities that might be used in manufacturing. Shortcomings of die-cast Mg are historically known, as are those of wrought products, and ICME is suggesting even greater emphasis on porosity reduction in die castings, as a key limiter of both ductility and fatigue life, at this point overwhelming improvements in basic mechanical properties of the metal as might arise for example from precipitation strengthening.

High Integrity Magnesium Automotive Components (AMD 601)

Field Technical Monitor: Richard J Osborne, General Motors Company
(248) 202-6963; e-mail: richard.osborne@gm.com

Introduction

The HIMAC project (AMD 601) addresses the near- and midterm metal casting development needs identified in both the project's original SOW and the previously published Magnesium Vision 2020 document [86] that was requested by DOE (FY 2005) and included in the final report of the Structural Cast Magnesium Development Project (AMD 111 and AMD 112). Understanding and eliminating the technical barriers that currently inhibit Mg casting production will move the automotive industry into a better position to realize emerging automotive Mg component needs, build needed Mg industry infrastructure, and develop tools that will be required to reduce the cost of Mg components and enable sustainable production requirements.

Casting Al components today involves process support systems such as thermal treatments, grain refinement, and models to identify hot tear and porosity to produce Al automotive components. None of these support systems have been successfully developed (or used) for casting Mg components, and consequently, they are termed "barriers" by the manufacturers. Without a proven support system using the technologies developed for the Al industry, the production of high integrity Mg automotive components will not be successful. These known manufacturing barriers will be investigated and developed for the HIMAC casting processes. The barriers were subdivided among the eight project tasks and assigned to industrial and/or academia personnel for investigations and solutions.

- Task 1: Squeeze casting process development
- Task 2: Low pressure casting process development
- Task 3: Thermal treatment of castings including research into stepped heat treatment and fluidized beds
- Task 4: Microstructure control during casting including grain refining and property improvement

- Task 5: Computer modeling and properties to enable prediction of casting quality and microstructure
- Task 6: Controlled molten metal transfer and filling
- Task 7: Emerging casting technologies
- Task 8: Technology transfer

The investigation, development, and conversion of existing, different types of Al casting processes that are identified in the HIMAC project to Mg will provide new manufacturing process information to suppliers of Mg components. In addition, the detailed results of the processes that have been converted to Mg will provide suppliers with some alternative choices for manufacturing Mg automotive components.

Approach

The goal of the HIMAC project was to investigate and develop several existing Al casting technologies and processes (e.g., squeeze casting and LPPM); to manufacture cast Mg automotive suspension components; to evaluate the potential of new emerging casting technologies for the use of Mg, specifically the ablation and T-Mag processes; and to investigate the controlled molten metal transfer of Mg into molds using an EMP (Table 1).

Table 1. Casting processes.

Supplier	Task	Casting process
Meridian	1	Squeeze casting process development
Contech	1	Squeeze casting process development
ATD	2	Low pressure casting process development
Marlatt Technologies	2	Low pressure casting process development
CMI Novacast	6	Controlled molten metal transfer and filling
Alotech LTD	7-A	Ablation process
T-Mag PTY LTD	7-B	T-Mag process

The development of these processes addressed the need to solve critical technology barriers, including microstructure control, porosity and hot-tearing, thermal treatments, and controlled mold filling, that was required to effectively manufacture a high-integrity cast Mg control arm that required high ductility and strength, low porosity, and freedom from objectionable oxides and inclusions. Identical Mg control arms were produced from all of the above processes using AM60 and/or AZ91 Mg alloys and were thermally treated, radiographically inspected, metallographically analyzed for internal cast integrity, and tested for static and cyclic material properties. The components were bench tested (static and fatigue) to destructive failure.

Results and Discussions

Casting and testing procedures were established for all processes to provide sufficient Mg castings for the manufacturing, testing, and evaluation phase of the project. Tooling, casting parameters, and modeling were implemented for each process to control metal flow, fill, porosity, and hot tears. Hundreds of castings were produced by the different processes for inspection and evaluation. Specific results include, but are not limited to, the following.

- Squeeze Casting Process: Meridian Lightweight Technologies used a squeeze casting machine that was part of its production facility and designed and manufactured a prototype Mg front lower control arm for the 2008 Chrysler Caliber SRT-4 vehicle. The results of Meridian’s work indicate that squeeze casting Mg is a feasible process for obtaining high integrity components which are suitable for automotive applications where heat treatment would be necessary to achieve enhanced material properties. With the exception of the x-ray levels, all project metrics were met, including casting appearance, completeness of fill, and freedom from hot tearing, and static tests met the component testing requirements. (FY 2010)
- Low Pressure Permanent Mold Casting Process: Solidification modeling was performed during the mold construction and revised as the casting process changed; machine and tooling were revised during the various casting trials as recommended by the various solidification and flow models provided by EKK Inc. The LPPM team successfully developed and cast components that met SOW requirements, developed a recuperative gas collection system that recycled the gases for the future, and developed the use of mold coatings for casting Mg with the LPPM process. The

castings that were produced had good appearance and minimum porosity and hot tears from both AM60 and AZ91 Mg alloys. The LPPM process proved successful and a viable casting process to manufacture quality structural lower control arms made from the AZ91 Mg alloy. At the end of the LPPM trials, the equipment was revised for the installation of the EMP. (FY 2010)

- Control Molten Metal Transfer and Filling: Completion of this process was a stretch goal as the EMP has been used for Al casting but not for Mg. CMI Novacast Inc. developed an EMP, transfer launder, cooling system, and control system as enabling technologies for improved integrity and quality of cast Mg components. All of the prototype equipment was delivered to the LPPM casting site and proved the feasibility of using the EMP as a Mg casting process. Fully developed castings were obtained; however, further development work was required to provide high integrity castings. Time and project funds limited the required number of tests to ultimately deliver castings of the quality that the HIMAC team required. Nevertheless, the results conclusively indicate the basic project goals were achieved: Mg control arms were produced in sufficient quantities for evaluation and testing. (FY 2010)

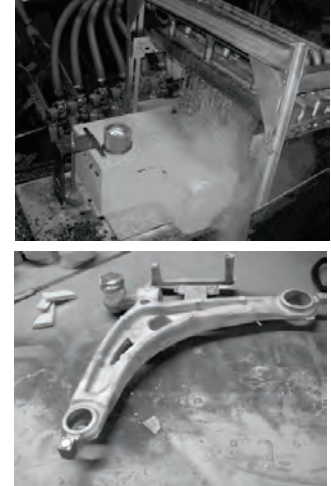


Figure 1. Ablation process: (a) ablation of a mold in progress; (b) ablation of control arm complete.

- Ablation Casting Process: Alotech Ltd. LLC had developed this new casting process (Figure 1) for cast Al automotive components but not for Mg until the HIMAC project. The process incorporates an aggregate mold and quiescent metal fill followed by rapid solidification rates (the mold is removed in under 120 seconds). The process concept is to recycle both the water soluble (aggregate) and the water that is used, making this a totally closed system for continued use. This part of the process was not yet completed at the time the HIMAC castings were made, but it is the ultimate goal of Alotech LLC to achieve complete recycling. This prototype casting process (as developed to date) has successfully demonstrated concept feasibility to cast Mg components with superior metallographic and material properties. (FY 2010)

- T-Mag Process: Researchers at the Commonwealth Scientific and Industrial Research Organization, Australia’s national science agency, developed the T-Mag permanent mold casting process, which is being commercialized by a consortium, T-Mag Pty Ltd. This process has many of the virtues of low pressure die casting (high casting quality from nonturbulent fill and high yield) but without the need to manage flow and pressurization control of furnace cover gas. The T-Mag process is a very well defined prototype process, and there should be minimum problems duplicating the existing process and escalating it to a full size production facility. Metallographic and material property results achieved for the HIMAC project are outstanding. (FY 2010)

- Testing and Evaluation: The computer model that was developed by the University of Iowa to predict porosity and hot tears was validated by comparing the predictions to measurements made on different types of Meridian Lightweight Inc. production type test castings. The measurements and predictions were found to be in good agreement. (FY 2010)

Table 2 indicates MSST’s involvement in this phase of the testing and evaluation. Material and metallographic properties of all HIMAC processes were obtained by excising coupons from the same area of each casting, and Table 2 indicates the tensile results. Extensive testing and evaluation results from MSST’s study are included in the HIMAC project final report posted on the United States Council for Automotive Research’s VROOM site.

Table 2. Summary of AZ 91 tensile results (Mississippi State University).

Process	Location	Side	$\sigma_{Y,2\%}$	σ_{uts}	$\epsilon_{elongation}$
LPPM	A	T	85.4	127.6	0.014
LPPM	A	B	77.3	137.7	0.024
LPPM	B	T	78.2	152.1	0.034
LPPM	B	B	91.5	223.3	0.055
Ablation	A	T	98.8	330.8	0.159
Ablation	A	B	89.1	288.4	0.126
Ablation	B	T	93.0	285.5	0.100
Ablation	B	B	104.2	328.0	0.166
Squeeze casting	A	T	102.0	185.2	0.036
Squeeze casting	A	B	82.8	100.2	0.018
Squeeze casting	B	T	97.9	173.6	0.025
Squeeze casting	B	B	87.3	118.2	0.018
T-Mag	A	T	87.0	210.0	0.060
T-Mag	A	B	95.1	200.6	0.047
T-Mag	B	T	98.3	191.3	0.058
T-Mag	B	B	80.5	228.7	0.078
LPPM (EMP)	A	T	91.9	233.4	0.073
LPPM (EMP)	A	T	101.3	143.4	0.017

X-ray results are not conclusive evidence to determine the best process, as the facilities ranged from full production shops (with limited time to experiment) to small prototype shops that were built just for the HIMAC Project. A summary would indicate the following.

- Task 1: Squeeze casting 0% Did not achieve ASTM E-155 (level 2 or less)
- Task 2: LPPM 89% Achieved ASTM E-155 (level 2 or less)
- Task 6: EMP 100% Did not achieve ASTM E-155 (level 2 or less)
- Task 7-A: Ablation 90% Achieved ASTM E-155 (level 2 or less)
- Task 7-B: T-Mag 95% Achieved ASTM E-155 (level 2 or less)

Note: The SOW for the project indicated the goal for the x-ray requirement was to achieve ASTM E-155 (level 2 or less). The squeeze casting and EMP processes interfaced with production equipment and there was insufficient time to fully achieve this x ray level requirement. However, all other aspects of these processes were achieved.

Conclusions

The objectives and deliverables of the HIMAC project have been met: new Mg alloy casting processes have been investigated and developed from existing Al processes and/or emerging processes; Mg casting barriers that were identified and prohibited casting of high integrity Mg automotive components have been solved, with solutions provided for use by manufacturers, and/or clearly identified for future research and development studies; modeling techniques have been provided to minimize hot tear and porosity in Mg components, and the success of this aspect of the project was proven when implemented in the squeeze casting process. Mass weight savings of 29% (steel versus Mg) was achieved from all processes using nonoptimized design criteria and AZ91 Mg alloy.

All five processes have provided hundreds of components for testing and evaluation, and the results of the project have already generated interest in doing further studies of several of the key HIMAC project processes from OEMs and universities that were involved. Neither cost studies nor a cost analysis/process were included as the processes that were developed varied from full production facilities in Canada to small prototype operations in Australia, Michigan, and Ohio, thus making a cost evaluation impractical.

Certainly, the information shown cannot tell the reader which process is the best, but there are clear indications of the potential of using certain processes for either sand or metal molds to achieve Mg automotive castings with high integrity (high ductility and strength, low porosity, free of objectionable oxides and inclusions) and cast Mg automotive chassis components using AM60 and/or AZ91 Mg alloys.

Development of Corrosion Inhibiting E-coat System for Body-in-White Assemblies (AMD 1001)

Principal Investigator: Matthew J. O'Keefe
Missouri University of Science and Technology, Materials Research Center
(573) 341-6764; e-mail: mjokeefe@mst.edu

Principal Investigator: Surender Maddela
Missouri University of Science and Technology, Materials Research Center
(573) 341-4358; e-mail: maddelas@mst.edu

Project Lead: Yar-Ming Wang
General Motors Company Research & Development Center
(586) 986-0762; e-mail: yar-ming.wang@gmail.com

Project Lead: Adam Stals
Chrysler Group LLC
(248) 576-7423; e-mail: as926@chrysler.com

Project Lead: Mike Pawlik
PPG
(412) 492-5393; e-mail: mpawlik@ppg.com

Principal Investigator: Matthew J. O'Keefe
Missouri University of Science and Technology, Materials Research Center
(573) 341-6764; e-mail: mjokeefe@mst.edu

Principal Investigator: Surender Maddela
Missouri University of Science and Technology, Materials Research Center
(573) 341-4358; e-mail: maddelas@mst.edu

Project Lead: Yar-Ming Wang
General Motors Company Research & Development Center
(586) 986-0762; e-mail: yar-ming.wang@gmail.com

Project Lead: Adam Stals
Chrysler Group LLC
(248) 576-7423; e-mail: as926@chrysler.com

Project Lead: Mike Pawlik
PPG
(412) 492-5393; e-mail: mpawlik@ppg.com

Introduction

Magnesium has a very negative standard electrode potential resulting in poor corrosion resistance in aqueous solution. The development of a robust paint-line compatible pretreatment process for Mg-intensive vehicles is critical to its expanded use in automotive body and chassis applications. In an automotive paint line, phosphate electrolytes are formulated to treat mixed metals such as galvanized steel and Al in body-in-white (BIW) assemblies. However, because of high solubility in the phosphate baths Mg alloys are not compatible with phosphate processes commonly used in automotive manufacturing [74]. To treat a mixed-metal BIW assembly, including Mg alloy parts, a new conversion coating process needs to be developed. The most popular and effective conversion coating has been a chromium based conversion coating. However, the use of chromate baths is restricted due to the high toxicity of the hexavalent chromium compounds [75]. Recently, research on environmental and nontoxic coating processes has led to the development of various novel conversion coating processes, especially in the case of Al alloys [76, 77]. Several researchers have demonstrated that treatments with aqueous solutions of rare-earth salts, especially cerium salts, can effectively inhibit the corrosion of metals [78, 79]. These studies revealed that corrosion protection can be attributed to the formation of a hydrated rare earth oxide film over the active (cathodic) sites on the metal surface. However, only a few researchers have reported the use of cerium based conversion coatings on Mg alloys [80–82]. The most difficult aspect of coating Mg is developing an appropriate pretreatment process; once a suitable pretreatment is in place, many metals can be coated [75]. Maddela et. al. and Zheng et. al. have demonstrated that pretreatments significantly change coating properties and corrosion resistance of Mg alloys [82, 83].

This project will leverage and extend patented corrosion inhibiting electrocoating (e-coating) technology for inorganic conversion coatings developed for Al based aerospace structures to dissimilar metal BIW vehicles [84, 85]. Incorporation of active, corrosion inhibiting rare-earth compounds into the electrocoat (e-coat) system will combine active and barrier passivation technology that is not currently used in the industry. This approach has been shown to be effective for inhomogeneous Al alloys that contain intermetallic compounds that form galvanic couples with the Al matrix. High strength Al alloys are similar to BIW assemblies in that they contain dissimilar metal components that set up galvanic couples which promote corrosion. To address this situation, rare-earth based conversion coatings have been shown to be effective at mitigating corrosion of metallic substrates.

Cerium based conversion coatings were deposited on Mg AZ91D and AZ31B alloys and friction stir welded Mg (AZ91D, AZ31B)-Al (7075-T6) couples. The corrosion protection of cerium based conversion coatings (CeCCs) on Mg and Mg-Al couples has been studied using potentiodynamic polarization measurements, electrochemical impedance spectroscopy, and salt fog testing. The corrosion results show that CeCCs enhance the corrosion resistance of Mg alloys. Preliminary results

show that cerium conversion coatings can be obtained on Mg-Al couples by a single coating process. CeCCs can significantly enhance the corrosion resistance of Mg-Al couples. The development of a robust paint-line compatible pretreatment process for Mg-intensive vehicles is critical to its expanded use in automotive body and chassis applications. The project “Development of Corrosion Inhibiting E-coat System for Body-in-White (BIW) Assemblies—AMD 1001,” in collaboration with the Missouri University of Science and Technology, Materials Research Center, was launched in September 2010. This project is divided into three major tasks as indicated below.

- Task I: Conversion coating development
 - Coating on individual alloys
 - Coating on binary alloys
 - Coating on BIW system
- Task II: E-coating on conversion coating development
 - Coating on individual alloys
 - Coating on binary alloys
 - Coating on BIW system
- Task III: Corrosion inhibiting e-coat formulation
 - Coating on individual alloys
 - Coating on binary alloys
 - Coating on BIW system

These tasks will assess the viability of developing a new pretreatment process for high volume production of BIW automotive structures containing Mg alloy parts. The stretch goal of the program is to incorporate corrosion inhibiting compounds into an e-coat formulation. This would provide a single coating process that has active corrosion protection of the BIW assembly.

Results and Discussions

Task I (conversion coating development) of the project was initiated in September 2010. The preliminary experiments were conducted on Mg (AZ91D, AZ31B) alloys, Al (6016, 7075) alloys, and FSW Mg-Al (AZ91D-7075, AZ31B-7075) couples. The cerium conversion coatings were deposited on alloys with different surface preparations, and different cerium deposition solutions (cerium chloride and cerium nitrate) were used. Optical images of cerium coated Mg alloys and Mg-Al couples before and after salt fog testing are shown in Figure 1 and Figure 2. The cerium conversion coatings enhanced the corrosion resistance of Mg alloys (Figure 1) and Mg-Al couples (Figure 2). It was demonstrated that cerium coatings can be deposited on Mg-Al couples by a single coating process.

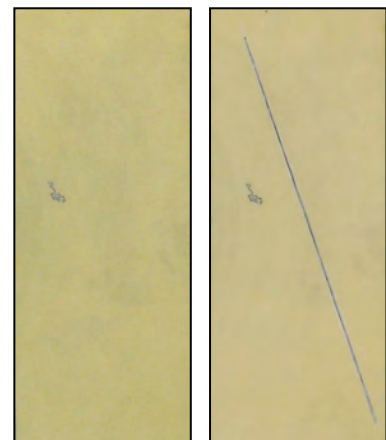


Figure 1. Optical images of salt fog tested cerium conversion coated AZ91D alloy panels with and without scribe: (a) one week and (b) one week after scribe.

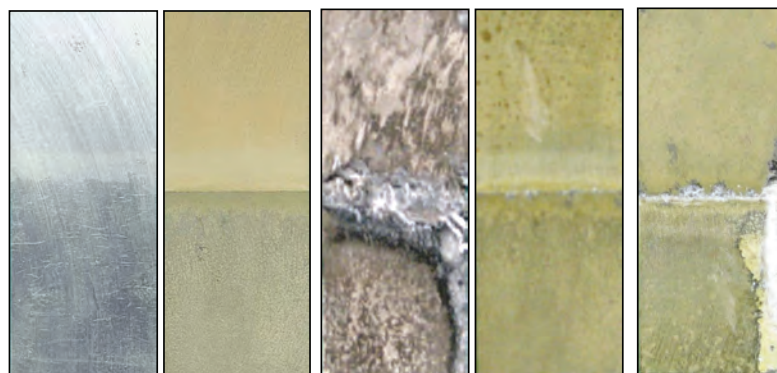


Figure 2. Optical images of Mg-Al couples before and after salt fog testing: (a) bare couple, (b) CeCC couple, (c) bare couple after 1 day of salt fog testing, (d) CeCC couple after 1 day salt fog testing, and (e) CeCC couple after 7 days of salt fog testing.

Conclusions

The following conclusions were derived based on the preliminary study.

- Cerium conversion coatings can be deposited on Mg-Al couples by a single coating process.
- CeCCs can significantly enhance the corrosion resistance of Mg alloys and Mg-Al couples.

Enabling Technologies

The implementation of many light metal applications is hindered because of a need for more development and/or a better understanding of enabling technologies to support those applications. For example, no matter how much weight a Mg front end may save compared to steel, this type of application will never be implemented in production if there are no robust, cost-effective means of joining the Mg front end structure to the steel BIW without experiencing galvanic corrosion. Similarly, this type of construction will not be implemented without a good understanding of the behavior of Mg in crash management situations. These types of technologies that are required to implement the use of light metals are referred to as “enabling technologies.” Much of the work funded by AMD falls into this category. The following are some examples.

- Development of an accelerated cosmetic corrosion test that correlates with field experience for Al automotive panels. This project will not save any weight on its own but helps to improve the confidence level of automakers so that they are more likely to use Al panels for savings of 35% to 50%.
- Development of ceramic coatings to eliminate galvanic corrosion problems associated with steel fasteners in Mg components. This technology does not save any weight on its own but could enable significantly increased use of Mg components to achieve weight savings of 40%–65%.
- Development of a better understanding of the effects of the initial alloy chemistry and subsequent manufacturing processes on the behavior of Mg/Mg alloys through ICME will enhance the ability to predict the behavior of Mg/Mg alloys and thus improve the confidence level of automakers in using them.

Additionally, the Mg front end project incorporates several enabling subtopics including crashworthiness, NVH, sheet forming, joining, corrosion, etc. that do nothing to reduce weight on their own but are required to ensure successful implementation of Mg structural assemblies.

Development of Steel Fastener Nano-Ceramic Coatings for Corrosion Protection of Magnesium Parts (AMD 704)

Project Lead: Richard Osborne, General Motors Company
(248) 202-6963; e-mail: richard.osborne@gm.com

Introduction

Magnesium has been identified as a structural automotive material that would enable automakers to meet fuel economy and emission requirements through “lightweighting.” As discussed in Magnesium Vision 2020 [86], galvanic corrosion is a significant barrier to the use of Mg in automotive applications, with the most common source of galvanic corrosion originating from fastening. This project identifies possible solutions including the development of impermeable coatings that would isolate a steel fastener (cathode) from the Mg (anode) [86]. The purpose of this project is to facilitate the use of lightweight Mg in automotive applications by developing and validating nano-ceramic coatings for steel fasteners that will inhibit galvanic corrosion between the fasteners and Mg components.

Approach

Phase I of the project, which ended in July 2010, had the following intended approach.

- Thin film coatings of ceramics will be used to electrically and effectively isolate steel bolts, nuts, and washers from Mg parts to stop the galvanic electric current to protect these Mg parts from galvanic corrosion.
- A design of experiments will be performed to select the ceramic materials, layer sequence, and film thickness for the thin coating layers.
- Comprehensive analyses through various testing of corrosion; characterization of mechanical property and material microstructure; and multiscale simulations at the atomic, nanoscale, and micron scale.
- Transfer knowledge and technology to industry for high volume process.

The results from Phase I were promising but did not achieve the original objectives. Phase II was initiated in August 2010 with two tasks, described as follows.

1. In Task 1, thin film nano-ceramic coatings will be deposited upon flat steel substrates. The galvanic corrosion performance of the coatings will be assessed using a galvanic current measurement with Al as the baseline.
2. Task 2 will only begin if Task 1 is successful. In this task, those coatings that successfully pass Task 1 will be applied to steel fasteners and tested using a modified VDA corrosion test, which will assess the ability of the coatings to isolate steel fasteners from Mg.

Results and Discussion

The initial direction from Phase I was to provide an effective low cost nano-ceramic coating and to establish a means of applying this coating to steel fasteners at automotive volumes. It had already been established that nano-ceramic coatings exhibited high strength and ductility, uncharacteristic of ceramic materials. However, substrate defects located on the surface of flat steel substrates were found to affect coating adhesion and were detrimental to coating performance. It was essential to characterize the effect of these defects on the nano-ceramic coatings and identify solutions before the coatings could be applied to fasteners and before refining the coating process for mass production. It was reasoned that if solutions could not be found for surface defects on flat substrates, then it would be even more unlikely that the coatings would perform well on complex 3D surfaces where forming defects would increase the potential for poor coating adhesion.

Silicon-nitride ceramic coatings were found to be effective in masking steel surface defects in thicknesses ranging from 80 nm to 800 nm. However, the coating strength and ductility did not appear sufficient to provide effective isolation under load where any cracks and fissures would induce corrosion. This led to the decision to evaluate the compound effect of multilayer nano-ceramic coatings. During the first two quarters of the 2010 fiscal year a number of coating combinations were evaluated, and it was found that multilayer nano-ceramic coatings performed better than single layer coatings. One multilayer coating in particular, silicon nitride, followed by Al oxide and a UV curable topcoat, performed the best in reducing galvanic corrosion between coated steel specimens and Mg. This work concluded Phase I of the project with results that were sufficient to justify additional research to define the optimum process parameters and fully characterize the performance of multilayer nano-ceramic coatings.

Phase II of the project was defined with the goal to establish the concept feasibility of coating steel fasteners with multilayer nano-ceramic coatings that performed as well as or better than Al with respect to galvanic current and corrosion. The galvanic couple between Al and Mg was set as the baseline for the project as this represents the most prevalent automotive strategy for isolating steel from Mg (i.e., the use of Al spacers). Phase II consists of two tasks: the first task is to measure the galvanic current between multilayer nano-ceramic coated steel and Mg and the second task is to measure the galvanic corrosion between multilayer nano-ceramic coated steel fasteners and steel using VDA (salt spray) testing. Phase II was approved, and work was begun in the fourth quarter of the fiscal year. At the conclusion of the 2010 fiscal year, a design of experiments was being conducted to rank the importance of coating variables and define a coating matrix to be tested in the 2011 fiscal year.

Conclusions

As a result of the project, the following have been concluded.

1. Single layer nano-ceramic coatings are not likely to succeed due mostly to substrate defects that are several orders of magnitude greater than the nano-sized ceramic particles that comprise the coating.
2. Effective multilayer nano-ceramic coatings using silicon nitride as a precoat to mask the surface defects are possible and show initial promise.

Conclusions

Consistent with its mission, AMD successfully completed work that includes demonstration of (1) the benefits of using Mg in powertrain components, (2) a corrosion test delivering good correlation to field performance of painted Al body panels, (3) a low cost alternative Al alloy (B206) for application in automotive suspension components, (4) predictive math based tools to describe performance properties that enable greater use of Al powder metal components, (5) process technologies needed to manufacture high integrity cast Mg automotive suspension components, (6) a Mg front end body structure design that delivers 50% mass reduction (compared to steel) while approaching cost neutrality and meeting current safety and performance requirements, and (7) material and manufacturing technologies enabling design and implementation of Mg body front end structures. These accomplishments address and resolve an array of technology gaps and challenges that exist and inhibit the implementation of new lightweight metals for high volume production application.

AMD Presentations/Publications/Patents

AMD 309—None

AMD 405

G.K. Sigworth, F. DeHart and S. Millhollen: "Use of High Strength Al Casting Alloys in Automotive Applications," pp. 313–322, *Light Metals 2001 Métaux Léger*, editors M. Sahoo and T.J. Lewis, Canadian Inst. Mining, Metallurgy and Petroleum, Montreal, Quebec, 2001.

G.K. Sigworth and F. DeHart: "Recent Developments in the High Strength Al-Copper Casting Alloy A206," *AFS Transactions* 2003, Vol. 111, pp. 341–354, 2003.

G.K. Sigworth, F. DeHart, J.F. Major and D. Donskoi: "Bulking Up Al Alloys," *Modern Casting*, pp. 40–41, May 2003.

G.K. Sigworth and J.F. Major: "Factors Influencing the Mechanical Properties of B206 Alloy Castings," *Light Metals* 2006, pp. 795–800 (2006).

J.F. Major and G.K. Sigworth: "Chemistry/Property Relationships in AA 206 Alloys," *Trans. American Foundry Society*, Vol. 114, pp. 117–128 (2006).

M. Manivannan, J.H. Sokolowski and D.O. Northwood: "Improving the Corrosion Resistance of a High Strength Al-Cu Alloy," paper presented at *Corrosion and Prevention 2008*, November 16–19, 2008, Wellington, New Zealand.

A. Rodríguez, R. Chávez and J. Hernández, Y. Raymond and F. Major: "The Effect of Solidification Conditions and Alloy Composition on the Castability and Mechanical Properties of B206 Alloy," *Trans. American Foundry Society*, Vol. 117, pp. 79–92 (2009).

D. Jean and J.F. Major: "Chemistry/Property Relationships in AA 206 Alloys: Fatigue Behavior," *Trans. American Foundry Society*, Vol. 117, pp. 103–112 (2009).

D, Jean, J.F. Major, J.H. Sokolowski, B. Warnock and W. Kazprzak: "Heat Treatment and Corrosion Resistance of B206 Al Alloy," *Trans. American Foundry Society*, Vol. 117, pp. 113–120 (2009).

AMD 410

Stone, T.W., Hammi, Y., Carino, R.L., Horstemeyer, M.F., 2009, "Modeling for Powder Metallurgy Component Design and Performance Prediction," PowderMet 2009 Conference, Las Vegas, NV, June 28–May 1.

Stone, T.W., Sanderow, H., Grewal, H., Hammi, Y., Allison, P., Solanki, K., Horstemeyer, M.F., 2009, "Process Modeling: Use of Uncertainty, Sensitivity and Optimization Techniques for Improved Understanding of Compaction Model Outputs," PowderMet 2009 Conference, Las Vegas, NV, June 28–July 1.

AMD 905—None

AMD 304

Powell, B.R., Testing of Magnesium Parts a Success. In Metal Casting Technology, 2010, [6], pp. 26–29.

Powell, B.R.; Opportunities and Challenges for the Use of Magnesium in Automotive Applications, at Lightweight Metals Symposium of the Canadian Conference of Metallurgists, Vancouver, BC, Canada, October 4, 2010.

Powell, B.R.; Miller, W.L.; Quinn, J.F.; Allison, J.E.; Hines, J.A.; and Ried, P.P.; The Magnesium Powertrain Cast Components Project, at the 2010DOE/NETL Review, Southfield, MI, May 13, 2010.

Powell, B.R.; Quinn, J.F.; Miller, W.L.; Quinn, J.F.; Allison, J.E.; Hines, J.A.; and Beals, R.; Magnesium Replacement of Al Cast Components in a Production V6 Engine to Effect Cost-Effective Mass Reduction, at the U.S. DOE DEER 2010 Conference, Detroit, MI, September 29, 2010.

AMD 601

Pokorny, M.G.; Monroe, C.A.; and Beckermann, C., Prediction of Deformation and Hot Tear Formation Using a Viscoplastic Model with Damage, in Shape Casting: The 3rd International Symposium, eds. J. Campbell, P.N. Crepeau and M. Tiryakioglu, TMS, Warrendale, PA, 2009, pp 265–272.

Xue Y; Horstemeyer MF; McDowell DL; El Kadiri H; Fan J, Microstructure-based multistage fatigue modeling of cast AE44 magnesium alloys, Int J of Fatigue 2007; 29: 666–76.

El, Kadiri.; Xue, Y.; Horstemeyer, M.F.; Jordan, B.; and Wang, P.; Fatigue Crack Growth Mechanisms in a Die Cast AM50 Alloy; Acta Materialia 2006; 54:5061–76.

Pokorny, M.; Monroe, C.; Beckermann, C.; Bichler, L.; Ravindran, C., Prediction of Hot Tear Formation in a Magnesium Alloy Permanent Mold Casting, Int. J. Metalcasting, Vol. 2, No. 4, 2008, pp. 41–53.

Saha, P.; Lohies, K.; Viswanathan, S.; Batson, R.G.; Gokhale, A.; A Systematic Study of the Grain Refinement of Magnesium by Zirconium; Magnesium Technology 2010 (ISBN: 978-0-87339-746-9, The Minerals, Metals, and Materials Society, Warrendale, PA; p 425) 2010.

Beckermann, C.; Prediction of Porosity and Hot Tears in Magnesium Castings; Material Science and Technologies; 2007 Conference, Detroit, MI September 2007.

Woycik, G.; Low Pressure Casting of Magnesium Alloys for Automotive Components; American Foundry Society-111th Metalcasting Congress, May 15–18, 2007.

Weiss, D.; Magnesium Casting Technology Update; American Foundry Society-111th Metalcasting Congress, May 15–18, 2007.

Szymanowski, B.; HIMAC, Magnesium Squeeze Casting Update; American Foundry Society-111th Metalcasting Congress, May 15–18, 2007.

Cox, B.; High Integrity Magnesium Automotive Components (HIMAC); American Foundry Society-111th Metalcasting Congress, May 15–18, 2007.

Woycik, G.; Marlatt, M.; Low Pressure Permanent Mold Casting of a Magnesium Lower Control Arm: AFS 6th International Conference on Permanent Mold Casting of Al and Magnesium; Frisco, TX. 2008.

Sheng, R.; Chen, S.; Nath, J.; Sponsored Research: Low Pressure Casting Process Simulation and Tooling Design for HIMAC's Magnesium Automotive Control Arm (08-148); CastExpo 2008.

Winardi, L.; Scarber, L.; Griffin, R.; Weiss, D.; Comparison of Gas Evolution Results from Chemically Bonded Cores In Contact with Magnesium and Al Melts (08-048); CastExpo 2008.

Jacques, R.; Jekl, J.; Development of the Squeeze Cast Process for the USCAR HIMAC Project. (08-165); CastExpo 2008.

Marlatt, M.; Woycik, G.; Kim, C.W.; Low Pressure Casting of a Magnesium Control Arm (08-166); CastExpo 2008.

Saha, P.; Lories, K.; Viswanathan, S.; Batson, R.G.; Gokhale, A.; A Systematic Study of the Grain Refinement of Magnesium by Zirconium; 2010 TMS Annual Meeting, Seattle, WA 2009.

113 Metal-casting Congress; Paris Hotel; Las Vegas, Nevada; April 7-10, 2009;

Panel 1: HIMAC Progress Review on Low Pressure and Squeeze Casting Processes (09-133); 113 Metal-casting Congress; Paris Hotel; Las Vegas, Nevada; April 7-10, 2009.

Marlatt, M.; Low Pressure Magnesium Casting of a Lower Control Arm; 113 Metal-casting Congress; Paris Hotel; Las Vegas, Nevada; April 7-10, 2009.

Kim, C.W.; Nitz, J.D.; Siersma, K.; HIMAC-Task #2 Support Low Pressure Simulation; 113 Metal-casting Congress; Paris Hotel; Las Vegas, Nevada; April 7-10, 2009.

Kim, C.W.; Siersma, K.; Modeling of Mg Squeeze Casting Sponsored Research: Low Pressure Casting; 13 Metal-casting Congress; Paris Hotel; Las Vegas, Nevada; April 7-10, 2009.

Panel 2: Process Simulation of Advanced Casting Processes & Materials (09-149)

Sholapurwalla, A.; Process Optimization of High Integrity Magnesium Control Arm; 113 Metal-casting Congress; Paris Hotel; Las Vegas, Nevada; April 7-10, 2009.

Shah, J.; Virtual Library of Cast Alloys; 113 Metal-casting Congress; Paris Hotel; Las Vegas, Nevada; April 7-10, 2009.

Starobin, A.; Simulation of Core Gas Evolution; 113 Metal-casting Congress; Paris Hotel; Las Vegas, Nevada; April 7-10, 2009.

Panel 3: New Approaches to Magnesium Grain Refining (09-162)

Cox, B.; New Approaches to Magnesium Grain Refining; 113 Metal-casting Congress; Paris Hotel; Las Vegas, Nevada; April 7-10, 2009.

Han, Q.; Ultrasonic Grain Refining; 113 Metal-casting Congress; Paris Hotel; Las Vegas, Nevada; April 7-10, 2009.

Sahoo, M.; Zavadil, R.; Sullivan, L.A.; Li, X.; Gokhale, A.; New Approaches to Magnesium Grain Refining; 113 Metal-casting Congress; Paris Hotel; Las Vegas, Nevada; April 7-10, 2009.

Saha, P.; Viswanathan, S.; Engineering an Efficient Grain Refiner for Magnesium Alloys; 113 Metal-casting Congress; Paris Hotel; Las Vegas, Nevada; April 7-10, 2009.

Invited Speakers

Beckermann, C.; Modeling of Deformation and Hot Tears; International Conference on Modeling of Casting, Welding, and Advanced Solidification Processes X11, Vancouver, Canada; June 2009.

Viswanathan, S.; Engineering an Efficient Grain Refiner for Magnesium Alloys; 113th Metalcasting Congress, Las Vegas, April 7-10, 2009.

Viswanathan, S.; Processing of Lightweight Alloys; Pacific Northwest National Laboratory, Richland, WA, June 30, 2008, Presentation.

Poster Presentations

Saha, P.; Shamsuzzoha, M.; Viswanathan, S.; Poster titled, Engineering Efficient Zirconium-Based Grain Refiners for Magnesium Alloys; Third Place in the 2008 International Metallographic Contest, Class 3 (Electron Microscopy—Transmission and Analytical) sponsored by the International Metallographic Society and ASM International.

Saha, P.; Viswanathan, S.; Poster Titled, Microstructural Characterization of Magnesium-Zirconium Alloys; Poster Winner at the 2008 AFS/FEF Student Technology Contest held in conjunction with the 2008 AFS CastExpo.

Saha, P.; Viswanathan, S.; Engineering an Efficient Zirconium-Based Grain Refiner for Magnesium Alloys, 113th Metalcasting Congress, Las Vegas; 2009.

Saha, P.; Viswanathan.; Determination of Mushy Zone Mechanical Properties of Magnesium Alloys Using a Gleeble, TMS Annual Meeting, San Francisco, CA, 2009.

Saha, P.; Shamsuzzoha, M.; Viswanathan, S.; Engineering Efficient Zirconium-Based Grain Refiners for Magnesium Alloys, 2008 International Metallographic Society Poster Contest—Class 3: Electron Microscopy, Transmission and Analytical, Microscopy & Microanalysis 2008 Meeting, Albuquerque, NM, August 3–7, 2008.

P. Saha and S. Viswanathan; Microstructural Characterization of Magnesium-Zirconium Alloys, 2008 AFS CastExpo, Atlanta, GA, 2008.

Saha, P.; Shamsuzzoha, M.; Viswanathan, S.; Microstructural Characterization of Magnesium-Zirconium Alloys, 2008 TMS Annual Meeting, New Orleans, LA; 2008.

AMD 603—None

AMD 604/904

Luo, A.A., Forsmark, J.H., Sun, X., Shook, S.O., Misiolek, W.Z., Mishra, R.K., Microstructure and Mechanical Properties of Magnesium Extrusion Alloys AM30, AZ31 and AZ61, in Magnesium Technology 2010, Agnew, S.R., Nyberg, E.A., Neelameggham, N.R. and Sillekens, W.H., eds., TMS, Warrendale, PA, 2010, TMS, Warrendale, PA, pp 553–558.

Luo, A.A., Forsmark, J.H., Sun, X., Shook, S.O., “Mechanical and Thermophysical Properties of Magnesium Alloy Extrusions,” SAE Technical Paper 2010-01-0214, SAE International, Warrendale, PA, 2010.

Wagner, D.A., Logan, S., Wang, K. and Skrzek, T., “Test Results and FEA Predictions from Magnesium AZ31 Sheet Beams in Bending and Axial Compression,” in Magnesium Technology 2010, Agnew, S.R., Nyberg, E.A., Neelameggham, N.R. and Sillekens, W.H., eds., TMS, Warrendale, PA, 2010, pp 547–553.

Wagner, D.A., Logan, S.D., Wang, K., and Skrzek, T., “FEA Predictions and Test Results from Magnesium Beams in Bending and Axial Compression,” SAE Technical Paper 2010-01-0405, SAE World Congress, April 12, 2010, Society of Automotive Engineers, Warrendale, PA.

Albinmousa, J., et al., Monotonic and Fatigue Behavior of Magnesium Extrusion Alloy AM30: An International Benchmark Test in the “Magnesium Front End Research and Development Project,” SAE Paper 2010-01-0407, Society of Automotive Engineers, Warrendale, PA, SAE 2010 World Congress, April 2010.

Yang, Q., Badarinarayan, H., Feasibility study on FSSW of Magnesium Alloys, in The proceedings of the 8th International Symposium on Friction Stir Welding, Timmendorfer Strand, Germany, May 18-20, 2010, TWI Ltd., UK, 2010.

AMD 703—See References

AMD 1001—None

AMD 704

L. Lin, C. Qu, R. Kasica, Q. Fang, R. Miller, E. Pierce, E. McCarty, J. Fan, D. Edwards, G. Wynick, and X. Wang, "Multilayer Coatings for Anti-Corrosion Applications," Abstract accepted by American Ceramic Society 2011 Daytona Meeting.

C. Qu, P. Li, J. Fan, D. Edwards, W. Schulze, G. Wynick, R. Miller, L. Lin, Q. Fang, K. Bryson, H. Rubin, and X. Wang, to appear in Proceedings of 34th International Conference on Advanced Ceramics & Composites (ICACC).

Y. Liu, C. Qu, R. Miller, D. Edwards, J. Fan, P. Li, E. Pierce, A. Geleil, G. Wynick, and X. Wang, "Comparison of oxide and nitride thin films—electrochemical impedance measurements and materials properties," Ceramic Transactions Volume 214, pages 131–145.

MS Graduate Theses (Alfred University)

- L. Lin, Evaluation of anti-corrosion behavior for multilayer thin film coatings, MSEE thesis, to be completed by Dec. 2010.
- C. Qu, Al oxide thin films as anti-corrosion layers, MSCE thesis, September 2009.
- Y. Liu, Silicon nitride and other oxide thin films on carbon steel substrates—anti-corrosion barrier layer application, December 2008.

AMD References

AMD 309

1. F. Bovard, J. Tardiff, T. Jafolla, D. McCune, G. Courval, K. Smith, S. Ramamurthy, R. Singleton, F. Vartolas, and J. Repp, "Cosmetic Corrosion Test for Al Autobody Panels: Final Report," SAE Paper No. 2010-01-0726, SAE 2010, April 2010.
2. F. Bovard, J. Tardiff, T. Jafolla, D. McCune, G. Courval, K. Smith, S. Ramamurthy, R. Singleton, F. Vartolas, and J. Repp, "Development of an Improved Test for Finished Al Autobody Panels," SAE Paper No. 2008-01-1156, SAE 2008, April 2008.
3. F. Bovard, J. Tardiff, T. Jafolla, D. McCune, G. Courval, K. Smith, F. Lee, S. Ramamurthy, J. Shaffer, F. Vartolas, and J. Repp, "Update on the Development of an Improved Test for Finished Al Autobody Panels," SAE Paper No. 2007-01-0417, SAE 2007, April 2007.
4. F. Bovard, J. Tardiff, T. Jafolla, D. McCune, G. Courval, K. Smith, F. Lee, F. Lutze, and J. Repp, "Development of an Improved Test for Finished Al Autobody Panels," SAE Paper No. 2005-01-0542, SAE 2005 Transactions Journal of Materials and Manufacturing, March 2005.
5. G. Courval, K. Smith, C. Meade, F. Lutze, F. Bovard, and T. Jafolla, "Development of an Improved Test for Finished Al Autobody Panels", SAE Paper No. 2003-01-1235, Proceedings of SAE World Congress, March 2003.
6. F. Bovard, J. Tardiff, T. Jafolla, D. McCune, G. Courval, K. Smith, S. Ramamurthy, R. Singleton, F. Vartolas, and J. Repp, "Update on the Development of an Improved Test for Finished Al Autobody Panels," SAE Paper No. 2009-01-0891, SAE 2009, April 2009.
7. SAE J2334, "Cosmetic Corrosion Lab Test," Society of Automotive Engineers, Warrendale, PA, June 1998.
8. F. Lee, B. Pourdeyhimi, and K. Adamsons, "Analysis of Coatings Appearance and Surface Defects Using Digital Image Capture/Processing/Analysis," The International Symposium on a Systems Approach to Service Life Prediction of Organic Coatings, Breckenridge, Co, September 14–19, 1997.
9. ASTM G85-98 Annex 2, "Cyclic Acidified Salt Fog Testing," Annual Book of ASTM Standards, Vol. 3.02, 2005.
10. ASTM G85-98 Annex 4, "Salt/SO₂ Spray Fog Testing," Annual Book of ASTM Standards, Vol. 3.02, 2005.

11. D. P. Doyle and T.E. Wright, "Rapid methods for Determining Atmospheric Corrosivity and Corrosion resistance," pp. 227–43, Atmospheric Corrosivity, edited by W.H. Ailor, 1982.
12. E.L. Colvin, et. al., "Filiform Corrosion of Al Auto Body Sheet in Accelerated and Outdoor Environments," SAE Paper No. 970735, Proceedings of SAE World Congress, Feb. 1997.
13. L.F. Vega, et. al. "Influence of Surface Treatments on Durability of Painted Al Alloys," SAE Paper No. 970731, Proceedings of SAE World Congress, Feb. 1997.
14. *AMD 405*
15. G.K. Sigworth: "Method for Grain Refinement of High Strength Al Casting Alloys," U.S. Patent 6,368,427, April 9, 2002; and U.S. Patent 6,645,321 B2, Nov. 11, 2003.
16. G.K. Sigworth, F. DeHart and S. Millhollen: "Use of High Strength Al Casting Alloys in Automotive Applications," pp. 313–322, Light Metals 2001 Métaux Léger, editors M. Sahoo and T.J. Lewis, Canadian Inst. Mining, Metallurgy and Petroleum, Montreal, Quebec, 2001.
17. G.K. Sigworth and F. DeHart: "Recent Developments in the High Strength Al-Copper Casting Alloy A206," AFS Transactions, 2003, paper 03-135.
18. G.K. Sigworth: Final Report for AMD 305, April 11, 2002.
19. W. D. Robertson: "Correlation of Mechanical Properties and Corrosion Resistance of 24S-type Al Alloys as Affected by High Temperature Precipitation," Trans. AIME, Vol. 166, pp. 216–227 (1946).
20. C.H. Cáceres, "A Phenomenological Approach to the Quality Index," Int. J. Cast Metals Research, Vol. 12, pp 367–375 (2000). According to the theory by Cáceres, the quality index in B206 alloy is given by the relationship: $Q = UTS + 270 \log E$, where Q and the UTS are given in MPa, and E is the elongation to fraction in the tensile specimen.
21. Jean and J.F. Major: "Chemistry/Property Relationships in AA 206 Alloys: Fatigue Behavior," Trans. American Foundry Society, Vol. 117, pp. 103–112 (2009).
22. G. Keshavaram, D. Seiler and D. Dewitt: "Al Alloys for Automotive Knuckle Castings," SAE paper 2000-01-1291.
- AMD 410—None*
- AMD 905*
23. K. Siegert, Aluminium, Vol. 80 # 7-8 (2004) 854.
24. A.J. Barnes, Mat. Sci. Forum, 170-172 (1994) 701.
25. J. G. Schroth in: Advances in Superplasticity and Superplastic Forming, edited by E. M. Taleff, P. A. Friedman, P. E. Krajewski, R. S. Mishra, and J. G. Schroth, TMS, Warrendale, PA, (2004) 9.
26. "Materials Progress: Forming/Processing." Advanced Materials & Processes, 157 (3), (2000) 19.
27. Materials Engineering, Vol. 88 # 5 (1978) 52.
28. L.R. Morris and R.A. George: SAE Paper 770206 (1977) 1.
29. R.A. Ayres, H.W. Lanning, B. Taylor, R. Heimbuch, and W.G. Brazier: SAE Paper 780180 (1978) 702.
30. R.C. Eissinger, N.H. Jewell, and J.L. Livermore: SAE Paper 770303 (1978) 1.
31. R.A. Ayres: Met. Trans., Vol. 8A (1977) 487.
32. R.A. Ayres and M.L. Wenner: Met. Trans., Vol 10A (1979) 41.
33. R.A. Ayres: Met. Trans., Vol. 10A (1979) 849.

34. D.V. Wilson: Sheet Metal Industries (1981) 313.
35. F. Shehata, M.J. Painter, and R. Pearce: J. of Metal. Tech., Vol. 2 (1978) p.279.
36. J.O. Kumpulainen, A.J. Ranta-Eskola, J. Mat. Eng. Tech., Vol. 105 (1983) 119.
37. F.A. Shehata: Key Eng. Mat., Vol. A4 (1983) 1.
38. G. L'esperance, M.H. Loretto, W.T. Roberts, D. Price, and D.V. Wilson: Met. Trans., Vol. 15A, 1984, 913-922.
39. M. Sugamata, J. Kaneko, H. Usagawa, and M. Suzuki, "Effect of Forming Temperature on Deep Drawability of Al Alloy Sheets," Advanced Technology of Plasticity, Second Int. Conf. on Technology of Plasticity, Stuttgart, Germany, Vol. 2 (1987) 1275.
40. A.M. Szacinski and P.F. Thomson: Materials Science and Technology, 1991, vol. 7, 37-41.
41. Y. Abe and M. Yoshida: Science and Engineering of Light Metals. RASELM '91, Tokyo, Japan, 1991, 643-648.
42. E.M. Taleff, D.R. Lesuer, and J. Wadsworth, Met. Mat. Trans. A, 27A#2 (1996) 343-352.
43. T. Naka and F. Yoshida, J. Mat. Proc. Tech., 89-90 (1999) 19-23.
44. T. Naka, G. Torikai, R. Hino, and F. Yoshida, J. Mat. Proc. Tech., 113 (2001) 648-653.
45. E.M. Taleff, P.J. Nevland, and P.E. Krajewski, Met. Mat. Trans A, 32A (2001) 1119-1130.
46. D. Li and A. K. Ghosh, Mat. Sci. and Eng. A, A352 (2003) 279-286.
47. P.E. Krajewski, SAE Paper 2005-01-1388, (2005)
48. D. Li and A.K. Ghosh, J. Mat. Proc. Tech., 145 (2004) 281-293.
49. L.A. Kren, Metal Forming Magazine, March 2005, 28-30.

AMD 304

50. Beals, R.S.; Liu, Z.-K.; Jones, J.W.; Mallick, P.K.; Emadi, D.; Schawm, D.; and Powell, B.R.; US Automotive Materials Partnership, Magnesium Powertrain Cast Components Project: Fundamental Research Summary, JOM, 2007, 59 [8] pp. 43-8.
51. USAMP; Summary of the Tensile Properties of Creep-Resistant Magnesium Alloys, NADCA Product Specification Standards for Die Castings, the North American Die Casting Association, 2009.
52. USAMP; Automotive Lightweight Materials Database, www.metalcastingvirtuallibrary, American Foundry Society, 2010.
53. Verbrugge, M.W.; Motivations Driving the Use of Magnesium in Automotive Applications, at Magnesium Technology Symposium 2007, TMS Annual Meeting, Orlando, FL, 2007.

AMD 601—None

AMD 603—None

AMD 604/904

54. Luo, Alan A., Nyberg, Eric A., Sadayappan, Kumar and Shi, Wenfang, A Canada-China-USA Collaborative Research and Development Project "Magnesium Front End Research and Development (MFERD)" 2007 Annual Progress Reports, Project Technical Committee, Hangzhou, China, April 2008.
55. Luo, Alan A., Nyberg, Eric A., Sadayappan, Kumar and Shi, Wenfang, A Canada-China-USA Collaborative Research and Development Project: "Magnesium Front End Research and Development (MFERD)" 2008 Annual Progress Reports, Project Technical Committee, Niagara-on-the-Lake, Canada, May 2009.

AMD 703

56. Allison, J.E., Backman, D. and Christodoulou, L., "Integrated Computational Materials Engineering: A New Paradigm for the Materials Profession," *Journal of Metals* 2006, 58 [11], 25.
57. Presentations from TMS 2010 Annual Meeting, Symposium on Magnesium ICME, Seattle, WA, February 15–19, 2010.
58. Allison, J.E., Liu, B., Boyle, K., Hector, L., McCune, R.C., "Integrated Computational Materials Engineering (ICME) for Magnesium: An International Pilot Project."
59. Hector, L.G., Wrobel, J., Kurzydowski, K., "Thermodynamic and Elastic Properties of La-X (X=Al,Mg) Intermetallic Compounds from First Principles Calculations."
60. Misiolek, W. Z., De-Pari, L., "Numerical Simulation of Direct Extrusion of Magnesium Alloys."
61. Marin, E.B., Horstemeyer, S., Bouvardi, C., Bammann, D. J., El Kadiri, H., Wang, P., "On Modeling the Extrusion Process of Magnesium Alloys."
62. Oppedal, A. L., El Kadiri, H., "Transmutation and accommodation effects by glide twinning."
63. Ma, Q., El Kadiri, H., "Plasticity in a Rod-Textured Extruded Mg AM30 Alloy."
64. Raeisinia, B., Agnew, S. R., "Effect of Grain-Matrix Interaction Stiffness on Slip System Hardening Parameters of a Viscoplastic Self-Consistent Polycrystal Model."
65. Dreyer, C., Hector, L.G., Agnew, S.R., "Extracting post-uniform constitutive behavior from high temperature tensile test data."
66. Ben-Artzyl, A., Hector, L. G., Krajewski, P., "Strain Field Measurement during Bending of Extruded Magnesium Alloys."
67. Haupt, T. A., "Cyberinfrastructure for Integrated Computational Material Engineering."
68. Huo, L., Han, Z., Liu B., "Two- and Three-Dimensional Cellular Automaton Models for Simulating Dendrite Morphology Evolution of Cast Magnesium Alloys."
69. Li, S.-J., Xiong, S.-M., Liu, B., Allison, J.E., "Numerical Simulation of Flow-Induced Air Entrapment Defects in the High Pressure Die Casting Process."
70. Shang, S.-L., Wang, Y., Liu, Z.-K., "ESPEI: Extensible, Self-optimizing Phase Equilibrium Infrastructure for Magnesium Alloys."
71. Li, M., Zhang, R., Allison, J.E., "Modeling Casting and Heat Treatment Effects on Microstructure in Super Vacuum Die Casting (SVDC) AZ91 Magnesium Alloy."
72. Shin, D., Wolverton, C., "First-Principles Study of Ternary Hcp Solid Solution Phases from Special Quasirandom Structures: Application to Mg-Al-X Alloys."
73. Polesak, F. J., Krajewski, P. E., Raeisinia, B., Agnew, S.R., "Experimental and Computational Simulation of the Post-Warm Forming Constitutive Behavior of AZ31."
74. Polesak, F. J., Krajewski, P.E., Raeisinia, B., Agnew, S.R., "Assessing and Modeling the Impact of Initial Microstructure on Dynamic Recrystallization of Sheets."

AMD 1001

75. G. Gao, M. Ricketts, "Evaluation of protective coatings on magnesium for phosphate process compatibility and galvanic corrosion prevention," SAE Technical Paper 010081, SAE International, Warrendale, PA, 2002.
76. J. E. Gray, B. Luan, "Protective coatings on magnesium and its alloys-a critical review," *Journal of Alloys and Compounds*, Vol.336, 2002, pp. 88–113.

77. W. G. Fahrenholtz, J. Zhou, M. J. O'Keefe, "Characterization of spontaneously formed cerium-based conversion coatings on Al," *Ceramic Engineering and Science Proceedings* (2002), 23(4), pp.469–476.
78. D. K. Heller, W. G. Fahrenholtz, M. J. O'Keefe, "The effect of post-treatment time and temperature on cerium-based conversion coatings on Al 2024-T3," *Corrosion Science* (2010), 52(2), pp. 360–368.
79. P. Yu, S. A. Hayes, T. O'Keefe, M. J. O'Keefe, J. O. Stoffer, "The phase stability of cerium species in aqueous system (Part II-A) the Ce (III/IV)-H₂O-H₂O₂/O₂ system equilibrium considerations," *Journal of the Electrochemical Society*, Vol. 153(1), 2006, pp. C74–79.
80. B. R. W. Hinton, D. R. Arnott, N. E. Ryan, "Cerium conversion coatings for the corrosion protection of Al," *Materials Forum*, 9(3), 1986, pp. 162–173.
81. A. L. Rudd, C. B. Breslin, F. Mansfeld, "The Corrosion protection afforded by rare earth conversion coatings applied to magnesium," *Corrosion Science*, Vol. 42, 2000, pp. 275–288.
82. K. Brunelli, M. Dabala, I. Calliari, M. Magrini, "Effect of HCl treatment on corrosion resistance of cerium-based conversion coatings on magnesium and magnesium alloys," *Corrosion Science*, Vol. 47, 2005, pp. 989–1000.
83. S. Maddela, M. J. O'Keefe, Y. M. Wang, H. H. Kuo, Influence of surface pretreatment on cerium-based conversion coating on Mg AZ91D alloy, *Corrosion*, 66(11), 2010, pp.115008/1-115008/8.
84. R. F. Zheng and C. H. Liang, "Conversion coating treatment for AZ91D magnesium alloys by a permanganate-REMS bath," *Materials and Corrosion*, Vol. 58, 2007, pp.193–197.
85. Stoffer et al., "Additive-assisted, cerium-based, corrosion-resistant e-coating," U.S. Patent 7,241,371, July 10, 2007.
86. E. Morris et al., "The use of inhibitors to improve the corrosion protection of E-coat systems on Al alloys: a combined electrochemical and neutral salt spray evaluation," *Polymer Materials Science and Engineering*, 78 (172) (Spring Meeting).

AMD 704

87. Magnesium Vision 2020: A North American Automotive Strategic Vision for Magnesium, 2006 USCAR Website, USCAR.ORG; <http://uscar.org/guest/publications.php>

C. Auto/Steel Partnership - U.S. Automotive Materials Partnership

Field Technical Monitor: Roger Heimbuch
Auto/Steel Partnership
2000 Town Center, Suite 320; Southfield, MI 48075
(248)945-4770; e-mail: rheimbuch@a-sp.org

Field Technical Monitor: Ronald Krupitzer
American Iron and Steel Institute
Steel Market Development Institute
2000 Town Center, Suite 320; Southfield, MI 48075
(248) 945-4761 ; e-mail: rkrupitzer@steel.org

Technology Area Development Manager: Carol Schutte
U.S. Department of Energy
1000 Independence Ave., S.W.; Washington, DC 20585
(202) 287-5371; e-mail: carol.schutte@ee.doe.gov

Field Project Officer: Joseph Renk
National Energy Technology Laboratory
626 Cochran Mill Road; P.O. Box 10940; Pittsburgh, PA 15236
(412)386-6406; e-mail: joseph.renk@netl.doe.gov

Contractor: Auto/Steel Partnership
Contract No.: DE-FC26-02OR22910

Objective

- *ASP050—Advanced High-Strength Steel Stamping:* Support development of formability simulation and fracture prediction tools. Study die processes and part design geometries to reduce/eliminate springback.
- *ASP061—Nonlinear Strain Path:* Deliver experimental data and associated predictive models for advanced high-strength steel (AHSS) under nonlinear strain path deformation.
- *ASP230—Tribology:* Deliver experimental data that will lead to improved die designs, die materials, and die surface treatments.
- *ASP350—Precision Flow Form Application Development:* Develop and demonstrate the Precision Flow Form Process to form steel components to reduce mass of cast iron parts by 50%.
- *ASP070—Joining Technologies:* Provide joining parameters and joint performance data for future applications of AHSS.
- *ASP160—Sheet Steel Fatigue:* Provide test data that describe the fatigue performance of base metal and welded joints of AHSS and sound durability assessment criteria.
- *ASP330—Vehicle Structural System Benchmarking:* Develop mass predictive statistical models for 16 closure and chassis structural subsystems and identify lightweight outliers.
- *ASP241—Future-Generation Passenger Compartment (FGPC):* Meet three objectives: (1) Replicate the findings of the FGPC Phase 1 project on a five-passenger, four-door high-production-volume donor vehicle by reducing the passenger compartment mass by 25% or more with a cost parity relative to the baseline while meeting all product requirements. (2) Perform concept development of a large truck cab with no B-pillar that combines an increase from 1.5 to 2.5 times in vehicle curb mass roof-strength criteria with weight parity [the objective of the Mass Efficient

Architecture for Roof Strength (MEARS) project]. (3) Evaluate the study of secondary mass saving on the FGPC solution.

- *ASP340—Lightweight Front Suspension:* Develop steel-intensive front lower control arm designs that meet the mass and performance of baseline forged Al design at 30% less cost and offer significant weight reduction when compared to traditional steel and cast iron designs.

Accomplishments

- *ASP050—Advanced High-Strength Steel Stamping:* Developed an edge fracture criteria that can be used in finite-element analysis (FEA) tools. Developed, published, and distributed the AHSS Application Design and Stamping Process .
- *ASP061—Nonlinear Strain Path:* Developed a test plan, sample preparation procedures, and data analyses techniques and templates. Data collection has begun, using Digital Image Correlation (DIC), on conventional and pre-strained tensile coupons. Investigation of temperature dependence has also started.
- *ASP230—Tribology:* Implemented the initial results from these tests; continuous improvement is critical to the successful application of AHSS.
- *ASP350—Precision Flow Form Application Development:* Initiated the design and FEA analyses.
- *ASP070—Joining Technologies:* Created and distributed a software application that allows original equipment manufacturers (OEMs) and suppliers to quantify and compare the manufacturing and business costs of various automotive welding and joining processes.
- *ASP160—Sheet Steel Fatigue:* Completed single lap shear, double lap shear, and start-stop weld joint testing.
- *ASP330—Vehicle Structural System Benchmarking:* Identified a statistical methodology to normalize mass comparisons and the current state-of-the-art mass performance for 16 structural subsystems and, in addition, developed power law predictive mass models for the structural subsystems.
- *ASP241—Future-Generation Passenger Compartment:* Accomplished the following: (1) The Phase 2 (Validation) project achieved a 39.8 kg (-15%) mass reduction in the optimized components of the combined passenger compartment and doors compared to the donor vehicle. (2) The MEARS lightweight solution with extensive use of AHSS combined with nylon inserts at critical locations enabled the performance to be increased from 1.8 times to 3.0 times while reducing mass by 4.4 kg. (3) The mass compounding study findings conclude that when all subsystems can be resized, a primary mass savings of 1 kg enables a secondary mass savings of 1.5 kg. When the powertrain has been fixed and is not available for resizing, the secondary mass savings is approximately 0.6 kg/kg.
- *ASP340—Lightweight Front Suspension:* Completed two stamped control arm designs and one forged design that met project objectives. The stamped designs met the target weight and met or exceeded performance targets. The project demonstrated that steel reduces suspension component weight and saves cost through design optimization.

Future Direction

- *ASP050—Advanced High Strength Steel Stamping:* Complete microstructure study on edge cracking.
- *ASP061—Nonlinear Strain Path:* Continue data generation for transient hardening, forming limits, and fracture and bake hardening. Select and develop models to represent the observed material behavior.
- *ASP230—Tribology:* Project closed FY 2010.
- *ASP350—Precision Flow Form Application Development:* Complete design of differential case, build tools, and acquire material.

- *ASP070—Joining Technologies*: Project closed FY 2010.
- *ASP160—Sheet Steel Fatigue*: Project closed FY 2010.
- *ASP330—Vehicle Structural System Benchmarking*: Project closed FY 2010.
- *ASP241—Future Generation Passenger Compartment*: Project closed FY 2010.
- *ASP340—Lightweight Front Suspension*: Project closed FY 2010.

Introduction

Advanced high-strength steels (AHSSs), because of their unique mechanical properties, have the potential to reduce vehicle mass. AHSSs differ from conventional mild steel and High-Strength Low-Alloy (HSLA) steels because they are produced using unique combinations of alloy composition and processing methods to achieve their high strength without compromising formability. There are four unique families of AHSSs with subgrades within each: Dual Phase, Complex Phase, TRIP, and Martensitic steels. Each family has unique properties (quasi-static, fatigue, and high strain rate) and manufacturing characteristics (joining, stamping, hydroforming, and precision flow forming), which need to be fully understood if the materials are to be successfully applied to high-volume automotive applications. To maximize the mass savings that can result from using these materials, focal design projects have been carried out to better define the manufacturing processing issues and needs to most effectively apply these new materials to reduce vehicle mass. Using design optimization tools, the Auto/Steel Partnership (A/SP) also demonstrated the need for even more advanced or next-generation steels. Work has focused on developing the critical manufacturing technologies necessary to produce parts using these materials economically (cost parity) on a high-volume basis. In addition, work has been done to understand the properties of these materials that are important to product durability and safety. These steels are 100% recyclable, and there are no known recyclability issues. The objective is to enable the use of advanced steels to create components and structures with mass reductions of 25% and greater to meet FreedomCAR goals.

Stamping is the most common way of transforming sheet steel into the complex shapes that make up the automobile. To be efficient and timely, the process to develop dies to convert sheet to complex shapes needs to incorporate sound product/process decisions with accurate math-based tools. The empirical knowledge base and math tools that had worked so effectively in designing dies for conventional steels were not adequate when applied to AHSSs. Over the past year, the focus of this task (Advanced High-Strength Steel Stamping-ASP050) has been to improve the springback and fracture predictability of the math-based tools used to design dies.

It is recognized that sheet metal follows nonlinear strain paths during forming operations and crash events and that nonlinearity is more important for AHSSs than lower strength steels. This task (Nonlinear Strain Path-ASP061) aims to deliver a comprehensive set of experimental data and predictive models for AHSSs under nonlinear strain path deformation. The models will include constitutive behavior, localized necking and fracture criteria for stamping and vehicle crashworthiness simulations. The results will enable more efficient vehicle design and more weight reduction opportunities, taking advantage of the rapid hardening behavior of AHSSs, and will accelerate the use of AHSSs by reducing the cost and time required for stamping die development.

AHSSs have been very destructive to stamping dies, and the problem has increased as the strength of the AHSSs has progressed from the 590 grades through the 780 grades and to the 980 grades. The task ASP230 (Tribology) aims to deliver information that will lead to improved die designs, die materials, and surface treatments that will allow continued commercial application of AHSSs for mass reduction.

Flow forming, a more recent advancement in the metal spinning technology, elevates metal spinning to a higher plateau. It differs dramatically from other types of spinning. For certain classes of parts, preliminary work suggests the process offers the potential of reducing mass by more than 50% over current technologies. This project (Precision Flow Forming-ASP350) is focused on demonstrating that flow-forming technology is capable of producing high-precision parts from sheet metal at thicknesses greater than 10 mm to attain major mass reduction.

Joining is a critical process in the high-volume production of automobiles. The AHSS Joining Technology Task (ASP070) has been aimed at providing the knowledge to assemble AHSSs into vehicles. For a variety of reasons, welds need to be repaired,

and a project completed this past year provides the information needed to select appropriate methods to do weld repairs. Because vehicle subassemblies are produced by many subcontractors, there is also a need for weld standards. Based on past work done under this task, a revised AWS/SAE D8.9M:2002 (Recommended Practices for Test Methods for Evaluating the Resistance Spot Welding Behavior of Automotive Sheet Steel Materials) has progressed to the final stage of balloting. Engineering data has also been generated to support a similar specification for gas-metal arc welding (GMAW).

As structural components are optimized and thinner gauge, higher strength materials are assessed, fatigue life of the component and the areas where loads are transferred become increasingly important considerations to ensure durability requirements are met. To assess the performance of a component in the design phase, the fatigue characteristics of the base material and the joints, where loads are transferred, must be known. The Sheet Steel Fatigue Task (ASP160) has essentially completed testing of various grades of steel as well as various grades of steel that have been spot welded, adhesively bonded, weld bonded, and metal inert gas (MIG) welded. The experimental data generated under this project have been used to validate fatigue modeling techniques.

Vehicle structure lightweighting programs generally claim mass reductions relative to a single reference point that is poorly defined relative to the current state of the art in current production. The current state of the art of structural mass performance and the metric by which designs can be compared are not known. In addition, a comparison of architectures, materials, and manufacturing strategies that result in best-in-class mass performance is not known. Such an understanding is critical to setting appropriate goals and comprehending the value of lightweighting projects. The Vehicle Structural Systems Benchmarking Task (ASP330) addresses these information gaps to provide a statistical reference for the relative mass reduction capability of materials, the current state of the art in mass reduction, and a basis by which comparisons can be made.

AHSSs have unique material properties and manufacturing characteristics. To maximize the mass reduction and minimize cost of utilizing the new material, the design needs to be optimized around the unique characteristics of the new materials. To better understand the mass reduction potential of AHSSs, focal design projects were conducted for the body-in-white (BIW) [ASP241– Future-Generation Passenger Compartment (FGPC)] and a chassis component (ASP340—Lightweight Front Suspension). The FPGC task resulted in an estimated 15% mass reduction on a subsystem that weighed 264.7 kg at cost parity.

The Lightweight Front Suspension task created a design that was equivalent in mass to AI design but reduced cost by approximately 30% at high-volume production.

Activity and Developments

Advanced High-Strength Steel Stamping—ASP 050

Principal Investigator: Changqing Du, Chrysler Group LLC
(248) 576-6680; e-mail: CD4@chrysler.com

Principal Investigator: Ching-Kuo Hsiung, General Motors Corporation
(586) 907-1015; e-mail: Ching-Kuo.hsiung@gm.com

Introduction

AHSSs are increasingly being used to deliver superior vehicle safety performance, while at the same time provide opportunities for mass reduction. FEA has been widely used in automotive industry for vehicle designs and manufacturing feasibility. However, two major challenges remain: (1) inability to accurately predict springback and deliver compensated stamping tool surface and (2) inability to predict shear fractures (stretching with bending) using conventional FEA analysis techniques, and this has resulted in significant issues during tryout of AHSS parts. To address these issues, the A/SP initiated

enabler projects, focusing on stamping experiments using production-intent tooling, with the results being compared to analyses conducted using computer (FEA) models. To date, various classes of automotive parts have been studied, which were fabricated from AHSSs with tensile strengths varying from 600 to 980 MPa.

Approach

- Springback prediction and Die Face Compensation – Finite-element modeling and correlation to experiment.
- AHSS Fracture – Characterization of fracture during stamping of AHSS to guide stamping process and steel development.

Results and Discussion

A compensation software package developed by the U.S. Automotive Materials Partnership (USAMP) was used to predict a compensated surface. The approach was to form DP780 parts using dies cut to the compensated surface. Parts were then measured and compared to the nominal target.

The results showed that “twisting” was not being compensated, perhaps caused by the compensation process, which was used to avoid the “die back draft” at the top of the B-pillar in the area that showed the twist.

Tests were also conducted as an evaluation of LS-Dyna material models. Two types of material models in the simulation were evaluated. Better results were achieved using Mat125 in LS-Dyna. Overall, in most critical areas, the shapes predicted by simulation correlate well with the real panel shape, except on some portions in the area of the flange.

B-Pillar—DP980 Formability

Die tryout was refocused on a DP980 formability evaluation. Ten different grades from different suppliers were run—five from North America steel companies and five from foreign steel companies.

Various results were achieved. The newest materials showed the best formability. Additional work was scheduled to be completed in calendar year 2010 including the following.

- Analysis from a GM lab: Tensile, Microscopy, Chemistry
- Surface chemistry and surface roughness
- Circle gridded blank and surface strain analysis
- Laser trim and scan for springback study

Edge Cracking—Large Cutout Panels

The objective of the project was to develop edge fracture criterion for large-radius stretched features. Sets of Chrysler LLC Edge-Cracking Experimental Dies were used (Figure 1).

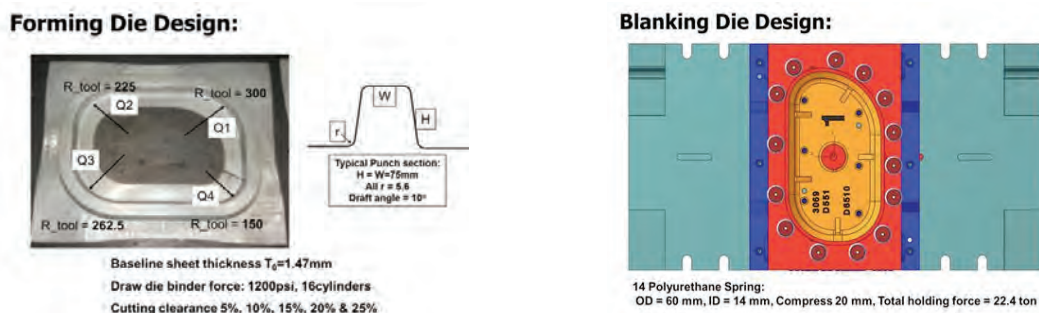


Figure 1. Edge cracking draw panel and blanking die design.

Thinning and edge fracture were characterized and correlated with process conditions. Nineteen materials were selected for the experimental tasks. Mechanical properties were tested by the GM Material Laboratory, 236 cracked samples were prepared at AutoDie International, LLC. Thinning measurements were conducted at Applied Engineering Technologies (AET) Inc.

Edge thinning limits have been proposed/measured for evaluating the edge stretching failure for AHSSs (up to 980 MPa) panels with interior cut (Figure 2).

The knowledge/data can be used in FEA evaluation, die tryout, and monitoring production parts. For the AHSS sheets in this study, the sheared edge thinning limits increase with reduced tensile strength, in general. No clear-cut relation was found regarding the effect of cutting clearance on edge thinning limit. The edge thinning limit for of TRIP780 is greater than that of DP780. The edge thinning stretched along rolling direction, marked as R (rolling direction) in Figure 2, is higher than that along the transverse direction, marked as T (transverse direction) in Figure 2.

Edge Cracking—Medium Cutout Panels

The flat punch hole expansion test and cut edge test is used to study edge fracture limits under various geometric, edge trimming, and material thickness conditions (Figure 3).

The same materials were used for both sets of edge cracking tests, and the results will be analyzed. The materials tested include DP780 and DP980 (1.0, 1.4, 1.8 mm) with four cutting clearances. Measurements, including edge thinning, are in process. Results are projected to be concluded in 2011.

Microstructure Study on Edge Cracking—Wayne State University

The characteristics and microstructure on sheared edge conditions have been investigated through edge cracking projects in cooperation with Wayne State University. The goal was to obtain a detailed understanding of edge fracture phenomena. Preliminary results are shown in Figure 4. The optical microscopy (OM) method was used to identify and measure the four zones on the sheared edge surfaces, Rollover, Burnish, Fracture, and Burr, as shown in Figure 4.

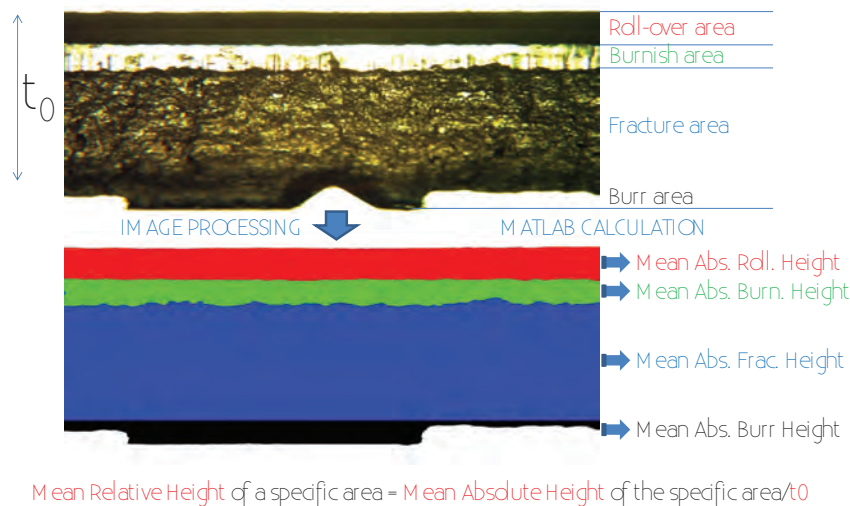


Figure 4. Sheared edge characteristic and measurement using optical microscopy.

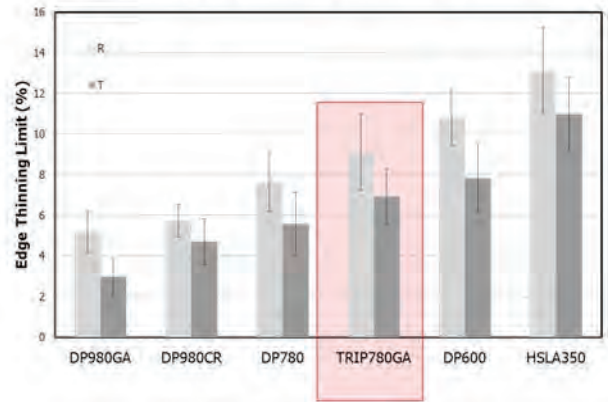


Figure 2. AHSS edge stretch limit for thinning.

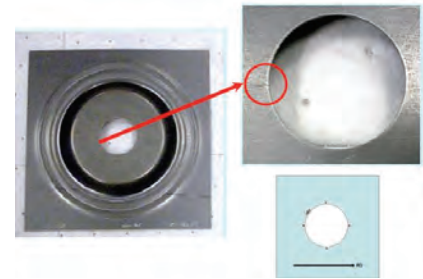


Figure 3. Medium cutout panel and large-size cutout measurement.

Figure 5 shows the trends of these four zones as the material tensile strength increases for a set of samples with a hole size of 80 mm in diameter.

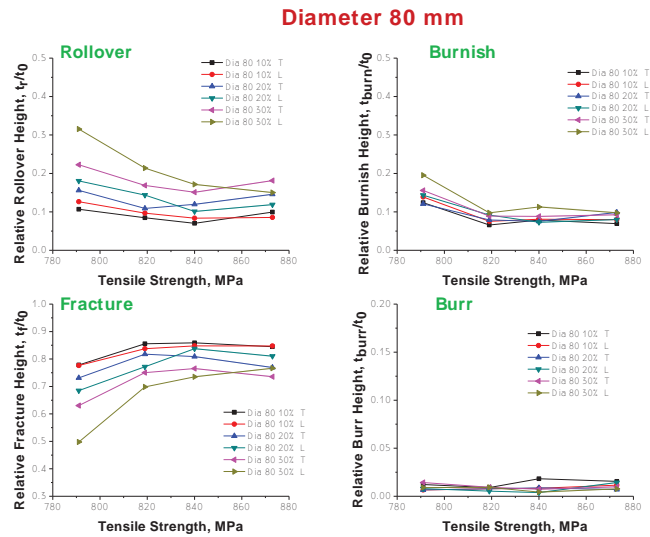


Figure 5. Trend of the four zones as material strength increases.

The investigation on the effects of characteristics and microstructure to the edge fractures is continuing at Wayne State University. The project will be completed in September 2011.

Blanking Force Study—Staged Punch

The objective of the blanking force study was to investigate the press force requirement when a Staged Punch is used for DP980 steel blanking. The approach was to conduct experimental testing to compare the press forces between a Flat Punch and a Staged Punch using an existing Chrysler Large Size Cutout blanking die sets. The results shows that the press force with the Staged Punch can be reduced by about 50% while the Cutting Noise Energy can be reduced by 36~77%.

Plane Strain Fracture Limits

The objective was to determine experimentally the plane strain formability of 50KSI HSS, DP600, DP780, DP980, and TRIP780 sheet metal as a function of pulling direction (0° and 90°) with respect to the rolling direction. The results of testing three samples of each of the five materials show significant different fracture strains in 50KSI HSS and Trip 780 samples only. The team determined that continued study is needed; that is, more samples of each material should be tested. This is shown in Figure 6.

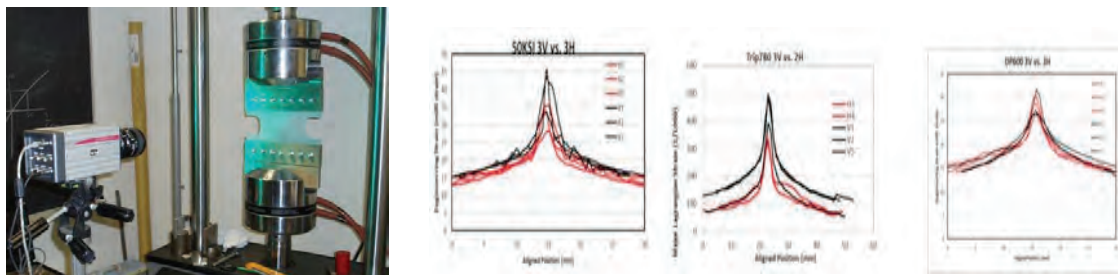


Figure 6. Digital Image Correlation measurement/experiment tensile test setup and major strain measurement.

Digital Image Correlation (DIC) Measurement on Hole Expansion—Oakland University

The project goal was to measure the strain distribution history up to edge fracture on a flat and a conical punch. The results from a total of nine test cases using six grades of materials were tabulated and graphed. The DIC results provided a detailed strain history data to be used for further study (Figure 7).

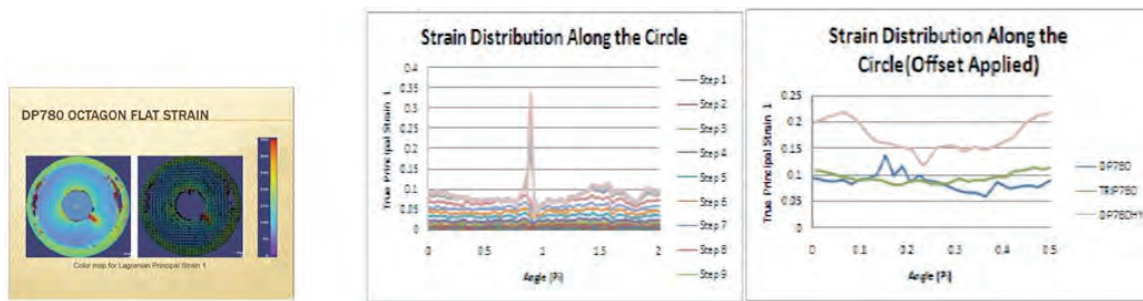


Figure 7. DIC strain measurement results.

Conclusion

The Shear Fracture Project and final report was completed by Edison Welding Institute in conjunction with the Ohio State University (OSU) in December 2009. Results show that stretch-bending fracture type can be predicted with knowledge of material and process variables. The FEA simulation results, using a OSU-proposed thermomechanical constitutive model, duplicated the fracture types observed in stretch-bending experiments within acceptable accuracy. FEA modeling at the microstructural level is also being investigated to determine if it provides value in predicting these fractures.

A Skid-line project was completed in July 2010. The results of this project provide experimental evidence and guidelines for OEM’s steel outer panel quality improvement.

The large-scale edge cracking project, using a production-scale die set, was completed in July 2010. Through this project, more than 250 samples of multiple grades of AHSS were tested, measured, and studied. The criterion of edge stretching without cracking has been established for AHSS stamping production. The medium-scale edge cracking project, using a 6 in. punch, was completed September 2010.

A DP980 B-Pillar forming and springback evaluation was completed September 2010. The results showed that five sets of DP980 steel sheets provided by five different steel suppliers were tested through the B-Pillar part draw die, the same die used for a DP780 B-Pillar part. The two DP980 steels from overseas steel suppliers performed well on formability and without die surface galling issues. The parts made by domestic steel suppliers had fractures in one or more locations. Die galling issues for non-coated steels or zinc powdering for zinc coating steels were observed after stamping one part in most of the domestic steel trails. The team is investigating an explanation for the differences between foreign steels and domestic steels.

Nonlinear Strain Path—ASP 061

Principal Investigator: Cedric Xia, Ph.D.; Ford Motor Company
(313) 845-2322; e-mail: zxia@ford.com

Principal Investigator: Thomas B. Stoughton, Ph.D.; General Motors Company
(586) 986-0630; e-mail: thomas.b.stoughton@gm.com

Principal Investigator: Chang-Qing Du, Ph.D.; Chrysler Group LLC
(248) 576-5197; e-mail: CD4@chrysler.com

Introduction

Current product performance simulations using commercial finite-element design packages for formability and crashworthiness generally assume that the vehicle body parts are not deformed at the start of the simulation, with a uniform thickness for a given part. For more accurate prediction and correlations of design intent to product manufacturing and performance, it is critical to incorporate prior manufacturing effects such as forming and bake hardening into product performance simulations with more reliable constitutive and fracture models so that the full potential of lightweighting can be realized. The Nonlinear Strain Path (NSP) project aims to deliver a comprehensive set of experimental data and associated predictive models for AHSS under nonlinear strain path deformations. The models include constitutive behavior, forming limit and fracture criteria for stamping/hydroforming simulations, and vehicle crashworthiness simulations. The materials of

focus are DP600 and DP780 grades, with DDQ and BH210 as baseline comparisons. Exploratory work will also be done on DP980 and TRIP780 grades. The developed and validated models will (1) enable efficient vehicle design for more weight reduction opportunities to take advantage of the rapid hardening behavior of AHSS and (2) enable the acceleration of AHSS usage by reducing the cost and time for AHSS manufacturing.

Approach

The collaborating partners include Chrysler Group LLC, Ford Motor Company, General Motors Company, ArcelorMittal, Severstal, and U.S. Steel, supported by up to a dozen test laboratories, finite-element modeling (FEM) software vendors and stamping technology vendors. The research is facilitated and coordinated by the National Center for Manufacturing Sciences (NCMS) which serves as Technical Project Administrator. The project team also includes experimental researchers and metallurgists at the National Institute of Standards and Technology (NIST). The approach is to conduct experiments under nonlinear deformation conditions to characterize the strain phenomena in AHSS sheet, and to identify the gaps between prediction and experiment. The team will then quantify the effects under representative experimental variations of deformation conditions encountered through the life of automotive sheet metal products from the stamping plant to the vehicle service. Data collection tasks will take full advantage of recent advances in Digital Image Correlation (DIC) technology in the experiments. DIC is an optical method that employs tracking and image registration techniques for accurate 2D and 3D measurements of deformations, displacement, and strain from the digital images. Based on the correlation results, the project will identify the best available advanced constitutive, forming limits, and fracture models applicable to nonlinear deformation of sheet steels. The best models from the validation will then be implemented in production software for stamping and crashworthiness.

Results and Discussion

The project was kicked off on September 29, 2009, and has made significant progress in FY 2010 as discussed below.

Experiment Planning and Material Testing

The NSP team developed a consensus test matrix addressing the boundaries encompassing both crash and formability applications of the strain data and drafted a consensus technical specification for tensile testing of six grades of AHSS using DIC apparatus. Specifications were also developed using consensus best practices for DIC data acquisition and detailed data analysis. A second supporting experimental plan was developed for temperature-dependent strain testing.

A Request for Proposal was issued in early March 2010 for competitively soliciting quotes from test laboratories with DIC and high-temperature strain testing capability. After evaluation, Oakland University (OU) was selected to perform DIC testing (approximately 900 tests) on conventional and pre-strained tensile test coupons, and Wayne State University (WSU) was selected to provide test support by investigating the temperature dependence of mechanical properties of steels within the range of DIC testing that addresses normal production stamping operations.

Material Sourcing

The three steel suppliers on the NSP team were contracted to procure and supply materials per the test specifications for DIC and temperature-dependent strain testing tasks. Preparation of gridded control and pre-strained tensile test coupons is under way, that is, uniaxial coupons by ArcelorMittal Lab and equi-biaxial test coupons by General Motors Research Lab.

Simulation Support

Livermore Software Technology Corporation (LSTC), the simulation software vendor, performed supporting finite-element analysis of several tensile test specimen sizes and configurations to provide recommendations of the optimum geometry that is compatible with the DIC and tensile test hardware. The optimal coupon for experimental collection of strain and deformation data is a variant of the ASTM E8 design.

Both DIC and temperature-dependent strain testing experiments were kicked off with OU and WSU, respectively, in August 2010. To date, DIC tests have been completed for DP980, DP 780, and TRIP 780 test samples (Non-bake hardening).

Figure 1 illustrates the five significant deformation location points in the necking region of a typical DIC tensile test coupon that are of interest to the NSP project.

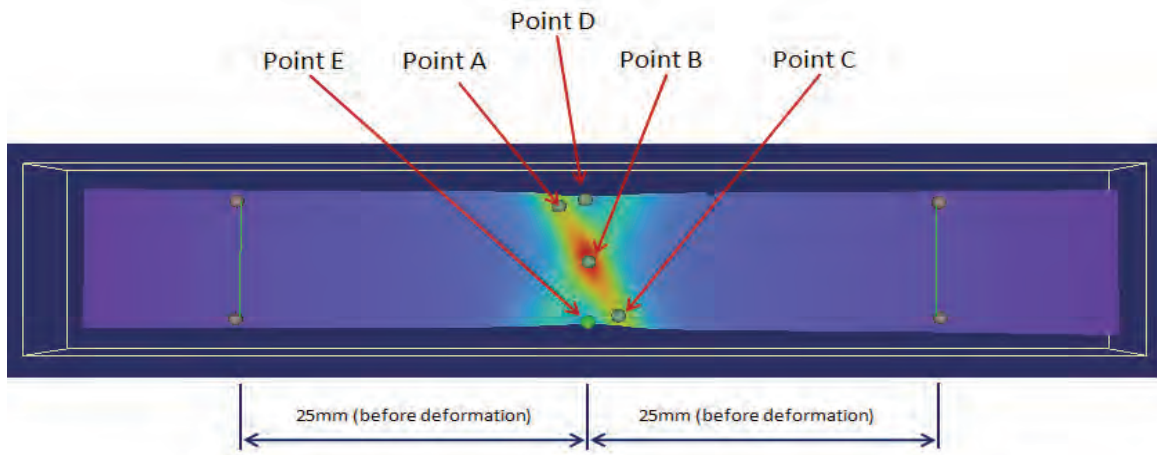


Figure 1. A typical DIC image for a tensile test coupon illustrating the five significant deformation points of interest in the necking area.

Conclusions

After developing consensus test plans, sample preparation procedures and data analyses techniques and templates, the NSP Project has begun data collection tasks for DIC testing and temperature-dependent strain for characterizing transient hardening and bake hardening under uniaxial/equi-biaxial strain path changes. DIC testing is expected to conclude in December 2010.

Tribology—ASP 230

Principal Investigator: Jody Hall, Ph.D., General Motors Company
(248) 670-8123; e-mail: jody.1.hall@gm.com

Introduction

The ability to fully realize the benefits of AHSS depends upon the ability to aggressively form these steels into parts that are a challenge to manufacture. These steels have been shown to cause die failures in early implementations. This project is intended to improve the tribological understanding of the interaction between AHSS, tooling, coatings, and the forming process so that the proper system can be selected to successfully manufacture automotive parts.

Approach

A/SP Tribology members designed a progressive die in which each operation is inserted in a way such that the die can test a myriad of different design conditions, materials, and surface treatments. In addition, a laboratory test was designed to determine the effectiveness of a coating or surface treatment more efficiently and cost-effectively than production. A coating fatigue test will be performed to determine if any correlation exists between the laboratory and progressive die experiment.

Results and Discussion

Progress Die Project—Phase 2

Phase II of the Progressive Die Project tested only trim and pierce conditions. Trimming and piercing are two types of necessary metal-cutting operations in the stamping process. Typically, a rectangular piece of sheet metal, called a blank, is fed into the first die for the forming operation to give the part its shape. Subsequent operations follow that trim the excess blank material from the formed part and cut holes in the panel so that additional parts can be attached later in the assembly operation.

A myriad of AHSS sheet metals were tested that included coated and uncoated materials. There were some results from Phase I that could not be analyzed visually. Optical Profilometry was used in Phase II to determine if a particular standard decreased the wear inflicted from AHSS when no wear was visible. wear.

The pierce in the first station tested 8%, 10%, 12%, and 15% clearance to determine which design allows for the smallest wear rate. Pierce clearance is the designed gap between the sidewalls of the punch and the button in the closed die position. The gap is a measured percentage of the sheet metal thickness. From the Optical Profilometry data in Table 1, 15% is the optimal pierce clearance for AHSS.

Table 1. Pierce clearance data

Break %	Original Surface	Post DP780 Roughness	Post DP980 Roughness	Post DP780 % wear	Post DP980 % wear
8	0.194 μm	0.145 μm	2.068 μm	75.3	711.4
10	0.204 μm	0.066 μm	1.050 μm	27.7	452.7
12	0.224 μm	0.043 μm	1.148 μm	22.5	436.8
15	0.131 μm	0.024 μm	0.705 μm	3.0	271.4

The second pierce station tested different pierce materials: AISI D2, AISI M2, and Vanadis® 4Extra. These materials represent typical tool steels used for cutting metal. The Optical Profilometry data in Table 2 shows that AISI M2 is the optimal material because it has the lowest amount of wear or material removal during this metal-cutting operation. The negative wear value indicated material transfer or buildup on the tooling.

Table 2. Pierce material data

Material	Original Surface	Post DP780 Roughness	Post DP980 Roughness	Post DP780 % wear	Post DP980 % wear
AISI D2	0.585 μm	0.155 μm	0.910 μm	26.5	123.0
AISI M2	1.644 μm	0.22 μm	0.377 μm	1.4	22.6
Vanadis® 4 Extra	0.629 μm	-0.056 μm	0.258 μm	-8.9	45.0

The trim station angle varied from -30° to 30° in 5° increments, and there were two pierce punches added in the last station piercing at the same angles.

Additional testing yielded results that showed the optimal trim angle falls between -20° and 20° while optimal pierce angle is between -15° and 15° . Also, the hardness of the die material showed direct correlation to material performance. This data will be shown in detail in the final report.

Coating Fatigue Test—Phase 2

Three different coatings from three different suppliers were evaluated on D2 substrate test coupons using the modified Coating Fatigue Test apparatus shown in Figure 1.

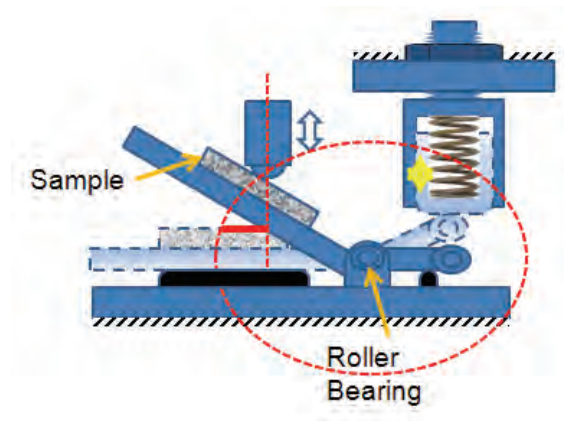


Figure 1. Coating Fatigue Test Phase II apparatus.

Each sample was evaluated for cohesive failures (chipping), adhesive failures (peeling), fatigue cracks, and material transfer. **Table 3** shows the summary of the results for each coating. Columns 2–4 show the severity of each of the failure mechanisms by peeling + chipping / fatigue crack / material transfer with the x’s indicating the severity of the observation of occurrence and the o’s indicating no evidence. The coatings are ranked in order of least to most failure mechanisms, or from 1–6. It was observed that the TiC coating performed the best as a result of having the least severe amount of failures present after 1500 cycles. As shown in **Figure 2**, TiAlN and CrN exhibited more wear than TiC and were more dependent on the supplier of the coating. The results show similar ranking of coating performance as was found in the results of the Phase I Progressive Die Wear Project. In the wear project, D2/TiC performed the best, and D2/TiAlN demonstrated only about half the number of cycles before severe wear occurred.

Table 3. Ranking of coating failures in included impact-sliding tests

Coating	Head	Middle	Tail	Total	Rank (impact)	Rank (sliding)	Rank (fatigue)	Overall Rank
A_TiAlN	xxx/xxx/o	0/xx/0	x/x/0	10	4	3	6	4
B_TiAlN	xxxx/xx/o	Xxxx/xx/xx	Xxx/o/o	17	6	6	5	6
A_CrN	xxxx/xxx/o	Xx/o/o	Xxx/o/o	12	5	5	4	5
B_CrN	xxx/xx/o	x/o/o	X/o/o	8	3	2	2	2
B_TiC	x/o/o	x/o/x	x/o/o	3	1	1	1	1
C_TiC	xx/xx/o	x/xo/x	Xxx/o/o	8	2	3	2	2

The results of the lab-scale Coating Fatigue Test demonstrated good correlation with the results from the production-scale Progressive Die Wear Project and will be used in the future to screen substrate material and coating combinations.

Conclusions

The Progressive Die Wear Test is a cost-effective test tool from which standards can be continuously improved. The original design that permits stations to be altered and/or replaced allows the tool to continue testing the multitude of conditions seen in stamping AHSS parts. The initial results from these tests are already being implemented, and their continuous improvements are critical to the successful application of AHSSs.

The Coating Fatigue Test adds components missing in most coating wear tests — stress and strain from fatigue. This test proved to be an effective and efficient way to initially evaluate material and coating combinations, which will assist in narrowing the search for cost-effective, quality coatings.

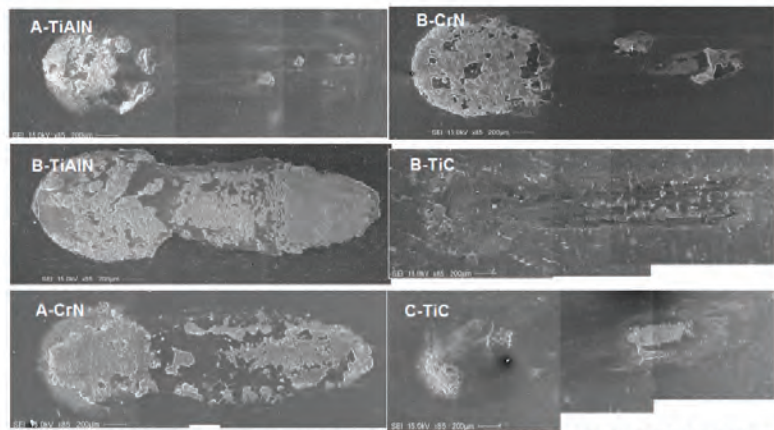


Figure 2. Summary of the impact-sliding tracks of six coatings after 1500 cycles.

Precision Flow Form—ASP 350

Principal Investigator: Todd Cleaver, Tech Knowledge
(734) 675-5562; e-mail: todd@techknowledgeAMD.com

Introduction

Flow forming is one of several types of metal spinning techniques used to produce round sheet metal products. Metal spinning has been known and evolving for centuries. All metal spinning processes use the same basic tools to shape metal. These tools include a lathe-type spinning machine, rollers, and a mandrel. The work piece, or blank, is normally a flat metal

disc or pre-form that is clamped between the mandrel and the machine's tail stock. Rollers are used to apply pressure to the rotating blank, forcing it, in successive passes, to take the shape of the mandrel, which is made to the inside dimensions of the part.

Flow forming, a more recent advancement in the technology, elevates metal spinning to a higher plateau. It differs dramatically from other types of spinning in that rather than shaping the metal by bending or compressing it, the metal is shaped by being forced to flow along the mandrel. Because of the high forming pressures involved, temperatures at the roller-work piece interface typically are 1000°F or higher, causing the metal to soften and flow, hence the name flow forming. Because the process changes the structure of the metal, drastic reductions in wall thickness can be achieved along with very fine accuracy.

Flow forming has been used successfully in the auto industry to produce clutch components with weight and cost advantages. Significant cost and weight opportunities can be achieved in other components as well, such as differential cases, if it can be demonstrated that the flow forming technology can deliver close tolerances with steel blanks of thicknesses over 10 mm (current state of the art). The combination of recent improvements in machine and control capabilities coupled with new control strategies and roller designs may deliver differential cases at net shape with weight savings of over 50% at a net cost savings as compared to the current cast iron. The weight savings vs cast iron will result from

- thinner walls due to higher strength,
- Consistency of wall thickness because there are no draft angles and no molten metal flow issues as in cast processes, and
- the weldable steel, which eliminates the need for bolted flanges.

Approach

Designed experiments will focus on developing the precision flow forming of distortion-free, functional cases and on a distortion free welding process. The outlined tasks are as follows.

1. Launch and Establish Test Criteria
2. Design Differential Case and Tooling
3. Build Tools
4. Acquire Materials
5. Flow Form Process Development
6. Welding Process Development
7. Assemble Differential Cases
8. Validation Testing
9. Information Dissemination and Reporting

Development work is planned to be performed at TransForm, a recognized leader in the application of flow form technology, and at Eaton, the leading supplier of differential cases in North America.

Results and Discussion

The original principal investigator, Linamar, chose to drop out of the project due to other business pressures in December 2009. The project team worked quickly to find other resources to achieve project goals. In March 2010, the project team agreed to a new plan with TransForm and Eaton. The differential case chosen was an Eaton product. TransForm is a recognized leader in the application of flow form technology, and Eaton is a leading supplier of differential cases in North America.

The project team confirmed test and project gate decision criteria in March 2010. Success criteria are all based on achieving equal or better stress and distortion levels at or near 50% weight reduction (flow form design vs nodular iron design). The

final product will be validated against standard bench tests as applied to current production differential cases.

Design and FEA analyses have been initiated by TransForm and Eaton. Progress has been interrupted by the inability to agree on terms and conditions between Eaton, Transform, and USAMP.

Conclusions

An enthusiastic team is in place, and conclusions will be reported as the project progresses.

Advanced High-Strength Steel Joining Technologies Project—ASP 070

Principal Investigator: John C. Bohr, General Motors Company
(810) 602-8276; e-mail: johnc.bohr@gm.com

Introduction

The primary objective of the High-Strength Steel Joining Technologies project team was to provide welding and joining expertise to support the A/SP lightweighting projects and to facilitate the increased use of AHSSs. A secondary goal of the project was to identify and remove barriers to the application of AHSSs to allow automotive manufacturers to reduce vehicle weight and enhance BIW performance.

Approach

As an enabling project we had to anticipate needs of the A/SP lightweighting projects and conduct applied research to address identified barriers and technology gaps. The focus was on materials classified as International Iron and Steel Institute (IISI) Groups 3 and 4 as well as specific materials recommended by the A/SP member companies. Whenever possible we utilized commercially available equipment or equipment typically found in existing manufacturing facilities for AHSS feasibility assessments. The team determined welding parameters to produce quality welds, and then statically and dynamically tested welds produced at these parameters to quantify individual weld structural performance. Process FEM was also used to predict weld quality characteristics and optimize weld process parameters. When used, simulation results were validated with experimental data.

Results and Discussion

Weld Repair and Joint Efficiency Project—Phase III

This work was the third and final phase of the A/SP Joining Technology Committee Joint Efficiency and Repair Welding project. The Phase III effort created a software application to allow automotive OEM’s and suppliers the ability to quantify and compare the manufacturing and business costs of various automotive welding and joining processes to support process selection decisions.

Based on a user-defined scenario (including materials to be joined, projected volume, and the desired joint efficiency), the application calculates system costs directly associated with the selected joining processes. The system cost calculation includes both fixed and variable costs (for a minimum 5 years) but with consideration given to differing organizations’ cost structures and labor rates (user inputs) (Figure 1).

After selecting the processes for the comparison, the user is prompted to review detailed cost collection sheets for fixed and variable costs associated with those processes. Default values may be edited by the users to more accurately represent their cost information (Figure 2).



Figure 1. A/SP cost comparison user-defined scenario.

Equipment Cost Worksheet Reset

Equipment List	Quantity	Total Equipment Cost
Power Supply	1	\$ 5,000
Wire Feeder/Torch	1	\$ 5,000
Fume Collector		
Enclosure		
Installation		

Total Equipment Cost is the total cost for each piece of equipment listed (cost of equipment times the number needed). The installation cost is included in the Total Equipment Cost.

Labor and Maintenance Cost Worksheet

Number of Weld Stations	1	FTE = Full Time Equivalent
Number of FTE Operators to Maintain Weld Station	0.10	
Number of FTE Operators Per Year	0.10	
Labor Rate, Operator	\$70	
Equipment Supplier Annual Maintenance	\$2,500	

Next Sheet

Previous Sheet

Next Sheet

Previous Sheet

Figure 2. Sample cost collection worksheets.

After the user has reviewed and modified, where necessary, the cost data, various charts and graphs are produced for the selected joining technologies. These outputs show the anticipated manufacturing costs for 5 years, the weld performance, and an intangibles ranking (Figure 3). A process cost comparison tool (pivot table) is also generated to allow users to view their data in different ways.

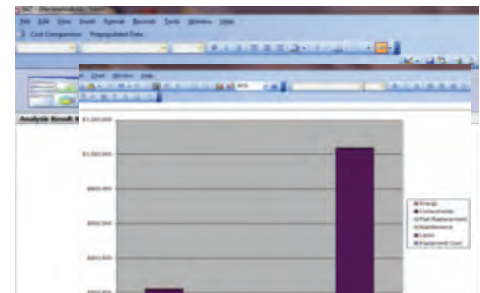


Figure 3. Sample cost comparison graph.

The A/SP Cost Comparison application is distributed on a CD and is required to be loaded to the user's computer. The minimum system requirements to run the application include Microsoft Access, Excel, and Word.

Spot Weld Material Weldability Characterization (ANSI/AWS D8.9M:201X)

The steel test procedures in AWS/SAE D8.9M:2002 (Recommended Practices for Test Methods for Evaluating the Resistance Spot Welding Behavior of Automotive Sheet Steel Materials) were developed for assessing the resistance spot weldability of IISI Groups 1 and 2 types of steels. Although the existing test procedures in Sections 10 (Endurance Test) and 11 (Weld Property Test) of D8.9M:2002 provide useful weldability characteristics, the project team has concurred that this information is incomplete in determining the weldability information necessary to characterize AHSSs.

A revised ANSI/AWS standard has been prepared to address the shortcomings of the existing Recommended Practice and now includes a consensus of standard laboratory test methods to characterize the spot weldability of all types of steel. During the last year, a draft ANSI/AWS standard has been balloted, commented on, and revised as deemed necessary by the project team. As of October 2010, ballots of the AWS D8D Automotive Resistance Welding Subcommittee and the AWS D8 Automotive Welding Committee have been successfully completed. The AWS Technical Activity Committee ballot should be complete by the end of 2010. We anticipate the updated American National Standard and American Welding Society publication to be issued in the first quarter of 2011.

Gas-Metal Arc Welding (GMAW) Weldability Characterization Task

The GMAW characterization of automotive sheet metal entails the identification and understanding of several key process variables. The task undertaken by the Joining Team subgroup in 2010 utilizes statistical analysis to screen several variables for their significance in the characterization process.

A specific Design of Experiment was developed to screen the chosen variables. Specimens were welded according to approved welding procedure specifications (WPS). Mechanical and metallurgical tests have been performed on all specimens. The Design of Experiment Statistical Analysis of Variance (ANOVA) is currently in progress. It is anticipated to be complete by the end of October 2010.

Information obtained from this project is to be used in the development of an industry standard for characterizing the weldability of steel when using GMAW or laser welding.

Conclusions

The work of the AHSS Joining Technologies team continues to demonstrate that steel, including the new AHSSs, can be welded by a multitude of joining processes. The work also has eliminated barriers and misperceptions about utilizing AHSSs for vehicle lightweighting. Automotive OEM and supplier welding expertise and knowledge have been significantly improved as a result of these project activities. Transition has begun on the identification of future projects focused on providing new welding and joining solutions for the automotive industry.

Sheet Steel Fatigue—ASP 160

Principal Investigator: A.K. Khosrovaneh, General Motors Company
(586) 907-5726; e-mail: ak.khosrovaneh@gm.com

Introduction

Future and near-future vehicle designs are faced with several stringent requirements that impose conflicting demands on the vehicle designers. Weight must be reduced while safety requirements are met and cost is contained. Advanced high-strength steels are currently the best material candidate for meeting these mandates at lower cost, compared with aluminum, magnesium, and plastics/composites. As structural components are optimized and thinner gauge, higher strength materials are assessed, fatigue life of the components and the areas where loads are transferred become increasingly important considerations. To assess the performance of a component in the design phase, the fatigue characteristics of the base material and the joints must be known. This project has nearly completed testing for various grades of steel as well as various grades of steel that have been spot welded, adhesively bonded, weld bonded, and MIG welded.

Approach

A number of different joint configurations were tested for the MIG-welded joints, including single lap shear, double lap shear, and start and stop. Great care was taken in this study to ensure that the geometry of the welds was consistent, not only within a given material lay-up but also between all of the specimens of a given type. This was done in order to substantially reduce life scatter and provide a better understanding of the role base material plays in the life of the GMAW joints.

Results and Discussion

Single lap-shear, double lap-shear, and start-stop weld joint testing has been completed. **Figure 1** shows the results for the single lap-shear tests. As can be seen from **Figure 1**, the tests results for stress ratio R of 0.1 and 0.3 are similar, which indicates that the mean stress has no effect on the MIG weld. In **Figure 2**, the scatter between DP590 GI and DP 590-GI is due to the weld profile. Also the scatter for DP590_HR_3.4 between 200,000 and 500,000 cycles are due to weld quality.

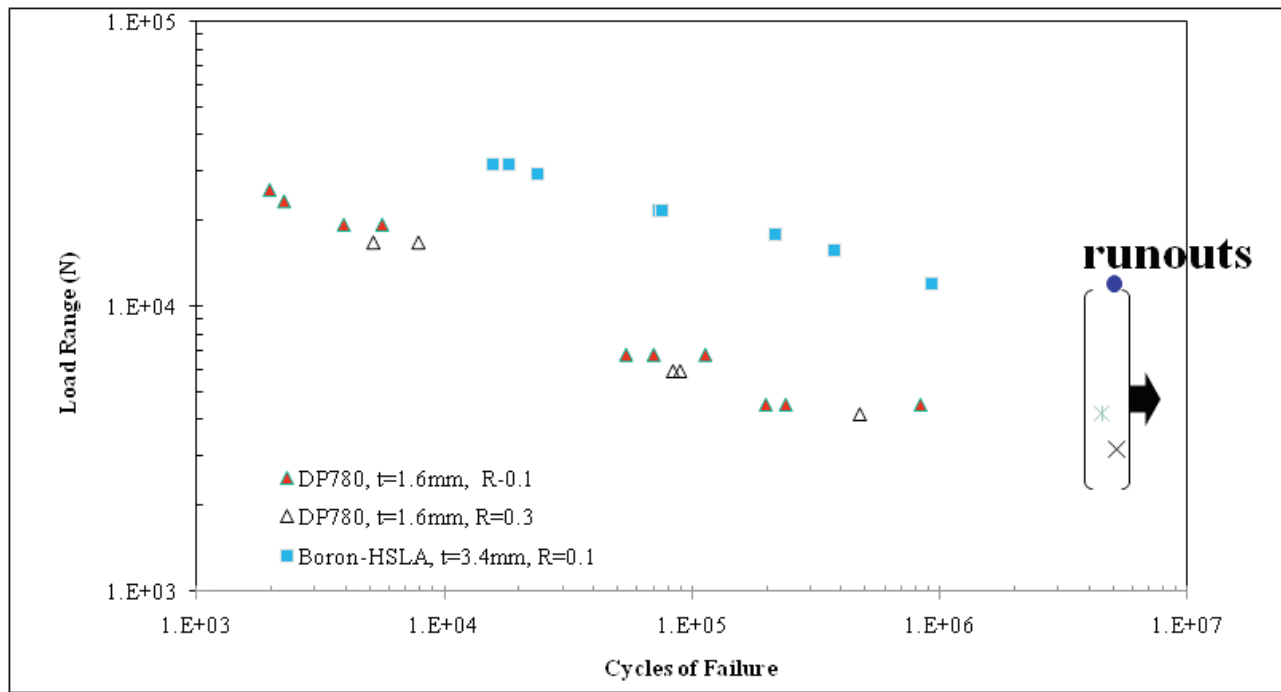


Figure 1. Single lap-shear test results.

The effect of weld starts and stops on fatigue performance was analyzed using the start-stop specimens. Weld starts tend to suffer from incomplete fusion and tend to be relatively flat compared to the center of the weld, and weld stops tend to have some mounding up of the weld metal because the welding torch pushes weld metal ahead of it. Figure 3 shows the fatigue results for the start-stop lap-shear specimens for Phase 2. Note that the data was normalized (dividing load by thickness) to remove thickness effects. Again, the observation made for lap-shear and double lap-shear tests may be made here as well. The parent metal strength does not appear to have a strong effect on the joints, nor does load ratio appear to affect the strength of the joints. Also, more scatter has been observed with the thinner material.

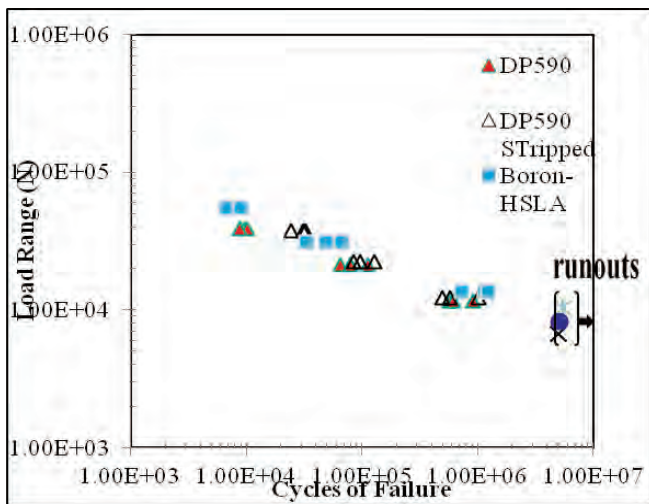


Figure 2. Double lap-shear test data showing the results for the double shear specimens at R = 0.1.

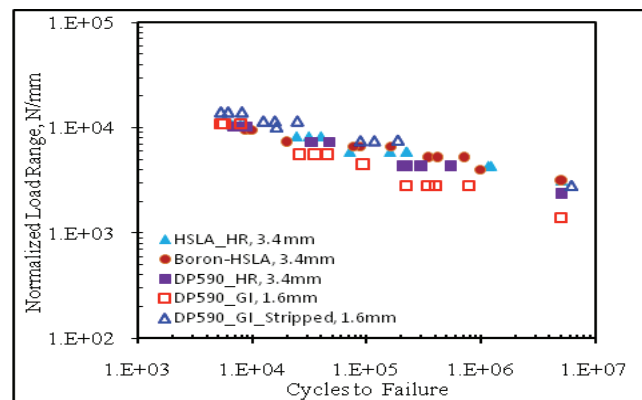


Figure 3. Fatigue test results for start-stop lap-shear specimens from Phase 2.

Also, in this study, the fatigue prediction methods for MIG welds that are available in the commercial software packages have been investigated. This study investigated the methods/algorithms in the nCode DesignLife approach and fe-safe Verity approach. The analysis reveals that both methods provided good correlation between test and analysis.

Figure 4 shows the predicted fatigue life obtained from DesignLife vs experimental fatigue life and fe-safe Verity versus experimental fatigue life for double-lap specimen configuration. As can be seen, in general there is a good correlation between analysis and test results. The 45 degree line indicates perfect correlation between the experiment and the analysis. Due to the scatter inherent in fatigue testing, lines which are a factor of 3 on either side of the perfect correlation line have also been plotted. A correlation is considered good if it lies within the factor of 3 scatter bands.

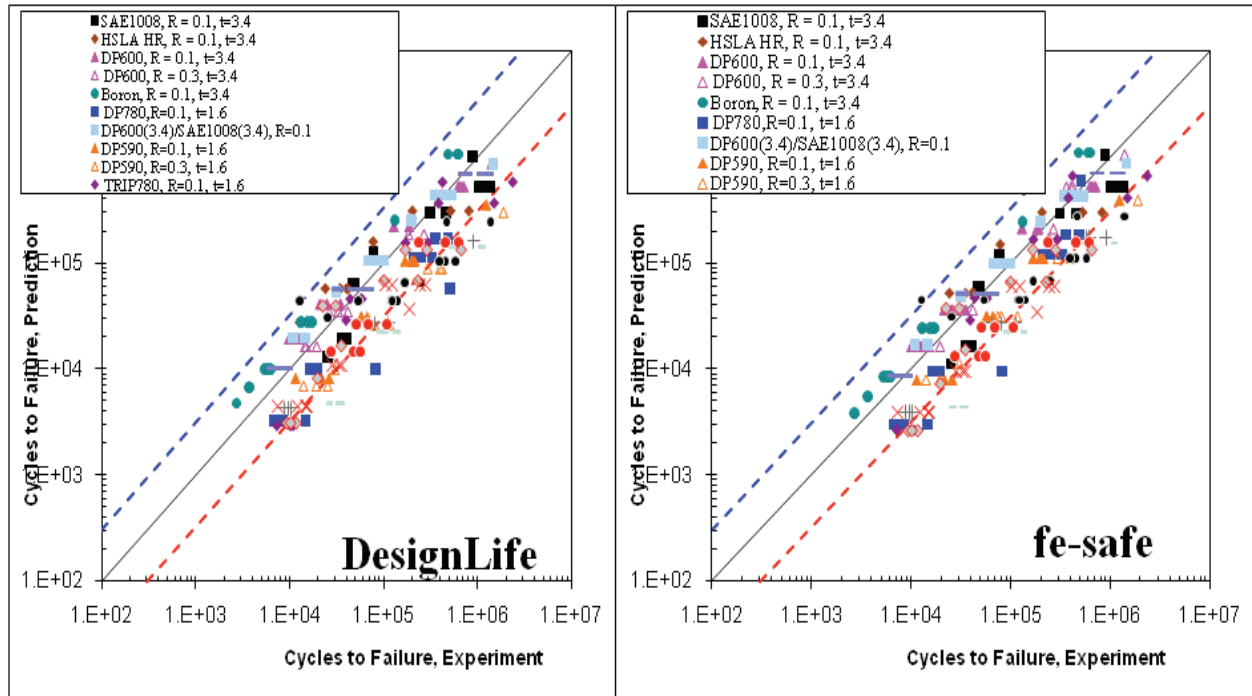


Figure 4. Analysis vs test data for double lap-shear specimen.

Conclusions

The following conclusions were drawn based on the 2010 Sheet Steel Fatigue project.

- For welded joints with reasonably similar weld geometries, parent metal strength does not affect the fatigue strength of welded joints.
- Sheet thickness is a more dominant factor in the fatigue strength of GMAW joints than any other factor in this study.
- Unlike the results of base metal tests, mean stress did not appear to significantly affect weld fatigue.
- Scatter was increased for thinner materials, especially for welds with dissimilar grades.
- Increased difficulty was observed in GMAW welding of very thin sheet.
- Joints with weld stops and starts did not have a significantly greater impact on joint fatigue performance than joints that had no starts and stops.

Benchmarking—ASP 330

Principal Investigator: Jody Shaw, United States Steel Corporation
(248) 267-2808; e-mail: jrshaw@uss.com

Introduction

Vehicle structure lightweighting programs often claim mass reductions relative to a single reference point that is undefined relative to the current state of the art in current production. The current state of the art of structural mass performance and the metric by which designs can be compared are not known. In addition, a comparison of architectures, materials, and manufacturing strategies that result in best-in-class mass performance is not known. Such an understanding is critical to setting appropriate goals and comprehending the value of lightweighting projects. The A/SP Benchmarking project will address these information gaps to provide a statistical reference for the relative mass reduction capability of materials, the current state of the art in mass reduction, and a basis by which comparisons can be made.

Approach

The study evaluated the structural mass of 16 closure and chassis structural subsystems by data mining a large (140+) vehicle teardown database using regression analysis to identify the attributes that correlate with system structural mass, identify the fleet average mass performance of each structural subsystem against significant attributes, develop mass predictive models for each structural subsystem, and identify lightweight outliers. A team of experts were assembled for each structural subsystem to identify candidate mass driving attributes and to evaluate the data. Regression analysis was utilized to identify attributes of statistical significance and to develop power law predictive models of subsystem typical mass as well as lightweight outliers. This enabled the identification of state-of-the-art lightweight outliers within the population of vehicles.

Results and Discussion

An example of the benchmarking report findings is provided for the front door. The expert group considered 13 geometrical, vehicle configurations and door component attributes that may correlate with structural mass. Regression analysis identified the door area as the dominant attribute for mass prediction. Less significant attributes were window regulator type and material. Figure 1 plots the door structural mass against the dominant attribute, door area, and identifies material types. Also plotted are the power law predictions for the typical steel, typical Al, and lightweight outliers. Graphs similar to Figure 1 are provided for all 16 structural systems investigated in the final benchmarking report.

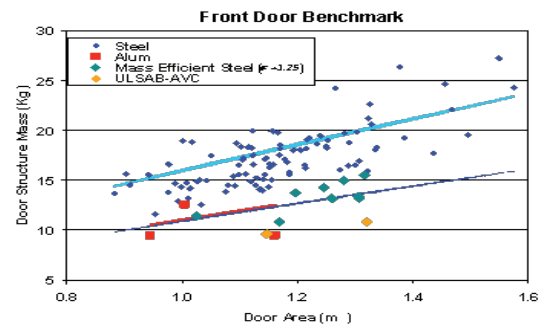


Figure 1. Structural door mass plotted against door area.

The studied revealed a wide mass bandwidth when measured against area. This scatter is attributed to variation in structural performance, material, and design efficiency. While the three Al door structures are significantly lighter than the average steel designs, there are steel designs that provide equivalent mass solutions as Al.

Figure 1 demonstrates the deliverable of establishing a mass normalized mass reference by which lightweighting studies can be benchmarked. An example is provided with the concept designs of the ULSAB-AVC program, which pushes the mass reduction envelope relative to the current state of the art.

The power law equations prediction for the nominal mass of the 16 structural subsystems is shown in Figure 2. The equations identify the component attributes with statistical significance. Figure 3 identifies the power law equations for low mass outliers when sufficient data points are available for statistical significance.

Subsystem	Estimation equation for nominal mass
A. Front door	$\hat{m} = 11.06(\text{Area}, \text{m}^2)^{0.897} \begin{cases} 1.41\text{Fe} \\ 1.00\text{Al} \end{cases} \begin{cases} 1 \text{ if linkage regulator} \\ 0.92 \text{ if other} \end{cases}$
B. Hood	$\hat{m} = 4.28(\text{Area}, \text{m}^2)^{1.24} \begin{cases} 1.65\text{Fe} \\ 1.00\text{Al} \end{cases}$
C. Deck lid	$\hat{m} = 5.039(\text{Area}, \text{m}^2)^{1.1766} \begin{cases} 1.67\text{Fe} \\ 1.00\text{Al} \end{cases}$
D. Hatchback	$\hat{m} = 2.712(\text{Area}, \text{m}^2)^{0.55} (\text{Depth}, \text{mm})^{0.277} \begin{cases} 1.35\text{Fe} \\ 1.00\text{Al} \end{cases}$
E. Lift gate	$\hat{m} = 7.283(\text{Area}, \text{m}^2)^{0.4429} (\text{Mounted mass}, \text{kg})^{0.1558} \begin{cases} 1.38\text{Fe} \\ 1.00\text{Al} \end{cases} \begin{cases} 0.827 \text{ License pocket} \\ 1.000 \text{ No pocket} \end{cases}$
F. Front suspension	$\hat{m} = 1.45(\text{FGAM}, \text{kg})^{0.4292} \begin{cases} 0.733\text{McPherson} \\ 1.000\text{SLA} \end{cases} \begin{cases} 0.881\text{Passenger} \\ 1.000\text{Utility} \end{cases}$
G. Knuckle	$\hat{m} = 0.343(\text{FGAM}, \text{kg})^{0.478} \begin{cases} 0.571\text{McPherson} \\ 1.00\text{SLA} \end{cases} \begin{cases} 1.67\text{Fe} \\ 1.00\text{Al} \end{cases}$
H. Lower Control Arm	McPherson Strut: $\hat{m} = 0.0102(\text{FGAM}, \text{kg})^{0.890} \begin{cases} 1.427\text{Fe} \\ 1.000\text{Al} \end{cases} \begin{cases} 1.390\text{Cast / Forged} \\ 1.202\text{StampedClosed} \\ 1.000\text{StampedOpen} \end{cases}$ Short and Long Arm (SLA): $\hat{m} = 0.002827(\text{FGAM}, \text{kg})^{1.059} (\text{LinkageRatio})^{2.786} \begin{cases} 1.49\text{Fe} \\ 1.00\text{Al} \end{cases}$
I. Rear suspension	$\hat{m}(\text{kg}) = 0.07144(\text{RGAM})^{0.90} \begin{cases} 1.16\text{FWD} \\ 1.00\text{RWD / AWD} \end{cases}$
J. Wheels	$\hat{m} = 0.000148(\text{Diameter}, \text{mm})^{1.296} (\text{Width}, \text{mm})^{0.652} \begin{cases} 1.16\text{Fe} \\ 1.00\text{Al} \end{cases}$
K. Front seat	$\hat{m} = 9.155 \text{ kg} \dots \sigma = 1.98 \text{ kg}$
L. IP Beam	$\hat{m} = 8.75 \begin{cases} 0.858\text{Steel} \\ 0.575\text{Alloy} \\ 1.000\text{Plastic} \end{cases}$
M. Front bumper	$\hat{m} = 7.375 \times 10^{-7} (\text{CurbMass}, \text{kg})^{0.57} (\text{BumperLength}, \text{mm})^{1.053} \cdot (\text{Rail Width}, \text{mm})^{0.587} \begin{cases} 1.49\text{Fe} \\ 1.00\text{Al} \end{cases} \begin{cases} 1.3 \text{ CrushCan} \\ 1.0 \text{ NoCrushCan} \end{cases}$
N. Rear bumper	$\hat{m} = 0.0063(\text{CurbMass}, \text{kg})^{0.374} \begin{cases} 1.457\text{Fe} \\ 1.000\text{Al} \end{cases}$
O. Exhaust system	$\hat{m} = 12.886(\text{Disp}, \text{liter})^{0.1776}$
P. Body in White	$\hat{m} = 3.418(\text{GVM}, \text{kg})^{0.452} (\text{Area}, \text{m}^2)^{0.599} \begin{cases} 1.000\text{Steel} \\ 0.704\text{Al} \end{cases} \begin{cases} 1.02\text{FWD} \\ 1.00\text{RWD} \\ 1.08\text{AWD} \end{cases}$

Figure 2. Structural subsystem power law.

A. Front door	$\dot{m}_{EFF} (kg) = \frac{11.06(Area, m^2)^{0.867} 1.41Fe}{(1.25)(1.146)} \left[\begin{array}{l} 1 \text{ if linkage regulator} \\ 0.92 \text{ if other} \end{array} \right]$
B. Hood	$\dot{m}_{EFF} = \frac{4.28(Area, m^2)^{1.34} 1.65Fe}{(1.2)(0.95)}$
C. Deck lid	$\dot{m}_{EFF} = \frac{5.039(Area, m^2)^{1.1766} 1.67Fe}{(1.12)(1)}$
D. Hatchback	$\dot{m}_{EFF} = \frac{2.712(Area, m^2)^{0.55} (Depth, mm)^{0.177} 1.35Fe}{(1.2)(1.1)}$
E. Lift gate	$\dot{m}_{EFF} = \frac{7.283(Area, m^2)^{0.4423} (Mounted\ mass, kg)^{0.5368} \left(\begin{array}{l} 0.827 \text{ license pocket} \\ 1.000 \text{ No pocket} \end{array} \right) 1.38Fe}{(1.15)(1)}$
F. Front susp.	not evaluated
G. Knuckle	McPherson Strut: $\dot{m}_{EFF} = \frac{0.343(FGAM, kg)^{0.473} (0.571McPherson) (1.67Fe)}{(1.2)(1)}$ Short and Long Arm (SLA): $\dot{m}_{EFF} = \frac{0.343(FGAM, kg)^{0.473} (1.00SLA) (1.00Al)}{(1.2)(1.1)}$
H. Lower Control Arm	McPherson Strut: $\dot{m}_{EFF} = \frac{0.0102((FGAM, kg)^{0.899} \left(\begin{array}{l} 1.390Castr/Forged \\ 1.202StampedClosed \\ 1.000StampedOpen \end{array} \right))}{(1.26)(1.15)}$ Short and Long Arm (SLA): $\dot{m}_{EFF} = \frac{0.002827(FGAM, kg)^{0.899} (LinkageRatio)^{2.766} (1.49Fe)}{(1.12)(0.95)}$
I. Rear susp.	not evaluated
J. Wheels	Steel: $\dot{m}_{EFF} = \frac{0.000148(Diameter, mm)^{1.266} (Width, mm)^{0.633} (1.16Fe)}{(1.192)(1.1)}$ Alum: $\dot{m}_{EFF} = \frac{0.000148(Diameter, mm)^{1.266} (Width, mm)^{0.633} (1.00Al)}{(1.192)(1)}$
K. Front seat	not evaluated
L. IP Beam	Steel: $\dot{m}_{EFF} = 5.19kg$, Alum: $\dot{m}_{EFF} = 3.37kg$
M. Front bumper	Steel: $\left[\frac{7.375 \times 10^{-7} (CurbMass, kg)^{0.55} (BumperLength, mm)^{1.053} (RailWidth, mm)^{0.387} (1.49Fe)}{(1.37)(1.5)} \right] \left(\begin{array}{l} 1.3 \text{ CrushCau} \\ 1.0 \text{ NoCrushCan} \end{array} \right)$ Alum: $\left[\frac{7.375 \times 10^{-7} (CurbMass, kg)^{0.55} (BumperLength, mm)^{1.053} (RailWidth, mm)^{0.387} (1.00Al)}{(1.37)(1.1)} \right] \left(\begin{array}{l} 1.3 \text{ CrushCau} \\ 1.0 \text{ NoCrushCan} \end{array} \right)$
N. Rear bumper	Steel: $\dot{m}_{EFF} = \frac{0.0063(CurbMass, kg)^{0.874} (1.457Fe)}{(1.48)(1.2)}$ Alum: $\dot{m}_{EFF} = \frac{0.0063(CurbMass, kg)^{0.874} (1.000Al)}{(1.48)(1.2)}$
O. Exhaust	not evaluated
P. Body in White	$\dot{m}_{EFF} = \frac{3.418(GVM, kg)^{0.438} (Area, m^2)^{0.599} \left(\begin{array}{l} 1.02FWD \\ 1.00RWD \\ 1.08AWD \end{array} \right) (1.00Steel)}{(1.094)(1)}$, (divide by 1.15 for ULSAB)

Figure 3. Structural subsystem lightweight power law equations.

There are many attributes that correlate with mass of the subsystem. Closures are dominated by the closure area, while suspension systems by gross axle weight. However in all cases, material (steel or Al) is a significant attribute in all subsystems where the material attribute is considered.

Figure 4 compares nominal Al, lightweight steel, and lightweight Al normalized against nominal steel. Conventional thinking is that Al provides a significant mass advantage over steel. However the actual mass reduction is highly dependent on the application, that is, structural subsystem with steel providing the lightweight solution in some cases and Al in others.

Nominal Al solutions provide, on average, a 32% mass reduction relative to nominal steel solutions; lightweight steel solutions provide, on average, a 28% mass reduction relative to nominal steel; and the lightest Al designs provide a 13% mass reduction relative to the lightweight steel designs.

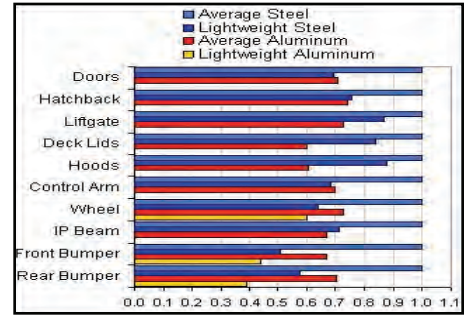


Figure 4. Material mass comparison.

Conclusions

The study identified a statistical methodology to normalize mass comparisons and the current state-of-the-art mass performance for 16 structural subsystems. This approach will allow a meaningful reference for mass reduction project to ensure such projects enhance the current state of the art. The project also developed power law predictive models for the structural subsystems.

This study concludes that lightweight Al designs provide, on average, a 13% mass reduction relative to lightweight steel designs.

The project also identified lightweight outliers. However it is not understood if these solutions were lightweight because of compromises in performance or because of greater structural efficiency. The project also did not define design and manufacturing strategies that result in lightweight designs. A Phase 2 of the benchmarking project is recommended to perform structural performance benchmarking and hardware teardowns to identify the design and manufacturing strategies that enable lightweight low-cost solutions.

Future Generation Passenger Compartment—Validation—ASP 241

Principal Investigator: Jody Shaw, United States Steel Corporation
(248) 267-2808; e-mail: jrshaw@uss.com

Principal Investigator: Joe Polewarczyk, General Motors Corporation
(586) 986-2157; e-mail: joseph.m.polewarczyk@gm.com

Introduction

The Future-Generation Passenger Compartment (FGPC)—Validation objectives are to replicate the findings of the FGPC Phase 1 project on a five-passenger, four-door high-production-volume donor vehicle reducing passenger compartment mass by 25% or more with cost parity relative to baseline while maintaining the structural performance in crash safety, stiffness and durability and architectural constraints. In addition, the MEARS project is the concept development of a large truck cab with no B-pillar that comprehends the increase from 1.5 to 2.5 times in vehicle curb mass roof-strength criteria with weight parity. Both projects will use AHSSs, advanced design optimization techniques, and advanced steel manufacturing while comprehending manufacturing feasibility. Last, a study of secondary mass saving will be investigated and evaluated on the FGPC solution.

Results and Discussion

The optimization methods applied to the FGPC Phase 2 (Validation) project achieved a 39.8 kg (–15%) mass reduction in the optimized components of the combined passenger compartment and doors compared to the donor vehicle. This was achieved with an aggressive use of AHSSs, as shown in Figure 1. A second evaluation and optimization applied continuous joining with structural adhesives to the spot-welded flanges of the FGPC solution. This increased structural performance in stiffness and crash and enabled additional mass reduction to 20%. Technical cost modeling was applied to the baseline, optimized design, and continuous joining design, predicting that this mass reduction could be accomplished at cost parity. The mass and cost comparisons are also shown in Figure 1.

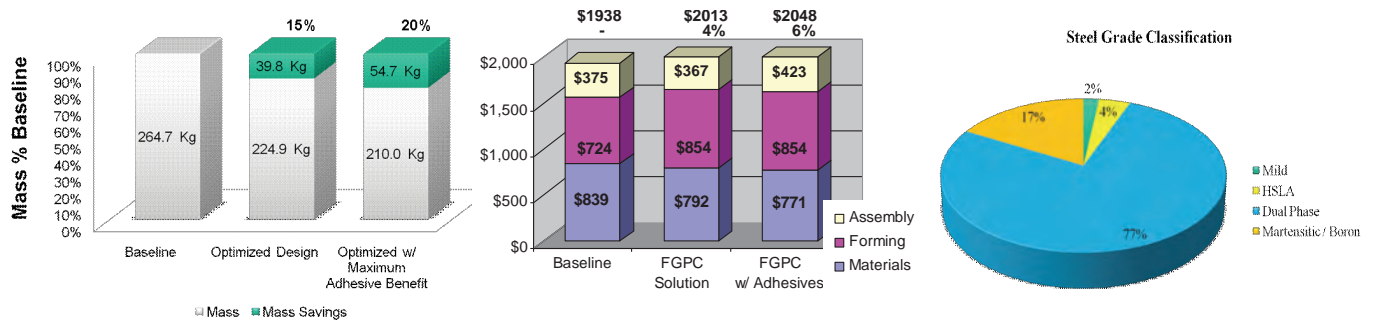


Figure 1. FGPC mass reduction and technical cost modeling results.

The MEARS project objective was to evaluate the impact of the changing roof strength regulations anticipated to increase from 1.5 times gross vehicle weight (GVW) to 2.5. It was found in the FGPC design that for sedans the IIHS side impact controlled the design, resulting in roof strength performance far exceeding the anticipated 2.5 times the requirement. It was felt and confirmed that a B-less pillar extended-cab pick-up truck design would be controlled by roof strength rather than by side impact. The objective of the study was to meet the anticipated 2.5 times criteria at weight parity with the baseline design with performance at 1.5 times. The study identified a broad band width of possible solutions that increase roof strength performance to 3.0 times. The lightweight solution with extensive use of AHSSs combined with nylon inserts at critical locations enabled the performance to be increased from 1.8 times to 3.0 times while reducing mass by 4.4 kg with a cost increase of \$69.48, as shown in Figure 1. The study also confirmed manufacturing feasibility. Many of the design attributes identified in this study were implemented in a production design shortly after the study.

Phase 1 of FGPC found mass body structure mass savings would increase from 30% to 40% when the curb weight was reduced by 20% (identified as mass compounding). This identified that structural mass could be reduced as other vehicle attributes (powertrain, interior, etc.) mass is reduced (Figure 2). The objective of this task was to develop a more comprehensive tool for evaluating the mass compounding effect. The study implemented regression analysis on a database of 112 vehicles including 33 sedans, 10 SUVs, 48 hatchbacks, and 12 vans.

Model	Normalized Load	Mass of Roof Structure (kg)
Donor	1.8	36.1
Phase II Final Design Concept	3.0	31.7

Figure 2. MEARS mass performance.

The study findings conclude that when all subsystems can be resized, a primary mass saving of 1 kg enables secondary mass savings of 1.5 kg. When the powertrain has been fixed and is not available for resizing, the secondary mass savings is approximately 0.6 kg/kg. The study also identified a mass estimation approach for each of the vehicle subsystems and the functional subsystems secondary-mass-savings coefficients, as shown in Figure 3, which were implemented into a vehicle mass configuration and mass compounding calculator. The influence coefficients for sedans are compared for the initial study of 33 vehicles (Old Report) and the findings from the A2MAC1 database (New Report), which are considered consistent with each other. This tool is being applied to concept vehicle programs today.

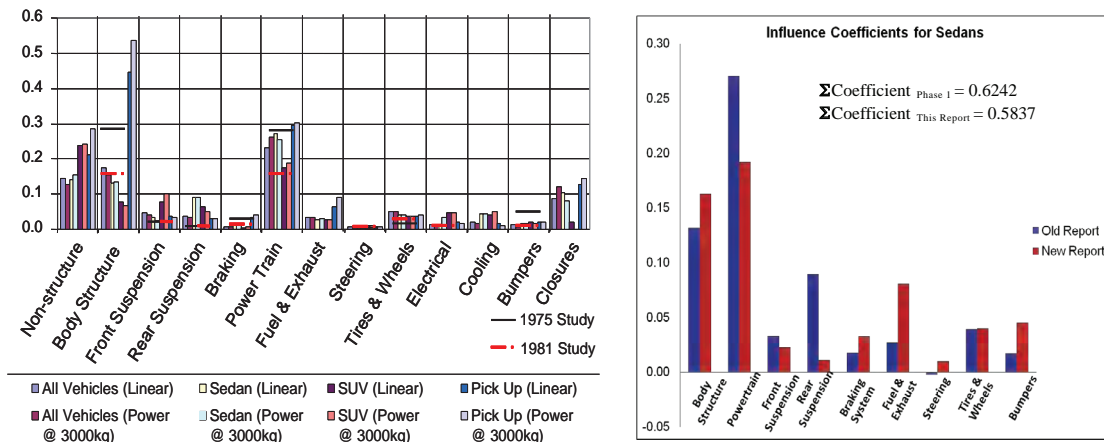


Figure 3. Preliminary vehicle subsystem relative mass and subsystem mass compounding coefficients.

Conclusions

The study provides an effective tool for estimating vehicle functional system mass and vehicle mass for the full range of vehicle types and sizes. Figure 4 presents the body structure mass for a vehicle included in the study. The study also enables an estimation of secondary mass savings of each functional structural system resulting from primary mass reduction if these subsystems are resized. This provides an effective tool for establishing mass targets early in the design cycle.

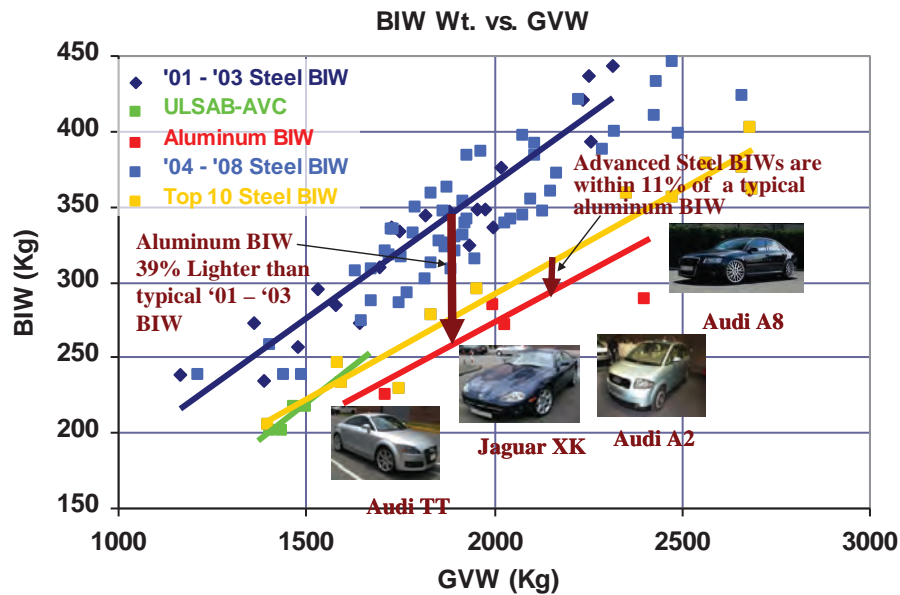


Figure 4. BIW weight vs gross vehicle weight.

Lightweight Front Suspension—ASP 340

Principal Investigator: Bart Depompolo, United States Steel Corporation
(248) 267-2756; e-mail: badepompolo@uss.com

Principal Investigator: Rich Salmon, General Motors Company
(586) 492-3814; e-mail: richard.j.salmon@gm.com

Introduction

The purpose of this 6 month project was to develop steel-intensive front lower control arm designs (one in sheet steel and one in bar steel) that meet the mass and performance of the baseline forged Al design at 30% less cost, and offer significant weight reduction when compared to traditional steel and cast iron designs.

Project Objectives

The project objective is to develop cost-effective designs and manufacturing processes to enable lightweight as-formed steel front lower control arms (sheet and forged alternatives) for a MacPherson Strut suspension system that meet the following criteria (Figure 1) without adversely impacting performance.

- Structural performance equivalent to the current-production (baseline) Al front lower control arms.
- Mass equivalent to the forged Al baseline lower control arm.
- Cost at 30% less than the forged Al baseline lower control arm.
- Must meet available package constraints.
- Complete technical assessment of suspension corrosion requirements and performance.

Approach

The team will design two steel lower control arms to meet the general requirements of the MacPhearson front suspension package of the baseline vehicle. The two solutions will be a sheet steel solution and a forged steel solution with attached ball joints. The designs must include the following.

- FE and CAD models that is readable in Catia and UG.
- Complete static and dynamic load analysis and performance assessment.
- Complete cost estimate of current production Al and steel solutions for production volumes of 30,000, 100,000 and 250,000 vehicles per year for 6 years.

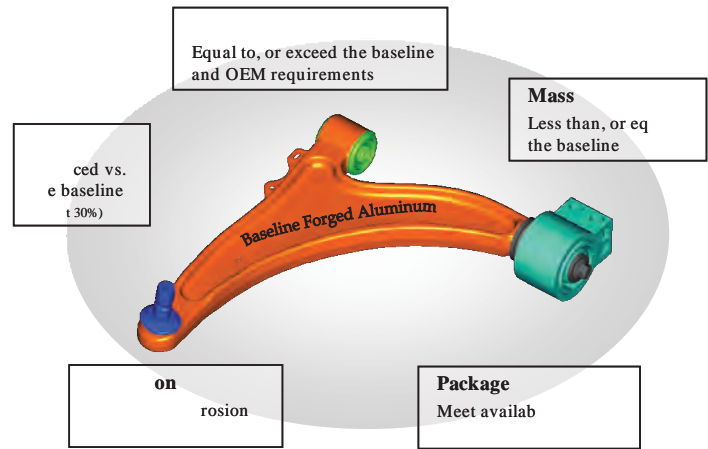


Figure 1. Front lower control arm design targets.

Results and Discussion

The baseline front lower control arm design is the current production Chevrolet Malibu/Buick Lacrosse Al cast/forged component design, as shown in Figure 2. The control arm is a challenging baseline component as it is one of the lightest weight designs as determined from a benchmarking study. The concept study will develop innovative steel designs, with sufficient use of leading-edge technology to achieve the greatest mass reduction while obtaining manufacturing feasibility. The design must provide efficient cost, weight, and performance solutions using new steel technologies. The project is structured in three phases—design, estimating, and technology transfer.



Figure 2. Chevy Malibu forged Al front lower control arm.

Development Process

An iterative optimization strategy was used to minimize the mass of each design while meeting the specified structural requirements. A schematic of the overall development strategy is shown in Figure 3. The optimization process resulted in two stamped steel control arm designs, referred to as the I-beam design and clamshell design, and the forged control arm design, which are described below and shown in Figures 4–6, respectively. All three designs met the design requirements with respect to performance.

The *clamshell design* features an upper and lower stamping, a bushing sleeve, a forged T-pin, and a riveted forged ball-joint housing. All components are assumed to be MIG welded, and the stampings are butt welded to maximize the component cross section.

The *I-beam design* features a web, inboard and forward flanges, a bushing sleeve, a bent tube, a forged T-pin, and a riveted forged ball-joint housing. Note that the ball-joint housing is supported in double shear via an additional reinforcement. All components are assumed to be MIG welded on one side.

The *forged design* used a minimum gage of 3 mm with machined bushing and ball-joint housing.

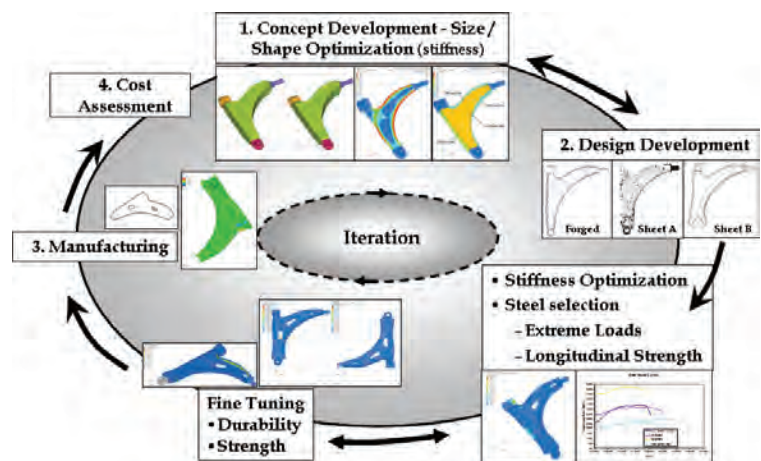


Figure 3. Development process diagram.

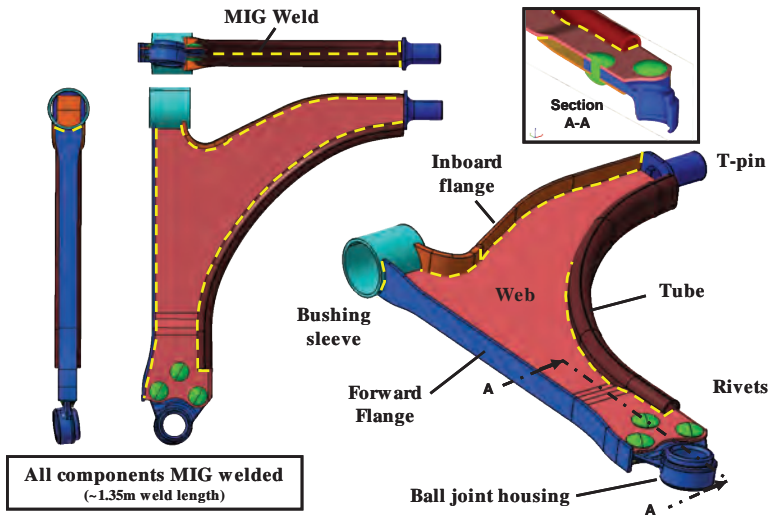


Figure 4. I-beam design concept.

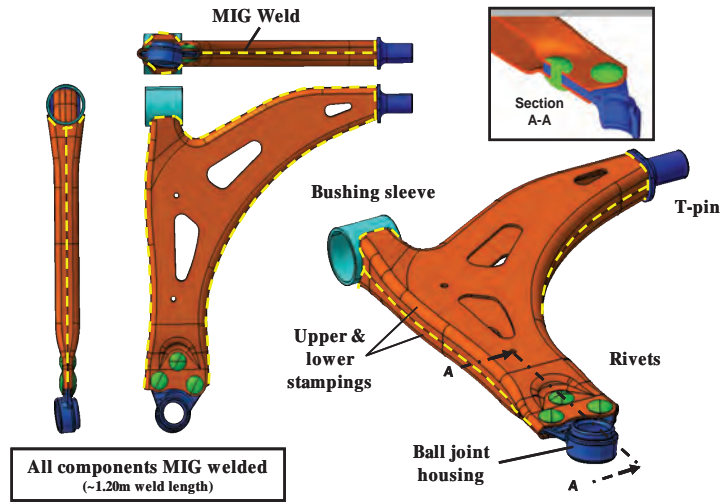


Figure 5. Clamshell design concept.

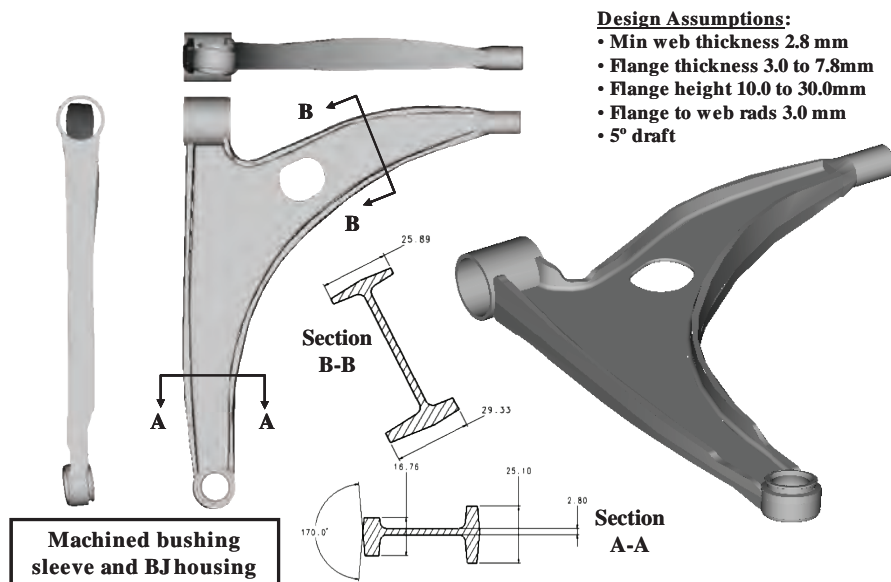


Figure 6. Forged design concept.

Mass Summary

The mass of clamshell design is equivalent to the 3.07 kg baseline assembly mass, while the I-beam and forged steel designs are 2% (0.05 kg) and 4% (0.13 kg) heavier, respectively.

Cost Estimate

The cost results indicate that the clamshell design has a comparable cost to the baseline at the lowest production volume and a 26% to 34% lower cost at the higher production volumes. The I-beam design has a higher cost at the lowest volume but offers a 10% to 21% lower cost for the two higher volumes. The capital and tooling costs for the steel control arm designs are higher than the forged Al baseline at low volume. However, these costs when amortized over increasing production volumes result in steel control arm costs decreasing more rapidly than the baseline.

Conclusions

The results of the study support the following conclusions.

- The Clamshell Design is predicted to have equivalent mass to the baseline assembly with up to a 34% cost reduction potential at a production volume of 250,000 vehicles per year. The design is deemed production feasible based on forming simulations and industry welding examples.
- The I-beam Design is predicted to have the highest buckling resistance and high stiffness with a 2% (0.05 kg) higher mass than the baseline assembly, with up to a 21% cost reduction potential at a production volume of 250,000 vehicles per year. The design is deemed production feasible based on typical welding process development and industry tube bending examples.
- The Forged Design is predicted to have the highest stiffness and durability performance (no welds) of all designs with a 4% (0.13 kg) higher mass than the baseline assembly, assuming an aggressive 3 mm minimum gage manufacturing target.

Conclusions

The project successfully delivered two stamped control arm designs and one forged design that met the project objectives. The two stamped designs met the target weight, met or exceeded the performance targets, and met cost targets. The forged design was within 4% of the target weight and met or exceeded performance targets.

This program demonstrated that it is possible to reduce suspension component weight and save cost using steel to optimize component designs. Automotive OEM interest, as demonstrated by requests for the final report and discussions with Multimatic, is evidence that the project results are significant and may have an impact on future suspension designs.

Presentations/Publications/Patents

Advanced High-Strength Steel Applications—Design and Stamping Process Guidelines, Auto/Steel Partnership, AHSS Applications Guidelines Project Team, January 2010.

Mooney, P. “Stamping 101,” A/SP Steel Technology Transfer, Henkel, September 28, 2010, Madison Heights, Michigan.

Sadogopan, S. “Stamping Technologies,” A/SP Steel Technology Transfer, Henkel, September 28, 2010, Madison Heights, Michigan.

Yan, B. “Shear Fracture of AHSS,” A/SP Steel Technology Transfer, Henkel, September 28, 2010, Madison Heights, Michigan.

ASP 230

Mulholland, T. Investigation of Tooling Durability for Advanced High-Strength Steel. Presented at the 2010 Great Designs in Steel Seminar, May 5, 2010, Livonia, Michigan.

Nie, X. and Su, J. F. Coating Impact Fatigue Test Phase I - Final Report, Auto/Steel Partnership Publication, Auto/Steel Partnership, Southfield, Michigan, April 2010.

Mulholland, T. "Tribology," National Energy Technology Laboratory/USAMP – Auto/Steel Partnership Semi-Annual Technical Review, May 11, 2010.

Nie, X. and Su J. F. Coating Impact Fatigue Test Phase II - Final Report, Auto/Steel Partnership Publication, Auto/Steel Partnership, Southfield, Michigan, July 2010.

Hall, J. N. et. al. "Investigation of Stamping Tooling Durability for Dual Phase Steels." In SAE World Congress Proceedings, SAE, Warrendale, Pennsylvania, April 2011.

ASP 350

Buchholz, K. "Steely Visions of Lightweight Parts." Published in Automotive Engineering International, October 2009.

ASP 070

Bohr, J.; Coon, T.; Jiang, C.; and Bzdok, M. A Comparative Study of Joint Efficiency for AHSS. Presented at Great Designs in Steel Seminar, Livonia, Michigan, May 5, 2010.

A/SP Joint Efficiency Phase III—Cost Comparison (CD). A software application distributed by the Auto/Steel Partnership, October 2010.

ASP 160

Mohan Iyengar, R.; Bonnen, J. J. F.; Young, E.; Maatz Jr., D. F.; Soter, M.; Amaya, M.; Citrin, K.; Khosrovaneh, A.; Link, T.; Schillaci, N.; and Shih, H.-S. "Influence of Weld Process Parameters on the Geometric Variability of the Gas-Metal Arc Welds," SAE Technical Paper Series 2009-01-1549, 2009 SAE World Congress Detroit, Michigan.

Bonnen, J. J. F.; Raghuram Mandapati Kang, H. T.; Mohan Iyengar, R.; Khosrovaneh, A. K.; Amaya, M.; Citrin, K.; and Shih, H. "Durability of Advanced High Strength Steel Gas Metal Arc Welds," SAE Paper No. 2009-01-0257, SAE, Warrendale, Pennsylvania.

Kang, H. T.; Mane, S.; Khosrovaneh, A. K.; Amaya, M.; Shih, H.; and Bonnen, J. J. F. "Durability of Advanced High Strength MIG Weld and Investigation on Some of the Methods Available on Predicting the Fatigue Life of MIG Welds in Body and Frame Automotive Structures," abstract accepted as a 2011 SAE paper.

Kang, H. T.; Mane, S.; Khosrovaneh, A. K.; Amaya, M.; Shih, H.; and Bonnen, J. J. F. "The Effect of Welding Dimensional Variability on Fatigue Life of Gas Metal Arc Welding Joints," abstract accepted as a 2011 SAE paper.

ASP 340

DePompolo, B. "Lightweight Suspension," 2009 DOE Project Review Meeting, October 28, 2009, Southfield, Michigan.

Kanelos, D. "Lightweight Suspensions/Lightweight Control Arm," A/SP Technology Transfer, Chrysler Tech Center, March 11, 2010, Auburn Hills, Michigan.

Fuchs, H. "Lightweight Suspension Front Lower Control Arm Design Optimization," Great Designs in Steel, May 5, 2010, Livonia, Michigan.

DePompolo, B. "AHSS Lightweight Suspension," National Energy Technology Laboratory/USAMP—Auto/Steel Partnership Semi-Annual Technical Review, May 11, 2010.

DePompolo, B. "Lightweight Suspension," 2010 DOE Project Review, October 6, 2010, Southfield, Michigan.

ASP 061

Yoshida, K.; Kuwabara, T.; and Kuroda, M. Path. Dependence of the forming limit stresses in a sheet metal. International Journal of Plasticity, March 2007, 23(3), 361–384.

D. Nondestructive Evaluation Steering Committee - U.S. Automotive Materials Partnership

Field Technical Monitor: Martin Jones
Ford Motor Company - NDE Lab
35750 Plymouth Road; Livonia, MI 48150-146
(313) 805-9184; e-mail: mjone147@ford.com

Field Technical Monitor: George Harmon
Chrysler Group LLC
Body Materials Engineering
Mail Code 482-00-11; 800 Chrysler Drive; Auburn Hills, MI 48326-2757
(248) 512-4840; e-mail: gjh8@chrysler.com

Field Technical Monitor: Leonid Lev
General Motors Company LLC
GM R&D and Planning
Mail Code 480-106-21; 30500 Mound Road; Warren, MI 48090-9055
(586) 986-7450; e-mail: leo.lev@gm.com

Technology Area Development Manager: Carol Schutte
U.S. Department of Energy
1000 Independence Ave., S.W.; Washington, DC 20585
(202) 287-5371; e-mail: carol.schutte@ee.doe.gov

Field Project Officer: Joseph Renk
National Energy Technology Laboratory
626 Cochran Mill Road; P.O. Box 10940; Pittsburgh, PA 15236
(412) 386-6406; e-mail: joseph.renk@netl.doe.gov

Contractor: U.S. Automotive Materials Partnership (USAMP)
Contract No.: DE-FC26-02OR22910

Objectives

- Support the introduction and use of lightweight materials in automotive vehicles by developing rapid, cost-effective inspection methods that ensure the strength and performance of new materials and joining methods.
- Develop resonant inspection (RI) procedures and prediction tools that will ensure the detection of discrepancies in high-strength, performance-critical permanent mold castings.
- Evaluate shearography as an inspection method for resistance spot welds (RSW).

Accomplishments

- Collected and used resonant inspection on more than 400 castings for two production knuckles. These test sets included typical production casting discrepancies and normal variations such as cavity to cavity and degating variability. The parts have all been radiographed, fluorescent penetrant inspected, and weighed, and many have been inspected by computed tomography (CT) and coordinate measuring machine. (FY 2010)
- Created heuristic RI sort modules for the knuckle test sets and statistically analyzed the resonance frequency shifts to determine repeatability, normal variability, and discrepancy sensitivities. This is among the first high-quality assessments of RI and the attributes that determine the probability of detection (POD) for different discrepancies. (FY 2010)

- Designed a novel tensile bar that is ASTM B557M compatible and has isolated resonances which will enable the direct comparison of resonance inspection frequency shifts to material strength and location of the discrepancy. More than 80 experimental cylinders have been cast and radiographed and will be machined into RI-modified ASTM B557M tensile bars. To date, these include shrinkage and oxide inclusion discrepancies. (FY 2010)
- Completed standardized process flow chart for developing RI plans for new parts including step-by-step inputs and outputs, equipment calibration, and statistics-based sample sizes. (FY 2010)
- Completed design of the finite element software that will optimize selection of inspection resonance frequencies and predict the probability of detection using computer aided design (CAD) and engineering inputs. (FY 2010)
- Launched the shearography of resistance spot welds project and reviewed the plan with the OEM community. (FY 2010)

Future Directions

- Complete the resonance inspection vs casting strength correlation study. This includes tensile bar machining, CT inspection, tensile testing, and metallography.
- Complete the finite element software for the simulation of resonance inspections and evaluate its performance using the two baseline knuckles.
- Prepare resistance spot weld coupons with variable button sizes, perform shearography, and evaluate the performance.

Introduction

Many new materials and joining methods are being explored and evaluated in the quest for lighter weight passenger and commercial vehicles. Often these materials and processes introduce new challenges to the quality of automotive structures and components due to their chemical reactivity, lower volumetric strengths, and “newness” in the automotive production environment. Nondestructive evaluations (NDEs) can often ensure the quality of these materials and also reduce their cost by replacing destructive tests with nondestructive ones. The Nondestructive Evaluation Steering Committee has worked with the other USAMP divisions to identify opportunities for using nondestructive testing (Harmon et al., 2006). The focus of these has been high-value, high-need, fast in-line inspections. In addition to collaboration on other projects, the Nondestructive Evaluation Steering Committee is currently sponsoring two focused projects.

The following sections outline the two current projects, which target high-integrity light metal castings and resistance spot welding (RSW). High-integrity light metal castings currently require 100% inspections and use methods that are expensive and may not detect all significant discrepancies. RSW currently relies on spot sampling and destructive tests which have relatively low confidence levels and incur high costs. These are both areas where NDE success can significantly improve vehicle quality and reduce costs, which are among the goals of the Lightweight Materials program.

Activity and Developments

NDE901—Reliability Tools for Resonance Inspection of Light Metal Castings

Principal Investigator: Martin Jones, Ford Motor Company - NDE Lab
 Phone: (313) 805-9184; e-mail: mjone147@ford.com

Introduction

There are many automotive castings that are either safety or performance critical to the vehicle and require 100% inspection with extremely high requirements for the confidence of reliability. These include many chassis and powertrain components.

Usually these have complex shapes and present extremely difficult inspection problems even with multiview x-ray systems or surface-only inspections such as dye-penetrants.

RI (also referred to as acoustic inspection) offers unique capabilities for these inspections. Sound in the range of 100 to 100,000 Hz can readily penetrate small to very large castings and is sensitive to heat treatment, porosity, cracks, and at least some oxide inclusions. RI also has significantly lower capital and piece costs than either radiographic testing (RT) or fluorescent penetrant inspection (FPI). In fact, RI is already used for 100% inspection of many castings such as knuckles, rocker arms, master cylinders, and brake calipers. Despite these advantages, RI has not achieved full automotive acceptance because the sensitivity and robustness cannot be ensured with current implementations.

Approach

Working with RI system vendors and casting vendors, we are developing new tools to improve the robustness of RI in production. Working with RI system vendors, we have a large pool of experience on current implementation processes and recurring issues. Working with casting vendors, we are generating three sets of castings that allow quantitative assessments of resonance frequency shift sensitivities and correlation to casting strength.

The first tool set establishes standard RI processes for the plant. This includes both a process work flow procedure to create the resonance inspection plan for a new part and a standardized procedure to ensure reliability and traceability of RI inspected parts when the RI plan is in production.

The second tool set is a finite element software program that uses the CAD model and the engineering performance requirements for a part and generates the inspection parameters and expected performance. The inspection parameters include the small set of inspection frequencies and a sort module that processes the measured frequency shifts to pass or fail a casting. This finite element model uses finite element submodels for the discrepancies to accurately predict frequency shifts. The program is being written with an acoustic system integrator and has a workbench of tools for verifying the stimulation with measured parts.

Results and Discussion

Standardized Processes

A detailed “Resonant Inspection Process Development Flow Chart” has been completed. This involved much iteration between RI vendors and casting experts to encompass current inspection and casting processes. The flow chart provides a checkoff process for establishing an RI plan. Each step in the process has defined inputs and outputs. The process begins with defining the engineering requirements such as the discrepancies and locations to be detected and the allowed part variation due to mold cavity, degating, or machining variation. This is followed by steps for collecting both good and discrepant parts and for validating an RI inspection plan. This flow chart was evaluated during the selection and inspection of the two production castings being used. To complete the standardization of RIs, it is also necessary to define what is required once the RI plan is implemented in production. This is essential to have reliability and traceability for the inspections. In FY 2009, a workshop was held to lay the foundation for this production document, which will be completed this year using the production inspection experience acquired during FY 2010.

Integrated Tools for POD to Critical Defects

There are three essential ingredients for predicting POD: (1) the sensitivity of the response to the size of the discrepancy: for RI, the response is the frequency shift of a resonance due to the discrepancy; (2) the noise in the frequency shifts due to all sources: these include measurement error (<1 part in 10,000) and resonance variability due to acceptable material variation (typically 1 part in 1,000); and (3) the sort module selected. The discrepancies to be included are shrink porosity, cracks, and oxide inclusions. Both a production knuckle and an experimental laboratory-cast cylinder are being used to develop the POD tools.

The material and resonance frequency variations of the knuckle have been extensively measured. [Table 1](#) and [Figure 1](#) describe the very small variations associated

Table 1. Measured knuckle property variation for a single mold cavity.

Property (# of knuckles)	Std dev/mean
Young’s modulus, E (4)	2,600 ppm
Shear modulus, G (4)	2,000 ppm
Density (4)	900 ppm
Mass (80)	900 ppm
Frequency (80)	370 ppm
Frequency (repeatability)	60 ppm

with knuckles made with a single mold cavity, during a single shift, and heat treated. The repeatability variation of RI is typically very low (<100 ppm).

The global frequency shifts associated with the discrepancies have now been quantified for three discrepancy classes (RT reject/FPI reject/no heat treatment) as seen in Figure 2. These shifts are expressed as the difference of the means for the subset of knuckles divided by the variability of the good knuckles. The frequency shifts are expressed in sigmas.

The knuckles without heat treatment are consistently and substantially (1 to 3 σ) shifted to lower frequencies as expected for a less stiff part. The x-ray discrepancies also show a shift to higher frequencies, as expected for mass reduction, especially for the upper modes. These shifts are only on the order of 1 σ and will be more difficult to detect with RI. The largest shifts were for the surface/FPI rejected parts. These are shifted to higher frequencies by as much as 5 σ at low frequencies and indicate a substantial loss of mass. The statistical significance of these shifts can be evaluated with a modified T test as shown in Figure 3: there are many resonances that could be used to detect each discrepancy type. The frequency shifts associated with gate height have also been measured and corroborated by finite

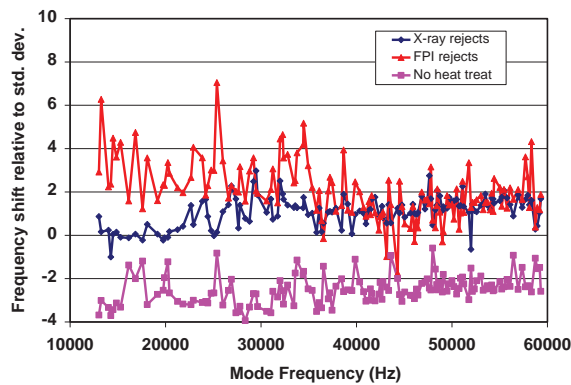


Figure 2. Resonance frequency shifts for different discrepancies in an automotive knuckle casting.

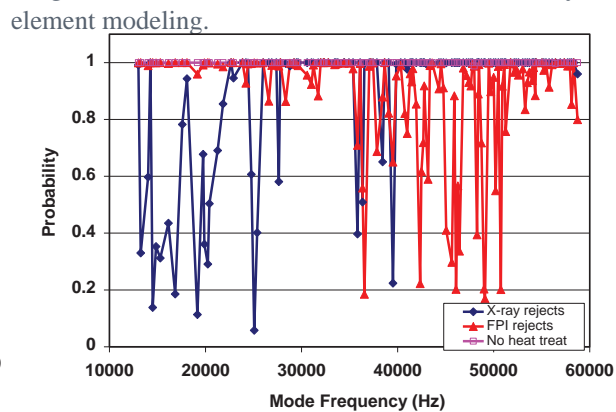


Figure 3. Probability of detection for discrepancies in an automotive knuckle at each resonance.

The knuckle resonance measurements have also been used to create heuristic sort modules using commercially available processes. These sort modules optimize the good/bad sort using the predefined good and bad assignments of training sets. These sort modules provide a baseline comparison to the physics based sort modules under development.

In addition to the automotive knuckle, a series of cylindrical castings with three different diameters have been cast at the Chrysler Technical Center. These allow different sizes and types of discrepancies to be positioned into ASTM B557M tensile bars that are machined from the cylinders. The tensile bars have been designed to have well separated, nondegenerate resonances. In addition to samples with shrink porosity and sponginess, samples with oxide films have now been cast. These are created by embedding oxidized Al “coins” in the sand mold. Samples with tight cracks will also be made by fatiguing the bars.

Finite Element Sort Modules

To have a useful predictive tool, it is necessary to integrate all the physics into a software tool bench. The overall design of the tool bench was completed. This includes the data structures; inputs, outputs, and processing algorithms for each module; and a graphical user interface. The simulation begins with the part design (CAD model), engineering requirements (peak loads and associated locations), and experimental resonance measurements for model validation. These inputs then must be converted into finite element models for the part and for discrepancies that would limit the performance of the part. A library of simulated good and discrepant parts is generated. This can be used by RI vendors to create heuristic sort modules before castings are available.

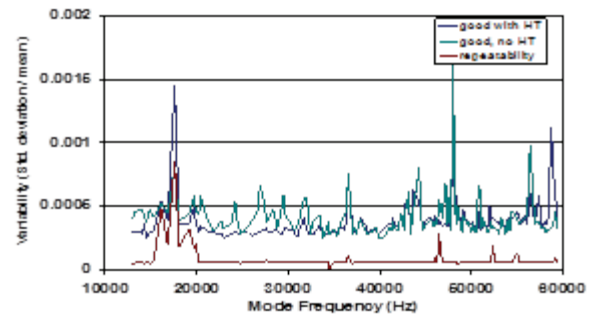


Figure 1. Frequency variation of 118 resonances with repeatability, heat treatment (HT), and no HT.

element modeling.

Conclusions

Good progress is being made on the project deliverables. The production casting portion of the project is largely completed. These castings have shown the systematic shifts associated with discrepancy and the detectability using single resonance sort modules. The cylindrical castings are being prepared for machining into tensile bars. The overall design of the sort module is complete and is being coded.

NDE1002—Shearographic Nondestructive Evaluation of Spot Welds for Lightweighting of the Vehicle

Principal Investigator: Lianxiang Yang, Oakland University
(248) 370-2283; e-mail: yang2@oakland.edu

Principal Investigator: Leonid C. Lev, General Motors Research and Planning
(586) 986-7450; e-mail: leo.lev@gm.com

Introduction

Resistance Spot Welding is the conventional joining method for body structures. When optimized, it produces strong, robust joints with low cost. While RSW reached its prominence with joining of mild steels, it has been adapted to newer lightweight metals ranging from the extremely strong advanced high-strength steels (AHSSs) to Al and magnesium. Because of the difficulties of keeping the weld process in control (weld-tip wear, weld-gun control, corrosion associated with cooling, etc.) RSW, even with mild and interstitial-free steels, requires frequent weld inspections, typically by tear downs (destructive testing). This is very expensive and has low sampling rates. RSW of lightweight materials is more critically needed because of increased weld brittleness and because of the high, variable conductivity of Al and magnesium.

There have been many attempts to perform NDE on spot welds. Single element ultrasonic inspections have been widely implemented, at least in Europe, but have not been successful on AHSS. A previous USAMP Automotive Metals Division project developed ultrasonic phased arrays that could simultaneously image the weld surface and the faying surface. While this technology generates the most detailed nondestructive picture of the weld, it was unsuccessful on galvanized low-carbon steels. Ultrasound was unable to differentiate the fused material in the heat-affected zones from the martensitic nugget that gives these welds substantive strength (Hopkins et al., 2010).

Approach

This project is designed to overcome past difficulties by using shearography to detect spatial variations in the stiffness of the weld. Shearography uses a coherent light source to illuminate the surface. The reflected light is split into two paths and then overlapped to generate a “sheared” interference pattern. As the part is stressed by a force or thermal source, the interference pattern will change. Digital shearography uses the difference between the strained and unstrained images to quantify the surface strains—typically the in-plane strain along one axis (Steinchen and Yang, 2003). Very small variations in strain can be detected. Optimal ways of stressing the resistance spot welds is one of the primary objectives. The spatial strain pattern will be compared with a finite element modeling-generated library of strain patterns to evaluate the size of the weld nugget.

Figure 4 shows preliminary results for two weld coupons with acceptable and undersized welds.

This technology has the advantages of being completely noncontact and having multiple commercial vendors. The project is a 3-year concept feasibility project.

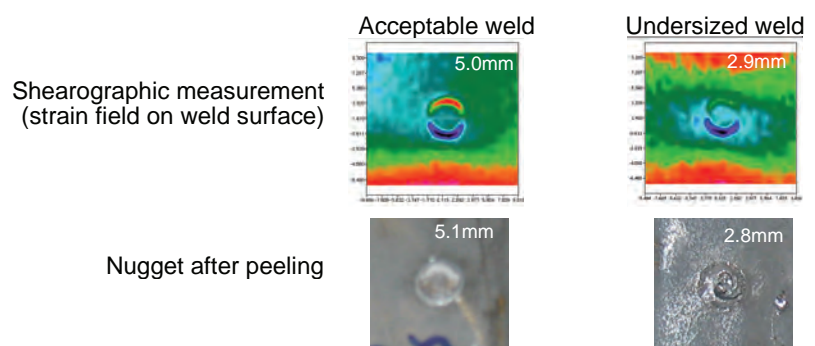


Figure 4. Shearographic images for two welds compared with the nugget size after the weld is peeled.

Results and Discussion

This project was approved by the USAMP Nondestructive Evaluation Steering Committee at the end of FY 2010, but no purchase orders have been issued.

Conclusions

Nondestructive testing can detect many of the discrepant conditions that reduce the quality of lightweight materials, components, and structures. Through systematic selection of methods, careful testing, and validation, nondestructive testing can help to enable the introduction and continued production of these energy-saving materials.

Presentations/Publications/Patents

Lai, C.; Sun, X.; Dasch, C.; Harmon, G.; Jones, M. Quantifying Resonance Inspection with Finite-Element-Based Modeling, *J. Sound and Vibration*, in press.

Jones, M. NDE 901—Reliability Tools for Resonance Inspection of Light Metal Castings, National Energy Technology Laboratory Semiannual Review, May 2010.

References

Harmon, G.; Dasch, C.; Mozurkewich, G.; Hopkins, D. Strategic Plan for Nondestructive Evaluation Development in the North American Automotive Industry, USCAR Website, 2006.

ASTM B557M, Standard Test Methods for Tension Testing Wrought and Cast Al- and Magnesium-Alloy Products; ASTM International, West Conshohocken, Pennsylvania, 2008.

Hopkins, D.; Mozurkewich, G.; Dasch, C. NDE Inspection of Resistance Spot Welds in Automotive Structures Using an Ultrasonic Phased Array, AMD409 Final Report, 2010.

E. Multi-Materials Vehicle - US Automotive Materials Partnership

Field Technical Monitor: David A. Wagner
Ford Motor Company
Ford Research and Advanced Engineering
2101 Village Road, MD 3137-RIC; Dearborn, MI 48121-2053
(313) 845-2547; e-mail: dwagner6@ford.com

Field Technical Monitor: Stephen D. Logan
Chrysler Group LLC
Materials Engineering
Mail Code 482-00-13, 800 Chrysler Drive; Auburn Hills, MI 48326-2757
(248) 512-9485; e-mail: sl16@chrysler.com

Field Technical Monitor: Joseph M. Polewarczyk
General Motors Corporation
GM, R&D and Planning
Mail Code 480-106-212, 30500 Mound Road; Warren, MI 48090-9055
(586) 907-2872; e-mail: joseph.m.polewarczyk@gm.com

Technology Area Development Manager: Carol Schutte
U.S. Department of Energy
1000 Independence Ave., S.W.; Washington, DC 20585
(202) 287-5371; e-mail: carol.schutte@ee.doe.gov

Field Project Officer: Joseph Renk
National Energy Technology Laboratory
626 Cochran Mill Road, P.O. Box 10940; Pittsburgh, PA 15236
(412)386-6406; e-mail: joseph.renk@netl.doe.gov

Contractor: U.S. Automotive Materials Partnership (USAMP)
Contract No.: DE-FC26-02OR22910

Objectives

- Conduct collaborative, precompetitive, high-risk research to develop the component technologies and direct research and development (R&D) in materials and processes that will enable the high volume production of multi-material vehicles (MMVs) that are half the mass of, as affordable as, more recyclable than, and with quality and durability equal to or better than current vehicles.
- Connect and relate USAMP's Auto/Steel Partnership (A/SP), Automotive Composites Consortium (ACC), and Automotive Metals Division (AMD) "seed" projects together in a multi-materials vehicle so that USAMP projects address vehicle level material integration issues as well as bulk materials issues.
- Establish vehicle technical specifications (crash performance, dynamic stiffness, durability, etc.) for a baseline donor vehicle for alignment of other USAMP projects.
- Archive the computer aided design (CAD) and computer aided engineering (CAE) models and analyses for the baseline donor vehicle and from each of the three seed projects for alignment of other USAMP projects.
- Establish baseline cost estimates for the steel baseline donor vehicle for alignment of other USAMP projects.
- Determine weight reduction required, using vehicle performance/fuel economy simulation analysis, to enable a current production seven passenger minivan and an eight passenger crossover utility vehicle (CUV) to achieve fuel economy

improvements of 40% to 45% and 20% to 25%, respectively, when retrofitted with smaller current production four cylinder engines and state-of-the-art transmissions, while maintaining the performance metrics of the current production vehicles.

Accomplishments

- Selected a baseline donor vehicle platform to serve as a benchmark to quantify and compare technology improvements. The vehicle was a large General Motors (GM) rear wheel drive passenger vehicle. (FY 2007)
- Created the MMV technical specification metrics for safety; ride and handling; durability; noise, vibration, and harshness (NVH); recyclability; serviceability; manufacturability; and selected vehicle use scenarios such as towing and shipping tie down. (FY 2007)
- Provided the CAD and CAE models plus the baseline vehicle analytical performance for the donor vehicle to the other teams. (FY 2008)
- Archived the CAD and CAE files for the baseline vehicle and the analyses. (FY 2008)
- Archived the CAD and CAE files from the three seed project alternative material designs for the A/SP steel passenger compartment, the AMD magnesium intensive front end, and the ACC composite underbody. (FY 2010)
- Provided the baseline cost model and requisite assumptions for determining the costs of the baseline donor steel vehicle. Costs for the steel baseline vehicle, with predominantly stamped parts, included part costs and assembly costs plus the investments required for both the parts and the assembly. These costs were used by other USAMP projects for comparisons with the alternative material designs. (FY 2009)
- Determined the weight reductions required, based on analyses of vehicle performance and fuel economy, to achieve targeted 40%–45% and 20%–25% respective fuel economy improvements for a seven passenger minivan and eight passenger CUV while maintaining performance comparable to the current production vehicles. For the two vehicles evaluated in this project, a seven passenger minivan and an eight passenger CUV, weight reductions between 11% and 50% are required, depending on aero improvements and engine technology, to meet the targeted 40%–45% and 20%–25% fuel economy improvements while maintaining performance in six customer driven metrics. (FY 2010)

Future Directions

- All of the subprojects within the Multi-Material Vehicle Research and Development Initiative have been completed.
- The MMV team will complete the fiscal year reports and the Cooperative Agreement final report.
- MMV efforts will continue in other groups within USAMP.
- For FY 2011, the Multi-Material Vehicle Research and Development Initiative has been disbanded.

Introduction

The Multi-Material Vehicle Research and Development Initiative was a USAMP umbrella focal project, supporting the FreedomCAR goals and timeline, with the primary objective of investigating vehicle weight reduction opportunities and issues associated with incorporating multiple materials in multiple locations within a vehicle structure.

The MMV R&D portfolio emphasized design, joining, corrosion, energy management, manufacturing processes, and other technologies that could facilitate mixed material systems that could support delivery of FreedomCAR goals by 2015. Recently the MMV team expanded its research efforts to analyze the weight reductions required for a seven passenger minivan and an eight passenger CUV to meet 40% and 25% fuel economy improvements, respectively, without degrading vehicle performance, while using currently available gasoline engine and transmission technology.

The MMV team focused on analytical, design, cost modeling, and benchmarking studies supporting the three seed project technologies. The longer term focus of future MMV projects within other USAMP groups will be on integration and joining/assembly technologies and associated process developments for manufacturing discrete parts and subassemblies in high volume.

The majority of the MMV efforts focused on supporting the three seed projects: the A/SP Future Generation Passenger Compartment Design and Optimization project, the AMD Magnesium Front End Design and Development project, and the ACC Composite Underbody project. Three of the four MMV projects provided the vehicle engineering metrics, the baseline CAD and CAE analyses, and the baseline cost model against which the alternative material project teams could compare their designs. This effort provided the consistent foundation for the three seed projects and formalized the metrics and costs.

The final project from the MMV team identified the weight savings required to meet fuel economy while maintaining critical full vehicle performance metrics such as 0 to 60 mph acceleration time and trailer tow grade capacity. With currently available modern engines, significant weight must be reduced from current vehicles to meet future fuel economy metrics. This project did not identify how the weight could be reduced from vehicles or whether the resulting vehicle architecture could meet all the federal safety requirements and typical customer durability requirements but rather provided insights into the required weight savings for two levels of fuel economy improvement.

Activity and Developments

MMV 702 Multi-Material Vehicle CAD/CAE Support

Principal Investigator: David A. Wagner, Ford Motor Company
(313) 845-2547; e-mail: dwagner6@ford.com

Principal Investigator: Stephen D. Logan, Chrysler Group LLC
(248) 512-9485; e-mail: sl16@chrysler.com

Principal Investigator: Joseph M. Polewarczyk, General Motors Corporation
(586) 907-2872; e-mail: joseph.m.polewarczyk@gm.com

Introduction

The donor vehicle platform, the GM unibody (body-frame-integral) rear wheel drive vehicle, has formed the baseline for the lightweighting technology improvements. The focus for the three initial technology seed projects addressing major lightweighting initiatives were A/SP's Future Generation Passenger Compartment (FGPC), the AMD 603 Magnesium Front End Design and Development project, and the ACC 007 Composite Underbody project. For FY 2010 the focus was on archiving the design and engineering performance information for the alternative material vehicle structures.

Approach

This project used a supplier, Multimatic Inc., as the archivist for the design information and engineering performance analyses from the three seed projects. Multimatic stored all of the data from the baseline vehicle and the three seed project alternative material designs. The archive included CAD files and CAE models and selected analyses for the baseline steel vehicle, the hes passenger compartment, the Mg intensive front end, and the composite underbody. These archived CAD and CAE files will be available to USAMP projects for 7 years.

Results and Discussion

The archived information included the CAD from the baseline steel vehicle plus the CAD information from the three alternative materials seed projects. [Figures 1, 2, and 3](#) show the designs.

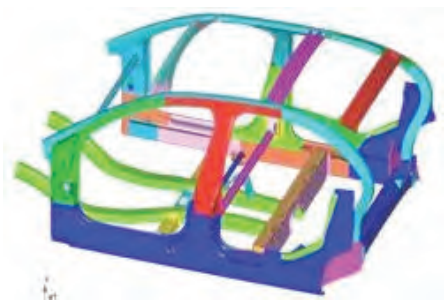


Figure 1. A/SP FGPC design.

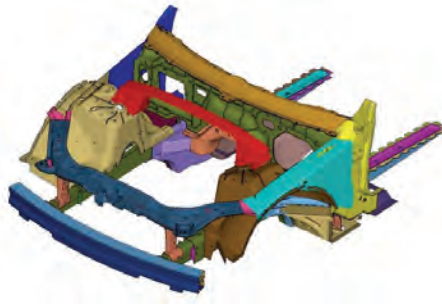


Figure 2. AMD magnesium (intensive) front end design.

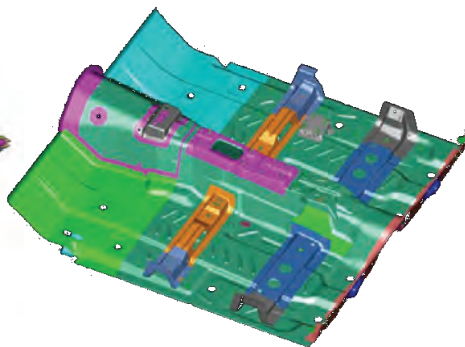


Figure 3. ACC composite underbody design

The CAE archive included the safety, durability, and NVH models and selected load cases for the baseline steel vehicle plus the three alternative materials seed projects.

Conclusions

Project completion in FY 2010 required archiving the design and engineering analysis information from the baseline steel vehicle plus the three alternative materials seed projects. These archived data will be available to future USAMP projects for 7 years. All efforts on this project are complete.

MMV 903 Lightweight 7+ Passenger Vehicle

Principal Investigator: David A. Wagner, Ford Motor Company
(313) 845-2547; e-mail: dwagner6@ford.com

Principal Investigator: Stephen D. Logan, Chrysler Group LLC
(248) 512-9485; e-mail: sl16@chrysler.com

Principal Investigator: Joseph M. Polewarczyk, General Motors Corporation
(586) 907-2872; e-mail: joseph.m.polewarczyk@gm.com

Introduction

The goal of the Lightweight 7+ Passenger Vehicle simulation project was to determine the weight reduction necessary to achieve fuel economy improvements of 40%–45% and 20%–25% for a baseline minivan and up-level CUV, respectively. Vehicle performance and towing capacity were not to be compromised from the current vehicle's capability. The project focused on a lighter weight vehicle, a reduced power engine, high efficiency transmission, reduced auxiliary loads, and improved aerodynamics. This project supported the overall MMV goal of identifying the weight reduction opportunities to achieve fuel economy improvements while maintaining vehicle capabilities.

Approach

The baseline vehicles selected for this study were a model year (MY) 2010 Chrysler Town & Country minivan and an up-level MY 2010 Chevrolet Traverse four wheel drive CUV. Two engine selections were made for each vehicle (a total of four engines), each with different peak power ratings. Using the vehicle simulation software GT-DRIVE from Gamma Technologies, the simulation models were first correlated to the two reference vehicles, with their standard production powertrains, for both fuel economy and performance.

A benchmarking activity was conducted by FEV with its large database of internally tested engines. This process was carried out to locate two engines of different power levels that were the most efficient within a specific peak power range. A transmission benchmarking activity was also carried out in the same manner to determine the most efficient solution from a driveline standpoint. Four engines were then selected by FEV, two for each vehicle, and the torque and fuel mapping data, as tested under laboratory conditions at FEV, were used as input for the next phases of the project.

Next, the models were updated with the newly selected powertrains, various transmission gear ratios and shift schedules, reduced auxiliary loads, and improved aerodynamics. An iterative weight reduction process was subsequently conducted. The vehicles were simulated at three distinct starting weight classes (before weight reductions): the US Environmental Protection Agency (EPA) equivalent test weight (ETW), classified as the vehicle base curb weight plus an additional 300 lb; the gross vehicle weight rating (GVWR), the vehicle curb weight plus additional passengers and luggage; and the gross combined weight rating (GCWR), the GVWR weight plus additional weight to account for trailer towing. A total of 480 unique vehicle models were simulated during the course of the analysis. The vehicle response curves versus vehicle weight for each powertrain were developed for each of six performance metrics at the appropriate vehicle weights. Additionally, the effects of improved aerodynamic designs were investigated by reducing the drag by 19% for the baseline minivan and by 6% for the up-level CUV.

The six performance criteria required of the newly configured vehicles were four acceleration tests (5 s distance, 0–30 mph, 0–60 mph, and 0–100 mph), hill climb ability at 55 mph, and top speed. The newly configured vehicles had to meet or exceed current production vehicle performance in these six customer relevant performance metrics.

Results and Discussion

The final results reveal that a significant amount of weight reduction is generally needed to achieve the desired fuel economy targets while maintaining performance comparable that of current production vehicles. [Tables 1 and 2](#) give the summary results from the seven passenger minivan and the up-level eight passenger CUV. For example, the curb weight of the baseline minivan, getting 24.3 mpg, must be reduced by 2,250 lb to a new curb weight of 2,257 lb to reach a fuel economy of 34 mpg using the 2.4 L inline four (I4) engine with original baseline aerodynamics ([Table 1](#)).

Table 1. Weight reduction for the baseline minivan to reach 40% fuel economy improvement

Baseline Minivan Curb weight = 4,507 lb 3.8 L V6 NA PFI OHV	2.4 L I4 PFI SOHC		1.6 L I4 TC DI DOHC	
	Original	Improved	Original	Improved
	Aero	Aero (19%)	Aero	Aero (19%)
Required weight reduction (lb)	2,250	1,750	1,000	500

Notes: V6 = V-architecture, six cylinders; NA = naturally aspirated; PFI = port fuel injection; OHV = overhead valve (pushrod); I4 = inline, four cylinders; SOHC = single overhead camshaft; TC = turbocharged; DI = direct injection; DOHC = dual overhead camshaft

Table 2. Weight reduction for the up-level CUV to reach 20% fuel economy improvement

Up-Level CUV Curb weight = 4,720 lb 3.6 L V6 NA DI DOHV	2.0 L I4 TC DI DOHC		3.2 L V6 NA DI DOHC	
	Original	Improved	Original	Improved
	Aero	Aero (6%)	Aero	Aero (6%)
Required weight reduction (lb)	2,000	2,000	2,000	2,000

Notes: V6 = V-architecture, six cylinders; NA = naturally aspirated; DI = direct injection; DOHV = dual overhead valves; I4 = inline, four cylinders; TC = turbocharged; DOHC = dual overhead camshaft

The fuel economy goal for the baseline minivan was to achieve an improvement of 40%–45% over the 2005 segment average of 24.3 mpg. This is the EPA combined “raw” fuel economy result from the FTP 75 (Federal Test Protocol, city) and HWFE (highway fuel economy) drive cycles, weighted based on a 55% city and 45% highway driving mix. These fuel economy numbers are not the same as what is posted on a new vehicle sales sticker or in the literature. The raw versus sticker fuel economy numbers can vary significantly due to supplemental cycles that account for air conditioning use and more aggressive highway speed and acceleration.

In conjunction with the fuel economy predictions, performance simulations were conducted. [Table 3](#) lists the 16 vehicle performance results for the baseline minivan. These values were then used as the target performance points for the prototype lightweight vehicle with reduced power engines.

Table 3. Baseline minivan vehicle performance metrics.

Vehicle performance	EPA ETW (4,750 lb)	GVWR (5,875 lb)	GCWR (7,000 lb)
5 s distance (ft)	156	138	124
0–30 mph time (s)	3.5	4.1	4.7
0–60 mph time (s)	10.4	12.4	14.5
0–100 mph time (s)	30.6	41.5	57.0
Max grade at 55 mph (%)	11.2	8.8	7.3
Top speed (mph)	126	Not applicable	Not applicable

Likewise for the up-level CUV, the vehicle performance in 16 different metrics was required to match the current production vehicle’s customer requirements. Table 4 lists the 16 vehicle performance results for the up-level CUV. These values were then used as the target performance points for the prototype lightweight vehicle with reduced power engines.

Table 4. Up-level CUV vehicle performance metrics.

Vehicle performance	EPA ETW (5,000 lb)	GVWR (6,500 lb)	GCWR (10,250 lb)
5 s distance (ft)	166	142	105
0–30 mph time (s)	3.3	4.0	5.7
0–60 mph time (s)	7.9	9.7	14.7
0–100 mph time (s)	20.9	26.7	43.6
Max grade at 55 mph (%)	12.8	9.6	5.6
Top speed (mph)	136	Not applicable	Not applicable

We began the analyses by matching the modeled vehicle performance for both the baseline minivan and the up-level CUV against published and proprietary performance data. Once the vehicle simulations with the GT-DRIVE software were in agreement with vehicle performance, the models were updated to include the new engines and dual clutch six-speed transmissions. Then the effects of low rolling resistance tires and reduced auxiliary loads were included in the models. At this point the effects of these improvements before any weight reductions were evaluated.

For the baseline minivan, the switch to the 2.4 L I4 NA engine alone achieved a 10% improvement in combined fuel economy. The transmission was the second best fuel economy enabler followed by the reduced auxiliary loads and then the low rolling resistance tires. Final fuel economy of this configuration improved 20% over the baseline vehicle. But peak power compared to the original 3.8 L V6 was about 23% less, so performance would suffer, and the accompanying 0–60 mph time increased more than 2 s [Figure 4(a)]. For the baseline minivan with the 1.6 L I4 TC engine with DI and variable intake cam phasing, the results were similar. This engine achieved a fuel economy increase of 19% with the engine change alone. Overall fuel economy improved 29% before any weight reductions [Figure 4(b)]. Vehicle weight reductions would then gain back the lost performance.

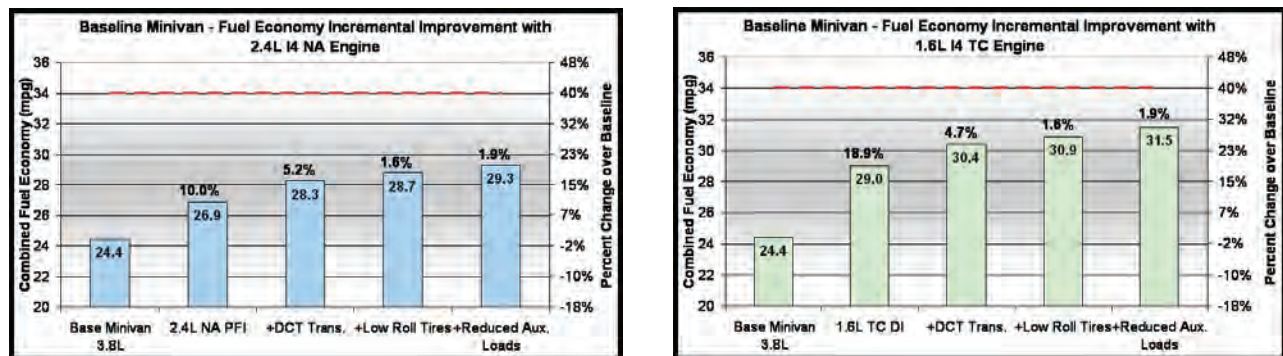


Figure 4. Baseline minivan fuel economy changes due to dual clutch transmission, low rolling resistance tires, reduced auxiliary loads, and (a) new 2.4 L engine or (b) new 1.6 L TC DI engine.

Fuel economy for the baseline minivan with the 2.4 L I4 engine, dual clutch transmission (DCT), low rolling resistance tires, and reduced auxiliary loads (electric power steering, and high-efficiency alternator) depends on vehicle weight and final drive gear ratio [Figure 5(a)]. The final drive gear in the transmission makes a difference in fuel economy (about 1–2 mpg) at a particular weight. A minimum of about 1,750 lb would need to be removed with the most fuel economic final drive selection to eclipse the 34 mpg target. The weight reduction required for the higher powered 1.6 L TC DI engine to meet the fuel economy target is less than for the 2.4 L engine [Figure 5(b)]. The final selections that meet all the fuel economy and performance targets for the baseline minivan for each engine are circled in Figures 5(a) and 5(b).

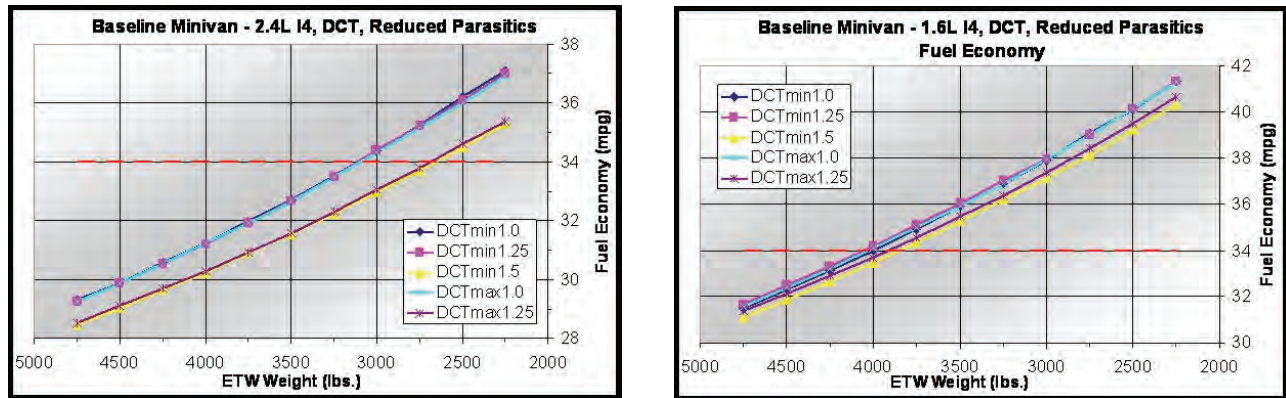


Figure 5. Baseline minivan fuel economy as a function of vehicle weight and final drive gear ratio for engines (a), 2.4 L I4 NA, and (b), 1.6 L I4 TC DI.

For the up-level CUV, the switch to the 2.0 L I4 TC engine alone improves fuel economy 10.5% with the total improvement reaching 15%. The reduction in power of roughly 30% means performance would suffer, and it is shown to reduce the 0–60 mph time by 2.3 s. The transmission change to a DCT does not show a significant increase in fuel economy. This was determined to be because the shift and torque converter lockup schedule for the 6T75 transmission was quite aggressive for maximizing fuel economy and the engine speed dropped below 1,500 rpm during cruise portions of the drive cycle on a regular basis. The reduced auxiliary loads and the low rolling resistance tires have a similar effect on the fuel economy of the CUV to that on the minivan. Final fuel economy of this configuration improved 15% over the baseline CUV vehicle [Figure 6(a)]. For the CUV, the 3.2 L V6 NA high power engine gives a modest improvement to fuel economy of just over 1%. Acceleration from 0–60 mph takes just over 1 s longer. Overall fuel economy improved only 6% before any weight reduction [Figure 6(b)]. Vehicle weight reductions would then gain back the lost performance.

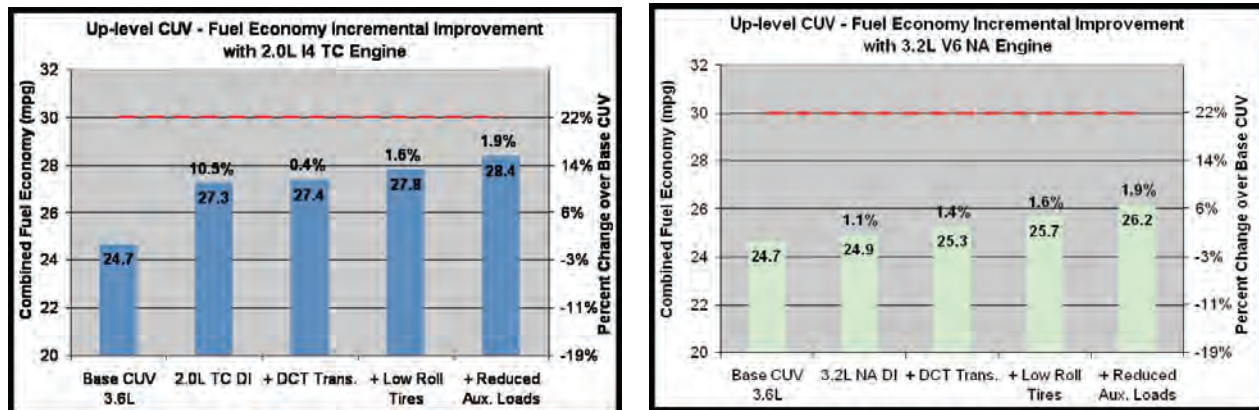


Figure 6. Up-level CUV fuel economy changes due to DCT, low rolling resistance tires, reduced auxiliary loads, and (a) new 2.0 L TC DI engine or (b) new 3.2 L V6 DI engine.

For the up-level CUV to achieve the performance targets at the GCWR (with trailer towing) rating, a significant weight reduction of 2,000 lb would be needed as a result of the lower power engines and the requirement to meet the fuel economy target of 20% improvement (~30 mpg). With this scenario, the fuel economy gains were quite impressive for the 2.0 L I4 TC engine, as shown in Figure 7(a), where the weight reduction required for the vehicle to surpass the 30 mpg target is

only about 500 lb. However for the 3.2 L V6 NA, DI engine, a 2,000 lb weight reduction would be needed to meet the fuel economy target. This weight reduction for the vehicle with the 3.2 L engine also meets all the GVWR and GCWR metrics. As with the plots for the baseline minivan, the circled points in Figures 7(a) and 7(b) indicate the final selection, where both fuel economy and all the performance targets were met.

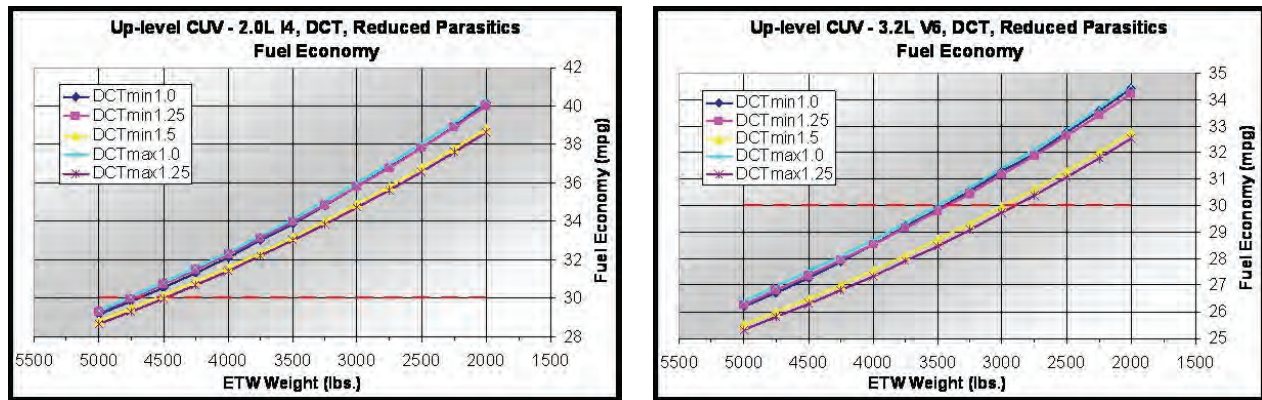


Figure 7. Up-level CUV fuel economy as a function of vehicle weight and final drive gear ratio for engine (a), a new 2.0 L TC DI engine, or (b), a new 3.2 L V6 DI engine.

Conclusions

To achieve aggressive fuel economy targets and not sacrifice vehicle performance with current gasoline engine-powertrain technology, a significant weight reduction is often necessary. Highly downsized (typically with the use of boosting), DI engines offer a unique opportunity for improved fuel economy by maintaining high specific loads at part load and acceptable vehicle performance due to their impressive specific output (brake mean effective pressure) capability. However, maintaining vehicle performance at GCWR can often require additional weight reduction as compared to the weight reduction required to meet fuel economy targets and vehicle performance at ETW and GVWR.

The amount of weight reduction required for the baseline minivan studied in this project was quite considerable with the lower powered 2.4 L engine compared to the more powerful and more efficient 1.6 L TC engine. There was quite a difference though in the technology used on both engines, and the 1.6 L would likely cost significantly more due to the added cost of the turbocharger and advanced fuel injection system. While this project did not consider the cost of different engine and transmission or weight saving technologies, future work could examine these aspects of vehicle design.

The up-level CUV with substitute engine and transmission selections needed a 2,000 lb weight reduction for all cases to either achieve performance targets (2.0 L engine) or fuel economy targets (3.2 L engine). With the 2.0 L engine, any attempt to minimize the weight reduction would result in noticeable towing performance reduction, which is unlikely to be acceptable to customers. In the case of the 3.2 L engine, weight reductions below 2,000 lb would proportionally reduce the fuel economy improvement.

It is important to note that this study did not consider how the weight reductions could be achieved or whether the resulting vehicle would meet the necessary safety, durability, NVH, vehicle dynamics, and other metrics. Additionally, this project did not address the cost and manufacturing implications of the suggested weight reductions.

Conclusions

The Multi-Material Research and Development Initiative successfully provided baseline vehicle information and common engineering and cost metrics for the three alternative materials seed projects during the 4 years, 2007 through 2010, of the project. Additionally, the final task of the MMV effort documented the weight savings required for a seven passenger minivan and an eight passenger CUV to meet 40% and 20% fuel economy improvements while maintaining current vehicle performance metrics. This effort identified the substantial weight reductions required (11% to 50%) to meet fuel economy and performance targets, even with improved aerodynamics and the best current production engines and transmissions.

The MMV project is now complete. All future multi-materials efforts will be contained within the ongoing USAMP divisions, the A/SP, the AMD, the ACC, and the Nondestructive Evaluation group.

Presentations/Publications/Patents

Zaluzec, M. M. and Wagner, D. A. Multi-materials Vehicle R&D Initiative, Project ID “LM009.” Presented at the 2010 DOE Hydrogen Program and Vehicle Technologies Program Annual Merit Review and Peer Evaluation Meeting, June 7–11, 2010, Wardman Park Marriott Hotel, Washington D.C.

5. Recycling

A. Recycling End-Of-Life Vehicles Of The Future - Argonne National Laboratory

Field Technical Monitor: Edward J. Daniels
Argonne National Laboratory
9700 S. Cass Ave.; Argonne, Illinois 60439
Phone: (630) 252-5279; e-mail: edaniels@anl.gov

Technology Area Development Manager: Dr. Carol Schutte
U.S. Department of Energy
1000 Independence Ave., S.W.; Washington, D.C. 20585
Phone: (202) 586-1022; e-mail: carol.schutte@ee.doe.gov

Contractor: Argonne National Laboratory
Contract No.: DE-AC02-06CH11357

Executive Summary

The objective of the recycling project is the development and demonstration of cost-effective automotive materials recycling strategies and technology to achieve the following.

- Eliminate any real or perceived recycling barriers that would preclude the use of advanced lightweighting automotive materials and improve the life-cycle energy use of vehicles.
- Enable the optimum recycling of all automotive materials by a market-driven infrastructure.

To achieve the objective, the following approach to research and development was used.

- Assess the critical needs for cost-effective recycling of automotive materials and components.
- Establish research priorities to enable cost-effective recycling of advanced automotive materials.
- Compile information in an accessible format regarding the status of existing and emerging recycling technologies.
- Communicate a collaborative industry/government approach to issues related to the recycling of automotive materials.
- Coordinate research with other agencies and stakeholders in the United States, Europe, and Asia.
- Benchmark the automotive materials recycling industry and technology.
- Develop and demonstrate technology for the recovery of polymers and other materials from shredder residue, identified as the most important priority for recycling technology development.
- Validate the technical and economic feasibility of the technology at an industrial shredder facility.

Objectives FY 2010

- Update the recycle bibliography (database) and the state-of-the-art technology review document and maintain and update the website.
- Complete work of the plastics cleaning task and prepare the final report.
- Prepare the dismantling task final report.
- Design, build, and operate a 20 ton/hr validation plant to establish the business case for the Argonne technology for recovery of polymers and materials from shredder residue.

Accomplishments FY 2010

- Updated the recycling bibliography database, state-of-the-art technology review document, and recycling website.
- Compiled and analyzed the data on plastics cleaning and prepared the task report.
- Prepared the dismantling task report.
- Evaluated validation plant performance and analyzed plant operational data, which demonstrated that the process is scalable and effectively recovers polymers and residual metals from shredder residue.

Future Direction

Complete the evaluation of the validation plant data, prepare and document the preferred process design based on operating experience from the validation plant, and re-confirm process economics.

Introduction

Today, end-of-life vehicles (ELVs) in the United States are profitably processed for materials and parts recycling by an existing infrastructure which include dismantlers, remanufacturers, and shredders. The dismantlers recover parts and materials that can be reused. A full range of components are remanufactured, allowing end users the opportunity to replace defective equipment at a cheaper cost and with less environmental impact. The shredders recover ferrous and nonferrous metals from the remaining auto “hulk.” The residual material, commonly referred to as “shredder residue,” is typically landfilled and contains advanced lightweighting materials such as polymers which are not presently recovered for recycle. The recyclability of these non-metals, primarily the polymers, of ELVs is limited both by the lack of commercially proven technologies to cost-effectively recover them and a lack of profitable post-use markets. As new lightweighting materials are developed for automotive applications, the number and complexity of ELVs is expected to increase, posing new challenges to the existing recycling infrastructure. Vehicles of the future will use greater amounts of advanced lightweighting materials (e.g., plastics, composites, high-strength steels, aluminum, and magnesium), more complex parts, including hybrid electric batteries, alternate fuel tanks, electronic controls, and “smart materials,” such as shape-memory polymeric alloys. Recycling of these advanced lightweighting materials will become increasingly important to the supply chain.

After assessing the critical needs, and establishing research priorities to enable cost-effective recycling of advanced materials, Argonne National Laboratory has focused its research on developing and evaluating technology to recover materials from shredder residue. Argonne characterized shredder residue from a number of sources to determine composition variability. A pilot plant was built and operated for processing shredder residues to recover materials for market evaluation and to provide “control” samples for testing of alternative technologies. Cost/performance analysis was conducted to establish the business case for recycling polymers and other materials from shredder residue. Throughout this process, Argonne held industry-focused workshops, communicated research results with automotive and recycling industries and other stakeholders, and coordinated research with stakeholders around the world. Argonne established and maintains a website for the dissemination

of ELV recycling information. Argonne developed and evaluated a number of technology options for recycling shredder residue. The research culminated in the design, construction, and operation of a full-scale (20 ton/hr) validation plant at an industrial shredder site. Construction of the validation plant was completed in September 2009, and the plant was started up in October 2009. Data from the plant are being analyzed and evaluated as the final step in the project.

Because the research has focused on the recovery of materials for reuse in automotive applications, research was also conducted to evaluate the physical properties of the recovered polymers. As polychlorinated biphenyls (PCBs) were identified as a residue in the recovered polymers, Argonne developed a process for removing this contamination from these materials. Supporting research has also been conducted to improve the operational and economic performance of the technology and to evaluate other market opportunities such as conversion of the recovered polymers and other organics to hydrocarbon fuels.

In addition to recovering polymeric materials from shredder residues, Argonne identified future R&D needs to further improve the recyclability of ELVs. Preliminary research was performed on recovering the residual oxide fraction in shredder residue, and on improving the separation of magnesium components from the nonferrous fraction currently recovered by industry and reused in aluminum alloys where the magnesium value is lost.

Activity and Developments

Recycling Technology Baseline Assessments and Planning: Vehicle Technologies Program (VTP 18068, 9046, 8775, 16637, 16634)

Principal Investigator: Bassam Jody, Argonne National Laboratory
Phone: (630) 252-4206; e-mail: bjody@anl.gov

Principal Investigator: John Hryn, Argonne National Laboratory
Phone: (630) 252-5894; e-mail: jhryn@anl.gov

Introduction

The objective of this effort was to establish R&D priorities and develop cost-effective automotive materials recycling strategies for the recycle program in collaboration with stakeholders. This included establishing the baseline or state of the art for automotive materials recovery/recycling technology, benchmarking the automotive materials recycling industry, and compiling information in an accessible format regarding the status of existing and emerging recycling technology and research.

Approach

A recycling research plan was prepared that served as a “working document” to guide the United States Department of Energy (DOE) in establishing priority goals for materials recycling, with an initial emphasis on lightweighting materials. The plan was developed in consultation with automotive manufacturers and recycling industries and other relevant organizations to identify critical recycling needs/barriers.

The state of the art of worldwide automotive materials recovery/recycling technologies was reviewed, and technology profiles of emerging automotive materials recycling technologies were developed. Dismantling opportunities that can increase recycling of automotive materials as new materials and components used in vehicles were identified.

Life-cycle studies to quantify the environmental impacts and benefits associated with various ELV recycling technologies were conducted.

A recycling website was established to enable dissemination of recycle information to all stakeholders.

Results and Discussions (in FY 2010)

Development and management of the R&D plan and ongoing efforts toward the milestones and the objectives continued in FY 2010. To that end, communications with the automobile makers, American Chemistry Council–Plastics Division (ACC-PD), Institute of Scrap Recycling Industries (ISRI), and technology developers were maintained. We also responded to numerous inquiries from automotive recyclers, technology developers, and entrepreneurs who are involved in automotive recycling and provided direct information relative to their requests and/or referred them to the recycling website.

The recycling website was updated with additional information, publications, and links (http://www.es.anl.gov/Energy_systems/CRADA_Team/index.html). As part of our outreach effort, we continued tracking international developments related to recycling ELVs. The database of recycle technologies was updated and reposted to the website. The technology review document (state of the art for recycling automotive materials) was also updated. The updated review is in final editing and will be posted to the website in FY 2011.

As assessment of the status and needs of the dismantling industry was completed.

Conclusions

This task serves as a planning and assessment task for the recycling project, including identification of knowledge gaps and research needs. By keeping in close contact with the stakeholders, the developed technology is streamlined to serve their needs. The updated bibliography of abstracts of automotive recycling papers and the updated state of the art of worldwide automotive materials recovery/recycling technology review documents provide recyclers and researchers with valuable resources and information for expediting new technologies for the recycling of automotive materials. The updated bibliography has been added to the website. The technology review document is undergoing final editing.

The dismantling report was prepared in FY 2010. The results revealed that newer and future vehicles are likely to contain expensive parts that will be cost-effective to dismantle and recover. These include electric batteries and some high-grade polymers and composites. Some of these materials may have to be dismantled not only for their material value but also for environmental reasons. New dismantling tools and personnel training will be required to efficiently recover the new materials.

New recycling technology needs were identified in 2008 during a workshop held with key stakeholders. Two of the high-priority research needs were proposed for further investigation, and preliminary work was performed in developing processes to recover magnesium from scrap aluminum.

Development of Technology for Recycling Polymers from Shredder Residue:

Principal Investigator: Bassam Jody, Argonne National Laboratory
Phone: (630) 252-4206; e-mail: bjody@anl.gov

Introduction

The objective of this task is to develop and demonstrate technology for the cost-effective recovery of polymers and other materials from post-shred residues. The research conducted culminated in the design, construction, and start-up of a full-scale field validation plant in 2009. Research conducted at Argonne's pilot plant provided data essential to establishing the business case for sustainable recycling of automotive materials from post-shred residue. Because the research has focused on the recovery of materials for reuse in automotive applications, extensive research was also conducted to evaluate the physical properties of the recovered polymers and to remove residual contamination such as PCBs from these materials. Supporting research has also been conducted to improve the economic performance of the materials recovery process technology and to evaluate other market opportunities such as conversion of materials to hydrocarbons for possible use as fuel or chemicals.

Approach

The approach followed in developing technology to recover materials from shredder residues consists of the following: shredder residues from different sources were processed in Argonne’s small-scale pilot plant to characterize materials compositions and variability, conceptual process systems were developed, alternative separation technologies were evaluated and benchmarked, and cost and performance analyses of alternative technologies were conducted. Physical properties of recovered polymers were determined to guide the development of the separation technology. Technology was tested and evaluated for removal of substances of concern from recovered polymers. Ultimately, a preferred process configuration for separation and recovery of materials from shredder residue was developed and validated in a large-scale plant at an industrial site.

Results and Discussions (in FY 2010)

Recycling Technology Validation

Recycling technology validation is needed to collect and analyze operation and performance field data in order to evaluate the plant’s performance and compare it to the plant’s design parameters, which were based on pilot plant data. A 20 ton/hr full-scale validation plant was designed. The validation plant was installed at a shredder site and was operated during FY 2010. At another shredder site, a series of auto shredding campaigns were conducted to benchmark the expected composition of materials and polymers from shredder residue as a function of obsolete auto age and type.

Start-up and debottlenecking of the 20 ton/hr plant occurred in FY 2010. To assess the performance of the plant, controlled and supervised runs were conducted, which included a large “mass balance” run using 160 tons of shredder residue. [Table 1](#) summarizes the results averaged from several analyzed large samples. The polymers recovered in the validation plant were less than those recovered in the Argonne small-scale pilot plant. The olefins fraction constituted about 3.2% of the shredder residue mass, which is about one-fourth what was previously obtained in multiple trials in the Argonne pilot plant. The rubber fraction amount was also lower than what was achieved in the pilot plant. This is most likely due to the type of source material that was processed in the shredder. Residual metals were recovered in the process. The amounts recovered in the validation plant were on the order of 5% to 10% of the shredder residue, which is about the same as what was achieved by Argonne’s small-scale pilot plant.

Samples from the three polymer fractions (olefins, styrenics, and rubber concentrate) were analyzed to determine composition. The results showed that the composition of the polymer fractions was about the same as that obtained in the pilot plant.

Table 1. Materials recovered from the mass balance test as mass percent of shredder residue.

Material	Mass %	Material	Mass %
Oversized heavies	8.7	Nonferrous metals, >1"	1.1
Polyolefin concentration	3.2	Nonferrous metals, <1" but >5 mm	1.0
Styrenics concentration	2.9	Nonferrous metals <5 mm	1.8
Rubber concentration	4.9	Total potential product streams	23.6

The “all auto” study was conducted to examine changing materials content of different types of vehicles. This information helps in the design of future material recovery facilities. The vehicles were de-polluted by draining all fluids, removing any batteries, and removing mercury switches. Tires and wheels were also removed, so along with them went the lead wheel weights (spare tires were not removed however). Anything that did not belong to the vehicle was also removed (e.g., clothes, garbage bags, etc.). Forty vehicles of each of four categories were shredded without mixing with any other source material, and samples of their shredder residues were processed and analyzed. The categories of vehicles were (1) late model domestics (Chrysler, Ford, and General Motors), (2) late model transplants (Honda, Toyota, and Nissan), (3) normal ELVs (pre-2000 domestic vehicles shredded currently), and (4) late-model federalized imports (Hyundai, Kia, Dae Woo, etc.). Each category of vehicles was processed individually. Samples of the resulting shredder residues (12 mm to 6 in. fraction) were processed in Argonne’s pilot plant and analyzed, and the results are summarized in [Figure 1](#).

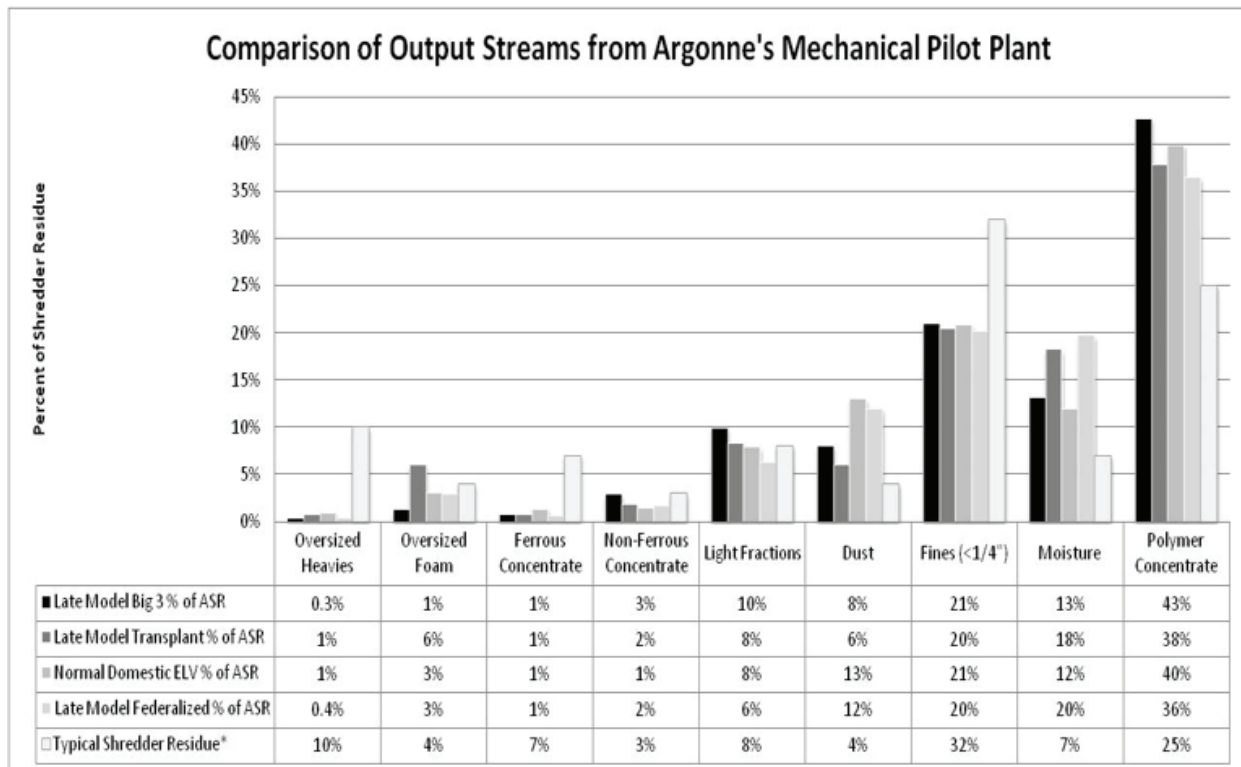


Figure 1. Output streams from Argonne's pilot plant for the different car categories.

The results show that the compositions of the fractions derived from the shredder residues from each of the four categories are similar and that these shredder residues contain approximately similar polymer contents (polymer concentrate and lights) when compared with the typical shredder residue. This is significant because a process that is designed to handle today's shredder residue will be able to handle shredder residue from recently built vehicles that will become obsolete in the future. The results of the polymer analysis are given in the next section.

Compatibility/Compounding Evaluation of Recovered Polymers

Argonne determined properties of recovered polymers and conducted blending and pelletizing trials of the recovered polymers and mold trials using recovered polymers from the pilot plant. The results showed that polymers recovered from shredder residue can be used to make quality auto parts. In FY 2010 compositional analysis of plastics recovered by the validation plant were evaluated as polymers as well as for use as cement kiln fuel.

Polymer samples produced by the validation plant were analyzed. The results are summarized in [Tables 2 and 3](#). The combined polyethylene (PE) and polypropylene (PP) in the olefins fraction is about the same as what was obtained in the pilot plant. The styrenics fraction is about 67% acrylonitrile-butadiene-styrene (ABS) and polystyrene (PS), which is comparable with the pilot plant results. The composition of the rubber fraction is consistent with that which was produced by the pilot plant. These results show that the Argonne process is capable of recovering the polymers and that the process can accommodate changes in the shredder residue compositions and reasonable changes in particle sizes.

Table 2. Composition (mass percent) of the polymer fractions produced by the validation plant and pilot plant.

Material	Validation Plant (mass%)			Pilot Plant (mass %)		
	Olefins	Styrenics	Rubber	Olefins	Styrenics	Rubber
Plastic	75	52	52	62	82	33
Rubber	11	12	42	10	17	57
Foam and fiber	4	31	1	7	0	5
Wood and others	10	5	5	21	1	5
Total	100	100	100	100	100	100

Table 3. Composition of the plastics fractions produced by the validation plant and pilot plant.

Material	Validation Plant			Pilot Plant		
	Olefins	Styrenics	Rubber	Olefins	Styrenics	Rubber
PP	42%	8%	6%	73%	10%	4%
PE	25%	1%	0%	20%	1%	3%
PS & ABS	1%	67%	22%	1%	52%	2%
Nylon	0%	5%	25%	0%	4%	31%
Filled PP	1%	7%	0%	5%	12%	5%
PC and PC/ABS	0%	1%	14%	0%	0%	27%
PVC	0%	0%	8%	0%	2%	14%
PPO	0%	4%	0%	0%	8%	0%
Others/Unknowns	31%	7%	25%	1%	11%	14%
Total:	100%	100%	100%	100%	100%	100%

The polymeric fractions recovered by the validation plant were reasonably similar in composition to those produced by the Argonne pilot plant. The polymers produced by the validation plant were not upgraded by further purification as was the olefin fraction produced in the pilot plant. It is assumed that the upgrading process would produce similar materials with similar properties, but this has not been confirmed.

Samples from the all auto study were also analyzed, and the results are shown in Figure 2. The results show that the compositions of the fractions derived from the 12 mm to 6in. size shredder residues from each of the four categories are similar and that these shredder residues contain similar polymer contents (polymer concentrate and lights) when compared with the typical shredder residue.

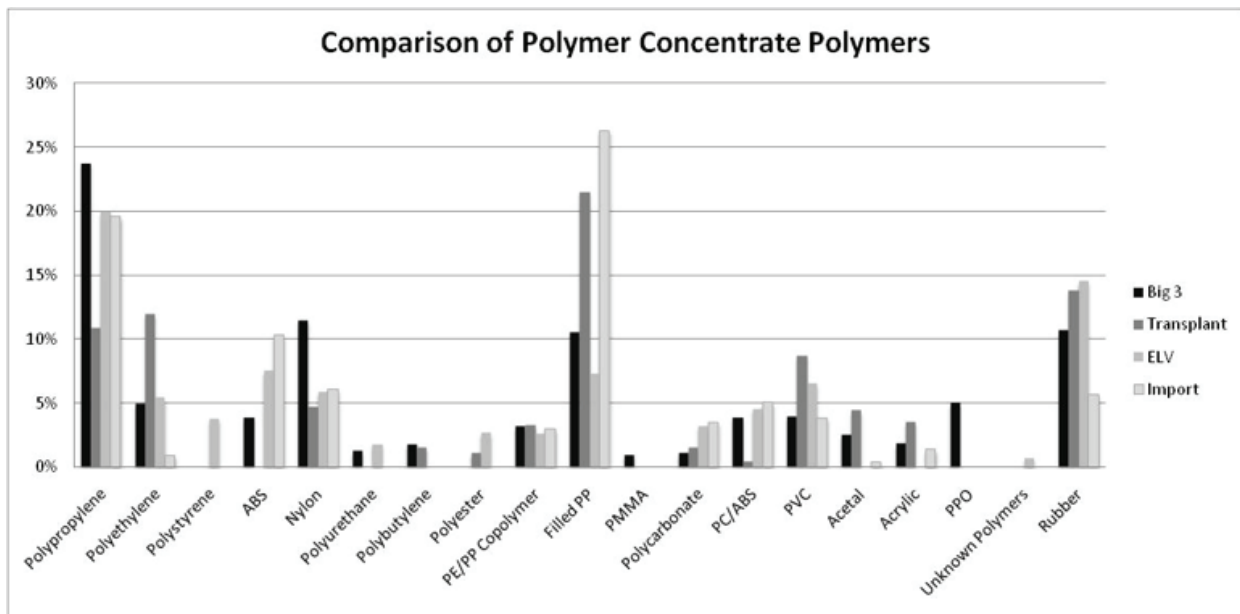


Figure 2. Composition of the polymer concentrate and polymers in the polymer concentrate generated from each of the four categories.

Because the recovered polymers contain residual PCBs, they were evaluated as potential fuel for cement kilns. The evaluation criteria include heating value, PCBs, mercury, chlorine, heavy metals, sulfur, and moisture content. The heating value of the recovered polymers is about 50% higher than most coals, and the moisture content and the sulfur content are both lower. The H/C ratio for the plastics is also double that for coal, which means less CO₂ emissions. Compared to coal, ash from these

polymers contains more calcium oxide because of the fillers in the plastics. It also contains more magnesium oxide but less silicon dioxide and aluminum oxide. Discussions with a cement kiln operator concluded that the recovered polymers can be used as a cement kiln fuel.

Development of Technology for Removal of PCBs and Other Substances of Concern (SOCs) from Shredder Residue

Typically, materials recovered from shredder residue contain residual PCBs. Under current EPA regulations, these materials cannot be reintroduced into commerce unless the PCBs can be removed to a concentration of less than 2 ppm. Therefore, development of a process that is economical, environmentally acceptable, and does not degrade the properties of the polymers, is extremely important. At present, there is no commercially available technology that can meet these criteria. Many chemical, thermal, and mechanical processes were tested in the laboratory at Argonne. In addition, Argonne developed a two-stage process that was successful in reducing the concentration of the PCBs on the recovered plastics to <2 ppm. However, the process is costly and resulted in the degradation of some of the mechanical properties of the polymers. Technologies developed by others and evaluated at Argonne have also not been demonstrated to be cost-effective.

Analysis of samples from the all auto work showed, as expected, that cars built after 1983 contain very low levels of PCBs. This could be a reason to expect the concentration of PCBs in shredder residue to decrease over time. Toxicity characteristic leaching procedure (TCLP) analysis of all auto samples also showed that most of the TCLP metals were not detectable. The average cadmium concentrations also dropped for the newer vehicles, 0.02 to 0.07 mg/L for the post-2000 categories from 0.22 mg/L for the pre-2000 category produced for the fine shredder residue and 0.32 mg/L for the coarse residue.

In summary, removing the PCBs from polymers recovered from shredder residue economically and without degrading the polymers has proven to be a challenge. This is at least partially due to the fact that some polymers are known to be excellent adsorbents of PCBs. The data gathered and obtained in the lab over the past few years were analyzed, and a task report has been prepared. The major conclusions are as follows.

- None of the washing solutions and solvents tested succeeded in reducing the concentration of PCBs below 2 ppm in a consistent fashion under practical and economical operating conditions. Many tests reduced the concentration from about 30 ppm to between 5 ppm and 15 ppm in a reasonable time and under practical operating conditions. Further reduction in the concentration of PCBs requires more extensive and prolonged treatment.
- As expected, the performance of the solvents was improved at higher temperatures.
- The rate of removal of the PCBs becomes very slow at concentrations below 5 ppm. This suggests that the PCBs are associated with the plastics by different mechanisms. Some of the PCBs are in the oils and dirt that are on the plastics, and some are adsorbed on the plastics and do not desorb easily during washing.
- The PCBs concentration was consistently reduced from 5–10 ppm to below 2 ppm upon desorption at high temperatures, typically around 250°C. These conditions degraded the plastics.

An economical process for removing the PCBs from shredder residue polymers has not yet been developed. High temperatures and high pressures and long residence times are likely to degrade the properties of the polymers and/or increase the cost. In the present regulatory environment, there is a need for a low-to-moderate temperature process that can remove the PCBs without degrading the polymers.

Recycling Metallic Oxides from Shredder Residue Fines

Previous research had shown that the oxide fines could serve as a viable source material of iron oxide for cement production and/or direct reduction to produce iron units for steelmaking. Therefore, the composition of fines recovered from the validation plant was compared to the composition of fines from our previous research to determine whether these market opportunities are still viable. However, the amount of magnetic fines in shredder residue has been decreasing as the shredders employ more powerful magnets in their operations, so the opportunity to economically recover these materials may be limited.

In FY 2010, fines generated from the validation plant were evaluated. However, work on the fines was limited because the plant did not consistently operate at production level. A screen having slots 4 mm × 25 mm (0.15 in. × 1.0 in.) in size was used to separate the fines. Nonferrous metals in this size range are not effectively removed by eddy current systems. The fines

material was analyzed and processed at Argonne to investigate if a potential product stream can be generated from these fines. The amount of these fines recovered in the validation plant depended on the wetness of the shredder residue and could vary significantly from day to day. The fines were not routinely weighed as part of the operating procedure for the plant. Results from a single test performed at the validation plant showed that the fines were about 26% of the weight of shredder residue. These fines contained some residual metals, glass, sand, rocks, and some pieces of polymers.

The fines were investigated at Argonne to determine their composition, and a conceptual process was developed to recover residual iron and iron oxides from the fines. The ferrous fraction produced from the fines material was 27% of the fines by weight. This fraction contained on average 50% ferrous metals, 5% nonferrous metals, and 45% other primarily inorganic material. Increasing the concentration of the ferrous material through the use of high intensity magnets may be necessary to produce a product fraction. The remaining 73% of the fines material were organics containing polymers, fibers, and foams.

The recovered amount of these fines from shredder residue is variable, depending on the moisture content of the starting material the composition of the feed material being shredded. After removal of the metals and inorganic materials, the mixed organics could be used as a fuel. Briquetting of the small-particle metals and polymers may be necessary.

Conclusions

The technical feasibility of recovering polymers and residual ferrous and nonferrous metals from shredder residue was demonstrated. The technology is in the process of being validated at a full-scale (20 ton/hr) validation plant at an industrial shredder. The process was determined to be robust and accommodating to changes in feed materials composition. PCBs were identified, a source of concern for the recovered materials, but technology was developed to reduce the PCB content to low levels while somewhat degrading material properties. A technically viable, cost-effective process that reduces the PCB content of recovered polymers to below threshold level without degrading the physical properties of the recovered polymers has yet been developed. An option for recovering metallic oxides from shredder residue was explored and if pursued to technology validation would further improve the economics of recycling ELVs.

Conclusions

The recycle project at Argonne successfully developed technology that advanced the state of the art in recycling automotive lightweighting materials by removing actual and perceived barriers to recycling advanced lightweighting automotive materials. Once validated, the technology will also enable optimum recycling for recovery of these polymeric materials, thereby successfully meeting the project objectives. The overall approach used to develop the technology, including performing initial assessments and benchmarks, identifying technology gaps, communicating and collaborating with industry and stakeholders, and ultimately developing the technology from bench to pilot to full scale with technology validation proved to be the correct course of action. Although the economic slowdown in the last 2 years has resulted in changes in both the feed material to the shredder and delays in technology implementation, the developed technology is robust and was able to accommodate changes in the composition of the shredder residue and moderate changes in the particle size of the polymers. While research has shown progress in the ability to remove residual contamination (i.e., PCBs) from the recovered polymers, complete removal of the PCBs is still not cost-effective and may degrade the physical properties of the recovered polymers. Nevertheless, the regulatory environment at some point may permit the reuse of these materials in automotive applications, as has been permitted for other recovered materials with low-threshold levels of PCB. In addition, the PCB content of recovered polymers will continue to decrease with time as pre-983 ELVs are shredded. However, the recovered plastics do have good properties as a fuel, including a heating value that is about 50% higher than that of coal. A cement kiln operator has evaluated the polymers and concluded that, unlike unprocessed shredder residue, the recovered polymers can be used as a fuel. Although this is not the preferred route for disposition of advanced lightweighting automotive polymeric materials, the technology developed demonstrates that these materials have value when recovered and need not be landfilled.

Presentations/Publications/Patents

Allen, T. Metal Recovery from Shredder Residue Fines. SAE Paper # 2007-01-0528, 2007 SAE World Congress, Detroit, Michigan, April 2007.

Binder, M.; Simon, N. L.; Duranceau, C. M.; Wheeler, C. S.; and Winslow, G. R. Modular Life Cycle Model — Basis for Analyzing the Environmental Performance of Different Vehicle End-of-Life Options. In Proc. of the 5th International Automobile Recycling Congress, Amsterdam, March 9–11, 2005.

Carpenter, J. A., Jr. Effects of Transportation on the Ecosystem, Ecomaterials and Ecoprocesses. In Proc. of the International Symposium on Ecomaterials and Ecoprocesses, August 24–27, 2003.

Carpenter, J. A., Jr.; Daniels, E. J.; Sklad, P. S.; Warren, C. D.; and Smith, M. T. The R&D of the FreedomCAR Materials Program. In Proc. Of the International Auto Body Congress, Novi, Michigan, September 19, 2006.

Daniels, E. J. Automotive Materials Recycling: A Status Report of U.S. DOE and Industry Collaboration, Ecomaterials and Ecoprocesses. In Proc. of the International Symposium on Ecomaterials and Ecoprocesses, August 24–27, 2003, Vancouver, BC, Canada, pp. 389–402.

Daniels, E. J. Industry and Government Collaboration to Facilitate Sustainable End-of-Life Vehicle Recycling. Present at the 2005 ASME International Mechanical Engineering Congress & Exposition, BRTD- 4: Sustainability Applications in Product Design and Manufacture, Orlando, Florida, November 5–11, 2005.

Daniels, E. J.; Carpenter, J. A., Jr.; Duranceau, C.; Fisher, M.; Wheeler, C.; and Winslow, G. Sustainable End-of-Life Vehicle Recycling: R&D Collaboration between Industry and the U.S. DOE, The Mineral, Metals & Materials Society, Journal of Metals, August 2004, 56(8), pp. 28–32.

Daniels, E. J.; Jody, B. J.; and Pomykala, Jr., J. A. Method and Apparatus for Separating Mixed Plastics Using Flotation Techniques, U. S. Patent # 7,255,233, August 2007.

Daniels, E. J.; Jody, B. J.; Pomykala, J. A. Jr.; and Spangenberg, J. S. Market Driven Technology Development for Sustainable End-of-Life Vehicle Recycling: A Perspective from the United States. Presented at the 6th International Automobile Recycling Congress, Amsterdam, Netherlands, March 15–17, 2006.

Duranceau, C. Market Driven Automotive Recycling in North America. Presented at the Institute of Scrap Recycling Industries Shredder Meeting, Dallas, Texas, October 30, 2004.

Duranceau, C.; Carpenter, J.; and Fisher, M. Market Driven Automotive Recycling in North America. Keynote at the 2004 International Car Recycling Workshop, American Plastics Council, May 19, 2004, Washington, D.C.

Green, J. A. S. Developing a Technical Roadmap for Automotive Lightweight Metals Recycling, Light Metal Age, December 2008.

Jody, B. J.; and Daniels, E. J. Technologies for Recycling Shredder Residue. SAE Paper # 2007- 01-0526, SAE World Congress, Detroit, Michigan, April 2007.

Jody, B. J.; Daniels, E. J.; and Pomykala, J. A., Jr. Processes for Recycling the Non-Metallic Portion of Obsolete Automobiles, U.S. Environment-2003 On-Line Conference, July 14–25, 2003.

Jody, B. J.; Pomykala, J. A., Jr.; and Daniels, E. J. Cost Effective Recovery of Thermoplastics From Mixed Scrap. Materials Technology, March 2003, 18(1), pp. 18–24.

Jody, B. J.; Pomykala, J. A., Jr.; and J. S. Spangenberg, J. S. Recycling End-of-Life-Vehicles of the Future, Energy Systems Division, Argonne National Laboratory, Report # ANL/ES-C0201801, December 1, 2009.

Jody, B. J.; Pomykala, J. A., Jr.; Daniels, E. J.; and Spangenberg, J. S. Process to wash polymers contaminated with polychlorinated biphenyls (PCBs). U.S. Patent # 7,525,010, April 2009.

Jody, B. J.; Pomykala, J. A., Jr.; Spangenberg, J. S.; and Daniels, E. J. Recycling of the Changing Automobile and Its

Impact on Sustainability. Accepted for presentation at the 2011 SAE World Congress, Detroit, Michigan, April 2011.

Jody, B. J.; Pomykala, J. A., Jr.; Spangenberg, J. S.; and Daniels, E. J. Impact of Recycling Automotive Lightweighting Materials on Sustainability. SAE paper # 2009-01-0317, SAE World Congress, Detroit, Michigan, April 2009.

Jody, B. J.; Pomykala, J. A., Jr.; Spangenberg, J. S.; and Daniels, E. J. Automotive Recycling in the United States: Energy Conservation and Environmental Benefits. *The Journal of Metals*, November 2007, 59(11), pp. 41–45.

Jody, B. J.; Pomykala, J. A., Jr.; Spangenberg, J. S.; and Daniels, E. J. Recovery and Recycling of Polymers from Shredder Residue. *Journal of Solid Waste Technology and Management*, November 2006, 23(4), pp. 228–236.

Jody, B. J.; Pomykala, Jr., J. A.; and Daniels, E. J. Process for the Recovery and Separation of Plastics, U.S. Patent # 6,599,950, July 2003.

Polyurethanes. Paper # SAE-2006-01-1579, SAE World Congress, Detroit, Michigan, April 2006.

Pomykala, J. A. Jr.; Jody, B. J.; and Daniels, E. J. Thermoplastic Separation and Recovery from Various Mixed Scrap by the Argonne Developed Froth Flotation Technology. In Proc. of the 13th Annual Global Plastics Environmental Conference (GPEC), Orlando, Florida, March 6–7, 2007.

Pomykala, J. A., Jr.; Jody, B. J.; Daniels, E. J.; and Greminger, J. Separation and Recovery of Thermoplastics From Mixed-Scrap Plastics. In Proc. of the 9th Annual Global Plastics Environmental Conference (GPEC), February 26–27, 2003, Detroit, Michigan, pp. 7–16.

Pomykala, J. A., Jr.; Jody, B. J.; Daniels, E. J.; Yang, J.; and Spangenberg, J. S. A Mechanical Separation Process to Recover Metals and Polymers from Shredder Residue. TMS 2007 Annual Meeting & Exhibition, Orlando, Florida, February 25–March 1, 2007.

Pomykala, J. A., Jr.; Jody, B. J.; Spangenberg, J. S.; and Daniels, E. J. Mass Balance and Composition Analysis of Shredder Residue. SAE Paper # 2007-01-0527, 2007 SAE World Congress, Detroit, Michigan, April 2007.

Pomykala, J. A., Jr.; Jody, B. J.; Spangenberg, J. S.; and Daniels, E. J. Mass Balance and Composition Analysis of Shredder Residue. SAE Paper # 2007-01-0527, 2007, SAE Transactions, *Journal of Materials & Manufacturing*, August 2008.

Sendjarevec, V.; Simon, N.; Duranceau, C.; Winslow, G.; Williams, R.; Wheeler, C.; Niemiec, S.; and Schomer, D. Screening Study to Evaluate Shredder Residue Materials, SAE Paper # 2004-01-0468, SAE World Congress, Detroit, Michigan, 2004.

Sendjarevic, I.; Sendjarevic, V.; Winslow, G. R.; Duranceau, C. M.; Simon, N. L.; and Niemiec, S. F.; and Wheeler, C. S. Overview of Washing Systems for Commercial Cleaning of Plastics Separated from Automotive Shredder Residue, SAE Paper # 2005-01-0851, Detroit, Michigan, April 2005.

Sendjarevic, V.; Sendjarevic, I.; Mayne, K.; Winslow, G. R.; Duranceau, C. M.; Simon, N. L.; and Wheeler, C. S. Recycling of Polyurethane Foams Recovered From Shredder Residue Via Glycolysis Process Into Polyurethanes, paper # SAE-2006-01-1579, SAE World Congress, Detroit, Michigan, April 2006.

Sendjarevic, V.; Sendjarevic, I.; Winslow, G. R.; Duranceau, C. M.; Simon, N. I.; and Wheeler, C. S. Chemical Recycling of Mixed Polyurethane Foam Recovered from Shredder Residue into Polyurethane Polyols, SAE paper # 2005-01-0850, SAE World Congress, Detroit, Michigan, April 2005.

Spangenberg, J. S.; Daniels, E. J.; Jody, B. J.; and Pomykala, J. A. Jr. Friction Based Material Sorter. U.S. Patent # 7,766,172 B2, August 2010.

Sullivan, J. L.; Wheeler, C. S.; and Simon, N. L. United States National Life Cycle Inventory Database Project, A Status Report, SAE Paper 2005-01-0852, SAE World Congress, Detroit, Michigan, April 2005.

Sullivan, R.; Hamilton, D.; and Carpenter, J. A., Jr. Automotive Technology: Looking Forward, Ecomaterials and Ecoprocesses. In Proc. of the International Symposium on Ecomaterials and Ecoprocesses, August 24–27, 2003, Vancouver, BC, Canada, pp. 49–67.

Wheeler, C. S.; Simon, N. L.; Binder, M.; Winslow, G. R.; and Duranceau, C. M. A Life Cycle Look at Making Oil from End-of-Life Vehicles. SAE paper # 2006-01-0374, SAE World Congress, Detroit, Michigan, 2006.

Wheeler, C. S.; Simon, N. L.; Duranceau, C. M.; Winslow, G. R.; and Binder, M. Modular Life Cycle Model of Vehicle End-of-Life Phase—Basis for Analysis of Environmental Performance, SAE Paper 2005-01-0847.

Winslow, G. R.; Appel, B. S.; Adams, T. N.; Simon, N. L.; Duranceau, C. M.; and Wheeler, C. S. Scale Up Study on Converting and Recycling Shredder Residue Into a Fuel Oil. SAE paper #2006-01-1580, SAE World Congress, Detroit, Michigan, 2006.

Winslow, G. R.; Appel, B. S.; Adams, T.; Simon, N. I.; Duranceau, C. M.; Wheeler, C. S.; and Sendjarevic, V. Recycling Shredder Residue Containing Plastics and Foam Using a Thermal Conversion Process, SAE Paper #2005-01-0848, Detroit, Michigan, April 2005.

Winslow, G. R.; Simon, N. L.; Duranceau, C. M.; Williams, R.; Wheeler, C. S.; Fisher, M.; Kistenmacher, A.; and VanHerpe, I. Advanced Separation of Plastics from Shredder Residue, SAE Paper # 2004-01-0469, Detroit, Michigan, April 2004.

Winslow, G. R.; Wheeler, C. S.; Williams, R. L.; Duranceau, C. M.; Simon, N. L.; and Schomer, D. R. Screening Study to Evaluate Shredder Residue Materials, SAE paper # 2004-01-0468, Detroit, Michigan, April 2004.

Winslow, G.R.; and Adams, T. Recycling Automotive Shredder Residue and Plastics Using the CWT Thermal Process. In Proc. of the 10th Annual Global Plastics Environmental Conference (GPEC), Detroit, Michigan, February 18, 2004.

6. Crosscutting

A. Cost Modeling - Oak Ridge National Laboratory

Field Technical Monitor: C. Dave Warren
Oak Ridge National Laboratory
1 Bethel Valley Road; Oak Ridge, TN 37831
(865) 574-9693; e-mail: warrencd@ornl.gov

Technology Area Development Manager: Carol Schutte
U.S. Department of Energy
1000 Independence Ave., S.W.; Washington, DC 20585
(202) 287-5371; e-mail: carol.shutte@ee.doe.gov

Contractor: Oak Ridge National Laboratory (ORNL)
Contract No.: DE-AC05-00OR22725

Objectives

- Assess the economic viability of new and existing lightweight materials technologies.
- Develop technical cost models to estimate the cost of lightweight materials technologies.

Accomplishments FY 2010

- Completed the cost-effectiveness analysis of a 50% body and chassis weight-reduction Lightweighting Materials (LM) goal for 2010. Carbon-fiber-reinforced polymer matrix composite (carbon-FRPMC) and magnesium (Mg) vehicle component applications would be necessary to achieve the weight-reduction goal.
- Completed the life-cycle analysis (LCA) comparison of the conventional Chinese Pidgeon process vs the solid oxygen-ion conducting membrane (SOM) primary Mg production technologies.
- Completed the cost-effectiveness analysis of four potential Mg continuous sheet manufacturing technologies under the Light Metals Processing and Manufacturing technology initiative.

Future Direction

- Develop a baseline multi-material vehicle cost model which could be used in subsequent years for development and validation of the cost-effectiveness of various multiyear LM body and chassis weight-reduction goals.
- Participate in Phase II of the Canada-China-U.S. collaborative Magnesium Front End Research and Development Project (MFERD) involving LCA with the focus on examination of fuel economy benefits of lightweighting in advanced powertrains such as pure hybrids, plug-in hybrids, and battery electric vehicles.

Technical Cost Modeling

Principal Investigator: Sujit Das, Oak Ridge National Laboratory
(865) 946-1222; e-mail: dass@ornl.gov

Primary Participant: Susan Schexnayder, University of Tennessee, Knoxville
(865) 974-5495; e-mail: schexnayder@utk.edu

Introduction

The cost modeling effort comprises a single task which supports both modeling of potential cost impacts of various technologies and modeling of other system-level materials replacement impacts. Individual efforts for this task are approved on a case-by-case basis at the discretion of DOE program management. In previous years, cost models were developed for the carbon fiber (CF) and Mg research portfolios. System level models for potential mass savings have been developed and are continually refined to provide program guidance for the cost-benefit analysis of various potential lightweighting technologies.

The LM component of the DOE Vehicle Technologies Program has a 50% weight-reduction goal for passenger vehicle body and chassis systems, with safety, performance, and recyclability comparable to 2002 vehicles. To achieve this long-term weight-reduction goal, LM has set annual intermediate weight-reduction goals, starting with 10% in FY 2007 and finally achieving 50% by FY 2010. Following previous years' studies of the cost effectiveness of the weight-reduction goals, the current work focuses on the 50% body and chassis weight-reduction goal of FY 2010.

Approach

The technical cost modeling task involves developing and modifying various component, material, and system level models to analyze and validate the effectiveness of different technical research efforts. The goals of those modeling efforts are as follows.

- Address the economic viability of LM technologies both at the specific component level and at the complete vehicle level.
- Use cost modeling to identify specific technology improvements and major cost drivers that are detrimental to the economic viability of those new technologies.
- Derive cost estimates based on a fair representation of the technical and economic parameters of each process step.
- Provide technical cost models and/or evaluations of the "realism" of cost projections of LM projects under consideration for LM funding.

Examine technical cost models of LM technologies that include Al sheet, CF precursor and precursor processing methods, and FRPMCs and examine methods of producing primary Al, Mg, and Ti, and Mg alloys with adequate high-temperature properties for powertrain applications.

Results and Discussion

Cost-Effectiveness of a 50% Body and Chassis Weight-Reduction Goal in Light Duty Vehicles

The cost-effectiveness of the LM 2010 body and chassis weight-reduction goal of 50% in light-duty vehicles was assessed based on the use of LM options for various body and chassis components under a plausible midsize vehicle scenario. The analysis focused on carbon-FRPMCs for body components to meet a significantly higher weight-reduction goal. Specific body systems considered for carbon-FRPMCs include body in white, panels, and front/rear bumpers. In addition, Mg was selected for several chassis components (i.e., cradle, corner suspension, steering and braking systems, and wheels) to achieve the total 50% weight reduction in body and chassis systems. The analysis also considered the effect of primary weight

savings of 50% on other vehicle components that can be resized while maintaining the same level of vehicle performance with the reduced vehicle weight. These weight savings are known as secondary weight savings. Because of secondary weight savings, total body and chassis weight savings are estimated to be 57%, whereas final vehicle weight savings are estimated to be about 35%. The cost-effectiveness of the 50% body and chassis weight reduction goal is estimated in terms of both vehicle retail price and life cycle cost using the detailed 35+ component level automotive system cost model developed by ORNL and Ibis Associates, Inc. Cost data for components considered for LM substitution were collected from recent major studies, thus reflecting the latest technology developments and material prices.

Including powertrain resizing and secondary body and chassis mass savings, the carbon-FRPMC LM vehicle that meets the LM 50% body and chassis weight savings goal is found to entail a \$373/vehicle increase in retail price (Figure 1). The higher cost is due primarily to the carbon FRPMC body system, which is \$1,424 more expensive than the baseline system—the effect of which is not completely offset by the powertrain cost savings of \$1,361/vehicle. However, with a significant cost savings of \$1,552/vehicle during the vehicle operation stage, life-cycle cost savings of \$1,212/vehicle are projected, assuming a gasoline price of \$3.00/gallon. It is estimated that if the price of Mg used in chassis components is reduced from the baseline price of \$4.44/kg to \$3.85/kg and CF price is reduced from the baseline price of \$17.60/kg to DOE’s long-term target value of \$11.00/kg, cost effectiveness at the vehicle retail price level could be achieved.

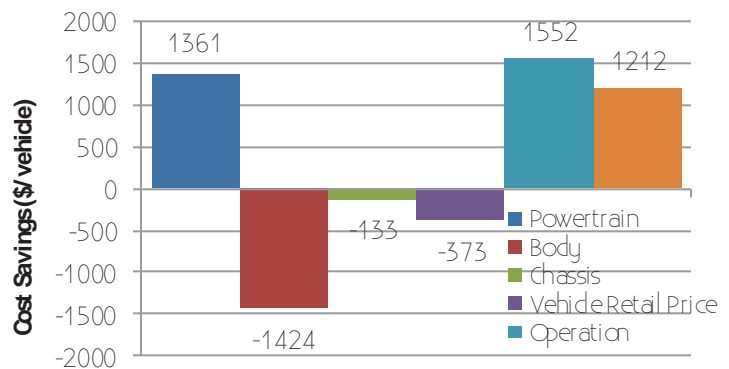


Figure 1. Estimated cost savings of 50% body and chassis weight-reduction scenario.

Findings in this analysis are consistent with previous findings that vehicles with high carbon-FRPMC content are higher priced than baseline vehicles. However, vehicle platform business decisions that promote low annual production volumes would facilitate the competitiveness of carbon-FRPMC body structures, as would economic incentives that reward lower mass designs. Lightweighting also improves the cost-effectiveness of advanced technology vehicles by lowering the powertrain cost while maintaining the performance, which has been considered in only a few of the latest studies and would be critical in the successful commercialization of LM technologies. Consideration of powertrain resizing, secondary mass savings, and life-cycle cost perspectives would therefore be important to maximize the fuel economy gains from a lightweight structure and to successfully achieve market penetration of lighter weight vehicles in the future.

Comparative Life-Cycle Assessment of Primary Magnesium Production

An alternative electrochemical primary Mg production technology developed by Boston University and known as the SOM process has been evaluated for comparison of life-cycle impacts with the metallothermic Chinese Pidgeon process. The Pidgeon process supplies 80% of the market demand for Mg today by replacing the capital-intensive electrolytic refining process used chiefly in the West. In the SOM process for Mg production, electrolysis is carried out in a molten salt bath at 1,150°C–1,300°C by passing a current through a flux containing Mg oxide (MgO), which is contained in a stainless steel crucible that works as the cathode. Although the oxide reduction in this process is electrochemical in nature, it replaces the intensive Mg chloride dehydration necessary for the conventional Mg electrolytic process with a simple Mg hydroxide or Mg carbonate (magnesite ore) calcining operation. The SOM cell anode includes a yttria-stabilized zirconia (YSZ) membrane and a contact material which provides electrical contact to the YSZ and catalyzes the anode reactions. Oxygen ions move through the inert YSZ membrane and are removed from the system in an anode either as water or carbon monoxide with carbon dioxide (CO₂).

LCA of the SOM primary Mg process was based on using the raw material, MgO, obtained from magnesite calcination. Life-cycle comparisons were made both at the Mg ingot level and for the Mg automotive front end considered under MFERD. The analysis estimates life-cycle primary energy used and greenhouse gas (GHG) emissions in terms of CO₂ equivalents. The latter was proposed by the International Panel on Climate Change. The life-cycle impacts for the Chinese Pidgeon process

were based on last year's MFERD life-cycle results, whereas for SOM the detailed life-cycle inventory data were collected and then life-cycle comparisons were made by using SimaPro, an LCA software package developed by PRé Consultants in the Netherlands.

Figure 2 shows the comparison of estimated primary energy consumed and the global warming potential in terms of kilograms of CO₂ equivalent for the major primary Mg production processes. Compared to Pidgeon, SOM technology looks favorable from both energy and emissions perspectives: the GHG emissions from the Pidgeon process were estimated to be 37 kg CO₂/kg compared to 4.9 kg CO₂/kg for SOM. Assuming that the electricity grid is relatively clean because a significant proportion of the energy supply is from hydroelectricity for both electrochemical processes, SOM looks considerably more favorable than the Western electrolytic process from an energy perspective. As one would expect, results for specific Mg applications such as front end parts show a trend similar to those for primary Mg production. Assuming the environmental processing parameters are unaffected when Metal Oxygen Separation Technologies, Inc., scales up the SOM process from laboratory-scale to demonstration-plant scale, SOM primary production technology appears to be an environmentally friendly technology.

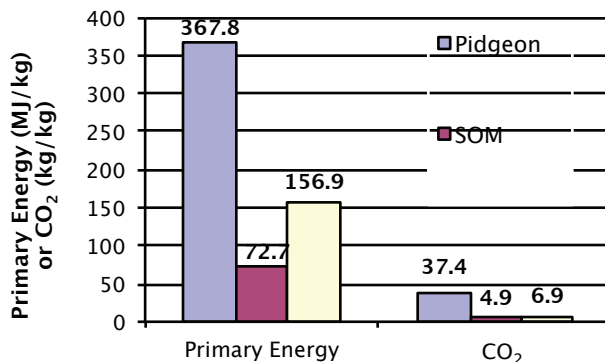


Figure 2. Life-cycle primary energy and GHG emissions of major competing primary Mg production technologies.

Light Metal Processing and Manufacturing Cost Modeling

Cost remains a major barrier to widespread use of automotive LM, although the pressure to use lightweight vehicles is greater than before because of new fuel economy emission regulations. The Light Metal Processing and Manufacturing initiative was undertaken to organize a comprehensive effort to prioritize and solve technical barriers in each stage of the life cycle of light metal components, including cost-effectiveness for automotive applications. The initial focus of this work was examination of the cost-effectiveness of several potential Mg sheet manufacturing technologies because the improved affordability of Mg sheet would tremendously help in vehicle lightweighting.

This assessment considered alternative Mg sheet manufacturing technologies—twin belt casting, twin roll casting, and thixomolded thermomechanical processing (TTMP)—and compared them to the baseline conventional direct chill casting. These alternative technologies are continuous strip rolling processes that combine solidification and hot rolling into one operation, thus eliminating or reducing the hot rolling needed for conventionally produced ingots and resulting in substantial savings in energy and cost. TTMP is a relatively novel Mg sheet-making approach based on the semisolid injection molding process currently being used for making Mg net-shape components. The thermomechanical processing produces the desired Mg sheet thickness using thixomolded blanks.

Figure 3 shows the estimated Mg sheet cost breakdown of three competing manufacturing technologies compared to the baseline conventional direct chill casting technology at an annual production volume of 10,000 tons and an AZ31 alloy price of \$2.10/lb. The twin roll casting technology offers the greatest cost advantage, with a final sheet cost of \$2.89/lb compared to the baseline sheet technology cost of \$3.80/lb. The TTMP technology is the least cost-effective technology (\$6.22/lb), and because this process requires Mg alloy granules, the metal cost itself is greater than the total sheet cost of two other competing technologies. The casting cost is also higher in this case because of a lower productivity rate of 4.6 lb/hr in. compared to 45 lb/hr-in. for the most cost-effective twin roll casting. In all cases, metal cost contributes the largest share (64%–85%) of the total cost for continuous Mg sheet. The cost results shown here demonstrate the relative competitiveness of Mg sheet manufacturing technologies without any considerations of profit in the final sheet price estimation.

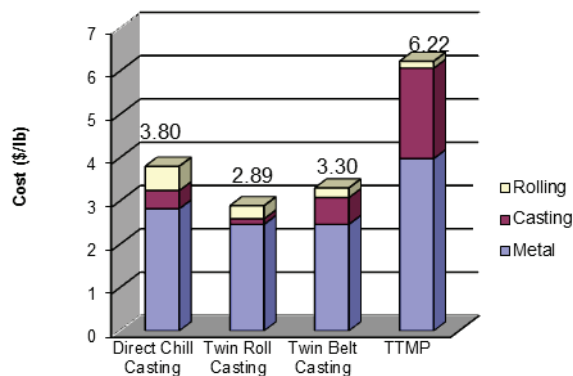


Figure 3. Estimated cost for Mg produced from four sheet-manufacturing technologies.

Because metal cost is such a large fraction of sheet cost, the viability of any continuous sheet casting technology will be maximized by casting as close to final thickness as microstructure and surface quality will allow. Development of alloys and processing schemes that allow higher reduction per pass (on the order of 50% reduction per pass) without edge cracking would also improve the viability of continuous sheet casting technologies.

Conclusions

Achieving the LM 2010 goal to reduce body and chassis weight by 50% is possible with life-cycle cost equivalence and only a small retail price increase. To achieve retail price equivalence, a combination of material price reduction and higher fuel price would be necessary. The alternative primary Mg production technology, SOM, appears to be a more favorable technology from the GHG emissions perspective compared to the conventional Western electrolytic and Chinese Pidgeon technologies. Twin roll casting technology appears to be the most promising technology among the alternatives considered for Mg sheet manufacturing; the viability of any continuous Mg sheet manufacturing technology will be dictated by maximum casting recovery.

Presentations/Publications/Patents

Das, S. Recycling and Lifecycle Issues for Light Weight Vehicles. In *Materials, Design and Manufacturing for Lightweight Vehicles*, Mallick, P. K., ed.; Woodhead Publishing: UK, 2010.

Dubreuil, A.; Bushi, L.; Das, S.; Tharumarajah, A.; and Gong, X. A Comparative Life Cycle Assessment of Magnesium Front End Autoparts; SAE Paper 2010-01-0275; Society of Automotive Engineers: Warrendale, Pennsylvania, 2010.

Ashley, S. Shedding Pounds on a Magnesium Diet. *Automotive Eng. International*, April 6, 2010, pp. 34–36.

Das, S. Importance of Economic Viability Assessment of Automotive Lightweight Materials. Invited presentation at the 3rd Annual Advanced Lightweight Materials for Vehicles conference, August 11–12, 2010, Detroit, Michigan.

B. Safety Data and Analysis - Lawrence Berkeley National Laboratory

Principal Investigator: Tom Wenzel
Lawrence Berkeley National Laboratory
1 Cyclotron Road, 90R4000; Berkeley, CA 94720
(510) 486-5753; e-mail: TPWenzel@lbl.gov

Technology Area Development Manager: Carol Schutte
U.S. Department of Energy
1000 Independence Ave., S.W.; Washington, DC 20585
(202) 287-5371; e-mail: carol.schutte@ee.doe.gov

Contractor: Lawrence Berkeley National Laboratory (LBNL)
Contract No.: DE-AC02-05CH11231

Objectives

- Work with interagency team [Department of Energy (DOE), Environmental Protection Agency (EPA), and National Highway Traffic Safety Administration (NHTSA)] to coordinate research on vehicle weight, size, and occupant safety of recent model light-duty vehicles, including detailed analyses of vehicle attributes and their respective influence on occupant risk. Analysis will guide the agencies in the application of mass reduction as an enabler for reducing fuel consumption and carbon dioxide (CO₂) emissions.
- Using a common dataset of vehicle attributes by vehicle year, make, and model, conduct a regression analysis of the relationship between vehicle weight and size and fatality risk per mileage-adjusted vehicle registration years, using fatality data from the Fatality Analysis Reporting System (FARS). This report will be authored by NHTSA, with contributions from by Lawrence Berkeley National Laboratory (LBNL).
- Using the same dataset of vehicle attributes, conduct a regression analysis of the relationship between vehicle weight and size and casualty risk per crash, using data on fatalities and serious injuries from police-reported crashes in roughly 14 states. This report will be authored by LBNL, with contributions from NHTSA.

Accomplishments

- Obtained vehicle wheelbase and track width measurements by vehicle year, make, and model from Motortrend website, Branham Automobile Reference Books, and other sources.
- Prepared a draft report comparing occupant risk by vehicle type and model using two measures of risk: fatality risk per vehicle registration year and casualty risk per police-reported crash. Report also examines potential sources of bias in state crash data and summarizes the effect of accounting for driver age/gender, driving behavior, and crash location on casualty risk.

Future Directions

- Evaluate whether database of vehicle attributes proposed by NHTSA provides sufficient detail to assess relationship between vehicle weight and risk.
- Assess whether results of logistic regression model using state casualty risk from five states differ from results of NHTSA model using national fatality risk.
- Replicate NHTSA logistic regression analysis of relationship between vehicle weight and size and fatality risk per vehicle registration year, using national FARS data, police-reported crashes from 14 states, R. L. Polk & Company registration data, and vehicle odometer data.

- Update database of casualty risk to include model year 2007 vehicles and police-reported crash data from an additional ten states.
- Conduct logistic regression analysis of relationship between vehicle weight and size and casualty risk per police-reported crash, using updated casualty risk database.

Introduction

For its updated analysis of the relationship between vehicle weight/footprint and safety, NHTSA and LBNL plan to use the same database of vehicle attributes by vehicle model year, make, model, and trim. The attributes to be analyzed include curb weight, footprint (wheelbase times track width), other vehicle measurements thought to influence safety (door sill height, bumper height, average height of force, etc.), and other attributes that vary by vehicle model (presence of electronic stability controls, side airbags, primary or secondary energy absorbing system, etc.).

However, NHTSA intends to replicate its 2003 analysis, which estimates fatality risk per registered vehicle-mile. Fatalities are taken from NHTSA's FARS; vehicle registrations from R. L. Polk & Company and annual vehicle mileage data are taken from CARFAX, state vehicle emission inspection and maintenance (I/M) test results, or National Automotive Sampling System General Estimates System (NASS GES). NHTSA intends to use its previous approach to derive non-fatal crashes for its statistical analysis: using non-culpable vehicles involved in all police-reported crashes from about 15 states, to allocate national vehicle registration years to combinations of crashes, drivers, and vehicles. The crash data will come from 15 states that include the vehicle identification number (VIN) in the data they provide to NHTSA's State Data System.

LBNL intends to analyze casualty (fatality and serious/incapacitating injury) risk per police-reported crash, using all crashes from the same 15 states. This is an extension of LBNL's earlier analysis of casualty risk using crash data from five states by obtaining data through 2007 to include model years 2005 through 2007 and by obtaining data for additional states that report VIN. Because the two agencies are planning to use different data and methodologies to assess the influence of vehicle weight and footprint on safety, it is important to understand how the different approaches compare.

LBNL analyzed the differences in the two approaches to estimating risk and examined several other aspects of casualty risk per police-reported crash. The results of the analysis are summarized as follows.

Activity and Developments

VIN Correction

The VINs provided in the state crash databases are truncated at 10 to 12 characters; without the full 17-digit VIN, we are not able to determine whether these truncated VINs represent legitimate combinations of numerals and characters. We used two pieces of information to determine whether each truncated VIN was valid: the model year reported in the databases independently of the VIN and a lookup table of over 50 million unique legitimate 17-character VINs from eight state inspection and maintenance programs throughout the country. After translating VIN position 10 to match the reported model year and comparing the truncated VINs with the database of full valid VINs to correct VIN positions 8 and 11, we increased the number of decodable VINs of model years 2000 to 2004 vehicles by 18%.

Comparison of Two Measures of Risk

We compared fatality risk per vehicle registration year and casualty risk per police-reported crash using the same data: all police-reported crashes in five states. For the most part, the trend in casualty risk by vehicle type is quite similar to that of fatality risk, when vehicle registration years are used as the measure of exposure; however, casualty risks are substantially lower than fatality risks for sports cars and for pickups.

The trend in casualty risk by vehicle type is similar regardless of whether vehicle registration years or police-reported crashes are used as the measure of exposure. Casualty risks for subcompact and compact cars are relatively higher per vehicle than per crash, while casualty risks for large and import luxury cars, minivans, large SUVs, and pickups are relatively lower per vehicle than per crash.

Casualty risks per vehicle registration year are remarkably consistent across four of the five states; the exception is Pennsylvania, which has much lower casualty risks than the other states, because it reports a category of injuries, moderate injuries, between serious/incapacitating injuries and minor injuries. On the other hand, the five states have dramatically different fatality risks per vehicle registration year. These differences could be attributable to small numbers of fatalities in certain vehicle types and states, distance from trauma centers, or the quality of care that might prevent serious injuries from becoming fatalities.

Casualty risks per police-reported crash are substantially higher in Florida and Maryland than in the other three states, across all vehicle types, in part because of which crashes are required to be reported in each state. When casualty risk per crash for individual vehicle types is indexed to the risk for all vehicles in each state, the relative risks by vehicle type are quite similar in the five states. The exceptions are high risks of sports cars in Pennsylvania and ¾ ton pickups in Pennsylvania and Missouri and low risks of midsize crossover SUVs in Pennsylvania.

The agreement between casualty risk per vehicle registration year and per crash, by vehicle model, is highest in Pennsylvania ($R^2 = 0.72$) and lowest in Maryland ($R^2 = 0.51$). Adjusting casualty risk per vehicle for annual mileage by vehicle model, using state I/M inspection records, slightly lowers the correlation with casualty risk per crash in each state. The agreement in casualty risk for 103 popular vehicle models among the five states varies substantially; the correlation among the five states is stronger for casualty risk per vehicle registration year (R^2 between 0.56 and 0.77, depending on state) than for casualty risk per crash (R^2 between 0.28 and 0.45, depending on state).

Accounting for Vehicle Miles Traveled

We analyzed average odometer readings of model year 2002 vehicles from 2008 and 2009 I/M records in four of the five states, as well as four additional states (California, Colorado, Ohio, and Wisconsin). Average odometer readings are highest in Missouri (87,330) and lowest in Maryland (79,523), a difference of about 10%. When indexed to the average odometer reading for all vehicle types in each state, the average odometer by vehicle type is quite similar across the four states. There is more variability across the states in terms of average miles driven for sports cars, import luxury cars, large SUVs, midsize car-based SUVs (CSUVs), and pickups than for other vehicle types. Using Illinois as the baseline state, the correlation of average odometer readings for the 103 most prevalent vehicle models is highest for Pennsylvania ($R^2 = 0.78$) and lowest for Maryland ($R^2 = 0.68$).

California's I/M program includes vehicles in rural as well as urban counties; vehicles registered in urban California counties are driven 5% fewer miles than vehicles registered in rural counties. Almost all vehicle types are driven less in urban counties than rural counties; the exceptions are 1 ton pickups and full-size vans. Since average odometer reading varies much more by vehicle type than by driving location, it is probably safe to assume that average mileage taken from vehicles registered in urban areas is representative of vehicles throughout a state.

For most vehicle types, adjusting for miles driven has little to no effect on casualty risk per vehicle registration year; however, adjusting for miles driven substantially increases casualty risk for sports cars by 30%, which are driven many fewer miles than other vehicles, and slightly reduces casualty risk for full-size vans and ¾ ton pickups.

Crash Involvement Rates

Crash involvement rates vary consistently by state, with Illinois and Missouri having relatively high crash rates (77 and 66 crashes, respectively, per 1,000 registered vehicle years) and Florida and Pennsylvania having relatively low crash rates (30 per 1,000 registered vehicle years). However, when crash frequencies for each vehicle type are indexed to the crash frequency for all vehicles in each state, the trends in indexed crash frequencies among vehicle types are similar across the five states. Some vehicle types have consistently higher crash involvement rates in each state (subcompact, compact cars), while others have consistently low crash rates (large cars, import luxury cars, minivans, large SUVs, midsize CSUVs, ½ and ¾ ton pickups). Sports cars do not have substantially higher crash frequency than other car models, which suggests that their high fatality and casualty risks are due to them being involved in more severe crashes, or to relatively poor crashworthiness compared to other cars. Using Missouri as the baseline state, the correlation (R^2) of crash rates for the 103 most prevalent vehicle models are between 0.81 and 0.85 in the four other states.

There is a strong correlation ($R^2 = 0.91$) between vehicle registration years and vehicles involved in police-reported crashes for vehicle models, indicating that crashes, rather than registrations, can be safely used as a measure of exposure; the correlation is not improved when one accounts for mileage by vehicle model. However, there is no correlation between

average odometer and crash frequency across vehicle types or models.

Effect on Casualty Risk

Calculating risk using all police-reported crashes, rather than vehicle registration years, as the measure of exposure changes the risk of certain vehicle types relative to that of other vehicle types. For example, subcompact and compact cars have higher crash involvement rates than midsize, large, and import luxury cars, so the difference in casualty risk between smaller and larger cars is dramatically reduced when the measure of exposure is changed from registration years to all police-reported crashes. On the other hand, midsize and large cars, and minivans, have relatively low crash involvement rates, so changing the measure of exposure to crashes increases their casualty risk relative to that of other vehicle types. Similarly, the relatively low crash involvement rates of large SUVs, crossover SUVs, and full-size pickups result in relatively higher casualty risks when the measure of exposure is changed from vehicle registration years to all police-reported crashes.

In general, changing the measure of exposure from registration years to all police-reported crashes reduces the sharp decline in casualty risk as car size increases. Casualty risk per crash does decrease as size increases, within each major vehicle type, but for cars and truck-based SUVs the decrease is not as large as when registration years is used as the measure of exposure.

Reporting Bias by States

We used NASS GES data to analyze whether casualty risks per crash from the five states and 12 other states that provide crash data and VINS are representative of national casualty risks per crash. For most vehicle types, casualty risks are highest in the five VIN states, followed by those in the 12 other VIN states, and lowest in the remaining states. The 12 other VIN states are most representative of national casualty risk for all vehicle types except pickups; national casualty risks for pickups fall between those in the VIN states and those in the non-VIN states. Based on this analysis of GES data, we would expect that calculating casualty risk using data from all of the SDS) VIN states will overstate national casualty risk, for all vehicle types. However, national GES casualty risks are remarkably similar to the casualty risks from all police-reported crashes in the five states for all vehicle types except pickup trucks, which have substantially lower casualty risks in the national GES data than in the police-reported crash data from the five states.

Another type of reporting bias is the criteria each state requires for a crash to be reported to police and included in the dataset provided to the NHTSA SDS. As mentioned previously, Florida has the highest casualty risk per crash of the five states; indexing the risk by vehicle type to the risk for all vehicles in each state is one method to eliminate the bias. In its 2003 report, NHTSA speculated that the high fatality rate in Florida (from FARS) was in part caused by a large number of high-risk young drivers in that state. However, Florida has an average, if not slightly low, fraction of young male drivers (and a slightly high fraction of elderly drivers) involved in all police-reported crashes, relative to the other states.

Reporting Bias by Drivers

We suspect that one-vehicle, non-rollover, non-injury crashes by pickup trucks are underreported. Pickup trucks have as high, or higher, crash rates in non-rollover, non-injury crashes than most vehicle types, particularly in non-I/M or rural counties. Crash rates for pickups are quite a bit lower in I/M or urban counties than in rural areas; this suggests that one-vehicle, non-injury crashes involving pickups may be underreported in urban areas; however, pickup crash rates in urban areas are still as high or higher than those for many other vehicle types.

Accounting for Driver Age and Gender

Elderly drivers (over 65 years old) have higher casualty risk than other drivers in virtually all vehicle types. For most vehicle types, young drivers (under 25 years old) have the same casualty risk as middle-aged drivers, and all drivers. Apparently calculating risk per police-reported crash accounts for much of the effect of poor driving behavior of young drivers that is observed in calculating risk per vehicle or vehicle-mile.

Accounting for Bad Driving Behavior

Driver age and gender is a crude measure of driving behavior; a more accurate measure would be the circumstances of the current crash and past driving record. We analyzed NHTSA's "bad driver rating" variable (based on whether alcohol, drugs, or reckless driving was involved in the current crash, as well as the driver's driving record over the last 3 years) by vehicle type and found that young males have the highest, and elderly drivers the lowest, bad driver rating across all vehicle types, using FARS data for model years 2003 through 2007. Young females have much lower bad driver ratings than young males;

this suggests that the higher casualty risks for women compared to men are the result of their relative frailty rather than risky driving behaviors on their part. Similarly, elderly drivers are very safe drivers, but they face high casualty risks because of their frailty.

The casualty risks for bad drivers are substantially higher than those for drivers who are not bad, for all vehicle types; this suggests that bad drivers are involved in a greater number of serious crashes, perhaps involving higher speeds, than not bad drivers. Bad drivers account for a greater increase in casualty risk for certain vehicle types (import luxury cars, SUVs, crossover SUVs, and pickups) than they do for most types of cars (including sports cars), minivans, and full-size vans.

Accounting for Crash Location

We used the population density of the county in which a crash occurred to assess the relationship between casualty risk and crash location. Casualty risk decreases as county population density increases, with the highest casualty risks in the most rural counties and the lowest risks in the most urban counties, for all vehicles types. However, because a large fraction of pickup trucks are driven in rural areas (22%, as opposed to 10% for other vehicle types), accounting for the population density of the county in which a crash occurs reduces the casualty risk in pickup trucks by about 15% relative to that of other vehicle types. Because crash frequency in rural counties is four times higher than in urban counties, the effect of driving in rural counties on casualty risk per crash is smaller (twice as high as in urban counties) than the effect on casualty risks per vehicle registration year (10 times as high in rural counties as in urban counties).

Accounting for General Quality of Vehicle Design

Using NASS GES, which reports the zip code on the driver's license, there clearly is a relationship between driver income (the median household income of the driver's zip code) and casualty risk per crash for cars, with casualty risk decreasing as driver income increases for each car type. In addition, risk consistently decreases as income increases for five of the 10 most prevalent vehicle models; however, there is no similar relationship for the other five prevalent vehicle models. Therefore it is not clear how strong the relationship between driver income and risk is when one accounts for vehicle model. The decrease in casualty risk as income increases is not the result of better driving behavior by drivers with higher incomes, as the percent of bad drivers does not increase with increasing income, with the possible exception of drivers with the highest incomes.

Conclusions

Our analysis of the two types of risk, fatality risk per vehicle registration year and casualty risk per police-reported crash indicates that there is reasonable agreement between the two types of risk, especially by vehicle type. Based on our analysis of data from five states, there is good agreement between fatality and casualty risk per registered vehicle across most vehicle types, although sports cars and pickup trucks have substantially lower casualty risk than fatality risk. Using police-reported crashes rather than vehicle registration years as the measure of exposure results in relatively lower casualty risks for subcompact and compact cars and relatively higher risk for large and import luxury cars, minivans, large SUVs, and ½ and ¾ ton pickups.

Adjusting casualty risks per registration year by the average odometer reading of individual vehicle models increases casualty risk of sports cars by about 30%, as sports cars are driven many fewer miles than other vehicle types. However, adjusting for mileage has no effect on the casualty risks of other vehicle types.

There is a strong correlation between vehicle registration years and the number of vehicles involved in police-reported crashes, by vehicle model. This indicates that crashes, rather than registration years, can be safely used as the measure of exposure.

Calculating risk using all police-reported crashes, rather than vehicle registration years, as the measure of exposure changes the risk of certain vehicle types relative to that of other vehicle types. For example, subcompact and compact cars have higher crash involvement rates than midsize, large, and import luxury cars, so the difference in casualty risk between smaller and larger cars is dramatically reduced when the measure of exposure is changed from registration years to all police-reported crashes. On the other hand, midsize and large cars and minivans have relatively low crash involvement rates, so changing the measure of exposure to crashes increases their casualty risk relative to that of other vehicle types. Similarly, the relatively low crash involvement rates of large SUVs, crossover SUVs, and full-size pickups results in relatively higher casualty risks

when the measure of exposure is changed from vehicle registration years to all police-reported crashes. In general, changing the measure of exposure from registration years to all police-reported crashes reduces the sharp decline in casualty risk as car size increases. Casualty risk per crash does decrease as size increases, within each major vehicle type, but for cars and truck-based SUVs the decrease is not as large as when registration years is used as the measure of exposure.

National GES casualty risks are remarkably similar to the casualty risks from all police-reported crashes in the five states for all vehicle types except pickup trucks, which suggests that the five-state casualty risks are representative of national casualty risks. However, pickup trucks do have substantially lower casualty risks in the national GES data than in the police-reported crash data from the five states.

Bias introduced by different states' definitions of police-reported crashes, or serious injury crashes can be addressed by indexing risk by vehicle type or model to the risk for all vehicles in that state. This bias can be addressed in the logistic regression model by introducing a dummy variable for each state. Analysis of crash frequencies of one-vehicle, non-rollover, non-injury crashes suggests that crashes involving pickup trucks are not underreported.

Elderly drivers (over 65 years old) have higher casualty risk than other drivers in virtually all vehicle types. For most vehicle types, young drivers (under 25 years old) have the same casualty risk as middle-aged drivers, and all drivers. Apparently calculating risk per police-reported crash accounts for much of the effect of poor driving behavior of young drivers that is observed in calculating risk per vehicle or vehicle-mile.

Driver age and gender is a crude measure of driving behavior; a more accurate measure would be the circumstances of the current crash and past driving record. Using NHTSA's "bad driver rating" variable and FARS data for model years 2003 through 2007, young males have the highest, and elderly drivers the lowest, bad driver rating across all vehicle types. Young females have much lower bad driver ratings than young males, suggesting that the higher casualty risks for women compared to men are the result of their relative frailty rather than risky driving behaviors on their part. Similarly, elderly drivers are very safe drivers, but they face high casualty risks because of their frailty.

Casualty risk decreases as county population density increases, with the highest casualty risks in the most rural counties, and the lowest risks in the most urban counties, for all vehicles types. However, because a large fraction of pickup trucks are driven in rural areas (22%, as opposed to 10% for other vehicle types), accounting for the population density of the county in which a crash occurs reduces the casualty risk in pickup trucks by about 15% relative to that of other vehicle types. Because crash frequency in rural counties is four times higher than in urban counties, the effect of driving in rural counties on casualty risk per crash is smaller (twice as high as in urban counties) than the effect on casualty risks per vehicle registration year (10 times as high in rural counties as in urban counties).

NASS GES data indicate that casualty risk per crash decreases as driver income increases, for each car type. Although risk consistently decreases as income increases for five of the 10 most prevalent vehicle models, there is no similar relationship for the other five prevalent vehicle models; therefore, it is not clear how strong the relationship between driver income and risk is when one accounts for vehicle model. The decrease in casualty risk as income increases is not the result of better driving behavior by drivers with higher incomes, as the percent of bad drivers does not increase with increasing income, with the possible exception of drivers with the highest incomes.

The study indicates that, for the most part, casualty risks per crash are similar to fatality risks per mileage-adjusted vehicle registration year, by vehicle type. We expect that the general agreement between casualty risk per crash and fatality risk per vehicle registration year will hold when we and NHTSA use updated vehicle curb weight by vehicle make and model in logistic regression models to determine the statistical relationship between vehicle weight and risk. These regression models are being developed to help inform NHTSA's analysis of the potential casualty and fatality risk associated with vehicle lightweighting. The models will ultimately be used to estimate the safety impacts of proposed upcoming NHTSA and EPA regulations on new vehicle fuel economy and tailpipe greenhouse gas emissions, respectively, where weight reduction technologies are expected to play an important role.

Presentations / Publications / Patents

Wenzel, T.P. Analysis of Casualty Risk per Police-Reported Crash for Model Year 2000 to 2004 Vehicles, using Crash Data from Five States. Draft report prepared for EERE, U.S. DOE, October 2010.

This document highlights work sponsored by agencies of the U.S. Government. Neither the U.S. Government nor any agency thereof, nor any of their employees, makes any warranty, express or implied, or assumes any legal liability or responsibility for the accuracy, completeness, or usefulness of any information, apparatus, product, or process disclosed, or represents that its use would not infringe privately owned rights. Reference herein to any specific commercial product, process, or service by trade name, trademark, manufacturer, or otherwise does not necessarily constitute or imply its endorsement, recommendation, or favoring by the U.S. Government or any agency thereof. The views and opinions of authors expressed herein do not necessarily state or reflect those of the U.S. Government or any agency thereof.

For more information
1-877-EERE-INFO (1.877.337.3463)
eere.energy.gov

DOE/EE-0577

January 2011

Printed with a renewable-source ink on paper containing
at least 50% wastepaper, including 10% post consumer waste.